

The Stability of Selected Psychoactive Drugs in Simulated Post-mortem Blood

by

Jared William Castle

BSc (Forensic and Analytical Science) (Hons)

*Thesis
Submitted to Flinders University
for the degree of*

Doctor of Philosophy

College of Science and Engineering

February 2020

DECLARATION

“I certify that this thesis:

1. does not incorporate without acknowledgment any material previously submitted for a degree or diploma in any university; and

2. to the best of my knowledge and belief, does not contain any material previously published or written by another person except where due reference is made in the text.”

Jared W. Castle

5th February 2020

This research was funded by the Ross Vining Grant from the Government of South Australia and was performed in collaboration with Forensic Science South Australia.

A large proportion of this research was performed within the Toxicology Laboratories at Forensic Science SA, with in kind support provided in the form of drug standards, chemicals, equipment, access to instrumentation, IT support, scientific guidance and research supervision.



Government of South Australia

Forensic Science SA

ACKNOWLEDGEMENTS

This has been a journey:

From Pasadena to Brompton to Nailsworth to Prospect to Richmond to St Kilda West to Kensington; from RACI to ANZFSS to FACTA to AAFS; and from Flinders to Forensic Science SA to the Victorian Institute of Forensic Medicine.

First and foremost, tremendous thanks to my primary supervisors, Paul Kirkbride and Danielle Butzbach, whose training, advice, and willingness to critique my work have been invaluable. Really, I couldn't have achieved this without your support and assistance. Special thanks to my co-supervisor, Frank Reith, without whose assistance in helping me navigate the complexities of microbial analyses I would have known not where to start. You reminded me there are times you need to relax and times you need to get on with it, even if you've got a full-time job to do. Thanks especially for the Fringe memories. For your enthusiasm and permission to write a chapter for *Forensic Microbiology*, thank you David Carter. I'm not alone in thinking our collaboration was a success! Thanks also to Claire Lenehan and Stewart Walker, for critical editing advice, and Sam Costello, for the inclination to offload faeces. Real fun...

I feel privileged to have carried out my studies and research at FSSA. It was a pleasure to work amongst you all, an exemplary team of individuals, most supportive and tolerant of my inquisitiveness, and I am so deeply grateful for the experience. I miss you all. Thanks to Peter Stockham for your help with instrumentation and Chris Kostakis for your willingness to accommodate me. Although challenging, I feel equally privileged to have been able to carry out the write up while working at the Victorian Institute of Forensic Medicine in the dream job I've been working toward for almost a decade, and desired for even longer (credit due also to my parents for allowing me to watch questionable material at the age of 5, sparking this mission in the first place). Thanks for taking a chance on me, a *graduate*, and thanks to those who have encouraged me to finish this beast and that make it such a great place to work. Thanks especially to Matt, whose enthusiasm for research and improvement is contagious, and whose willingness to teach me has been, and no doubt will continue to be, both of great motivation and benefit. Thanks also to staff and students at CSIRO Land & Water for always being there to help me out – I think you all had to tolerate the worst of my stupid questions during my candidature.

I acknowledge the financial support of Flinders University, who enabled me to attend not one but two overseas conferences. This led to some incredible memories (Seattle and the obligatory post-international-conference *vacation*) and some not so incredible memories (food poisoning

in Auckland). An Australian Government Research Training Program Scholarship was also provided as a stipend throughout the duration of candidature.

Beyond academia: thanks Emma, for the help when I felt like I was falling off a cliff; thanks now-Dr Phil, for our study sessions, which provided a nice change of venue for me to stare at a screen; thanks Andy, for our well timed Blue Mountain trip and late-game advice; thanks to my Adelaide board game, hiking, and beach buddies (cheers Cameron, Luke), offering me sweet respite; thanks to all the musos, for compositions that kept me sane during the mundane realities of formatting and pushed me onward during the challenges of research; and lastly...

... a world of gratitude to James. It's hard to imagine what the tail end of this journey would have been like without your support.

Well, it's been a real team effort this PhD-thing but...as this is a thesis and not a phone book I can't prattle on forever. I do want to explicitly *not* thank my appendix though. Good riddance.

"This is all we have when we die." – Tommy Rogers¹

¹ Between the Buried and Me, Lyrics to "White Walls". *Colors*, 2007.

SUMMARY

The presence or absence of psychoactive medication in post-mortem specimens is important to establish to determine medication adherence or potential drug intoxication in coronial investigations. This thesis examined the stability of 17 selected antipsychotic and antidepressant drugs. Liquid chromatography coupled to diode array detection (LC-DAD) analytical methods were optimised and validated for the analysis of these drugs in human whole blood. Drug stability was assessed in blood preserved (with 2 % w/v sodium fluoride) and unpreserved; and inoculated (with faecal microorganisms) or non-inoculated. Their stability was evaluated at: -20 °C and 4 °C, to simulate specimen/body storage; room temperature, relevant to specimen handling; and 37 °C, relevant post-death and in warm climates.

Dominant microorganisms present in inoculated blood specimens throughout the 37 °C experiments were identified using 16S rRNA sequencing as previously reported dominant species in post-mortem specimens, indicating the methodology used to simulate post-mortem blood was suitable. Preservation did not prevent community changes over time in all preserved specimens, indicating sodium fluoride alone may not limit microbial activity for some species. There was a significant difference between microbial communities based on temperature, sodium fluoride presence, and the interaction between these factors, indicating that communities present in authentic post-mortem specimens may vary depending on the environment of the body after death, the time at which specimens are collected, and how specimens are stored and handled.

The greater instability of chlorpromazine, fluphenazine, prochlorperazine, and flupentixol, and reduced formation of some degradation products, at -20 °C than at 4 °C, after a year, indicates it may be preferable to refrigerate and not freeze specimens. N-dealkylation degradation products were detected for many drugs. However, this degradative pathway is unlikely to affect the interpretation of casework analyses unless degradation rates are considerably enhanced in authentic post-mortem specimens.

Lurasidone degraded until undetected in inoculated, unpreserved blood specimens stored at room temperature and 37 °C. Degradation products were characterised by liquid chromatography coupled to quadrupole-time-of-flight-mass-spectrometry (LC-QTOF-MS), followed by comparison to standards synthesised by Tristan Fraser [1]. Unambiguous identification was not achieved. Nevertheless, the major degradation product was detected in retrospectively analysed casework data. Risperidone, which degraded at a similar rate in the

same experiments, is known to degrade in post-mortem specimens until only its degradation product may be detected [2, 3]. The major lurasidone degradation product should therefore be included in coronial screening methods as a marker of lurasidone administration. FSSA now utilises the major lurasidone degradation product to indicate cases where lurasidone concentrations may be underestimated.

Ziprasidone was unstable in all blood specimens stored at room temperature and 37 °C. It was indicated that ziprasidone may react with carbonyl species present in blood, and that the resultant degradation products may further degrade due to microbial activity and then degrade to unknown products. This highlights that ziprasidone may not be reliably detected in post-mortem casework. Due to limited casework data available for review, it remains to be determined if the degradation products detected should be used as indicators of the ante-mortem administration of ziprasidone.

PUBLICATIONS

Book chapter:

Jared W. Castle, Danielle M. Butzbach, G. Stewart Walker, Claire E. Lenehan, Frank Reith & K. Paul Kirkbride

“Microbial impacts in postmortem toxicology”. In book: Forensic Microbiology. pp. 212-244 (2017)*

Communications:

Jared Castle

“Research Hub: Investigating prescription drug degradation by microbes using a simulated post-mortem blood model”. In FACTA News (August 2017). p. 2

Jared W. Castle, Danielle Butzbach, Stewart Walker, Claire Lenehan, Frank Reith, Sam Costello & Paul Kirkbride

“Best Oral Presentation Runner-Up: Jared Castle
Antipsychotic drug degradation in a simulated post-mortem blood model: A summary”. In FACTA News (December 2017). p. 4-5

Journal publications in preparation:

Jared W. Castle, Danielle M. Butzbach, G. Stewart Walker, Claire E. Lenehan, Sam P. Costello & K. Paul Kirkbride

“Stability of 17 psychoactive drugs in a ‘simulated post-mortem blood’ model”

Jared W. Castle, Tristan Fraser, Danielle M. Butzbach, G. Stewart Walker, Claire E. Lenehan, K. Paul Kirkbride

“Microbial degradation products of lurasidone”

Jared W. Castle, Danielle M. Butzbach, G. Stewart Walker, Claire E. Lenehan, K. Paul Kirkbride

“*In vitro* degradation of ziprasidone in human whole blood”

Conference papers:

Jared W. Castle, Danielle M. Butzbach, G. Stewart Walker, Claire E. Lenehan, Frank Reith, Sam Costello & K. Paul Kirkbride

“Prescription drug degradation in a simulated post-mortem blood model”

Oral Presentation at the American Academy of Forensic Sciences 70th Annual Scientific Meeting held in Seattle, United States, 19-24th February, 2018.

Jared W. Castle, Danielle M. Butzbach, G. Stewart Walker, Claire E. Lenehan, Frank Reith, Sam Costello & K. Paul Kirkbride

“Antipsychotic drug degradation in a simulated post-mortem blood model”**

Oral Presentation at the Forensic and Clinical Toxicology Association Inc. Meeting held in Melbourne, Australia, 19-22nd November, 2017.

Jared W. Castle, Danielle M. Butzbach, G. Stewart Walker, Claire E. Lenehan, Frank Reith, Sam Costello & K. Paul Kirkbride

“An optimised LC-UV method for the analysis of antipsychotics in blood”

Poster Presentation at the Australian and New Zealand Forensic Science Society 23rd International Symposium on the Forensic Sciences held in Auckland, New Zealand, 18-22nd September, 2016.

*Awarded the Australian and New Zealand Policing Advisory Agency/National Institute of Forensic Science Best Chapter in a Book award for 2017.

**Awarded by the Forensic and Clinical Toxicology Association Inc. committee runner up best oral presentation.

CONTENTS

Declaration	i
Acknowledgements	iii
Summary	v
Publications	vii
Contents	ix
Figures	xii
Tables	xxiii
Equations	xxvii
Abbreviations	xxviii
Chapter 1 - General introduction	1
1.1 Post-mortem toxicology: background	1
1.2 Post-mortem decomposition.....	1
1.3 Challenges in post-mortem toxicology	5
1.4 Antidepressant and antipsychotic drugs.....	8
1.5 Analytical techniques.....	16
1.6 Analysis of microbial communities.....	21
1.7 Research overview.....	24
Chapter 2 - Post-mortem drug stability	28
2.1 Overview	28
2.2 “Microbial impacts in postmortem toxicology”	29
2.3 Addendum	54
Chapter 3 - Materials & instrumentation	57
3.1 Chemicals.....	57
3.2 Materials.....	60
3.3 Instrumentation	62
3.4 Data analysis.....	64
Chapter 4 - Method development & validation	66
4.1 Outline.....	66
4.2 Final method.....	66
4.3 Method optimisation.....	67

4.4	Method validation	78
4.5	Conclusions	93
Chapter 5 - Drug stability in aqueous solutions		95
5.1	Outline.....	95
5.2	Monitoring chromophores by UV-Vis spectroscopy.....	95
5.3	LC-DAD monitoring of hydrolysis.....	99
5.4	Ziprasidone and lurasidone hydrolysis.....	101
5.5	Qualitative LC-QTOF-MS analysis	103
5.6	Conclusions	108
Chapter 6 - Drug stability in human whole blood		109
6.1	Outline.....	109
6.2	Overview of experiments	109
6.3	Drug stability results and discussion	121
6.4	Microbial analyses results and discussion.....	139
6.5	UV-Vis spectroscopy of blood specimens.....	147
6.6	Conclusions	149
Chapter 7 - Degradation products in blood experiments		152
7.1	Outline.....	152
7.2	LC-QTOF-MS analyses of blood experimental extracts.....	152
7.3	Conclusions	167
Chapter 8 - Lurasidone degradation products.....		168
8.1	Outline.....	168
8.2	Identification of degradation products	168
8.3	Qualitative blood experiment.....	194
8.4	Hydrolysis of lurasidone in ante-mortem blood	196
8.5	Post-mortem casework analysis	198
8.6	Conclusions	202
Chapter 9 - Ziprasidone degradation products		204
9.1	Outline.....	204
9.2	LC-DAD and LC-QTOF-MS analyses of blood experiment extracts	204

9.3	Deuterated ethanol experiment	229
9.4	Solvent reactivity	237
9.5	Post-mortem casework analysis	243
9.6	Conclusions	244
Chapter 10 - Conclusions and future work.....		247
10.1	Conclusions	247
10.2	Future work.....	250
Appendix A - Identification of prochlorperazine stock impurity.....		255
A.1	Identification of prochlorperazine stock impurity	255
Appendix B - Blood experiments data.....		259
B.1	Data normalisation	259
B.2	Risperidone degradation.....	261
B.3	Drug degradation in the week experiments.....	262
B.4	Drug degradation in the longer-term experiments.....	265
Appendix C - Microbial communities		273
C.1	Sequencing results	273
C.2	Community comparisons	274
C.3	Taxa relative abundance.....	275
Appendix D - Degradation products		288
D.1	N-dealkylation degradation products	288
D.2	Sulfoxide degradation products	298
References.....		300

FIGURES

Figure 1-1: Structure of antidepressant drugs investigated.....	15
Figure 1-2: Structure of first-generation antipsychotics investigated.....	15
Figure 1-3: Structure of second-generation antipsychotics investigated.....	15
Figure 4-1: Optimised separation of analytes as two drug sets using method A.....	70
Figure 4-2: Optimised separation of “A drugs” using method A.....	70
Figure 4-3: Optimised separation of “B drugs” using method B.....	71
Figure 4-4: UV-Vis absorbance spectra of a) ZUCL and co-eluting adjacent peak and inset, chromatogram and b) peaks identified as CHLO-SO and PROC-SO.....	71
Figure 4-5: Extraction recovery experiment protocols.....	73
Figure 4-6: AMIS peak shape under a variety of conditions.....	75
Figure 4-7: UV-Vis absorbance spectrum of unknown peak at RT=13.7 min following unbuffered LLE from human whole blood.....	77
Figure 4-8: Standard deviation and variance of instrument responses vs. concentration plot for PROC.....	82
Figure 4-9: Initial and adjusted RT of “A drugs” using Method A.....	92
Figure 4-10: Initial and adjusted RT of “B drugs” using Method B.....	93
Figure 5-1: UV spectra of HALO over time in a) pH = 7 solution and b) pH = 11 solution.....	97
Figure 5-2: UV spectra of CLOM over time in a) pH = 7 solution and b) pH = 11 solution.....	97
Figure 5-3: UV spectra of ZIPR over time in a) pH = 7 solution and b) pH = 11 solution.....	98
Figure 5-4: UV spectra of LURA over time in a) pH = 7 solution and b) pH = 11 solution.....	98
Figure 5-5: ARIP degradation in neutral aqueous solution over time.....	101
Figure 5-6: UV-Vis spectra of ZIPR and alkaline degradation products.....	103
Figure 5-7: Extracted ion chromatograms for PERI and PERI-AMD.....	105
Figure 5-8: Proposed fragmentation pathway for PERI and PERI-AMD.....	106
Figure 5-9: MS/MS spectra for a) PERI and b) PERI-AMD. Collision energy = 20 eV.....	107
Figure 5-10: Extracted ion chromatograms of ZIPR (black) and ZIPR alkaline hydrolysis products (coloured).....	107

Figure 6-1: Aqueous blood layer of sub-samples from experiment WA following collection of the organic layer. Note the cherry red colour for #6 and #2.	120
Figure 6-2: Concentration change (%) of AMIT in a,b,c) unpreserved and d) preserved blood specimens incubated at a) 37 °C for 7 days in experiment WA, b) room temperature for 12 months in experiment YA, and c-d) room temperature for 7 months in experiment YB.....	122
Figure 6-3: Relative concentration change (%) of RISP in blood specimens incubated at 37 °C for 7 days in experiment WA.....	123
Figure 6-4: Relative concentration change (%) of RISP in a) experiment WBI and b) experiment WB2 blood specimens incubated at 37 °C for 7 days.....	124
Figure 6-5: Relative concentration change (%) of CHLO in blood specimens incubated at 37 °C for 7 days in experiment WA.	125
Figure 6-6: Relative concentration change (%) of A analytes in blood specimens incubated at 37 °C for 7 days in experiment WA.....	125
Figure 6-7: Relative concentration change (%) of B analytes in blood specimens incubated at 37 °C for 7 days in experiment WBI and WB2.	125
Figure 6-8: Relative concentration change (%) of LURA in a) experiment WBI and b) experiment WB2 and in blood specimens incubated at 37 °C for 7 days.	126
Figure 6-9: Relative concentration change (%) of ZIPR in a) experiment WBI and b) experiment WB2 and in blood specimens incubated at 37 °C for 7 days.	127
Figure 6-10: Relative concentration change (%) of A analytes in blood specimens incubated at a) -20 °C, b) 4 °C, and c) room temperature for 12 months in experiment YA.	128
Figure 6-11: Relative concentration change (%) of B analytes in blood specimens incubated at a) -20 °C, b) 4 °C, and c) room temperature for 7 months in experiment YB.	129
Figure 6-12: Relative concentration change (%) of a,c,e) LURA and b,d,f) ZIPR in blood specimens incubated at a,b) -20 °C, c,d) 4 °C, and e,f) room temperature for 7 months in experiment YB.	130
Figure 6-13: Relative response to LORA for a) CHLO-SO, b) PROC-SO, and c) PERA in blood specimens incubated at 37 °C for 7 days in experiment WA.....	132
Figure 6-14: Relative response to LORA for a-c) CHLO-SO, d-f) PROC-SO, and (g-i) PERA in blood specimens incubated at a,d,g) -20 °C, b,e,h) 4 °C, and c,f,i) room temperature for 12 months in experiment YA.	134

Figure 6-15: UV-Vis absorbance spectra of three unknown peaks eluting in experiment YA. .	135
Figure 6-16: Microbial diversity index scatterplots.....	141
Figure 6-17: Most abundant species present in specimens.....	143
Figure 6-18: Hierarchical cluster dendrogram of specimens.....	144
Figure 6-19: PCoA plot of specimens.....	145
Figure 6-20: CO-Hb (%) in unpreserved blood specimens of the a) week-long experiments (WA, WBI, and WB2) and b) longer experiments (YA and YB).	148
Figure 6-21: CO-Hb (%) in unpreserved blood specimens of the a) experiment WA, inoculated with drugs and b) experiment YB microbial matrix controls.....	148
Figure 6-22: UV-Vis spectra of blood specimens.....	149
Figure 7-1: Proposed MS/MS fragmentation pathway for AMIT, NORT, and NORT-AC.....	155
Figure 7-2: Chromatogram of an extract collected from an inoculated, unpreserved blood specimen stored at room temperature for 12 months in experiment YA.	161
Figure 7-3: Relative response of AMIT and NORT over time in experiment YA in a) non-inoculated, unpreserved specimens, b) non-inoculated, preserved specimens, c) inoculated, unpreserved specimens, and d) inoculated, preserved specimens.	164
Figure 7-4: Relative response of FLPH and FLPH-SO over time in experiment YA in a) non-inoculated, unpreserved specimens, b) non-inoculated, preserved specimens, c) inoculated, unpreserved specimens, and d) inoculated, preserved specimens.	165
Figure 8-1: Structure of <i>cis</i> -N-debenzothiazole lurasidone.	170
Figure 8-2: Synthetic scheme for N-debenzothiazole lurasidone.	170
Figure 8-3: Extracted ion chromatograms of LURA and possible degradation products in a seven month extract of an inoculated, unpreserved room temperature blood specimen.	171
Figure 8-4: Relative response of LURA and 360.265 m/z degradation product over time in inoculated, unpreserved blood specimens for a) week experiment B1 and b) week experiment B2.	172
Figure 8-5: Relative response of LURA and 360.265 m/z degradation product over time in preserved and unpreserved, non-inoculated blood specimens and preserved, inoculated blood specimens for a) week experiment B1 and b) week experiment B2.	173

Figure 8-6: Relative response of LURA and 388.259 m/z degradation product over time in inoculated, unpreserved blood specimens for a) week experiment B1 and b) week experiment B2.	174
Figure 8-7: Relative response of LURA and 402.275 m/z degradation product over time in inoculated, unpreserved blood specimens for week experiment B1.	174
Figure 8-8: Relative response of LURA and 360.265 m/z degradation product over time in seven-month experiment in a) non-inoculated, unpreserved specimens, b) non-inoculated, preserved specimens, c) inoculated, unpreserved specimens, and d) inoculated, preserved specimens.	175
Figure 8-9: Relative response of LURA and 388.259 m/z degradation product over time in seven-month experiment in inoculated, unpreserved specimens.	176
Figure 8-10: Relative response of LURA and 460.281 m/z degradation product over time in seven-month experiment in inoculated, unpreserved specimens.	176
Figure 8-11: Relative response of LURA and 402.275 m/z degradation product over time in seven-month experiment in a) non-inoculated, unpreserved specimens, b) non-inoculated, preserved specimens, c) inoculated, unpreserved specimens, and d) inoculated, preserved specimens.	177
Figure 8-12: Relative response of LURA and 430.306 m/z degradation product over time in seven-month experiment in a) non-inoculated, unpreserved specimens, b) non-inoculated, preserved specimens, c) inoculated, unpreserved specimens, and d) inoculated, preserved specimens.	178
Figure 8-13: MS spectra with generated molecular formula showing predicted isotope ratios in red for: a) LURA and the major 360.265 m/z degradation product.	179
Figure 8-14: MS spectra with generated molecular formula showing predicted isotope ratios in red for degradation products with m/z of a) 388.259, and b) 402.275 c) 430.306 and d) 460.281.	180
Figure 8-15: Extracted ion chromatogram of LURA-SO.	181
Figure 8-16: MS spectra with generated molecular formula showing predicted isotope ratios in red boxes for LURA-SO.	181
Figure 8-17: Relative response of LURA and LURA-SO over time in seven-month experiment in a) non-inoculated, unpreserved specimens, b) non-inoculated, preserved specimens, c) inoculated, unpreserved specimens, and d) inoculated, preserved specimens.	183

Figure 8-18: Chemical structure of a) DPI and b) DP2 and DP3 as postulated by Kumar Talluri <i>et al.</i> [432].	184
Figure 8-19: MS/MS spectra for: a) LURA; and degradation products with m/z of b) 360.265, c) 388.259, and d) 402.275. Collision energy = 40 eV.	185
Figure 8-20: MS/MS spectra for: a) 430.306 m/z degradation product, b) 460.281 m/z degradation product, and c) LURA-SO. Collision energy = 40 eV.	186
Figure 8-21: Proposed MS/MS fragmentation pathway for LURA and ND-LURA.	188
Figure 8-22: Proposed degradation of LURA via a) 1,2-benzisothiazole reduction and subsequent b) amidine hydrolysis of reductively cleaved LURA to yield the degradation product ND-LURA.	189
Figure 8-23: Structure of a) ziprasidone and b) ziprasidone metabolite M4A.	190
Figure 8-24: MS/MS spectra for a) the 360.265 m/z degradation product and b) <i>trans</i> -ND-LURA. Collision energy = 40 eV.	192
Figure 8-25: Extracted ion chromatograms of synthesised ND-LURA and 360.265 m/z degradation product.	193
Figure 8-26: Structural isomers of C ₂₁ H ₃₃ N ₃ O ₂ .	194
Figure 8-27: Chemical structure of buspirone.	195
Figure 8-28: Non-refrigerated interval (NRI) and ratio of 360.265 m/z degradation product to LURA data for post-mortem cases.	200
Figure 9-1: UV-Vis absorbance spectra of ZIPR and suspected ZIPR degradants in blood experiments.	205
Figure 9-2: Relative response of unknown peaks eluting near AMIT in first week-long blood experiment (WBI) using B drugs: a) before AMIT, and b) after AMIT.	205
Figure 9-3: Relative response of ZIPR and 439.135 m/z degradation products over time in inoculated, unpreserved blood specimens for a) week experiment B1 and b) week experiment B2.	208
Figure 9-4: Relative response of ZIPR and a-b) 439.135 m/z and c-d) 455.132 m/z degradation products over time in preserved and unpreserved, non-inoculated blood specimens and preserved, inoculated blood specimens for a,c) week experiment B1 and b,d) week experiment B2.	210

Figure 9-5: Relative response of ZIPR and the suspected ZIPR degradation products 439.135 m/z and 441.152 m/z over time in inoculated, unpreserved blood specimens for a) week experiment B1 and b) week experiment B2.....	211
Figure 9-6: Relative response of ZIPR and 439.135 m/z degradation product over time in seven-month experiment in a) non-inoculated, unpreserved specimens, b) non-inoculated, preserved specimens, c) inoculated, unpreserved specimens, and d) inoculated, preserved specimens.	212
Figure 9-7: Relative response of ZIPR and 441.152 m/z degradation product over time in seven-month experiment in a) non-inoculated, unpreserved specimens, b) non-inoculated, preserved specimens, c) inoculated, unpreserved specimens, and d) inoculated, preserved specimens.	213
Figure 9-8: Relative response of ZIPR and 455.132 m/z degradation product over time in seven-month experiment in a) non-inoculated, unpreserved specimens, b) non-inoculated, preserved specimens, c) inoculated, unpreserved specimens, and d) inoculated, preserved specimens.	214
Figure 9-9: Extracted ion chromatograms of ZIPR and suspected degradation products.	215
Figure 9-10: MS spectra with generated molecular formula showing predicted isotope ratios in red boxes for ZIPR.	215
Figure 9-11: MS spectra with generated molecular formula showing predicted isotope ratios in red boxes for the suspected ZIPR degradants of m/z: a) 439.135, b) 441.152, and c) 455.132.	216
Figure 9-12: Extracted ion chromatogram of 429.115 m/z degradant.	217
Figure 9-13: MS spectrum with generated molecular formula showing predicted isotope ratios in red boxes for 429.115 m/z degradant.....	217
Figure 9-14: Relative response of ZIPR and 429.115 m/z degradation product over time in seven-month experiment in a) non-inoculated, unpreserved specimens, b) non-inoculated, preserved specimens, c) inoculated, unpreserved specimens, and d) inoculated, preserved specimens.	218
Figure 9-15: MS/MS spectra for a) ZIPR and the suspected degradants of m/z: b) 439.135, c) 441.152, and d) 455.132. Collision energy = 40 eV.	220
Figure 9-16: MS/MS spectra for 429.115 m/z degradant. Collision energy = 40 eV.....	221
Figure 9-17: Structural isomers of C ₂₃ H ₂₃ ClN ₄ OS: a) 1-vinyl-ziprasidone, b) 3-vinyl-ziprasidone, c) spiro[cyclopropane-1,3']-ziprasidone, and d) 3-ethylidene-ziprasidone.	223
Figure 9-18: Proposed MS/MS fragmentation pathway for ZIPR and the 439.135 m/z (3E-ZIPR) degradation products.	225

Figure 9-19: Proposed MS/MS fragmentation pathway for 441.152 m/z (3A-ZIPR degradation product).	226
Figure 9-20: Structural isomers of C ₂₃ H ₂₃ ClN ₄ O ₂ S: a) 3-ethylidene ziprasidone sulfoxide, b) 1-acetyl-ziprasidone, c) 3-acetyl-ziprasidone, and d) 2-acetyl-ziprasidone.	227
Figure 9-21: Chemical structure of unobserved theoretical degradants a) N-debenzothiazole-3-ethyl-ziprasidone and b) N-debenzothiazole-3-ethylidene-ziprasidone.	227
Figure 9-22: Structure and pathway of formation of hypothetical ZIPR species.	228
Figure 9-23: UV-Vis absorbance spectra of additional peaks observed in deuterated experiment compared to a) early eluting 439.135 m/z peak and b) later eluting 439.135 m/z peak observed in non-deuterated experiments.	232
Figure 9-24: Extracted ion chromatograms of suspected deuterated degradants of ZIPR.	232
Figure 9-25: MS spectra with generated molecular formula showing predicted isotope ratios in red boxes for degradants of m/z a) 440.142 and b) 456.137.	233
Figure 9-26: Relative response of ZIPR and degradants of m/z a) 440.142 and b) 456.137 over time in preserved and unpreserved, non-inoculated blood specimens for deuterated experiment.	234
Figure 9-27: MS/MS spectra for degradants of m/z a) 440.142 and b) 456.137. Collision energy = 40 eV.	235
Figure 9-28: Hypothesised product following the reaction of ZIPR with acetone (3-(propan-2-ylidene)-ziprasidone).	237
Figure 9-29: UV-Vis absorbance spectra of 439.135 m/z peak in blood and peak detected in week-long acetaldehyde experiment.	238
Figure 9-30: UV-Vis absorbance spectra of peaks detected during a) initial analyses, b) after two hours, c) after six hours, and d) from ten hours. ZIPR shown for comparison only.	240
Figure 10-1: Structure of a) perospirone and b) postulated microbial degradation product of perospirone.	253
Figure 10-2: Structure of a) ropinirole and b-c) postulated degradation products of ropinirole.	253
Figure 10-3: Structure of a) roluperidone and b-c) postulated degradation products of roluperidone.	254

Figure A-1: UV-Vis absorbance spectra of PROC (solid line) and impurity at RT=16.6 min (dotted line).....	255
Figure A-2: MS spectra with generated molecular formula showing predicted isotope ratios as red boxes for a) PROC and b) PERA. Observed ion signal intensities are shown as lines within the boxes.....	256
Figure A-3: MS/MS spectra for a) PROC and b) PERA. Collision energy = 20 eV.....	257
Figure A-4: Possible fragmentation pathway of PROC and PERA.....	257
Figure B-1: Concentration change (%) of AMIT in a,c,e) preserved and b,d) unpreserved blood specimens incubated at 37 °C for 7 days in a) experiment WA, b-c) experiment WBI, and d-e) experiment WB2.	259
Figure B-2: Concentration change (%) of AMIT in a,c,e,g) preserved and b,d,f,h) unpreserved blood specimens incubated for 12 months a-b) at -20 °C and c-d) 4 °C in experiment YA and incubated for 7 months e-f) at -20 °C and g-h) 4 °C in experiment YB.....	260
Figure B-3: Relative concentration change (%) of RISP in blood specimens incubated at a) -20 °C, b) 4 °C, and c) room temperature for 12 months in experiment YA and at d) -20 °C, e) 4 °C, and f) room temperature for 7 months in experiment YB.....	261
Figure B-4: Relative concentration change (%) of a) ASEN, b) CLOZ, c) FLPH, d) FLTX, e) HALO, f) PERI, g) PROC, and h) QUET in blood specimens incubated at 37 °C for 7 days in experiment WA.....	262
Figure B-5: Relative concentration change (%) of a-b) ARIP, c-d) CLOM, and e-f) DOTH, and g-h) MIRT in blood specimens incubated at 37 °C for 7 days in a,c,e,g) experiment WBI and b,d,f,h) experiment WB2.	263
Figure B-6: Relative concentration change (%) of a-b) MOCL and c-d) TRIF in blood specimens incubated at 37 °C for 7 days in a,c) experiment WBI and b,d) experiment WB2.	264
Figure B-7: Relative concentration change (%) of a,c,e) ASEN and b,d,f) CHLO in blood specimens incubated at a,b) -20 °C, c,d) 4 °C, and e,f) room temperature for 12 months in experiment YA.....	265
Figure B-8: Relative concentration change (%) of a,c,e) CLOZ and b,d,f) FLPH in blood specimens incubated at a,b) -20 °C, c,d) 4 °C, and e,f) room temperature for 12 months in experiment YA.....	266

Figure B-9: Relative concentration change (%) of a,c,e) FLTX and b,d,f) HALO in blood specimens incubated at a,b) -20 °C, c,d) 4 °C, and e,f) room temperature for 12 months in experiment YA.....	267
Figure B-10: Relative concentration change (%) of a,c,e) PERI and b,d,f) PROC in blood specimens incubated at a,b) -20 °C, c,d) 4 °C, and e,f) room temperature for 12 months in experiment YA.....	268
Figure B-11: Relative concentration change (%) of QUET in blood specimens incubated at a) -20 °C, b) 4 °C, and c) room temperature for 12 months in experiment YA.....	269
Figure B-12: Relative concentration change (%) of a,c,e) ARIP and b,d,f) CLOM in blood specimens incubated at a,b) -20 °C, c,d) 4 °C, and e,f) room temperature for 7 months in experiment YB.....	270
Figure B-13: Relative concentration change (%) of a,c,e) DOTM and b,d,f) MIRT in blood specimens incubated at a,b) -20 °C, c,d) 4 °C, and e,f) room temperature for 7 months in experiment YB.....	271
Figure B-14: Relative concentration change (%) of a,c,e) MOCL and b,d,f) TRIF in blood specimens incubated at a,b) -20 °C, c,d) 4 °C, and e,f) room temperature for 7 months in experiment YB.....	272
Figure C-1: Relative abundance of prokaryotic phyla in experiment specimens.....	276
Figure C-2: Order abundance of phylum Firmicutes in specimens.....	277
Figure C-3: Family abundance of order Clostridiales (of phylum Firmicutes) in specimens...	278
Figure C-4: Species abundance of family Clostridiaceae (of order Clostridiales of class Clostridia of phylum Firmicutes) in specimens.....	278
Figure C-5: Species abundance of family Lachnospiraceae (of order Clostridiales of class Clostridia of phylum Firmicutes) in specimens.....	279
Figure C-6: Species abundance of family Tissierellaceae (of order Clostridiales of class Clostridia of phylum Firmicutes) in specimens.....	280
Figure C-7: Species abundance of family Ruminococcaceae (of order Clostridiales of class Clostridia of phylum Firmicutes) in specimens.....	280
Figure C-8: Species abundance of order Lactobacillales (of class Bacilli of phylum Firmicutes) in specimens.....	281
Figure C-9: Family abundance of phylum Bacteroidetes in specimens.....	282

Figure C-10: Species abundance of family Bacteroidaceae (of order Bacteroidales of class Bacteroidia of phylum Bacteroidetes) in specimens.....	283
Figure C-11: Order abundance of phylum Actinobacteria in specimens.....	284
Figure C-12: Species abundance of order Coriobacteriales (of phylum Actinobacteria) in specimens.	285
Figure C-13: Species abundance of order Bifidobacteriales (of phylum Actinobacteria) in specimens.	285
Figure C-14: Order abundance of phylum Proteobacteria in specimens.....	286
Figure D-1: Relative response of CHLO and NOR-CHLO over time in year experiment in a) non-inoculated, unpreserved specimens, b) non-inoculated, preserved specimens, c) inoculated, unpreserved specimens, and d) inoculated, preserved specimens.	289
Figure D-2: Relative response of QUET and NOR-QUET over time in year experiment in a) non-inoculated, unpreserved specimens, b) non-inoculated, preserved specimens, c) inoculated, unpreserved specimens, and d) inoculated, preserved specimens.	290
Figure D-3: Relative response of CLOZ and NOR-CLOZ over time in year experiment in a) non-inoculated, unpreserved specimens, b) non-inoculated, preserved specimens, c) inoculated, unpreserved specimens, and d) inoculated, preserved specimens.	291
Figure D-4: Relative response of FLPH and DA-FLPH over time in year experiment in a) non-inoculated, unpreserved specimens, b) non-inoculated, preserved specimens, c) inoculated, unpreserved specimens, and d) inoculated, preserved specimens.	292
Figure D-5: Relative response of AMIT and NORT over time in experiment YB in a) non-inoculated, unpreserved specimens, b) non-inoculated, preserved specimens, c) inoculated, unpreserved specimens, and d) inoculated, preserved specimens.	293
Figure D-6: Relative response of CLOM and NOR-CLOM over time in seven-month experiment in a) non-inoculated, unpreserved specimens, b) non-inoculated, preserved specimens, c) inoculated, unpreserved specimens, and d) inoculated, preserved specimens.....	294
Figure D-7: Relative response of MIRT and NOR-MIRT over time in seven-month experiment in a) non-inoculated, unpreserved specimens, b) non-inoculated, preserved specimens, c) inoculated, unpreserved specimens, and d) inoculated, preserved specimens.....	295

Figure D-8: Relative response of DOTH and NORD over time in seven-month experiment in a) non-inoculated, unpreserved specimens, b) non-inoculated, preserved specimens, c) inoculated, unpreserved specimens, and d) inoculated, preserved specimens.296

Figure D-9: Relative response of TRIF and NOR-TRIF over time in seven-month experiment in a) non-inoculated, unpreserved specimens, b) non-inoculated, preserved specimens, c) inoculated, unpreserved specimens, and d) inoculated, preserved specimens.297

Figure D-10: Relative response of PERI and PERI-SO over time in seven-month experiment in a) non-inoculated, unpreserved specimens, b) non-inoculated, preserved specimens, c) inoculated, unpreserved specimens, and d) inoculated, preserved specimens.298

Figure D-11: Relative response of TRIF and TRIF-SO over time in seven-month experiment in a) non-inoculated, unpreserved specimens, b) non-inoculated, preserved specimens, c) inoculated, unpreserved specimens, and d) inoculated, preserved specimens.299

TABLES

Table 1-1: Total scripts filled for antidepressants in Australia during 2015 calendar year.	9
Table 1-2: Total scripts filled for antipsychotics in Australia during 2015 calendar year.....	12
Table 2-1: Some functionalities found susceptible to microbial metabolism.....	31
Table 3-1: Source and purity of reagents.	57
Table 3-2: Drug standards purity, supplier, and solvent used in stock solutions.	58
Table 4-1: Conditions tested for LC-DAD system.	68
Table 4-2: Solvent gradient for liquid chromatography method.	69
Table 4-3: Wavelength monitored (λ) and retention time (RT) for the analytes.....	72
Table 4-4: Working solutions used for initial extraction recovery experiments.....	73
Table 4-5: Extraction recoveries (%) for analytes for each extraction method.	74
Table 4-6: Working solutions used for revised extraction efficiency experiments.	76
Table 4-7: Extraction recoveries (%) of analytes for revised unbuffered LLE method.....	77
Table 4-8: Retention time (min) and identity of unknown peak following unbuffered LLE from blood.....	78
Table 4-9: Working solutions used for method validation.	78
Table 4-10: Predicted and calculated y-residuals for unweighted and $1/x^2$ -weighted PROC calibration curves.....	83
Table 4-11: Linearity data, LLOQ, and LOD for analytes using HPLC method A.....	83
Table 4-12: Linearity data, LLOQ, and LOD for CHLO, FLTX, and FLPH using HPLC method A.	84
Table 4-13: Linearity data, LLOQ, and LOD for analytes using HPLC method B.	84
Table 4-14: Accuracy and precision data for CHLO, FLTX, and FLPH using HPLC method A.	85
Table 4-15: Accuracy and precision data for analytes using HPLC method A.....	86
Table 4-16: Accuracy and precision data for analytes using HPLC method B.....	87
Table 4-17: Analyte stability during extraction.	88
Table 4-18: Analyte stability on auto-sampler after 33 hours for Method A drugs.	89
Table 4-19: Analyte stability on auto-sampler after 18 hours for Method B drugs.....	89

Table 4-20: Analyte stability on auto-sampler during Chapter 6 blood experiments for Method A drugs.....	90
Table 4-21: Analyte stability on auto-sampler during Chapter 6 blood experiments for Method B drugs.....	90
Table 4-22: Analyte stability after three freeze-thaw cycles in preserved whole blood.....	91
Table 4-23: LURA and RISP stability after three freeze-thaw cycles.	91
Table 4-24: Initial and adjusted retention times (RT) for analytes and impurities.	92
Table 5-1: Summary of UV-Vis spectroscopy results.	96
Table 5-2: Drugs in the Set A and Set B solutions.	99
Table 5-3: AMIS signal changes (%) after ~5 days at room temperature.....	100
Table 5-4: Summary of analyte aqueous stability after 5 days at room temperature determined during LC-DAD monitoring experiment.....	100
Table 5-5: Summary of AMIT stability over 75 hours in aqueous solutions analysed by LC-DAD HPLC Method A.	102
Table 5-6: Summary of ZIPR and LURA stability over 24 hours in aqueous solutions analysed by LC-DAD HPLC Method B.	103
Table 5-7: LC-QTOF-MS data for analytes.....	104
Table 5-8: MS/MS data for PERI and PERI-AMD.	106
Table 5-9: MS data for ZIPR and alkaline hydrolysis degradants.	108
Table 6-1: Blood experiments specimen types overview.....	110
Table 6-2: Reported ante-mortem plasma therapeutic concentrations of drugs and approximate concentrations used in blood experiments.	111
Table 6-3: Cell counts by microscopy using a Petroff Hausser Counting Chamber for experiment WB2 and YB inoculate.	139
Table 6-4: Sequenced sample ID nomenclature.	140
Table 7-1: LC-QTOF-MS data for parent compounds, N-dealkylation degradants, N-dealkylation standards, and synthesised acetyl derivatives for possible and confirmed N-dealkylation degradation products.	156
Table 7-2: MS/MS data for parent compounds, N-dealkylation degradants and synthesised acetyl derivatives for confirmed N-dealkylation degradation products.	157

Table 7-3: MS/MS data for parent compounds, N-dealkylation degradants and synthesised acetyl derivatives for possible N-dealkylation degradation products.....	158
Table 7-4: LC-QTOF-MS data for parent drugs and their possible sulfoxides.....	160
Table 7-5: MS/MS data for parent drugs and their possible sulfoxides.....	160
Table 8-1: MS data for LURA and degradation products.....	182
Table 8-2: MS/MS data for LURA, LURA-SO and degradation products.....	187
Table 8-3: MS/MS data for synthesised ND-LURA and major 360.265 m/z degradation product detected in blood experiments.....	192
Table 8-4: LC-QTOF-MS data for synthesised ND-LURA and major 360.265 m/z degradation product detected in blood experiments.....	193
Table 8-5: Response ratio of 360.265 m/z compound to LURA in non-inoculated controls after five weeks at room temperature following alkaline LLE.....	197
Table 8-6: Ratio response of 360.265 m/z degradation product to LURA in non-inoculated blood specimens after five weeks at room temperature following unbuffered LLE.....	198
Table 8-7: Ratio response of 360.265 m/z degradation product to LURA in inoculated blood specimens after five weeks at room temperature following unbuffered LLE.....	198
Table 8-8: Case details for post-mortem cases with LURA detected.....	200
Table 9-1: 439.135 m/z relative response and 439.135 m/z/ZIPR ratios observed in experimental blood extracts during the first week experiment compared to the mean observed in calibrators and QCs.....	208
Table 9-2: MS data for ZIPR and possible ZIPR degradants.....	219
Table 9-3: MS/MS data for ZIPR and suspected degradants.....	222
Table 9-4: Hypothesised ZIPR degradation products chemical information.....	229
Table 9-5: Calculated molecular formulae and precursor ions for predicted deuterated analogues of 3-ethylidene-ziprasidone.....	230
Table 9-6: Deuterated ethanol experiment design.....	231
Table 9-7: MS data for deuterated degradants of ZIPR.....	233
Table 9-8: MS/MS data for deuterated degradants of ZIPR.....	235
Table 9-9: Summary of LC-DAD chromatogram data in short acetaldehyde experiment.....	239
Table 9-10: LC-QTOF-MS data for acetaldehyde degradants of ZIPR.....	241

Table 9-11: MS data for acetone degradants of ZIPR.....	242
Table 9-12: Overview of ZIPR and solvent reactivity.	242
Table 9-13: Case details for post-mortem cases with ZIPR detected.....	244
Table A-1: MS data for PROC and PERA.	257
Table A-2: MS/MS data at 20 eV for PROC and PERA.....	258
Table C-1: DNA sequencing details.....	273
Table C-2: Two-way PERMANOVA results for microbial community analyses.	274

EQUATIONS

Equation 3-1: Calculation for mass accuracy.....	64
Equation 3-2: Calculation for the mean.	64
Equation 3-3: Calculation for the standard deviation.....	65
Equation 3-4: Calculation for Welch’s t-test.....	65
Equation 4-1: Extraction recovery calculations.....	73
Equation 4-2: Calculation for accuracy.....	79
Equation 4-3: Calculation for intra-day and inter-day precision (as coefficient of variation (C.V.)) [203].	79
Equation 6-1: Calculations used to normalise data to AMIT.....	114
Equation 6-2: Uncertainty calculations for drug quantification data.....	115
Equation 6-3: Simpson’s Reciprocal Index (1/D) calculation [232].....	118
Equation 6-4: Shannon-Wiener Index (H) calculation [232].....	118
Equation 6-5: Effective number of species (ENoS) calculation [443].	118
Equation 6-6: Bray-Curtis similarity (BCS) calculation [445].	119
Equation 6-7: Percent carboxyhaemoglobin determination from UV-Vis spectroscopy.....	120
Equation 6-8: Uncertainty calculations for CO-Hb data.....	121

ABBREVIATIONS

6-MAM	6-monoacetylmorphine
ACP	2-amino-5-chloropyridine
ADP	adenosine diphosphate
AGRF	Australian Genome Research Facility
ATP	adenosine triphosphate
BPC	base peak chromatogram
BZP	<i>N</i> -benzylpiperazine
C/P	cardiac/peripheral
CO-Hb	carboxy-haemoglobin
DAD	diode array detector
EDTA	ethylenediaminetetraacetic acid
EIC	extracted ion chromatogram
EME	ecgonine methyl ester
ENoS	effective number of species
EPSE	extrapyramidal (parkinsonian) side effects
ESI	electrospray ionisation
EtG	ethyl glucuronide
EtS	ethyl sulfate
FGA	first-generation antipsychotic
FMT	faecal microbiota transplant
FSSA	Forensic Science SA
GABA	γ -aminobutyric acid
GC-MS	gas chromatography-mass spectrometry
GHB	γ -hydroxybutyrate
GMF	generated molecular formula
HCl	hydrochloric acid
IS	internal standard
LC-DAD	liquid chromatography
LC-DAD buffer mix	1:4 ethanol:25 mM ammonium formate buffer (pH = 3.6)
LC-MS	liquid chromatography-mass spectrometry
LLE	liquid-liquid extraction
LLOQ	lower limit of quantitation
LOD	limit of detection
M3G	morphine-3-glucuronide
M3S	morphine-3-sulfate
M6G	morphine-6-glucuronide
MAOI	monoamine oxidase inhibitor
MDA	3,4-methylenedioxyamphetamine
MDEA	3,4-methylenedioxyethylamphetamine
MDF	Mass Defect Filtering
MDMA	3,4-methylenedioxymethamphetamine
MFE	Molecular Feature Extraction
MS	mass spectrometry
NaSSA	noradrenergic and specific serotonergic antidepressant

NDRI	norepinephrine and dopamine reuptake inhibitor
NGS	next-generation sequencing
NH ₃	ammonia
NIFS	National Institute of Forensic Science
NMS	neuroleptic malignant syndrome
NPS	new/novel psychoactive substances
OTU	operational taxonomic unit
PCoA	principle coordinate analysis
PCR	polymerase chain reaction
PMI	post-mortem interval
PMR	post-mortem redistribution
PPT	protein precipitation
QC	quality control
QTOF-MS	quadrupole-time-of-flight mass spectrometer
RIMA	reversible inhibitor of monoamine oxidase A
SGA	second-generation antipsychotic
SNRI	serotonin and norepinephrine reuptake inhibitor
sp.	species (singular)
spp.	species (plural)
SSRI	serotonin selective reuptake inhibitor
TCA	tricyclic antidepressant
THC	Δ ⁹ -tetrahydrocannabinol
THC-COOH	11-nor-9-carboxy-Δ ⁹ -tetrahydrocannabinol
UV-Vis	ultra-violet and visible

Common drugs:

AMIS	amisulpride	MIRT	mirtazapine
AMIT	amitriptyline	MOCL	moclobemide
ARIP	aripiprazole	PERA	perazine
ASEN	asenapine	PERI	pericyazine
CHLO	chlorpromazine	PROC	prochlorperazine
CLOZ	clozapine	QUET	quetiapine
DOTH	dothiepin	RISP	risperidone
FLPH	fluphenazine	SERT	sertraline
FLTX	flupentixol	TRIF	trifluoperazine
HALO	haloperidol	TRIM	trimeprazine
LORA	loratadine	ZIPR	ziprasidone
LURA	lurasidone	ZUCL	zuclopenthixol

CHAPTER I - GENERAL INTRODUCTION

1.1 Post-mortem toxicology: background

Post-mortem toxicology serves the purpose of establishing if any drugs or poisons may have been present or absent peri-mortem that could have contributed towards the cause of death in an individual [4]. This information, complimentary to post-mortem histology and autopsy results, is required to assist forensic pathologists in determining decedent cause/manner of death. Accurate cause/manner of death findings may be contingent on the toxicological analysis of post-mortem specimens, and numerous studies have illustrated this [5-8], establishing post-mortem toxicology as an essential component of death investigations.

Data acquisition and interpretation in post-mortem toxicology is complicated by numerous issues including cadaver decomposition, drug redistribution after death, and the instability of drugs and poisons in decomposing cadavers, in the specimens collected therefrom, and throughout analysis. An overview of post-mortem decomposition is provided below with an emphasis on microbial involvement. Following this, key interpretative challenges in post-mortem toxicology are addressed, with drug instability in post-mortem specimens addressed in Chapter 2.

1.2 Post-mortem decomposition

Following cessation of respiratory and cardiovascular systems, cells become unable to acquire and utilise oxygen from the environment for adenosine triphosphate (ATP) production. Consequently, vital metabolic and homeostatic processes that rely on the energy released from the exergonic hydrolysis of ATP become unable to proceed [9]. Instead, adenosine diphosphate (ADP) and lactic acid by-products are formed, lowering the pH of the cytoplasm and triggering a process termed autolysis, whereby hydrolytic enzymes are released from the lysosome, vacuole and plasma membranes are digested and cellular contents are released [4, 10-12].

Heteroorganotrophic² microorganisms also degrade cadavers in a process called putrefaction [14]. During life, the host immune system and mucus produced within the body hinder the translocation of microorganisms from the gastrointestinal tract to the lymphatic and circulatory system [15]. After death, these protections fail and microorganisms migrate by enzymatic

² Heteroorganotrophic organisms consume organic compounds to produce inorganic compounds (e.g. humans) [13].

digestion of membranes that surround the internal organs [10, 16, 17]. Once translocated, aerobic respiration of facultative anaerobes³ presumably depletes tissues of any remaining oxygen, leading to anoxic conditions. Consequently, a decrease in the growth and presence of obligate aerobes, such as *Staphylococcus sp.*, and an increase in the growth of obligate anaerobes, such as *Clostridium perfringens* and *Bacteroides sp.*, is observed [11, 16-25]. Because of the hypoxic environment, the participation of fungi in putrefaction is thought to be initially limited to the digestion of external surfaces, as, excluding facultative anaerobic yeasts such as *Candida spp.*, most fungi are obligate aerobes [10].

Cadaver putrefaction leads to acidification of the environment, due to protein degradation [12], and evolves gaseous metabolic by-products, including hydrogen sulphide, carbon dioxide, methane, ammonia, sulfur dioxide, and hydrogen, leading to abdominal distention and the eventual purging of body fluids out of any open wounds and orifices due to pressure build-up [10, 11]. The exact putrefactive chemicals produced is dependent on the species of microorganisms present, a variable that is itself dependent on factors such as temperature, humidity, environment, and the initial microbial community at the time of death [26].

Once the integrity of the skin is compromised the corpse is a more favourable habitat for aerobic organisms, and extracorporeal microorganisms, such as *Pseudomonas sp.*, abundant in soil, can more readily assist in putrefaction [26]. Scavenging animals may also create wounds that allow for oxygen permeation and transmit oral microorganisms [26]. Other macrofauna, attracted by volatile putrefactive compounds, such as insects and their larvae, also introduce enzymes capable of degrading compounds otherwise resistant to degradation such as collagen and keratin [4, 10, 26].

Oxygen plays a significant role in the ability of microorganisms to decompose a body. If the environment is anoxic, digestion of organic matter is only possible by fermentation, leading to the formation of short chain acids and alcohols, as well as previously specified putrefactive gases [26, 27]. Due to the prevention of fatty acid oxidation, anaerobic and humid environments are associated with the formation of adipocere, a soft, greasy, white-reddish brown substance (also known as “grave wax”) that consists of a mixture of polyhydroxy fatty acids, fat, and soap [11, 26, 27]. Thus, the further underground that a body is buried the slower the expected rate of decomposition due to decreasing concentrations of oxygen [10, 11]. As microorganisms require

³ Obligate aerobes require oxygen for respiration and so can only grow in an oxygenated environment; obligate anaerobes ferment organic compounds for energy and cannot grow in an oxygenated environment; and facultative anaerobes can both aerobically respire and anaerobically ferment organic compounds [13].

water for respiration, hot and dry environments can alternatively lead to preservation by mummification [11, 14]. Aerobically respiring microorganisms enable all organic matter to be degraded to a mixture of carbon dioxide, water, sulfates and nitrates, leaving only a skeletonised corpse [27].

The rate of putrefaction depends upon the climate (e.g. summer or winter) and environment (e.g. indoors, outdoors, clothed, unclothed) in which a body is left to decay [10, 14]. Bodies with the same approximate post-mortem interval⁴ (PMI)) may also degrade with remarkable variability depending on the cause of death and the health of the individual at the time of their death with conditions such as obesity, diabetes mellitus, HIV/AIDS, and sepsis noted to increase decomposition rates [28, 29].

1.2.1 Microbial life after death

The community of microorganisms inhabiting an individual after death will initially be as during peri-mortem. During life, microorganisms inhabit not only the human gut but also skin, conjunctiva, the nose, and genitalia [18, 30]. In the human gut they function as key mutualists, metabolising complex sugars into substrates accessible for metabolism by humans and synthesising biotin (Vitamin B₇) [30]. A comprehensive review by Rajilić-Stojanović and de Vos in 2014, with data collated since 1896, reported that 1057 culturable species had been identified in the human gastrointestinal tract, with Bacteria significantly dominant (957 species) in comparison to Archaea (8 species) and Eukarya (92 species) [31]. A later rebirth in culture-based methods combined with matrix-assisted laser desorption/ionization–time of flight mass spectrometry and 16S rRNA sequencing (culturomics) as of 2016 had increased the number of known microorganism species in the human gut to 1525 [32]. Actinobacteria, Bacteroidetes, Firmicutes, and Proteobacteria are the most prevalent bacterial phyla, the methanogenic Euryarchaeota are the most prevalent archaeal phyla, and fungi of the *Candida* genus dominate the human gastrointestinal tract [31]. Studies have shown that age and geography affect microbial diversity [33, 34]. Reasons for variations in the human gut microbiome between individuals have also been attributed to medical conditions, such as obesity [35, 36], Parkinson’s disease [37], and type 2 diabetes [38], and medications and diet have also been found to have an impact on the prevalence of particular microorganisms [39, 40].

Many studies have identified the species of bacteria and fungi associated with decomposing cadavers, often with the goal of determining whether particular species can serve as markers for

⁴ The post-mortem interval is the elapsed time between death and post-mortem examination.

burial sites or to assess whether death was due to infection [20, 21, 41-50]. Recently there has also been interest in determining whether changes in the abundance of particular microorganisms within the cadaver may be linked to time since death [24, 51, 52].

Traditionally, microscopic analysis and culturing have been used to determine species presence [46, 48, 50, 53]. Identification of species by inter-species genetic variation, following culturing, has also been used to compliment traditional techniques in more recent studies [42, 43]. However, these approaches are unlikely to have provided a complete overview of the organisms present in post-mortem specimens, as evidenced by the fact that species previously indistinguishable by their morphology or unable to grow under traditional and limited culture conditions have now been discovered and are distinguishable through sequencing and culturomics analyses [54-58]. This “next-generation sequencing” (NGS) has been utilised for post-mortem microbiome research since 2013 [20, 23, 59-65]. Culturomics approaches have not yet been used to determine the microbial community of post-mortem specimens.

Key findings of post-mortem microbiome research have been that as decomposition progresses anaerobic bacteria dominate, diversity is reduced, and the community between individuals and across body sites, though different during early stage decomposition, become more similar over time [24]. In a study by Hyde *et al.* the dominant phyla in mouth and most skin samples of pre-purge human cadavers was found to be Proteobacteria followed by Firmicutes [20, 64]. As decomposition progressed the trend was usually that Proteobacteria and Actinobacteria became less abundant and more abundant, respectively, with Firmicutes dominant during post-purge decomposition [20, 64]. However, this research only encompassed the decomposition of four donated bodies without the following: consistent or known medical histories; causes of death and whether individuals were of considerably different weight and age [20, 64]. Similar results were obtained in a study by Pechal *et al.*, examining swine decomposition, wherein mouth and skin were initially dominated by Proteobacteria pre-bloat but were surpassed by Firmicutes post-bloat [59]. A study investigating the aquatic decomposition of two swine carcasses also shows that skin biofilms are initially dominated by Proteobacteria during early stage decomposition and that succession by Firmicutes is accompanied with decreasing Proteobacteria abundance [65]. The increasing dominance of Firmicutes over Proteobacteria in these studies is expected, as the former species is comprised of obligate anaerobes and the latter facultative anaerobes [13]. Numerous studies have found that, of the Firmicutes species, *Clostridium* spp. dominate [25, 64]. Interestingly, the introduction of oxygen into the abdominal

cavity of mice whilst studying the post-mortem microbiome produced different results, with Proteobacteria dominating post-purge and a reduction in body habitat diversity [23].

The fungi dominant in human post-mortem specimens, as determined by a combined culturing and genetic identification approach utilised by Martínez-Ramírez *et al.* on samples obtained from 105 human cadavers, are of the genera *Candida*, *Aspergillus*, and *Penicillium*, which also dominate during life [31, 42, 50]. In the same study severely decomposed cadavers were also noted to host species of the genera *Mucor* and *Trichoderma* and the absence of *Rhodotorula* species, all of which may be present during life [31, 36, 42, 66]. Preferential utilisation of different forms of nitrogen (i.e. mineral or organic) across species is apparent by the detection of different fungi after proteolysis is complete [44].

Of the Archaea, it has been suggested that methanogens in particular may be involved in decomposition [24].

1.3 Challenges in post-mortem toxicology

1.3.1 Post-mortem redistribution

Drugs may redistribute after death, due to release from decomposing tissues and proteins, as well as diffusion processes [67]. Different arteries and veins are subject to differing elevations in drug concentrations depending on their location in the body as drug redistribute from the gut, lungs, myocardium, and liver into surrounding tissues and blood vessels [68-70]. The extent to which a drug will redistribute is thought to be dependent on the physiochemical properties of the drug with the key factors identified to influence redistribution drug lipophilicity, ionisation state, and volume of distribution⁵ [70]. For example, it is generally accepted that basic and highly lipophilic drugs, such as tricyclic antidepressants, exhibit significant redistribution that is reflective of their high volume of distribution and thus higher concentrations in body tissues [71-73].

As blood is often the specimen of choice for the measurement of drug concentrations, it is of utmost importance to collect blood from a site where post-mortem redistribution (PMR) is minimised. Generally, peripheral blood from the femoral vein is collected, as numerous studies have shown that PMR may be minimised in this location compared to central sites such as cardiac and pulmonary veins [69, 74-76]. It is not straight forward to assess whether PMR may occur for a given drug. Post-mortem cardiac/peripheral (C/P) blood ratios and liver/peripheral

⁵ Volume of distribution is a theoretical volume that represents how accurately drug plasma concentrations reflect drug tissue concentrations. $V_D = [\text{total drug}]/[\text{total plasma}]$ [71]

blood ratios have been used [72, 77]. However, this approach assumes that peripheral blood concentrations are not influenced by redistribution phenomenon, which may be a false premise for particular drugs [78-80]. The potential for drugs to redistribute post-mortem can also be assessed through studies where numerous blood samples are collected post-mortem at different times and tested [78-82]. However, these approaches may also be flawed due to the collection of blood samples after drug redistribution has occurred or improper sample collection. Post-mortem drug degradation may also be a confounding factor.

1.3.2 Specimen collection

The specimens available for collection are dependent on decomposition progression (1.2). Although a preferred specimen, blood may be absent, and internal organs or putrefactive fluids may need to be analysed. Furthermore, some authors advocate the quantification of drugs in other specimens such as liver due to PMR affecting femoral blood concentrations for some drugs [82, 83]. Regardless of the specimen analysed an understanding of PMR and ante-mortem drug distribution is important for correct specimen collection and data interpretation [74].

If possible, in addition to blood, liver samples are commonly collected with a preference for the right lobe to minimise the effect of PMR on analysis, as diffusion of drugs from gastric contents into the left lobe can occur [74]. It has been found that post-mortem liver samples are more often sterile than post-mortem blood, however, blood is a more homogenous matrix and therefore easier to analyse [84, 85]. Brain tissue is a specimen that has recently garnered interest due to both the high concentration of lipophilic drugs, a slower rate of putrefaction than other tissues (perhaps due to the blood-brain barrier preventing microbial translocation), and low PMR [49, 86]. Its use is challenged, however, by the uneven distribution of drugs in brain tissue [87]. Other specimens, such as urine, bile, stomach contents, hair, nails, and vitreous humour (see Chapter 2), have limited or specialised applications. As waste products, both bile and urine are of limited utility due to extensive metabolism of parent drugs [67]. However, it has been advised that bile could be a useful specimen to analyse as a complement to other post-mortem specimens [88]. Urine may also be unavailable in many cases due to peri-mortem voiding of the bladder, drug excretion is impacted by urinary pH variations, and drugs detected may be more representative of drug administration ante-mortem than peri-mortem (particularly for acute overdoses) [67]. Stomach contents are useful due to minimal metabolism of drugs and the potential for finding the remains of any tablets if a drug has been ingested [67]. Hair and nails can also be useful specimens due to their uptake of drugs during growth, thus allowing for the

determination of exposure weeks or months later [89, 90]. Both specimens are also well-preserved, due to keratinases required for their digestion [11].

1.3.3 Pharmacokinetic and pharmacogenetic considerations

Despite its shortcomings due to PMR, blood remains the most convenient specimen for interpretative reasons, as therapeutic concentrations, which are lacking for other specimens, are readily available in literature for many drugs of interest [67]. However, pharmacological data is based on measurements of drug concentrations in plasma, whereas in post-mortem toxicology drug concentrations are measured in whole blood [67]. Published data that are representative of non-toxic drug concentrations in post-mortem specimens is most appropriate for comparative purposes when determining whether a drug may have contributed to the cause of death [91-94]. However, genetic diversity between individuals, as well as the age of an individual, leads to variations in enzyme expression, leading to differences in drug metabolism [67, 95-98]. Age may also influence many other factors such as the extent to which a drug is protein bound or undergoes gut metabolism [96, 97]. Consequently, a therapeutic dose in one individual may not be sufficient in another or alternatively could even cause adverse side effects and death [67, 99]. Some classes of drugs, infamously the opioids, also result in tolerance within individuals, necessitating the intake of increasing doses over time in order for that individual to experience the same pharmacological effect [95]. Therefore, drug concentrations that could be interpreted as toxic may not necessarily be so in a tolerant individual. Drugs may also inhibit their own metabolism if administered at a dose high enough to saturate metabolising enzymes and may slow or enhance the rate of metabolism of other drugs [67, 100, 101]. As drug combinations are often found in decedents these interactions are important to understand [95, 102].

Whether death was due to acute ingestion of a drug may be elucidated from the analysis of multiple specimens, allowing for the determination as to whether most of the drug was unabsorbed in the stomach or metabolised and excreted into the urine for example. To assist in interpreting toxicology results some authors also advocate the analysis of parent drug and metabolites to indicate acute intoxication [103, 104].

1.3.4 Drug instability

The detection of drugs in post-mortem specimens is dependent upon their stability in the preanalytical phase in cadavers and post-mortem specimens and throughout analytical procedures. Degradation of drugs and metabolites is possible due to chemical instability or microbial activity. This may lead to decreased drug concentrations, increased drug

concentrations (e.g. from conjugate hydrolysis), or even complete degradation. Therefore, knowledge of the stability of drugs and metabolites in post-mortem specimens is essential to ensure known degradation products, if any, are included in screening methods and to enable informed interpretation of analytical results. As the focus of the research in this thesis, drug stability is covered in detail in Chapter 2.

1.4 Antidepressant and antipsychotic drugs

Antidepressant and antipsychotic drugs may be used to compliment counselling-based methods of treating mental illness or in cases where psychological treatment alone has been ineffective or is otherwise inaccessible for a patient [100]. Individuals with mental illnesses that may be prescribed these drugs have greater mortality rates than the general population, and in particular, an increased risk of suicidal behaviour [105, 106]. These drugs, and their use in drug combinations, can lead to impairment or death [107-109]. Prescription medicines may also be maliciously administered [110], particularly those with sedation as a side effect [111-113]. It may also be necessary to determine if individuals prescribed these medications were non-adherent at the time of an incident. Therefore, the detection of these drugs in coronial toxicology casework is to be expected and numerous studies have examined the frequency of their presence [114-116].

Such studies may underrepresent true frequencies of antipsychotic and antidepressant drug use if degradation of the drugs occurs post-mortem. Across 235 suicide cases (2012-2015) analysed at the Institute of Legal Medicine of the Charité-University Medicine Berlin and 1436 non-overdose suicide cases (1997-2006) analysed at the NSW Department of Forensic Medicine, suicide was most common at home (63.8 % and 61.1 %, respectively) [115, 116]. Deaths at home may increase the time it takes for the bodies to be discovered, particularly if the individuals are socially isolated, and therefore increase the opportune time during which microbial drug degradation may occur to reduce drugs to concentrations beneath the detection limit of analytical methods. In the NSW study, only 34.9 % of decedents with known psychosis were positive for antipsychotic drugs [115]. Without knowledge of the stability of these drugs during the post-mortem interval it cannot be stated that non-detection indicates non-adherence. If degradation of these drugs may occur, overdose or adverse drug reaction deaths may also not be identified and data concerning drug usage trends may be compromised in post-mortem toxicology-based epidemiological studies which may serve to inform prescription policies or drug monitoring programs.

1.4.1 Antidepressants

Antidepressants are indicated for the treatment of affective disorders such as major depression disorder and obsessive-compulsive disorder [100]. Hypotheses for their therapeutic mode of action include their involvement in monoamine neurotransmission and the stimulation of neuroplasticity [117].

Older classes of antidepressants discovered in the 1950s include monoamine oxidase inhibitors (MAOIs) and tricyclic antidepressants (TCAs) [117]. MAOIs bind irreversibly to monoamine oxidase, preventing the breakdown of its substrates (e.g. dopamine, norepinephrine, serotonin, tyramine) until the enzyme is re-synthesised [118]. In contrast to MAOIs, TCAs consist of agents with varying serotonin and norepinephrine reuptake inhibition properties [109]. More commonly used antidepressants in Australia are the serotonin selective reuptake inhibitors (SSRIs) and serotonin and norepinephrine reuptake inhibitors (SNRIs) (Table 1-1). Other non-serotonergic antidepressants used include: bupropion, a norepinephrine and dopamine reuptake inhibitor (NDRI), although such usage is off-label in Australia [119, 120]; and mirtazapine and mianserin, which, despite their classification as noradrenergic and specific serotonergic antidepressants (NaSSA), possess no demonstrable serotonergic activity [121, 122]. Indeed, mirtazapine's antagonism of 5-HT_{2A} receptors may be of use in treating serotonin toxicity (see below) [121, 123].

Table 1-1: Total scripts filled for antidepressants in Australia during 2015 calendar year.

Antidepressant	Classification	Total scripts*	Antidepressant	Classification	Total scripts*
Sertraline	SSRI	3,628,007	Dothiepin	TCA	415,167
Escitalopram	SSRI	3,515,659	Doxepin	TCA	234,919
Venlafaxine	SNRI	2,882,485	Nortriptyline	TCA	148,226
Mirtazapine	NaSSA	2,112,824	Moclobemide	RIMA	117,074
Amitriptyline	TCA	2,089,481	Clomipramine	TCA	74,363
Desvenlafaxine	SNRI	2,036,598	Reboxetine	NRI	49,672
Citalopram	SSRI	1,738,614	Mianserin	NaSSA	44,888
Fluoxetine	SSRI	1,640,461	Tranlycypromine	MAOI	17,739
Duloxetine	SNRI	1,479,299	Bupropion [†]	NDRI	16,297
Paroxetine	SSRI	1,050,057	Imipramine	TCA	14,563
Fluvoxamine	SSRI	429,190	Phenelzine	MAOI	7,127

*Data representative of drugs prescribed under the Pharmaceutical Benefits Scheme and Repatriation Pharmaceutical Benefits Scheme only [124]; [†]Although classified as an antidepressant by the Australian Statistics on Medicines, bupropion is only indicated for smoking cessation in Australia [120] and therefore its usage as an antidepressant is off-label and not covered by the Pharmaceutical Benefits Scheme. Bolded drugs investigated in this thesis.

Side effects associated with antidepressants vary depending on drug pharmacology and may include sexual dysfunction, sleepiness, insomnia, weight gain, weight loss, dry mouth, nausea,

migraine, seizures, and excessive sweating [125, 126]. Potentially fatal side effects include: gastrointestinal bleeding; hyponatremia; hepatic necrosis; and ventricular arrhythmias [118, 125, 127]. The use of MAOIs may also lead to potentially fatal hypertensive crises, due to the inhibited metabolism of dietary tyramine, and hepatic necrosis [118]. Reversible inhibitors of monoamine oxidase A (RIMA) have not been reported to induce hypertensive crises, such as from dietary tyramine [101], as monoamines are able to displace the drugs or otherwise reactivate monoamine oxidase after inhibition [118]. SSRIs, SNRIs, and mirtazapine are considered to be safer than TCAs when taken in overdose due to lower fatal-toxicity indices⁶, hazard indices⁷, and case fatality rates reported for these substances in literature [125]. Nevertheless, SSRIs may inhibit their own metabolism and the metabolism of other serotonergic drugs, leading to elevated intra-synaptic serotonin levels and subsequent serotonin toxicity [128, 129]. This condition is potentially fatal and is associated with physical symptoms such as mydriasis, akathisia, tremor, clonus, muscular hypertonicity, and hyperthermia [130]. Fatalities typically involve serotonergic drug combinations, such as the combination of MAOIs with: SSRIs, SNRIs, clomipramine [109, 131], ipramine, and the opioid analgesics tramadol, dextromethorphan, and pethidine [128]. Overdoses of bupropion are associated with seizures, status epilepticus, and may cause death *via* cardiac arrest [132, 133]. Mirtazapine appears to be relatively safe in overdose, with self-resolving tachycardia, hypertension, and CNS depression exhibited [134-137]. Nevertheless, at least six reported fatalities have been attributed to mirtazapine intoxication [94].

1.4.2 Antipsychotics

Antipsychotics are indicated for the treatment of psychosis associated with affective disorders (e.g. bipolar disorder, anxiety disorders, and treatment resistant depression) and schizophrenia [100, 138]. In addition to these indications, antipsychotics may be prescribed off-label to treat other conditions such as anxiety [139], insomnia [140], dementia, obsessive-compulsive disorder, and post-traumatic stress disorder [141, 142]. Quetiapine has also been implicated as a drug that may be administered to facilitate sexual assault [111-113] and with recreational uses [143-145].

Antipsychotics are commonly classified as first-generation (typical) antipsychotics (FGA) and second-generation (atypical) antipsychotics (SGA). FGAs, such as the phenothiazines, thioxanthenes and butyrophenones, achieve their therapeutic action primarily through antagonism of mesolimbic D₂-dopamine receptors, relieving psychotic symptoms such as

⁶ The fatal-toxicity index of a drug is defined as the number of deaths per million prescriptions.

⁷ The hazard index of a drug is defined as the number of major or fatal outcomes per 1000 ingestions.

delusions, hallucinations, and thought disorder (known as the positive symptoms of schizophrenia) [100, 138, 146]. Unfortunately, this antagonism can exacerbate the negative symptoms of schizophrenia (anhedonia, loss of motivation, and apathy) [138]. Furthermore, antagonism of other D₂ receptors throughout the brain can also lead to adverse extrapyramidal (parkinsonian) side effects (EPSE), such as muscle cramps, restlessness, tremor, tardive dyskinesia, as well as the potentially fatal neuroleptic malignant syndrome (NMS) [100, 138, 146]. Most FGAs also exhibit varying degrees of M₁-muscarinic cholinergic receptor antagonism and may also be antagonists of H₁-histamine receptors and α₁-adrenergic receptors, leading to side effects of sedation, weight gain, decreased blood pressure, dry mouth, constipation, and blurred vision [138].

SGAs have more complex pharmacological profiles (characteristically lesser dopamine receptor antagonism or partial agonism as well as antagonism of 5-HT_{2A}-serotonin receptors) and are associated with a lesser incidence of EPSE and considered to better treat the negative symptoms of schizophrenia [100, 138, 146-148]. However, a meta-analysis of clinical trial data suggests that some SGAs are no better at treating positive and negative symptoms, and that some, such as quetiapine, may be less efficient than FGA at treating the positive symptoms [149]. The use of SGAs is also associated with metabolic side effects leading to weight gain, type 2 diabetes mellitus, and may cause life-threatening ketoacidosis and hyperglycaemic hyperosmolar syndrome [147, 148, 150, 151]. Clozapine in particular is associated with: risks of seizures (requiring titration dosing) [152]; agranulocytosis and myocarditis, both of which can be fatal (the former necessitating blood monitoring [153, 154]); and the potentially fatal reduction of peristalsis [155]. SGAs are more often prescribed in Australia than FGAs (Table 1-2).

Compared to non-users, an increase in the frequency of sudden cardiac death is observed for users of either FGAs or SGAs [108]. The frequency of cardiotoxicity when using thioridazine (a first-generation phenothiazine antipsychotic) ultimately lead to its withdrawal from the global market in 2005 [156]. In the elderly, antipsychotic use is also associated with an increased risk of falls from orthostatic hypotension, fatal pneumonia, stroke, and deep vein thrombosis [157, 158]. Antipsychotics can also impair the ability of a body to cool down by suppression of sweating and increased blood flow to the skin due to vasodilation [159, 160]. As such, the use of antipsychotics is correlated with heat-related deaths [161, 162]. Hypothermia may also result following antipsychotic administration, particularly following initiation of treatment [159, 163]. However, having a psychiatric illness reportedly triples the risk of death during a heat wave [164], and there is evidence that thermodyregulation may be a symptom of schizophrenia [165].

The reason for correlations between antipsychotic use and heat-related deaths may also not be due to thermodyregulation alone but also confounding variables such as poverty, inadequate housing, social isolation, cognitive impairment, and inappropriate behavioural responses to heat.

Table 1-2: Total scripts filed for antipsychotics in Australia during 2015 calendar year.

Antipsychotic	Generation	Classification	Total scripts*
Olanzapine	SGA	Tricyclic	1,052,620
Quetiapine	SGA	Tricyclic	988,541
Prochlorperazine	FGA	Phenothiazine	827,673
Risperidone	SGA	Benzisoxazolepiperazine	648,076
Clozapine	SGA	Tricyclic	301,466
Aripiprazole	SGA	Phenylpiperazine	215,646
Paliperidone	SGA	Benzisoxazolepiperazine	177,319
Lithium ⁺	-	-	164,615
Haloperidol	FGA	Butyrophenone	89,909
Amisulpride	SGA	Benzamide	88,386
Chlorpromazine	FGA	Phenothiazine	73,047
Pericyazine	FGA	Phenothiazine	50,127
Ziprasidone	SGA	Benzisothiazolepiperazine	39,207
Zuclopenthixol	FGA	Thioxanthene	32,603
Asenapine	SGA	Tricyclic	31,089
Trifluoperazine	FGA	Phenothiazine	24,700
Flupentixol	FGA	Thioxanthene	13,436
Fluphenazine	FGA	Phenothiazine	7,448
Lurasidone	SGA	Benzisothiazolepiperazine	1,450

**Data representative of drugs prescribed under the Pharmaceutical Benefits Scheme and Repatriation Pharmaceutical Benefits Scheme only [124]; ⁺Although classified as an antipsychotic by the Australian Statistics on Medicines, lithium is indicated for mood disorders in Australia and not psychosis [166]. Bolded drugs investigated in this thesis.*

The issues with current antipsychotic medications in treating schizophrenia were highlighted in 2005 by the results from the Clinical Antipsychotic Trials of Intervention Effectiveness (CATIE) study, which revealed that only 371 out of 1432 patients (26 %) completed an 18 month regimen of treatment, predominantly discontinuing due to poor efficacy or intolerable side effects [148]. The adverse and sometimes toxic or fatal side effects of antipsychotic medications, as well as their inability to adequately treat the negative symptoms of schizophrenia, stimulates future research to explore other approaches to treat psychosis [167].

1.4.3 Polypharmacy and drug interactions

Co-administration of multiple antipsychotics is common [168, 169]. Given the cardiac side effects of some antipsychotics it is therefore possible that polypharmacy may increase mortality. However, this has not been conclusively established [170]. Amongst Australian veterans prescribed multiple antipsychotics and older than 65 years (n = 365) the most frequently co-

prescribed antipsychotics were risperidone (45.4 %), quetiapine (44.4 %), olanzapine (28.2 %), haloperidol (22.4 %), and pericyazine (5.8 %) [171].

In some cases, such as to treat psychotic depression, antidepressants and antipsychotics may be co-prescribed [172]. Based on prescription data stored on the Medicare Department of Human Services Pharmacy Claims database, over a two-year period (2010-2012) quetiapine was more commonly co-administered with an antidepressant than on its own among 15-59 year-olds in Australia [173, 174]. Other atypical antipsychotics such as olanzapine, risperidone, and aripiprazole were also commonly co-administered with antidepressants [173, 174]. For patients older than 44 years, co-administration was more common than single drug administration [173].

Inhibition of cytochrome P-450 enzymes by an adjuvant antidepressant or antipsychotic may lead to elevated concentrations of another antipsychotic or antidepressant (and vice versa) [101, 175]. In some cases this may necessitate dose reductions or increases to avoid adverse side effects or to maintain therapeutic effects [101]. There is a risk of life-threatening torsade de pointes⁸ if either the antidepressant or antipsychotic may prolong the QTc interval [101, 176, 177]. Other potentially fatal side effects include: status epilepticus, if drugs that lower the seizure threshold are combined (such as olanzapine and mirtazapine); paralytic ileus, if drugs that reduce peristalsis are combined (such as chlorpromazine with amitriptyline or nortriptyline); and hepatic encephalopathy (as reported following treatment with trifluoperazine and trazodone) [101]. The use of atypical antipsychotics in combination with antidepressants has also been reported to result in ST. One mechanism by which this is hypothesised to occur is the selective antagonism of 5-HT₂ and 5-HT₃ receptors by antipsychotic drugs leading to the selective activation of 5-HT_{1A} receptors [178]. Olanzapine and risperidone are such drugs that have been reported to cause ST with concurrent antidepressant usage [179, 180]. Some antipsychotic drugs such as ziprasidone, quetiapine, and aripiprazole are also partial agonists of 5-HT_{1A} receptors [181]. Of these drugs, ziprasidone and quetiapine have been implicated in case reports as causing serotonin toxicity when taken with antidepressants [182, 183]. However, the diagnosis in a poisoning case involving aripiprazole and fluoxetine (an SSRI) was NMS, with serotonin toxicity unable to be decisively ruled out [184]. Serotonin toxicity and NMS are differential diagnoses [130, 185].

Drugs other than antidepressants and antipsychotics may also behave as cytochrome P-450 enzyme inducers or inhibitors, resulting in decreased or increased concentrations of parent

⁸ Torsade de pointes refers to a distinctive form of tachycardia which may progress to cardiac arrhythmia.

drugs and metabolites, respectively [101]. For example, cigarette smoking induces CYP1A2, which metabolises clozapine to the inactive metabolite clozapine N-oxide [186]. Therefore, if a patient were to stop smoking, concentrations of the active drug, clozapine, would become elevated and this could lead to adverse side effects [100]. Drug-drug interactions may also occur after administration of a drug has ceased, due to prolonged half-lives of the drug or its metabolites. For example, fluoxetine and its active metabolite norfluoxetine have half-lives of 1-3 days and 7-15 days, respectively [101, 187]. Therefore, wash-out periods may be required before therapy with other drugs can commence due to the enzyme inhibition and the subsequent risk of adverse side effects such as ST [188]. Potentially fatal additive toxicity may also result from multiple drugs having similar biological effects, such as reducing peristalsis or bone marrow suppression [101].

1.4.4 Drugs investigated in this thesis

Selected antidepressants and antipsychotics (Figure 1-1 to Figure 1-3) required further investigation regarding their susceptibility to microbially degrade in a post-mortem blood environment and to determine if any degradation products form that should be used as marker compounds in instances where a parent drug may degrade below analytical detection limits.

The drugs investigated in this thesis were selected based on: their usage in Australia (see Table 1-1 and Table 1-2); past studies indicating drug instability in some post-mortem blood specimens but without identification of any degradation products (chiefly, DOTH and CHLO) (past studies are detailed in Chapter 2); structural similarities with CHLO (*i.e.* the phenothiazine antipsychotics and FLTX (Figure 1-2 (a-f))); for CLOZ, variable increases and decreases in post-mortem concentrations inter-individual, suggesting possible degradation and/or redistribution [78]; and for ZIPR and LURA, structural similarity with risperidone (RISP), a drug known to degrade to undetectable levels in post-mortem specimens [2, 3].

It is important to note that, due to PMR (1.3.1), it cannot be concluded that concentrations in authentic post-mortem specimens will correspond to peri-mortem concentrations, even if drugs are stable in post-mortem specimens. While peripheral blood collection can minimise the effects of PMR on determined blood concentrations [69, 74-76] PMR has still been indicated as possibly affecting femoral blood concentrations of CHLO [78], CLOZ [78], FLTX [80], and MIRT [79] in studies comparing femoral blood concentrations in specimens collected after death at multiple time points. Prior to these studies it was postulated that MIRT exhibits minimal post-mortem redistribution, based on congruent post-mortem central and peripheral blood

concentrations [136, 137]. This highlights the aforementioned difficulties of assessing whether PMR may occur for a drug using experimental data.

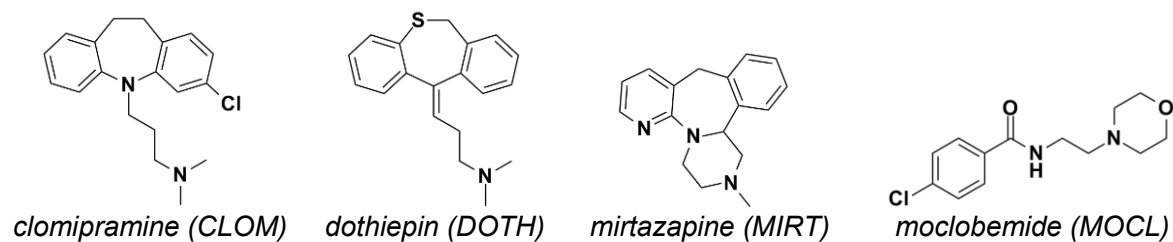


Figure 1-1: Structure of antidepressant drugs investigated.

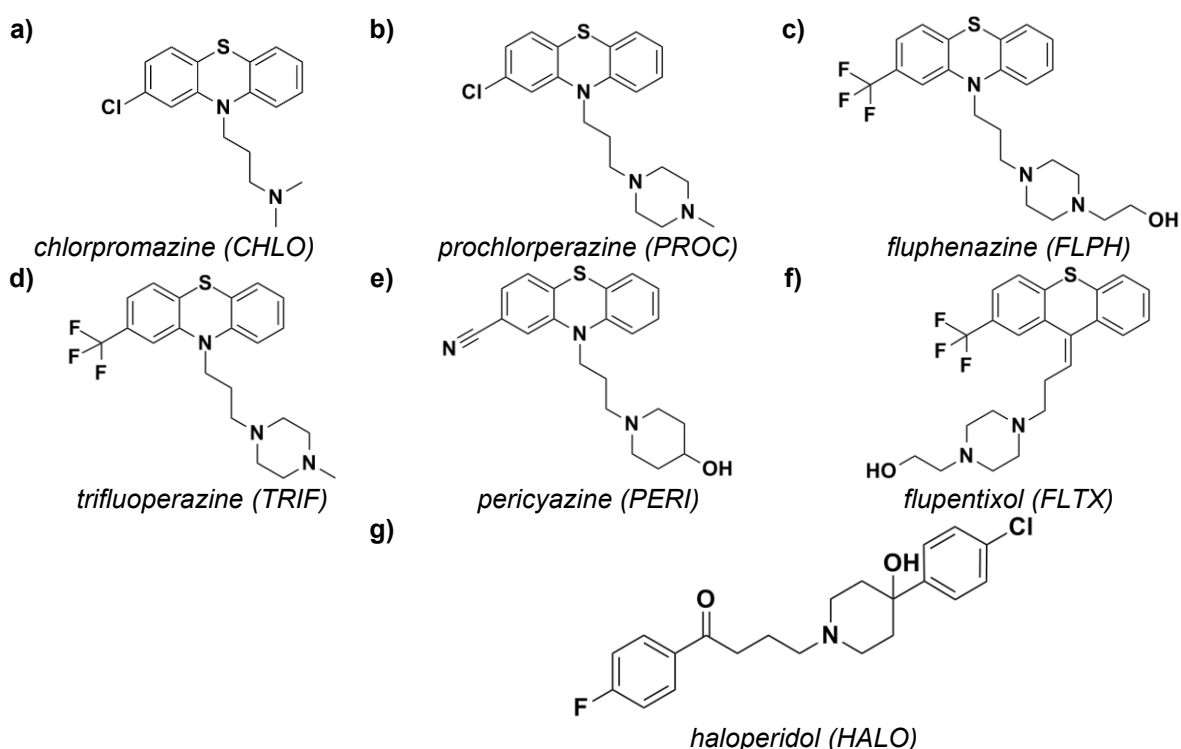


Figure 1-2: Structure of first-generation antipsychotics investigated.
Classification: (a-e) phenothiazine, (f) thioxanthene, and (g) butyrophenone.

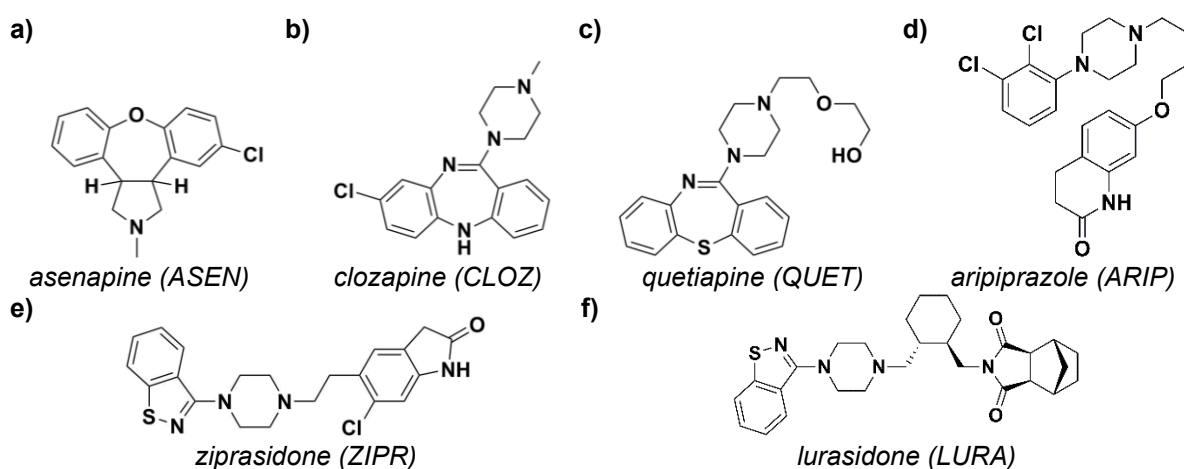


Figure 1-3: Structure of second-generation antipsychotics investigated.

Classification: (a-c) tricyclic, (d) phenylpiperazine, and (e-f) benzisothiazolepiperazine.

Using a model, and defining literature C/P ratios [189] as “observed PMR”, lipophilicity and halogenated groups were considered most predictive of observed PMR [190]. Therefore PERI, PROC, FLPH, and TRIF may also undergo a post-mortem redistribution that could affect femoral blood concentrations, due to possessing the lipophilic phenothiazine moiety present in CHLO.

Drugs for which femoral blood concentrations between the post-admission-pre-autopsy interval have been found to be steady are HALO [78], QUET [78], and DOTH [191]. Based on C/P ratios ARIP is not considered subject to PMR [153]. Furthermore, post-mortem femoral blood concentrations of ARIP in 25 cases approximated *in vivo* plasma/serum concentrations, leading Skov *et al.* to conclude that “major post-mortem concentration increases” would be unlikely in femoral blood [192]. CLOM is considered subject to post-mortem redistribution based on C/P ratios [193]. The post-mortem redistribution behaviour of ASEN, LURA, and ZIPR has not yet been studied.

1.5 Analytical techniques

There are many analytical techniques that may be used in forensic toxicology, including immunoassay techniques, ultra-violet and infrared spectroscopy, and inductively coupled plasma-mass spectrometry [194]. For the targeted quantification of small molecules, as in this thesis, gas chromatography and liquid chromatography coupled to mass spectrometry are commonly utilised.

1.5.1 Sample extraction and clean-up

The analysis of post-mortem specimens proceeds with the extraction of the analytes of interest away from unwanted matrix components (specimen matrices may contain many interfering components such as endogenous proteins, lipids, cells, and putrefactive compounds [195]) and concentration to a level appropriate for instrumental analysis. Tissue specimens require homogenisation or enzymatic digestion prior to analyte extraction [67]. The effectiveness of analyte recovery and sample clean-up depends on the extraction technique and target analytes. The research presented in this thesis was carried out in partnership with Forensic Science SA (FSSA), where liquid-liquid extraction (LLE) is currently the preferred method for the extraction of acidic and basic drugs [196].

1.5.1.1 Liquid-liquid extraction

LLE exploits solubility and pKa differences amongst compounds by their preferential partitioning in two immiscible liquid phases. Usually, one phase is aqueous and the other

organic, allowing for the extraction of neutral compounds (which partition into the organic phase) from ionic compounds (which partition into the aqueous phase) [197]. The pH of the aqueous phase can be manipulated in order to optimise the extraction of compounds into organic solvents by shifting the dissociation equilibrium in favour of unionised species [197]. An inappropriate pH can not only lead to inefficient extraction of an analyte but also decomposition through hydrolysis or rearrangement reactions [198, 199]. Back-extraction (a LLE on the phase collected from an initial LLE) may also be performed to further separate unwanted components co-extracted together with analytes [67]. This technique reduces extraction recovery but can be useful when analysing decomposed blood and liver specimens [200]. Once in an organic phase, concentration of analytes is performed by evaporating the solvent and reconstituting the residue in a known volume of buffer/solvent for subsequent analysis. It is also possible to perform organic-organic extractions to separate drugs from lipids [67].

1.5.1.2 Protein precipitation

Protein precipitation (PPT) is a more straight-forward extraction technique than LLE, in which a chemical reagent (e.g. barium chloride, zinc sulfate, or tungstic acid) or solvent (e.g. acetonitrile) is added to the specimen to induce the precipitation of proteins, enabling the recovery of analytes from the supernatant [67]. Protein precipitation is effectuated by the reduction of protein hydration layers and the hydrophilic and hydrophobic electrostatic attractions of amino acid residues causing proteins to aggregate [201]. This technique is inherently less selective than other extraction techniques that may target analytes and exclude matrix components on the basis of their lipophilicity and pKa. Nevertheless, this technique is useful for extracting a variety of drugs (acidic, neutral, or basic) and it has utility in forensic laboratories [202].

1.5.2 Drug identification and quantification

When analysing specimens in post-mortem toxicology often high-throughput screening methods are utilised in order to determine those positive for any tested drugs or analytes and therefore those that warrant further quantitative analysis. The analytes detected, and the concentrations at which they are quantifiable, for a given analytical method is dictated by the sample extraction method and the instrumentation used. To ensure methods perform reliably validation must be performed to evaluate relevant parameters (as detailed in the Scientific Working Group for Forensic Toxicology (SWGTOX) Standard Practices for Method Validation in Forensic Toxicology standard [203]).

1.5.2.1 Chromatographic separation followed by mass spectrometry

The use of liquid or gas chromatography followed by mass spectrometry is common in post-mortem toxicology laboratories for both screening and quantification. As a chromatographic technique⁹, liquid-chromatography separates molecules by their different partitioning between the chromatographic column (the stationary phase) and the elution solvent (the mobile phase) [204]. For some analytes, gas-chromatography may be utilised, which separates compounds based on their differential partition between a gaseous mobile phase and a solid stationary phase. The mechanism of separation for both techniques is similar: analytes with a greater affinity for the stationary phase will elute later than those with lesser affinity. Separated constituents that elute from the chromatographic column are then analysed by one of many mass spectrometry techniques. These techniques follow the general principle of ionising the analytes, fragmenting their chemical structure, and filtering ions using electromagnetic fields [205].

The use of chromatography followed by mass spectrometry adheres to the recommendation to use two different physiochemical techniques when identifying compounds in a forensic science context [67]. The former technique provides data regarding how an analyte is retained during a chromatographic method (the retention time, characteristic of how the analyte interacts with the stationary and mobile phases), and the latter technique provides mass spectral data for chemical structure elucidation. For both techniques, comparison of analyte retention time and mass spectral data with known standards analysed by the same method concurrently is required for confirmatory identification [206].

For analytes to be analysed by gas chromatography coupled to mass spectrometry (GC-MS) they must be both of high enough vapour pressure and thermally stable or derivatised into a compound that meets these criteria. If not, thermal degradation or reactions between multiple analytes in the injection port may occur [207]. For these reasons, there is a growing preference to use liquid chromatography coupled to mass spectrometry (LC-MS) over GC-MS in toxicology laboratories, which can enable the screening and quantification of hundreds of analytes in a single acquisition method [208, 209]. If using high resolution mass spectrometry it is also possible to use less abundant isotopes to extend the linear range of a method [210]. The use of multiple mass spectrometers in tandem is also common in toxicology because they can enhance the selectivity and limits of detection by means of selective mass filtration and multiple ion

⁹ Chromatographic techniques separate mixtures based on the different physiochemical properties of constituent molecules.

reaction monitoring [211].

In this thesis, a liquid-chromatograph-quadrupole-time-of-flight mass spectrometer (LC-QTOF-MS) was used for qualitative purposes. The chromatographic method used in conjunction with this instrument used a reverse-phase (non-polar) column with an aqueous phase and an organic phase used to perform gradient elution. For gradient elution methods, mobile phases are mixed prior to flowing through the column, and the ratio at which they are mixed changed throughout the run. When used with a reverse-phase column gradient elution proceeds with the aqueous phase at first dominating and the contribution of the organic phase increasing over time. In this way, the affinity for the analytes to the stationary and mobile phase is dynamic, with compounds of high polarity eluting early in the run due to low affinity for the stationary phase compared to the mobile phase when it has a low proportion of organic solvent. During gradient elution the mobile phase becomes less polar due to the increasing proportion of organic solvent and compounds of lower and lower polarity sequentially elute for analysis. In order to analyse the eluate by a QTOF-MS it must be vapourised and ionised and therefore the mobile phase must be volatile [206].

Electrospray ionisation (ESI) is the common ionisation technique utilised for forensic analyses [206]. This technique occurs at atmospheric pressure and is achieved by applying a high voltage to the eluate to form charged droplets [212]. Due to the high temperatures employed these droplets reduce in size as the solvent evaporates and Coulombic repulsion causes the droplets to disintegrate into smaller droplets [212]. Subsequent droplet reduction and disintegration occurs until gaseous ions are produced that then enter the mass spectrometer, guided by pressure differentials and an electric field [212]. Inside the mass spectrometer a high vacuum is maintained [212]. In a QTOF-MS, this enables the ions that enter to be filtered and separated at high resolution based on their mass to charge ratios (m/z) using a quadrupole, hexapole (collision cell)¹⁰ and a time of flight sector. The quadrupole can be configured to screen for specific ions (i.e. the m/z range for the analytes of interest) and the collision cell to fragment those ions for subsequent separation by time-of-flight [213].

The collision cell may fragment ions as specified in the acquisition method or, if operating the instrument in a Data Dependent Acquisition mode, such as auto-MS/MS, may fragment ions when they are detected in excess of a threshold ion count [206]. This latter application allows for the retrospective analysis of collected data. This is useful if additional compounds have been

¹⁰ A quadrupole consists of four rods with oscillating electromagnetic fields. A hexapole consists of six rods with oscillating electromagnetic fields.

added to the screening database, which are then suspected of having been present in previously analysed samples. This strategy has been applied to establish the presence of bacterial degradation products and novel psychoactive substances (NPS) in past toxicology casework [2, 206, 214, 215].

The fragmentation of analytes that may be realised using mass spectrometric techniques can assist in the structural elucidation of novel compounds. However, MS/MS spectra between analytes may be similar if they share the same chemical formulae and chemical moieties, such as is the case with the β -methylphenylethylamines, which are positional isomers of amphetamines [216]. This highlights that the theoretical determination of chemical structures from mass spectrometric analyses of unknowns alone is not conclusive. Unfortunately, the presence of compounds at low concentrations in post-mortem specimens limits and can prevent the use of traditional techniques used to characterise unknown compounds, such as infrared spectroscopy, ultra-violet spectroscopy, x-ray crystallography, and nuclear magnetic resonance techniques. Therefore, the accepted method of determining the identity of an unknown compound is to ensure its resolution from isomeric analytes in the chromatographic method and comparison of retention time and mass spectral data to concurrently analysed known standards.

There are well-documented concerns regarding the use of LC-MS techniques in both clinical and post-mortem toxicology [211, 217-219]. Co-eluting compounds in a complex matrix such as blood can result in ion suppression or enhancement, impacting upon the quantitative validity of the results obtained. Numerous mechanisms are thought to cause suppression, more generally termed “matrix effects”, including competition between analyte and matrix components for charge acquisition, competition between analyte and matrix components for migration to droplet surfaces for gas emission, non-volatile matrix components limiting droplet evaporation or precipitating analytes, and neutralisation of analyte ions by other charged ions in gas-phase reactions [220]. Enhancement may result from matrix components that increase the ability for analytes to acquire charge [220]. Due to matrix variability, matrix effects are not consistent inter- and intra-patients [221]. Methods to combat matrix effects include: altering the chromatographic separation so that the analytes of interest elute further in the run, thereby avoiding the solvent front or other co-eluting interferants; optimising the extraction technique to reduce the amount of matrix components present; and using stable isotopically labelled analogues as internal standards for analytes [217, 222]. The use of a labelled IS is ideal to account for matrix effects but it is essential that the labelled analogues have an identical retention time

to the analytes being quantified [205, 211, 222]. It also may not be possible in the case of novel analytes to obtain certified stable isotopically labelled analogues [211].

A prior study by Butzbach *et al.* highlights how other analytical techniques may be more appropriate for quantitative investigations into post-mortem drug stability. In their study, sertraline concentrations appeared to decrease in liver macerate specimens with increasing putrefaction, implying possible degradation [223]. However, sertraline response decreases were later attributed to a putrefactive by-product of microbial metabolism leading to ion suppression [223].

1.5.2.2 Other methods of detection

Though mass spectrometry is the dominant detection method in post-mortem toxicology laboratories there are other techniques that may be coupled to chromatographic separation.

Coupling ultra-violet and visible (UV-Vis) detection to chromatography is possible if analytes contain chromophores and limits of detection are suitably low. Modern LC-UV techniques utilise a diode array detector (DAD) which disperses light transmitted through the eluent/analyte toward an array of light-sensitive diodes which can measure many wavelengths at once [224]. Data are collected as a 3D spectrochromatogram and this may allow for the assessment of peak purity when determining if components arising from matrix degradation are co-eluting with analytes and altering signal intensities. As analysis by a DAD is a non-destructive technique, it is also possible to collect fractions eluting from an LC-DAD system for further characterisation using other analytical techniques if necessary. For example, mass spectrometric analyses of fractions may assist in the qualitative identification of unknown peaks.

LC-UV techniques are not as sensitive or selective as LC-MS, but there is no requirement to use expensive labelled ISs due to matrix effects (nor would this be possible due to coelution).

1.6 Analysis of microbial communities

1.6.1 Cell counts

One of the simplest techniques to count the number of microbial cells in a sample is the use of a counting chamber, such as the Petroff-Hausser Counting Chamber, in combination with optical microscopy. Using counting chambers, a known volume of microorganisms is placed into an area of known size. In practice, this is achieved by pipetting a sample between the space of a slide and coverslip. On the slide is a fixed grid, a subsection of which is used to count all the microorganisms viewed. Extrapolation to the number of microorganisms present within a

sample or culture is then achieved once dilution factors and the counting chamber cell depth are taken into account [13].

1.6.2 Taxa identification

Initial approaches to determine the human gut microbiota utilised culturing techniques whereby microorganisms were inoculated in a growth medium (usually contained with an agar gel) under specific conditions and a series of tests were then performed to determine the identity of the organisms isolated [18]. These techniques were able to deduce the increasingly anaerobic nature of microorganisms from the ileum to the colon [225, 226]. The advent of metagenomic analysis following the development of DNA sequencing technology, bioinformatics software, and the establishment of genomic databases, has since allowed for a more comprehensive identification of the human microbiome. The power of these techniques, including 16S rRNA sequencing, to elucidate the community of microorganisms that live within and on humans, has led to the discovery of many species that could not be cultivated previously [54, 56, 57].

1.6.2.1 16S rRNA sequencing

16S rRNA sequencing allows for the determination of the microbial communities present in a sample by comparison of amplified and sequenced 16S rRNA genes (amplicon reads) with a reference database, such as GreenGenes [227]. This method enables taxa identification down to the genus level and sometimes the species level. The 16S rRNA gene is utilised because of its omnipresence in bacteria and archaea, coding for a small subunit (16S) of ribosomal RNA [228, 229]. This gene contains both conserved regions (i.e. regions where sequences are identical across taxa) and variable regions (i.e. regions where sequences differ across taxa), allowing the DNA of many taxa to be amplified using universal primers and enabling taxonomic resolution for identification purposes [228, 229].

Identification of the community of microorganisms within a sample proceeds by the extraction of genomic DNA. Many kits are commercially available for extracting nucleic acids from different sample types (e.g. soil, faeces, and blood). Irrespective of the extraction protocol, all methods achieve their goal of purifying the nucleic acid of interest by cell lysis and then removal of any unwanted substances by a series of wash steps prior to nucleic acid elution in an aqueous solution [230]. The removal of matrix components is necessary in order to obtain DNA of sufficient purity for subsequent amplification and sequencing. Gene sequences from taxonomic ranks can then be selectively amplified and sequenced using one of many NGS technologies.

Among these, the Illumina MiSeq platform is considered preferable for 16S rRNA sequencing [228].

Illumina MiSeq proceeds by initially fragmenting the template DNA into shorter sequences and then attaching oligonucleotide adapters (or 'tags'). Following this, the DNA is denatured and washed across a proprietary flow cell surface coated with adapter-complimentary oligonucleotides to which the tags hybridise [231]. The oligonucleotides in the flow cell are complimentary to both the 5' and 3' adapters of the DNA, this results in the formation of 'bridges', wherein single-stranded template DNA is bound at both the 5' and 3' sites (i.e., both ends of the strand) to the flow cell [231]. The template DNA is then amplified using DNA polymerase and the double-stranded product denatured [231]. Sequencing is then performed in tandem with DNA synthesis in a proprietary process, using fluorescently-labelled deoxynucleoside triphosphates (i.e. the A, C, T, and G bases of DNA) [231]. As each nucleotide is added a laser excites the fluorescent labels on the nucleotide bases and each base produces a distinct colour, indicating the bases to which the nucleotides have bound to on the template DNA [231]. This synthesis process is repeated for the complimentary DNA template to produce reverse reads. The sequences relate to the fragments of DNA that are produced in the first step of the process; these fragmentary sequences must then be 'reassembled' to yield the sequence of the intact DNA strands present in the sample. This is done by identifying overlaps (clustering) at the ends of contiguous fragments of DNA (contigs) by aligning forward and reverse reads, to reassemble the DNA template as amplicon reads. These amplicon reads are then classified into operational taxonomic units (OTUs) based on sequence similarity prior to taxonomic assignment using the chosen database.

1.6.3 Community comparisons

Having established the identity of community taxa in samples, microbial diversity can be assessed within and between samples using diversity indices and multivariate analyses. Diversity indices consider richness (the number of OTUs present) and evenness (the equitability of OTU abundance) to assign a numerical value that characterises the microbial diversity of a sample [232]. It is not possible to compare the diversity indices of different samples without consideration of the variable sequencing reads used to obtain the data [228]. Normalisation methods may be used to remove these biases but given large effect sizes the analysis of unnormalised data may be valid [233].

It was of greater interest in this thesis to compare the similarity of different communities based on the taxa detected. Because of the complexity of sequencing data the similarity of different

communities is commonly visually explored using cluster dendrograms (in which samples are group based on similarity as clusters that then group with other clusters) and ordination plots (composed of principal coordinates that represent data variability as 2D or 3D scatterplots) [234, 235]. Cluster analysis and ordination both require a coefficient that measures the similarity between samples, such as Bray-Curtis similarity, which is a quantitative similarity index based on sequence abundance for each OTU [234, 235]. Observed relationships between variables are considered significant only following statistical analyses such as PERMANOVA (permutational multivariate analysis of variance) [236].

1.7 Research overview

1.7.1 Project aim

The aim of this thesis was to determine if any degradation products should be included in coronial toxicology screening methods for the investigated psychoactive drugs. To achieve this, the objectives were:

1. Develop LC-DAD methods for the quantitative analysis of the drugs in whole blood, with appropriate method validation in the field of forensic toxicology [203] (Chapter 4);
2. Identify those drugs that may degrade in aqueous solutions, to assist in establishing whether any degradation of the drugs may be attributable to hydrolysis reactions in whole blood (Chapter 5);
3. Establish whether microbial degradation of selected psychoactive drugs may occur and the effect of sodium fluoride on the degradation of these drugs, achieved by assessing the stability of the drugs in non-inoculated and inoculated (simulated post-mortem) human whole blood, preserved (with 2 % w/v sodium fluoride) and unpreserved (Chapter 6);
4. Determine the microbial communities present in the simulated post-mortem blood specimens, to confirm the appropriateness of the simulation (and also to compare the effect of sodium fluoride and temperature on the thriving communities in whole blood) (Chapter 6);
5. Characterise the degradation products present in the blood experiments and determine their presence in authentic post-mortem blood specimens (Chapter 7, Chapter 8, and Chapter 9).

1.7.2 Experimental overview

The experiments carried out in this thesis allowed for the determination of the likely stability

and degradation of selected psychoactive drugs in post-mortem blood, both in collected specimens and in decomposing cadavers, using a simulated model. The drugs selected were important candidates to investigate regarding their susceptibility to microbially degrade (see 1.4.4).

In this research, human whole blood was the specimen in which drug stability was investigated. Due to legislation in place in South Australia, the use of human post-mortem blood for research purposes is forbidden unless the deceased did not object to such research using their post-mortem tissue during life [237]. Furthermore, all people deemed senior available next of kin must consent to the research being performed [237]. Because of this restriction to experimental protocols, previous research carried at FSSA thus involved inoculating bacteria collected from porcine caecal contents into porcine blood in order to simulate human post-mortem blood [223]. However, despite use of potassium oxalate as an anticoagulant, the use of porcine blood as a matrix resulted in coagulation of the blood after 4-7 days, thus preventing an extended assessment of drug stability [223]. In this thesis, simulation was alternatively achieved using ante-mortem human whole blood spiked with human faeces as a faecal microbiota transplant (FMT) slurry. The slurry used was pooled from nine human donors to address known inter-human variance in gut microbiomes. Faecal matter was chosen as the microorganisms present are representatives of the gastrointestinal tract, which may translocate after death into blood. Microorganisms constitute between 25-54 % of the mass of dry faeces [238, 239]. By inoculating a community of microorganisms, rather than individual species, the expectation is that the stability of the analytes will be determined in the presence of species that may have different xenobiotic metabolism pathways. One concern regarding this approach was that faecal samples are expected to contain microorganisms more representative of the large intestine than earlier habitats in the digestive process, and are therefore unlikely to represent all the microbiota that may translocate from the gastrointestinal tract [238]. Nevertheless: studies on the microbial composition of the human gut are commonly carried out using faecal samples [30, 33, 37-39, 54, 56, 58, 240, 241]; microbial density is greatest in the large intestine of the gastrointestinal tract [242]; and the microorganisms that proliferate during putrefaction are most likely to derive from the large intestine due to their obligate or facultative anaerobic nature [226]. The use of ante-mortem human whole blood spiked with a FMT slurry was therefore deemed appropriate to approximate a post-mortem blood matrix in which drugs could be exposed to microorganisms relevant during putrefaction.

The concentration of microorganisms in post-mortem blood has been scarcely researched, with the only reported asymptotic value of 3-3.5 million organisms/ml or /g determined for bacteria within 24-30 hours post-mortem [48]. There is no protocol in the literature that details the simulation of post-mortem blood using human faeces of FMT slurry to afford reproducible inoculation.

Experiments were carried out using sodium fluoride (2% w/v) as a preservative and using no preservatives (a pseudo-simulation of PMI conditions). Numerous controls used were: a blood matrix control, consisting of the ante-mortem blood alone; non-inoculated-drug controls, wherein the blood was spiked with the drugs but not inoculated with microorganisms, to enable differentiation between chemical instability in the matrix and microbial decomposition of the drugs; and drug-free controls, wherein the blood was inoculated with the microorganisms but not spiked with the drugs, to exclude interference from the microbial matrix. Specimens spiked with the drugs contained amitriptyline (AMIT) as a negative control and risperidone (RISP) as a positive control due to their respective putrefactive stability and instability [2, 195]. The duration of the stability study was over seven months for specimens kept at and below room temperature. This long time period was chosen because forensic toxicology laboratories may store specimens for extended durations (refrigerated at 4 °C or frozen below -20 °C) to allow for further testing if later requested.

The stability of drugs in blood at temperatures pertaining to sample freezer storage (-20 °C), sample refrigerator storage/mortuary storage (4 °C), specimen receipt/handling (room temperature), and a higher temperature (37 °C) was determined. The higher temperature was chosen as an expected optimum for the respiration of gastrointestinal microorganisms due to their colonisation of the human gut. The room temperature specimens were also expected to test the stability of the drugs against different species of microorganisms than those respiring at 37 °C. Thus, the communities of microorganisms present before inoculation and at the end of the study duration for both the control and experimental specimens at 37 °C and room temperature were determined. This also enabled extrapolation as to whether the sodium fluoride (2 % w/v) preservative impacted the growth of microorganisms in comparison to the experiments carried out without any preservative present, as would be expected. The Diversity Profiling service at the Australian Genome Research Facility (AGRF) was utilised for this purpose, amplifying and sequencing bacterial and archaeal DNA using 16S rRNA sequencing in conjunction with Illumina MiSeq. The prokaryotic universal primers 341F and 806R were used [243]. Shotgun metagenomic sequencing, which classifies taxa based on all genes present and

not just the 16S rRNA gene, may identify up to twice the number of species in a sample compared to 16S rRNA sequencing [244]. However, this approach was more expensive and also would have precluded the use of human blood as a matrix, due to the subsequent reduction of sequencing depth expected from co-sequencing microbial and matrix DNA [228].

Drug degradation in the specimens was analysed by LC-DAD quantitatively and LC-QTOF-MS qualitatively. LC-DAD was used quantitatively due to the limitations associated with LC-MS regarding matrix effects in highly putrefied samples without using stable isotopically labelled analogues and the thermal instability of analytes (preventing the use of GC-MS techniques) (see 1.5.2). Qualitative analysis using LC-QTOF-MS allowed for the identification and monitoring of degradation products arising from drug degradation in the blood specimens. Retrospective data analysis of casework was then performed to confirm if these degradants may be present and if there was evidence they could be utilised as markers of drug administration for cases in which the parent drugs have degraded.

1.7.3 Biosafety and ethics

The use of ante-mortem blood and FMT slurry, that may contain PC2 microorganisms, was approved by the Flinders University Institutional Biosafety Committee (approval number 2015-04). The Committee did not approve the growth and isolation of microorganisms from these specimens using agar plates. The Southern Adelaide Flinders Clinical Human Research Ethics Committee at Flinders University/Flinders Medical Centre approved the use of de-identified stool samples obtained from another study (RAH Protocol No: 121218) and approved the use of ante-mortem blood obtained from the Australian Red Cross Blood Service (approval number 215.15). The Australian Red Cross Blood Service and FSSA have an agreement whereby donated human ante-mortem blood may be acquired for research purposes. The FSSA Research and Development Committee approved the use of blood obtained from the Australian Red Cross Blood Service in this project (approval number TOX 15-03). The Southern Adelaide Flinders Clinical Human Research Ethics Committee approved the use of de-identified casework instrument data files and toxicology and autopsy notes concerning such cases (approval number 123.18). The FSSA Research and Development Committee also approved the use of this data (approval number TOX 17-02).

CHAPTER 2 - POST-MORTEM DRUG STABILITY

2.1 Overview

A substantial section of this chapter is taken from a publication “*Microbial impacts in postmortem toxicology*” that was prepared as part of the literature review process of this PhD candidature. This publication provides necessary context for the work performed in this thesis, discussing how microorganisms affect the practice of post-mortem toxicology through the decomposition of the human body and their degradation of drugs and metabolites. This publication details examples of microbially mediated drug degradation and the experimental approaches that have been utilised (as of July 2016) to determine if microorganisms may be responsible for drug or metabolite degradation. This publication has been reformatted in the style of this thesis. Reference details have been merged with the thesis. The content is otherwise as published, with permission obtained from John Wiley & Sons Ltd for thesis inclusion. The authors were awarded the Australian and New Zealand Policing Advisory Agency/National Institute of Forensic Science “Best Chapter in a Book” award for 2017 for the publication.

Jared Castle’s contribution to the publication was to review the literature on the following topics: post-mortem degradation, chemical functionalities prone to decomposition/microbial metabolism, prior experimental methodology to determine drug stability in ante-mortem and post-mortem specimens, and the degradation of specific drugs. Jared Castle was responsible for the synthesis of the majority (85 %) of the text.

Publication details:

“Microbial impacts in postmortem toxicology”. In book: *Forensic Microbiology*. pp. 212-244 (2017)

Jared W. Castle¹, Danielle M. Butzbach², G. Stewart Walker¹, Claire E. Lenehan¹, Frank Reith^{3,4} and K. Paul Kirkbride¹

¹ School of Chemical and Physical Sciences, Flinders University, Adelaide, South Australia, Australia

² Toxicology Section, Forensic Science SA, Adelaide, South Australia, Australia

³ School of Biological Sciences, Sprigg Geobiology Centre, University of Adelaide, Adelaide, South Australia, Australia

⁴ CSIRO Land and Water, Environmental Contaminant Mitigation and Technologies, PMB2, Adelaide, South Australia, Australia

Copyright notice for “Forensic Microbiology”:

Forensic Microbiology, First Edition. Edited by David O. Carter, Jeffery K. Tomberlin, M. Eric Benbow and Jessica L. Metcalf.

This edition first published 2017 © 2017 John Wiley & Sons Ltd

All rights reserved. No part of this publication may be reproduced, stored in a retrieval system, or transmitted, in any form or by any means, electronic, mechanical, photocopying, recording or otherwise, except as permitted by law. Advice on how to obtain permission to reuse material from this title is available at <http://www.wiley.com/go/permissions>

2.2 “Microbial impacts in postmortem toxicology”

2.2.1 Introduction

Forensic toxicologists are required to determine the drugs and poisons present in an individual in order to assist law enforcement, the coroner or criminal courts in establishing cause of death, manner of death, or potential impairment of an individual. Screening methods in postmortem toxicology rely on the identification of drugs and known metabolites.

Therefore, any phenomenon that leads to the inaccurate identification or quantification of drugs or poisons in postmortem specimens is of great concern. In particular, the collection and analysis of postmortem specimens is often hindered by the (i) decomposition of the human body and (ii) sometimes rapid degradation of the very substances that have caused the death of the individual — both processes that are largely mediated by microorganisms. Partial or complete conversion of a drug or metabolite into another compound could result in that drug not being detected, and/or create challenges in interpretation, particularly if potentially toxic concentrations or drug combinations were present. In the worst-case scenario, an incorrect determination of what substances were present at death, and their concentrations, may lead to erroneous “cause/manner of death” findings. This could have further repercussions in legal proceedings, for example, in court trials and insurance claims. Furthermore, the presence or absence of drugs causing impairment of an individual may not be able to be established, or incorrect medication adherence determined.

Thus, knowing the stability of any drugs or poisons under investigation is imperative to ensure the following: (i) appropriate degradation products are screened; (ii) appropriate storage conditions are employed; and (iii) results obtained can be analyzed, presented, and interpreted with confidence. In addition, toxicology laboratories are required by law to store case specimens for an extended length of time to enable reanalysis if requested, and so knowledge of the stability of drugs over this time period is important. This chapter reviews the literature that

covers the impact of microbial activity on the amount of drug, poison, or their metabolites present in postmortem tissues and fluids.

2.2.2 Microbial factors complicating postmortem toxicological analyses

2.2.2.1 Cadaver decomposition and specimen contamination

Decomposition predominantly occurs through the action of heterotrophic microorganisms present in an individual after their death (i.e., putrefaction) [10]. Cadaver decomposition, and the microbial community shifts that occur throughout, is discussed in Chapters 2, 8, and 10¹¹. In many cases, particularly those of sudden or unexpected death, only postmortem specimens are available for analysis in postmortem toxicology. Thus, specimen selection is partially dependent upon how far putrefaction has progressed. Each specimen type has its own distinct advantages and disadvantages; in some cases, a combination thereof can be valuable in elucidating the role of a drug or poison in the death of an individual.

The postmortem migration of gastrointestinal microorganisms (see Chapter 8¹²) into the lymphatic and circulatory system decreases the likelihood of obtaining sterile specimens commonly collected at autopsy, such as blood, liver, and urine [10, 16, 17]. The pH of postmortem blood becomes mildly acidic during the autolytic phase of early decomposition before becoming mildly alkaline during putrefaction [246]. Thus, microorganisms that thrive in such environments are expected to dominate in blood, provided they are capable of fermentation or anaerobic respiration. Despite microbial contamination, the use of blood is usually most convenient because pharmacological data concerning drug concentrations found during antemortem therapeutic drug monitoring and potentially fatal and nonfatal drug concentrations found in postmortem specimens are available [91-94, 192, 247-249].

Putrefactive amines such as tyramine, tryptamine, and 2-phenylethylamine are produced from the degradation of proteins [195]. These amines could interfere with the detection of some drugs (i.e., amphetamines) in decomposing specimens analyzed by some immunoassays and gas chromatography with nitrogen–phosphorus detection. However, the use of modern and more selective analytical techniques has reduced the extent of such interference.

¹¹ These chapters are those present in the *Forensic Microbiology* book. Chapter 2: [245]; Chapter 8: [15]; Chapter 10: [24].

¹² This chapter is that present in the *Forensic Microbiology* book. Chapter 8: [15].

2.2.3 Postmortem drug and metabolite degradation

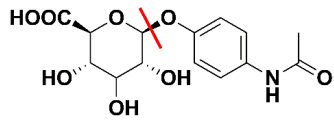
Along with the body, some drugs and metabolites may microbially degrade during the time between death and specimen collection at autopsy (the postmortem interval, PMI). This is of particular concern if the body has been exposed to warm enough temperatures to favor microbial growth, as this increases the likelihood of degradation prior to autopsy. Similarly, drugs and metabolites may continue to microbially degrade in collected specimens before analysis.

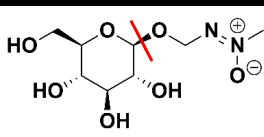
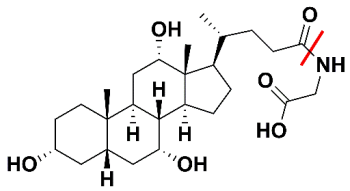
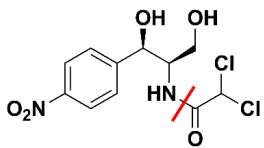
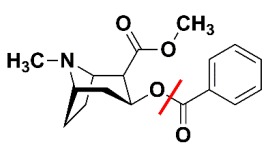
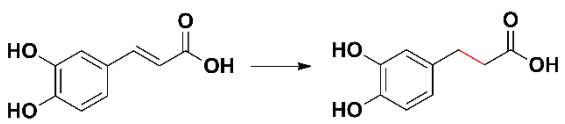
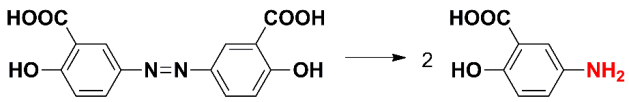
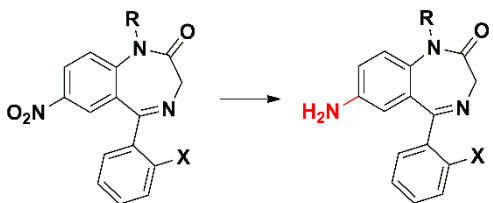
Gastrointestinal microorganisms that translocate into the lymphatic and circulatory system after death have the ability to carry out a diverse array of xenobiotic metabolic reactions (see Chapters 8 and 9). Numerous reviews describe the nature of these reactions and the substrates affected [250-252]. Microbial and mammalian metabolic pathways can sometimes be similar, for example fungi, particularly *Cunninghamella* spp., have been used as model organisms in pharmacological studies instead of laboratory animals and *in vitro* models [253, 254].

Chemical functional groups prone to decomposition, although not necessarily due to microbial activity, were established in a landmark study published by Stevens [195]. In these experiments, human liver macerates spiked with drugs were placed outside, with protection from rain but not necrophagous flies. Nitro groups, N-oxides, oximes, thionosulfur groups, heterocyclic sulfur atoms, and amine and hydroxyl functionality on an aromatic ring were determined to be the chemical functionalities most prone to decomposition. Metabolism by bacteria carried by blow flies was suggested and direct inoculation using fecal bacteria reportedly increased degradation rates (however, no data were provided).

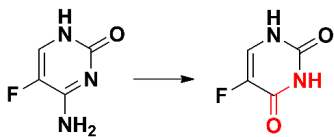
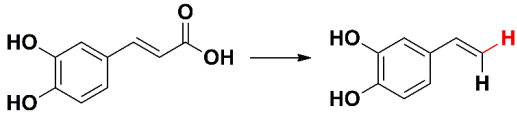
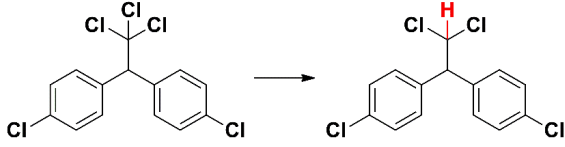
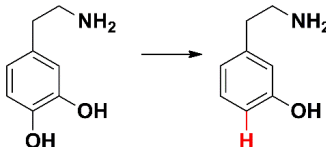
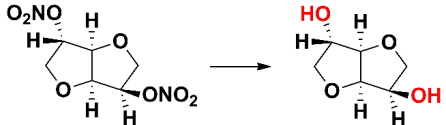
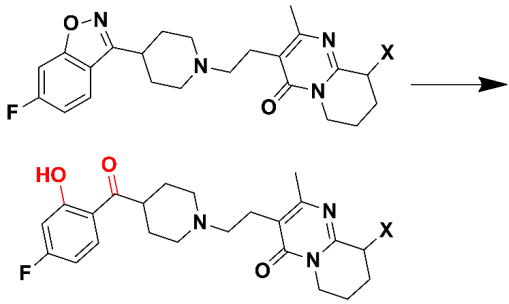
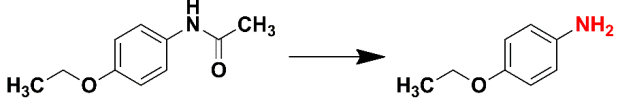
Data from studies investigating the microbial metabolism of drugs in the gastrointestinal tract support the results of Stevens [195], showing that many reactions in which functional groups are interconverted, added, or removed may take place [250, 251, 255]. Some functionalities that are found susceptible to microbial metabolism are shown in Table 2-1.

Table 2-1: Some functionalities found susceptible to microbial metabolism.

Reaction	Example	References
Hydrolysis of Glucuronide conjugates	 paracetamol glucuronide	[256, 257]

Reaction	Example	References
Glycoside conjugates	 <p>cycasin → methylazoxymethanol</p>	[258]
Glycine conjugates	 <p>glycocholic acid</p>	[259]
Amides	 <p>chloramphenicol</p>	[260]
Esters	 <p>cocaine → ecgonine methyl ester</p>	[261]
Reduction of		
Alkenes	 <p>caffeic acid → dihydrocaffeic acid</p>	[262]
Azo groups	 <p>olsalazine → 5-aminosalicylic acid</p>	[263]
Nitro groups	 <p>X=F (flunitrazepam), Cl (clonazepam), H (nitrazepam)</p>	[264]

Reaction	Example	References
Nitroalkenes	<p>nizatidine</p>	[265]
Sulfoxides	<p>omeprazole → omeprazole sulphide</p>	[266]
Functionalisation		
Aromatisation	<p>shikimic acid → protocatechuic acid</p>	[250]
Esterification	Esterification of coprostanone	[267]
Hydroxylation	<p>BII78 dihydroxylation</p>	[253]
N-Acetylation	<p>5-aminosalicylic acid → N-acetyl-5-aminosalicylic acid</p>	[268]

Reaction	Example	References
Other		
Deamination	 <p>flucytosine → 5-fluorouracil</p>	[269]
Decarboxylation	 <p>caffeic acid → 4-vinylcatechol</p>	[270]
Dehalogenation	 <p>DDT → DDD</p>	[271]
Dehydroxylation	 <p>dopamine → m-tyramine</p>	[272]
Denitration	 <p>isorbide dinitrate → isorbide</p>	[273]
Heterocyclic ring scission	 <p>X=H (risperidone), OH (paliperidone)</p>	[2, 223]
N-Deacetylation	 <p>phenacetin → p-phenetidine</p>	[274]

Reaction	Example	References
N-Demethylation	 <p>methamphetamine → amphetamine</p>	[275]

2.2.4 Precautions taken to limit microbial impacts

Chemical preservatives may be added to postmortem specimens in order to limit further microbial action, with sodium fluoride (2% w/v) most commonly used. Its preservative action is primarily achieved by fluoride ions inhibiting enolase and H⁺/ATPase [276]. Dual inhibition of these enzymes both prevents the catabolism of carbohydrates for adenosine triphosphate (ATP) production and leads to acidification in the cytoplasm, further reducing enzyme activity [276]. Other enzymes also inhibited by fluoride include blood cholinesterase (which is only partially inhibited), whose activity otherwise remains in postmortem specimens containing only citrate and facilitates the hydrolysis of cocaine to ecgonine methyl ester (EME) [277, 278]. However, the efficiency of sodium fluoride in minimizing the degradation of different drugs is variable and, in the case of organophosphorus pesticides, its use may lead to accelerated degradation [279-281]. Because sodium fluoride may both stabilize and degrade drugs, the collection of multiple aliquots of blood is therefore preferred to enable the storage of both preserved and unpreserved specimens. Other preservatives, such as sodium azide, have been used; however, its high reactivity with carbonyl compounds prevents its practical use [282].

Postmortem toxicology specimens are stored at low temperatures in order to decrease the rate of microbial metabolism. In a mortuary, corpses are commonly stored at 4 °C. Autopsy specimens are then generally stored at -20 °C, a temperature that is considered to inhibit the growth of most microorganisms [283]. Yet the relationships between temperature, microorganisms, and enzyme activity are complex and merit more research. One particularly complicated factor is that many microorganisms release enzymes extracellularly to break down substrates that then cross the cell membrane. This means that while a microbe might cease activity at a particular temperature regime, the extracellular enzymes might remain active.

2.2.5 Experimental protocols used to investigate postmortem drug and metabolite degradation due to microbial activity

There have been numerous studies investigating the stability of drugs during postmortem decomposition that emphasize the role of microbes in specimen degradation. Some

experiments have been carried out by monitoring concentration changes within decaying cadavers; however, in these situations it is inherently unclear whether changes may be attributed to drug decomposition, redistribution, or a combination thereof [284]. Therefore, *in vitro* studies are most commonly carried out. In addition to human specimens, research has also been performed using surrogate tissue and blood derived from pigs, rats, or other mammals. This is becoming more commonplace following an investigation in the late 1990s in the United Kingdom regarding organs and other specimens being retained after autopsy without the next-of-kin's consent or knowledge [285].

Where local legislation and ethical constraints prevent the use of postmortem specimens for research purposes, a common compromise is to inoculate sterile specimens with cultured species in order to simulate postmortem conditions. This species-specific approach, regardless of the blood matrix chosen, has proven invaluable in predicting analyte stability in real postmortem cases, and even in discovering important microbial degradation products whose significance may have otherwise remained unknown [2]. While effective, this approach does not account for the presence of microbial communities in postmortem specimens, where there will be complex interspecies interactions [11, 26, 286]. Some microorganisms may also be unable to carry out all of the enzymatic steps required to degrade an analyte to the extent that could be observed in postmortem blood, or may produce metabolites that other species do not [223, 253, 262, 287]. Collecting the postmortem blood of animals for use as a model may also be limited due to matrix and microbiome variations from human specimens [288-290]. Studies using only one source of blood matrix, such as a blood donation from an individual, have been found to be subject to interindividual variation [291].

Research investigating postmortem fungal metabolism has seldom ventured beyond exploring the postmortem production of ethanol by fermentation [22, 292, 293]. Of note is the work carried out by Martínez-Ramírez and colleagues, wherein the fungal metabolism of the four psychoactive drugs amitriptyline, mirtazapine, promethazine, zolpidem, and the beta-blocker metoprolol was assessed using fungi found to colonize cadavers [287, 294, 295]. In the case of four of the five drugs studied, metabolites previously unreported in mammals formed; of the 28 fungal strains tested, all produced metabolites found in mammals and 18 produced novel metabolites in growth medium [287]. One of these novel metabolites, a hydroxy zolpidem, was subsequently detected in 2 of 33 reanalyzed postmortem case samples, confirming that postmortem fungal degradation of drugs is possible in postmortem specimens [295].

Assessment of drug stability in sterilized specimens or antemortem whole blood provides information that is necessary to determine whether degradation observed in postmortem specimens, simulated or not, is a result of microbial metabolism, enzymatic degradation, or instability in the matrix toward chemical processes such as hydrolysis. However, appropriate abiotic controls have not been included in many studies where casework specimens have been analyzed over time due to the nature of the experiments.

2.2.6 Examples of microbially mediated drug degradation

In the following discussion, the current literature on the stability of specific drugs and their metabolites in postmortem specimens is reviewed, highlighting potential interpretative issues that may be of consequence following drug or metabolite degradation and production. The significance of potential microbial contributions is highlighted by comparison to stability studies in sterile specimens and antemortem whole blood, where possible.

2.2.6.1 Drugs

Alcohol (ethanol)

Alcohol is the dominant drug encountered in many countries and is routinely determined in postmortem toxicology. Ethanol can be produced postmortem by the fermentation of sugars by bacteria and yeasts [22, 26, 296]. It is also possible for some microorganisms, for example, *Pseudomonas* spp. and *Serratia marcescens*, to consume ethanol, thus lowering the concentration found in blood at autopsy [297]. Postmortem blood concentrations averaging 0.36 g/100 mL (0.36% w/v) are usually present if acute intoxication was the cause of death [296]. In cases where ethanol is produced postmortem, concentrations are usually less than <0.03 g/100 mL [296]. However, there are case studies where concentrations as high as 0.19 g/100 mL [296] and 0.22 g/100 mL have been attributed to postmortem production [298]. This means that determining whether blood alcohol concentrations were from antemortem ingestion or from postmortem production can prove very difficult, especially if decomposition is advanced. In some jurisdictions, any alcohol in the blood is proscribed, and thus ethanol synthesis by microbes postmortem could be problematic for any investigation.

To gauge the extent of the potential problem, Gilliland and Bost showed that in a retrospective survey of 286 autopsies, no alcohol was detected in 39 cases (14%), consumption was attributed to 130 cases (45%), endogenous alcohol production was indicated in 55 cases (19%), and the source of alcohol was unable to be determined in 62 cases (22%) [299]. Therefore, of the 247

cases that tested positive to alcohol, up to 117 (or 41%) could have had the source of ethanol misidentified from blood alcohol concentrations alone [299].

The greater likelihood of vitreous humor and urine remaining sterile has led to many laboratories testing for ethanol in these specimens. Different alcohol levels in these fluids can be indicative of postmortem ethanol production [296, 299]. For example, the absence, or a lower concentration, of ethanol in the vitreous humor compared to the blood indicates postmortem production of alcohol in the blood [296]. The concentration of ethanol in vitreous humor averages about 1.2 times that of the blood concentration [296]. For cases involving severe trauma, such as fatal aviation accidents, blood or urine may be unavailable; thus, the concentration of ethanol in alternative tissue specimens becomes particularly relevant [300]. A fermentation study by Lewis *et al.* (2004) showed that ethanol formed between 22 and 75 mg/hg (0.022–0.075 g/100 mg), after 96 hours at 4 °C, and 19 and 84 mg/hg (0.19–0.084 g/100 mg), after 48 hours at 25 °C, in unpreserved macerated muscle and kidney specimens. In fluoride-preserved specimens, no ethanol was formed [300].

Because of the challenges surrounding the interpretation of postmortem ethanol levels, the metabolites ethyl glucuronide (EtG) and ethyl sulfate (EtS) have been explored as potential marker chemicals for the ingestion of ethanol. However, both false-negative and false-positive results for EtG are possible: given sufficient decomposition, complete bacterial hydrolysis of EtG can take place (due to the action of β -glucuronidase-possessing bacteria, such as *Escherichia coli*) [301], or EtG may be produced from ethanol that has been synthesized postmortem [302]. In antemortem unpreserved urine, it was found that 5 days of storage at 22 °C resulted in EtG either becoming undetectable, increasing in concentration, or being synthesized and then degraded [302]. EtG was found to completely degrade within a day in some bacterially contaminated unpreserved urine specimens [303]; however in another study, Schloegl *et al.* found no degradation over 5 weeks in urine when stored at 4 °C [304]. In unpreserved postmortem blood, Høiseth *et al.* showed that EtG completely degraded in some of the specimens as early as 11 days at 30 °C and 3 days at 40° C [301]. EtG was found to be stable in fluoride-preserved specimens compared to corresponding experiments in unpreserved specimens, with no concentration changes reported after 5 days at 22 °C in antemortem urine or after 18 days at room temperature in postmortem blood [301, 303]. Schloegl *et al.* also examined EtG stability in postmortem liver and muscle tissue (not specified if preserved or unpreserved) and found that room temperature storage for 4 weeks resulted in decreases in concentration of 28% on average [304]. As with ethanol, the use of vitreous humor or urine as

complimentary specimens to blood may be beneficial, as EtG has been found to not always be present in all specimens [305].

Studies on EtS are less frequent—it appears that only one study [306] has shown its degradation in microbial growth medium, but not in human tissues [303, 305, 307]. Concentrations of EtS have not been found to change in studies performed using urine in which uropathogens were present [303, 308]. Thus, the presence of both EtG and EtS or EtS alone is considered to be a strong indicator of perimortem ingestion of ethanol [309]. However, the slower excretion of the glucuronide and sulfate conjugates means they can be present days after ethanol ingestion, and conjugate concentrations do not correlate with ethanol concentrations; thus results must be cautiously interpreted [305, 310].

Amphetamines

Methamphetamine can be metabolized by gastrointestinal microbes (sourced from guinea - pig cecal and fecal contents) to yield amphetamine, with species of the genera *Enterobacterium*, *Enterococcus*, *Lactobacillus*, *Clostridium*, and *Bacteroides* capable of performing the *N*-demethylation (Table 2-1) [275]. Therefore, microbial degradation of methamphetamine is plausible in postmortem specimens. However, in rabbit unpreserved postmortem blood, liver, and skeletal muscle stored for 2 years at 25 °C, methamphetamine concentrations did not decrease significantly, indicating stability [311]. Amphetamine concentrations in the same specimens increased in liver, however, presumably from degradation of another methamphetamine metabolite [311]. In human antemortem preserved blood stored at ambient temperature, these amphetamines decreased in concentration; however, there was no clear trend of degradation over a 5-year period [312]. Holmgren *et al.* found no significant amphetamine concentration changes in preserved postmortem blood specimen stored for a year at -20 °C [313]. A longer study by Karinen *et al.* under the same conditions reanalyzed specimens after 16–18 years, finding that amphetamine concentrations remained within 30% of their initial concentration in 11 out of 16 specimens [314]. In a study by Zaitsev *et al.*, antemortem urine specimens were collected and all found to be contaminated with bacteria to differing degrees [282]. The urines were spiked with methamphetamine and amphetamine, then stored at 4 or 25 °C, with either no treatment, addition of sodium azide, or filter-sterilized using a 0.2 µm membrane [282]. Only specimens stored at 25 °C without treatment resulted in losses of 44% and 32% for amphetamine and methamphetamine, respectively, after 150 days [282].

One study has examined 3,4-methylenedioxymethamphetamine (MDMA), 3,4-methylenedioxyethylamphetamine (MDEA), and 3,4-methylenedioxyamphetamine (MDA) in serum, whole blood, water, and urine at -20, 4, and 20 °C, with no observable decrease in concentrations after 21 weeks [315]. However, the presence or absence of microbes was not mentioned. Another study found no concentration changes for methamphetamine, amphetamine, MDMA, MDA, ephedrine, and pseudoephedrine in urine specimens stored at both -20 and 4 °C after 24 months (for filtration-sterilized specimens) and 6 months (non-sterilized specimens). Filtration-sterilized specimens of the aforementioned drugs, excluding pseudoephedrine, stored for 7 days at 37 °C gave statistically insignificant losses, apart from MDMA where losses were practically insignificant (1.8%). All specimens contained sodium azide (0.1% w/v) [316]. Wenholz *et al.* found MDMA to be moderately stable in putrefying porcine liver, with only some losses in liver at room temperature compared to aqueous controls [317]. No significant change to MDMA concentrations were observed in two postmortem blood specimens stored for 16–18 years at -20 °C [314]. However, in one specimen from the same study, MDA disappeared and there was a 56% increase in the concentration of amphetamine, suggesting MDA degrades to amphetamine.

Antidepressants

The tricyclic antidepressant dothiepin has been reported to completely degrade in putrefying human liver macerates within 3 days [195]. Subsequent investigations where bacteria were inoculated into unpreserved blood (both antemortem and postmortem) have found that the decomposition of dothiepin is not mediated by either *Clostridium perfringens* or *Proteus mirabilis*, bacteria that are observed in postmortem blood [318]. Another study found that no degradation occurred in postmortem blood inoculated with human fecal bacteria and incubated at 23 °C for 7 days, yet rabbit fecal bacteria degraded dothiepin by 24% in a paired experiment [191]. It is therefore possible that the degradation in the liver macerates reported by Stevens resulted from instability in the liver matrix or potential degradation by microorganisms introduced by blow flies or other contamination [195]. Other tricyclic antidepressants that have been studied and determined to be stable during putrefaction include doxepin, amitriptyline, and imipramine [195]. However, Lutfi found that amitriptyline and imipramine exhibited losses of 84 and 69% in postmortem blood stored at 25 °C for a year, with decreasing losses at lower temperatures [319]. It was not specified whether specimens were preserved or not. Holmgren *et al.* found amitriptyline and clomipramine to be stable in preserved postmortem blood specimens stored for a year at -20 °C [313].

The monoamine oxidase inhibitor tranylcypromine was observed to decrease in concentration in blood in a case study with obvious signs of putrefaction, indicating microbial activity. The researchers further investigated that finding by spiking tranylcypromine into antemortem blood under nonsterile conditions and incubating it at 37 °C for up to 48 hours, by which time only 42% of the drug remained [320].

The serotonin-selective reuptake inhibitor antidepressants citalopram, paroxetine, sertraline, fluoxetine, and venlafaxine have been found to be stable for 57 days in putrefying porcine liver [84, 223]. In this same study, fluvoxamine was found to significantly decrease in concentration; however, this may be at least partially due to chemically mediated hydrolysis [84, 223]. In a different study [321], fluoxetine decreased in concentration in blood, urine, and liver stored at 4 and 25 °C. The maximum loss was in liver at 25 °C with a 36% decrease in concentration over 90 days. However, no information about the presence of microbes or evidence of putrefaction was reported. In a study by Holmgren *et al.*, losses of 28%, although not statistically significant, were observed for fluoxetine in preserved postmortem blood specimens stored for a year at -20 °C [313]. However, another study by Karinen *et al.* found losses of fluoxetine under the same conditions to reach 61% after 16–18 years of storage [314]. Holmgren *et al.* found citalopram and sertraline to be stable in preserved postmortem blood specimens stored for a year at -20 °C [313].

The microbial contribution to the degradation of trazodone is unknown. McIntyre *et al.* found degradation up to 20% after 8 months of storage at 4 °C in preserved postmortem whole blood [322]. Blood in this study was collected from deceased who exhibited no obvious signs of decomposition.

Antipsychotics

Butzbach *et al.* found that the microbial degradation of both paliperidone and risperidone to their 2-hydroxybenzoyl degradation products is possible in unpreserved porcine blood inoculated with bacterial species cultured from porcine cecum contents (Table 2-1) [2]. They also found that within 2 days at 37 °C, degradation was complete and that losses were >40% after almost 4 days at 20 °C, whereas the drugs were stable in sterile controls under the same conditions and in the inoculated specimens at 7 °C [2]. The addition of sodium fluoride was successful in minimizing the formation of the 2-hydroxybenzoyl microbial degradation product of risperidone to trace levels and preventing further degradation *in vitro* [223]. In postmortem cases, the presence of these degradation products in the absence of the parent drugs has been

reported [2, 3, 223]. Based on mass spectral data Taylor and Elliott also suggested that a dihydroxyrisperidone ring scission degradation product was present in the urine, presumably from microbial degradation of the dihydroxy metabolite of risperidone [3]. This compound had previously only been reported as present in feces [323, 324]. Reference standards were not available to enable any quantification of the degradation products in toxicological analyses of postmortem blood; consequently, for the Taylor and Elliot case, it was only possible to state that the decedent did ingest risperidone some time before death [3]. In comparison to the decomposing blood studies, risperidone losses in preserved antemortem whole blood were only about 30% in a 20-week study by Saar *et al.* at temperatures up to 20 ° C, further implicating microorganisms in the aforementioned cases as the dominant factor leading to the degradation observed [291]. In the same study, paliperidone losses did not exceed 29% after 10 weeks at 20 °C.

Thioridazine concentrations have been reported to both increase and decrease in postmortem blood. Batziris *et al.* reported that thioridazine degrades more rapidly in putrefying blood in comparison to antemortem blood. It was found that *P. mirabilis* and *C. perfringens* were not responsible for drug losses in unpreserved blood after 8 hours of storage at 37 °C [318]. Previously, Stevens reported that thioridazine completely degraded within 5 days when spiked into liver left to putrefy under environmental conditions [195]. Holmgren *et al.* reported about 40% increase in thioridazine concentrations (n = 5) when postmortem femoral blood specimens were stored at -20 °C for a year, suggesting possible conversion from a sulfoxide metabolite, even with potassium fluoride (1% w/v) used as a preservative [313]. No experiments have been performed yet to confirm that this conversion occurs and whether or not microbial activity is the cause.

There are contradicting results in the literature regarding the stability of chlorpromazine in both ante- and postmortem specimens, making it unclear whether microorganisms are pivotal to its decomposition or chemical instability may be responsible. Saar *et al.* found that after 20 weeks in preserved antemortem blood 65–70%, 35%, and about 50% losses of chlorpromazine occurred for storage at -20 °C, 4 °C, and 20 °C, respectively [291]. On the other hand, McKay *et al.* found chlorpromazine to be stable in unpreserved antemortem blood after 12 weeks at -20 °C [325]. Chlorpromazine has been found to degrade at room temperature in unpreserved postmortem blood, urine, liver, kidney, and brain specimens, with refrigeration considerably reducing losses (in blood at room temperature: 75% losses after 3 months, trace levels, or undetectable after 6 months) [326]. Lutfi still observed chlorpromazine after 1 year in

postmortem blood, although only at 30% of the initial concentration [319]. Chlorpromazine losses in refrigerated unpreserved postmortem blood did not exceed 25% after 6 months, which would suggest, in light of the prior discussed antemortem study by Saar *et al.*, that factors other than microorganism activity may play a role in the decrease in chlorpromazine concentrations [326]. However, in the putrefying liver study by Stevens, chlorpromazine was found to degrade completely in two separate specimens after 17 and 36 days [195]. Batziris *et al.* also found chlorpromazine degraded more rapidly in postmortem blood than in antemortem whole blood [318]. Duffort *et al.* found no degradation of chlorpromazine; however, there was no difference in the extent of degradation in preserved and unpreserved blood specimens [327]. These authors also reported on the stability of 15 other antipsychotics and 21 antidepressants. Unfortunately, whether the matrix used was ante- or postmortem blood was not clearly specified for any drug, making conclusions regarding microbe involvement difficult to draw.

The involvement of microorganisms in olanzapine degradation is unknown. Experimental evidence suggests that chemical degradation is the primary mechanism by which losses occur. Saar *et al.* observed 100% losses in preserved antemortem blood specimens (20 weeks at -60 °C) and 100% losses in stock solutions of olanzapine have been observed for both room temperature and refrigerated (4-6 °C) storage [291, 328, 329].

Benzodiazepines

The conversion of nitrobenzodiazepines to their 7-aminometabolites (Table 2-1) occurs in both ante- and postmortem blood, although the rate appears to increase significantly in the latter due to microbial activity. In unpreserved postmortem blood, flunitrazepam and clonazepam decreased in concentration by 96% and 89%, respectively, within 8 hours at 22 °C. In comparison, flunitrazepam and clonazepam decreased by 50% and 15%, respectively, after 10 days in unpreserved sterile whole blood at 22 °C [264, 330]. In an earlier study using bacterially contaminated postmortem blood, complete degradation of flunitrazepam, nitrazepam, and clonazepam occurred within 2, 3, and 4 hours, respectively [264]. The addition of 1% sodium fluoride reduced the rate of conversion, with 24%, 46%, and 60% remaining, respectively, after 6 hours. Addition of 1% sodium fluoride to bacterially contaminated whole fresh blood reduced the rate of bacterial conversion of flunitrazepam by 95%, 92%, and 65% for *C. perfringens*, *Staphylococcus aureus*, and *Bacillus cereus*, respectively [264]. Skopp *et al.* found it took up to 240 days for flunitrazepam to completely degrade in unpreserved antemortem whole blood stored at 4 °C [331]. In a separate study by El Mahjoub and Staub, complete degradation was observed within 168 days in unpreserved antemortem whole blood stored at room temperature

[332]. Work by Pépin *et al.* later found flunitrazepam, nitrazepam, and clonazepam to degrade more rapidly at -20 and 4 °C in unpreserved postmortem blood, in contrast to the Robertson and Drummer studies under these conditions [333]. The large variation between the results of both sets of experiments suggests that there could be some difference in the postmortem blood matrix or microbial communities present. A longterm study by Karinen *et al.* found that flunitrazepam and clonazepam concentrations after 16–18 years of storage at -20 °C did not significantly decrease compared to concentrations initially determined in preserved postmortem blood [314].

The 7-aminometabolites, which may be present due to human or microbial metabolism, may also subsequently degrade. In bacterially-contaminated unpreserved postmortem blood, losses of between 10 and 20% were reported after 45 hours of storage at 22 °C for the 7-aminometabolites of flunitrazepam, nitrazepam, and clonazepam [330]. As with the parent benzodiazepines, degradation of the 7-aminometabolites also occurred in the study by Pépin *et al.* [333]. In preserved postmortem blood stored for a year at -20 °C, an average loss of about 50% ($n = 10$) was reported for 7-aminonitrazepam [313]. For other benzodiazepines and their metabolites (diazepam, nordiazepam, flunitrazepam, and 7-aminoflunitrazepam), concentrations changes were statistically insignificant [313].

Temazepam also degrades more readily in postmortem rather than antemortem specimens. Al-Hadidi and Oliver reported up to about 50% degradation of the drug when stored at 5 and 25 °C for a year in unpreserved antemortem blood, whereas Lutfi reported 62 and 70% losses for storage of the drug at the same temperatures and for the same time but in postmortem blood (addition of a preservative was unspecified) [319, 334].

The instability of the *N*-oxide benzodiazepines, chlordiazepoxide, and demoxepam in postmortem specimens has been addressed in various studies. For chlordiazepoxide, sodium fluoride has proven effective in significantly slowing degradation rates at both 4 and 25 °C in postmortem blood [335], while in another study, the same amount of loss at 4 °C in unpreserved postmortem blood took approximately six times as long to be achieved in preserved postmortem blood [336]. At lower temperatures of -80 and -20 °C degradation was inhibited, with stability observed after 24 weeks in postmortem bile, blood, and vitreous humor, in both preserved and unpreserved specimens. Degradation products were identified as demoxepam, nordiazepam, and desoxychlordiazepoxide [195, 335, 336]. Desmethyl-desoxychlordiazepoxide has also been observed in sudden deaths involving chlordiazepoxide, presumably a breakdown product of the metabolite norchlordiazepoxide [337]. Regarding demoxepam, Pépin *et al.* reported its

disappearance in unpreserved postmortem blood after 1 month of storage at 25 °C [333]. Losses of 97% were reported after 6 months at 4 °C. Stevens determined in experiments using putrefying human liver macerate that both chlordiazepoxide and demoxepam degraded completely within 3 days [195]. For nordiazepam, the following losses were reported: 27% and 88% (75 days in unpreserved postmortem blood at 4 °C and 25 °C, respectively); 30% and 60% losses (50 days in unpreserved postmortem liver at 4 °C and 25 °C, respectively) [335]. Concentration changes of 30% for nordiazepam were reported by Karinen *et al.* for 20 preserved postmortem blood specimens stored for 16–18 years at –20 °C, although statistically insignificant [314].

Degradation of the triazolo benzodiazepines appears less enhanced in postmortem blood in comparison to the nitro and *N*-oxide benzodiazepines. Alprazolam has been found to degrade by 15% and 30% in unpreserved postmortem blood stored at –20 °C and 25 °C, respectively, after 2 months [333]. Comparatively, alprazolam remained stable after a year of storage at 25 °C in packed red blood cells reconstituted in isotonic saline [338]. In the same experiment, estazolam was also found to be stable, with no apparent change in stability for specimens with sodium fluoride present. In unpreserved postmortem blood, a loss of 30% after 8 weeks at 25 °C was reported by Pépin *et al.* [333]. Results from Zaitso *et al.* indicate that the enhanced degradation observed may not be due to microbial action, as they found no notable difference in estazolam stability in antemortem urine specimens that underwent filtration sterilisation compared to those that did not [282]. The effectiveness of this sterilization technique was demonstrated by its ability to preserve nitrazepam, which, as previously discussed, degrades microbially within hours at room temperature [282, 330].

In a recent investigation into the stability of benzodiazepines in Reinforced Clostridial Medium, Martindale *et al.* (2015) suggested that *E. coli* and *Bacteroides fragilis* may have metabolized flunitrazepam and diazepam to minor human metabolites [339]. It was also suggested that *C. perfringens* may secrete compounds that prevent the degradation of diazepam, as it is degraded in the matrix without *C. perfringens* present. This apparent stabilization was observed even when a mixed culture of all three bacterial species was used. These experiments highlight the advantage of performing experiments with microbial communities rather than isolated species.

Diazepam has been observed to be stable in unpreserved postmortem blood, brain, and liver stored at 4 and 25 °C for 3–5 months [335]. Stevens also found diazepam to be stable in putrefying human liver macerates [195]. However, diazepam has been reported as unstable in unpreserved blood. Skopp *et al.* reported losses of about 45% for antemortem specimens stored

for 240 days at 4 °C [331]; Pépin *et al.* found 25% and 50% losses for postmortem specimens stored for 2 months at 4 °C and 25 °C, respectively [333]; and Lutfi reported 68% losses for postmortem specimens stored for a year at 25 °C [319]. A long-term study found diazepam concentrations to predominantly remain within 30% of their initial concentration after 16–18 years in preserved postmortem blood stored at –20 °C [314].

For other benzodiazepines, such as bromazepam, clobazam, flurazepam, lorazepam, and midazolam, degradation does not appear to be enhanced in postmortem specimens compared to antemortem specimens [195, 331–333, 335, 336].

Cannabis

In fresh antemortem blood and plasma, Johnson *et al.* found THC (Δ^9 -tetrahydrocannabinol) and THC-COOH (11-nor-9-carboxy- Δ^9 -tetrahydrocannabinol) to be stable at room temperature for 32 days, with significant decreases for THC after that point [340]. No information regarding sterility was provided. Holmgren *et al.* reported a significant decrease in THC concentrations (about 66%) after storage at –20 °C for 1 year in preserved postmortem femoral blood [313]. Skopp and Pötsch performed a study examining THC-COO-glucuronide in the urine of cannabis users [341]. The glucuronide was hydrolyzed to form THC-COOH at 20 and 40 °C without preservatives; and it was noted that after 10 days, signs of microbial growth were observed in half of the urine specimens. While this is likely partially due to microorganisms hydrolyzing the glucuronide, the pH of the urine was also a factor [341]. Decreases in THC-COO-glucuronide concentrations were observed by Scheidweiler *et al.* in preserved antemortem blood stored at –20 °C, 4 °C, and room temperature for 12, 12, and 1 week, respectively [342]. No concurrent significant increases in THC-COOH concentrations were reported. To our knowledge, no studies have been performed to examine whether bacteria or fungi found in human remains can specifically degrade THC or THC-COOH.

Cocaine

Some fungi and bacteria have been found to be able to hydrolyze cocaine to ecgonine methyl ester (EME). Notably, this includes *Aspergillus niger*, which is a fungus that is found in the gastrointestinal tract (Table 2-1) [31, 261, 343]. However, nonmicrobial hydrolysis is also possible: the methyl ester moiety of cocaine may chemically hydrolyze *in vitro* in neutral and alkaline conditions to benzoylecgonine (BE) or the phenyl ester may, by the action of blood cholinesterase, hydrolyze to produce EME [278, 344]. Even with sodium fluoride (1% w/v), which inhibits cholinesterase, complete cocaine degradation was observed by Baselt *et al.* in preserved antemortem sheep blood after 1 year at 4 °C [345]. Cocaine in antemortem whole

blood adjusted to a pH of 5 was found to be considerably more stable than at pH 10 [278]. BE or EME may also degrade to produce ecgonine.

When cocaine and ethanol are concurrently consumed, cocaethylene is formed as a metabolite. There are indications that cocaethylene might be formed by microbes; however, this has not been observed to occur *in vitro* [346]. In the absence of other cocaine metabolites, analyzing for ecgonine and cocaethylene is advised [312, 346, 347].

***γ*-Hydroxybutyrate**

γ-Hydroxybutyrate (GHB) is produced in the body at low levels as an endogenous metabolite of *γ*-aminobutyric acid (GABA), and this necessitates the use of interpretive cutoff values to discriminate between endogenous levels and those arising from ingestion [348]. Endogenous GHB levels are not expected to exceed 5 mg/L and 10 mg/L in antemortem blood and urine, respectively. For postmortem specimens, greater cutoff values have been advised – 30 mg/L and 10 mg/L for femoral blood and urine, respectively [349]. However, values above these cutoffs are possible and may be as high as 193 (mean = 30 mg/L in that study) and 217 mg/L (mean = 56 mg/L in that study) in postmortem femoral blood and urine, respectively, for specimens collected from deceased where GHB use was not suspected [350-352]. On the other hand, blood concentrations of GHB in GHB-related deaths can be as low as 18 and 9 mg/L for single drug and poly-drug overdose deaths, respectively [353]. As a consequence, elevated levels in other specimens such as urine, vitreous humor, or brain, or evidence from the scene, are necessary to identify the cause of death as GHB-related [353].

Decreases in GHB concentrations following initial increases have been observed in unpreserved postmortem blood [354]. Addition of fluoride has been shown to result in specimens that are stable for at least 6 months at 4 °C and confidently reanalyzed up to 7 years later if stored at –20 °C without detrimentally affecting the interpretation of GHB concentrations [355, 356]. Postmortem specimens have been found to be stable when stored at –20 °C for at least 2 years; however, there was no mention whether any preservative was used or not [357]. Though the precise cause of the rising and then falling concentrations is not clear, microbes are implicated as it has been observed that greater concentration changes take place in postmortem blood rather than antemortem serum [354]. One untested hypothesis is that the metabolite GHB-glucuronide, which has a longer elimination half-life than GHB, is slowly hydrolyzed back into GHB [358]. This may be mediated by microbial enzymes. Another hypothesis includes the degradation of putrescine, both an endogenous chemical and one that is produced from putrefactive amino acid degradation, to GABA and its subsequent degradation to GHB [26, 359].

Interpretation of GHB concentrations is complex; low levels are expected due to the drug's rapid elimination, and at these levels it is difficult to establish whether concentrations are endogenous, result from consumption, or from postmortem production. As GHB is labile in the absence of preservatives at room temperature (i.e., during the PMI or incorrectly stored antemortem specimens), an alternative biomarker for GHB consumption that can both afford greater sensitivity and behave more predictably is sought after. Recently, GHB sulfate has been discovered as a metabolite which, analogous to EtS in ethanol analysis, may be resistant to microbial degradation and thus more valuable than GHB or GHB glucuronide alone in inferring endogenous or administered GHB for postmortem specimens [360]. Further work is necessary to establish endogenous levels of GHB sulfate, as well as whether microbes may have an impact upon conjugate concentrations.

Opiates

Concentrations of 6-monoacetylmorphine (6-MAM) — the key metabolite that indicates heroin consumption — have been found to decrease in femoral blood between body receipt at the mortuary and autopsy, with an average time interval of 64 hours [79]. Høiseith *et al.* found that in both ante- and postmortem blood, 6-MAM was detected in only 4 of 19 cases in a subsequent reanalysis (between 4.2 and 9.4 years later) despite storage with sodium fluoride and at -20°C [361]. Papoutsis *et al.* found that losses of 6-MAM were significant after storage for 3 months, with about 35% losses reported in preserved antemortem whole blood [362]. 6-MAM may be found in preserved vitreous humor even when it is no longer detectable in preserved postmortem blood, similar to ethanol [305, 313]. A significant microbiological component to the instability of 6-MAM is implied by the results of Zaitso *et al.*, in which sodium azide and filtration sterilization decreased and prevented, respectively, 6-MAM degradation in antemortem urine [282].

Compared to 6-MAM, morphine and codeine are more stable. Insignificant changes to their concentrations were found in preserved postmortem blood stored at -20°C after 1 year [313]), in ante- and postmortem blood at -20°C after 9 years [361], and less than 30% change for most preserved postmortem specimens reanalyzed after 16–18 years at -20°C [314]. Another year-long study found that morphine concentrations in postmortem blood exhibited losses of 15–24% when stored between -20 and 25°C — no mention was made as to the use of preservatives or anticoagulants in this study [363]. Stevens observed no degradation of morphine in putrefying human liver macerates after 29 days [195].

The situation relating to overall change in morphine concentrations over time appears dependent upon hydrolysis of its glucuronides [312, 364]. A study by Moriya and Hashimoto found that postmortem blood and urine specimens, but not liver, maintained morphine glucuronide concentrations when stored at 4 °C, 18–22 °C (room temperature), and 37 °C over a period of 10 days (no use of preservatives mentioned by the authors) [365]. Longer-term studies in four specimens of postmortem blood have shown that morphine and its glucuronides are stable if stored at –20 °C (no use of preservatives mentioned by the authors) [366]. At 4 °C significant changes in concentration were observed for morphine-3-glucuronide (M3G) in postmortem blood, which averaged about 20% losses after 124 days of storage [366]. Morphine-6-glucuronide (M6G) and morphine concentrations were more notably affected by storage at 20 °C in postmortem blood, wherein both were ultimately reduced to undetectable levels in two of four cases [366]. M3G concentrations became undetectable by the 124th day also, although no specimens were analyzed between the 70th and 124th day [366]. Giorgi and Meeker reported that in preserved antemortem blood stored at ambient temperature, morphine concentrations decreased in specimens stored for 2 years, increased in specimens stored for 3 years, and decreased in specimens stored for 5 years [312]. Skopp *et al.* in their study found that in the postmortem blood specimens, concentrations increased during the first 70 days for two of four cases and then became undetectable in two of the four cases; however, they did not mention whether preservatives were used [366].

New Psychoactive Substances

New psychoactive substances (NPS) encompass a variety of drugs that may be further classified by their chemical structure (e.g., the cathinones, phenethylamines, tryptamines, and piperazines) or psychotropic effects (e.g., stimulants, hallucinogens, entactogens, synthetic opioids, sedatives, and cannabimimetics) [367, 368]. Despite the proliferation of NPS and their involvement in fatalities, there is a lack of information regarding their stability toward microbial degradation; as of early 2016, only mephedrone (4-methyl methcathinone) and *N*-benzylpiperazine (BZP) have been studied.

Studies on mephedrone show that microbial activity could be contributing toward its degradation. Johnson and Botch-Jones reported 30% losses and >50% losses of mephedrone after 7 and 14 days of storage, respectively, in whole blood at 4 °C. At room temperature, mephedrone was undetectable after 7 days — the presence or absence of sodium fluoride was not mentioned [369]. Degradation rates were slower in a subsequent study that indicated mephedrone was more stable in antemortem blood compared to postmortem blood. The use of

sodium fluoride with potassium oxalate (1.67%/0.2%) as a preservative was also found to be preferred to no preservative at all [370]. After 185 days, specimens stored at $-20\text{ }^{\circ}\text{C}$ in sodium fluoride preserved antemortem blood resulted in losses of 6.6%, whereas preserved postmortem blood specimens showed losses of 9.1% [370]. Complete mephedrone degradation was observed within 94 and 59 days at temperatures of $4\text{ }^{\circ}\text{C}$ and $20\text{ }^{\circ}\text{C}$, respectively, for both ante- and postmortem specimens [370]. Greater than 30% losses were observed for mephedrone in putrefying porcine liver after 30 days and 14 days at $4\text{ }^{\circ}\text{C}$ and room temperature, respectively [317]. Degradation in the putrefying porcine liver was significantly greater than in aqueous controls.

Wenholz *et al.* investigated BZP stability in putrefying porcine liver and water at 4 and $20\text{ }^{\circ}\text{C}$ after 14, 30, and 90 days, finding significantly greater degradation of BZP in the putrefying samples after 14 days and 90 days for the samples stored at $4\text{ }^{\circ}\text{C}$ and $20\text{ }^{\circ}\text{C}$, respectively [317]. Degradation differences between the two matrices in all other analysed samples were insignificant, indicating that microbial activity is likely not crucial for the degradation of BZP.

Other drugs

Paracetamol concentrations have been found to increase in preserved and unpreserved postmortem blood specimens, with corresponding decreases in concentration of the glucuronide metabolite. Storage of casework specimens below $-15\text{ }^{\circ}\text{C}$ is effective in inhibiting the conversion of paracetamol glucuronide to paracetamol, regardless of whether a preservative is used [256]. In unpreserved postmortem blood, this hydrolysis was complete within 3 days at room temperature, whereas in postmortem blood preserved with sodium fluoride (2% w/v), the rate is reduced such that an approximate 50% reduction in instrument response was observed after 5 days [256, 257]. Thus, sodium fluoride is efficient in reducing the rate of paracetamol-glucuronide degradation but does not completely prevent degradation from occurring. In comparison, unpreserved sterile antemortem blood showed no conversion of the glucuronide to the parent drug after 48 hours of incubation at $37\text{ }^{\circ}\text{C}$, although some degradation of the glucuronide was observed after 8 weeks storage at 20 and $30\text{ }^{\circ}\text{C}$ in preserved antemortem blood [256, 257].

Thai *et al.* added 20 bacterial species to sterile antemortem unpreserved blood incubated at $37\text{ }^{\circ}\text{C}$ and found that paracetamol glucuronide completely degraded within 10 hours, with a corresponding increase in response for paracetamol [256]. Paracetamol glucuronide was then spiked into sterile antemortem unpreserved blood and portions inoculated with individual bacterial species with incubation at $37\text{ }^{\circ}\text{C}$, and it was found that 10 of the species produced

paracetamol within 24 hours and at 48 hours paracetamol was detected for another two species. An abiotic control with aqueous solutions of paracetamol glucuronide confirmed that bacteria are crucially involved in the hydrolysis of the glucuronide to the parent drug (Table 2-1) [256, 257]. No degradation of the sulfate or mercapturate metabolites was reported [256, 257].

The stability of anti-asthmatic β 2-agonists was investigated by Couper and Drummer in preserved postmortem blood [371]. While salbutamol and terbutaline were found to be stable after 1 week at 23 °C, 6 months at 4 °C, and 1–2 years at –20 °C, fenoterol degradation was significant under all three conditions (losses of 83%, 93%, and 66%, respectively). Structurally, fenoterol differs from salbutamol and terbutaline by the presence of an additional phenolic group, with its degradation potentially attributed to oxidation at this site. Furthermore, as there were no observed increases in salbutamol concentration over 2 years, the authors also hypothesized that the sulfate metabolite of salbutamol might not degrade back into the parent drug.

Trihexyphenidyl was found to degrade slowly in postmortem blood and urine over a 6-month period at 25 °C giving maximal losses of 12.8% [372]. Postmortem blood and urine specimens analyzed over the same period and stored at 4 and –20 °C were stable. Antemortem blood and urine specimens were collected from four people receiving trihexyphenidyl, with no change in concentrations after storage at 4 °C for 6 months.

Valproic acid has been found to degrade in postmortem blood stored at 4 °C and 20 °C, resulting in losses of about 25% and 85%, respectively, over 28 days [373]. It appears that chemical hydrolysis is the dominant mechanism of zopiclone degradation with the rate of formation of 2-amino-5-chloropyridine (ACP), the only known degradation product of zopiclone and its metabolites, occurring most rapidly in alkaline conditions [374]. Pounder and Davies observed no degradation of zopiclone in unpreserved postmortem blood inoculated with fecal bacteria after 10 days at 23 °C [375]. Other studies, in both ante- and postmortem blood have found that zopiclone does degrade. After 8 days of storage at 20 °C, zopiclone losses were 75%, and hydrolysis was complete after 1 week of storage at 40 °C in unpreserved antemortem blood [376]. In preserved antemortem blood, complete degradation was reported after ~25 days storage at 20 °C, and ~50% decreases after almost 1 year of storage at –20 °C [377]. In unpreserved postmortem blood, the degradation of zopiclone is similar to its degradation in preserved antemortem blood [333]. Furthermore, in preserved postmortem blood, losses >20% have been observed after 12 months of storage at –20 °C by Holmgren *et al.* [313], whereas no significant degradation was observed by Nilsson *et al.* in preserved antemortem blood [378].

2.2.6.2 Poisons

Cyanide

Obtaining meaningful quantitative results for cyanide is complicated by the possibility of increasing or decreasing postmortem concentrations. Lokan *et al.* suggested that bacterial species such as *Pseudomonas aeruginosa* could utilize glycine as a substrate to form cyanide [379]. A more recent review highlighted that these changes may also be attributed to the formation of cyanide from endogenous thiocyanate, or the degradation of cyanide to thiocyanate or ammonium formate, or the reaction between cyanide with aldehydes and polysulfides [380]. Later, McAllister *et al.* found that changes in cyanide concentrations could be prevented using sodium fluoride (2% w/v), whereas average increases of 35% were reported in unpreserved specimens after 25–30 days at 4 °C [381].

Ethylene glycol

Although ethylene glycol is not an endogenous compound, its presence is not uncommon in human blood and urine due to environmental exposure [382-385]. Threefold increases in ethylene glycol concentrations are possible after 7 days of storage in unpreserved whole blood spiked with putrefying blood (10% v/v) at 26–28 °C [384]. However, the microbial production of ethylene glycol is unlikely to have significant consequences on determining ethylene glycol poisoning as the cause of death. Ethylene glycol poisoning results in characteristic findings at autopsy and blood concentrations greater than those reported in the study by Wurita *et al.* [189, 384, 386-388].

Formic acid

Formic acid is a toxic metabolite of formaldehyde and methanol, and is responsible for decreased vision and blindness associated with methanol poisoning. As with ethylene glycol and GHB, background levels of formic acid are present in both ante- and postmortem specimens, even when methanol or formaldehyde ingestion antemortem has been definitively excluded [389]. This occurs due to consuming foods and drinks that contain trace quantities of methanol and formaldehyde [390]. The increase in formic acid concentrations in putrefying specimens is well established, having been explored as a marker for the estimation of PMI [12]. Cases have been reported where formic acid concentrations have exceeded the likely fatal concentration of 0.5 g/L despite the absence of methanol or formaldehyde ingestion ante mortem, presumably due to protein and amino acid degradation by microbes [12, 389, 391, 392]. In urine specimens separately inoculated with *Enterococci* and *E. coli*, formic acid concentrations have been observed to both increase, presumably from citric acid, and decrease when stored at room

temperature and 37 °C, at a rate dependent on pH [393]. Storage with sodium fluoride as a preservative was sufficient in preventing further significant formic acid synthesis in putrefying blood and urine stored at 4 °C for 3–4 months [389]. Thus, the postmortem production of formic acid may only be significant during the PMI although further work needs to be performed in order to determine this.

2.2.7 Concluding remarks

Many drugs, poisons, and their metabolites are unstable in postmortem specimens. Having an understanding of the microbial contribution to this instability due to the near-pervasive presence of microorganisms in postmortem specimens is crucial for the interpretation of casework results in forensic toxicology. Despite the use of preservative agents and frozen storage conditions after specimen collection to inhibit both enzymatic and microbial activity, changes in drug concentrations are still observed. This may be because either the microbes or enzymatic processes are not inhibited by the preservation methods or because abiotic processes are responsible, such as chemical hydrolysis. The use of preservatives and frozen storage also cannot counteract the degradation of drugs that occurs during the PMI prior to specimen collection at autopsy.

Although microbial degradation often results in the loss of drugs and/or their metabolites, for those drugs that have conjugate metabolites, microbial activity may result in the formation of the parent drug, thus increasing its concentration over time. Several instances are reported where both microbial production and degradation of drugs and metabolites take place concurrently [302, 354]. Thus, the overall drug concentration outcome over time may be complex and depends upon the kinetics of competing processes.

Whereas a good body of knowledge is available in regard to drug decomposition kinetics, there is less information available concerning drug production kinetics. It therefore follows that a more extensive study of the conversion of glucuronides and other conjugates into their parent drug in the presence of microbes is a research priority. Such investigations are encouraged by prior studies in literature where the hydrolysis rate of glucuronide metabolites has been found to increase in postmortem blood compared to antemortem blood [256, 257, 394, 395]. Furthermore, in some laboratories, enzymatic or chemical hydrolysis of glucuronide conjugates is deliberately carried out to hydrolyze the conjugates back into the parent drug in order to achieve greater analytical sensitivity or longer detection windows. If conjugates are lost as a result of microbial action, then that is important information for the forensic toxicologist.

Another avenue for further research would be to determine whether there are undiscovered sulfate metabolites of those drugs that are known to undergo glucuronidation. Both EtS and paracetamol sulfate have been observed to be stable in putrefying environments [256, 257, 305]. Therefore, other sulfate metabolites may also be resistant to microbial activity and thus useful markers of antemortem drug use. This would particularly be the case if concentrations of the parent drug or other metabolites fluctuate.

Experimental approaches that investigate how the entire microbial community present in postmortem specimens impact drug and metabolite concentrations are required to ensure meaningful toxicology result interpretations. Postmortem specimens are ecological systems, and forensic toxicology would benefit greatly if these microbial habitats were understood in more detail. Further clarification regarding which microorganisms are responsible for degradation may be achieved utilizing high-throughput sequencing to investigate microbial community structure in conjunction with culture-dependent methods such as matrix-assisted laser desorption/ionization time-of-flight mass spectrometry (culturomics).

2.3 Addendum

At the time of this publication it was emphasised that sulfate metabolites appear to be stable during putrefaction and therefore that sulfate metabolites may be useful markers of antemortem drug use. Since this publication a study by Liu *et al.* investigated the stability of ethanol biomarkers, including EtS, in unpreserved post-mortem blood specimens stored at -20, 4, 25, and 37 °C [396]. Supporting prior studies, EtG was found to degrade in ethanol-positive tissues at 25 and 37 °C whereas EtS was stable at all temperatures. It was also stressed in the Chapter section headed “5.1.8 γ -hydroxybutyrate” that endogenous levels of GHB-sulfate were required to be established prior to its use as a marker in post-mortem specimens for ante-mortem GHB administration. It has since been established by Piper *et al.* that endogenous GHB-sulfate levels may overlap with post-administration levels [397]. Similarly, GHB-glucuronide levels were determined to be similar between control groups and patients treated with GHB-sodium salt in two different studies [398, 399]. Therefore, unfortunately, neither GHB conjugate is suitable for use as a marker of GHB administration. Further, Watanabe *et al.* have discovered that sulfate metabolites of AM2201 are produced by *Cunninghamella elegans*, a fungus, in culture conditions [400]. However, it remains to be established if fungi associated with post-mortem remains may perform this biotransformation in authentic post-mortem specimens.

It was also stated that the morphine glucuronide conjugates hydrolysing may explain increasing morphine concentrations over time, as is established for paracetamol [256, 257, 395]. Since this

publication Staeheli *et al.* have investigated the redistribution and stability of morphine and its conjugate metabolites [401]. These authors found that there was no correlation between morphine and M3G or morphine and morphine-3-sulfate (M3S) concentrations changes in femoral blood collected at two time points after death, with the decedents stored at 5 °C between each sampling [401]. In heart blood, a positive correlation was observed, attributed to the redistribution of morphine and its conjugates into heart blood [401]. The time between the initial and secondary sampling ranged from 18-29 hours, therefore, it may be that this time period and the temperature did not enable significant degradation of the conjugates [401]. Relatedly, buprenorphine-glucuronide and norbuprenorphine-glucuronide do appear to convert back to their parent compounds over time in blood specimens stored at 5 °C, with the parent compounds detected after 2 weeks in ante-mortem blood specimens containing sodium fluoride [402]. The authors recommended against long-term storage of blood specimens containing buprenorphine at 5 °C due to this hydrolysis [402].

Studies have tested the utility of antioxidant agents in preventing the degradation of drugs. Saar *et al.* found that ascorbic acid approximately halved the rate of olanzapine degradation in preserved whole blood specimens and prevented the formation of its oxidative degradation product, 2-hydroxymethyl-olanzapine, in aqueous solutions [403]. Ascorbic acid has also been found to enhance the stability of buprenorphine in whole blood specimens stored at -20 °C, with losses after 20 weeks no greater than the error of the methods used [402]. In comparison, 90 % losses were observed in specimens containing sodium fluoride and potassium oxalate and 69 % losses in specimens containing sodium fluoride, sodium ethylenediaminetetraacetic acid (EDTA), citric acid, and sodium citrate, given the same time period [402]. The stability of THC is similarly improved in preserved whole blood specimens if ascorbic acid is present [404]. In specimens without ascorbic acid losses up to 95 % after 19 weeks storage at -20 °C have been observed [404]. In authentic post-mortem blood preserved and stored at -20 °C for a year ~66 % losses were observed [313]. In the Sørensen & Hasselstrøm study, ascorbic acid added to blood specimens before incubation yielded no significant degradation [404]. For propofol, 50 % losses were observed by Sørensen & Hasselstrøm in preserved whole blood specimens stored at -20 °C for ~50 days. As with THC, in specimens containing ascorbic acid, sodium metabisulfite, or glutathione no significant degradation was observed [404, 405]. These studies suggest that it may be useful to mix post-mortem blood specimens with an antioxidant upon collection to prevent such degradation from occurring. However, as with sodium fluoride, the collected specimen should not replace a collected unpreserved post-mortem blood specimen, as there is limited evidence that ascorbic acid may increase the rate of glucuronide hydrolysis [402].

It was stated in the Chapter section headed “5.1.10 New Psychoactive Substances” that the degradation of mephedrone may be assisted by microbial activity. Further work has indicated that other synthetic cathinones [406, 407] and mephedrone metabolites [408] are also unstable in ante-mortem whole blood matrices, indicating chemical instability. Future research may investigate the stability of synthetic cathinones in post-mortem blood, however, differences in degradation rates may be practically insignificant as observed in the Busardò *et al.* study [370].

It is possible that other 1,2-benzisoxazole drugs may also form degradation products analogous to HB-RISP in post-mortem specimens. Indeed, zonisamide and iloperidone have both been reported to undergo reductive cleavage followed by imine hydrolysis to form 2-hydroxybenzoyl metabolites [409-411]. However, while the reduction of risperidone and zonisamide has been reported to occur due to microorganisms the similar transformation of iloperidone has thus far only been attributed to liver enzymes [409-411]. The formation of any metabolites of zonisamide and iloperidone as microbial degradation products in post-mortem specimens has not yet been established. It is therefore currently unknown if their 2-hydroxybenzoyl metabolites should be screened in these specimens to mitigate the risk of not detecting their parent drugs.

CHAPTER 3 - MATERIALS & INSTRUMENTATION

3.1 Chemicals

3.1.1 Reagents

All reagents used are detailed in Table 3-1. Where known, information regarding supplier and location of origin has been specified for chemicals and equipment.

Water for aqueous mobile phases used with the Agilent 1100 Series LC-DAD was distilled using Labglass Pty Ltd distillation apparatus (Brisbane, QLD, Australia), for LC-QTOF-MS buffer preparation was Milli-Q purified (Bayswater, VIC, Australia), for polymerase chain reaction (PCR) and DNA extraction purposes was nuclease-free water (Promega), and for other chemical analysis purposes was glass distilled unless otherwise stated.

Universal primers 27F [412] and 1492R [413] were used to amplify the 16S rRNA genes of extracted DNA in a PCR to confirm successful DNA extraction prior to amplification using primers 341F and 806R [243] and sequencing using the Illumina MiSeq platform at the AGRF (Melbourne, Australia).

Table 3-1: Source and purity of reagents.

Reagent	Supplier	Grade/Purity
27F primer	IDT®	-
1492R primer	IDT®	-
Acetaldehyde	Sigma-Aldrich	(99.5 %)
Acetic acid (glacial)	ChemSupply	80 %
Acetic anhydride	Sigma-Aldrich	99 %
Acetonitrile	Fischer Chemical	Optima® (99.9 %)
Acetone	Stennick Scientific	99.8 %
Agarose I	Astral Scientific	-
Ammonia (NH ₃)	ChemSupply	Analytical (30 %)
Ammonium formate	Stennick Scientific	Analytical
Difco™ Nutrient Broth	BD	-
<i>N</i> -butyl chloride (n-BuCl)	ChemSupply	Analytical (99.5 %)
Crystal violet dye	Commission Dyers	-
Disodium hydrogen orthophosphate	Ajax Finechem	-
100bp DNA ladder	Biotium	-
Ethanol	Ajax Finechem	Analytical (99.5 %)
Ethanol-d ₆	Sigma-Aldrich	Anhydrous >99.5 atom % D
Ethyl acetate	ChemSupply	99 %
Formic acid, for LC-DAD buffer	Univar	Analytical (90 %)
Formic acid, for LC-QTOF-MS buffer	Fischer Chemical	Optima® (99.9 %)
6x Gel Loading Dye buffer	Fischer Chemical	

Reagent	Supplier	Grade/Purity
GelRed™ Nucleic Acid Gel Stain, 10,000x in H2O	Biotium	-
Glutaraldehyde	Sigma-Aldrich	25 %, molecular biology
Glycerol	Sigma-Aldrich	>99 %, molecular biology
GoTaq® HotStart Colorless Master Mix M5138	Promega™	-
Hydrochloric acid (HCl)	Stennick Scientific	32% w/v
Magnesium sulfate (anhydrous)	Scharlau	98 %
Methanol	ChemSupply	Analytical (99.5 %)
Nuclease-free water	Promega™	-
Potassium oxalate	Sigma-Aldrich	-
Propan-2-ol	ChemSupply	Analytical (99.5 %)
Sodium bicarbonate	Sigma-Aldrich	Analytical
Sodium carbonate (anhydrous)	Univar	Analytical
Sodium chloride	-	-
Sodium dihydrogen orthophosphate	Ajax Finechem	-
Sodium dithionite	ChemSupply	88 %
Sodium fluoride	Univar	Analytical (99.0 %)
Sodium sulfate (anhydrous)	BDH Chemicals	Analytical (99.5 %)
TAE buffer	ThermoFisher Scientific	-

Grade/purity intentionally blank if not stated by supplier.

3.1.2 Drug solutions

3.1.2.1 Standard solutions

Separate analyte stock standard solutions and quality control (QC) solutions were prepared at concentrations between 500-1200 µg/mL in acetone, ethanol, or methanol from powdered standards (Table 3-2) by staff members at FSSA and stored at -20 °C or prepared from certified reference material ampoules sourced from commercial suppliers. National Institute of Forensic Science (NIFS) standards were not certified reference materials (“N”). Different scientists using different sources of powdered standard or certified ampoules were used to prepare stock and QC solutions, where possible.

Table 3-2: Drug standards purity, supplier, and solvent used in stock solutions.

Drug standard	as	Abbreviation	Supplier	Grade/Purity (%)	Solvent in stock solutions
Amisulpride		AMIS	NIFS	99.2 (N)	Ethanol
Amitriptyline	HCl	AMIT	NIFS	99.7 (N)	Ethanol
Aripiprazole		ARIP	NIFS	99.9 (N)	1:1 acetone: ethanol
Asenapine	maleate	ASEN	NIFS	99.8 (N)	Ethanol
Chlorpromazine	HCl	CHLO	NIFS	N	Ethanol
Clomipramine		CLOM	NIFS	98.8 (N)	Ethanol
Clozapine		CLOZ	NIFS	N	Ethanol

Drug standard	as	Abbreviation	Supplier	Grade/Purity (%)	Solvent in stock solutions
			Cerilliant	Certified	
Dothiepin		DOTH	NIFS LGC	N Certified	Ethanol
Flupentixol	dihydrochloride	FLTX	Sigma Toronto Research Chemicals	98.4 (N) 99.94 certified	Ethanol
Fluphenazine	HCl	FLPH	NIFS	98.4 (N)	Ethanol
Haloperidol		HALO	NIFS Cerilliant	N Certified	Ethanol
Loratadine		LORA	NIFS	N	Ethanol
Lurasidone		LURA	NIFS Cerilliant	N Certified	Ethanol
Mirtazapine		MIRT	NIFS	N	Ethanol
Moclobemide		MOCL	NIFS	N	Ethanol
Pericyazine		PERI	NIFS	N	Ethanol
Prochlorperazine		PROC	NIFS	99.6 (N)	0.1 M HCl / Ethanol
Quetiapine		QUET	NIFS	99.9 (N)	Ethanol
Risperidone		RISP	NIFS	N	Ethanol
Sertraline		SERT	NIFS	N	Ethanol
Trifluoperazine		TRIF	NIFS	N	Ethanol
Trimeprazine	tartrate	TRIM	May & Baker	N	Ethanol
Ziprasidone	mesylate trihydrate	ZIPR	Lipomed Cerilliant NIFS	Certified Certified 73.5 (N)	Methanol
Zuclopenthixol	dihydrochloride	ZUCL	NIFS Chiron	98.9 (N) Certified	Ethanol

N: non-certified material. Where purity not stated assumed to be 100 %.

3.1.2.2 Working stock and QC solutions

Mixed working stock and QC solutions were prepared at concentrations of c. 20-30 µg/mL by dilution of the stock and QC standard solutions in ethanol, respectively. Working stock solutions were used during extraction efficiency experiments, method validation, and as calibrants for the preparation of calibration curves. Working QC solutions were used to validate the calibration curves and determine the accuracy and precision of the analytical method. When not in use these solutions were stored at -20 °C.

3.1.2.3 Internal standards

Internal standard (IS) solutions at a concentration of c. 20 µg/mL were prepared by dilution of the appropriate stock standard in ethanol. When not in use these solutions were stored at -20 °C. Drugs used as an IS are noted where relevant.

3.2 Materials

3.2.1 Laboratory equipment

3.2.1.1 Analytical equipment

To prepare drug solutions (see 3.1.2) A-grade volumetric glassware and precision glass syringes were used (SGE, Melbourne, Australia).

The digital pH meter used for LC-DAD buffer preparation was a PHM 83 Autocal pH meter (Radiometer, Copenhagen, Denmark), calibrated using Scharlau buffer standards at pH 4 and 7 obtained from Southern Cross Science (Edwardstown, SA, Australia) prior to use. These mobile phases were filtered using Agilent 0.45 µm nylon filter membranes (part number 9301-0895) (Sydney, NSW, Australia).

Sterile polystyrene Sarstedt tubes (5 mL and 10 mL) were obtained from Adela Scientific (Thebarton, SA, Australia). 1.5 mL sterile screw cap tubes were obtained from Axygen Scientific (Union City, CA, US). UV-Cuvette Macro Brand® cuvettes were obtained from Sigma-Aldrich.

Sterile Luer-Slip plastic syringes and 0.2 µm syringe filters were obtained from Sigma-Aldrich and Sartorius Stedim (Dandenong South, VIC, Australia). Biosphere® Quality Tips were obtained from Sarstedt (Mawson Lakes, SA, Australia). From Adela Scientific, 200 µL Axygen Maxymum Recovery sterile wide bore aerosol barrier tips and 200 µL Zap™ Premier sterile wide bore aerosol barrier tips were obtained (Thebarton, SA, Australia).

S.E.M mechanical rollers and Ratek mechanical rollers were supplied by Adela Scientific (Thebarton, SA, Australia) and Stennick Scientific (Melrose Park, SA, Australia). The centrifuge used was a Beckman Allegra™ 6 Centrifuge. Solvent evaporators were Cerex® 48™ sample concentrators supplied by SPEware (Baldwin Park, CA, USA), using nitrogen (N₂) as the flow gas. Limited volume glass autosampler vials were obtained from Agilent Technologies (Mulgrave, VIC, Australia).

For the incubation of blood specimens at 37 °C a S.E.M BTC-9000 incubation oven was used.

Micro10 (Unident, Geneva, Switzerland) was used to decontaminate glassware exposed to biological material prior to cleaning.

3.2.1.2 Microbiology equipment

Sterile inoculating loops were purchased from Sigma-Aldrich. Columbia Blood Agar plates, Sabouraud Dextrose Agar plates, AnaeroGen™ atmosphere generation system, anaerobic

atmosphere generation satchets (AA0025), and anaerobic indicators (BR0055) were obtained from Oxoid (Thebarton, SA, Australia). For the incubation of agar plates at 37 °C a Medile Medizintechnik TD066 tissue drying oven obtained from HD Scientific Supplies Pty Ltd (Wetherill Park, NSW, Australia) was used.

The MoBio/QIAamp PowerSoil® DNA Isolation Kit (obtained from Geneworks (Thebarton, SA, Australia)) was used to extract DNA from the FMT and blood specimens. For DNA extraction an MP Biomedicals FastPrep-24™ Classic homogeniser and an Heraeus Megafuge 8R centrifuge were used. An Applied Biosystems Verti 96 Well Thermal Cycler was used for PCR (Applied Biosystems, California, USA).

3.2.2 Biological material

3.2.2.1 Ante-mortem blood

Ante-mortem whole blood obtained from the Australian Red Cross Blood Service was preserved with citrate, phosphate, dextrose and adenine as an anticoagulant [414]. Dextrose, citrate, and phosphate are all naturally present in ante-mortem blood and therefore expected to be present in authentic post-mortem blood. The levels at which these substances will be present in authentic post-mortem specimens is expected to vary depending on the medical state of the decedent at their time of death and post-mortem changes. In particular, dextrose levels may decrease post-mortem due to bacteria and fungi utilising it as an energy source for fermentation or glycolysis reactions [13, 22]. Adenine is a nucleobase added to blood transfusion products to maintain red cell ATP levels [415]. Adenine may have both inhibiting and stimulating effects on microbial growth [416]. For further details regarding biosafety and ethics approval refer to 1.7.3. Before use, blood was screened for the presence of drugs by a member of staff at FSSA.

Blood was stored in 50 mL Sarstedt plastic pots (Mawson Lakes, SA, Australia) at -20 °C. Blood was tested for sterility using Columbia Horse Blood Agar plates and incubating aerobically and anaerobically at 37 °C. Blood was considered sterile if no growth was observed after five days incubation.

3.2.2.2 Human stool

Faeces from nine healthy human donors were collected and prepared as faecal microbiota transplant (FMT) specimens (25 % fresh stool, 65 % saline, 10 % glycerol) as previously detailed for a *Clostridium difficile* study [417]. Refer to 1.7.3 Biosafety and ethics for further details. Exclusion criteria for the donors was extensive, with discrimination on the basis of age, BMI, past medical history, and current health (for more detail refer to [417]). The FMT specimens

were then mixed together, with the addition of water (sterilised by filtration with a Luer-Slip plastic syringe and 0.2 µm filters) to aid stirring. The mixed FMT specimens were stored in 50 mL Sarstedt plastic pots (Mawson Lakes, SA, Australia) at -80 °C and transported between CSIRO Land & Water and FSSA using dry ice (BOC Gas & Gear, Mile End South, SA, Australia).

3.2.2.3 Microbial cultures

The bacteria *Escherichia coli* and the fungi *Aspergillus brasiliensis* (formerly *A. niger*) were sourced from Southern Biological (Scoresby, VIC, Australia). Sub-cultures of the obtained stocks were prepared in 0.9 % sodium chloride and 50 % glycerol stocks (as recommended [418]).

Bacterial subcultures were grown by inoculating (150 µL) of the supplied stock in BD Difco™ Nutrient Broth. Subcultures were incubated at 37 °C for at least one day with shaking at 120 rpm until cell growth was visibly observed. Following centrifugation (10 minutes at 1774 x *g* and 10 °C), supernatants were discarded and cell pellets washed with 0.9 % NaCl (15 mL) by vortexing. Centrifugation, supernatant discarding, and washing was repeated twice more. After the final lot of supernatants were discarded the cell pellets were then reconstituted in 0.9 % NaCl by vortexing and aliquots added to the autoclaved glycerol to prepare 50 % glycerol stocks. For later sub-culturing, bacteria were also stored at 4 °C in the 0.9 % NaCl solution.

Fungi were plated onto Sabouraud Dextrose Agar plates and incubated at 28 °C for three days in the dark. After incubation, plates were irrigated with 0.9 % NaCl and aliquots added to the autoclaved glycerol to prepare 50 % glycerol stocks.

Prior to use, glycerol and BD Difco™ Nutrient Broth were autoclaved in Schott Flasks and Corning vials, respectively, at 121°C and 15 psi for 15 minutes. Excess broth prepared was stored at room temperature to allow for visual assessment of any contamination. Glycerol stocks were stored at -80 °C at Waite Campus prior to transport on ice to FSSA whereupon they were stored in 4 °C fridges prior to plating.

3.3 Instrumentation

3.3.1 Agilent 1100 Series LC-DAD

For quantitative experiments, an Agilent 1100 Series LC-DAD (Agilent Technologies Australia, Mulgrave, VIC, Australia) was employed, fitted with a Kinetex EVO C18 100Å 100 x 3.0 mm, 2.6 µm column and a SecurityGuard™ Cartridge Gemini C18 4 x 2.0 mm guard column (Phenomenex Australia, Lane Cove, NSW, Australia). The software used with this instrument

was Agilent Technologies ChemStation for LC 3D systems Rev. B.04.01 (482). See 4.3.1 for details regarding chromatographic and detection conditions employed.

3.3.2 Agilent 1200 Series HPLC and Agilent 6520 LC-QTOF-MS

For qualitative experiments, chromatographic separation was achieved using an Agilent 1200 Series HPLC, fitted with an Acquity BEH C18 130Å 50 x 3.0 mm, 1.7 µm column (Waters, Rydalmere, NSW, Australia) and SecurityGuard™ 4.0 mm, 3.0 mm I.D guard column (Phenomenex Australia, Lane Cove, NSW, Australia). The mass spectrometer used was an Agilent 6520 Series LC-QTOF-MS. The software used with this instrument for data acquisition was Agilent Technologies MassHunter Workstation LC/MS Data Acquisition for 6200 series TOF/6500 series QTOF (version B.05.01).

3.3.2.1 Chromatographic conditions

Gradient elution was performed with acetonitrile (A) and 0.1 % formic acid (B). Mobile phases were LC-MS grade and Milli-Q water used. No membrane filtration of phases was performed. Initial conditions were 10 % A at a flow rate of 0.35 mL/min. A then increased to 50 % between 0 and 8.0 min, further increased to 95 % between 8.0 and 10.0 min, then was held at 95 % until 10.1 min. For the remainder of the run the flow rate increased to 0.4 mL/min. Between 10.1 and 10.2 min A increased to 100 % and was then held at 100 % until 12.0 min. Post-run equilibration lasted 4.0 min. Column temperature was maintained at 30 °C. The injection volume for samples ranged from 0.5-4 µL with a needle wash program prior to each injection.

3.3.2.2 Mass spectrometer conditions

The mass spectrometer was operated in positive ESI mode. 2 GHz extended dynamic range mode was used, producing resolution of 7000-8000 at 322.0841 m/z. Source parameters were: gas temperature 350 °C; drying gas flow 10 L/min; nebulizer pressure 50 psi; capillary voltage 3000 V; fragmentor voltage 125 V; skimmer voltage 65; octopole peak RF 750. Continual mass calibration was done by infusing a calibration reference mass solution into the source *via* a second nebulizer. Data dependent auto-MS/MS mode was used to acquire MS and MS/MS data. [M+H]⁺ ions exceeding a threshold of 5000 ion counts ions were fragmented. The scan rate for both MS and MS/MS modes was 3.21 spectra/sec. Mass ranges were 100-1000 m/z and 40-700 m/z for MS and MS/MS, respectively. A narrow isolation window width was used (~1.3 m/z). For fragmentation, collision energies were 20-60 eV.

3.3.2.3 Data analysis

Agilent Technologies MassHunter Workstation Qualitative Analysis (version B.07.00 Service Pack 2) software was used to analyse LC-QTOF-MS data. To assist in the identification of compounds, mass accuracies were determined for generated molecular formula (GMF) as detailed in Equation 3-1.

Equation 3-1: Calculation for mass accuracy.

$$\delta \text{ (ppm)} = \frac{(m/z_c - m/z_o)}{m/z_c} \times 10^6$$

$$\delta \text{ (mDa)} = (m/z_c - m/z_o) \times 1000$$

where m/z_c = calculated m/z and m/z_o = observed m/z

3.4 Data analysis

Microsoft® Excel (Office 2010, 2013, and 365) was used for the analysis of LC-DAD, LC-QTOF-MS, and UV-Vis spectrophotometer data, secondary to instrument software. Data analysis and visualisation was aided by Daniel's XL Toolbox add-in for Excel, version 7.2.13 [419]. For multivariate analyses of microbial communities PAST was used (version 3.22) [420]. Common equations used are provided below for calculation of the mean (Equation 3-2) and standard deviation (Equation 3-3). Welch's t-test (Equation 3-4) was used to compare data sets and test the hypothesis that they were significantly different (*i.e.* to determine if the mean of each population is significantly different) [421]. Welch's t-test was used as it does not make assumptions regarding the variance of datasets and so is appropriate when comparing datasets with both equal and unequal variances, provided normally distributed data [421]. The difference between data sets was considered significant if $p < 0.05$. Other equations used are detailed where relevant.

Equation 3-2: Calculation for the mean.

$$x = \frac{\sum x_i}{n}$$

where x_i = individual value and n = total number of values

Equation 3-3: Calculation for the standard deviation.

$$s = \sqrt{\frac{\sum(x_i - x)^2}{(n - 1)}}$$

where x_i = individual value, x = mean,

and n = total number of values

Equation 3-4: Calculation for Welch's t-test.

$$t = \frac{x_1 - x_2}{\sqrt{\frac{s_1^2}{n_1} + \frac{s_2^2}{n_2}}}$$

where x = data set mean, s^2 = variance,

and n = total number of values

CHAPTER 4 - METHOD DEVELOPMENT & VALIDATION

4.1 Outline

LC-DAD methods were developed and validated for the quantitative analysis of 17 psychoactive drugs in human whole blood. A variety of chromatographic techniques to analyse for antipsychotics and antidepressants in putrefying blood were initially considered. Liquid chromatography methods in conjunction with a diode array detector were selected due to: i) the possession of chromophores by all of the drugs investigated; ii) the unpredictable matrix effects associated with the analysis of putrefactive specimens by LC-MS; and iii) the thermal instability of some of the analytes (ARIP, RISP, ZIPR, and LURA), which prevented analyses by GC-MS. Method development proceeded by first optimising chromatographic conditions and analyte detection followed by extraction method optimisation. Method validation then proceeded, following published guidelines [203, 218].

Chemicals and materials used were as listed in Chapter 3. Ante-mortem human whole blood as detailed in 3.2.2.1 was used as the sample matrix. Drug standards and drug solutions were obtained and prepared as specified in 3.1.2. An Agilent 1100 Series LC-DAD was used as detailed in 3.3.1 with a Kinetex EVO C18 100Å 100 x 3.0 mm, 2.6 µm column and a SecurityGuard™ Cartridge Gemini C18 4 x 2.0 mm guard column (Phenomenex Australia, Lane Cove, NSW, Australia).

4.2 Final method

4.2.1 Quality control

For each day when experimental blood specimens were analysed a six-point calibration curve was produced with duplicate QCs at low, medium, and high concentrations spiked and extracted. A zero blank (IS without blood) and a blood blank (with IS) were also concurrently extracted. QCs were analysed following the calibration curve, then reinjected every 15 to 18 samples and at the end of a sequence. To confirm the stability of the drugs on the auto-sampler throughout each experimental run the relative responses of the drugs in the initial QC injections were compared to the relative responses of the drugs in the reinjections (see 4.4.1.6).

4.2.2 Unbuffered LLE

IS solution (50 µL) and water (1.45 mL) were briefly vortexed together in a screw-capped borosilicate tube. Blood or specimen extract (100 µL) and then n-BuCl (5 mL) were added with

vortexing following each addition. The tubes were then placed on a mechanical roller (15 minutes at 20 rpm), followed by centrifugation (10 minutes at 1409 x g). After centrifugation the organic layer was collected and evaporated to just dryness under N₂ at 40 °C. The residue was then reconstituted in ethanol (50 µL), with vortexing, and transferred to a limited volume autosampler vial for LC-DAD analysis.

4.2.3 LC-DAD analysis

Mobile phases and gradient programs were as described in Table 4-2 for each respective method. Chromatographic instrumentation, column details, and acquisition and processing software were as detailed in 3.3.1. Parameters were: column temperature 40 °C; flow-rate 0.8 mL/min; injection volume 4 µL; post-run time 4 min. Analytes were detected and peak area and height integrated at the wavelengths specified in Table 4-3. Data analysis was performed using Microsoft® Excel.

4.3 Method optimisation

4.3.1 Instrumentation

4.3.1.1 Chromatography

To optimise the separation of analytes, a variety of mobile phase combinations were trialled utilising gradient methods (Table 4-1). For each mobile phase combination numerous gradient profiles were trialled. Methods with increasing runtimes had accordingly more gradual gradients.

Poor peak symmetry and separation were obtained using mobile phase combinations other than acetonitrile with ammonium formate buffer (pH adjusted using formic acid to 3.5 or 3.6) (10 mM or 25 mM). Ammonium formate buffer at a concentration of 25 mM was superior to 10 mM in stabilising the retention time of analytes when 3.5 ± 0.2 pH unit buffer variations were trialled. As the difference between the retention time shifts was minimal between 3.5 and 3.7 pH units compared to 3.5 and 3.3 pH units the ammonium formate buffer was henceforth adjusted to 3.6 using formic acid (10 % v/v).

Once a suitable mobile phase combination was determined the gradient profile was as described in Table 4-2. Drugs included in the suite of analytes after initial development of the method required a slight alteration of the gradient to obtain peaks without fronting. This altered method is referred to in text as Method B, with the change to Method A as noted in Table 4-2.

Table 4-1: Conditions tested for LC-DAD system.

Mobile phases	Flowrate (mL/min)	Temp. (°C)	Runtime (min)	Comments/changes from prior condition
Methanol/0.1 % formic acid in water	0.5	30	19	Ghost peaks; peak tailing & shouldering
0.1 % formic acid in methanol/0.1 % formic acid in water	0.5	30	19	No peak shouldering; increasing baseline over run
Acetonitrile/0.1 % formic acid in water	0.5	30	19	No ghost peaks; improved peak symmetry; coelution of analytes
Acetonitrile/0.1 % formic acid in water	0.8	30	19	Peak fronting for early eluting analytes
0.1% formic acid in acetonitrile/0.1 % formic acid in water	0.8	30	19	As above
Acetonitrile/25 mM ammonium formate buffer (pH = 3.47)	0.8	40	19	Improved peak shapes
Acetonitrile/25 mM ammonium formate buffer (pH = 3.5)	0.8	40	25	Slight coelution of fewer analytes (particularly HALO and PERI)
Acetonitrile/25 mM ammonium formate buffer (pH = 3.5)	0.8	40	26	Improved separation of all analytes

Bold text indicates the major modifications between each condition tested.

To efficiently separate the analytes a slow gradient increase of the organic phase was required, with a run time of 26 minutes plus 4 minutes post-time. Despite this extended run time, HALO and PERI were not fully resolved, with slight coelution that necessitated their quantification using peak height rather than peak area. These antipsychotics are structurally diverse, with HALO a butyrophenone and PERI a phenothiazine (Figure 1-2). However, both possess a hydroxy-piperazine moiety, in HALO di-substituted and in PERI terminal. An LC-MS method developed to separate 30 antipsychotics optimised the elution of HALO and PERI with similar retention times of 8.3 and 8.2 min, respectively [422]. In the LC-MS method by Saar *et al.* the similar retention times of HALO and PERI were not an issue due to the use of multiple reaction monitoring transitions unique to each analyte [422]. In the LC-DAD method employed in this thesis these drugs were quantified at different wavelengths (Table 4-3) and quantification using peak height afforded accuracy and precision fit for purpose for this research (Table 4-11 and Table 4-15).

Table 4-2: Solvent gradient for liquid chromatography method.

Time (min)	% acetonitrile	% 25 mM ammonium formate buffer (pH = 3.6)
0	5	95
1	5 (method A) / 20 (method B)	95 (method A) / 80 (method B)
11	25	75
12	25	75
20	50	50
22	90	10
24	90	10
25	5	95

A slow gradient was also chosen to limit the potential for the coelution of any potential degradants with the drugs. Flow rate and column temperature were set to 0.8 mL/min and 40 °C, respectively. An injection volume of 4 µL was used.

The chromatogram for drugs initially separated using Method A is shown in Figure 4-1. AMIT and RISP were included as an inter-aliquot control and microbial control (see 6.2.1), respectively, and are indicated as controls in Figure 4-1.

As can be seen from the chromatogram, all analytes were resolved from each other when the drugs were split into two sets. Using one set of drugs alone resulted in the coelution of: ZIPR and QUET; HALO and PERI; and ZUCL and PROC. Therefore, these drugs were segregated where possible in the final two methods employed. In these two methods, the IS was changed from TRIM to LORA and AMIS excluded from blood experiments (for more information regarding the reason behind these decisions refer to 4.3.2.2). Method A was used with one set of drugs, termed “A drugs”, and method B used with another, termed “B drugs”. Chromatograms are depicted in Figure 4-2 and Figure 4-3 for these methods. HALO and PERI were included in the same method, pending successful validation of their quantification using peak height, due to the inclusion of the co-eluting DOTH in Method B. ZUCL was excluded due to close elution with CLOM and PROC and its structural similarity with FLTX. Peaks for all analytes approximated Gaussian curves, with slight tailing.

For the thioxanthene antipsychotic drugs, ZUCL and FLTX, partially co-eluting peaks (shown for ZUCL in Figure 4-4 (a) (inset)) with identical UV-Vis spectra were observed (Figure 4-4 (a) depicts the spectra of ZUCL observed). Rop found that both isomers of ZUCL have similar UV-Vis absorbance spectra [423]. Therefore, it was hypothesised that the dual ZUCL peaks and FLTX shoulder were the *cis* and *trans* isomers of ZUCL and FLTX. The presence of both isomers for either drug was not considered to be an issue, as integration of both could be performed to

give a sum of total ZUCL and FLTX. In the case of ZUCL it is expected that the *cis* isomer was the dominant peak integrated, due to ZUCL being marketed as the active *cis* isomer of clopenthixol [424].

The presence of minor amounts of chlorpromazine-sulfoxide (CHLO-SO) and prochlorperazine-sulfoxide (PROC-SO) in CHLO and PROC drug stocks, respectively, was postulated following comparison of the observed UV-Vis absorbance spectra with that previously reported by Butzbach [223] (Figure 4-4 (b)).

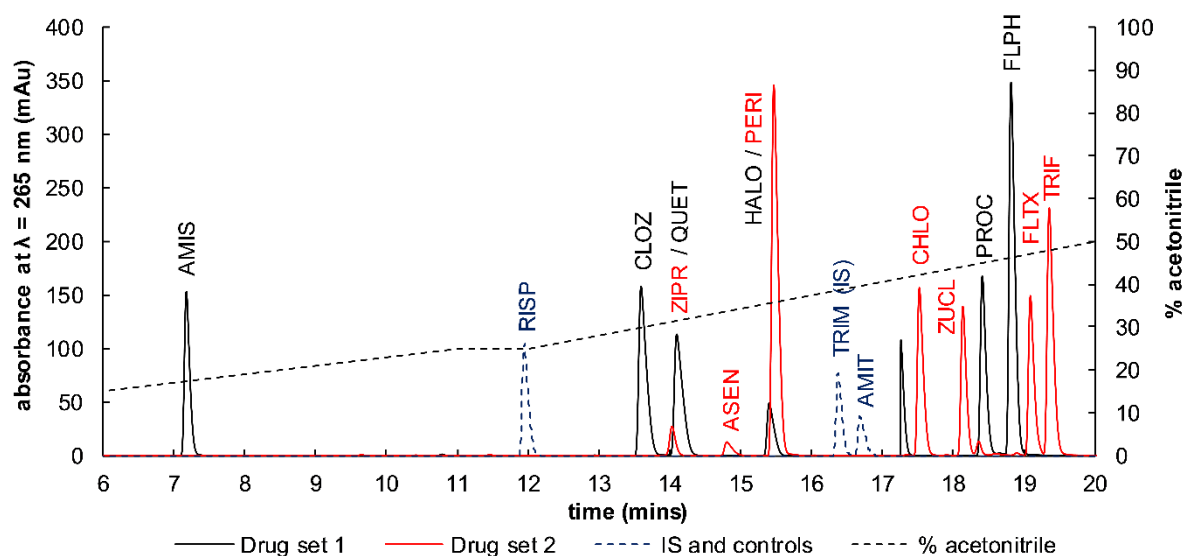


Figure 4-1: Optimised separation of analytes as two drug sets using method A.
Secondary axis: percentage (%) of acetonitrile in mobile phase.

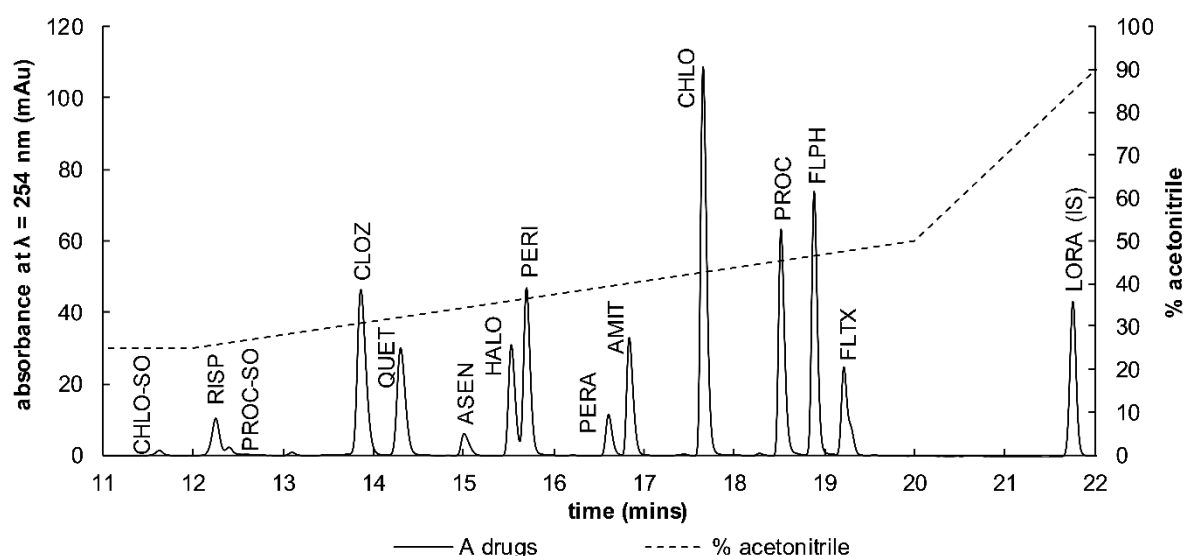


Figure 4-2: Optimised separation of “A drugs” using method A.
Secondary axis: percentage (%) of acetonitrile in mobile phase.

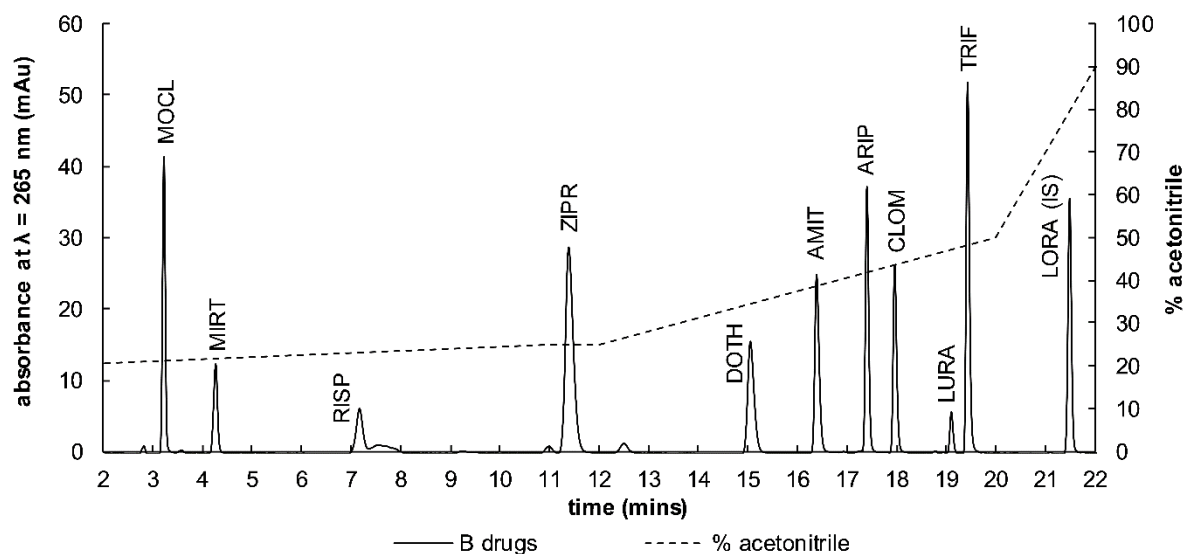


Figure 4-3: Optimised separation of “B drugs” using method B.

Secondary axis: percentage (%) of acetonitrile in mobile phase.

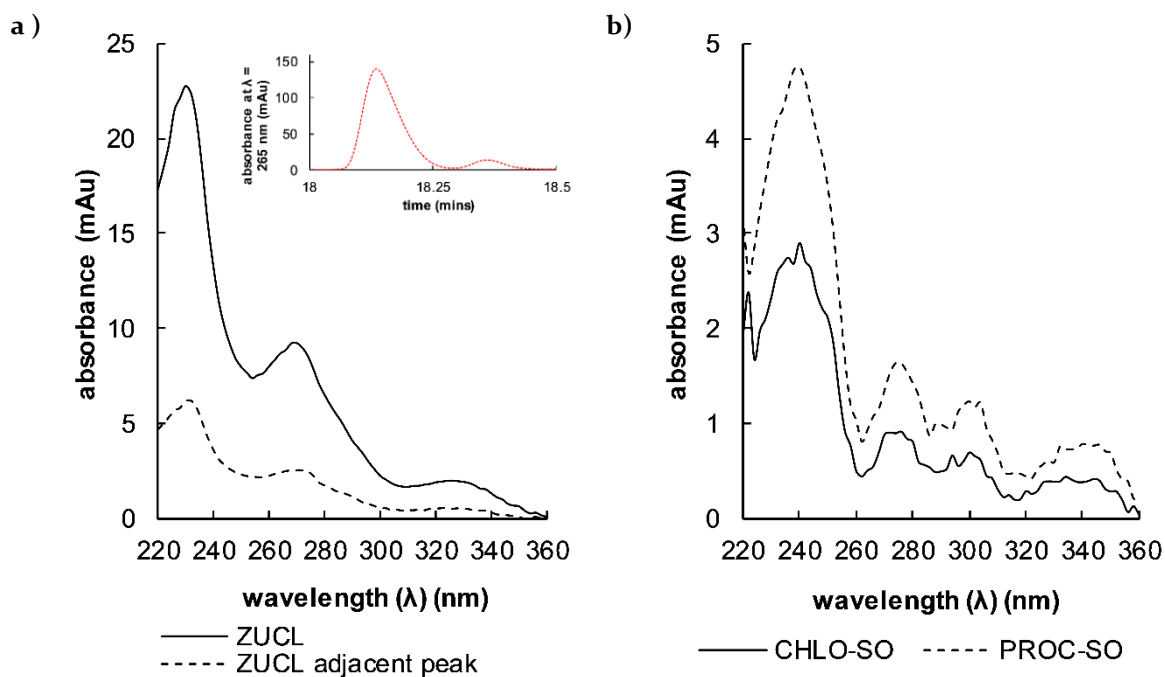


Figure 4-4: UV-Vis absorbance spectra of a) ZUCL and co-eluting adjacent peak and inset, chromatogram and b) peaks identified as CHLO-SO and PROC-SO.

4.3.1.2 UV detection

The software used with the Agilent 1100 Series HPLC-DAD allows for five wavelengths to be simultaneously acquired for later quantitative data analysis. Acquiring at the wavelength corresponding to absorption maxima of analytes generally affords optimal signal-to-noise, provided the absorption maxima is free of endogenous interferences and that the mobile phase does not also absorb at the same wavelength. Therefore, wavelength values were initially set to those that would approximate the absorption maxima of the analytes observed during initial method development and aqueous stability experiments (5.3). Detection wavelengths were then selected for each analyte based on greatest response and appropriately compromised to allow sensitive quantification of all analytes without interferences. Absorbance spectra were collected between 220-360 nm.

The retention time and wavelengths at which the drugs were integrated are noted in Table 4-3.

Table 4-3: Wavelength monitored (λ) and retention time (RT) for the analytes.

Method A			Method B		
Analyte	λ (nm)	RT (min)	Analyte	λ (nm)	RT (min)
AMIS	280	7.0	MOCL	245	3.3
CHLO-SO ⁺	245	11.2	MIRT	290	4.4
RISP	280	12.2	RISP	275	7.0
PROC-SO ⁺	245	12.3	HB-RISP	254	7.5
HB-RISP	254	12.3	ZIPR	245	11.0
CLOZ	245	13.9	DOTH	245	14.7
QUET	245	14.3	AMIT	254	16.2
ZIPR	245	14.4	ARIP	254	17.3
ASEN	245	15.0	SERT (IS [^])	275	17.5
HALO	245	15.5	CLOM	254	17.9
PERI	265	15.7	LURA	245	19.1
PERA~	254	16.6	TRIF	254	19.5
TRIM (IS)	245	16.6	LORA (IS)	245	21.6
AMIT	254	16.9			
CHLO	254	17.6			
ZUCL	245	18.3/18.5*			
PROC	254	18.5			
FLPH	254	18.9			
FLTX	254	19.2*			
TRIF	254	19.4			
LORA (IS)	245	21.7			

⁺Postulated from UV absorbance spectra, present as impurity in stock solutions; [^]only used as an IS for LORA extraction efficiency experiments; ~presumptive identification (see Appendix A); *hypothesised mix of *cis* and *trans* isomers.

4.3.2 Initial extraction methods

4.3.2.1 Experimental

Ethanollic working solutions of the drugs (~20 µg/mL, except for ZIPR and ASEN which were prepared at ~30 µg/mL) were prepared in two sets from previously prepared stock standard solutions (3.1.2) (Table 4-4). An IS solution of TRIM (~20 µg/mL) was also prepared. These solutions were used in subsequent extraction recovery experiments (Figure 4-5). For these experiments, greater than five replicates were analysed as recommended in literature [218].

Table 4-4: Working solutions used for initial extraction recovery experiments.

Set A	AMIS	AMIT	ARIP	CLOZ	FLPH	HALO	PROC	QUET	RISP
Set B	ASEN	CHLO	FLTX	PERI	TRIF	ZIPR	ZUCL		

Extraction recoveries were determined using Equation 4-1. Within the final extract, drug concentrations were ~10 µg/mL.

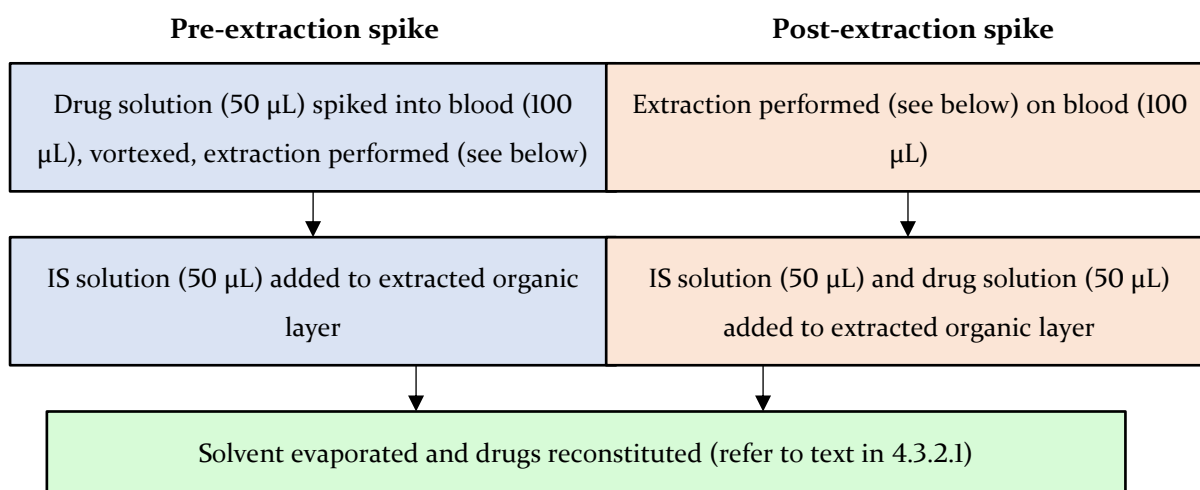


Figure 4-5: Extraction recovery experiment protocols.

IS = internal standard.

Equation 4-1: Extraction recovery calculations.

$$\text{extraction recovery (\%)} = \frac{\left(\frac{\text{area of "pre extraction spike" DRUG}}{\text{area of IS}} \right)}{\left(\frac{\text{area of "post extraction spike" DRUG}}{\text{area of IS}} \right)}$$

It is advantageous for the reconstitution solvent to be of similar composition to the mobile phase to prevent the reconstitution solvent from interfering with column-analyte adsorption [224]. Therefore, a 1:4 dilution of ethanol in 25 mM ammonium formate buffer (pH = 3.6) (LC-DAD buffer mix) was first selected. A preliminary screening of drug stability in aqueous solution

found that the drugs were most stable in acidic solution at pH = 3 (Chapter 5), and so drug degradation was not expected to be an issue using the acidic LC-DAD buffer mix.

Alkaline and unbuffered LLE methods were trialled, based on those utilised by the Toxicology laboratories at FSSA [196]. For the alkaline LLE: Set A or Set B working solution (50 µL) and blood (100 µL) were briefly vortexed together in a borosilicate screw-cap extraction tube. Water (1.2 mL) and aqueous NH₃ (30% w/v, 250 µL) were then added followed by vortexing (5 sec), then n-BuCl (5 mL) was added. The tubes were capped then placed on a mechanical roller (15 minutes at 20 rpm), followed by centrifugation (10 minutes at 1409 x g). If an emulsion or gel formed after the centrifugation step, a 1:1 mixture of sodium carbonate:sodium bicarbonate (~100 mg) was added followed by brief shaking, prior to further centrifugation (10 minutes at 1409 x g). After centrifugation the organic layer was transferred to a disposable borosilicate test tube. IS solution (50 µL) was added prior to evaporation of organic solvent under N₂ at 40 °C. The residue was then reconstituted in 1:4 ethanol:buffer mix (100 µL), with vortexing (5 sec), transferred to a limited-volume glass autosampler vial and capped. Water was substituted for aqueous NH₃ in the unbuffered extraction.

4.3.2.2 Results and discussion

Satisfactory recoveries (> 70%) were obtained for most analytes, regardless of extraction method (Table 4-5).

Table 4-5: Extraction recoveries (%) for analytes for each extraction method.

Analyte	Mean extraction recovery (n = 7) (%) [Range, C.V. (%)]	
	Alkaline LLE	Unbuffered LLE
AMIS	77.6 [54.0-92.8, 18.4]	8.4 [7.3-10.8, 13.6]
AMIT	87.0 [72-99, 10.1]	99.4 [84.6-126.6, 14.5]
ARIP	82.2 [62-96, 13.9]	102.8 [85.9-139.4, 16.8]
ASEN	86.9 [70-118, 18.5]	88.1 [75.0-97.9, 10.4]
CHLO	66.2 [54-90, 18.8]	75.2 [61.9-88.0, 13.4]
CLOZ	81.3 [64.8-93.7, 11.3]	99.2 [86.6-125.0, 13.6]
FLPH	74.2 [48.1-89.4, 18.3]	95.9 [82.4-129.6, 16.1]
FLTX	85.8 [68.5-120.2, 19.5]	86.3 [73.1-101.4, 13.0]
HALO	88.9 [77.4-99.2, 8.9]	103.5 [86.1-135.0, 15.8]
PERI	72.8 [57.8-97.4, 19.2]	86.8 [78.2-94.1, 6.0]
PROC	70.5 [41.3-91.3, 21.5]	85.8 [75.3-114.3, 15.2]
QUET	88.1 [73.9-99.0, 11.3]	101.5 [87.0-128.6, 14.3]
RISP	87.1 [73.0-102.7, 12.8]	101.6 [85.7-130.4, 14.9]
TRIF	70.6 [55.8-99.1, 21.9]	77.8 [62.1-91.4, 16.6]
ZIPR	58.2 [39.9-88.8, 27.5]	87.6 [74.7-99.0, 10.5]
ZUCL	86.0 [68.8-122.2, 20.8]	84.9 [72.4-100.4, 12.3]

C.V. = coefficient of variation.

The unbuffered LLE method was preferred due to lower recoveries obtained for most analytes using the alkaline LLE method (Table 4-5). Furthermore: the use of an unbuffered LLE method was found to be more convenient when analysing these drugs in comparison to alkaline LLE, due to no emulsions forming post-centrifugation; many analytes were subsequently observed to be unstable in alkaline solutions (see Chapter 5); and the phenothiazine drugs are known to oxidise in alkaline blood [223, 425, 426].

For AMIS, the alkaline LLE method would be preferred due to poor recovery by unbuffered LLE. However, in order to analyse AMIS by the LC-DAD method it was found that the reconstitution solvent could not be 100 % ethanol due to AMIS eluting as two peaks, presumably due to the ethanol behaving as a mobile phase (Figure 4-6). Using premade LC-DAD buffer mix as a reconstitution solvent or dissolution in 1 part ethanol followed by 4 parts buffer eradicated this phenomenon (Figure 4-6) but during subsequent method validation it was found that this choice of diluent yielded calibration curves with unacceptable ($R^2 < 0.99$) linearity. This was the case for unweighted and $1/x^2$ weighted linear calibration models. Variable reconstitution may also explain the large range in extraction recoveries obtained for analytes compared to revised methods (Table 4-5 and Table 4-7). An injection method to dilute samples reconstituted in buffer alone with ethanol at a ratio of 1:3 (4 μ L sample in buffer:12 μ L ethanol in a vial) was not successful in improving AMIS elution (Figure 4-6). Working with greater volumes in the injector program resulted in drops forming at the tip of the needle, indicating an injection capacity limitation. An alternative solution was to work with smaller volumes, but this would require greater concentrations of drugs to be spiked into blood. Therefore, for the above reasons, AMIS was excluded from the final LC-DAD method and not studied in the blood experiments performed in Chapter 6.

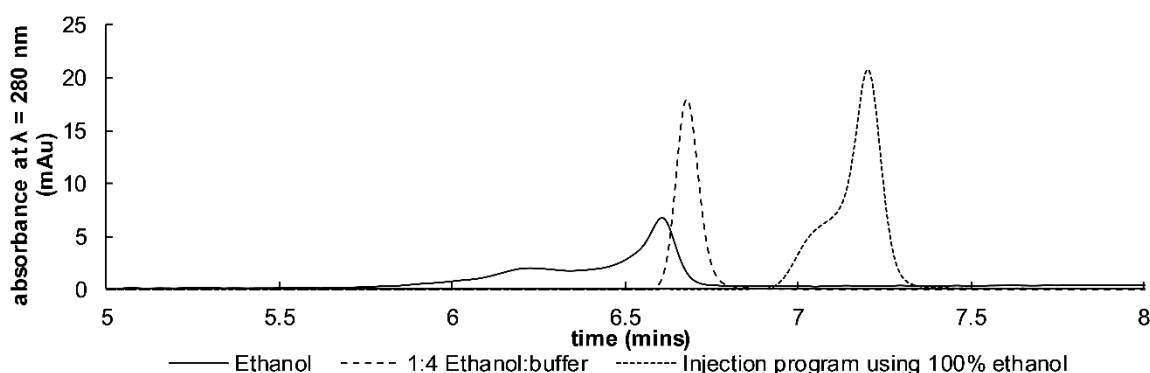


Figure 4-6: AMIS peak shape under a variety of conditions.

Several other changes were also implemented: the IS was changed from TRIM to LORA, due to i) the coelution of TRIM with an impurity of prochlorperazine (PROC) present in a later prepared stock solution (see Appendix A) and ii) subsequent concerns a polar degradation product in the Chapter 6 experiments may coelute with an IS; the volume of reconstitution solvent was reduced from 100 μ L to 50 μ L, to concentrate analytes from the blood samples during extraction; and the reconstitution solvent was changed from the LC-DAD buffer mix to 100 % ethanol.

4.3.3 Revised unbuffered LLE method

4.3.3.1 Experimental

Ethanollic working solutions of the drugs (\sim 20 μ g/mL) were prepared in three separate sets (except for ZIPR, ASEN, and LURA which were prepared at \sim 30 μ g/mL) from previously prepared stock standard solutions (3.1.2) (Table 4-6). An IS solution of LORA (\sim 20 μ g/mL) was also prepared. These solutions were used in all subsequent extraction recovery experiments.

Table 4-6: Working solutions used for revised extraction efficiency experiments.

Set A	AMIT	ARIP	CLOZ	FLPH	HALO	PROC	QUET	RISP
Set B	ASEN	CHLO	FLT	PERI	TRIF	ZIPR	ZUCL	
Set C	CLOM	DOTH	LURA	MIRT	MOCL			

Extraction recoveries were determined as detailed in section 4.3.2.1. SERT was the IS used in conjunction with LORA to determine extraction recovery. Drug concentrations were \sim 3 μ g/mL in the reconstituted extract.

Set A, Set B, or Set C working solutions (15 μ L), blood (100 μ L), and water (1.45 mL) were briefly vortexed together in a borosilicate tube. n-BuCl (5 mL) was added to the tubes, which were then capped, and placed on a mechanical roller (15 minutes at 20 rpm), followed by centrifugation (10 minutes at 1409 \times g). After centrifugation the organic layer was transferred to a disposable glass test tube. IS solution (50 μ L) was added prior to evaporation of organic solvent under N₂ at 40 °C. The residue was then reconstituted in ethanol (50 μ L) with vortexing, transferred to a limited volume autosampler vial and capped.

4.3.3.2 Results

High recoveries were obtained for all analytes, except for LURA, PROC and TRIF, for which recoveries were considered sufficient for the method (Table 4-7). The unbuffered LLE method trialled previously used LC-DAD buffer mix (100 μ L) as the reconstitution solvent (see 4.3.2.1).

This revised unbuffered LLE method used ethanol (50 μ L) and was found to reconstitute analytes with greater precision (Table 4-5 and Table 4-7). Therefore, method validation proceeded using this method.

Table 4-7: Extraction recoveries (%) of analytes for revised unbuffered LLE method.

Analyte	Mean recovery (%) [Range, C.V. (%)]	Analyte	Mean recovery (%) [Range, C.V. (%)]
AMIT	96.8 [92.9-101.5, 2.6]	LURA	59.0 [51.7-65.6, 7.7]
ARIP	94.7 [90.1-101.1, 3.6]	MIRT*	98.7 [96.4-102.9, 2.5]
ASEN*	97.5 [91.3-103.9, 4.8]	MOCL*	87.1 [85.5-90.6, 1.9]
CHLO*	80.9 [75.2-85.3, 4.2]	PERI*	90.1 [83.1-95.7, 5.0]
CLOM	96.1 [84.8-99.9, 5.3]	PROC	74.3 [68.5-77.3, 3.8]
CLOZ	91.5 [87.6-94.2, 2.4]	QUET	95.9 [92.8-102.0, 3.4]
DOTH	96.1 [86.3-99.7, 4.7]	RISP	98.9 [87.4-110.5, 8.2]
FLPH	83.9 [76.9-92.6, 5.8]	TRIF*	75.6 [68.7-83.1, 6.1]
FLTX*	94.7 [88.7-99.1, 3.7]	ZIPR*	91.9 [87.9-96.3, 3.4]
HALO	95.8 [92.4-97.7, 1.8]	ZUCL*	94.8 [88.4-97.8, 3.8]
LORA (IS)	96.8 [87.3-99.0, 4.0]		

n = 7 or *n = 6. C.V. = coefficient of variation.

4.3.4 Additional peaks following extraction

During the extraction efficiency experiments, a small peak with UV-Vis absorbance spectrum similar to CHLO-SO and PROC-SO (Figure 4-4 (b)), not previously detected from neat standard analysis, was detected (Figure 4-7) at a retention time of 13.7 min.

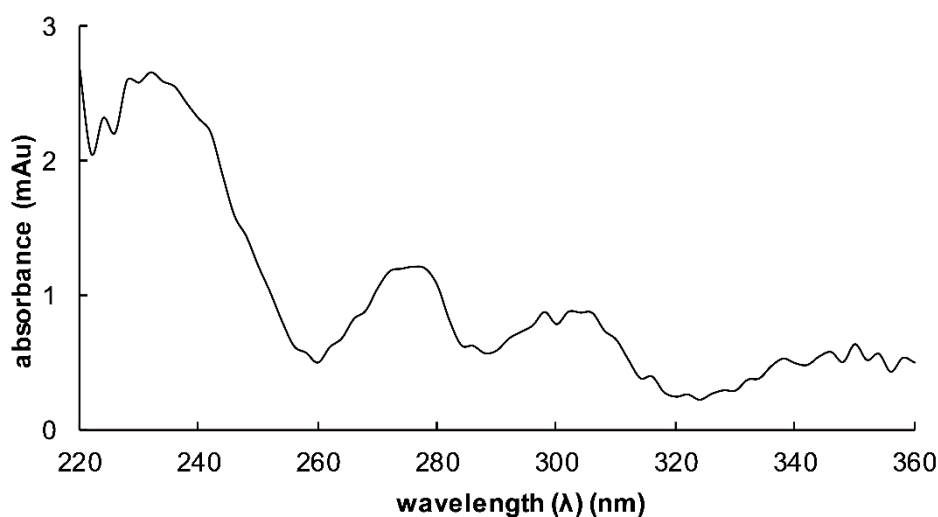


Figure 4-7: UV-Vis absorbance spectrum of unknown peak at RT=13.7 min following unbuffered LLE from human whole blood.

To determine which drug corresponded to the additional peak present, each drug was spiked individually into blood (100 μ L) at a concentration of \sim 10 μ g/mL and extracted by the unbuffered LLE method (4.3.3.1).

The additional peak present was identified as a degradant of TRIF, due to its formation in blood spiked with TRIF. The presence of a large absorption maximum around 230-240 nm, and a series of smaller maxima at ~270 nm and ~300 nm, in the UV-Vis spectrum of the degradant (Figure 4-7) is similar to the UV-Vis spectra of CHLO-SO and PROC-SO (Figure 4-4 (b)). This suggests that the degradant is probably trifluoperazine-sulfoxide (TRIF-SO) (Table 4-8). Sulfoxides of the other phenothiazine drugs, FLPH and PERI, were not detected in the LC-DAD method.

Table 4-8: Retention time (min) and identity of unknown peak following unbuffered LLE from blood.

Parent drug	Degradant/impurity	RT (min)
TRIF	TRIF-SO ⁺	13.7 (Method A) / 11.4 (Method B)

⁺Postulated from characteristic UV absorbance spectra (Figure 4-7).

The concurrent oxidation of phenothiazine drugs to phenothiazine-sulfoxides has previously been reported to occur during extraction from whole blood [223, 425-427]. For CHLO, it has been reported that this conversion is greater in blood made alkaline [425, 426]. The oxidation of CHLO to CHLO-SO occurs *in vitro* in whole blood and it appears that this conversion may be catalysed by haemoglobin [428]. Campbell *et al.* have also theorised that haemoglobin may be involved in phenothiazine oxidation, as they observed greater oxidation of promethazine and CHLO in whole blood compared to bone tissue extracts [427].

Given reproducible extraction conditions the extent of sulfoxide oxidation was not expected to significantly impede subsequent method validation. However, the response of the sulfoxides detected was monitored in blood experiments, particularly given the purported transformation of sulfoxide containing drugs to their sulfides by gut microorganisms [266, 429].

4.4 Method validation

4.4.1 Experimental

Two working solutions were prepared from drug stocks as indicated in 3.1.2.2 (Table 4-9). These working solutions were used for method validation unless otherwise indicated.

Table 4-9: Working solutions used for method validation.

Set A	AMIT	ASEN	CHLO	CLOZ	HALO	FLPH	FLTX	PERI	PROC	QUET	RISP
Set B	AMIT	ARIP	CLOM	DOTH	LURA	MIRT	MOCL	RISP	TRIF	ZIPR	

Accuracy was calculated as indicated in Equation 4-2. Intra and inter-day precision were calculated as recommended in literature, following the ANOVA approach specified by the Scientific Working Group for Forensic Toxicology (SWGTOX) (Equation 4-3) [203, 218].

Equation 4-2: Calculation for accuracy.

$$\text{Accuracy (\%)} = \frac{(C_m - C_n)}{C_n} \times 100 \%$$

where C_m = mean measured concentration and C_n = nominal concentration

Equation 4-3: Calculation for intra-day and inter-day precision (as coefficient of variation (C.V.)) [203].

$$\text{intra-day precision (\%)} = \left(\frac{\sqrt{MS_{wgS}}}{C_m} \right) \times 100 \%$$

$$\text{inter-day precision (\%)} = \left(\frac{\sqrt{\frac{MS_{bg} + (n - 1) \times MS_{wg}}{n}}}{C_m} \right) \times 100 \%$$

where MS_{wg} = mean square within groups from ANOVA table,

C_m = mean measured concentration,

MS_{bg} = mean square between groups from ANOVA table, and

n = number of replicates in each group

4.4.1.1 Selectivity

Method validation guidelines in forensic toxicology recommend the analysis of blank matrix samples from a minimum of 10 different sources in order to determine if common matrix interferences may affect analyte quantification [203]. As the methods presented in this thesis were to be used only in this research project, only the ante-mortem blood to be used in subsequent experiments was analysed to determine if any interferences may impact analyte quantification. Similarly, the use of a therapeutic drug as IS, contrary to recommended guidelines [218], was considered acceptable in this instance as LORA should not feasibly result from the degradation of any of the drugs investigated.

4.4.1.2 Linearity

It is recommended that calibrators be matrix-based for bioanalytical methods [218]. The environment of the blood matrix used during the experiments in Chapter 6 was expected to be dynamic, due to the presence of microorganisms degrading endogenous material as the experiments progressed. Linearity was therefore tested by spiking drugs in the ante-mortem

human whole blood used to prepare the inoculated blood matrix, which was prepared fresh at the start of each experiment in Chapter 6 and section 8.3. International guidelines followed were the use of at least four different concentrations, greater than five replicates per level, and assessment of the heteroscedasticity of the data to determine if a weighting factor should be used [203, 218]. Six-point calibration curves were constructed by spiking the drugs at concentration ranges of ~1-15 µg/mL, depending on the analyte.

HALO and PERI were quantified using peak height due to mutual coelution. RISP was quantified using peak height in samples where PROC was also present due to slight coelution with PROC-SO. AMIT (in Method B), CHLO, FLTX, and FLPH were initially quantified using peak area but later coelution with degradation products (see Chapter 6) necessitated re-analysis of validation data to determine if peak height was appropriate for quantification.

4.4.1.3 Limit of detection (LOD) & lower limit of quantification (LLOQ)

To determine the LOD, drugs were spiked at decreasing concentrations (as recommended in literature [218]) in triplicate and the LOD defined as the concentration below which identification of analytes using their retention time and UV-Vis spectra was not possible. The LLOQ was defined as the concentration of the lowest calibrator.

4.4.1.4 Accuracy and precision

Ethanol QC solutions of the drugs (~20 µg/mL) were prepared in two separate sets (except for ZIPR and ASEN which were prepared at ~30 µg/mL) as with the working solutions prepared (Table 4-9). On different days, a single calibration curve was produced using the working solutions and duplicate QCs extracted at low, medium, and high concentrations (~2, 5, and 9.1 µg/mL, respectively). Three different concentrations were used as recommended by international guidelines, and accuracy and precision at these concentrations assessed over more than eight days [203, 218]. Intra-day and inter-day accuracies and coefficient of variations (C.V.s) were then determined. Inter-day C.V.s were determined to take into account both intra- and inter-day components of imprecision as recommended in literature [218]. Accuracy and precision were considered acceptable if within ± 20 %, as recommended by the SWGTOX [203].

4.4.1.5 Process sample stability

The stability of the drugs during the extraction process was assessed at two stages: 1) prior to n-BuCl addition, but with water added (testing stability in diluted blood); and 2) after n-BuCl addition, post-rolling but pre-centrifugation (testing stability in n-BuCl). For both experiments, samples remained at room temperature for two hours prior to continuing the extraction

procedure. Extraction recoveries for these delayed samples were determined relative to the recoveries of samples extracted without delay. To determine the stability of the IS LORA during the extraction method SERT was used as the IS (added as an IS post-extraction as indicated in Figure 4-5). Set B drug concentrations were ~6 µg/mL in blood and Set A drug concentrations were ~3 µg/mL in blood. Drugs were considered stable if extraction recoveries in delayed samples were within ± 20 % of the extraction recoveries of samples extracted without delay.

4.4.1.6 Auto-sampler stability

The stability of the drugs in the reconstitution solvent (i.e. ethanol) was assessed by reinjecting sample extracts 18-33 hours after the initial injection. The relative responses of the drugs in the initial injection were compared to the relative responses of the drugs at 18-33 hours, with results expressed as percentage deviation from the initial injection. Thus, a negative value indicates a percentage decrease in the relative response at the time of the initial injection. For Method A drugs, amber vials were used, due to concerns regarding the photostability of phenothiazines [430]. For Method B drugs, stability was assessed in both amber and clear vials. Data from reinjected QCs run throughout the experiments as indicated in 4.2.1 were also processed in the same way. The auto-sampler was not temperature controlled. Drugs were considered stable if responses were within ± 20 % of the initial injection.

4.4.1.7 Freeze-thaw stability

The stability of the drugs during three freeze-thaw cycles, as advised [203, 218], in preserved ante-mortem whole blood, was assessed. Sodium fluoride (20 mg) was weighed into 5 and 10 mL sterile polystyrene Sarstedt tubes and Set A, Set B, or Set C (Table 4-6) working solution (200 µL) added followed by evaporation of organic solvent under N₂ at 40 °C. Blood (1 mL) was then added, with vortexing, to give a final concentration of 2 % w/v for sodium fluoride and ~4 µg/mL for the drugs (except for ZIPR and LURA which were spiked at ~6 µg/mL). Tubes were also placed on a mechanical roller to ensure thorough mixing (15 minutes at 20 rpm), followed by additional vortexing. An initial extraction ($t = 0$ days) was performed as outlined in 4.2.2.

The first cycle consisted of storing the samples at -20 °C for 24 hours followed by room temperature for one-hour to thaw, mechanical rolling of the tubes (15 minutes at 20 rpm), vortexing, and then extraction. Each subsequent cycle consisted of storing the samples at -20 °C for ~20 hours followed by room temperature for one hour. Freeze-thaw cycles and extraction were carried out on consecutive days. The initial relative responses of the drugs prior to storing the samples at -20 °C were compared with the relative responses of the drugs after each freeze-thaw cycle, with results expressed as percentage deviation from the initial injection. Thus, a

negative value indicates a percentage decrease in the relative response compared to the initial injection. Analytes were considered stable after three freeze-thaw cycles if they were within $\pm 10\%$ of the initial drug response [218].

4.4.2 Results

4.4.2.1 Selectivity

There were no interferences in the blank ante-mortem blood with any of the analytes.

4.4.2.2 Linearity, limit of detection (LOD) & lower limit of quantification (LLOQ)

Calibration curve data were heteroscedastic, with larger variance in instrument response with increasing concentration (see example for PROC in Figure 4-8), common to analytical toxicology methods with concentration ranges across multiple orders of magnitude [203]. To prevent the larger concentrations skewing any determined least-squares regression analysis, and therefore lowering the accuracy and precision of any data acquired at the lower end of the calibration range, a weighting factor was required. Selection of the correct weighting factor to apply was determined from the relationship between i) the standard deviation of relative response and concentration and ii) the variance of relative response vs. concentration and the calculation of y -residuals¹³, as recommended in literature [203, 431].

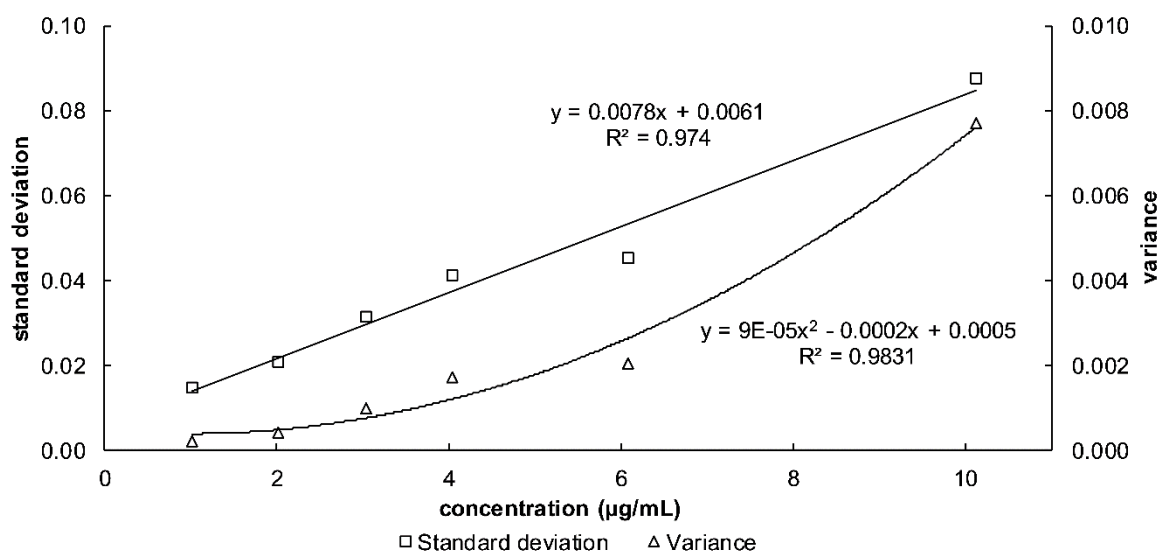


Figure 4-8: Standard deviation and variance of instrument responses vs. concentration plot for PROC.

n = 18.

¹³ Y-residuals are the differences between predicted y -values (nominal values based on the calibration) and observed y -values (instrument response) for the calibration model.

A linear relationship between standard deviation and concentration, with a concave upward quadratic relationship between variance and concentration was observed for analytes, indicating a weighting factor of $1/x^2$ should be applied (see example for PROC in Figure 4-8) [431]. Predicted y-values (nominal values based on the calibration model) were determined for analytes using unweighted and $1/x^2$ -weighted linear calibration models. The smaller the residuals the better the fit of the calibration model. From the obtained residuals (see example for PROC in Table 4-10) it can be seen that the $1/x^2$ -weighted calibration model provides a better fit for the lower end of the calibration range.

Table 4-10: Predicted and calculated y-residuals for unweighted and $1/x^2$ -weighted PROC calibration curves.

Concentration ($\mu\text{g/mL}$)	Mean observed y value	Unweighted model		$1/x^2$ -weighted model	
		Predicted y value	Mean y- residual	Predicted y value	Mean y- residual
1.0123	0.1230	0.1186	0.004	0.1237	-0.002
2.0246	0.2966	0.2863	0.008	0.2908	0.003
3.0369	0.4609	0.4539	0.005	0.4578	0.001
4.0492	0.6049	0.6215	-0.020	0.6249	-0.025
6.0739	0.9619	0.9568	-0.000	0.9590	-0.003
10.1231	1.6409	1.6274	0.005	1.6273	0.005

n = 18.

Reproducible linear calibration curves were obtained when quantifying HALO, PERI and RISP using peak height (see Table 4-II). The linear range, curve fit, LLOQ, and LOD details for all analytes are shown in Table 4-II and Table 4-13. Upper limits of the linear ranges were a nominal concentration set for the research project, not the upper limit of the method itself.

Table 4-II: Linearity data, LLOQ, and LOD for analytes using HPLC method A.

Analyte	Linear range ($\mu\text{g/mL}$)	R^2 (n=18)	LLOQ ($\mu\text{g/mL}$)	Acc. (%) @ LLOQ (n = 2)	LOD ($\mu\text{g/mL}$)
AMIT	1.01-10.12	0.9995	1.012	21.7	0.607
ASEN	1.51-15.08	0.9997	1.508	5.9	1.206
CLOZ	1.00-10.00	0.9998	1.000	16.6	0.400
HALO ⁺	1.02-10.24	0.9995	1.024	20.6	0.410
PERI ⁺	1.01-10.05	0.9998	1.005	11.5	0.402
PROC	1.01-10.12	0.9997	1.012	2.4	0.405
QUET	1.03-10.29	0.9999	1.029	17.6	0.412
RISP ⁺	1.00-10.00	0.9994	1.000	10.4	0.800

⁺Calibration model constructed using peak height; LLOQ = lower limit of quantification; LOD = limit of detection; Acc. = accuracy.

For most drugs, less than $\pm 20\%$ accuracy as recommended by international guidelines [203, 218] was obtained at the concentration of the lowest calibrator (Table 4-II, Table 4-12 and Table

4-13). For RISP, accuracy was 24.5 % at 1.006 µg/mL for HPLC Method B. This drug was included in these methods as a control to confirm that microorganisms were successfully inoculated and respiring in the blood experiments performed in Chapter 6. Accurate quantification of RISP at this concentration was not requisite, as it was spiked in the blood specimens at a higher concentration of ~6 µg/mL to enable its degradation over time to be determined. Therefore, the method was fit for purpose.

Table 4-12: Linearity data, LLOQ, and LOD for CHLO, FLTX, and FLPH using HPLC method A.

Analyte	Linear range (µg/mL)	R ² (n=18)	LLOQ (µg/mL)	Acc. (%) @ LLOQ (n = 2)	LOD (µg/mL)
<i>Integration by peak area</i>					
CHLO	1.00-10.05	0.9998	1.005	14.4	0.402
FLPH	1.02-10.16	0.9997	1.016	11.6	0.406
FLTX	1.01-10.12	0.9999	1.012	5.0	0.405
<i>Integration by peak height</i>					
CHLO	1.00-10.05	0.9991	1.005	14.0	0.402
FLPH	1.02-10.16	0.9994	1.016	10.6	0.406
FLTX	1.01-10.12	0.9991	1.012	-6.3	0.405

LLOQ = lower limit of quantification; LOD = limit of detection; Acc. = accuracy.

Table 4-13: Linearity data, LLOQ, and LOD for analytes using HPLC method B.

Analyte	Linear range (µg/mL)	R ² (n=16)	LLOQ (µg/mL)	Acc. (%) @ LLOQ (n = 2)	LOD (µg/mL)
AMIT ⁺	1.03-10.28	0.9992	1.028	2.5	0.617
ARIP	1.04-10.38	0.9994	1.038	-4.0	0.415
CLOM	1.04-10.36	0.9995	1.036	-4.0	0.414
DOTH	1.03-10.29	0.9993	1.029	11.2	0.824
LURA	1.53-15.33	0.9986	1.533	9.9	0.920
MIRT	1.05-10.45	0.9993	1.045	-0.4	0.418
MOCL	1.04-10.44	0.9994	1.044	1.3	0.209
RISP	1.01-10.06	0.9981	1.006	24.5	0.805
TRIF	1.04-10.44	0.9992	1.044	9.5	0.418
ZIPR	1.51-15.12	0.9996	1.512	2.0	0.605

⁺Calibration model constructed using peak height; LLOQ = lower limit of quantification; LOD = limit of detection; Acc. = accuracy.

AMIT and HALO for HPLC Method A also afforded accuracies at the LLOQ exceeding 20 %. AMIT was included in these methods if aliquot or recovery variations throughout the experiment required correction to an IS within specimens. As AMIT was to be spiked at a concentration of ~6 µg/mL the decrease in the accuracy of AMIT at the LLOQ was not significant for its use in this research.

4.4.2.3 Accuracy and precision

For all analytes, inter-day accuracy and precision was within $\pm 15\%$ (Table 4-14, Table 4-15 and Table 4-16). On one day, intra-day accuracy exceeded recommended limits [203] for RISP, AMIT, and ZIPR, and on three days for LURA. For AMIT, low and medium QC concentrations did not fulfil validation criteria on the same day. Inter-day accuracy for the AMIT high QC on the same day was within $\pm 10\%$. The reason for this is unclear.

The concentration of AMIT spiked in the blood experiments (Chapter 6) was $\sim 6\ \mu\text{g/mL}$, closest to the medium QC with a nominal concentration of $4.971\ \mu\text{g/mL}$. On the day where validation criterion was exceeded the accuracy of the medium AMIT QC was determined to be 21.2% , with one replicate of the duplicate medium QC reading high. As AMIT was used to normalise data (see 6.2.3.2) it was noted that on this day calculated relative concentration changes (%) may be underestimated.

Table 4-14: Accuracy and precision data for CHLO, FLTX, and FLPH using HPLC method A.

Analyte	Nominal concentration ($\mu\text{g/mL}$)	Intra-day (n = 8) [^]		Inter-day (n = 8)	
		Mean acc. [Range] (%)	C.V. (%)	Acc. (%)	C.V. (%)
		<i>Integration by peak area</i>			
CHLO	2.077	-0.1 [-2.4 - 2.7]	2.8	-0.1	2.6
	5.192	-1.8 [-4.4 - 0.6]	3.1	-1.8	2.8
	9.345	-0.3 [-2.6 - 1.3]	3.0	-0.3	2.5
FLTX	2.075	-6.4 [-9.8 - -4.2]	3.7	-6.4	3.2
	5.187	-9.8 [-14.3 - -6.7]	4.5	-9.8	4.0
	9.336	-8.1 [-5.8 - -10.2]	2.8	-8.1	2.6
FLPH	2.093	-1.4 [-4.5 - 2.1]	4.6	-1.4	3.9
	5.234	-3.5 [-8.1 - 0.3]	4.4	-3.5	4.2
	9.420	-0.6 [-3.0 - 1.1]	2.7	-0.6	2.5
		<i>Integration by peak height</i>			
CHLO	2.077	4.9 [-8.5 - 13.7]	2.6	4.9	8.6
	5.192	1.4 [-13.0 - 7.2]	3.5	1.4	7.6
	9.345	-5.0 [-16.3 - 1.4]	6.7	-5.0	8.7
FLTX	2.075	-12.1 [-18.6 - -8.6]	1.4	-12.1	3.7
	5.187	5.8 [-15.3 - -16.7]	3.3	5.8	9.7
	9.336	5.8 [-0.3 - 13.4]	2.7	5.8	4.5
FLPH	2.093	6.1 [-0.8 - 10.9]	2.3	6.1	3.8
	5.234	3.4 [-0.8 - 9.0]	3.8	3.4	4.3
	9.420	1.4 [-0.9 - 4.0]	2.6	1.4	2.7

[^]Two replicates at each concentration level per day; Acc. = accuracy; C.V. = coefficient of variation. Bold values used in uncertainty calculations (see 6.2.3.3).

Table 4-15: Accuracy and precision data for analytes using HPLC method A.

Analyte	Nominal concentration (µg/mL)	Intra-day (n = 16) [^]		Inter-day (n = 16)	
		Mean acc. [Range] (%)	C.V. (%)	Acc. (%)	C.V. (%)
AMIT	2.089	7.4 [2.2 - 15.4]	1.7	7.4	4.3
	5.223	3.3 [-1.2 - 9.6]	2.5	3.3	4.0
	9.401	2.3 [-2.1 - 7.0]	2.9	2.3	3.3
ASEN	3.073	2.6 [-4.6 - 9.4]	1.8	2.6	4.3
	7.683	-1.2 [-7.0 - 4.4]	2.8	-1.2	4.3
	13.830	-2.7 [-9.3 - 4.9]	3.0	-2.7	4.5
CLOZ	2.068	8.0 [2.2 - 14.7]	1.5	8.0	3.8
	5.170	4.2 [-0.2 - 11.1]	3.0	4.2	4.1
	9.306	4.0 [-0.8 - 10.1]	3.0	4.0	3.3
HALO ⁺	2.000	10.2 [3.9 - 18.1]	2.2	10.2	4.7
	5.000	6.2 [-1.4 - 13.3]	3.8	6.2	5.3
	9.000	5.1 [1.2 - 10.6]	2.6	5.1	3.0
PERI ⁺	2.216	4.1 [-2.9 - 12.9]	3.8	4.1	5.4
	5.540	2.0 [-4.0 - 8.9]	4.0	2.0	5.3
	9.972	1.8 [-0.9 - 6.3]	2.6	1.8	2.5
PROC	2.012	-8.5 [-15.6 - -2.4]	2.8	-8.5	5.3
	5.030	-11.9 [-17.1 - -6.4]	3.8	-11.9	4.5
	9.055	-10.9 [-14.3 - -7.7]	3.2	-10.9	3.2
QUET	2.024	7.8 [1.7 - 16.0]	2.0	7.8	3.8
	5.059	4.3 [-0.7 - 11.6]	2.8	4.3	4.0
	9.106	3.8 [-1.4 - 10.2]	2.6	3.8	3.3
RISP ⁺	2.087	0.4 [-9.8 - 12.8]	7.8	0.4	9.1
	5.219	-1.2 [-10.0 - 6.5]	5.2	-1.2	6.5
	9.393	2.2 [-3.3 - 7.5]	3.5	2.2	3.6

[^]Two replicates at each concentration level per day; ⁺calibration model constructed using peak height. Acc. = accuracy; C.V. = coefficient of variation. Bold values used in uncertainty calculations (see 6.2.3.3).

For LURA, mean intra-day accuracy at all concentrations was within $\pm 6\%$ except for the days where LURA inexplicably exceeded validation criteria. The reason for the erratic behaviour of LURA is unknown. These compounds were in a mixed solution with the other drugs as part of Method A or Method B which did not show these variations, thereby eliminating spiking error as the cause of the behaviour. All LURA validation data were therefore used when determining the uncertainty of measurements for the blood experiments in Chapter 6. For RISP, one medium QC was excluded due to a single instance of coelution with a previously un-observed peak.

Table 4-16: Accuracy and precision data for analytes using HPLC method B.

Analyte	Nominal concentration (µg/mL)	Intra-day (n = 18) [^]		Inter-day (n = 18)	
		Mean acc. [Range] (%)	C.V. (%)	Acc. (%)	C.V. (%)
AMIT ⁺	1.988	8.2 [-5.7 - 33.8] [#]	2.7	8.2	8.2
	4.971	3.5 [-3.9 - 21.2] [#]	2.8	3.5	6.6
	8.947	-1.0 [-7.0 - 7.6]	2.6	-1.0	5.4
ARIP	2.043	3.2 [-7.5 - 12.9]	3.0	3.2	4.7
	5.107	1.2 [-7.2 - 7.6]	2.3	1.2	4.3
	9.193	1.2 [-5.5 - 9.1]	2.8	1.2	5.2
CLOM	1.981	-3.7 [-14.0 - 3.5]	2.4	-3.7	4.6
	4.952	-7.3 [-15.6 - -0.3]	2.7	-7.3	4.5
	8.914	-7.2 [-14.3 - -0.4]	2.5	-7.2	4.6
DOTH	2.029	12.6 [0.9 - 18.2]	2.8	12.6	4.2
	5.072	9.9 [0.1 - 17.7]	2.6	9.9	4.2
	9.129	10.5 [0.4 - 19.2]	2.5	10.5	4.9
LURA	3.000	6.9 [-6.7 - 22.4] [#]	11.1	6.9	11.3
	7.500	9.2 [-4.0 - 44.8] ^s	11.7	9.2	14.1
	13.500	4.7 [-13.2 - 37.9] ^{&}	9.7	4.7	12.9
MIRT	1.994	-2.8 [-12.3 - 4.3]	2.7	-2.8	4.6
	4.985	-6.0 [-13.6 - 0.8]	2.8	-6.0	4.2
	8.974	-6.1 [-16.0 - 1.2]	3.0	-6.1	5.0
MOCL	1.982	1.3 [-9.0 - 9.4]	2.6	1.3	4.5
	4.956	-1.5 [-9.3 - 6.1]	2.6	-1.5	4.5
	8.920	-1.8 [-11.8 - 6.5]	2.8	-1.8	5.1
RISP	1.988	-1.5 [-14.6 - 9.1]	10.3	-1.5	10.2
	4.970 (n=17) ⁻	-2.4 [-11.3 - 4.6]	3.3	-2.4	5.6
	8.946	-2.0 [-10.3 - 13.4]	3.8	-2.0	8.1
TRIF	1.964	5.6 [-4.4 - 14.5]	3.0	5.6	5.0
	4.909	4.5 [-4.9 - 13.5]	2.2	4.5	4.5
	8.836	6.2 [-3.2 - 15.1]	3.2	6.2	5.8
ZIPR	2.965	6.0 [-3.9 - 12.5]	2.9	6.0	4.3
	7.413	4.4 [-4.5 - 10.4]	2.6	4.4	4.3
	13.343	4.0 [-16.7 - 12.7]	7.0	4.0	8.0

[^]Two replicates at each concentration level per day; ⁺calibration model constructed using peak height; ⁻sporadic coelution with unknown component prevented quantification; [#]one result or [&]two results or ^sthree results exceeded validation criteria. Acc. = accuracy; C.V. = coefficient of variation. Bold values used in uncertainty calculations (see 6.2.3.3).

4.4.2.4 Process sample stability

All analytes were stable (no losses greater than 20 %) in diluted blood and n-BuCl for two hours (Table 4-17).

Table 4-17: Analyte stability during extraction.

Analyte	Mean recovery after 2 hours (%) [Range, C.V.]		Analyte	Mean recovery after 2 hours (%) [Range, C.V.]	
	Diluted blood	n-BuCl		Diluted blood	n-BuCl
AMIT	101.6 [98.0-105.3, 2.2]*	103.8 [97.5-109.0, 3.9]	LURA	112.4 [90.1-139.4, 16.3]	101.9 [86.1-113.3, 8.4]
ARIP	105.2 [92.6-113.8, 7.1]*	107.0 [95.5-113.9, 7.6]	MIRT	98.4 [94.6-103.5, 4.0]^	98.2 [81.7-105.5, 8.2]
ASEN	95.8 [93.6-101.2, 3.4]^	97.6 [87.8-104.1, 5.3]	MOCL	100.9 [98.5-106.1, 2.6]	98.8 [83.3-108.9, 8.0]
CHLO	102.2 [97.6-110.2, 5.1]^	103.6 [98.3-112.2, 5.8]	PERI	110.8 [98.6-115.8, 6.4]^	111.9 [92.7-125.1, 10.5]
CLOM	98.3 [95.6-106.4, 3.9]	97.1 [83.1-108.8, 8.0]	PROC	101.8 [92.5-111.5, 6.2]*	105.3 [94.2-114.2, 7.2]
CLOZ	101.5 [95.6-110.3, 4.8]*	104.6 [98.2-110.8, 4.3]	QUET	105.7 [98.9-114.7, 5.3]*	104.2 [95.5-110.3, 5.8]
DOTH	98.0 [95.2-105.5, 3.6]	97.5 [83.1-107.9, 7.7]	RISP	106.7 [82.2-123.8, 15.3]*	109.5 [91.2-123.1, 12.0]
FLPH	105.6 [93.7-113.3, 6.8]*	107.4 [94.5-115.9, 7.8]	TRIF	103.3 [95.1-111.6, 6.9]^	103.0 [94.2-114.3, 7.1]
FLTX	107.6 [99.2-113.5, 5.5]	110.3 [95.6-122.6, 9.3]	ZIPR	100.7 [92.0-107.5, 5.9]^	106.5 [96.0-116.6, 7.3]
HALO	103.6 [93.1-112.7, 6.5]*	105.8 [97.6-110.6, 5.4]	ZUCL	107.7 [98.1-112.0, 5.2]^	111.8 [95.3-129.5, 11.2]
LORA	101.2 [91.8-108.5, 6.1]	105.0 [97.4-114.1, 5.3]			

n = 7, *n = 6, or ^n = 5 (replicates excluded due to mis-injection). C.V. = coefficient of variation.

For LURA and RISP, greater than $\pm 10\%$ standard deviations were observed for diluted blood samples. While it was expected that LURA may not be stable during the unbuffered LLE method, due to its instability in neutral aqueous solutions (see Chapter 5), the range of recoveries for LURA was found to be 90 – 139 %. It is not known why recoveries appear to have increased considerably for this analyte after two hours in diluted blood. In the same two replicates where recoveries were approximately 130 % for LURA the other analytes gave recoveries of $\sim 100\%$. Due to this, diluted blood was extracted with n-BuCl without delay.

4.4.2.5 Auto-sampler stability

All analytes yielded results within the deviation criteria of no more than $\pm 20\%$ over 33 hours (for the Method A drugs) (Table 4-18) and 18 hours (for the Method B drugs) (Table 4-19). There was no observed difference between Method B analyte stability in amber or clear vials (Table 4-19). For most drugs, deviations exceeding $\pm 5\%$ were not observed. For ZIPR, up to 8.7 % losses in analyte response after 18 hours were observed (Table 4-19). For RISP, up to 18.5 % losses in analyte response were observed after 33 hours (Table 4-18). This was not of practical concern,

as RISP was included in experiments as a control to monitor if its bacterial degradation product, HB-RISP, formed in microbially inoculated specimens rather than to assess the stability of RISP.

Table 4-18: Analyte stability on auto-sampler after 33 hours for Method A drugs.

Analyte	Amber vials
	Mean deviation (%) [Range]
AMIT	-0.2 [-2.5 – 4.3]
ASEN	1.0 [-0.6 – 3.0]
CHLO	0.7 [-0.2 – 1.4]
CLOZ	-3.2 [-5.0 – -1.5]
FLPH	1.1 [-1.2 – 3.0]
FLTX	1.8 [0.9 – 4.1]
HALO	0.1 [-0.5 – 0.7]
PERI	0.6 [0.1 – 1.0]
PROC	-0.2 [-1.2 – 1.3]
QUET	-1.0 [-2.6 – -0.3]
RISP	-7.4 [-18.5 – -3.5]

n = 7.

Table 4-19: Analyte stability on auto-sampler after 18 hours for Method B drugs.

Analyte	Amber vials	Clear vials
	Mean deviation (%) [Range]	Mean deviation (%) [Range]
AMIT	-0.6 [-1.2 – 0.3]	-0.4 [-1.3 – 0.3]
ARIP	0.1 [-0.3 – 0.6]	0.1 [-0.3 – 0.6]
CLOM	-0.2 [-1.4 – 0.9]	0.2 [-0.6 – 1.4]
DOTH	-0.1 [-0.6 – 0.6]	0.5 [-0.6 – 1.4]
LURA	0.6 [-1.0 – 2.0]	1.3 [0.4 – 2.6]
MIRT	-0.2 [-0.8 – 0.8]	-0.2 [-1.0 – 1.1]
MOCL	-0.5 [-1.4 – 0.4]	-0.8 [-1.1 – -0.4]
RISP	-10.8 [-15.4 – -4.2]	-2.2 [-5.3 – 0.4]
TRIF	0.6 [-0.9 – 2.4]	1.3 [0.4 – 2.3]
ZIPR	-4.1 [-8.6 – 0.0]	-4.5 [-8.7 – -2.3]

n = 7.

Deviations exceeding $\pm 5\%$ were observed for all analytes in the reinjected QCs of the blood experiments in Chapter 6 (Table 4-20 and Table 4-21). RISP was the only analyte for which a deviation less than -20% was observed (Table 4-20). Deviations greater than 20% were observed in different samples on different days with an increase in relative response of up to 35.2% over time for the lowest concentration QC (Table 4-21). In a different sample, and on one day of analysis, increases in relative response for the lowest concentration QC for FLTX were also observed ranging from 25.9% - 42.0% for repeated injections. Both RISP and FLTX were quantified using peak height, which is more susceptible than peak area to variations in peak shape. However, such deviations were not observed for the other drugs quantified using peak height (*i.e.* CHLO, HALO, PERI, and FLPH) all of which elute between RISP and FLTX (see Figure 4-2). Furthermore, the extremes observed for RISP and FLTX were in different samples.

Table 4-20: Analyte stability on auto-sampler during Chapter 6 blood experiments for Method A drugs.

Analyte	Nominal conc. (µg/mL)	Mean deviation (%) [Range, S.D.] t ₂ = 11-40 hours	Analyte	Nominal conc. (µg/mL)	Mean deviation (%) [Range, S.D.] t ₂ = 11-40 hours
AMIT	2.089	0.8 [-1.7-3.1, 1.0]	HALO	2.000	-0.8 [-8.8-3.2, 2.5]
	5.223	0.5 [-2.3-3.4, 1.0]		5.000	-1.3 [-9.4-3.9., 2.6]
	9.401	0.4 [-5.6-3.5, 1.3]		9.000	-1.0 [-8.4-2.8, 2.1]
ASEN	3.073	1.8 [-9.8-10.3, 3.6]	PERI	2.216	-1.2 [-8.5-3.1, 2.6]
	7.683	0.0 [-5.6-3.5, 1.6]		5.540	-1.3 [-9.9-4.2, 3.0]
	13.830	0.3 [-5.2-5.0, 1.6]		9.972	-0.7 [-8.8-4.7, 2.4]
CHLO	2.077	-1.8 [-11.3-3.0, 2.9]	PROC	2.012	-0.1 [-2.6-2.5, 1.2]
	5.192	-2.0 [-12.3-2.9, 3.6]		5.030	0.4 [-2.6-4.5, 1.2]
	9.345	-2.0 [-12.2-1.6, 3.2]		9.055	0.1 [-5.4-2.8, 1.4]
CLOZ	2.068	0.8 [-2.2-3.7, 1.2]	QUET	2.024	0.7 [-3.8-4.3, 1.8]
	5.170	0.5 [-2.9-3.5, 1.2]		5.059	0.3 [-3.0-2.6, 1.1]
	9.306	0.5 [-5.4-5.0, 1.4]		9.106	0.3 [-5.5-2.4, 1.2]
FLPH	2.093	-1.3 [-11.0-2.8, 3.1]	RISP	2.087	0.2 [-20.3-11.5, 5.9]
	5.234	-1.5 [-11.4-2.5, 3.1]		5.219	1.0 [-20.0-13.7, 6.0]
	9.420	-1.5 [-11.3-2.3, 2.8]		9.393	0.6 [-17.2-6.6, 5.2]
FLTX	2.075	2.4 [-10.8-42.0, 11.6]			
	5.187	-1.3 [-8.6-3.0, 2.8]			
	9.336	-0.9 [-9.9-3.5, 2.7]			

S.D. = standard deviation, n = 55 for low concentrations (one low replicate not reinjected due to instrument demand), n = 56 for medium and high concentrations. t₂ = reinjection time after initial injection.

Table 4-21: Analyte stability on auto-sampler during Chapter 6 blood experiments for Method B drugs.

Analyte	Nominal conc. (µg/mL)	Mean deviation (%) [Range, S.D.] t ₂ = 13-42 hours	Analyte	Nominal conc. (µg/mL)	Mean deviation (%) [Range, S.D.] t ₂ = 13-42 hours
AMIT	1.988	-0.1 [-10.4-13.8, 4.5]	MIRT	1.994	-0.4 [-4.6-4.6, 1.6]
	4.971	-0.8 [-7.2-7.4, 3.5]		4.985	-0.4 [-3.4-3.2, 1.2]
	8.947	0.0 [-9.4-15.9, 6.2]		8.974	-0.4 [-15.1-3.7, 2.6]
ARIP	2.043	0.2 [-1.7-2.6, 1.2]	MOCL	1.982	-0.1 [-2.7-2.0, 1.0]
	5.107	0.4 [-1.9-2.8, 1.0]		4.956	0.0 [-2.7-2.4, 1.1]
	9.193	0.2 [-14.1-3.8, 2.5]		8.920	0.0 [-14.2-3.6, 2.5]
CLOM	1.981	0.1 [-3.0-4.2, 1.4]	RISP	1.988	2.6 [-13.1-35.2, 8.6]
	4.952	0.1 [-2.5-3.1, 1.1]		4.970	0.3 [-6.0-5.7, 1.8]
	8.914	-0.1 [-14.4-3.4, 2.5]		8.946	0.1 [-14.7-5.0, 2.7]
DOTH	2.029	-0.3 [-5.3-2.6, 1.5]	TRIF	1.964	0.2 [-6.8-6.7, 2.4]
	5.072	-0.2 [-2.8-2.0, 1.2]		4.909	0.2 [-2.1-3.8, 1.5]
	9.129	-0.2 [-13.9-3.1, 2.4]		8.836	-0.1 [-14.0-3.6, 2.5]
LURA	3.000	-1.3 [-12.7-13.7, 4.8]	ZIPR	2.965	0.0 [-2.4-2.2, 1.0]
	7.500	-0.6 [-4.4-4.3, 1.9]		7.413	0.3 [-4.7-5.9, 1.7]
	13.500	-0.5 [-14.6-3.7, 2.5]		13.343	0.4 [-14.3-4.0, 2.7]

S.D. = standard deviation, n = 56 for low concentrations, except RISP, where n = 55 (due to coelution with an unknown peak), n = 55 for medium concentrations (one replicate of a duplicate excluded due to a mis-injection), except RISP, where n = 54 (due to coelution with an unknown peak), and n = 56 for high concentrations. t₂ = reinjection time after initial injection.

No data obtained from the blood experiments in Chapter 6 was excluded. This was justified as concentrations for RISP and FLTX were closer to the medium QC than the low QC which demonstrated acceptable (within $\pm 20\%$) autosampler stability.

4.4.2.6 Freeze-thaw stability

Deviations in the response of AMIT, CHLO, CLOZ, HALO, PROC, QUET, and ZIPR when analysed after the third freeze-thaw cycle were within $\pm 10\%$ (Table 4-22). Analytes that deviated within $\pm 15\%$ were ASEN, FLPH, FLTX, PERI, TRIF, and ZUCL; within $\pm 20\%$ were ARIP, MIRT, MOCL; and greater than $\pm 20\%$ were CLOM, DOTH, LURA, and RISP. LURA and RISP were considered to be unstable during freeze-thaw as mean deviations exceeded $\pm 10\%$. For both LURA and RISP, stability in each replicate varied considerably (Table 4-23). In one sample up to 93.7% losses of LURA occurred. Therefore, LURA and RISP cannot be reliably quantified following numerous freeze-thaw cycles. This is an important finding regarding laboratory storage of specimens.

Table 4-22: Analyte stability after three freeze-thaw cycles in preserved whole blood.

Analyte	Mean deviation (%) [Range]	Analyte	Mean deviation (%) [Range]
AMIT	2.6 [-2.3 – 6.4]	LURA	-39.3 [-93.7 – 9.6]
ARIP	-9.7 [-18.6 – 0.0]	MIRT	-3.8 [-18.4 – 5.4]
ASEN	0.3 [-11.1 – 7.0]	MOCL	2.6 [-15.5 – 15.4]
CHLO	-1.0 [-5.5 – 4.0]	PERI	-5.6 [-12.3 – 9.8]
CLOM	-5.8 [-24.2 – 5.2]	PROC	-3.9 [-9.8 – 1.3]
CLOZ	-2.8 [-7.3 – 2.3]	QUET	-3.1 [-5.0 – 1.0]
DOTH	-5.1 [-24.2 – 4.5]	RISP	-13.1 [-29.6 – -2.5]
FLPH	-7.8 [-12.1 – -0.8]	TRIF	-6.5 [-13.4 – -0.7]
FLTX	-4.2 [-11.1 – 3.2]	ZIPR	-3.9 [-8.9 – 2.1]
HALO	-3.1 [-9.2 – 2.6]	ZUCL	-5.6 [-12.7 – 1.7]

Table 4-23: LURA and RISP stability after three freeze-thaw cycles.

Replicate	Deviation (%)	
	LURA	RISP
1	-44.9	-11.0
2	-38.6	-2.5
3	-18.4	-13.0
4	9.6	-12.9
5	-93.7	-29.6
6	-49.5	-9.6

4.4.3 Retention time changes

Following maintenance on the HPLC to regrease the pump pistons retention times shifted (Table 4-24, Figure 4-9, and Figure 4-10).

Table 4-24: Initial and adjusted retention times (RT) for analytes and impurities.

Method A			Method B		
Analyte	Initial RT (min)	Adjusted RT (min)	Analyte	Initial RT (min)	Adjusted RT (min)
CHLO-SO ⁺	11.2	11.0	MOCL	3.3	3.1
PROC-SO ⁺	12.0	11.8	MIRT	4.4	4.0
RISP	12.2	11.6	RISP	7.0	5.8
HB-RISP	12.3	11.6	HB-RISP	7.5	5.8
TRIF-SO ⁺	13.7	11.7	TRIF-SO ⁺	11.4	8.3
CLOZ	13.9	13.1	ZIPR	11.0	8.6
QUET	14.3	13.4	DOTH	14.7	11.7
ASEN	15.0	14.0	AMIT	16.2	14.1
HALO	15.5	14.7	ARIP	17.3	16.2
PERI	15.7	14.9	CLOM	17.9	16.8
PERA	16.6	15.9	LURA	19.1	18.3
AMIT	16.9	16.1	TRIF	19.5	18.7
CHLO	17.6	17.0	LORA	21.6	20.9
PROC	18.5	17.9			
FLPH	18.9	18.3			
FLTX	19.2*	18.6/18.8*			
LORA	21.7	21.1			

⁺Postulated from characteristic UV absorbance spectra; *suspected mix of cis and trans isomers.

The quality control procedures performed in 4.2.1 confirmed that these retention time shifts did not negatively impact quantification of the analytes in their respective methods.

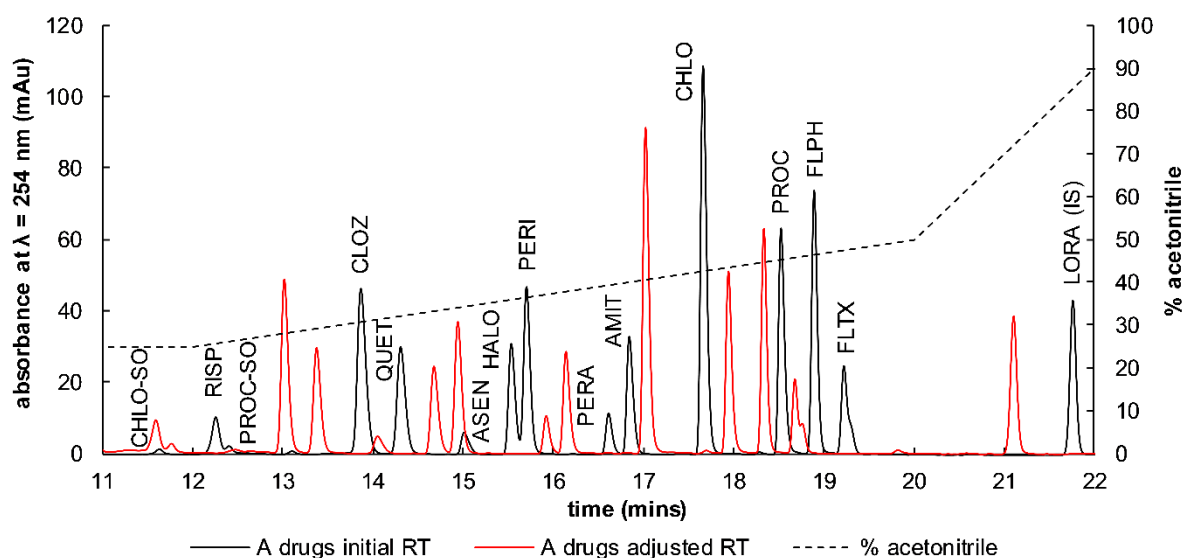


Figure 4-9: Initial and adjusted RT of “A drugs” using Method A.

% of mobile phase consisting of acetonitrile is displayed as secondary axis.

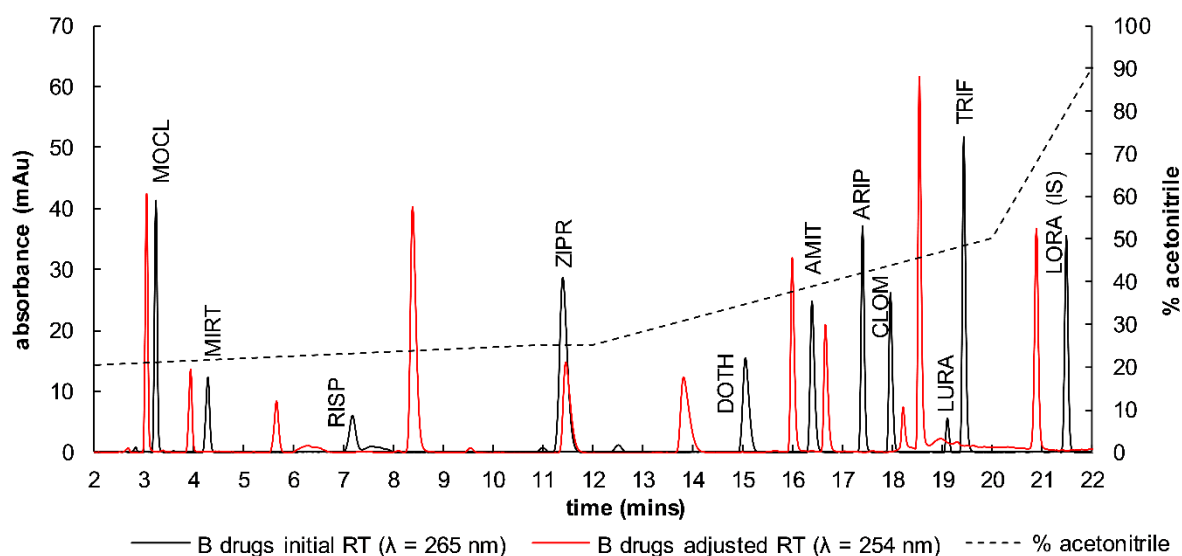


Figure 4-10: Initial and adjusted RT of “B drugs” using Method B.
% of mobile phase consisting of acetonitrile is displayed as secondary axis.

4.4.4 Discussion

Results exceeding the recommended SWGTOX guidelines regarding accuracy and precision were obtained for AMIT, RISP, and LURA on at least one occasion for each analyte [203]. For LURA, validation data was particularly poor on three occasions, but otherwise good inter-day accuracy and precision was achieved. The reason for this behaviour, as well as for LURA’s apparent greater extraction when allowed to remain in diluted blood for an extended time and LURA’s poor freeze-thaw instability, is unknown. Acceptable validation criteria were obtained for all phenothiazine analytes, despite suspecting TRIF-SO formation during unbuffered LLE of TRIF from ante-mortem human whole blood (4.3.4). The likely explanation for this is that the conversion rates of drugs to sulfoxide degradants were similar for both calibrators and QCs during extraction, due to similar extraction conditions.

4.5 Conclusions

LC-DAD methods were developed and validated for the analysis of 13 antipsychotic and 4 antidepressant drugs in human whole blood following unbuffered LLE. Although concerns regarding matrix effects precluded the use of LC-MS techniques for this research liquid chromatography methods using UV as a detection method may also be easily compromised by matrix components interfering with analyte detection. Using ante-mortem human whole blood this was found to be an issue for RISP on one occasion, preventing its quantification in a QC extract. Subsequent experiments detailed in Chapter 6 also found that components in a degrading blood matrix interfered with some other analytes. Despite efforts to separate analytes using a longer run-time, some degradants were also found to coelute with analytes,

necessitating quantification using peak height, and re-analysis of prior validation data to determine the error associated with such quantification.

Steps were taken to minimise the negative impact of extraction instability on the analysis of these drugs through the use of an unbuffered LLE method. AMIS was excluded in the final method due to requiring alkaline extraction and an aqueous reconstitution solvent for analysis which prohibited successful method validation of other drugs, presumably due to solubility issues. Initially, the IS was TRIM. This was changed to LORA following the detection of an impurity that was present in a later PROC stock solution.

Sulfoxide impurities were present in the stock solutions of CHLO and PROC. These sulfoxides were co-extracted by the unbuffered LLE method, which also resulted in the detection of TRIF-SO. This may indicate that the drugs are oxidised during stock solution preparation, in the stock solutions over time, or during extraction. It may also be the case that the sulfoxides are present as impurities in the powdered drug standards. As carrying out the extraction in an anoxic environment was not a practical solution it was accepted that some degree of oxidation may occur. Method validation established this phenomenon did not have a detrimental effect on the quantification of these analytes.

RISP, AMIT, LURA and ZIPR were only partially validated in accordance with suggested guidelines for accuracy and precision [203, 218]. LURA and RISP were also not found to be stable after three freeze-thaw cycles. Nevertheless, LURA and ZIPR were still subsequently included in experiments with the caveat of greater uncertainty regarding their true concentrations.

CHAPTER 5 - DRUG STABILITY IN AQUEOUS SOLUTIONS

5.1 Outline

Complimentary to the investigation of the microbial degradation of drugs, the selected psychoactive drugs investigated in this thesis were also tested for their stability in aqueous solutions. This work was performed to guide degradation product searches in the blood experiments, as hydrolysis reactions are known to occur in blood [223].

Chemicals, materials, and instrumentation were used as listed in Chapter 3. Throughout this chapter MColorpHast™ pH 0-14 Universal Indicator strips (Merck KGaA) (Darmstadt, Germany) were used to determine the required volume of acid or base to add to aqueous solutions to achieve the desired pH and used to test the pH of each solution. Unless otherwise specified, vials and equipment were not sterilised prior to use.

5.2 Monitoring chromophores by UV-Vis spectroscopy

5.2.1 Experimental and instrumentation

To assess the susceptibility of the drugs to hydrolyse, each drug (Figure 4-2 and Figure 4-3) was added to an acidic (pH = 1), neutral, and alkaline (pH = 11) solution. Each solution contained water (3 mL), for the acidic solution, HCl (100 µL, 32 % w/v) and for the alkaline solution, aqueous NH₃ (100 µL, 30 % w/v). In addition to the drugs of interest, whose stability was under investigation, control drugs AMIT (inter-aliquot standard) and RISP (microbe control) were also tested, as well as the ISs TRIM and LORA.

UV spectra were collected between 220 to 370 nm at a rate of 300 nm/min and a data interval of 0.5 nm, using a Varian Cary 50 Bio UV-Visible Spectrophotometer (Varian, Palo Alto, California, USA) in conjunction with the Scan application (software version: 3.00 (182)). Brand UV-macro cuvettes (Sigma-Aldrich) were used and spectra baseline corrected to the cuvette absorbance with water. The acidic, neutral, and alkaline solutions without any drugs added were scanned at the analysed wavelengths and found to give no absorbance. Data were collected every hour for the first 3 hours after mixing, then at 5, 7, 243 or 245 hours, and 648 hours (27 days). The experiments were performed at room temperature, with samples stored away from light between analysis.

Drugs were considered to degrade if there was a reduction in signal absorbance over time or if there were shifts in the maximum wavelengths of absorbance.

5.2.2 Results

The nine drugs whose chromophores were found to be stable over time in all aqueous solutions were ZUCL, QUET, AMIT, RISP, MOCL, MIRT, FLTX, and CLOZ. All drugs were stable in acidic solution after 7 to 24 hours (Table 5-1).

Table 5-1: Summary of UV-Vis spectroscopy results.

Analyte	Stability after 7 hr / 10 d / ~27 d			Analyte	Stability after 24 hr		
	pH=1	pH=7	pH=11		pH=1	pH=7	pH=11
CHLO	✓	✓/✗/✗	✗	ARIP	✓	✗	✗
FLPH	✓/✗/✗	✓/✗/✗	✓/✓/✗	MOCL	✓	✓	✓
PERI	✓/✗/✗	✓/✓/✗	✓/✗/✗	MIRT	✓	✓	✓
PROC	✓	✗	✗	LURA	✓	✗✗	✗✗
PROM	✓/✗/✗	✓	✓/✓/✗	LORA	✓	✗	✗
TRIF	✓/✓/✗	✓/✗/✗	✗	HALO	✓	✗✗	✗✗
ZUCL	✓	✓	✓	FLTX	✓	✓	✓
QUET	✓	✓	✓	DOTH	✓	✗	✗
ZIPR	✓	✗✗	✗✗	CLOZ	✓	✓	✓
AMIT	✓	✓	✓	CLOM	✓	✗✗	✗✗
RISP	✓	✓	✓	ASEN	✓	✗	✗
TRIM	✓/✗/✗	✗	✗				

✓ = no change in signal intensity of wavelength maxima, ✗ = reduction in signal intensity of wavelength maxima, ✗✗ = notable reduction in signal intensity and/or shift in wavelength maxima.

Reduction in signal intensity was observed for some drugs after the extended time of 10 and 27 days. The drugs that were unstable in neutral solution, CHLO, FLPH, PROC, THIO, ZIPR, ARIP, LURA, LORA, HALO, DOTH, CLOM, and ASEN, were also unstable in alkaline solution. HALO and CLOM demonstrated a rapid decrease in absorbance at their wavelengths of maximum absorbance (Figure 5-1 and Figure 5-2). For the two 1,2-benzisothiazolepiperazines, ZIPR and LURA, their wavelengths of maximum absorbance were no longer present in neutral solution (Figure 5-3 (a) and Figure 5-4 (b)). This was also apparent for LURA in alkaline solution. Alkaline solutions of ZIPR demonstrated a blue shift of the wavelength maxima over time.

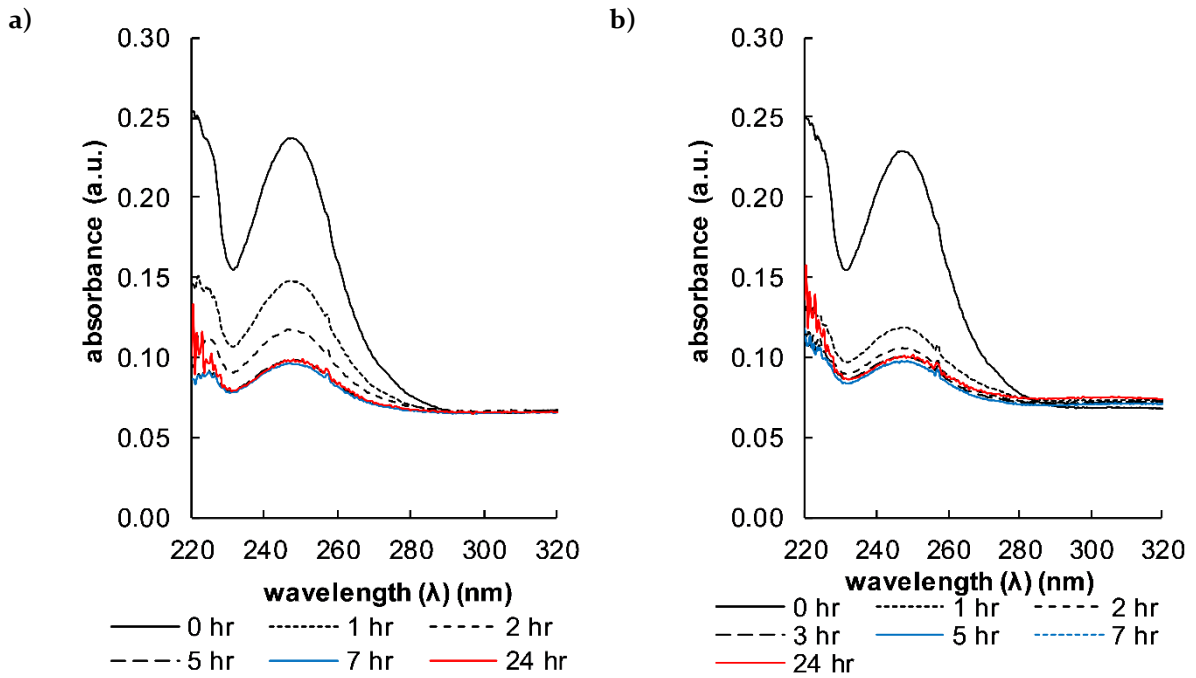


Figure 5-1: UV spectra of HALO over time in a) pH = 7 solution and b) pH = 11 solution.

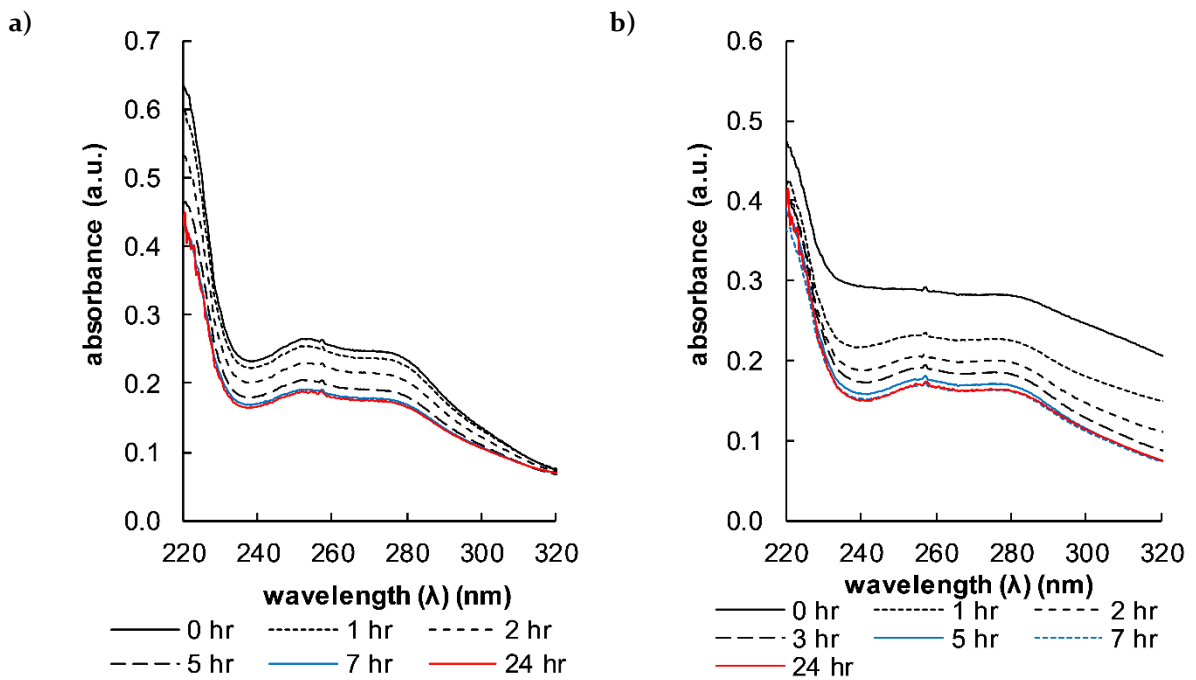


Figure 5-2: UV spectra of CLOM over time in a) pH = 7 solution and b) pH = 11 solution.

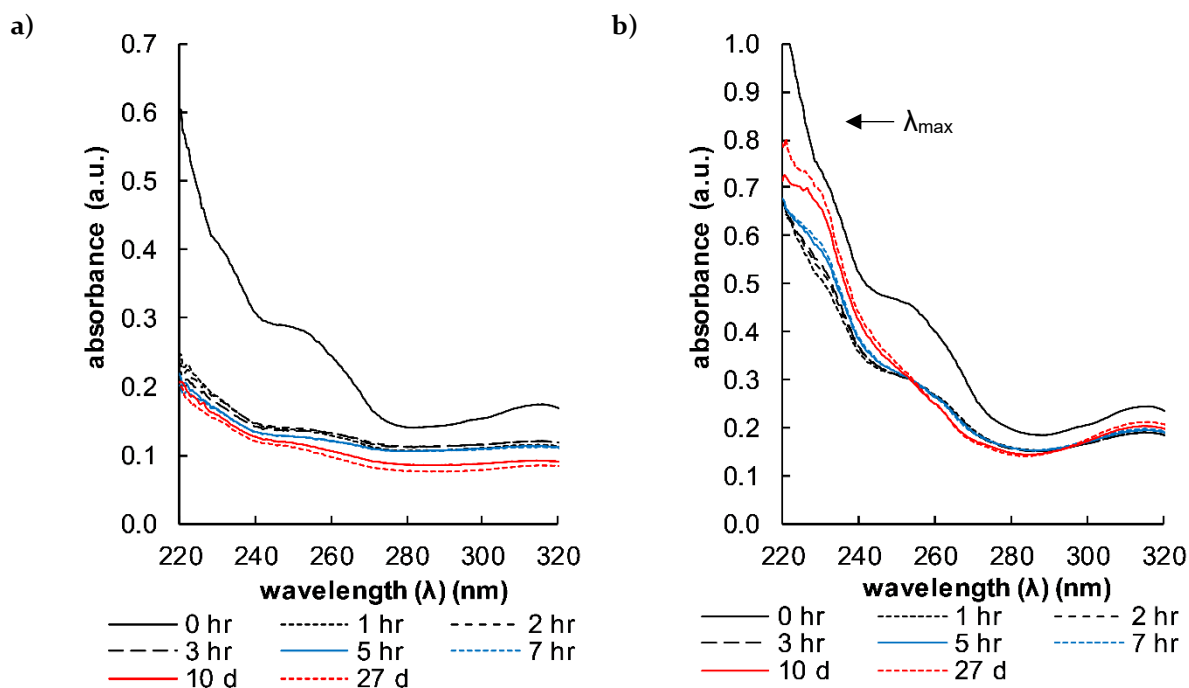


Figure 5-3: UV spectra of ZIPR over time in a) pH = 7 solution and b) pH = 11 solution.

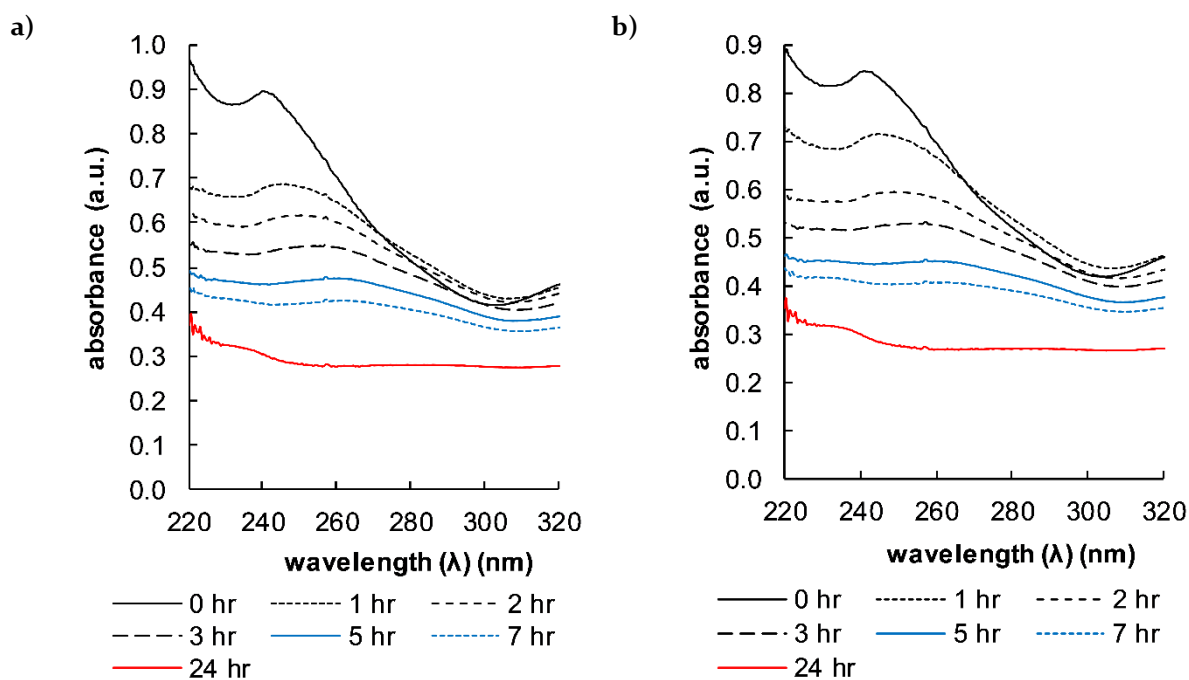


Figure 5-4: UV spectra of LURA over time in a) pH = 7 solution and b) pH = 11 solution.

The UV-Vis monitoring of drug degradation was informative regarding the degradation of the drugs into compounds with differing chromophores. However, if drug degradation does not occur at the chromophore, or does not alter the conjugated system of the parent drug, the UV-

Vis spectra may not change. Therefore, chromatographic techniques were subsequently utilised to investigate their degradation.

5.3 LC-DAD monitoring of hydrolysis

5.3.1 Experimental

Each drug, as part of set A or set B (Table 5-2), was added to an acidic (pH = 3), neutral, and alkaline (pH = 10) solution in triplicate. Control acidic, neutral, and alkaline solutions were simultaneously prepared. Organic solvent was removed from combined working solutions by evaporation under N₂ at 40 °C prior to the addition of water with vortexing. pH adjustment was achieved using HCl (15 µL, 0.18 M) and aqueous NH₃ (30 µL, 30 % w/v) for the acidic and alkaline solutions, respectively. Each solution contained water to make up a total volume of 1 mL. After mixing, samples were transferred into clear glass vials and stored in the LC-DAD autosampler at room temperature.

Table 5-2: Drugs in the Set A and Set B solutions.

Set A	AMIS	RISP	CLOZ	QUET	HALO	TRIM	AMIT	ARIP	PROC
Set B	AMIS	ZIPR	ASEN	PERI	CHLO	ZUCL	FLTX	TRIF	

Previous experiments indicated AMIS may be stable (data not shown, see Table 5-3 for intra-experiment validation) under the three conditions to be trialled and thus it was added to both sets to be used as an internal control to monitor the degradation of the other analytes.

Using HPLC Method A as described in Chapter 4 (chromatogram displayed in Figure 4-2) analysis was carried out after mixing, then approximately every three hours for eight measurements, and then after 5 days (120 hours). Relative changes to the peak area of analytes compared to AMIS, and the formation of additional peaks over time were noted. Relative response changes greater than 20 % across all replicates were considered indicative of degradation.

5.3.2 Results

AMIS was stable in all conditions as expected (Table 5-3). Results for other drugs are summarised in Table 5-4.

Table 5-3: AMIS signal changes (%) after ~5 days at room temperature.

Set A			Set B		
pH			pH		
3	7	10	3	7	10
100.3 ± 0.6	100.1 ± 0.8	98.9 ± 0.2	100.0 ± 1.0	99.8 ± 0.7	99.2 ± 0.5

Error is ± S.D., n = 3.

Table 5-4: Summary of analyte aqueous stability after 5 days at room temperature determined during LC-DAD monitoring experiment.

Analyte	pH			Analyte	pH		
	3	7	10		3	7	10
RISP	✓	✓	✓	ZIPR	✓	✓	✖✖ (1/3) ✖✖✖ (2/3)
CLOZ	✓	✓	✖	ASEN	✓	✓	✓
QUET	✓	✓	✓	PERI	✓	✓	✓
HALO	✓	✓	✖✖ (1/3) ✖✖✖ (2/3)	CHLO	✓	✓	✓
TRIM	✓	✓	✖	ZUCL	✓	✓	✓
AMIT	✓	✓	✖✖	FLTX	✓	✓	✓
ARIP	✓	✓ (1/3) ✖✖ (2/3)	✖	TRIF	✓	✓	✓
PROC	✓	✓	✖				
FLPH	✓	✓	✖				

✓ = stable, ✖ = unstable (> 20 % relative response change), ✖✖ = (> 50 % relative response change), ✖✖✖ = (> 80 % relative response change). (1/3) = one of three replicates; (2/3) = two of three replicates.

ZIPR and HALO did not appear to degrade in neutral solution. However, in the UV-Vis monitoring experiment a considerable reduction in signal intensity for HALO and ZIPR was observed within 7 hours (Figure 5-1 (a) and Figure 5-3 (a)). TRIM, PROC, and FLPH also did not appear to degrade in neutral solution, where reductions in signal intensity of wavelength maxima were observed in the UV-Vis monitoring experiment. Other drugs with losses less than 20 % in the LC-DAD experiment but reductions in signal intensity noted during the UV-Vis monitoring experiment were ASEN, PERI and CHLO. CLOZ and AMIT appeared stable by the UV-Vis monitoring experiment. However, in the LC-DAD experiment losses were greater than 20 % and 50 % in alkaline conditions for CLOZ and AMIT, respectively. This may be explained by degradation at a site other than their chromophores, however no degradation products were detected. ARIP, ZUCL, and FLTX results were consistent with the UV-Vis monitoring experiment.

ARIP relative response decreases in neutral solution were in two replicates ~80 % and in one replicate there was no decrease (Figure 5-5). Given the absence of any degradation in one

replicate it was considered that two of the three replicates may have been contaminated with an environmental microorganism that may degrade ARIP. No degradation of ARIP was apparent in a repeat experiment, in which amber vials were sterilised prior to preparing the solutions (Figure 5-5). Possible microbial degradation of ARIP in human whole blood was subsequently assessed in experiments performed in Chapter 6.

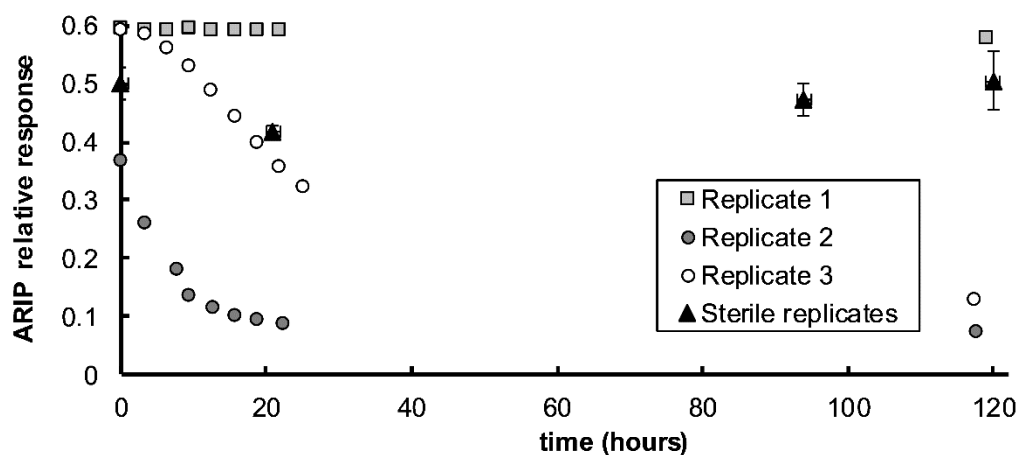


Figure 5-5: ARIP degradation in neutral aqueous solution over time.

Non-sterile, transparent vials (Replicates 1-3) and sterile, amber vials (error bars are S.D., $n = 3$, except for at 120 hrs where $n = 2$).

ZUCL was found to inter-convert between the *cis* and *trans* isomers in one replicate of the alkaline solution. Initially, the ratio of the earlier eluting ZUCL isomer to the later eluting isomer was 0.16 and after ~5 days was observed to be 0.85. Interestingly, *in vitro* *cis/trans* isomerisation has previously been reported to occur for ZUCL in post-mortem blood [423].

5.4 Ziprasidone and lurasidone hydrolysis

5.4.1 Experimental

The stability of ZIPR and LURA in aqueous solutions was investigated using the LC-DAD Method B detailed in Chapter 4. Based on the observed stability of AMIT and CLOZ during UV-Vis monitoring of their chromophores they were considered candidates as internal controls.

AMIT and CLOZ were added to acidic ($\text{pH} = 3$), neutral, and alkaline ($\text{pH} = 10$) solutions in triplicate in sterile 2.5 mL Eppendorf tubes. Control acidic, neutral, and alkaline solutions were simultaneously prepared. pH adjustment was achieved using HCl (15 μL , 0.18 M) and aqueous NH_3 (15 μL , 30 % w/v) for the acidic and alkaline solutions, respectively. Each solution contained water to make up a total volume of 0.5 mL. The concentration of AMIT and CLOZ in these solutions was ~32 $\mu\text{g/mL}$.

These solutions were then further diluted by aliquoting 50 μL into autosampler vials and diluting using HCl (150 μL , 0.025 M), water (150 μL), and aqueous NH_3 (150 μL , 7.5 % w/v), for acidic, neutral, and alkaline conditions, respectively. Final drug concentrations were ~ 6.4 $\mu\text{g}/\text{mL}$. These solutions were then analysed using HPLC Method A at time zero, after 24 hours, after 48 hours, and after 75 hours. Due to a mis-injection, data for one replicate at T0 for the alkaline solution of AMIT and CLOZ was not obtained. Therefore, only duplicate results are reported for the alkaline samples.

AMIT was suitable for use as a control in neutral and alkaline solutions for up to 75 hours based on static response changes over time (Table 5-5). This was of greater duration than the time in which ZIPR and LURA were observed to degrade by UV-Vis monitoring of their chromophores (Table 5-1).

Table 5-5: Summary of AMIT stability over 75 hours in aqueous solutions analysed by LC-DAD HPLC Method A.

time (hours)	AMIT relative to CLOZ response change (%)			AMIT absolute signal change (%)		
	pH			pH		
	3	7	11	3	7	11
24	104.0 \pm 1.0	100.0 \pm 0.3	100.4 \pm 0.3	111.8 \pm 5.6	105.3 \pm 3.8	101.6 \pm 0.5
48	105.5 \pm 0.8	98.8 \pm 0.7	100.4 \pm 0.3	114.2 \pm 6.0	104.6 \pm 4.8	100.8 \pm 0.8
75	117.8 \pm 1.4	98.1 \pm 0.9	99.2 \pm 1.2	116.3 \pm 5.8	103.4 \pm 4.0	100.2 \pm 0.3

Error is \pm S.D., n = 3, except for pH = 11 where n = 2.

AMIT and ZIPR or LURA were prepared as indicated above for AMIT and CLOZ in acidic, neutral, and alkaline solutions, and subsequently diluted in autosampler vials for analysis using HPLC Method B. In the autosampler vials concentrations were ~ 6.4 $\mu\text{g}/\text{mL}$ for AMIT, ~ 9.6 $\mu\text{g}/\text{mL}$ for ZIPR, and ~ 12 $\mu\text{g}/\text{mL}$ for LURA. Analysis was performed at time zero, after 6 hours, and after 24 hours.

5.4.2 Results

Results were consistent with the UV-Vis monitoring experiment, indicating that ZIPR and LURA both degrade in neutral and alkaline conditions after 24 hours (Table 5-6). Degradation was most pronounced for ZIPR, which in alkaline solutions produced degradation products detected by the LC-DAD method at time zero (Figure 5-6). The detection of degradation products at different retention times to ZIPR and with different UV-Vis spectra was expected, given the shift in wavelength maxima observed in alkaline solutions of ZIPR during the UV-Vis monitoring experiment (Figure 5-3 (b)). No additional chromatographic peaks were observed in neutral solutions of ZIPR. No additional peaks were observed to form as LURA degraded, consistent

with the apparent elimination of absorption maxima observed in neutral and alkaline solutions of LURA during the UV-Vis monitoring experiment (Figure 5-4).

These neutral and alkaline solutions of LURA and ZIPR were subsequently analysed by LC-QTOF-MS (see 5.5), using the instrumentation and method detailed in 3.3.2.

Table 5-6: Summary of ZIPR and LURA stability over 24 hours in aqueous solutions analysed by LC-DAD HPLC Method B.

	pH		
	3	7	11
time (hours)	ZIPR absolute signal change (%)	ZIPR relative to AMIT response change (%)	
6	97.3 ± 1.8	43.0 ± 14.8	36.2 ± 12.0
24	96.6 ± 2.1	43.1 ± 13.0	9.8 ± 2.0
time (hours)	LURA absolute signal change (%)	LURA relative to AMIT response change (%)	
6	98.3 ± 2.1	95.5 ± 6.2	90.0 ± 15.0
24	93.7 ± 3.8	84.2 ± 4.8	74.2 ± 15.6

Error is ± S.D., n = 3.

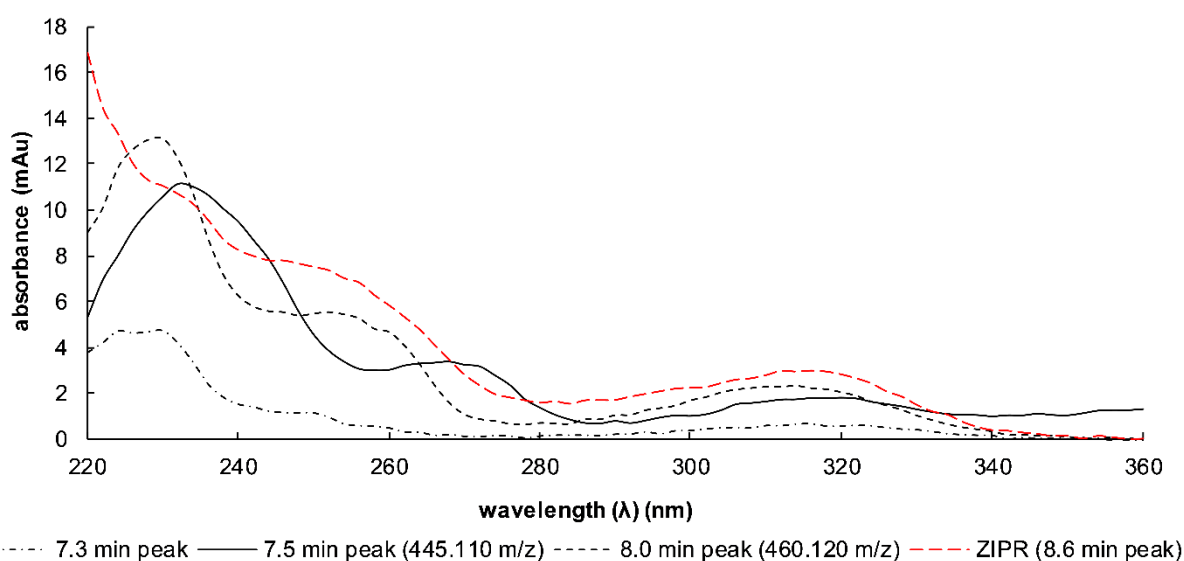


Figure 5-6: UV-Vis spectra of ZIPR and alkaline degradation products.

The compounds eluting at 7.5 and 8.0 min were identified by manual fraction collection from the LC-DAD and subsequent LC-QTOF-MS analysis (see 5.5).

5.5 Qualitative LC-QTOF-MS analysis

5.5.1 Experimental

All drugs investigated in this thesis (1.4.4) and AMIT, RISP, ZUCL, and LORA, were added to individual acidic (pH = 3), neutral, and alkaline (pH = 11) solutions. Each solution contained water (3 mL), for the acidic solution HCl (100 µL, 32 % w/v), and for the alkaline solution

aqueous NH₃ (100 µL, 30 % w/v). Final drug concentrations ranged from 3-5 µg/mL. Blank solutions without drugs were also prepared. An Agilent 1200 Series HPLC and Agilent 6520 Series LC-QTOF-MS (3.3.2) was used to analyse the samples qualitatively after storing them for 7 days at room temperature. This time was chosen based on observed degradation when monitoring chromophores by UV-Vis (5.2.2). Drug stocks were also diluted with ethanol and analysed.

Extracted ion chromatograms (EICs) were obtained for known analytes using their calculated accurate masses for their precursor ions (Table 5-7). Agilent MassHunter software was used to generate molecular formulae for precursor ions. Analyte identity was verified by comparison to known retention times using the method and established MS/MS fragmentation patterns, and comparison to the FSSA in-house database.

Table 5-7: LC-QTOF-MS data for analytes.

Analyte	Retention time (min)	Measured precursor ion (m/z)	Calculated precursor ion (m/z)	GMF precursor ion	Mass accuracy (δ) (ppm)	Mass accuracy (δ) (mDa)
MOCL	4.30	269.1058	269.1051	[C ₁₃ H ₁₇ ClN ₂ O ₂]H ⁺	-2.6	-0.7
MIRT	4.58	266.1658	266.1651	[C ₁₇ H ₁₉ N ₃]H ⁺	-2.6	-0.7
RISP	5.86	411.2196	411.2191	[C ₂₃ H ₂₇ FN ₄ O ₂]H ⁺	-1.2	-0.5
CLOZ	6.07	327.1373	327.1371	[C ₁₈ H ₁₉ ClN ₄]H ⁺	-0.6	-0.2
QUET	6.67	384.1737	384.1740	[C ₂₁ H ₂₅ N ₃ O ₂ S]H ⁺	0.8	0.3
ZIPR	6.92	413.1211	413.1197	[C ₂₁ H ₂₁ ClN ₄ OS]H ⁺	-3.4	-1.4
ASEN	7.57	286.1006	286.0993	[C ₁₇ H ₁₆ ClNO]H ⁺	-4.5	-1.3
HALO	7.57	376.1481	376.1474	[C ₂₁ H ₂₃ ClFNO ₂]H ⁺	-1.9	-0.7
PERI	7.57	366.1636	366.1635	[C ₂₁ H ₂₃ N ₃ OS]H ⁺	-0.3	-0.1
DOTH	7.95	296.1472	296.1468	[C ₁₉ H ₂₁ NS]H ⁺	-1.4	-0.4
ARIP	8.17	448.1531	448.1553	[C ₂₃ H ₂₇ Cl ₂ N ₃ O ₂]H ⁺	4.9	2.2
AMIT	8.35	278.1910	278.1903	[C ₂₀ H ₂₃ N]H ⁺	-2.5	-0.7
ZUCL	8.50	401.1455	401.1449	[C ₂₂ H ₂₅ ClN ₂ OS]H ⁺	-1.5	-0.6
PROC	8.51	374.1460	374.1452	[C ₂₀ H ₂₄ ClN ₃ S]H ⁺	-2.1	-0.8
LORA	8.74	383.1518	383.1521	[C ₂₂ H ₂₃ ClN ₂ O ₂]H ⁺	0.8	0.3
CHLO	8.77	319.1031	319.1030	[C ₁₇ H ₁₉ ClN ₂ S]H ⁺	-0.3	-0.1
FLPH	8.80	438.1824	438.1821	[C ₂₂ H ₂₆ F ₃ N ₃ OS]H ⁺	-0.7	-0.3
CLOM	8.98	315.1628	315.1623	[C ₁₉ H ₂₃ ClN ₂]H ⁺	-1.6	-0.5
FLTX	9.10	435.1712	435.1713	[C ₂₃ H ₂₅ F ₃ N ₂ OS]H ⁺	0.2	0.1
TRIF	9.20	408.1724	408.1716	[C ₂₁ H ₂₄ F ₃ N ₃ S]H ⁺	-2.0	-0.8
LURA	9.20	493.2645	493.2631	[C ₂₈ H ₃₆ N ₄ O ₂ S]H ⁺	-2.8	-1.4

GMF = generated molecular formula. Mass accuracies determined from single injection.

Initial screening for degradation products involved interrogation of the base peak chromatogram (BPC) across the 100-1000 m/z range. Following this, Molecular Feature Extraction (MFE) was used. MFE identifies precursor ions that are likely from a compound

present above a threshold ion count with co-eluting ions related to that precursor ion (e.g. isotopes, sodium or potassium adducts, dimers). Data were filtered to display compounds with a height greater than 2000 counts and these compounds examined to determine if they may be degradants of the parent drugs. Only compounds not detected in drug stocks are reported.

5.5.2 Results

Drugs for which no degradation products were identified in aqueous solutions were: CLOZ, MOCL, QUET, MIRT, HALO, RISP, ARIP, ZUCL, FLTX, and LORA. The succinimide hydrolysed degradant of LURA reported to form under alkaline hydrolysis by Kumar Talluri *et al.* was detected [432]. A precursor ion of m/z 335.0982 and generated molecular formula (GMF) $[C_{17}H_{19}ClN_2OS]H^+$ (calculated: 335.0979 m/z , $\delta = -0.9$ ppm (-0.3 mDa)) was detected in all solutions of CHLO. The m/z of this compound was 15.9951 m/z greater than CHLO, indicating the presence of an additional oxygen atom compared to CHLO (calculated mass of oxygen atom: 15.9949 Da, $\delta = -0.2$ mDa). However, due to the low response for this compound the fragments in the MS/MS spectra could not be identified. It is possible the compound is CHLO-SO. It is also suspected that the sulfoxides of TRIF and PROC were detected in TRIF and PROC solutions, however, the same precursor ions were also present in the respective drug stocks.

A compound giving a precursor ion of m/z 384.1747 and GMF $[C_{21}H_{25}N_3O_2S]H^+$ (calculated: 384.1740 m/z , $\delta = -1.8$ ppm (-0.7 mDa)) was detected in the alkaline PERI solution (Figure 5-7). This compound was tentatively identified as an amide (PERI-AMD, see Figure 5-8 for the proposed structure), arising *via* hydrolysis of the nitrile moiety of PERI. This identification was based on: the 98.096, 114.090, and 142.122 m/z product ions in common with PERI indicating no degradation on the alkyl chain of PERI; the m/z difference of 18.0111 between precursor ions indicating addition of two hydrogen atoms and one oxygen atom to PERI (calculated mass of H_2O : 18.0106 Da, $\delta = -0.5$ mDa); and absence of the 237.0487 m/z product ion characteristic of the aryl-cyanide-substituted-phenothiazine moiety of PERI (Figure 5-9 and Table 5-8).

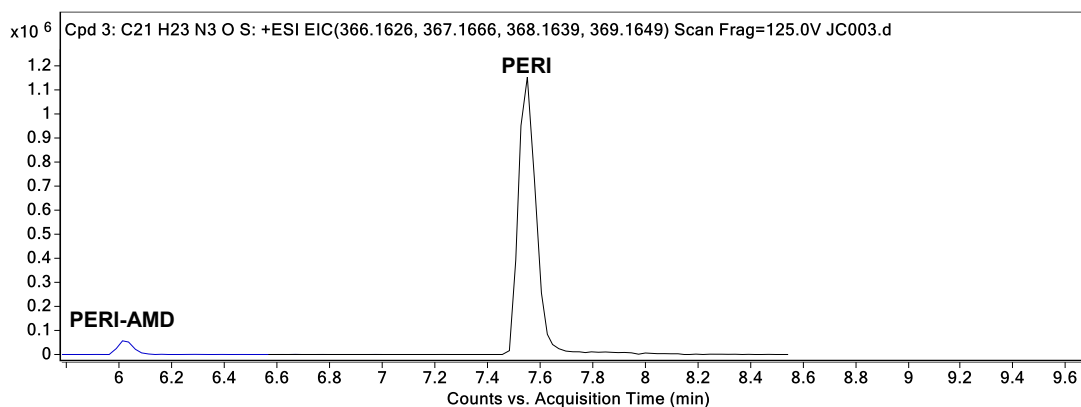


Figure 5-7: Extracted ion chromatograms for PERI and PERI-AMD.

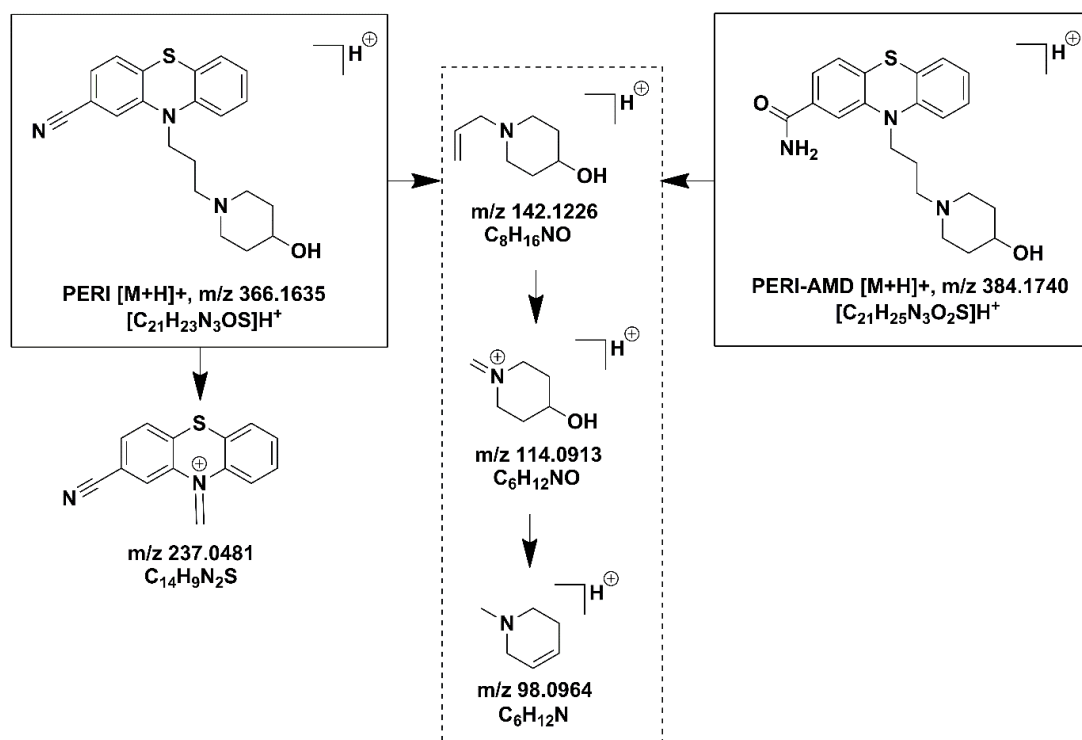


Figure 5-8: Proposed fragmentation pathway for PERI and PERI-AMD.

Fragments in common with PERI and PERI-AMD indicated by dotted-line box; m/z are calculated accurate mass/charge values.

Table 5-8: MS/MS data for PERI and PERI-AMD.

Analyte	Precursor ion (m/z)	Product ions (m/z)	GMF product ions	Calculated accurate mass (m/z)	Mass accuracy (δ) (ppm)	Mass accuracy (δ) (mDa)
PERI	366.1636	98.0960	C ₆ H ₁₂ N	98.0964	4.1	0.4
		114.0904	C ₆ H ₁₂ NO	114.0913	7.9	0.9
		142.1214	C ₈ H ₁₆ NO	142.1226	8.4	1.2
		237.0487	C ₁₄ H ₉ N ₂ S	237.0481	-2.5	-0.6
		366.1627	[C ₂₁ H ₂₃ N ₃ OS]H ⁺	366.1635	2.2	0.8
PERI-AMD	384.1747	98.0980	C ₆ H ₁₂ N	98.0964	-16.3	-1.6
		114.0898	C ₆ H ₁₂ NO	114.0913	13.1	1.5
		142.1236	C ₈ H ₁₆ NO	142.1226	-7.0	-1.0
		255.0450	C ₁₄ H ₁₁ N ₂ OS	255.0587	53.7	13.7
		384.1742	[C ₂₁ H ₂₅ N ₃ O ₂ S]H ⁺	384.1740	-0.5	-0.2

GMF = generated molecular formula. Mass accuracies determined from single injection.

The poor mass accuracy for the GMF of the 255.0450 m/z product ion of PERI-AMD may be due to low MS/MS response (Figure 5-9 (b)).

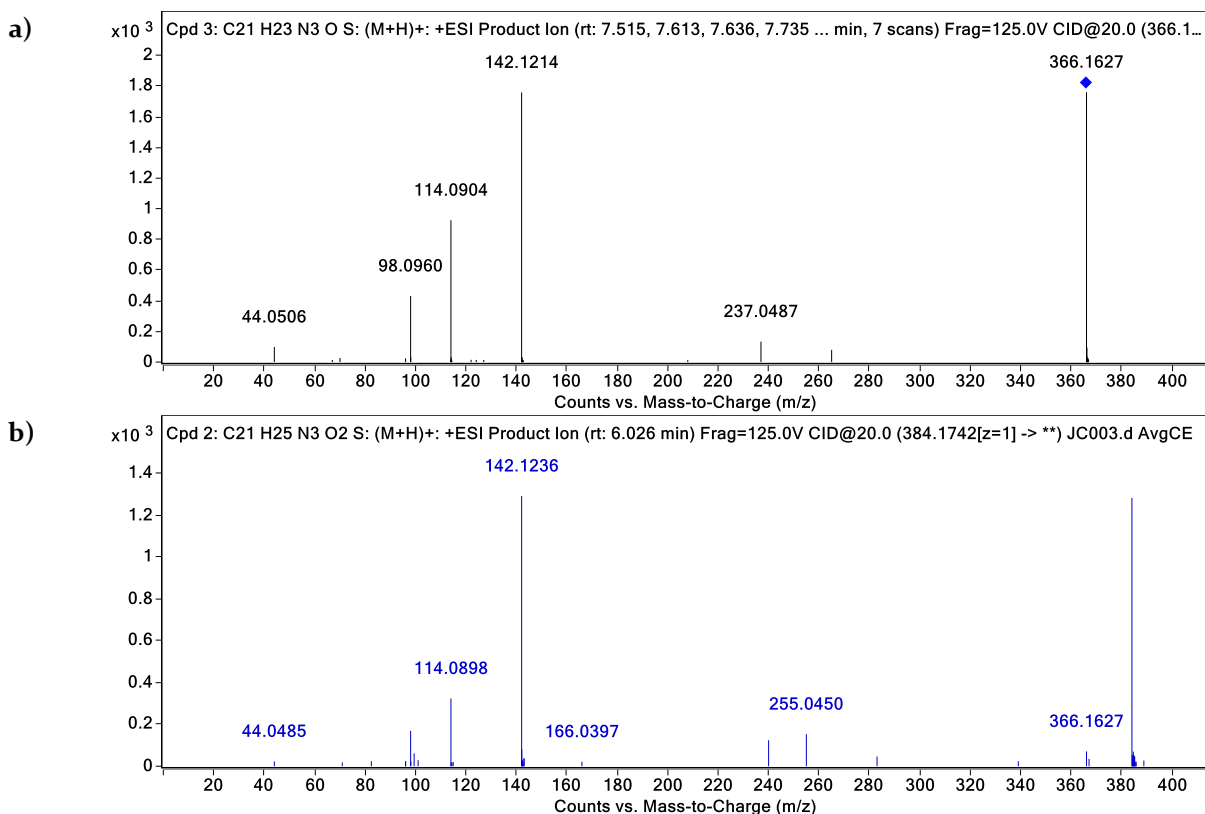


Figure 5-9: MS/MS spectra for a) PERI and b) PERI-AMD. Collision energy = 20 eV.

Numerous precursor ions were detected in alkaline ZIPR solutions that were possible alkaline degradation products (Figure 5-10). For these degradants, GMF were in good agreement with the observed masses and the isotope patterns observed in the MS spectra and indicated that chlorine atom(s) were present. The UV-Vis spectra of two of the four degradants were identified by manual fraction collection of LC-DAD Method B extracts from the LC-DAD ZIPR hydrolysis experiment followed by LC-QTOF-MS analysis. The delay between detector response and elution of a crystal violet dye solution out of the waste tubing was taken into consideration when manually collecting fractions.

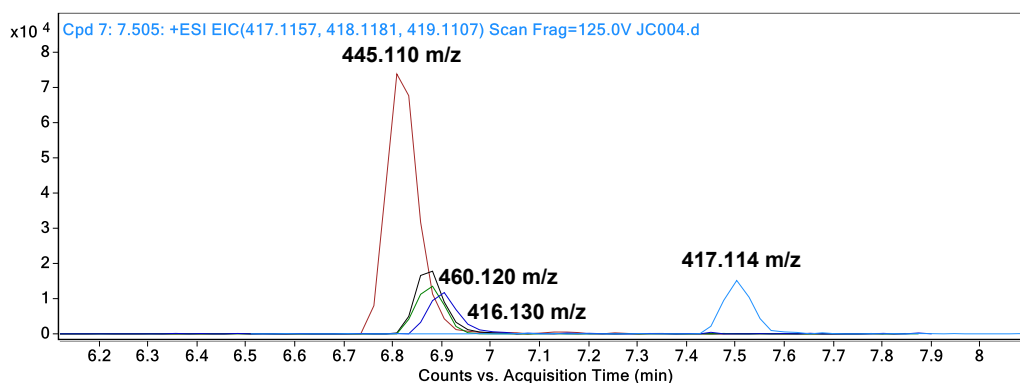


Figure 5-10: Extracted ion chromatograms of ZIPR (black) and ZIPR alkaline hydrolysis products (coloured).

Table 5-9: MS data for ZIPR and alkaline hydrolysis degradants.

Analyte	Measured [M+H] ⁺ (m/z)	Calculated [M+H] ⁺ (m/z)	GMF precursor ion	Mass accuracy (δ) (ppm)	Mass accuracy (δ) (mDa)
ZIPR	413.1190	413.1197	[C ₂₁ H ₂₁ ClN ₄ OS]H ⁺	1.7	0.7
416.130 m/z	416.1288	416.1306	[C ₂₀ H ₂₂ ClN ₅ OS]H ⁺	4.3	1.8
417.114 m/z	417.1138	417.1147	[C ₂₀ H ₂₁ ClN ₄ O ₂ S]H ⁺	2.2	0.9
445.110 m/z	445.1095	445.1096	[C₂₁H₂₁ClN₄O₃S]H⁺	0.2	0.1
460.120 m/z	460.1199	460.1205	[C₂₁H₂₂ClN₅O₃S]H⁺	1.3	0.6

GMF = generated molecular formulae. Analytes in bold were detected in LC-DAD Method B also (Figure 5-6). Mass accuracies determined from single injection.

5.6 Conclusions

The aim of the experiments in this chapter was to examine the stability of drugs in simple acidic and alkaline aqueous solutions before examination of their stability in blood (Chapter 6). All drugs were stable in acidic solutions. The drugs CLOM, HALO, LURA, and ZIPR were particularly unstable in neutral and alkaline solutions. This is of relevance to the extraction of these drugs from blood, as a neutral or alkaline environment is required to increase their solubility in organic solvents. A neutral extraction method was selected due to the greater stability of ZIPR in neutral solution.

By LC-QTOF-MS analysis, 4 major alkaline degradation products were detected for ZIPR and 1 for PERI. The identity of the ZIPR degradants is unclear. For PERI, the degradation product was tentatively identified as an amide-derivative, formed by simple hydrolysis of the nitrile moiety. This compound has not been reported before as a hydrolysis degradation product of PERI. The precursor ions corresponding to these degradation products were subsequently targeted in LC-QTOF-MS analysis of extracts from the blood experiments to determine if they may be present and therefore if these drugs may hydrolyse in human whole blood.

CHAPTER 6 - DRUG STABILITY IN HUMAN WHOLE BLOOD

6.1 Outline

The stability of 17 psychoactive drugs was investigated in human whole blood with and without faecal microorganisms and preservatives across a temperature range of -20 °C to 37 °C. Experimentation using non-inoculated controls and preserved specimens for all incubation temperatures was necessary to assess whether microbial activity in inoculated, unpreserved specimens may be the cause of any observed drug degradation. The preservatives added were equivalent to those used in post-mortem toxicology specimens. The extraction method and validated LC-DAD methods (see Chapter 4) were used to analyse specimens.

Human faecal microorganisms were selected to simulate a post-mortem blood microbial community, due to the abundance of anaerobic species in faeces [238, 239, 241] and the translocation of gut microorganisms into the bloodstream after death [15]. The identity of the microorganisms inoculated and dominating blood specimens was determined by 16S rRNA sequencing. Colour changes observed during the experiments were investigated by UV-Vis spectrophotometry.

6.1.1 Instrumentation

An Agilent 1100 Series HPLC-DAD and Agilent 1200 Series HPLC with Agilent 6520 LC-QTOF-MS in auto-MS/MS mode were used as detailed in 3.3.

6.1.2 Materials

Chemicals and materials were used as listed in Chapter 3. Ante-mortem human whole blood and faeces were sourced as detailed in 3.2.2. Microorganism cultures were obtained and prepared for use as described in 3.2.2.3. Drug standards and drug solutions were obtained and prepared as specified in 3.1.2.

6.2 Overview of experiments

6.2.1 Study design

The experimental design for all blood experiments consisted of matrix controls, non-inoculated control specimens, and inoculated drug specimens (Table 6-1). Inoculated specimens (#2-3, #6-7) were inoculated with microorganisms from the mixed faecal microbiota transplant (FMT)

specimens (3.2.2.2). Sodium fluoride (2 % w/v) was used as a preservative for preserved specimens (#3, #5, #7).

Table 6-1: Blood experiments specimen types overview.

Specimen type:	Blood matrix	Microbial matrix		Non-inoculated drug controls		Inoculated drug specimens	
<i>Specimen #</i>	<i>1</i>	<i>2</i>	<i>3</i>	<i>4</i>	<i>5</i>	<i>6</i>	<i>7</i>
Microorganisms		✓	✓			✓	✓
Preservatives*			✓		✓		✓
Drugs				✓	✓	✓	✓

*Preserved with 2 % w/v NaF.

Initially, week-long experiments were performed for each drug set (A or B, Table 4-9). These specimens were incubated at 37 °C in the dark. Although microorganisms have variable optimum growth temperatures [13] it was expected that the microorganisms in faeces would have an optimum growth temperature approximating the temperature of the human body. This temperature was therefore chosen to assess drug stability in an environment where endogenous microbial activity may be greatest and therefore maximise the possibility of determining whether the drugs may be microbially degraded. This temperature also corresponds to summertime temperatures across much of Australia.

Following this, longer experiments were performed to determine drug stability at -20 °C, 4 °C, and room temperature for a time period of 7-12 months. These experiments had potassium oxalate monohydrate added (0.2 % w/v) as an anticoagulant. These temperatures are more reflective of what post-mortem blood may be exposed to during autopsy, specimen receipt/handling, and specimen/cadaver storage. The formation of different microbial degradation products of drugs at these temperatures compared to 37 °C experiments is a theoretical possibility, due to the cooler environments favouring the growth of different microorganisms and differences in the xenobiotic metabolism of different microorganisms. It is also possible that extracellular microbial enzymes may remain active at lower temperatures [433].

Freezing temperatures, such as -20 °C, are generally considered to inhibit bacterial growth and so minimal microbial degradation of drugs at this temperature was hypothesised [283]. Nevertheless, it is necessary to know the long-term stability of drugs at refrigerated and frozen temperatures in case reanalysis of specimens is required. Previous studies have indicated that degradation rates of some organic molecules may be greater in frozen rather than liquid states [291, 434, 435]. Greater degradation of analytes stored in frozen specimens may be partially attributed to repeated freeze-thaw cycles.

Inoculated drug specimens and non-inoculated drug controls were prepared in triplicate for all experiments. Microbial matrix and blood matrix controls were prepared in singlicate for experiment WA and YA (week-long, A-drugs = WA; 12-month long, A drugs = YA). For experiment WBI (week-long, B-drugs, experiment 1 = WBI) and WB2 (experiment 2 = WB2) blood matrix and microbial matrix specimens were prepared in singlicate whereas for experiment YB (7-month long, B drugs = YB) they were prepared in triplicate.

The validated LC-DAD methods employed for this research necessitated the use of suprathreshold drug concentrations to enable drug detection (Table 6-2). This was considered an acceptable approach to minimise the use of ante-mortem human whole blood. Using the LC-DAD methods, the alternative approach would have involved extraction of greater quantities of ante-mortem human whole blood to enable greater concentration of analytes and potential degradation products during extraction and reconstitution.

Table 6-2: Reported ante-mortem plasma therapeutic concentrations of drugs and approximate concentrations used in blood experiments.

Drug	Therapeutic plasma concentration (mg/L)	Reference	Approximate blood concentration (mg/L)
ASEN	0.002-0.005	[248]	9.0
CHLO	0.03-0.5	[248]	6.0
CLOZ	0.1-0.6	[248]	6.0
FLPH	0.001-0.01	[248]	6.0
FLTX	0.001-0.01	[248]	6.0
HALO	0.005-0.017	[248]	6.0
PERI	0.005-0.03	[248]	6.0
PROC	0.01-0.05	[248]	6.0
QUET	0.1-0.5	[248]	6.0-8.0
ARIP	0.15-0.5	[248]	6.0
CLOM	0.02-0.4	[248]	6.0
DOTH	0.02-0.1	[248]	6.0
LURA	< 0.1	[153]	9.0
MIRT	0.03-0.3	[248]	6.0
MOCL	0.3-3	[248]	6.0
TRIF	0.001-0.05	[248]	6.0
ZIPR	0.05-0.2	[248]	9.0
RISP	0.002-0.02	[248]	6.0
AMIT	0.05-0.3	[248]	6.0

Percent decreases in concentration changes over time in prior drug stability studies have been found to be independent to the initial concentration spiked [291, 436]. Therefore, simultaneous experiments to spike drugs at different concentrations were not performed.

RISP was included in all experiments to monitor the formation of its known bacterial degradation product, HB-RISP [223]. In prior experiments, this degradation product was not observed to form in sterile blood controls [223]. HB-RISP was therefore a marker for the successful inoculation and respiration of microorganisms in the inoculated drug specimens.

AMIT was included in both sets of drugs if aliquot variation required subsequent correction to a standard within the sample (i.e. an inter-aliquot standard). As noted previously, AMIT is expected to be stable in post-mortem specimens [195]. A past study has successfully utilised AMIT to account for aliquot variance [84].

Prior to use in blood experiments, ante-mortem human whole blood was plated on Columbia Blood Agar plates incubated aerobically and anaerobically at 37 °C in the dark to assess matrix sterility. Anaerobic conditions were achieved using an AnaeroGen™ atmosphere generation system in conjunction with anaerobic atmosphere generation sachets. An anaerobic indicator was present to verify anaerobic conditions. Blood was only used in experiments if no colonies were present after five days of incubation.

Throughout this chapter the experimental specimens are referred to as specimens, the aliquots taken during extraction as sub-samples, and the sub-samples following the extraction procedure as extracts.

6.2.2 Specimen preparation

Ante-mortem blood (5 mL) was aliquoted into 5 mL sterile polystyrene Sarstedt tubes using a sterile plastic syringe. Drugs were spiked by removing organic solvent from ~32-75 µg/mL working solutions, depending on the analyte, under N₂ at 40 °C followed by reconstitution in ethanol (1.5 mL). Reconstituted drugs were then aliquoted (100 µL) into the sterile tubes using Luer-Slip plastic syringes with 0.2 µm filters. For preserved specimens, sodium fluoride (100 mg) was first weighed into tubes before the addition of blood. For longer experiment specimens, potassium oxalate monohydrate (10 mg) was also weighed to all tubes before the addition of blood.

Microorganisms were inoculated into specimens #2-3 and #6-7 (Table 6-1). This was achieved for the A drug experiments and experiment WBI by using sterile inoculating loops to transfer the FMT slurry after thawing. For experiment WBI there were incongruent rates of degradation between replicates in inoculated, unpreserved specimens. This indicated that the number or identity of the microorganisms inoculated may have varied between each replicate. Therefore, a repeat week experiment for the B drugs was performed. For this experiment (WB2) and a

seven-month experiment with the B drugs the FMT slurry was further diluted with filter-sterilised water (3 mL) (using Luer-Slip plastic syringes with 0.2 µm filters), vortexed to mix, and aliquoted (50 µL) into relevant specimen tubes. The same solution of FMT slurry was used to prepare fixed samples (see 6.2.5.1) to determine the number of cells inoculated in the inoculated, unpreserved specimens.

Prepared blood specimens were vortexed, rolled, vortexed, and initial sub-samples collected (4.2.2). Wide-bore sterilised pipette tips with filters were used to collect sub-samples. Immediately following sub-sampling, specimens were incubated at 37 °C, 4 °C, and -20 °C, or stored at room temperature to achieve the appropriate temperature for each experiment and specimen condition type.

6.2.3 Sample extraction and LC-DAD analysis

Sub-samples from specimen tubes were collected by placing the specimens on a mechanical roller (30 minutes at 25 rpm) followed by vortexing each specimen prior to collecting aliquots. Extraction was performed as described (4.2.2). After collecting aliquots, specimens were returned to the appropriate temperature in the dark. Specimens were analysed up to 7 days after incubation for the week-long experiments. For experiment YA, sub-samples for quantification were collected after 4, 8, 13, 25, 41, and 51 weeks. For experiment YB, sub-samples for quantification were collected after 1, 5, 21, and 32 weeks (shorter due to time constraints).

6.2.3.1 Quality control

QCs samples were prepared and analysed as previously described (4.2.1).

6.2.3.2 Normalisation of data

Aliquot variation was observed, despite rolling and vortexing samples prior to extraction to homogenise the specimens. Change in concentration values were therefore normalised using AMIT present in the specimens as an “inter-aliquot standard” (Equation 6-1).

Data normalised to AMIT is presented as a “relative concentration change (%)”. Data not normalised to AMIT is presented as a “concentration change (%)”.

In doing this, any fluctuation in AMIT concentrations is considered a variation not due to AMIT degradation but non-homogeneity of specimens. Normalising the relative response of the other drugs to the relative response of AMIT is assumed to compensate for these variations. Normalisation using AMIT has been previously performed in microbial drug degradation studies and its choice as an inter-aliquot standard in this research was based on its observed

resistance to microbially degrade in liver and blood specimens [84, 195, 437]. Both concentration change and relative concentration change (normalised to AMIT) plots were inspected for all analytes to ensure erroneous normalisation was not performed. Normalisation of change in concentration data to AMIT was not performed in specimens where: i) AMIT's apparent degradation product (and ante-mortem metabolite), nortriptyline (NORT), was detected by the LC-DAD method; and/or ii) in specimens where the AMIT change in concentration was greater than 20 %, indicating possible instability.

Equation 6-1: Calculations used to normalise data to AMIT.

$$\text{relative detector response of DRUG} = \frac{\text{detector response of DRUG}}{\text{detector response of IS}}$$

$$= \frac{\text{concentration of DRUG} - y \text{ intercept of DRUG calibration curve}}{\text{slope of DRUG calibration curve}}$$

$$\begin{aligned} &\text{change in concentration of DRUG at time X relative to time 0 (\%)} \\ &= \left(\frac{\text{concentration of DRUG at time X}}{\text{concentration of DRUG at time 0}} \right) \times 100 \% \end{aligned}$$

$$\begin{aligned} &\text{normalised change in concentration of DRUG at time X relative to time 0 (\%)} \\ &= \left(\frac{\text{change in concentration of DRUG at time X relative to time 0}}{\text{change in concentration of AMIT at time X relative to time 0}} \right) \times 100 \% \end{aligned}$$

6.2.3.3 Uncertainty calculations

The uncertainty associated with calculated concentrations was determined from the square root of the sum of the squares of the C.V. of the method uncertainty and the C.V. of concentration changes (or normalised “relative” concentration changes) for replicates. Method uncertainty was established based on the QC which yielded the largest inter-day C.V. (%) value observed during method validation (refer to 4.4.2.3). A coverage factor of 2 was then applied to afford a 95.45 % confidence interval for the data, as per the Joint Committee for Guides in Metrology [438] (Equation 6-2). These uncertainty values were used to plot error bars for LC-DAD data except where otherwise specified. For instances where a drug was not detected by LC-DAD analysis, or replicates plotted individually, the uncertainty was given based on 2 times the inter-day C.V only to give a confidence level of 95.45 %.

Differences in drug stability between specimens and different temperature conditions were considered “significant” at a confidence level of 95.45 %.

Equation 6-2: Uncertainty calculations for drug quantification data.

$$\begin{aligned} & \text{uncertainty for analyte conc. change (\%)} \\ & 2 \times \text{analyte conc. change mean (\%)} \\ & \times \sqrt{\left(\frac{\text{QC concentration interday standard deviation}}{\text{QC concentration overall mean}}\right)^2 + \left(\frac{\text{analyte conc. change standard deviation}}{\text{analyte conc. change mean}}\right)^2} \end{aligned}$$

6.2.4 LC-QTOF-MS screening for degradation products

Experiment extracts from the blood experiments were screened for degradation products using an Agilent 1200 Series HPLC and Agilent 6520 Series LC-QTOF-MS (see Chapter 7).

6.2.5 Microbial analyses

6.2.5.1 Cell counts

Diluted FMT slurries were prepared for the WB2 and YB experiments (see 6.2.2). In addition to aliquoting 50 μL into relevant blood specimens during specimen preparation, aliquots (50 μL) in triplicate were fixed in an aqueous solution (1 mL) of glutaraldehyde (2.5 % v/v) in sterile Eppendorf tubes (30 minutes in the dark). Water used was filter-sterilised using Luer-Slip plastic syringes with 0.2 μm filters. Fixed specimens were then stored at $-20\text{ }^\circ\text{C}$.

Fixed solutions were visually inspected using a Leitz Laborlux S optical microscope following vortexing. Cell counts of the inoculate were obtained using a Petroff Hausser Counting Chamber.

6.2.5.2 Sterility

At the conclusion of the week-long experiments, and throughout the longer experiments, non-inoculated specimens (#1 and #4-5) were plated on Columbia Blood Agar and Sabouraud Dextrose Agar to test for microbial contamination of the specimens. This was performed ~28-29 weeks into experiment YA, and after the final sub-sample was collected for quantification at the conclusion of experiment YA and YB. Columbia Blood Agar is a non-selective media that supports the growth of fastidious anaerobes [418]. Sabouraud Dextrose Agar was used in addition to test selectively for fungal contamination [439]. *E. coli* and *A. brasiliensis* were used as positive control organisms for Columbia Blood Agar and Sabouraud Dextrose Agar, respectively, by directly inoculating from previously prepared glycerol stocks (3.2.2.3).

Columbia Blood Agar plates were incubated at $37\text{ }^\circ\text{C}$ in the dark under both aerobic and anaerobic conditions. Sabouraud Dextrose Agar plates were incubated at $37\text{ }^\circ\text{C}$ in the dark aerobically. After five days, incubation plates were visibly inspected for colony growth. Archaeal

contamination was not assessed due to the lack of commercially available culture media and stringent nutritional and atmospheric requirements for successful growth [440].

6.2.5.3 Viability

Approval to plate inoculated, unpreserved specimens to test for bacterial viability was denied by the Flinders University Institutional Biosafety Committee due to the risks associated with the isolated amplification of PC2 risk organisms. Because of this restriction, an alternative approach to determine bacteria viability at the end of the week-long experiments was required.

To test viability in the week-long experiments, RISP was re-spiked into inoculated, unpreserved specimens after nine days incubation at 37 °C. Organic solvent was removed from the RISP stock (~20 µg/mL) under N₂ at 40 °C followed by reconstitution in ethanol (500 µL) and spiking using Luer-Slip plastic syringes with 0.2 µm filters to give a final concentration of ~3 µg/mL in the specimens. Specimen extracts were collected (see 6.2.3) to confirm successful re-spiking of RISP and extracts five days later collected to determine if RISP had degraded over this period. Degradation of the repeat spike of RISP over time was interpreted as confirmation of bacteria successfully respiring in samples and degrading re-spiked RISP, indicating that bacteria remained viable in the specimens throughout the duration of the week experiments.

6.2.5.4 Communities

Validating the DNA extraction

DNA from FMT specimens were extracted in duplicate using the MoBio PowerFecal® DNA Isolation Kit. This kit was chosen as previous research indicates that it affords reproducible high quality and yields of DNA from human stool samples compared to other DNA extraction kits [34]. As a positive control, *E. coli* DNA was extracted concurrently by first centrifuging (10 minutes at 4000 rpm) the sub-culture (3.2.2.3) and using the precipitated cell mass in the extraction.

The extraction procedure was varied from the specified protocol in the instruction manual supplied with the kit [441]. After heating the tubes at 65 °C for 10 minutes (step 5 in the protocol), contents were homogenised using FastPrep™-24 Classic (20 seconds at 4 m/s). After homogenisation, tubes were once more heated at 65 °C for 10 minutes. The remainder of the protocol from step 7 was followed, using ultra-pure water instead of Solution C6 to elute the DNA.

Gel electrophoresis was used to test for successful DNA extraction. Extracted DNA was stained

with loading dye and run on a 1 % agarose gel (1 hour at 100 V). Quantification was attempted using NanoDrop, but, excluding the *E. coli* positive control, poor UV-Vis spectra and 260/280 ratios were obtained. Poor absorbance ratios are not indicative of whether sequencing will be successful [442]. Therefore, PCR amplification of the 16S rRNA gene was performed to determine if inhibitors remained present that would prevent later DNA amplification and Illumina MiSeq sequencing at the AGRF. PCR was performed on DNA extracted from: FMT specimens, faecal-blood hybrids, and the *E. coli* positive control DNA.

For the PCR, GoTaq® HotStart polymerase was used at a final concentration of 1 x and GoTaq® Reaction buffer (pH = 8.5) added to afford DNTPs and MgCl₂ at a concentration of 200 µM and 2 mM, respectively. 27F and 1492R primers were used at a concentration of 0.4 µM. Extracted DNA was added to samples (1 µL). Nuclease-free water was added to make sample volumes up to 25 µL. Contents were mixed by pipetting and sample tubes centrifuged briefly. An Applied Biosystems Verti 96 Well Thermal Cycler was used to carry out the PCR (Stage 1: 95 °C for 5 minutes; Stage 2 (repeated 35 times): 95 °C for 1 minute, 55 °C for 1 minute, 72 °C for 90 seconds; Stage 3: 72 °C for 7 minutes, cool down to 14 °C). Successful DNA amplification was confirmed by staining DNA with loading dye and running on a 1 % agarose gel (1 hr at 100 V).

DNA extraction and 16S rRNA sequencing

DNA from FMT specimens was extracted in duplicate for sequencing the day before commencing all experiments. Gel electrophoresis was used to test for successful DNA extraction, as indicated above. After extraction, faecal specimens were immediately returned to a -80 °C freezer. For the week-long experiments, aliquots (400 µL) were collected from inoculated specimens (#2-3, #6-7) on the seventh day of the experiments. For the longer experiments, DNA was collected at a minimum at the final timepoint of the experiment. Extracted DNA was stored at -80 °C prior to 16S rRNA sequencing (primers: 341F – 806 R) using the Illumina MiSeq platform at the AGRF. Experiment WB2 DNA was not sent for sequencing due to financial constraints.

Data analysis

The Diversity Profiling Service at the AGRF identified OTUs up to the species level using the GreenGenes database [227]. Data obtained from the AGRF was further processed by removing OTUs classified as “Unassigned” and with less than 10 sequence reads in a sample.

Diversity indices calculated were Simpson’s Reciprocal Index (1/D) (Equation 6-3) and the Shannon-Wiener Index (H) (Equation 6-4). These indices differ in how they consider species

richness (the number of OTUs detected) and evenness (how similarly abundant each OTU is) as contributing to diversity [232]. Simpson's Reciprocal Index is weighted toward more dominant species and increases as evenness increases, such as in the situation where numerous taxa are co-dominant [232]. The Shannon-Wiener Index increases with increasing species richness and evenness [232]. Determined Shannon-Wiener indices were converted to effective number of species (ENoS) (or Hill numbers) to facilitate more intuitive comparisons between the diversity of different samples (Equation 6-5) [443].

Equation 6-3: Simpson's Reciprocal Index (1/D) calculation [232].

$$1/D = \frac{1}{\left(\frac{\sum n(n-1)}{N(N-1)}\right)}$$

where: N = total number of reads,

and n = number of reads for each OTU individually

Equation 6-4: Shannon-Wiener Index (H) calculation [232].

$$H = - \sum \left(\frac{n}{N} \times \ln \left(\frac{n}{N} \right) \right)$$

where: N = total number of reads,

and n = number of reads for each OTU individually

Equation 6-5: Effective number of species (ENoS) calculation [443].

$$ENoS = e^H$$

where: H = Shannon Wiener Index

To compare the relative abundance of different OTUs between samples further processing was required due to the nature of the data supplied by the AGRF and the sequencing of DNA extracts across multiple Illumina MiSeq runs. In the Diversity Profiling reports, OTUs were assigned unique reference numbers intra-run only and taxon assigned unambiguously but undefined in Greengenes were given identical consensus lineages intra- and inter-run. This meant that to the merge the data obtained from different runs into one table identical consensus lineages were first required to be merged into a single "(undefined)" category. For example, if multiple OTUs in a sample were classified as "k__Bacteria; p__Actinobacteria; c__Coriobacteriia; o__Coriobacteriales; f__Coriobacteriaceae; g__; s__" by AGRF then the sum of reads for all of these OTUs was the value used for the taxon, reported as "Bacteria - Actinobacteria -

Coriobacteriia – Coriobacteriales – Coriobacteriaceae – (undefined) – (undefined)”. This transformation of the data enabled qualitative comparisons between microbial communities across all samples. Multivariate statistical analyses were performed following fourth root data transformation to “downweight the influence of the more abundant taxa” [444]. Bray-Curtis similarity [445] was the coefficient calculated for the transformed data for all multivariate analyses (Equation 6-6).

Equation 6-6: Bray-Curtis similarity (BCS) calculation [445].

$$BCS_{ab} = 1 - BCD_{ab}$$

where: BCD_{ab} = Bray Curtis dissimilarity between sample a and sample b,

$$BCD_{ab} = 1 - \frac{2 \times C_{ab}}{S_a + S_b}$$

where: C_{ab} = sum of lesser reads for each OTU found in both samples,

and S = total number of reads in a sample

Two-way PERMANOVA tests [236] were performed for comparison of factors (specimen type, preservative, temperature, time, and drug set). The PERMANOVA was run with 9999 permutations (lowest p-value possible: 0.0001). Results were considered significant if $p < 0.05$. To visualise the similarities between the microbial communities across all samples a hierarchical cluster dendrogram clustered by UPGMA (unweighted pair group method with arithmetic mean) and a PCoA (principal coordinate analysis) ordination plot were constructed.

Due to the nature of Illumina MiSeq technology only the dominant microorganisms present in specimens will be detected (e.g. for detection in faeces, it has been reported that bacteria must be present at concentrations greater than 10^6 colony-forming units/g [446]). Consequently, it is important to note that it may not necessarily be the case that the microorganisms detected are responsible for any drug degradation observed in the blood experiments. This phenomenon may also account for taxon detection in the blood specimens otherwise not identified in the initial FMT specimens inoculated into the blood if the environment and incubation affect community structure.

6.2.6 Carboxyhaemoglobin analysis and UV-Vis spectrophotometry

During the first week-long experiment (WA) it was observed that diluted specimens containing microorganisms but not preservative (#2, #6) underwent a visible colour change from their dark red colour at experiment start to a brighter cherry red. By visual observation this colour was

noticeably different to the colour of both preserved samples (dark green) and unpreserved sterile samples (dark brown) (Figure 6-1).

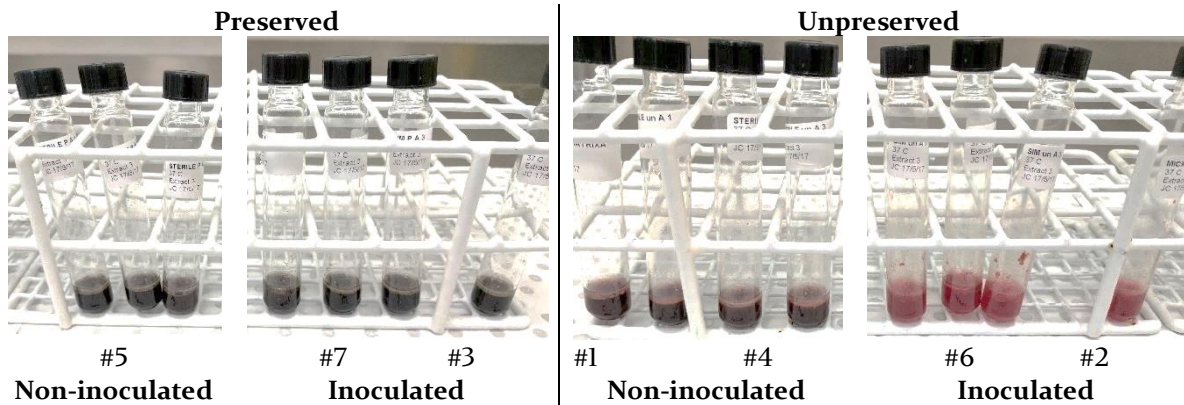


Figure 6-1: Aqueous blood layer of sub-samples from experiment WA following collection of the organic layer. Note the cherry red colour for #6 and #2.

#Numbers indicate specimen type (refer to Table 6-1).

Sub-samples for carboxyhaemoglobin (CO-Hb) analysis (100 μ L) were collected from all unpreserved specimens throughout experiments and stored at -20°C prior to analysis. For experiment WA, sub-samples for CO-Hb analysis were collected three, seven and nine days after the experiment commencement. For experiments WBI and WB2 sub-samples were collected with the initial extract, after two days, and after seven days. For experiment WB2, sub-samples were also collected after four days. For experiment YA, sub-samples were collected after two, three, six, nine, and twelve months and stored at -20°C . For experiment YB CO-Hb sub-samples were collected at the start of the experiment and upon conclusion.

CO-Hb analysis was performed using the UV-Vis spectroscopy method used at FSSA [196]. Aliquots (25 μ L) from the unpreserved samples were haemolysed and sodium dithionite used to reduce oxyhaemoglobin and methaemoglobin to deoxy-haemoglobin [447]. This allows for the absorbance ratios between the wavelength maxima for reduced haemoglobin ($\lambda_{\text{max}} = 432$ nm) and CO-Hb ($\lambda_{\text{max}} = 420$ nm) to be measured and determination of the CO-Hb content in the blood (Equation 6-7) [447].

Equation 6-7: Percent carboxyhaemoglobin determination from UV-Vis spectroscopy.

$$\% \text{CO-Hb} = \left(\frac{1 - (R \times 1.333)}{(R \times -0.8543) - 0.9939} \right) \times 100 \%$$

$$\text{where } R = \frac{\text{Abs}_{\lambda=420\text{nm}} - \text{Abs}_{\lambda=500\text{nm}}}{\text{Abs}_{\lambda=432\text{nm}} - \text{Abs}_{\lambda=500\text{nm}}}$$

Method performance was assessed by analysing a blank blood and a QC (at $>50\%$ CO-Hb) at the beginning and end of each analysis.

The C.V. of results from conditions #1, #2, #4, and #6 (Table 6-1) were determined and the uncertainty in the measured results determined as in Equation 6-2. Method uncertainty is specified as $\pm 11.6\%$ for CO-Hb concentrations greater than 10 % and $\pm 21.6\%$ for CO-Hb concentrations less than 10 % (confidence level = 95 %) [196]. Uncertainty values were used to plot error bars. For replicates plotted individually the uncertainty was the method uncertainty only.

Equation 6-8: Uncertainty calculations for CO-Hb data.

$$\text{uncertainty of CO-Hb (\%)} = \% \text{ CO-Hb mean} \times \sqrt{\left(1.96 \times \frac{\text{method uncertainty} + \text{specimen CO-Hb standard deviation}}{\text{specimen CO-Hb mean}}\right)^2}$$

In addition to CO-Hb analysis, blood sub-samples from specimens and the ante-mortem blood were diluted with water and their UV-Vis spectra collected from 240 to 700 nm at a rate of 300 nm/min and a data interval of 0.5 nm, using a Varian Cary 50 Bio UV-Visible Spectrophotometer (Varian, Palo Alto, California, USA) in conjunction with the Scan application (software version: 3.00 (182)). Brand UV-macro cuvettes (Sigma-Aldrich) were used and spectra baseline corrected to the cuvette absorbance with water.

6.3 Drug stability results and discussion

6.3.1 Data normalisation

For all experiments, concentration changes of AMIT over time indicated that aliquot variations in sampling of blood specimens contributed to variable instrument response relative to the IS, LORA (Figure 6-2). The consistently observed increases in AMIT concentration for some specimens in the experiments may be attributed to non-homogeneous distribution of drugs throughout blood specimens during experiment commencement. The reason for the sporadic nature of this, despite the identical preparation and sampling protocol for each specimen, is unknown and could not be attributed to the variable protein binding of the drugs. For experiment WA, the uncertainty for analyte concentrations in non-inoculated, unpreserved specimens was subsequently greater than for other conditions. Analytes in the initial extract for one replicate of the non-inoculated, preserved specimens in experiment WBI yielded low concentrations. For all subsequent extracts, responses were comparable to the other replicates. This may indicate that homogenisation of the specimen was not successful prior to the initial sub-sampling or the initial sub-sample contained a small clot that was present prior to drug spiking. Data for all analytes is therefore presented as a relative concentration change normalised to AMIT (6.2.3.2). Two of the replicates for the non-inoculated, preserved

specimens in experiment WB2 were very viscous, such that data for these replicates were not considered reliable and were excluded. The reason for the viscosity of the blood is suspected to be due to clotting, as no potassium oxalate was added to these specimens.

For experiment YA, there was a clear downward trend in AMIT concentration change in inoculated, unpreserved specimens stored at room temperature indicating that AMIT may be degrading in these specimens (Figure 6-2 (b)). For these specimens, concentration changes for drugs were not normalised to AMIT. Due to this observed instability of AMIT in experiment YA, data for inoculated, unpreserved specimens stored at room temperature were not normalised to AMIT in experiment YB as well (Figure 6-2 (c)). Concentration changes for some drugs and AMIT in non-inoculated, unpreserved specimens stored at room temperature also indicated some degradation may be occurring (Figure 6-2 (c)). For these specimens, data were not normalised to AMIT.

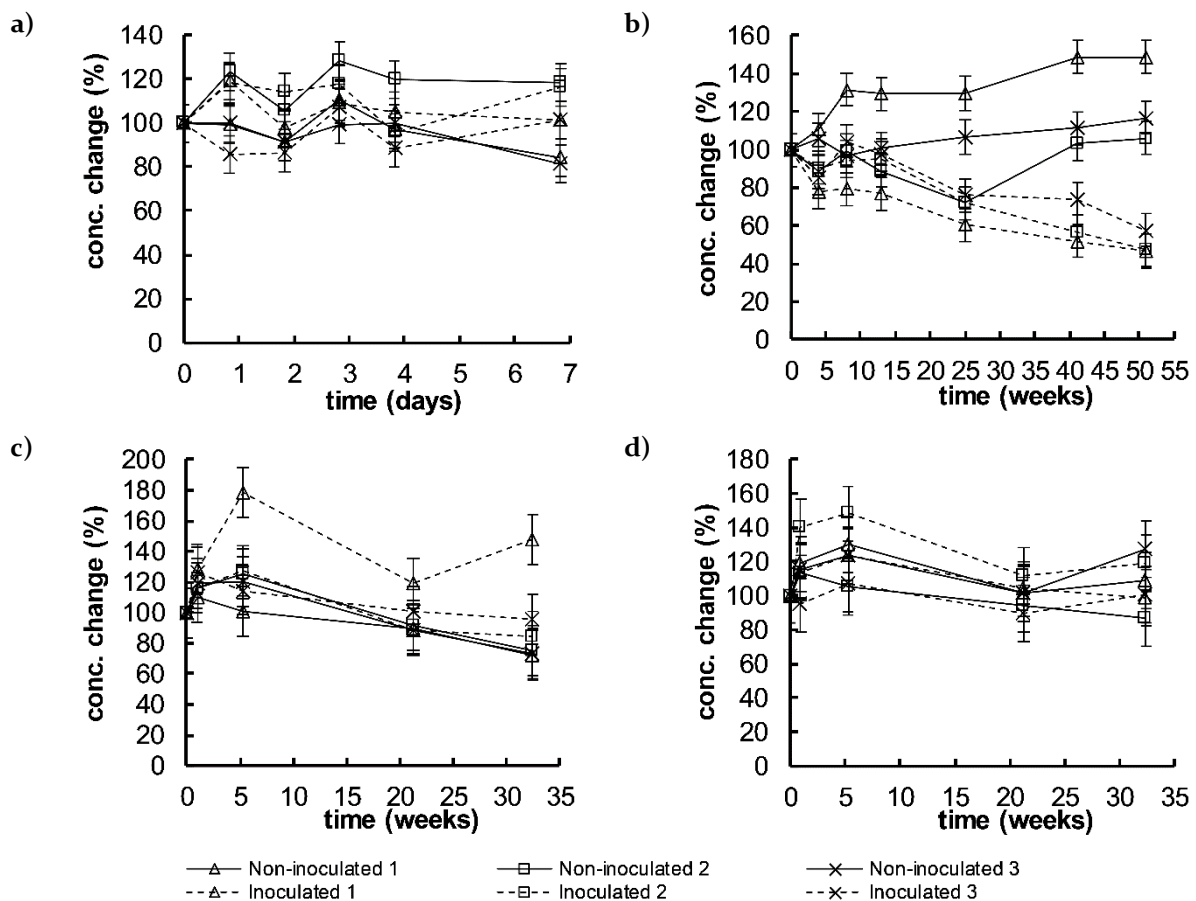


Figure 6-2: Concentration change (%) of AMIT in a,b,c) unpreserved and d) preserved blood specimens incubated at a) 37 °C for 7 days in experiment WA, b) room temperature for 12 months in experiment YA, and c-d) room temperature for 7 months in experiment YB.

Error bars are \pm uncertainty (6.2.3.3). Similar fluctuations were observed for all specimens throughout the experiments (Figure B-1 and Figure B-2).

6.3.2 Matrix degradation

In unpreserved and preserved inoculated blood specimens stored at room temperature and 37 °C degradation of the blood matrices was apparent by the appearance of numerous peaks that were not present in the unpreserved blood matrix controls. These peaks appeared in room temperature specimens after 4 weeks. At this time, the cherry-red colourations previously observed for specimens in the week experiments were once more observed in diluted subsamples of the room temperature specimens (Figure 6-1). After 8 weeks, a peak also appeared in the blood matrix. Some of these matrix degradants eluted close to CHLO, FLTX, and FLPH in experiment YA. Therefore, quantification of these drugs using peak height was post hoc validated. No degradative peaks before the IS were observed in specimens incubated at -20 °C and 4 °C.

Quantification of MIRT was not possible after ~1 day and after ~3 days in inoculated, preserved specimens in experiment WB1 and WB2, respectively, due to coelution with a matrix degradation product also present in the microbial matrix preserved specimens. Due to this coelution, in preserved specimens stored at room temperature, non-inoculated and inoculated, quantification was not possible after ~5 weeks. In inoculated, unpreserved specimens, quantification was not possible after ~32 weeks.

6.3.3 Risperidone degradation

RISP degradation below the LOD in all extracts of inoculated, unpreserved specimens incubated at 37 °C and room temperature corresponded to the detection of HB-RISP (Figure 6-3 and Figure 6-4). This confirmed that the inoculation and respiration of the microorganisms in blood was successful. RISP was stable at 4 °C and -20 °C as may be expected from its reported stability in porcine blood at 7 °C (Figure B-3) [2].

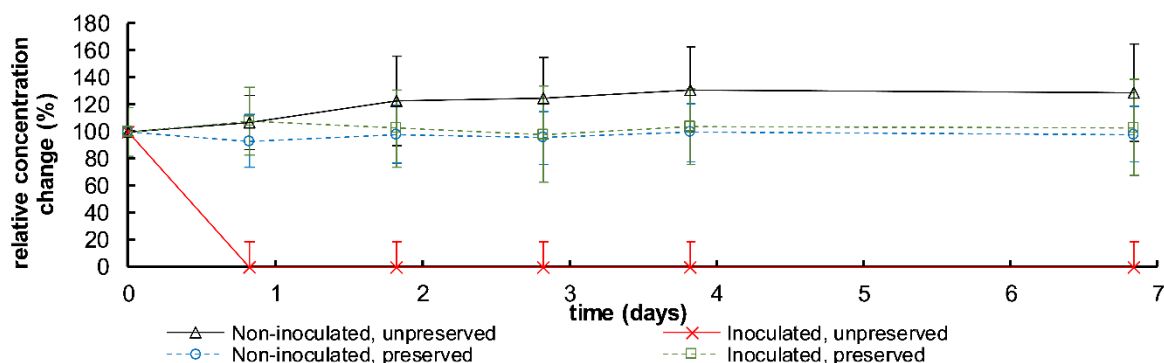


Figure 6-3: Relative concentration change (%) of RISP in blood specimens incubated at 37 °C for 7 days in experiment WA.

Error bars are ± uncertainty (6.2.3.3).

In experiment WA, after ~1 day RISP was no longer detected in all replicates. Unlike experiment WA, the rate at which RISP was degraded to undetectable levels varied from ~2 to ~7 days after inoculation in experiment WBI (Figure 6-4 (a)). This prompted a repeat of the experiment to try and prepare specimens with a more reproducible concentration of microorganisms. However, this did not result in more concordant degradation rates (Figure 6-4 (b)). One possible reason for this may be the nature of the diluted FMT specimens, and the adherence of cells to fibrous matter, which may have still resulted in heterogenous inoculation. Other reasons may be variable lag phases for the microorganisms in the different replicates or the inoculation of communities with different relative abundances of taxa that degrade RISP. RISP was undetected in inoculated, unpreserved specimens after 4 weeks for experiment YA and 5 weeks for experiment YB (Figure B-3).

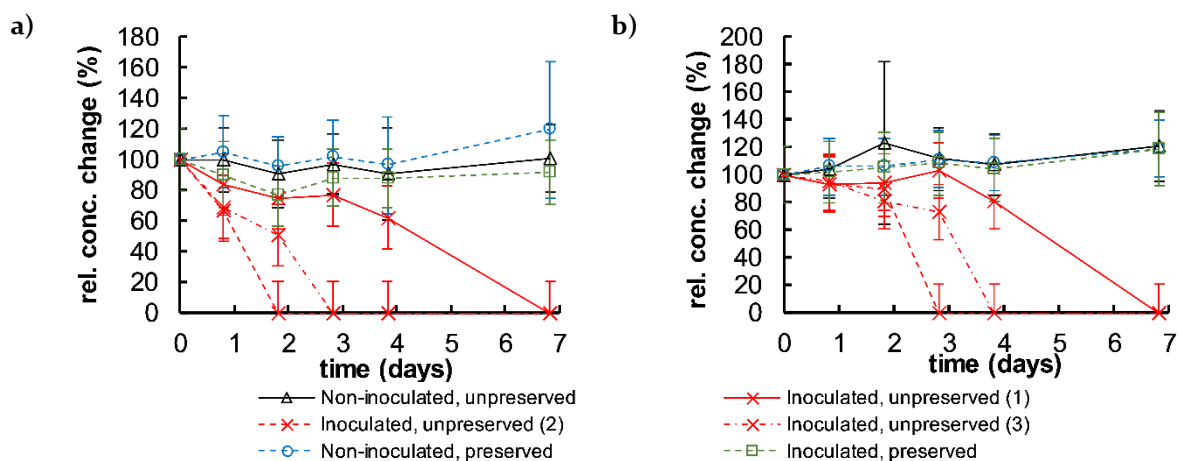


Figure 6-4: Relative concentration change (%) of RISP in a) experiment WBI and b) experiment WB2 blood specimens incubated at 37 °C for 7 days.

Inoculated, unpreserved specimens are plotted individually. Non-inoculated, preserved specimens are triplicate in experiment WBI and singlicate in experiment WB2. Error bars are \pm uncertainty (6.2.3.3).

6.3.4 Drug degradation in the week-long experiments at 37 °C

Except for LURA and ZIPR, none of the investigated drugs exhibited greater than 20 % losses in any of the blood specimens across the three experiments (Figure 6-5, Figure 6-6, and Figure 6-7).

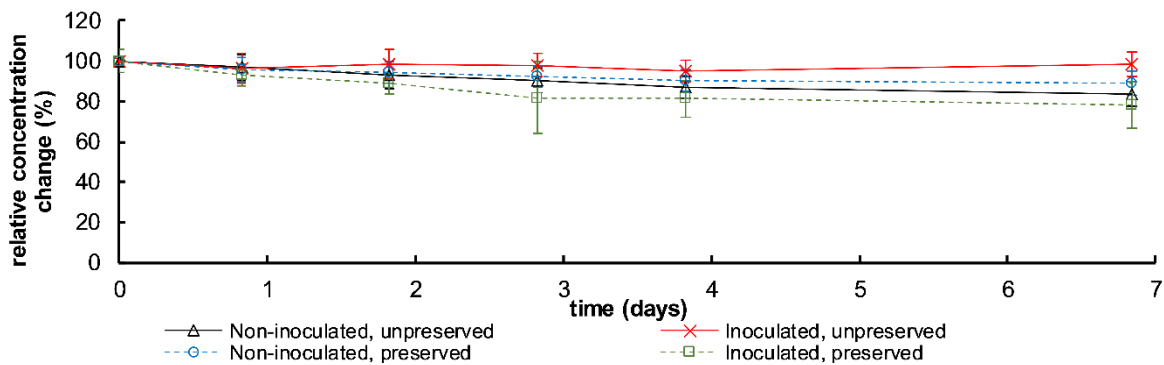


Figure 6-5: Relative concentration change (%) of CHLO in blood specimens incubated at 37 °C for 7 days in experiment WA.

Error bars are ± uncertainty (6.2.3.3). This graph is representative of data obtained for all other stable drugs (see B.3) in experiment WA, WBI, and WB2.

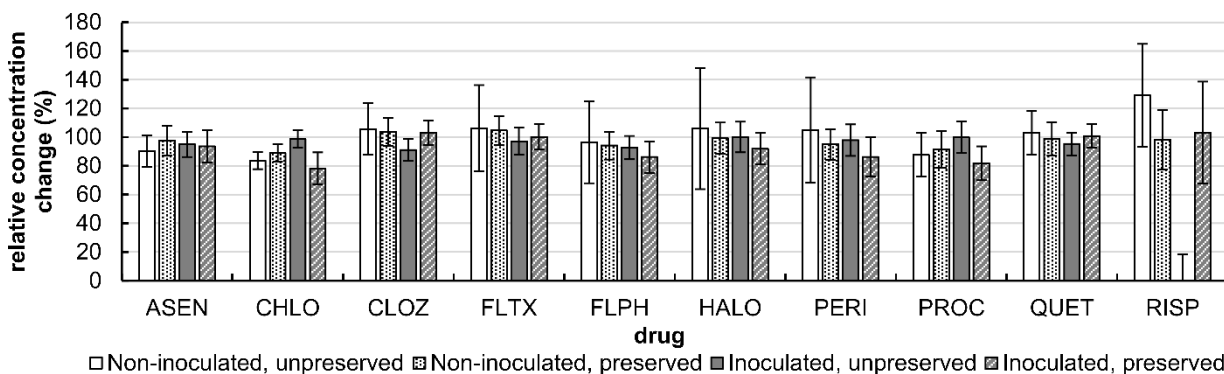


Figure 6-6: Relative concentration change (%) of A analytes in blood specimens incubated at 37 °C for 7 days in experiment WA.

Error bars are ± uncertainty (6.2.3.3).

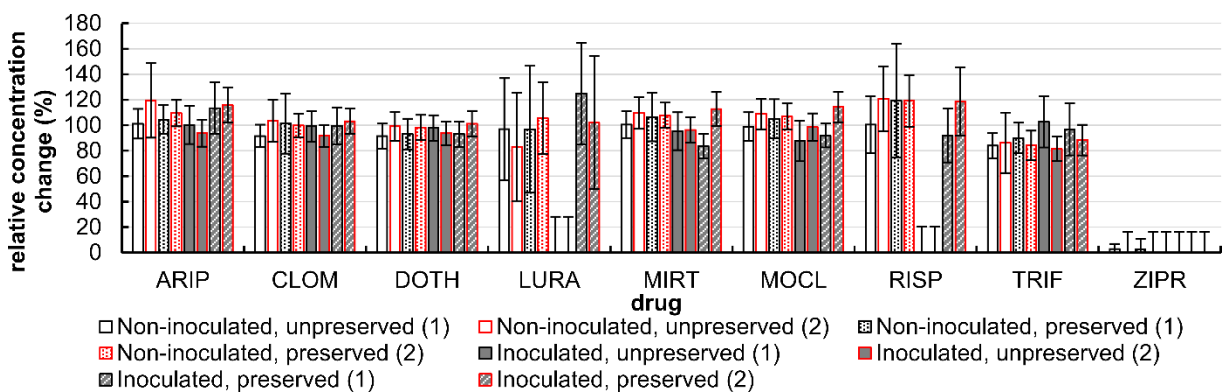


Figure 6-7: Relative concentration change (%) of B analytes in blood specimens incubated at 37 °C for 7 days in experiment WBI and WB2.

MIRT relative concentration changes reported up to 1 day and 3 days in inoculated, preserved specimens in WBI and WB2, respectively. Error bars are ± uncertainty (6.2.3.3).

LURA, similar to RISP, became undetectable in inoculated, unpreserved specimens, and did not demonstrate significant degradation in any other specimen types (Figure 6-8). The days on which LURA was not detected were also the same as when RISP became undetectable. As noted above, it was thought that issues regarding the reproducibility of inoculating microorganisms into the inoculated, unpreserved specimens led to a variation in the rate at which RISP was degraded to HB-RISP by bacteria across replicates. As this rate of degradation was seemingly shared by LURA in both experiments it is suggested that LURA may be microbially degrading as well.

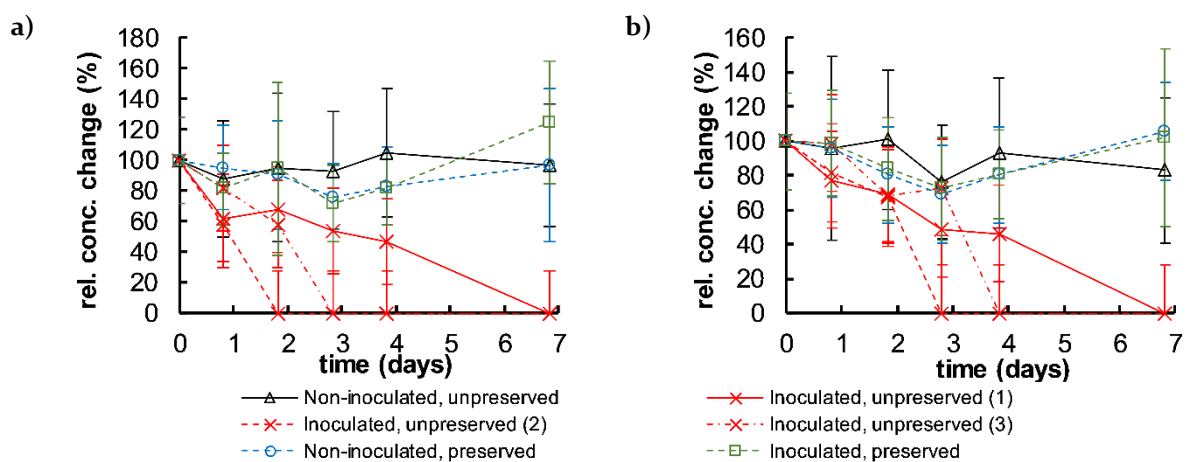


Figure 6-8: Relative concentration change (%) of LURA in a) experiment WB1 and b) experiment WB2 and in blood specimens incubated at 37 °C for 7 days.

Inoculated, unpreserved specimens are plotted individually. Non-inoculated, preserved specimens are triplicate in experiment WB1 and singlicate in experiment WB2. Error bars are \pm uncertainty (6.2.3.3).

ZIPR appeared as though it may share this same rate of degradation in inoculated, unpreserved specimens in experiment WB1 (Figure 6-9 (a)). However, degradation to undetectable levels was more rapid in the repeat experiment (Figure 6-9 (b)). ZIPR was also reduced to undetectable levels in all but the final extracts of the non-inoculated unpreserved and preserved specimens in experiment WB1. For these extracts, only traces of ZIPR remained, with losses averaging 97%. These results indicated that ZIPR was not necessarily degrading due to microbial activity alone or at all in blood specimens, and that degradation may have been leading to different degradation products in the different specimens.

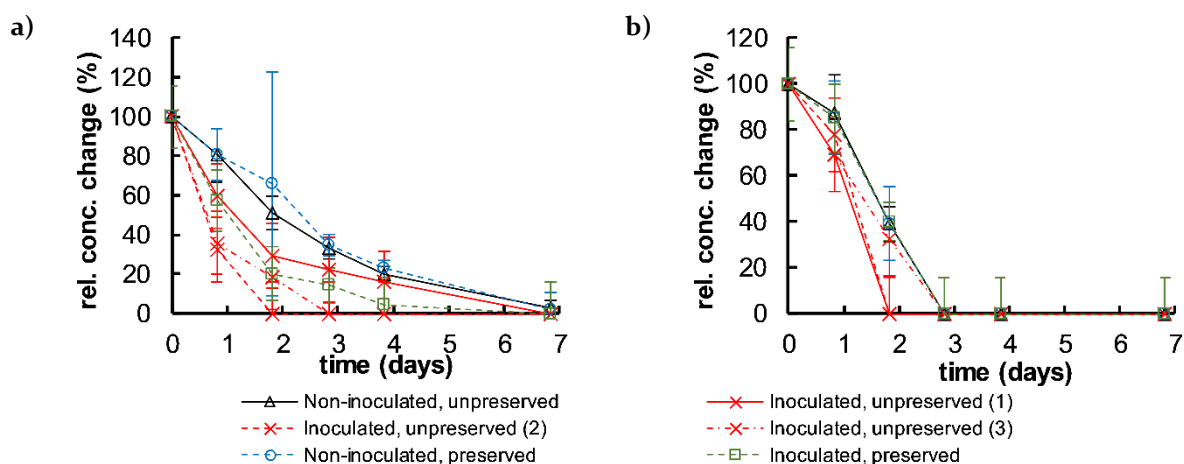


Figure 6-9: Relative concentration change (%) of ZIPR in a) experiment WB1 and b) experiment WB2 and in blood specimens incubated at 37 °C for 7 days.

Inoculated, unpreserved specimens are plotted individually. Non-inoculated, preserved specimens are triplicate in experiment WB1 and singlicate in experiment WB2. Error bars are \pm uncertainty (6.2.3.3).

6.3.5 Drug degradation in the longer-term experiments at room temperature, 4 °C and -20 °C

For relative concentration change (%) over time figures for each drug refer to B.4. Drug degradation results are summarised in Figure 6-10 and Figure 6-11.

ASEN appeared as though it may be degrading over time in inoculated, unpreserved specimens stored at room temperature (Figure B-7 (e)). However, quantification was not possible for extracts collected ~52 weeks into the experiment, due to coelution with an unknown compound with a UV-Vis spectrum similar to the phenothiazine-sulfoxides (Figure 4-4 (b)).

Of the A drugs, ASEN, CHLO, FLPH, FLTX, and PROC were all significantly more stable in inoculated, preserved specimens incubated at -20 °C compared to non-inoculated specimens (Figure 6-10 (a)). Significant losses greater than 20 % were observed for CHLO and PROC in non-inoculated specimens. Significant FLTX losses were greater than 20 % in non-inoculated, preserved specimens. The different extent of degradation in preserved and unpreserved non-inoculated specimens for these drugs was not significant (Figure 6-10 (a)). FLPH degradation was greater than 20 % in non-inoculated specimens but measurement uncertainty indicated this result was not significant.

PERI was the only phenothiazine found to be stable in all specimens incubated at -20 °C (Figure 6-10 (a)). PERI differs from the other phenothiazines, CHLO, PROC, and FLPH by: i) an aryl-nitrile substituent instead of an aryl-trifluoromethyl group for FLPH and FLTX and an aryl-

chlorine for CHLO and PROC; and ii) no disubstituted piperazine moiety. However, QUET and CLOZ both contain disubstituted piperazine functionality, and both drugs appear to be stable in -20 °C specimens. This indicates that degradation may be occurring due to the aryl-substituents. If so, the aryl-trifluoromethyl group in FLTX could account for its instability. TRIF contains in common with FLTX and FLPH an aryl-trifluoromethyl group and was the only B drug where significant losses exceeded 20 % at -20 °C in any specimen. Such losses were observed in all non-inoculated specimens and inoculated, unpreserved specimens (Figure 6-11 (a)). This indicates degradation may be occurring at this moiety. However, dechlorination of CHLO and PROC is unlikely to be occurring, as there was no increase in the response of perazine (PERA) (dechlorinated-PROC) (see later discussion in section 6.3.6) in these specimens and no detection of promazine (PROM) (dechlorinated-CHLO). Furthermore, the precursor ion expected for a dechlorinated-CLOZ derivative (calculated m/z of $[M+H]^+ = 293.1761$) was also not detected by LC-QTOF-MS analysis (see Chapter 7).

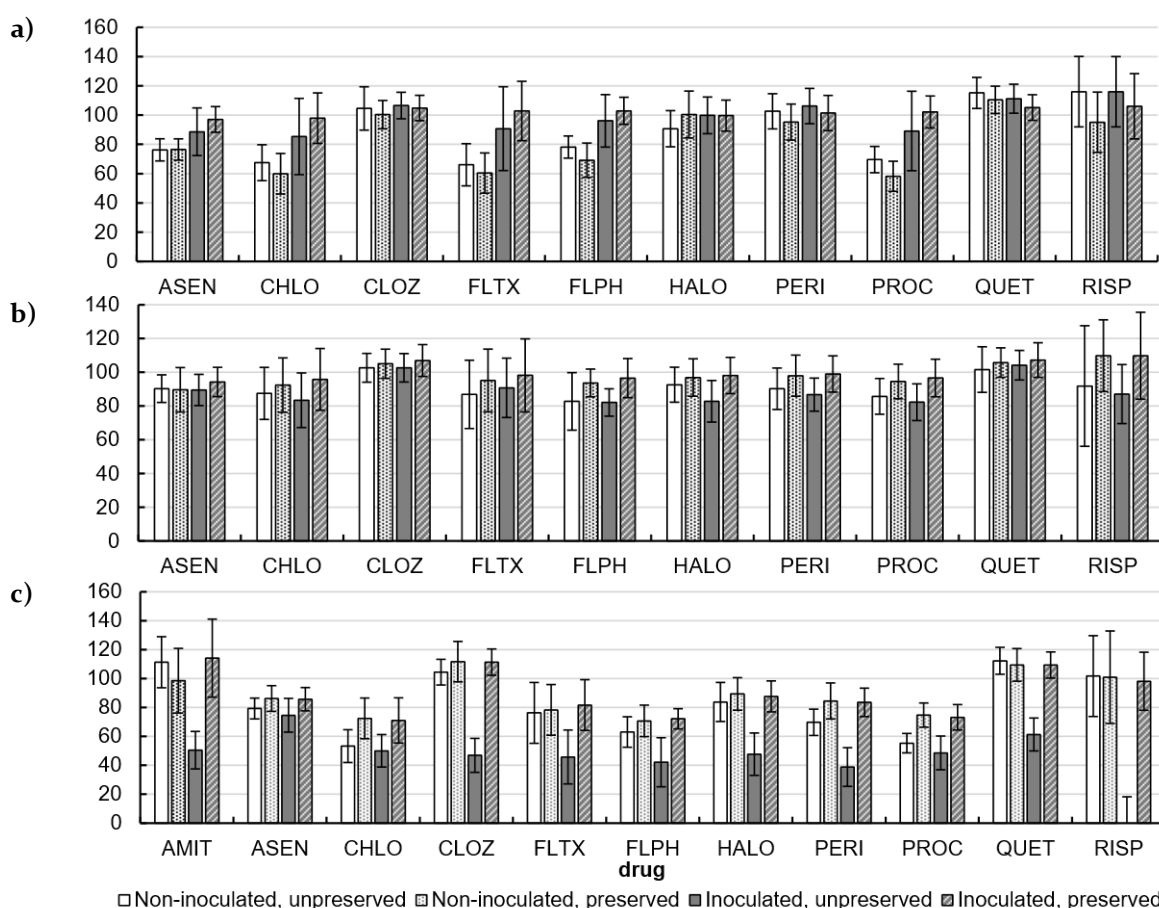


Figure 6-10: Relative concentration change (%) of A analytes in blood specimens incubated at a) -20 °C, b) 4 °C, and c) room temperature for 12 months in experiment YA. Y-axis is concentration change (%) for inoculated, unpreserved, room temperature specimens and relative concentration change (%) for all other specimens. ASEN concentration changes only reported up to ~41 weeks in inoculated, unpreserved specimens stored at room temperature. Error bars are \pm uncertainty (6.2.3.3).

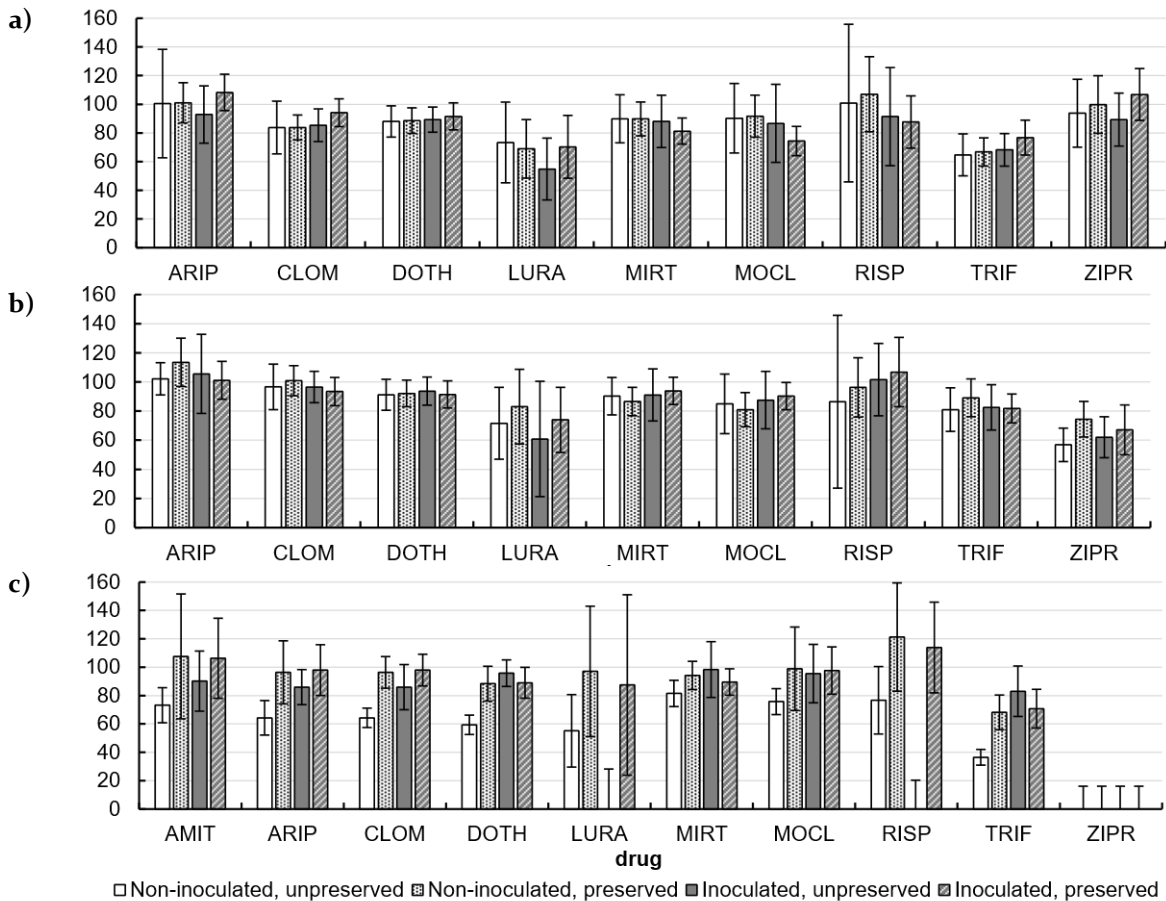


Figure 6-II: Relative concentration change (%) of B analytes in blood specimens incubated at a) -20 °C, b) 4 °C, and c) room temperature for 7 months in experiment YB. Y-axis is concentration change (%) for non-inoculated and inoculated, unpreserved, room temperature specimens and relative concentration change for all other specimens. MIRT concentration changes only reported up to ~1 week for preserved specimens stored at room temperature and up to ~32 weeks in inoculated, unpreserved specimens as noted in text. Error bars are \pm uncertainty (6.2.3.3).

For specimens incubated at 4 °C, statistically significant losses did not exceed 20 % for any of the drugs (Figure 6-10 (b) and Figure 6-II (b)) except for ZIPR in unpreserved specimens (Figure 6-12 (e)). In room temperature specimens, greater than 80 % losses for ZIPR were observed in inoculated, unpreserved specimens after ~5 weeks (Figure 6-12 (f)). After ~21 weeks, ZIPR was not detected in any of the room temperature specimens. Mean LURA losses were greater than 20 % in most specimens incubated at -20 °C or 4 °C (Figure 6-II (a-b)). However, the large method uncertainty associated with LURA meant only losses greater than 20 % in inoculated, unpreserved specimens were significant and no significant difference between specimens could be demonstrated (Figure 6-12 (a-c)). Degradation at -20 °C may have resulted from instability during freeze-thaw, as observed during method validation (4.4.2.6). LURA was reduced to undetectable concentrations in inoculated, unpreserved specimens stored at room temperature from ~5-21 weeks (Figure 6-12 (c)), similar to RISP.

DOTH and TRIF losses exceeded 30 % after 7 months storage at room temperature in non-inoculated, unpreserved specimens. This degradation was significantly greater than the losses observed in the other specimens (Figure 6-II (c)). ARIP and CLOM losses were greater than 20 % in the same specimens. For ARIP, losses were only significant compared to inoculated, preserved specimens (Figure 6-II (c)). For CLOM, losses were significant compared to all preserved specimens (Figure 6-II (c)).

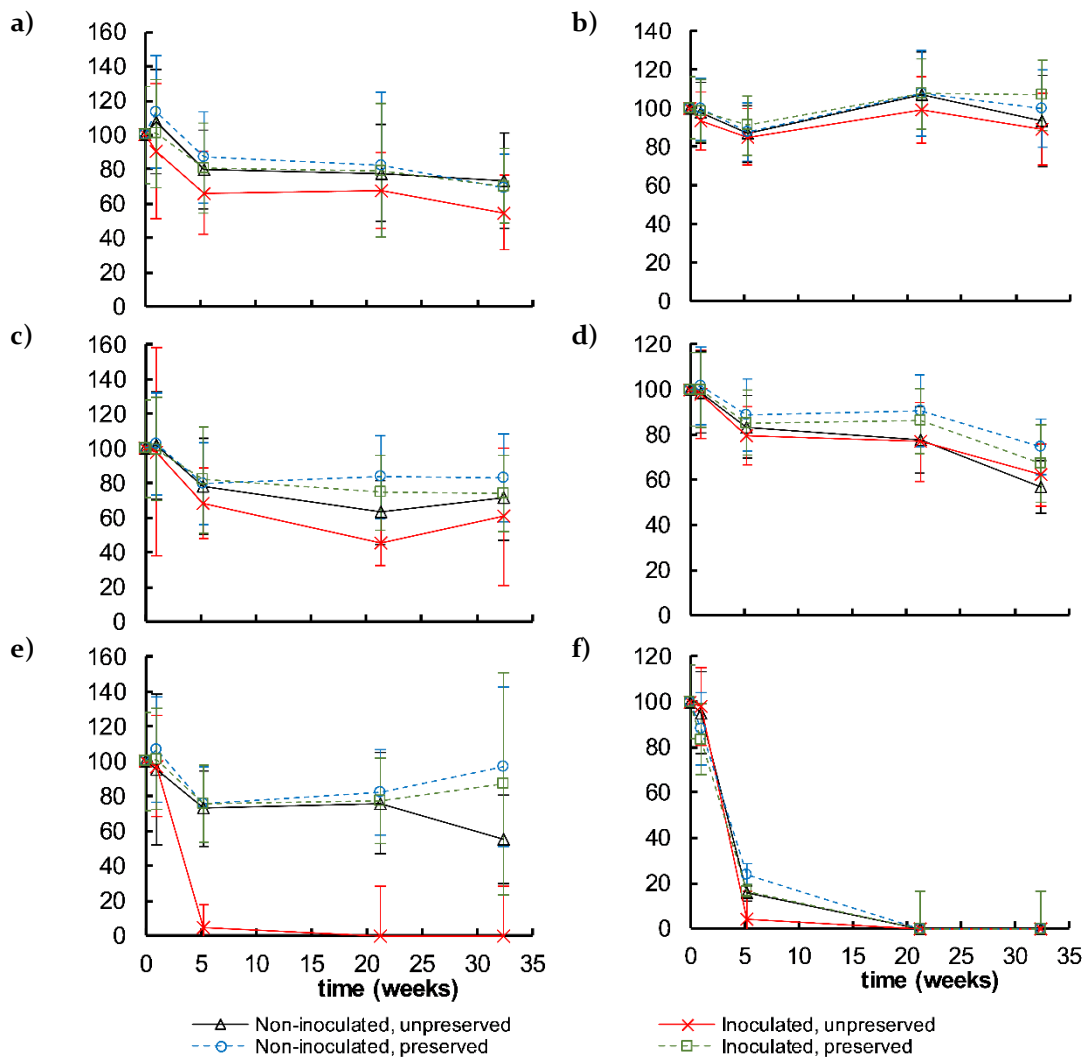


Figure 6-12: Relative concentration change (%) of a,c,e) LURA and b,d,f) ZIPR in blood specimens incubated at a,b) -20 °C, c,d) 4 °C, and e,f) room temperature for 7 months in experiment YB.

Y-axis is concentration change (%) for non-inoculated and inoculated, unpreserved, room temperature specimens and relative concentration change for all other specimens. Error bars are \pm uncertainty (6.2.3.3).

Losses for ASEN were not significantly greater than 20 % for any combination of temperature and specimen (Figure 6-10). AMIT, CLOZ, HALO, PERI, and QUET were found to be significantly more unstable after 12 months at room temperature in inoculated, unpreserved

specimens compared to other specimens (Figure 6-10 (c)). PROC was significantly more unstable in unpreserved, room temperature specimens compared to preserved, room temperature specimens (Figure 6-10 (c)). FLPH was significantly more unstable in inoculated, unpreserved specimens compared to preserved, room temperature specimens (Figure 6-10 (c)). Greatest mean losses of FLTX were obtained in inoculated, unpreserved specimens, however, these results were not significant (Figure 6-10 (c)).

In non-inoculated, unpreserved specimens CHLO, DOTH, PROC, and TRIF degraded more significantly at room temperature than at 4 °C. In these same specimens: DOTH, PERI, and TRIF also degraded more significantly at room temperature than at -20 °C; significantly greater than 20 % losses were observed for CHLO and PROC at -20 °C and room temperature; and significantly greater than 20 % losses were observed for ARIP, CLOM, and FLPH at room temperature (Figure 6-10). In preserved specimens, FLPH and PROC degraded more significantly at -20 °C and room temperature than at 4 °C (Figure 6-10). In non-inoculated, preserved specimens: CHLO, FLTX, and PROC degraded significantly by more than 20 % stored at -20 °C; and PROC and FLPH were significantly more stable at 4 °C than at room temperature (Figure 6-10). For inoculated, unpreserved specimens, significant degradation at room temperature was observed for CLOZ, FLPH, PROC, HALO, PERI, and QUET compared to -20 °C and 4 °C; and for CHLO and FLTX compared to 4 °C (Figure 6-10). Losses for CLOZ, FLPH, and PERI were significantly greater than 40 %. In inoculated, preserved specimens, significant losses greater than 20 % were obtained for FLPH stored at room temperature only (Figure 6-10). In these specimens, FLPH and PROC were significantly more unstable at room temperature compared to -20 °C and 4 °C.

In all specimens, ZIPR degraded until no longer detected at room temperature (Figure 6-12 (d-f)). The extent of ZIPR degradation at 4 °C compared to -20 °C was significant in non-inoculated, unpreserved and inoculated, preserved specimens (Figure 6-11). LURA was more significantly degraded at room temperature than at -20 °C in inoculated, unpreserved specimens (Figure 6-11). Losses for LURA in these specimens were greater than 20 % at -20 °C.

6.3.6 Degradation products detected by LC-DAD

6.3.6.1 Sulfoxide formation and dechlorination

The responses of CHLO-SO and PROC-SO were also determined over time throughout the experiments. In the week-long experiment, a trend appeared for the sulfoxide metabolites increasing in blood specimens over time, and at a greater rate in preserved specimens compared to unpreserved specimens (Figure 6-13 (a-b)).

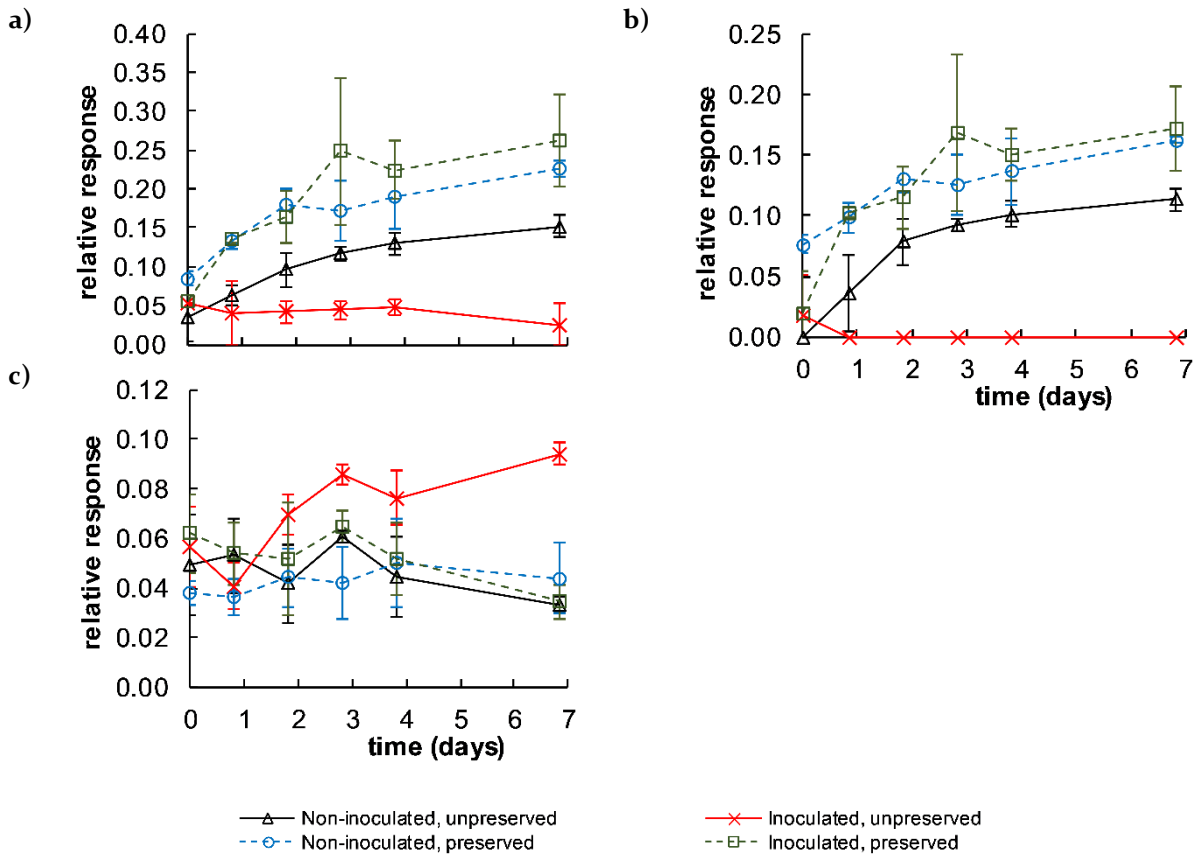


Figure 6-13: Relative response to LORA for a) CHLO-SO, b) PROC-SO, and c) PERA in blood specimens incubated at 37 °C for 7 days in experiment WA.

Error bars are \pm S.D., $n = 3$, except for PERA inoculated, unpreserved $n = 2$ at ~ 2 days.

The difference between the response of CHLO-SO and PROC-SO in non-inoculated unpreserved and preserved specimens was significant (Welch's t-test: $p < 0.02$). CHLO and PROC degradation and CHLO-SO and PROC-SO response were greatest in inoculated, preserved specimens (Figure 6-5 (b) and Figure 6-13 (a-b)). However, CHLO and PROC were not significantly less stable in any of the blood specimens. In all specimens, mean relative concentration changes (%) for CHLO and PROC were not less than 80 % (i.e. losses not greater than 20 %), indicating that the propensity for these drugs to form sulfoxide metabolites would likely have little impact on casework results and interpretation. In inoculated, unpreserved specimens, no increase in the relative response of CHLO-SO was observed over time and PROC-SO was not detected other than in the initial extract. This is consistent with the expectation that the inoculated microorganisms would preferentially respire aerobically, if able, to deplete oxygen levels in blood, limiting sulfoxide formation.

These results indicate that sulfoxide formation may occur not just during the unbuffered LLE as proposed in Chapter 4. Non-detection of PROC-SO in all but the initial extract may be due to its presence in blood $< LOD$.

No significant variation (Welch's t-test: $p > 0.05$) was observed for the relative response of PERA, an impurity present in the PROC stock (Appendix A), over time in extracts from any of the blood specimens (Figure 6-13 (c)). As noted above, PROC did not measurably degrade over time in inoculated, unpreserved specimens.

In the year experiment, the greatest losses of CHLO and PROC obtained in non-inoculated, preserved specimens stored at $-20\text{ }^{\circ}\text{C}$ correlated with greater amounts of CHLO-SO and PROC-SO detected over time compared to other specimens (Figure 6-14 (a-f)). This differs from the greatest responses of CHLO-SO and PROC-SO having been obtained in inoculated, preserved specimens in the week experiment (Figure 6-13 (a-b)). The response of CHLO-SO and PROC-SO in non-inoculated preserved and unpreserved specimens was significantly different (Welch's t-test: $p < 0.05$). Relative responses of CHLO-SO and PROC-SO in specimens incubated at $4\text{ }^{\circ}\text{C}$ were less than all other specimens, and the detection of both CHLO-SO and PROC-SO was sporadic. The fluctuating detection of CHLO-SO and PROC-SO may be due to their presence near their unknown LOD in the method. Losses were also statistically similar for CHLO and PROC in non-inoculated and inoculated, unpreserved specimens stored at room temperature (Figure 6-10 (c)). This implies degradation of CHLO and PROC to their sulfoxides may be occurring in non-inoculated, unpreserved specimens but that a different degradation product is formed in inoculated, unpreserved specimens. Minimal detection of the sulfoxides in room temperature inoculated, unpreserved specimens was comparable to their detection in the $37\text{ }^{\circ}\text{C}$ week experiment.

The quantification of PERA was not possible after ~ 25 weeks in room temperature, inoculated, unpreserved specimens, due to coelution with a compound later identified as nortriptyline (NORT) (see Chapter 7). As with the week experiment, there was no significant variation in PERA relative response over time in extracts of any blood specimens (Figure 6-14 (g-i)). This provides further support that dechlorination of PROC to yield PERA is not likely to occur in blood specimens and, as no significant increases were observed in the inoculated, unpreserved specimens, by extrapolation post-mortem blood.

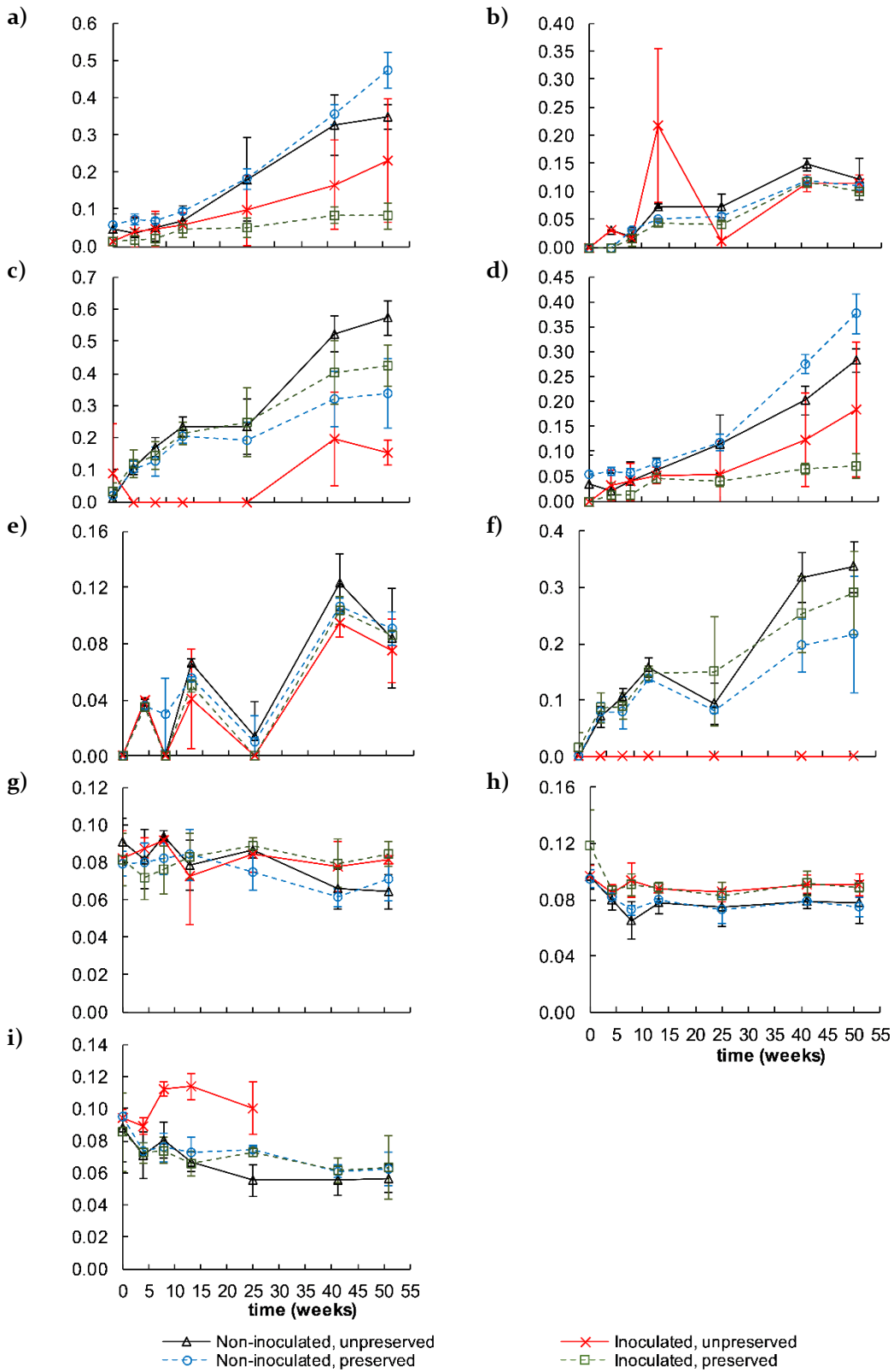


Figure 6-14: Relative response to LORA for a-c) CHLO-SO, d-f) PROC-SO, and (g-i) PERA in blood specimens incubated at a,d,g) -20 °C, b,e,h) 4 °C, and c,f,i) room temperature for 12 months in experiment YA.

Y-axis is relative response. Outlier obtained for one replicate at ~13 weeks for CHLO-SO (4 °C, inoculated, unpreserved). Error bars are ± S.D., n = 3.

6.3.6.2 Unknown peaks

During experiment YA, chromatographic peaks were detected in inoculated, unpreserved specimens that were not present in the microbial matrix or blood matrix controls, indicating they may be drug degradation products. From UV-Vis spectra, it appears that there may be multiple compounds co-eluting to produce the peaks at 16.8 min and 18.5 min or that the chromophores of the parent drugs are altered during degradation (Figure 6-15). Manual fraction collection followed by LC-QTOF-MS analysis of these peaks is detailed in Chapter 7.

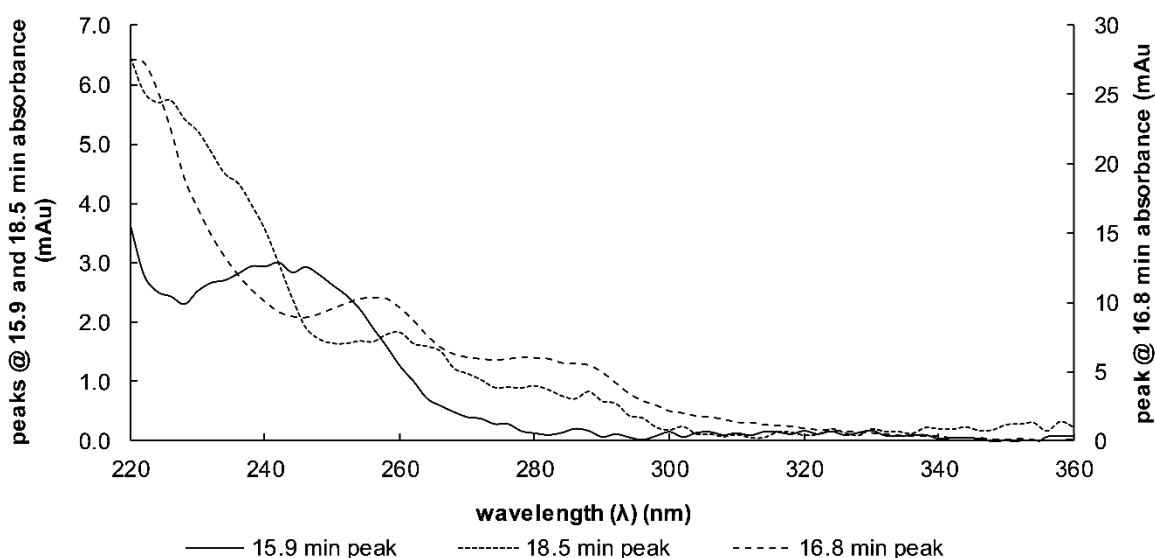


Figure 6-15: UV-Vis absorbance spectra of three unknown peaks eluting in experiment YA.

6.3.7 Comparative discussion of degradation

The stability of some of the drugs investigated in this study has previously been assessed in post-mortem specimens or in non-inoculated ante-mortem human whole blood. The experimental design used in this research also involved non-inoculated blood specimens as necessary controls to assist in determining the propensity of drugs to be microbially degraded.

ARIP, ASEN, CLOZ, FLPH, HALO, QUET, and TRIF have all been previously reported as stable in preserved ante-mortem whole blood by Saar *et al.*, who found losses for these drugs did not exceed 15 % after 10 weeks at -60 °C, -20 °C, 4 °C, and 20 °C [291]. The work in this thesis has established that none of these drugs are expected to degrade by key microbial species that may be present in post-mortem blood. Results of the week-long experiments in this thesis at 37 °C also support the findings in the Saar *et al.* study that these drugs are stable in a blood matrix. The lower temperature experiments performed in this thesis were of longer duration than in

the Saar *et al.* study and indicate some of these drugs are unstable (> 15 % losses) after extended storage at -20 °C and room temperature. The phenothiazines, FLPH and TRIF, were both found to have losses exceeding 15 % after a year and seven months, respectively, in the non-inoculated, unpreserved specimens. In non-inoculated, preserved specimens: TRIF losses were greater than 20 % and FLPH losses were greater than 15 %. At room temperature, losses of FLPH were also greater than 20 % in the inoculated specimens. In inoculated, preserved specimens stored at room temperature TRIF losses were greater than 15 %.

CLOZ was reported as stable by Saar *et al.* in preserved ante-mortem human whole blood stored at -20 °C, 4 °C, and room temperature for 20 weeks [291], Duffort *et al.* in preserved human whole blood (unknown if ante- or post-mortem) stored at -20 °C, 4 °C, and ambient temperature for seven days to six months [327], and Holmgren *et al.* in 4 preserved post-mortem femoral blood specimens re-analysed after 12 months storage at -20 °C [313]. Consistent with these prior studies, in the present study, CLOZ was found to be stable in preserved specimens stored at room temperature for a year. However, in inoculated, unpreserved specimens greater than 40 % losses were observed after this time, indicating possible microbial degradation. If not microbial degradation, it may be that microbial alteration of the blood environment is resulting in chemical instability.

QUET and HALO also exhibited instability in inoculated, unpreserved specimens (> 30 % losses) stored at room temperature for a year. Duffort *et al.* reported that FLPH and HALO were unstable in both preserved and unpreserved human whole blood stored at -20 °C, 4 °C, and ambient temperature [327]. For the degradation of the psychiatric medications investigated in this study it was unknown whether the matrix tested was ante- or post-mortem and concentrations of sodium fluoride in preserved specimens were variable within the range of 0.1-2 % w/v and unspecified [327]. Therefore, it is possible that the concentration of sodium fluoride in some specimens was not enough for a preservative effect [297, 448, 449]. In their report, losses greater than: 50 % were observed after 6 months stored at -20 °C; 60% after 6 months at 4 °C; and greater than 40 % after only a month at room temperature [327]. Degradation of these drugs was remarkably different in the experiments in this thesis, and no degradation was observed at -20 °C and 4 °C for any of the specimens. It may be that the instability of HALO may be partially attributable to hydrolysis reactions given its instability in neutral and alkaline aqueous solutions (5.2.2), however, if so, it is surprising that HALO was seemingly stable in all other specimens.

ARIP was also unstable (> 20 % losses) after seven months in non-inoculated, unpreserved specimens stored at room temperature.

No prior studies have investigated LURA stability in human whole blood. As in this study, ZIPR was previously reported by Saar *et al.* to degrade at 20 °C in preserved ante-mortem human whole blood [291].

ZUCL was investigated by Saar *et al.* and observed to be stable after 10 weeks in preserved ante-mortem whole blood stored at -60 °C, -20 °C, 4 °C, and 20 °C [291]. ZUCL is a thioxanthene structurally similar to FLTX. FLTX was not stable when stored at -20 °C in non-inoculated specimens, or when stored at room temperature in inoculated, unpreserved specimens.

CHLO, in common with some other phenothiazines, FLPH and PROC, degraded by more than 15 % in all -20 °C and room temperature specimens after a year. Greater degradation at -20 °C than 4 °C was consistent with observations by Saar *et al.* [291]. However, the extent of degradation in the experiments in this thesis (up to 40 % losses after 12 months in inoculated, unpreserved specimens at room temperature) was lesser compared to other reports of CHLO instability in blood stored at room temperature in literature. Coutselinis *et al.* found CHLO to degrade until undetected after 6 months in unpreserved post-mortem blood [326]. Lutfi found 70 % losses after 12 months in post-mortem blood (unspecified if preserved or unpreserved) [319] and Duffort *et al.* reported over 40 % losses after just a month in preserved and unpreserved human whole blood [327]. Batziris *et al.* reported that CHLO was stable in blood inoculated with *C. perfringens* and incubated for a day at 37 °C [318]. In the 37 °C week experiments, in which *C. perfringens* dominated inoculated, unpreserved specimens, CHLO was also observed to be stable. Enhanced losses in authentic post-mortem blood specimens may therefore indicate that the model in this thesis did not accurately simulate the post-mortem blood environment of these cases or did not contain the microorganism responsible for CHLO degradation, if its degradation occurs by microbial activity.

In this study, DOTH was found to be stable in most specimens regardless of preservative or microorganisms. Results were consistent with previous studies which reported no degradation of DOTH in blood inoculated with *C. perfringens* (after 24 hours at 37 °C) and in post-mortem blood inoculated with human faecal bacteria (after seven days at 37 °C) [191, 318]. However, Duffort *et al.* reported greater than 75 % losses in both unpreserved and preserved human whole blood after 1 month at room temperature, and 6 months at 4 and -20 °C [327]. DOTH has also been reported to completely degrade in putrefying liver macerates [195]. Losses exceeded 30 %

in non-inoculated, unpreserved specimens stored at room temperature for 7 months in this thesis.

MIRT was observed to be stable in all specimens, although coelution with matrix degradants prevented its quantification throughout the full duration of the experiments. MIRT was considered to be stable by Holmgren *et al* in preserved post-mortem blood stored at -20 °C for a year and by Duffort *et al.* in blood stored at -20 °C and 4 °C for six months, and ambient temperature for a month [313, 327]. CLOM was stable in all specimens except for non-inoculated, unpreserved specimens at room temperature, with losses greater than 20 % after 7 months. Holmgren *et al.* reported that CLOM was stable for a year in preserved post-mortem blood specimens stored at -20 °C, which was consistent with results of these experiments [313]. Results for CLOM stability at -20 °C and 4 °C were also consistent with results of Duffort *et al.*, who found CLOM stable at -20 °C and 4 °C for 6 months in blood specimens [327]. Duffort *et al.* also reported greater than 20 % losses in ambient temperatures specimens as soon as after one month [327].

MOCL was generally stable in all specimens, although greater than 15 % losses were observed in -20 °C inoculated, preserved specimens and room temperature non-inoculated, unpreserved specimens stored for 7 months. This was considerably less than the 45 % and greater losses of MOCL at 4 °C and -20 °C reported by Duffort *et al.* after 6 months in preserved and unpreserved blood specimens [327]. However, as discussed previously, the sodium fluoride concentrations and ante- or post-mortem nature of the matrix was not known in the Duffort *et al.* study [327].

Amongst room temperature specimens, losses greater than 20 % were observed for ARIP, CLOM, DOTH, and TRIF in only non-inoculated, unpreserved specimens. The absence of colonies following plating of these specimens on agar, and the stability of RISP, likely indicates degradation of these drugs did not result from microbial contamination but chemical instability in the matrix. CLOM was previously indicated to be unstable in aqueous neutral and alkaline solutions (5.2.2).

The apparent degradation of AMIT prevented the valid normalisation of concentration changes of drugs to AMIT concentration changes in some specimens. AMIT has been reported as a stable drug in putrefying liver macerates that were stored outside with exposure to necrophagous blow flies and rain protection [195]. It is also reportedly stable in preserved post-mortem blood when stored at -20 °C for at least one year [313], which is consistent with results from experiment YA. Butzbach also found the drug stable in bacterially inoculated porcine blood incubated at 37 °C

for up to 11 days [223]. Not contradictory to these studies, Lutfi found losses of 84 % in post-mortem blood (unknown if preserved or not) stored at 25 °C for a year [319]. This latter study likely best approximates the conditions of the specimens where AMIT degradation was greatest observed (i.e. inoculated, unpreserved specimens stored at room temperature in experiment YA and YB). Surprisingly, AMIT also degraded along with other drugs in the non-inoculated, unpreserved specimens stored at room temperature in experiment YB. No bacteria or fungi were found to have contaminated these specimens that grew on Columbia Blood or Sabouraud Dextrose Agar. It is unknown what the cause of AMIT degradation in this specimen may be. Peculiarly, AMIT did not degrade similarly in the non-inoculated, unpreserved specimens stored at room temperature in experiment YA, indicating the environment in the YB specimens was more amenable to its degradation.

6.4 Microbial analyses results and discussion

6.4.1 Sterility, viability, and cell counts

Inoculates of the non-inoculated specimens did not grow colonies on the Columbia Blood and Sabouraud Dextrose Agar plates over five days (6.2.5.2), indicating that microbial contamination of these specimens during specimen preparation and sampling was not probable. RISP spiked after a week into inoculated, unpreserved specimens in the week-long experiments once more degraded (6.2.5.3), indicating bacteria successfully respired throughout the duration of these experiments.

For experiment WB2 and YB, optical microscopy of the fixed diluted FMT specimens revealed the presence of fibrous tissue around which cells were clustering. Therefore, the attempt to homogenise the FMT specimens prior to inoculation was considered unsuccessful. This is evident from the cell counts obtained (Table 6-3).

Table 6-3: Cell counts by microscopy using a Petroff Hausser Counting Chamber for experiment WB2 and YB inoculate.

WB2		Number of cells per mL (x 50,000)			
replicate	1	2	3	Mean	
1	20	36	48	35	
2	45	24	20	30	
3	46	28	34	36	Grand mean: 34
YB					
replicate	1	2	3	Mean	
1	8	26	44	26	
2	21	35	26	27	
3	12	68	42	41	Grand mean: 31

6.4.2 Sequencing results

A guide to sample ID nomenclature is provided in Table 6-4.

Table 6-4: Sequenced sample ID nomenclature.

Letter/number	Description
W	Week experiment
Y	7- or 12-month (year) experiment
A	Samples collected as part of Week experiment A
B	Samples collected as part of Week experiment B
3	Samples collected after 3 months at room temperature
6	Samples collected after 6 months at room temperature
7	Samples collected after 7 months at room temperature
12	Samples collected after 12 months at room temperature
II / I2	Samples collected from FMT specimens the day before inoculation in experiments
C	Samples collected from microbial matrix “control” specimens (see Table 6-1, #2-3)
S	Samples collected from inoculated drug “sample” specimens (see Table 6-1, #6-7)
UN	Unpreserved specimens (see Table 6-1, #2, #6)
P	Preserved specimens (see Table 6-1, #3, #7)

Obtained reads for specimens ranged from 11,327 to 174,810 (Table C-1). DNA extraction was not successful to enable sequencing for WB_CUN1, WB_CP2, WB_CP3, WB_SPI, WB_SP2, WB_SP3, YA_3-SPI, YA_3-SP2, YA_3-SP3. The reason for this is unknown, although may be due to low microorganism concentrations in the preserved specimens. Results for WA_SP3 indicated contamination during extraction due to significantly greater OTUs detected (808). Therefore, this sample was excluded from further analyses.

Across all samples, $\sim 100.00 \pm 0.01$ % (S.D.) of sequences were defined at the order level, 97.72 ± 3.38 % (S.D) at the family level, 70.76 ± 21.14 % (S.D) at the genus level, and 28.24 ± 17.25 % (S.D) at the species level. Two-hundred-and-three OTUs remained, after combining the data from numerous sequencing runs to determine inter-sample variations in microbial communities. Bacterial OTUs were obtained belonging to 9 phyla, 21 classes, 28 orders, 56 families, 82 genera, and 34 species. These figures exclude undefined orders, families, genera, and species, which before combining runs may have been undefined but unambiguously assigned as multiple taxa. Archaeal OTUs were undefined *Methanosphaera sp.* and *Methanobrevibacter spp.* (2 different OTUs) and, in sample YA_6-CUN and YA_12-CUN, an undefined *Methanomassiliicoccus sp.*. All genera have members known to inhabit the human gastrointestinal tract [31].

6.4.3 Community comparisons

Diversity indices were calculated as described in 6.2.5.4. From plots of species richness versus sequence reads obtained for each sample it could be seen that with increasing sequencing depth a greater number of OTUs were detected (Figure 6-16 (a)). Despite this, greater species richness was consistently observed in the FMT samples compared to other samples with comparable sequencing reads, indicating the different specimen types may have variable species richness reflective of the environment and not the sequencing process. All other diversity indices produced comparable results with the diversity of the communities generally proceeding from most diverse in the FMT specimens, to sometimes less diverse in preserved blood specimens, and to least diverse in the unpreserved blood specimens (Figure 6-16).

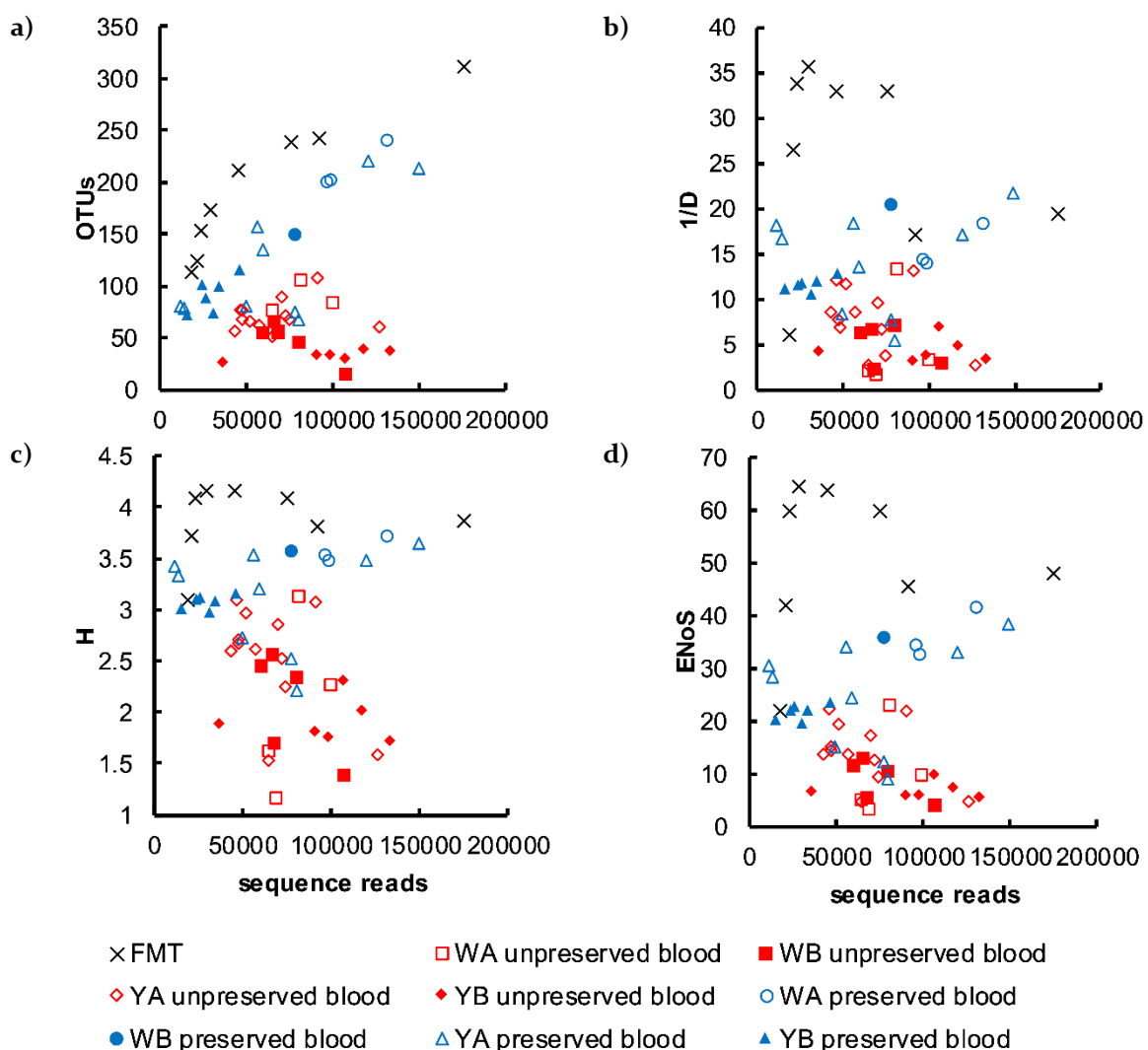


Figure 6-16: Microbial diversity index scatterplots.

a) Species richness (number of OTUs), b) Simpson's Reciprocal Index (1/D), c) Shannon-Wiener Index (H), and d) effective number of species (ENoS) vs. sequence reads.

The observation that unpreserved blood specimens were generally less diverse than preserved blood specimens and FMT specimens is also apparent from a graph identifying the taxa present with a relative abundance greater than 30 % (Figure 6-17). FMT specimens were generally not dominated by any one taxon. Exceptions are WA_I2, where a *Ruminococcus* sp. was particularly dominant at ~40 %, and YA_II and YA_I2, where a Ruminococcaceae taxon accounted for over 30 % of all reads. For experiment WA, unpreserved blood specimens were overwhelmingly dominated by *C. perfringens*, with only 40 % of other reads attributed to other taxa. For experiment WBI, *C. perfringens* was not dominant in one replicate (WB_SUN1). In the longer-experiments, unpreserved specimens after seven and twelve months had less than 60 % of total reads attributed to taxa with less than 30 % relative abundance.

For more detail regarding the OTUs identified in specimens see C.3.

By cluster analysis, the specimen type generally had the greatest impact on the similarity of the microbial communities detected in the specimens followed by the presence or absence of sodium fluoride in the blood specimens and the temperature at which blood specimens were incubated (Figure 6-18). However, WB_CUN3 and the YA_CP specimens did not cluster in accordance with these generalisations. Construction of a PCoA (principal coordinate analysis) ordination plot using Bray-Curtis similarities also visualised this (Figure 6-19).

More specifically: the WA and YA, and WB and YB specimens produced separate clusters with similarities greater than 80 %; separate clusters were formed between WA and WB unpreserved blood specimens with a similarity for samples within the clusters greater than 70 %; and most 37 °C unpreserved blood specimens clustered together with a similarity greater than 60 % as did the preserved blood specimens and FMT specimens. Therefore, in common with the diversity index calculations, preserved blood specimens and FMT specimens were more similar than unpreserved blood specimens. YA and YB unpreserved blood specimens clustered in two groups with similarities greater than 60 % and 50 %, respectively. Combined, all room temperature unpreserved blood specimens clustered together with similarities greater than 50 %.

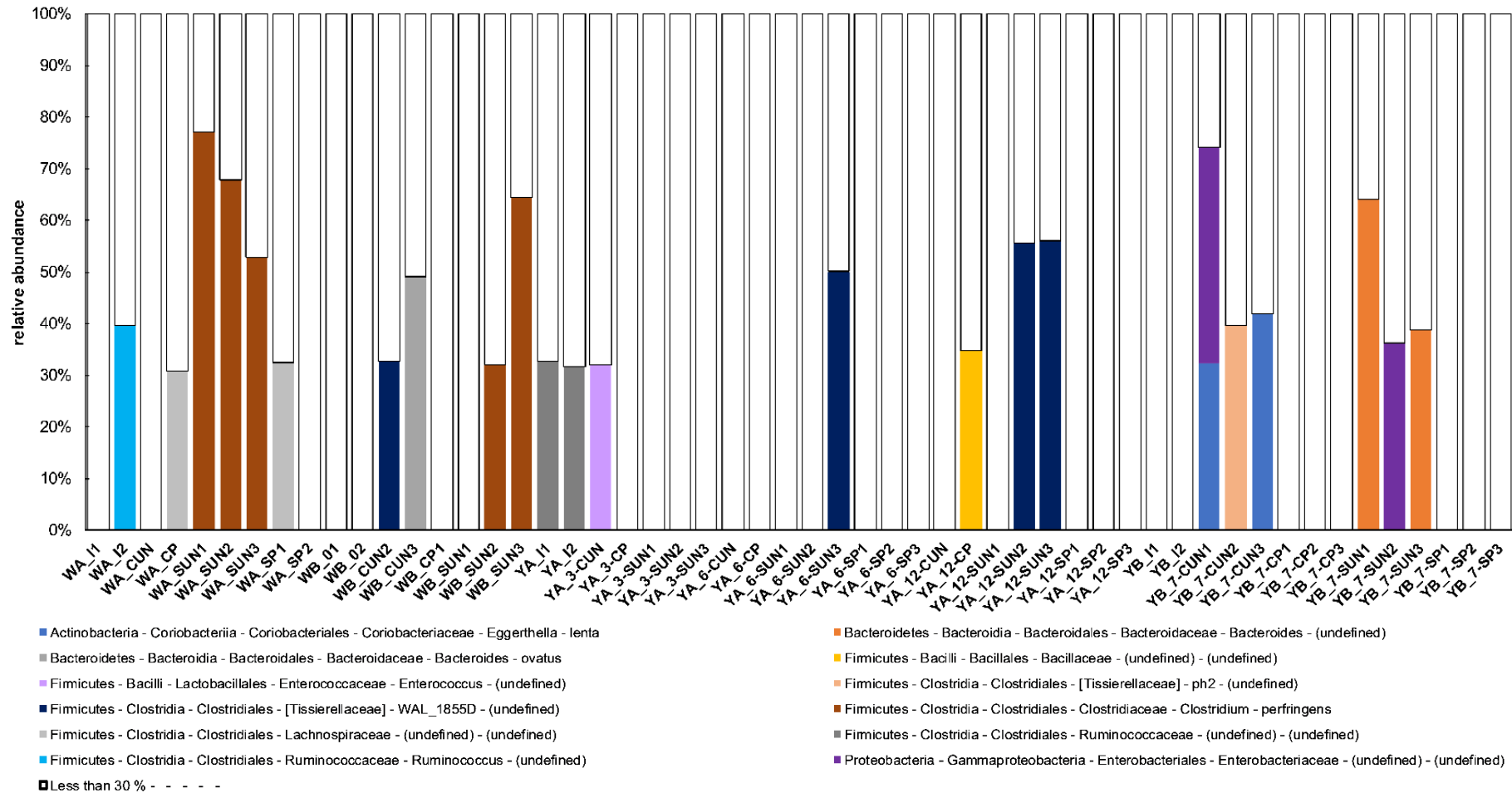


Figure 6-17: Most abundant species present in specimens.
Species with less than 30 % relative abundance are grouped together as “Less than 30 %”.

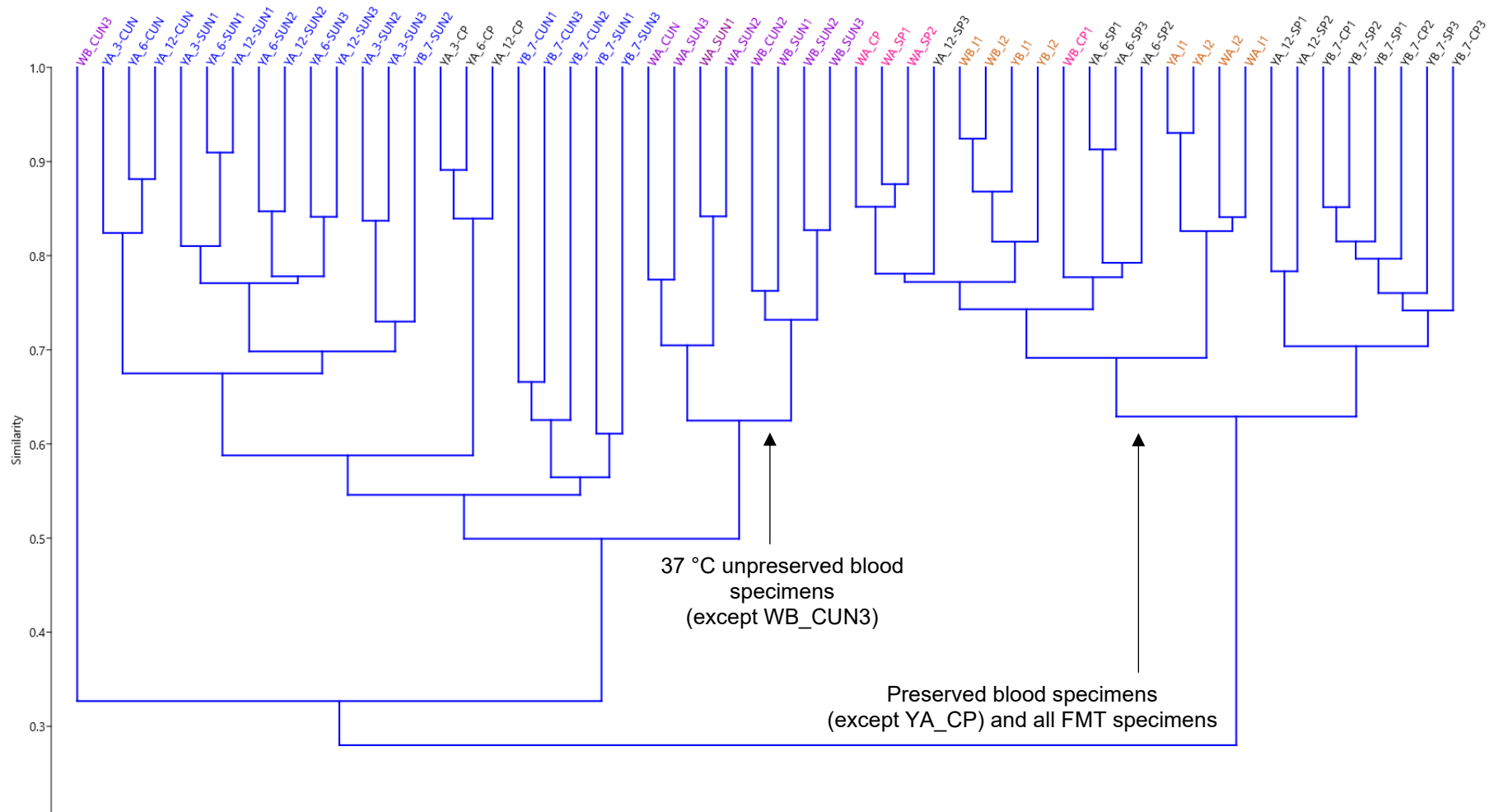


Figure 6-18: Hierarchical cluster dendrogram of specimens. Similarity calculated using Bray-Curtis similarity. Clustering method is UPGMA (unweighted pair group method with arithmetic mean).

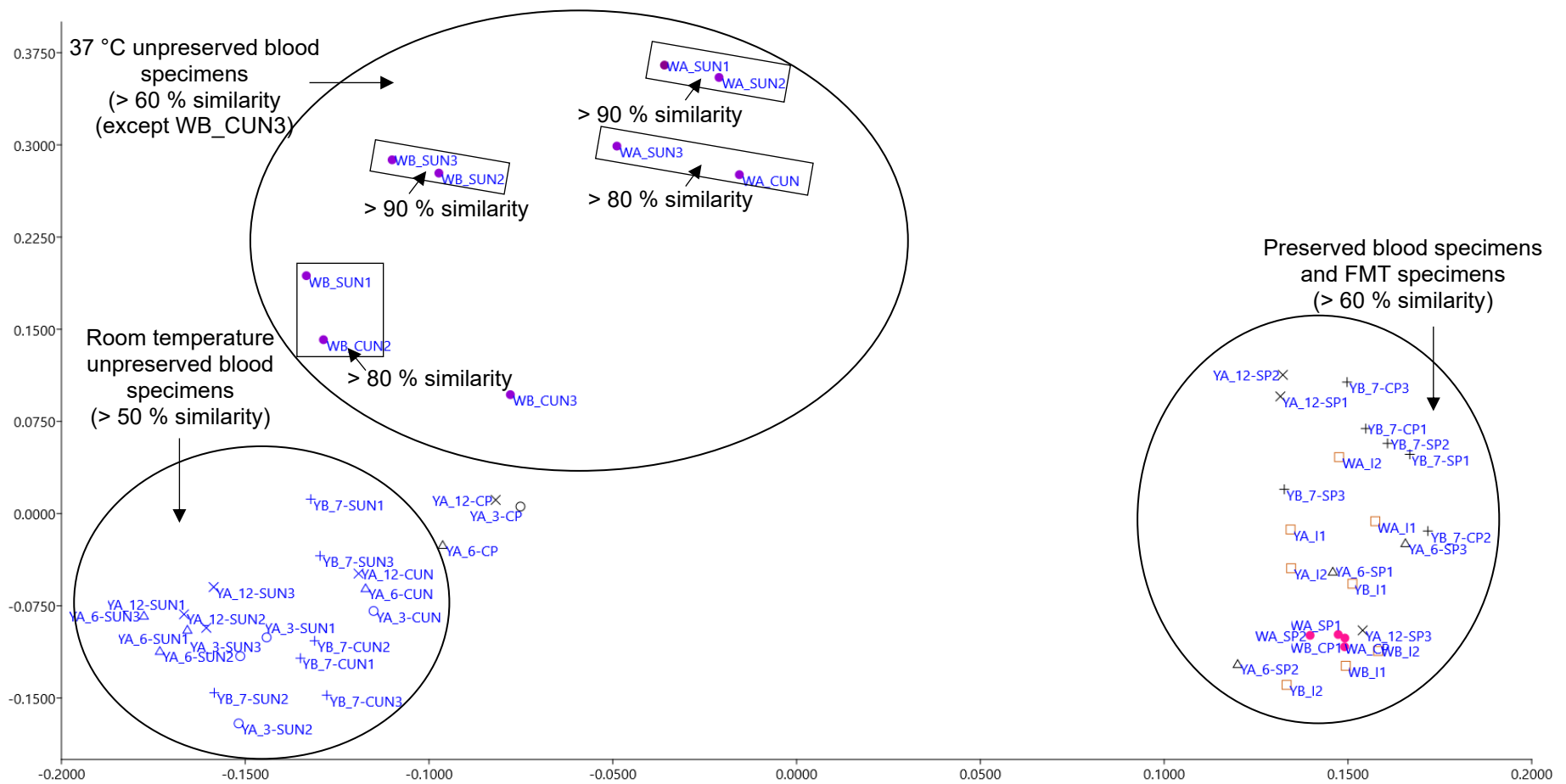


Figure 6-19: PCoA plot of specimens.

Similarity calculated using Bray-Curtis similarity. Similarity (%) values determined from cluster analysis (Figure 6-18).

6.4.4 Discussion

For most inoculated, unpreserved specimens incubated at 37 °C *C. perfringens* was the dominant microorganism detected. In one of these specimens a greater abundance of *B. fragilis* was noted followed closely by undefined *Bacteroides* sp. and undefined Proteobacteria taxa of the Enterobacteriaceae family. No taxa in this specimen solely accounted for over 25 % of the total abundance. The *B. fragilis*-dominated replicate took the longest for RISP, LURA, and ZIPR to reach undetectable levels. However, rates may differ due to variable concentrations of microorganisms inoculated, rather than the different communities.

Clostridium spp. are known to dominate post-mortem specimens [24, 25], and *B. fragilis* is an inhabitant of the gastrointestinal tract that may also translocate post-mortem [31]. *Bacteroides* sp. have been identified in post-mortem blood [330]. Other co-dominant taxa in this specimen were also facultative and obligate anaerobes which may also be present in post-mortem specimens, as they are part of the human microbiome [31]. The dominance of *C. perfringens* in most of the experimental specimens may be attributed to its rapid replication rate at 37 °C, which is reportedly as low as 10 minutes in ground beef [450]. The growth of *B. fragilis* was likely supported by the presence of haem as this is known to stimulate its growth in anaerobic conditions [451]. These results support the experimental plan as adequately imitating the immediate post-death post-mortem environment of blood and the proposition that in post-mortem blood these drugs will be stable from microbial, enzymatic, and hydrolytic degradation.

This outcome indicates that the routine introduction of oxygen during specimen sampling did not hinder the growth of anaerobic microorganisms, as both *C. perfringens* and *B. fragilis* are obligate anaerobes. This was expected, as oxygen gradients that form when culturing microorganisms would likely also become established in the blood specimens. Therefore, future studies investigating the stability of drugs by forensically relevant post-mortem microorganisms need not utilise an exclusively anoxic environment allowing for greater ease of specimen handling and sub-sampling.

Inoculated, unpreserved, room temperature specimens were more favourable toward the growth of Actinobacteria and Bacteroidetes taxa. After three months, *Enterococcus* spp., *Bacteroides* spp. and Enterobacteriaceae were dominant. From six months onwards, Clostridiales species became increasingly dominant (Figure C-1 and Figure C-2). However, members of the other taxa were still detected after twelve months. In comparison, inoculated, preserved, room temperature specimens were dominated by Lachnospiraceae and Ruminococcaceae taxa throughout the experiment.

Preserved specimens, regardless of temperature, afforded microbial communities most comparable to communities present in the FMT specimens, indicating microbial community composition did not change drastically. However, in many cases DNA extraction was not successful from preserved blood specimens for unknown reasons. From the data obtained the efficacy of 2 % w/v sodium fluoride to preserve post-mortem blood specimens is generally supported, as community stasis was most probably a result of hindered metabolism and growth. However, in the preserved microbial matrix control specimens of experiment YA communities with greater similarity to other unpreserved specimens were observed, indicating that in some cases preservation with 2 % w/v sodium fluoride was not as effective (Figure 6-18). Despite this, no colonies were observed on Columbia Blood Agar plates for these specimens. This may indicate that preservation in these specimens was not as effective against those species over an extended time interval. Given this, it may be a possibility that authentic post-mortem blood specimens from different individuals may be inconsistently preserved if the conditions that allowed for microbial growth and community shift in the experimental specimens are in place.

In total, at least 150 species were present in the blood specimens (73 in the unpreserved blood specimens) that may have affected drug degradation. There was a significant interaction between the preservative status of the blood specimens and the temperature at which the blood specimens were stored, with significantly different microbial communities favoured at 37 °C and room temperature in unpreserved specimens. Therefore, the drugs investigated in this thesis were tested for their stability against different microbial communities.

One caveat is that the microbial communities present in the inoculated specimens of this experiment may not represent all microorganisms that may be in post-mortem blood specimens. In particular, it may be the case that microorganisms translocate from other parts of the digestive tract that are not excreted in faeces and thus were not represented in these blood experiments [238].

6.5 UV-Vis spectroscopy of blood specimens

During experiments, inoculated, unpreserved blood was observed to undergo a colour change that was thought to be due to carboxyhaemoglobin formation due to the colour of diluted blood extracts (Figure 6-1). Extracts were therefore collected from unpreserved specimens for CO-Hb analysis using the UV-Vis spectroscopy method detailed in 6.2.6.

In both week experiments there was no significant formation of CO-Hb over time (Figure 6-20 (a)). The absence of absorbance between 610 and 630 nm in the unpreserved blood specimens

also indicated there was not a detectable amount of sulphaemoglobin present. Therefore, it could not be concluded that CO-Hb formation was responsible for the color change observed. In experiment YA there was a trend toward increasing CO-Hb concentrations over time (Figure 6-20 (b)), more apparent when considering replicates individually (Figure 6-21 (a)). In experiment YB CO-Hb concentrations only increased significantly in one replicate of the microbial matrix specimens (Figure 6-21 (b)).

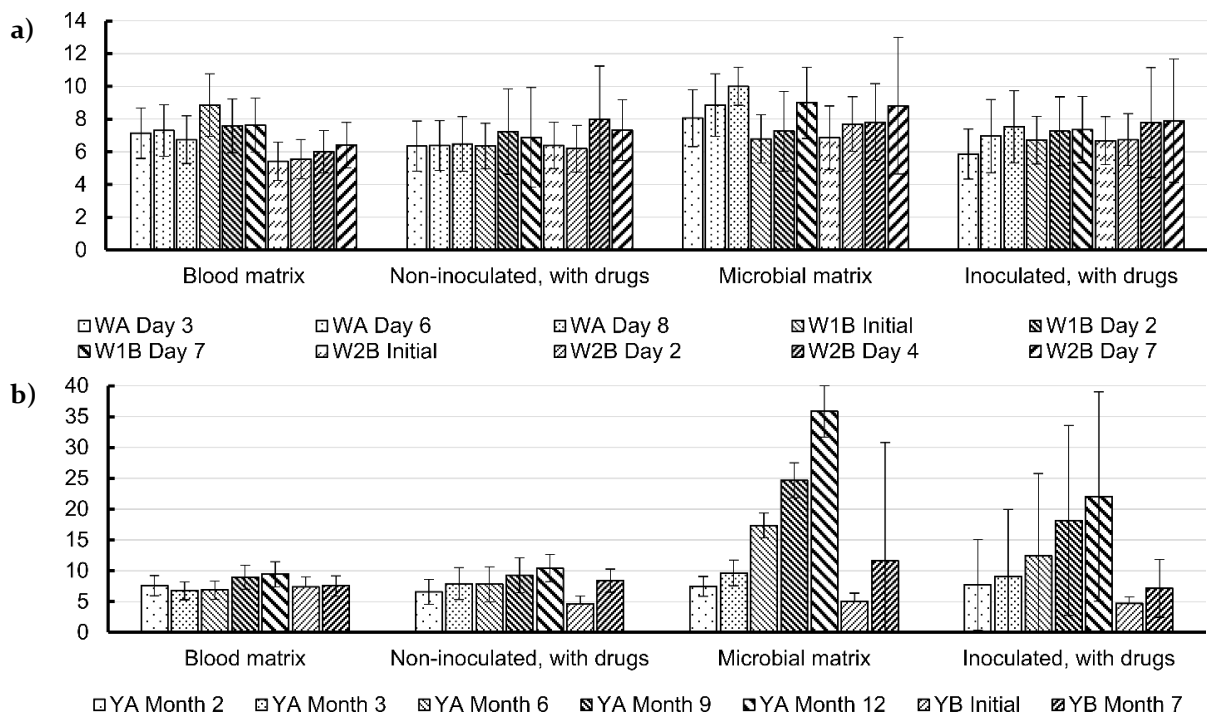


Figure 6-20: CO-Hb (%) in unpreserved blood specimens of the a) week-long experiments (WA, W1B, and W2) and b) longer experiments (YA and YB).

Y-axis is CO-Hb (%). X-axis is unpreserved specimen type. Error bars are \pm uncertainty (6.2.6); $n = 3$ for WA, YA, WB, and YB non-inoculated, with drugs, and inoculated, with drugs specimens, $n = 1$ for blood matrix and WA and YA microbial matrix specimens, $n = 3$ for WB and YB microbial matrix specimens.

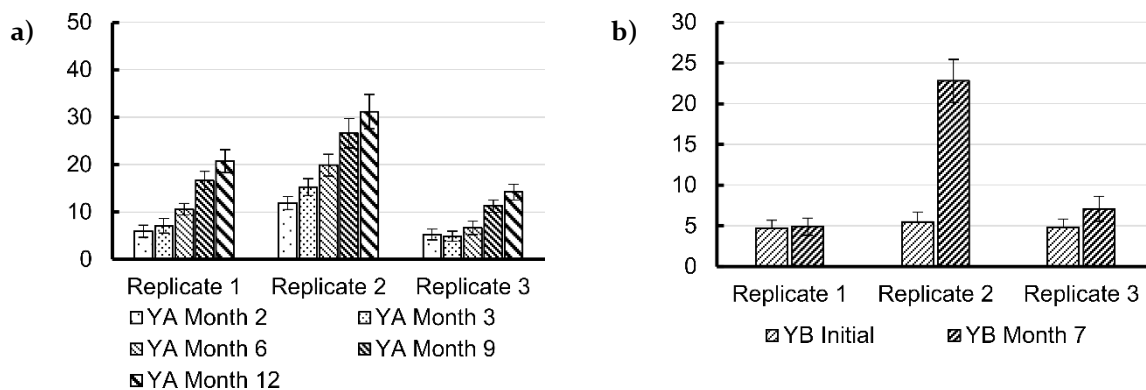


Figure 6-21: CO-Hb (%) in unpreserved blood specimens of the a) experiment WA, inoculated with drugs and b) experiment YB microbial matrix controls.

Y-axis is CO-Hb (%). X-axis is replicate number. Error bars are \pm uncertainty (6.2.6); $n = 3$.

Comparison amongst the UV-Vis spectra obtained for the diluted experimental blood specimens and ante-mortem blood found that inoculated, unpreserved blood specimens demonstrated a clear red shift towards 433 nm from 413 nm for the Soret band of haemoglobin (400-436 nm) characteristic of deoxyhaemoglobin (Figure 6-22) [452, 453]. This red shift was not present in inoculated, preserved specimens. Deoxyhaemoglobin is also reported to have a broad band in place of the α and β bands observed at 540 and 574 nm [454]. The α and β bands were not clearly distinguished in the inoculated, unpreserved (WKA, 37° C, 1 month) and inoculated, preserved (WKA, 37 °C, 1 month) spectra (Figure 6-22 (inset)). They were present in the ante-mortem blood, blood matrix specimen, and inoculated, unpreserved spectrum collected towards the end of the year experiment (YRA, r.t., 11 months). It appears that in inoculated, unpreserved specimens that deoxyhaemoglobin may be forming, and this may partially explain the brighter red colour of these specimens in the experiments.

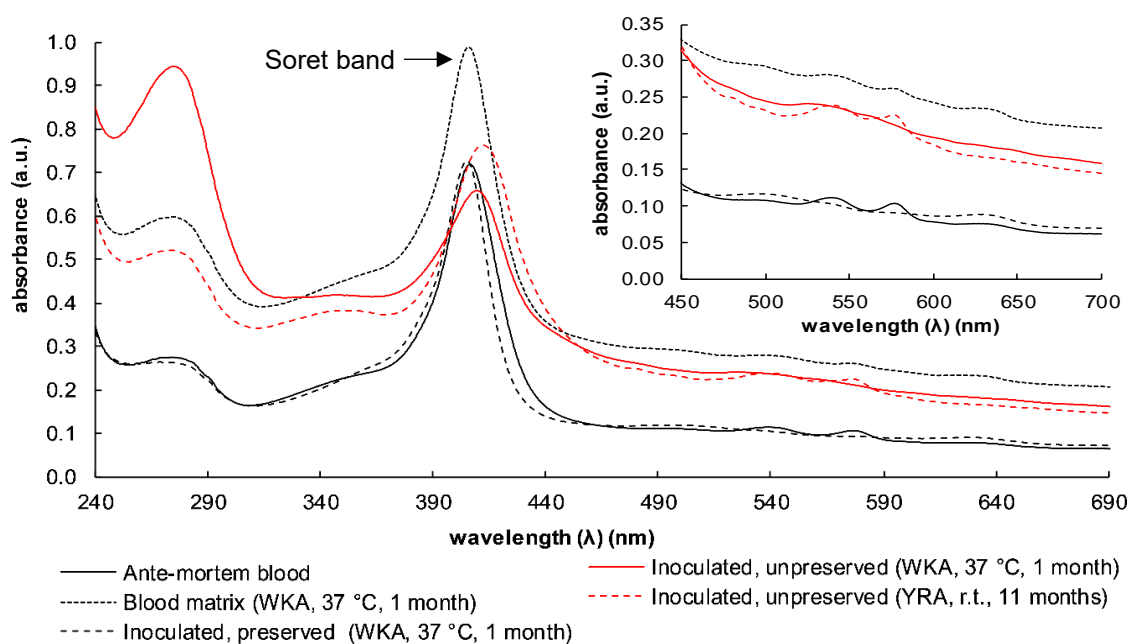


Figure 6-22: UV-Vis spectra of blood specimens.

6.6 Conclusions

The stability of 17 psychoactive drugs were investigated in ante-mortem human whole blood with and without forensically relevant microorganisms and preservatives present. The microorganisms inoculated in the experiments were sourced from FMT specimens and expected to be relevant to a post-mortem blood environment due to the migration of gastrointestinal bacteria into the circulatory system after death. The forensic relevance of the inoculated microorganisms was confirmed by 16S rRNA sequencing of the inoculated specimens incubated at room temperature and 37 °C.

ARIP, ASEN, CHLO, CLOM, CLOZ, DOTH, FLTX, FLPH, HALO, MOCL, PERI, PROC, QUET, and TRIF did not degrade significantly with no more than 20 % losses at 37 °C after a week or within a month at room temperature, in both inoculated and non-inoculated human whole blood, regardless of whether specimens were preserved or unpreserved. This indicates that these drugs may be stable in post-mortem blood and against key microbial species that may be present. MIRT was stable in all unpreserved specimens for these timeframes. In preserved specimens, coelution with matrix degradants prevented assessment of MIRT stability throughout the experiments. However, it is not possible to conclude from any observed stability that concentrations may remain steady in post-mortem blood after death as PMR may still affect the interpretation of post-mortem blood concentrations for some of these drugs (see discussion in 1.4.4). Furthermore, AMIT, CHLO, CLOZ, FLTX, FLPH, HALO, PERI, PROC, and QUET exhibited instability in inoculated, unpreserved room temperature specimens over extended timeframes which may be attributable or partially attributable to microbial activity. For CLOZ, HALO, and PERI degradation was significant compared to other non-inoculated and preserved specimens, indicating potential microbial degradation. Investigations to identify the degradation products correlated with the degradation of these drugs is detailed in Chapter 7.

LURA was determined to be degrading due to microbial activity, as its rate of degradation was similar to the transformation of RISP to the microbial degradant, HB-RISP in inoculated, unpreserved specimens at room temperature and 37 °C. Further supporting this conclusion, LURA did not degrade in non-inoculated specimens or in inoculated specimens incubated at temperatures considered to inhibit microbial activity, although the large method error may be obscuring some instability at 4 °C. ZIPR degraded until undetected in all blood specimens incubated at 37 °C and room temperature, with significantly greater instability at 4 °C than -20 °C also observed. This indicated instability in the whole blood matrix.

The degradation of LURA in inoculated, unpreserved blood specimens, and the degradation of ZIPR in all blood specimens, regardless of microorganism or preservative status, indicate that concentrations of these drugs in post-mortem blood may not be expected to reliably represent peri-mortem concentrations. Degradation rates for both LURA and ZIPR were comparable to RISP, which is known to degrade in post-mortem blood until only its degradation product, HB-RISP, may be detected [2, 3]. The observed degradation of LURA and ZIPR was therefore significant and warranted further investigation to determine the identity of the possible degradation products of LURA and ZIPR as it may be the case that only their degradation

products would be detected in casework to support the peri-mortem presence of LURA and ZIPR. Chapter 8 and Chapter 9 detail this work.

When stored at lower temperatures (-20 °C, 4 °C, and room temperature) and over a longer time period (seven to twelve months) drugs otherwise stable in the week-long 37 °C experiments were found to degrade. In particular, the long-term storage of blood specimens as non-frozen was supported by the significantly enhanced stability of CHLO, FLPH, PROC, and FLTX at 4 °C than at -20 °C in non-inoculated, preserved specimens after a year of storage. Theoretically, 4 °C is the ideal temperature for the storage of post-mortem specimens containing these drugs, as it limits microbial growth without freezing the matrix and potentially subjecting drugs to degradation during freeze-thaw cycles. However, there are other drugs which are more stable at -20 °C than at 4 °C and therefore it cannot be recommended that all blood specimens collected for drug analysis be stored at 4 °C [403, 406, 407]. Furthermore, it was also indicated that frozen storage or repeated freeze-thaw cycles of CHLO and PROC in human whole blood may accelerate sulfoxide formation, whereas microbial respiration may limit sulfoxide formation. Further work is necessary to establish this, as the LC-DAD method used in thesis was not validated for the analysis of the sulfoxides, which were detected near their suspected LOD. Dechlorination of the aryl chloride, PROC, to form PERA, was found to be insignificant in all specimens. It may be that the dechlorination of aryl chlorides as a class may not occur in post-mortem specimens.

CHAPTER 7 - DEGRADATION PRODUCTS IN BLOOD EXPERIMENTS

7.1 Outline

In the blood experiments detailed in Chapter 6 numerous antidepressant and antipsychotic drugs were found to be unstable in whole blood specimens stored for seven to twelve months. In experiment YA, additional peaks in the chromatogram were also noted to form in inoculated, unpreserved specimens spiked with drugs, indicating that they may be drug degradation products (see 6.3.6.2). This chapter details the analyses of experiment extracts and collected LC-DAD fractions by LC-QTOF-MS to identify and monitor the degradation products forming during the Chapter 6 blood experiments.

The degradation products for LURA and ZIPR are discussed in Chapter 8 and Chapter 9, respectively.

Chemicals, materials, and instrumentation were used as listed in Chapter 3.

7.2 LC-QTOF-MS analyses of blood experimental extracts

7.2.1 Experimental

An Agilent 1200 Series HPLC and Agilent 6520 Series LC-QTOF-MS (configured as described in 3.3.2) was used to screen experiment extracts for degradation products that may not have been detected by the LC-DAD method as well as manually collected LC-DAD fractions. Calibrator, QC, and blank samples were analysed concurrently with specimen extracts. Extracts from 6.2.3 were diluted with 375 μ L of ethanol, vortexed, and centrifuged prior to LC-QTOF-MS analysis. Initially, final and initial week extracts were analysed to determine if subsequent LC-QTOF-MS analysis of extracts throughout the experiments was warranted. For the longer experiments, LC-QTOF-MS analysis was performed routinely following LC-DAD analysis.

7.2.1.1 MS data analysis

EICs were obtained of analytes from their known masses (Table 5-7). GMF for precursor ions were obtained using Agilent MassHunter software.

BPCs were interrogated across the 100-1000 m/z range. Following this, MFE was used as described in 5.5.1. The degradants detected during the qualitative LC-QTOF-MS hydrolysis experiments (5.5.2) were targeted. Mass defect filtering (MDF) was also applied when searching the data. The mass defect is effectively the decimal numbers of a precursor ion mass/charge

value. MDF filtering therefore searches for precursor ions with similar mass defects, as the mass defect change is minimal when minor changes are made to the compounds structure. Drug metabolites can have similar mass defects to their parent drugs (often less than ± 50 mDa) and therefore MDF allows for the targeted identification of drug degradation products and metabolites [455]. A tolerance of ± 100 mDa was applied when analysing the MS data. Mass spectra presented are those following MFE.

The response of the degradants over time in blood specimens was determined. In experiment YA and YB, AMIT degraded in some specimens and so could not be used to account for inter-aliquot variations. Therefore, “relative responses” are relative to LORA for all specimens in these experiments, facilitating inter-specimen comparisons of degradant formation. Differences between the mean relative responses were tested for significance using Welch’s t-test (Equation 3-4), with results where $p < 0.05$ considered significant.

7.2.1.2 MS/MS data analysis

GMF and calculated accurate masses were determined for the product ions of degradants and their parent analytes, enabling structures to be hypothesised.

7.2.1.3 Manual fraction collection

To identify the compounds responsible for the LC-DAD peaks appearing during experiment YA (see 6.3.6.2), manual fraction collection followed by LC-QTOF-MS analysis was carried out. Fractions were collected into borosilicate tubes. Collected fractions were concentrated at 40 °C under N₂ to remove acetonitrile from the fractions, followed by alkaline extraction performed using water (1.2 mL) and aqueous NH₃ (250 μ L, 30 % v/v), with vortexing before n-BuCl (5 mL) was then added. Tubes were placed on a mechanical roller (15 minutes at 20 rpm), followed by centrifugation (10 minutes at 1409 $\times g$). After centrifugation the organic layer was collected and evaporated to just dryness under N₂ at 40 °C. Ethanol (50 μ L) was used to reconstitute the residue with vortexing, then analysed by LC-QTOF-MS.

7.2.1.4 Acetylation

Specimens containing the degradation products were extracted and derivatised by acetylation to determine if the degradation products contained nucleophilic functionalities such as alcohols, thiols, or primary or secondary amines [456]. Acetylation was performed by collecting subsamples of blood specimens and transferring the n-BuCl supernatant following centrifugation in the unbuffered LLE method (4.2.2) into a borosilicate tube containing anhydrous sodium sulfate (100 mg) prior to the evaporation and reconstitution steps of the extraction procedure.

Following transfer of the extraction solvent, acetic anhydride (1 mL) and glacial acetic acid (2 mL) were added. The tubes were briefly vortexed, loosely sealed, and then heated at 50 °C for 22 hours. After allowing the tubes to cool they were then centrifuged (10 mins at 3000 rpm) and the organic solvent was transferred to a clean test tube and evaporated under N₂ at 40 °C. The residue was reconstituted in ethanol (400 µL) with vortexing and analysed by LC-QTOF-MS.

7.2.1.5 Standard comparison

Standards of the suspected degradants, where possible, were run alongside collected fractions and experimental extracts to confirm their identity by retention time, accurate mass, and MS/MS spectra.

7.2.2 Results

7.2.2.1 Degradation product identification

Precursor ions corresponding to the m/z ratios expected of the desmethyl metabolites of AMIT, CHLO, CLOM, DOTH, and TRIF were detected in Day 7 extracts of the week-long experiments. However, these were not significant degradation products as evidenced by the stability of the parent drugs (see Figure 6-5 and B.3). In the longer-term experiments (seven months for YB, twelve months for YA) these precursor ions were detected with greater relative responses. In addition, precursor ions corresponding to the m/z ratios expected of the N-dealkylation metabolites of CLOZ, MIRT, QUET, and FLPH were also detected. Support for the identity of all these precursor ions as N-dealkylation degradation products included: i) MS/MS product ions in common with parent drug three-membered ring structures and ii) identification of compounds in the acetylated extracts 42.0101 m/z units greater than the degradants, indicating that the degradants contained a functional group capable of acetylation (e.g. a secondary amine following N-dealkylation) (see Figure 7-1 for AMIT and nortriptyline (NORT) as an exemplar). There was also in common a m/z difference between the precursor ions of the parent compounds and the purported N-dealkylation degradation products consistent with a methylene group (calculated mass for CH₂: 14.0157 Da) for NORT, nor-chlorpromazine (NOR-CHLO), nor-clomipramine (NOR-CLOM), northiaden (NORD), nor-mirtazapine (NOR-MIRT), nor-trifluoperazine (NOR-TRIF), and nor-clozapine (NOR-CLOZ) (Table 7-1). Major product ions ~14.0157 m/z units lesser than their parent compounds were also observed for NORT, NOR-CHLO, NOR-CLOM, NORD, and NOR-CLOZ (Table 7-2 and Table 7-3). Mass accuracies were poor ($\delta = > 5$ mDa) for some product ions, potentially due to low response on the LC-QTOF-MS.

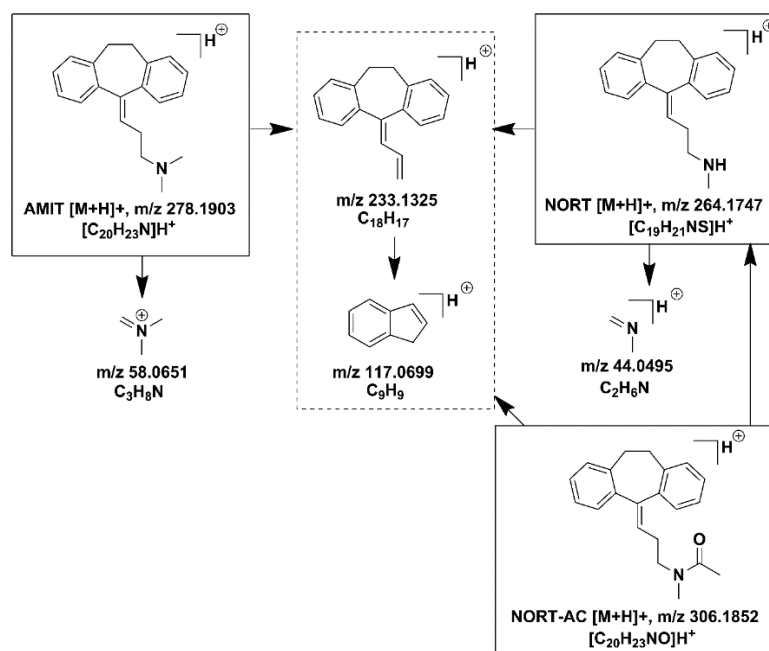


Figure 7-1: Proposed MS/MS fragmentation pathway for AMIT, NORT, and NORT-AC. Fragments in common between compounds indicated by dotted-line box; m/z are calculated accurate mass values.

The presence of NORT, NOR-CLOM, NOR-MIRT, and NOR-QUET in experiments was confirmed by comparison to concurrently run standards (Table 7-1). For NOR-CHLO, NORD, NOR-TRIF, NOR-CLOZ, and desethylalcohol-fluphenazine (DA-FLPH) no reference standards were available to confirm their identity. There was also limited evidence that desethylalcohol-flupentixol (DA-FLTX) (precursor ion: 391.1452 m/z, GMF of C₂₁H₂₁F₃N₂S (calculated [M+H]⁺ = 391.1450 m/z, δ = -0.5 ppm (-0.2 mDa); retention time = 8.65 min) was forming. It is not unreasonable to postulate the formation of this degradant in the same specimens in which NORT and NOR-QUET were also confirmed to be detected and in those where DA-FLPH was presumptively identified. However, no reference standards were readily available to confirm its identity and only two product ions consistent with the ring structure of FLTX were able to be presumptively identified. A compound with a precursor ion 42.011 m/z units greater than 391.1452 m/z was also detected (GMF: C₂₃H₂₃F₃N₂OS calculated 433.1561 m/z, δ = -1.2 ppm (-0.5 mDa); retention time = 8.91 min), indicating that acetylation of the 391.1452 m/z compound likely occurred. Interestingly, N-dealkylated degradation products of ASEN and PROC were not detected.

Table 7-1: LC-QTOF-MS data for parent compounds, N-dealkylation degradants, N-dealkylation standards, and synthesised acetyl derivatives for possible and confirmed N-dealkylation degradation products.

Analyte	Retention time (min)	Measured [M+H] ⁺ (m/z)	Calculated [M+H] ⁺ (m/z)	GMF product ions	Mass accuracy (δ) (ppm)	Mass accuracy (δ) (mDa)
AMIT	8.35	278.1908	278.1903	[C ₂₀ H ₂₃ N]H ⁺	-1.8	-0.5
NORT	8.20	264.1752	264.1747	[C ₁₉ H ₂₁ N]H ⁺	-1.9	-0.5
NORT standard	8.20	264.1751	264.1747	[C ₁₉ H ₂₁ N]H ⁺	-1.5	-0.4
NORT-AC	10.9	306.1855	306.1852	[C ₂₁ H ₂₃ NO]H ⁺	-1.0	-0.3
QUET	6.67	384.1744	384.1740	[C ₂₁ H ₂₅ N ₃ O ₂ S]H ⁺	-1.0	-0.4
NOR-QUET	6.29	296.1217	296.1216	[C ₁₇ H ₁₇ N ₃ S]H ⁺	-0.3	-0.1
NOR-QUET standard	6.29	296.1218	296.1216	[C ₁₇ H ₁₇ N ₃ S]H ⁺	-0.7	-0.2
NOR-QUET-AC	6.17	338.1325	338.1322	[C ₁₉ H ₁₉ N ₃ OS]H ⁺	-0.9	-0.3
CLOM	8.98	315.1631	315.1623	[C ₁₉ H ₂₃ ClN ₂]H ⁺	-2.5	-0.8
NOR-CLOM	8.77	301.1468	301.1466	[C ₁₈ H ₂₁ ClN ₂]H ⁺	-0.7	-0.2
NOR-CLOM standard	8.77	301.1472	301.1466	[C ₁₈ H ₂₁ ClN ₂]H ⁺	-2.0	-0.6
NOR-CLOM-AC	11.2	343.1570	343.1572	[C ₂₀ H ₂₃ ClN ₂ O]H ⁺	0.6	0.2
MIRT	4.58	266.1657	266.1652	[C ₁₇ H ₁₉ N ₃]H ⁺	-1.9	-0.5
NOR-MIRT	4.09	252.1496	252.1495	[C ₁₆ H ₁₇ N ₃]H ⁺	-0.4	-0.1
NOR-MIRT standard	4.09	252.1499	252.1495	[C ₁₆ H ₁₇ N ₃]H ⁺	-1.6	-0.4
NOR-MIRT-AC	5.22	294.1596	294.1601	[C ₁₈ H ₁₉ N ₃ O]H ⁺	1.7	0.5
CHLO	8.77	319.1039	319.1030	[C ₁₇ H ₁₉ ClN ₂ S]H ⁺	-2.8	-0.9
NOR-CHLO	8.53	305.0880	305.0874	[C ₁₆ H ₁₇ ClN ₂ S]H ⁺	-2.0	-0.6
NOR-CHLO-AC	11.1	347.0972	347.0979	[C ₁₈ H ₁₉ ClN ₂ OS]H ⁺	2.0	0.7
DOTH	7.95	296.1473	296.1467	[C ₁₉ H ₂₁ NS]H ⁺	-2.0	-0.6
NORD	7.79	282.1313	282.1311	[C ₁₈ H ₁₉ NS]H ⁺	-0.7	-0.2
NORD-AC	10.6	324.1415	324.1417	[C ₂₀ H ₂₁ NOS]H ⁺	0.6	0.2
TRIF	9.20	408.1725	408.1716	[C ₂₁ H ₂₄ F ₃ N ₃ S]H ⁺	-2.2	-0.9
NOR-TRIF	8.27	394.1567	394.1559	[C ₂₀ H ₂₂ F ₃ N ₃ S]H ⁺	-2.0	-0.8
NOR-TRIF-AC	8.92	436.1662	436.1665	[C ₂₂ H ₂₄ F ₃ N ₃ OS]H ⁺	0.7	0.3
CLOZ	6.07	327.1376	327.1371	[C ₁₈ H ₁₉ ClN ₄]H ⁺	-1.5	-0.5
NOR-CLOZ	5.57	313.1211	313.1215	[C ₁₇ H ₁₇ ClN ₄]H ⁺	1.3	0.4
NOR-CLOZ-AC	6.90	355.1321	355.1320	[C ₁₉ H ₁₉ ClN ₄ O]H ⁺	-0.3	-0.1
FLPH	8.80	438.1824	438.1821	[C ₂₂ H ₂₆ F ₃ N ₃ OS]H ⁺	-0.7	-0.3
DA-FLPH	8.24	394.1557	394.1559	[C ₂₀ H ₂₂ F ₃ N ₃ S]H ⁺	0.5	0.2
DA-FLPH-AC	8.91	436.1667	436.1665	[C ₂₂ H ₂₄ F ₃ N ₃ OS]H ⁺	-0.5	-0.2

GMF = generated molecular formulae. Mass accuracies determined from single injection.

Table 7-2: MS/MS data for parent compounds, N-dealkylation degradants and synthesised acetyl derivatives for confirmed N-dealkylation degradation products.

Analyte	Precursor ion (m/z)	Product ions (m/z)	GMF product ions	Calculated accurate mass (m/z)	Mass accuracy (δ) (ppm)	Mass accuracy (δ) (mDa)
AMIT	278.1908	58.0645	C ₃ H ₈ N	58.0651	10.3	0.6
		84.0805	C ₅ H ₁₀ N	84.0808	3.6	0.3
		91.0542	C ₇ H ₇	91.0542	0.0	0.0
		105.0688	C ₈ H ₉	105.0699	10.5	1.1
		117.0687	C ₉ H ₉	117.0699	10.3	1.2
		191.0838	C ₁₅ H ₁₁	191.0855	8.9	1.7
		218.1092	C ₁₇ H ₁₄	218.1090	-0.9	-0.2
		233.1316	C ₁₈ H ₁₇	233.1325	3.9	0.9
		278.1894	[C ₂₀ H ₂₃ N]H ⁺	278.1903	3.2	0.9
NORT	264.1752	44.0507	C ₂ H ₆ N	44.0495	-27.2	-1.2
		91.0539	C ₇ H ₇	91.0542	3.3	0.3
		105.0696	C ₈ H ₉	105.0699	2.9	0.3
		117.0694	C ₉ H ₉	117.0699	4.3	0.5
		191.0877	C ₁₅ H ₁₁	191.0855	-11.5	-2.2
		218.1128	C ₁₇ H ₁₄	218.1090	-17.4	-3.8
		233.1301	C ₁₈ H ₁₇	233.1325	10.3	2.4
NORT-AC	306.1855	44.0494	C ₂ H ₆ N	44.0495	2.3	0.1
		58.0644	C ₃ H ₈ N	58.0651	12.1	0.7
		91.0537	C ₇ H ₇	91.0542	5.5	0.5
		105.0696	C ₈ H ₉	105.0699	2.9	0.3
		117.0675	C ₉ H ₉	117.0699	20.5	2.4
		191.0827	C ₁₅ H ₁₁	191.0855	14.7	2.8
		218.1043	C ₁₇ H ₁₄	218.1090	21.5	4.7
		233.1346	C ₁₈ H ₁₇	233.1325	-9.0	-2.1
QUET	384.1744	70.0656	C ₄ H ₈ N	70.0651	-7.1	-0.5
		158.1170	C ₈ H ₁₆ NO	158.1176	3.8	0.6
		221.1064	C ₁₅ H ₁₃ N ₂	221.1073	4.1	0.9
		253.0783	C ₁₅ H ₁₃ N ₂ S	253.0794	4.3	1.1
		279.0935	C ₁₇ H ₁₅ N ₂ S	279.0950	5.4	1.5
		384.1721	[C ₂₁ H ₂₅ N ₃ O ₂ S]H ⁺	384.1740	4.9	1.9
NOR-QUET	296.1217	70.0654	C ₄ H ₈ N	70.0651	-4.3	-0.3
		221.1071	C ₁₅ H ₁₃ N ₂	221.1073	0.9	0.2
		253.0798	C ₁₅ H ₁₃ N ₂ S	253.0794	-1.6	-0.4
		279.0910	C ₁₇ H ₁₅ N ₂ S	279.0950	14.3	4.0
		296.1229	[C ₁₇ H ₁₇ N ₃ S]H ⁺	296.1216	-4.4	-1.3
NOR-QUET-AC	338.1325	86.0588	C ₄ H ₈ NO	86.0600	13.9	1.2
		253.0783	C ₁₅ H ₁₃ N ₂ S	253.0794	4.3	1.1
		296.1163	C ₁₇ H ₁₈ N ₃ S	296.1216	17.9	5.3
		338.1324	[C ₁₉ H ₁₉ N ₃ OS]H ⁺	338.1322	-0.6	-0.2
CLOM	315.1631	58.0657	C ₃ H ₈ N	58.0651	-10.3	-0.6
		86.0967	C ₅ H ₁₂ N	86.0964	-3.5	-0.3
		242.0730	C ₁₅ H ₁₃ CIN	242.0731	0.4	0.1
NOR-CLOM	301.1468	44.0504	C ₂ H ₆ N	44.0495	-20.4	-0.9
		72.0819	C ₄ H ₁₀ N	72.0808	-15.3	-1.1
		242.0670	C ₁₅ H ₁₃ CIN	242.0731	25.2	6.1
NOR-CLOM-AC	343.1570	44.0510	C ₂ H ₆ N	44.0495	-34.1	-1.5
		86.0602	C ₄ H ₈ NO	86.0600	-2.3	-0.2
		114.0895	C ₆ H ₁₂ NO	114.0913	15.8	1.8
MIRT	266.1657	72.0811	C ₄ H ₁₀ N	72.0808	-4.2	-0.3
		195.0913	C ₁₃ H ₁₁ N ₂	195.0917	2.1	0.4
		209.1065	C ₁₄ H ₁₃ N ₂	209.1073	3.8	0.8

Analyte	Precursor ion (m/z)	Product ions (m/z)	GMF product ions	Calculated accurate mass (m/z)	Mass accuracy (δ) (ppm)	Mass accuracy (δ) (mDa)
		266.1656	[C ₁₇ H ₁₉ N ₃] ⁺ H ⁺	266.1652	-1.5	-0.4
NOR-MIRT	252.1496	195.0941	C ₁₃ H ₁₁ N ₂	195.0917	-12.3	-2.4
		209.1075	C ₁₄ H ₁₃ N ₂	209.1073	-1.0	-0.2
		252.1546	[C ₁₆ H ₁₇ N ₃] ⁺ H ⁺	252.1495	-20.2	-5.1
NOR-MIRT-AC	294.1596	86.0602	C ₄ H ₈ NO	86.0600	-2.3	-0.2
		195.0888	C ₁₃ H ₁₁ N ₂	195.0917	14.9	2.9
		209.1067	C ₁₄ H ₁₃ N ₂	209.1073	2.9	0.6
		252.1468	C ₁₆ H ₁₈ N ₃	252.1495	10.7	2.7
		294.1561	[C ₁₈ H ₁₉ N ₃ O] ⁺ H ⁺	294.1601	13.6	4.0

GMF = generated molecular formulae. Mass accuracies determined from single injection.

Table 7-3: MS/MS data for parent compounds, N-dealkylation degradants and synthesised acetyl derivatives for possible N-dealkylation degradation products.

Analyte	Precursor ion (m/z)	Product ions (m/z)	GMF product ions	Calculated accurate mass (m/z)	Mass accuracy (δ) (ppm)	Mass accuracy (δ) (mDa)
CHLO	319.1039	58.0658	C ₃ H ₈ N	58.0651	-12.1	-0.7
		86.0967	C ₅ H ₁₂ N	86.0964	-3.5	-0.3
		214.0379	C ₁₃ H ₉ CIN	214.0418	18.2	3.9
		246.0099	C ₁₃ H ₉ CINS	246.0139	16.3	4.0
		319.1004	[C ₁₇ H ₁₉ CIN ₂ S] ⁺ H ⁺	319.1030	8.1	2.6
NOR-CHLO	305.0880	44.0505	C ₂ H ₆ N	44.0495	-22.7	-1.0
		72.0805	C ₄ H ₁₀ N	72.0808	4.2	0.3
		214.0398	C ₁₃ H ₉ CIN	214.0418	9.3	2.0
NOR-CHLO-AC	347.0972	44.0510	C ₂ H ₆ N	44.0495	-34.1	-1.5
		86.0603	C ₄ H ₈ NO	86.0600	-3.5	-0.3
		114.0907	C ₆ H ₁₂ NO	114.0913	5.3	0.6
DOTH	296.1473	58.0659	C ₃ H ₈ N	58.0651	-13.8	-0.8
		117.0693	C ₉ H ₉	117.0699	5.1	0.6
		147.0256	C ₉ H ₇ S	147.0263	4.8	0.7
		191.0842	C ₁₅ H ₁₁	191.0855	6.8	1.3
		251.0917	C ₁₆ H ₁₁ S	251.0889	-11.2	-2.8
		296.1446	[C ₁₉ H ₂₁ NS] ⁺ H ⁺	296.1467	7.1	2.1
NORD	282.1313	44.0486	C ₂ H ₆ N	44.0495	20.4	0.9
		91.0526	C ₄ H ₁₁ S	91.0576	54.9	5.0
		147.0214	C ₉ H ₇ S	147.0263	33.3	4.9
		191.0868	C ₁₅ H ₁₁	191.0855	-6.8	-1.3
		251.0865	C ₁₆ H ₁₁ S	251.0889	9.6	2.4
		282.1323	[C ₁₈ H ₁₉ NS] ⁺ H ⁺	282.1311	-4.3	-1.2
NORD-AC	324.1415	44.0502	C ₂ H ₆ N	44.0495	-15.9	-0.7
		117.0714	C ₉ H ₉	117.0699	-12.8	-1.5
		251.0837	C ₁₆ H ₁₁ S	251.0889	20.7	5.2
		282.1232	C ₁₈ H ₂₀ NS	282.1311	28.0	7.9
TRIF	408.1725	70.0655	C ₄ H ₈ N	70.0651	-5.7	-0.4
		113.1064	C ₆ H ₁₃ N ₂	113.1073	8.0	0.9
		141.1372	C ₈ H ₁₇ N ₂	141.1386	9.9	1.4
		248.0693	C ₁₄ H ₉ F ₃ N	248.0682	-4.4	-1.1
		280.0343	C ₁₄ H ₉ F ₃ NS	280.0402	21.1	5.9
		408.1719	[C ₂₁ H ₂₄ F ₃ N ₃ S] ⁺ H ⁺	408.1716	-0.7	-0.3
NOR-TRIF	394.1567	56.0514	C ₃ H ₆ N	56.0495	-33.9	-1.9
		70.0613	C ₄ H ₈ N	70.0651	54.2	3.8
		99.0907	C ₅ H ₁₁ N ₂	99.0917	10.1	1.0

Analyte	Precursor ion (m/z)	Product ions (m/z)	GMF product ions	Calculated accurate mass (m/z)	Mass accuracy (δ) (ppm)	Mass accuracy (δ) (mDa)
		127.1214	C ₇ H ₁₅ N ₂	127.1230	12.6	1.6
		248.0743	C ₁₄ H ₉ F ₃ N	248.0682	-24.6	-6.1
		280.0400	C ₁₄ H ₉ F ₃ NS	280.0402	0.7	0.2
NOR-TRIF-AC	436.1660	112.0749	C ₆ H ₁₀ NO	112.0757	7.1	0.8
		127.1245	C ₇ H ₁₅ N ₂	127.1230	-11.8	-1.5
		141.1018	C ₇ H ₁₃ N ₂ O	141.1022	2.8	0.4
		169.1322	C ₉ H ₁₇ N ₂ O	169.1335	7.7	1.3
		248.0651	C ₁₄ H ₉ F ₃ N	248.0682	12.5	3.1
		280.0383	C ₁₄ H ₉ F ₃ NS	280.0402	6.8	1.9
		436.1647	[C ₂₂ H ₂₄ F ₃ N ₃ OS]H ⁺	436.1665	4.1	1.8
CLOZ	327.1376	84.0796	C ₅ H ₁₀ N	84.0808	14.3	1.2
		192.0679	C ₁₃ H ₈ N ₂	192.0682	1.6	0.3
		227.0349	C ₁₃ H ₈ ClN ₂	227.0371	9.7	2.2
		270.0779	C ₁₅ H ₁₃ ClN ₃	270.0793	5.2	1.4
		296.0930	C ₁₇ H ₁₅ ClN ₃	296.0949	6.4	1.9
		327.1353	[C ₁₈ H ₁₉ ClN ₄]H ⁺	327.1371	5.5	1.8
NOR-CLOZ	313.1211	70.0659	C ₄ H ₈ N	70.0651	-11.4	-0.8
		192.0680	C ₁₃ H ₈ N ₂	192.0682	1.0	0.2
		227.0438	C ₁₃ H ₈ ClN ₂	227.0371	-29.5	-6.7
		270.0766	C ₁₅ H ₁₃ ClN ₃	270.0793	10.0	2.7
		296.0916	C ₁₇ H ₁₅ ClN ₃	296.0949	11.1	3.3
		313.1205	[C ₁₇ H ₁₇ ClN ₄]H ⁺	313.1215	3.2	1.0
NOR-CLOZ-AC	355.1321	84.0807	C ₅ H ₁₀ N	84.0808	1.2	0.1
		192.0654	C ₁₃ H ₈ N ₂	192.0682	14.6	2.8
		227.0364	C ₁₃ H ₈ ClN ₂	227.0371	3.1	0.7
		255.0311	C ₁₅ H ₃ N ₄ O	255.0301	-3.9	-1.0
		270.0794	C ₁₈ H ₁₀ N ₂ O	270.0788	-2.2	-0.6
		298.0745	C ₁₆ H ₁₃ ClN ₃ O	298.0742	-1.0	-0.3
		355.1297	[C ₁₉ H ₁₉ ClN ₄ O]H ⁺	355.1320	6.5	2.3
FLPH	438.1833	70.0655	C ₄ H ₈ N	70.0651	-5.7	-0.4
		84.0793	C ₅ H ₁₀ N	84.0808	17.8	1.5
		100.0757	C ₅ H ₁₀ NO	100.0757	0.0	0.0
		143.1178	C ₇ H ₁₅ N ₂ O	143.1179	0.7	0.1
		171.1470	C ₉ H ₁₉ N ₂ O	171.1497	15.8	2.7
		248.0668	C ₁₄ H ₉ F ₃ N	248.0682	5.6	1.4
		280.0373	C ₁₄ H ₉ F ₃ NS	280.0402	10.4	2.9
		438.1810	[C ₂₂ H ₂₆ F ₃ N ₃ OS]H ⁺	438.1821	2.5	1.1
DA-FLPH	394.1557	44.0503	C ₂ H ₆ N	44.0495	-18.2	-0.8
		56.0500	C ₃ H ₆ N	56.0495	-8.9	-0.5
		70.0658	C ₄ H ₈ N	70.0651	-10.0	-0.7
		99.0907	C ₅ H ₁₁ N ₂	99.0917	10.1	1.0
		127.1229	C ₇ H ₁₅ N ₂	127.1230	0.8	0.1
		248.0646	C ₁₄ H ₉ F ₃ N	248.0682	14.5	3.6
		280.0385	C ₁₄ H ₉ F ₃ NS	280.0402	6.1	1.7
		394.1535	[C ₂₀ H ₂₂ F ₃ N ₃ S]H ⁺	394.1559	6.1	2.4
DA-FLPH-AC	436.1667	99.0906	C ₅ H ₁₁ N ₂	99.0917	11.1	1.1
		112.0768	C ₆ H ₁₀ NO	112.0757	-9.8	-1.1
		127.1236	C ₇ H ₁₅ N ₂	127.1230	-4.7	-0.6
		141.1027	C ₇ H ₁₃ N ₂ O	141.1022	-3.5	-0.5
		169.1369	C ₉ H ₁₇ N ₂ O	169.1335	-20.1	-3.4
		280.0376	C ₁₄ H ₉ F ₃ NS	280.0402	9.3	2.6
		436.1662	[C ₂₂ H ₂₆ F ₃ N ₃ OS]H ⁺	436.1665	0.7	0.3

GMF = generated molecular formulae. Mass accuracies determined from single injection.

Precursor ions with GMF consistent with the sulfoxides of PERI, FLPH, and TRIF were detected in week-long experiments and longer-term experiments (Table 7-4). Shared ions in MS/MS spectra assisted in assigning degradants to parent drugs (Table 7-5). In the absence of UV-Vis data, these compounds could have also been aromatic hydroxylation products or N-oxides, as these compounds would afford the same precursor ions, GMF, and similar MS/MS spectra. However, no compounds with precursor ions 42.011 m/z greater were detected in acetylated extracts as expected from O-acetylation. From the formation of CHLO-SO and PROC-SO over time in blood specimens (6.3.6.1) the likely identity of these precursor ions was also as sulfoxide degradants although unambiguous identification was not achieved.

PERI-AMD and the alkaline ZIPR degradation products detailed in 5.5.2 were not detected. However, if the alkaline ZIPR degradants contained functionalities that may have been ionised during the unbuffered LLE (e.g. carboxylic acid, alcohol, or primary amine functionality) extraction recoveries were expected to have been low.

Manual LC-DAD fraction collection followed by LC-QTOF-MS analysis allowed the correlation between LC-DAD peaks and LC-QTOF-MS peaks in the inoculated, unpreserved blood specimen extracts to be assigned (Figure 7-2). The peak before AMIT was identified as NORT, confirmed by standard comparison, whereas the peak before CHLO and the peak between FLPH and FLTX were presumptively identified as NOR-CHLO and DA-FLPH, respectively.

Table 7-4: LC-QTOF-MS data for parent drugs and their possible sulfoxides.

Analyte	Retention time (min)	Measured [M+H] ⁺ (m/z)	Calculated [M+H] ⁺ (m/z)	GMF product ions	Mass accuracy (δ) (ppm)	Mass accuracy (δ) (mDa)
PERI	7.57	366.1636	366.1635	[C ₂₁ H ₂₃ N ₃ OS]H ⁺	-0.3	-0.1
PERI-SO	5.17	382.1580	382.1584	[C ₂₁ H ₂₃ N ₃ O ₂ S]H ⁺	1.0	0.4
FLPH	8.80	438.1824	438.1821	[C ₂₂ H ₂₆ F ₃ N ₃ OS]H ⁺	-0.7	-0.3
FLPH-SO	6.14	454.1768	454.1771	[C ₂₂ H ₂₆ F ₃ N ₃ O ₂ S]H ⁺	0.7	0.3
TRIF	9.20	408.1725	408.1716	[C ₂₁ H ₂₄ F ₃ N ₃ S]H ⁺	-2.2	-0.9
TRIF-SO	6.26	424.1668	424.1665	[C ₂₁ H ₂₄ F ₃ N ₃ OS]H ⁺	-0.7	-0.3

GMF = generated molecular formulae. Mass accuracies determined from single injection.

Table 7-5: MS/MS data for parent drugs and their possible sulfoxides.

Analyte	Precursor ion (m/z)	Product ions (m/z)	GMF product ions	Calculated accurate mass (m/z)	Mass accuracy (δ) (ppm)	Mass accuracy (δ) (mDa)
PERI	366.1636	98.0960	C ₆ H ₁₂ N	98.0964	4.1	0.4
		114.0904	C ₆ H ₁₂ NO	114.0913	7.9	0.9
		142.1214	C ₈ H ₁₆ NO	142.1226	8.4	1.2
		237.0487	C ₁₄ H ₉ N ₂ S	237.0481	-2.5	-0.6
		366.1627	[C ₂₁ H ₂₃ N ₃ OS]H ⁺	366.1635	2.2	0.8

Analyte	Precursor ion (m/z)	Product ions (m/z)	GMF product ions	Calculated accurate mass (m/z)	Mass accuracy (δ) (ppm)	Mass accuracy (δ) (mDa)
PERI-SO	382.1580	98.0959	C ₆ H ₁₂ N	98.0964	5.1	0.5
		114.0917	C ₆ H ₁₂ NO	114.0913	-3.5	-0.4
		142.1244	C ₈ H ₁₆ NO	142.1226	-12.7	-1.8
FLPH	438.1824	70.0655	C ₄ H ₈ N	70.0651	-5.7	-0.4
		84.0793	C ₅ H ₁₀ N	84.0808	17.8	1.5
		100.0757	C ₅ H ₁₀ NO	100.0757	0.0	0.0
		143.1178	C ₇ H ₁₅ N ₂ O	143.1179	0.7	0.1
		171.1470	C ₉ H ₁₉ N ₂ O	171.1497	15.8	2.7
		248.0668	C ₁₄ H ₉ F ₃ N	248.0682	5.6	1.4
		280.0373	C ₁₄ H ₉ F ₃ NS	280.0402	10.4	2.9
		438.1810	[C ₂₂ H ₂₆ F ₃ N ₃ OS]H ⁺	438.1821	2.5	1.1
FLPH-SO	454.1768	70.0656	C ₄ H ₈ N	70.0651	-7.1	-0.5
		100.0733	C ₅ H ₁₀ NO	100.0757	24.0	2.4
		143.1170	C ₇ H ₁₅ N ₂ O	143.1179	6.3	0.9
		171.1476	C ₉ H ₁₉ N ₂ O	171.1497	12.3	2.1
		280.0384	C ₁₄ H ₉ F ₃ NS	280.0402	6.4	1.8
		454.1771	[C ₂₂ H ₂₆ F ₃ N ₃ O ₂ S]H ⁺	454.1771	0.0	0.0
TRIF	408.1725	70.0655	C ₄ H ₈ N	70.0651	-5.7	-0.4
		113.1064	C ₆ H ₁₃ N ₂	113.1073	8.0	0.9
		141.1372	C ₈ H ₁₇ N ₂	141.1386	9.9	1.4
		248.0693	C ₁₄ H ₉ F ₃ N	248.0682	-4.4	-1.1
		280.0343	C ₁₄ H ₉ F ₃ NS	280.0402	21.1	5.9
		408.1719	[C ₂₁ H ₂₄ F ₃ N ₃ S]H ⁺	408.1716	-0.7	-0.3
TRIF-SO	424.1668	70.0663	C ₄ H ₈ N	70.0651	-17.1	-1.2
		113.1058	C ₆ H ₁₃ N ₂	113.1073	13.3	1.5
		141.1383	C ₈ H ₁₇ N ₂	141.1386	2.1	0.3
		280.0404	C ₁₄ H ₉ F ₃ NS	280.0402	-0.7	-0.2
		424.1653	[C ₂₁ H ₂₄ F ₃ N ₃ OS]H ⁺	424.1665	2.8	1.2

GMF = generated molecular formulae. Mass accuracies determined from single injection.

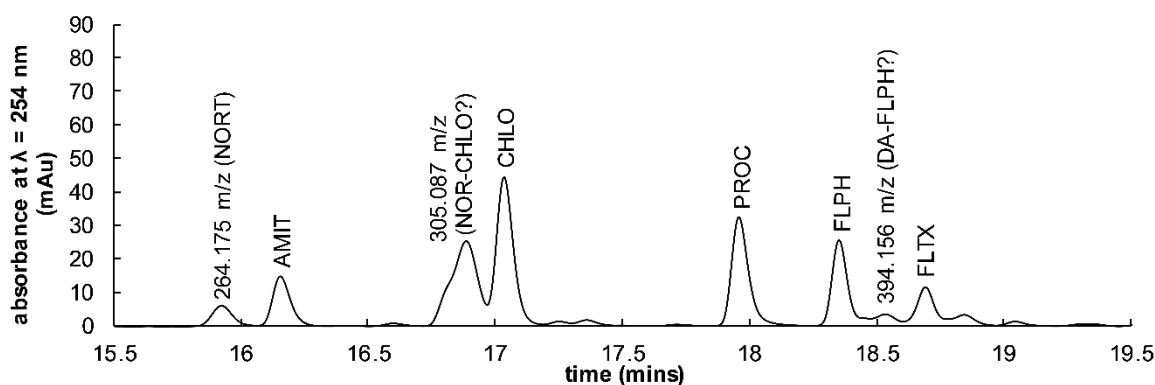


Figure 7-2: Chromatogram of an extract collected from an inoculated, unpreserved blood specimen stored at room temperature for 12 months in experiment YA.

Note: 305.087 m/z appeared to coelute with an unidentified compound.

7.2.2.2 Degradation product formation over time

The precursor ions of the N-dealkylation degradation products and possible sulfoxides were also detected in calibrator and QC extracts, although rarely with auto-MS/MS spectra acquired. Therefore, these compounds may be present as impurities in the stocks, working solutions used,

or otherwise form during extraction from blood. In particular, the sulfoxide metabolites may have formed during the heated evaporation step of the LLE, as Campbell *et al.* reported occurred for CHLO and promethazine in sample preparation techniques involving heated evaporation of organic solvent [427]. Even so, the trend for the relative response of the N-dealkylation and sulfoxide products to increase over time in the longer-term experiments indicates these compounds formed over time in the experimental blood specimens (Figure 7-3 and Figure 7-4).

For the N-dealkylation products the most important finding was that greatest responses were observed in extracts of the room temperature, inoculated, unpreserved specimens in both experiment YA and YB, indicating more of the degradants formed in these specimens over time than in other specimens. When comparing the specimen type and temperature where maximum responses were observed, greater formation in room temperature, inoculated, unpreserved specimens was significant for: NORT (YA), NOR-QUET, NOR-CHLO, DA-FLPH, and NORD compared to non-inoculated, unpreserved specimens at -20 °C; NORT (YA), NOR-CLOZ, NOR-QUET, NOR-CHLO, DA-FLPH, NORD, and NOR-CLOM compared to non-inoculated, preserved specimens at 4 °C; and NORT (YA), NOR-CHLO, NORD, and NOR-CLOM compared to inoculated, preserved specimens at room temperature.

Lowest responses were obtained for the N-dealkylation degradation products in specimens stored at 4 °C, regardless of preservative or inoculation state. Greater responses at room temperature and -20 °C than at 4 °C were significant for: NORT (YA and YB) in non-inoculated, unpreserved specimens; NORT (YB), NORD, and NOR-CLOM in inoculated, unpreserved specimens; and NORT (YB) and NOR-CLOM in inoculated, preserved specimens. There was no significant difference in the responses of the N-dealkylation degradation products in non-inoculated specimens stored at -20 °C compared to their response in the 4 °C and -20 °C inoculated, unpreserved specimens.

Another trend observed for the N-dealkylation degradation products was that the optimum temperature for their formation in non-inoculated specimens was at -20 °C, whereas in inoculated specimens it was at room temperature. In non-inoculated, unpreserved specimens, greater responses were significant for: NOR-CHLO and NORD at -20 °C than room temperature or 4 °C; DA-FLPH at -20 °C than room temperature; and NORT (YA and YB) at -20 °C than 4 °C. In non-inoculated, preserved specimens, greater responses were significant for: NORT (YA) and NOR-CHLO at -20 °C than room temperature or 4 °C; NOR-CLOZ and NOR-QUET at -20 °C than room temperature; and NORT (YB) and NORD at -20 than 4 °C. In inoculated, unpreserved specimens, greater responses were significant for: NOR-CLOZ, NOR-CHLO, and DA-FLPH at

room temperature than -20 °C and 4 °C; and NOR-QUET, NORT (YB), NORD, and NOR-CLOM at room temperature than -20 °C. In inoculated, preserved specimens, greater responses were significant for: NORT (YA) and NOR-CHLO at room temperature than -20 °C and 4 °C; and NORT (YB) and NOR-CLOM at room temperature than 4 °C.

NORT and NOR-CHLO were detected with auto-MS/MS spectra acquired in all specimen types (Figure 7-3 and Figure D-1). For NOR-MIRT, NOR-TRIF, and DA-FLTX, auto-MS/MS spectra were only acquired from ~21-25 weeks in inoculated, unpreserved specimens stored at room temperature (see D.1). For NOR-QUET, NOR-CLOZ, and DA-FLPH auto-MS/MS spectra were not acquired for most specimens throughout the experiment (D.1). For inoculated, preserved specimens, auto-MS/MS spectra were not acquired at all for NOR-QUET and NOR-CLOZ.

It was notable that greater proportions of the N-dealkylation degradation products were present in extracts of the room temperature, inoculated, unpreserved specimens than any other temperature and specimen combination, consistent with the specimen and temperature at which drug degradation was observed to be the greatest (6.3.5). Formation in the other specimens also indicates this transformation may be occurring due to metabolism in the blood, possibly catalysed by haemoglobin [457], but occurs at an enhanced rate in inoculated, unpreserved specimens due to microbial activity or otherwise microbial alteration of the blood matrix. The microbial communities of the experiment YA specimens were dynamic (see C.3) with *Enterococcus* spp., *Bacteroides* spp. and Enterobacteriaceae dominant after three months and an increasing dominance of Clostridiales from six months. For experiment YB, taxa of the Enterobacteriaceae family, *Bacteroides* spp., and an *Enterococcus* sp. were detected as constituting greater than 30 % of the total relative abundance of all taxa after seven months. These taxa have previously been reported to demethylate methamphetamine to produce amphetamine [275]. N-dealkylation of AMIT has also been reported in *in vitro* experiments by numerous fungal species [287], some of which may have been present in the FMT specimens (such as *Candida albicans*) and therefore the blood specimens, although this was not tested. Importantly, *Bacteroides* sp. have also been identified in post-mortem blood so it may be that N-dealkylation of drugs may also occur in authentic post-mortem specimens [330].

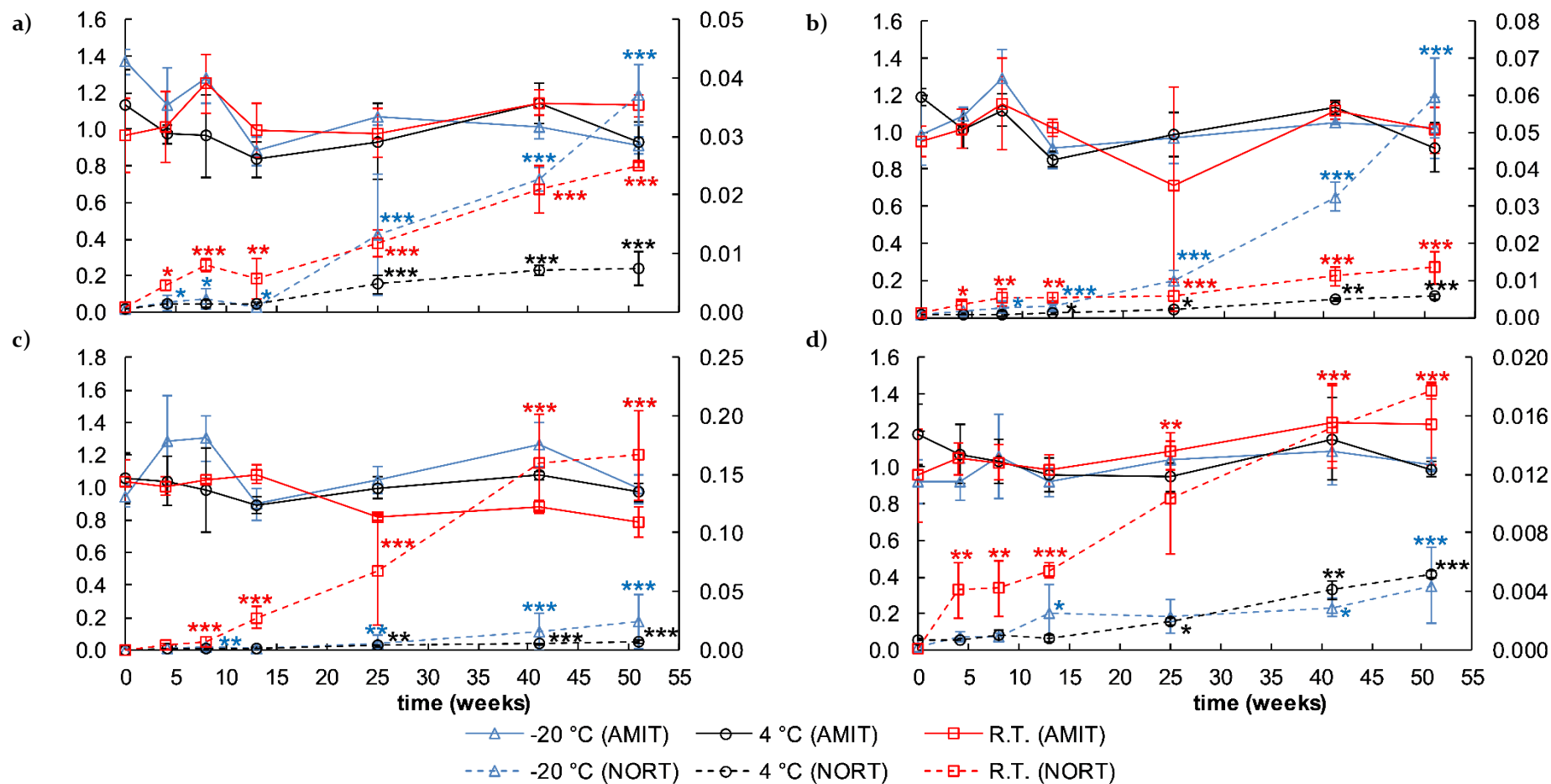


Figure 7-3: Relative response of AMIT and NORT over time in experiment YA in a) non-inoculated, unpreserved specimens, b) non-inoculated, preserved specimens, c) inoculated, unpreserved specimens, and d) inoculated, preserved specimens.

Primary Y-axis is mean AMIT relative response. Secondary Y-axis is mean NORT relative response. Asterisks indicate the acquisition of MS/MS spectra for NORT in: * one replicate; ** two replicates; *** all three replicates. Error bars are \pm S.D., n = 3.

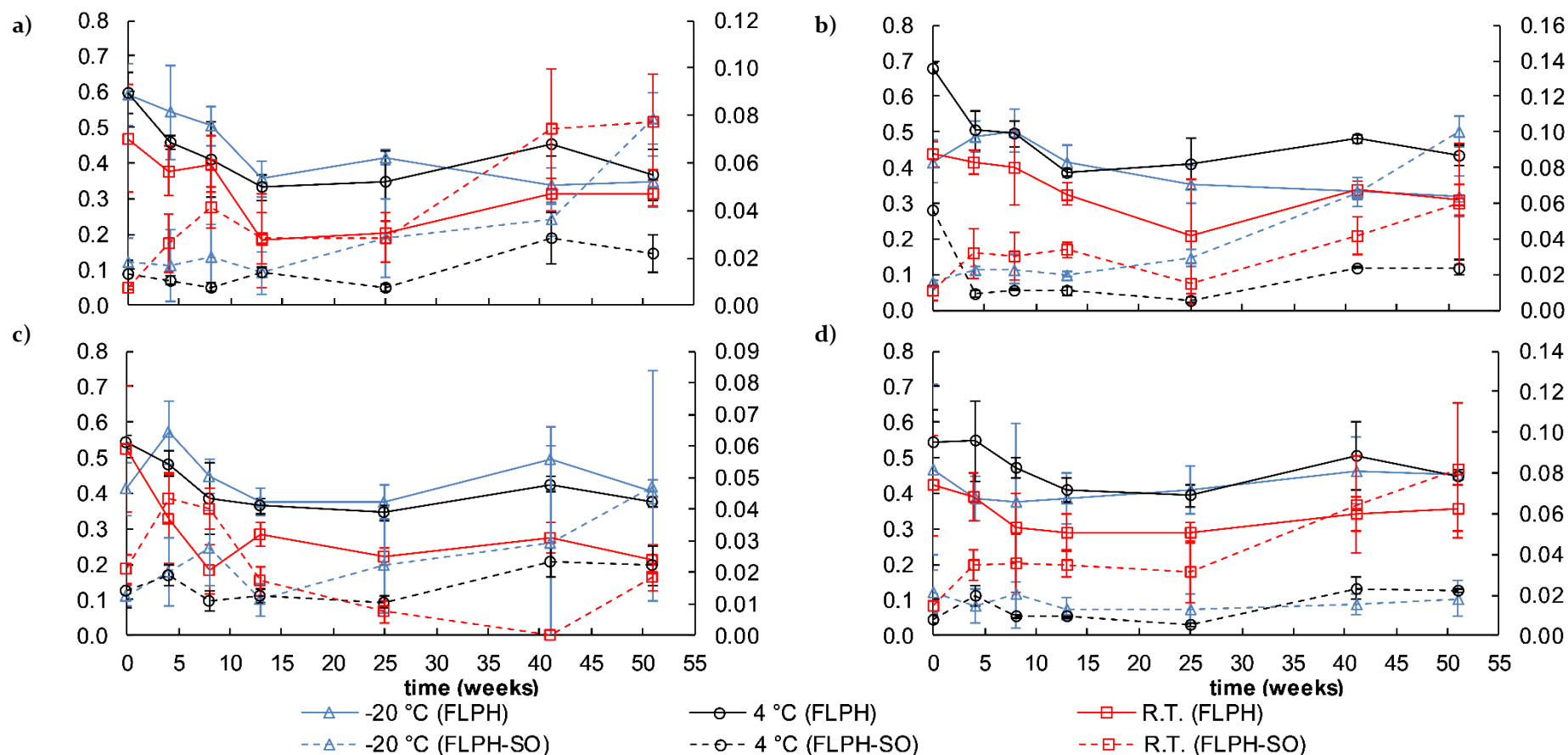


Figure 7-4: Relative response of FLPH and FLPH-SO over time in experiment YA in a) non-inoculated, unpreserved specimens, b) non-inoculated, preserved specimens, c) inoculated, unpreserved specimens, and d) inoculated, preserved specimens.

Primary Y-axis is mean FLPH relative response. Secondary Y-axis is mean FLPH-SO relative response. Auto-MS/MS spectra acquired for FLPH-SO in all specimens except for: T0 room temperature, non-inoculated, preserved specimens (x3), non-inoculated, unpreserved specimens (2x), T0 -20 °C, non-inoculated, unpreserved specimens (x2), and a T0 4 °C, inoculated, unpreserved specimen. Error bars are \pm S.D., $n = 3$.

There was a significant difference between the relative response of FLPH-SO and TRIF-SO at the start and end of the week experiments in: non-inoculated, unpreserved specimens; inoculated, preserved specimens (only in experiment WB2 for TRIF-SO; and non-inoculated, preserved specimens (only in experiment WBI for TRIF-SO).

In common with the N-dealkylation degradation products, it appeared sulfoxide formation was favoured more at -20 °C and room temperature than at 4 °C in the longer-term experiments (Figure 7-4 and D.2). For TRIF-SO, lowest relative responses were obtained in inoculated, unpreserved specimens, comparable to those at 4 °C in the other specimen types. The 4 °C specimens for the sulfoxides detected in experiment YA (PERI-SO and FLPH-SO) similarly had lowest responses, however, this was not significant. Significant differences in the longer-term experiments in common with what was observed for CHLO-SO and PROC-SO by LC-DAD analysis (6.3.6.1) were: the greater response of FLPH-SO in non-inoculated, unpreserved specimens at -20 °C compared to 4 °C and at room temperature compared to 4 °C; and the greater response of FLPH-SO in non-inoculated, preserved specimens at -20 °C compared to 4 °C. TRIF-SO formation was also significantly greater in non-inoculated, unpreserved specimens compared to inoculated, unpreserved specimens stored at room temperature (Figure D-II).

The enhancement of sulfoxide and N-dealkylation formation in -20 °C and room temperature non-inoculated specimens compared to 4 °C specimens may be attributed to the degradation of blood proteins that may otherwise inhibit these degradative pathways. Inhibition of sulfoxide formation by proteins in whole blood has previously been hypothesised by Traficante *et al.* who found the conversion of CHLO to CHLO-SO in whole blood *in vitro* was reduced by plasma but not protein-free plasma supernatant [428]. Unlike the N-dealkylation degradation products, with which maximal formation was observed in inoculated, unpreserved specimens, the sulfoxides were least abundant in these same specimens. If haemoglobin is involved in sulfoxide formation, as theorised [427, 428], it may be that haemoglobin was degraded in the inoculated, unpreserved specimens by microorganisms sequestering the haem or iron. Iron is an essential element for microbial metabolism and many bacteria and fungi possess a variety of haem uptake mechanisms and degradation pathways [458, 459]. Furthermore, haem may be used as a cofactor in intracellular reactions, and some taxa, such as Bacteroides, which dominated many of the blood specimens (6.4.4), require exogenous haem for growth [451, 458]. Decreased formation of sulfoxides in these specimens may also be due to degradation of another matrix component, likely attributable to microbial activity.

7.3 Conclusions

The identification of NORT, NOR-CLOM, NOR-MIRT, and NOR-QUET in extracts of experimental blood specimens by LC-QTOF-MS analysis was confirmed by comparison to concurrently run standards. Possible N-dealkylated degradation products of CLOZ, DOTH, CHLO, QUET, TRIF, and FLPH were also detected. Possible sulfoxide metabolites of PERI, FLPH and TRIF were detected.

Optimum formation of the N-dealkylation degradation products occurred in inoculated, unpreserved specimens, whereas the sulfoxide products were minimally formed in these specimens, indicating microbial activity may effectuate and inhibit their formation, respectively. These degradation products may also result from human metabolism [153]. Therefore, artefactual increases *in vitro* of N-dealkylation degradation products could have the potential to confound toxicology interpretations if their formation is practically significant. However, although the microorganisms detected in the inoculated, unpreserved specimens may be present in post-mortem blood, the slow rate of formation of the N-dealkylation degradation products and sulfoxide metabolites indicates there may be no relevant impact on the analysis of blood specimens for the parent drugs. However, in the blood experiments performed in Chapter 6, each drug was present at supra-therapeutic concentrations, and in combination with other drugs. It may be the case that microbial enzymes responsible for dealkylation of the drugs were saturated or inhibited, because of the multiple drugs and their high concentrations. If this is the case, degradation rates may actually be enhanced in authentic post-mortem blood specimens, and the degradation of these drugs to their dealkylation degradation products may affect their concentrations to a more relevant extent. Regardless, storage of specimens at 4 °C was found to considerably reduce the formation of these degradants.

CHAPTER 8 - LURASIDONE DEGRADATION PRODUCTS

8.1 Outline

The degradation of LURA by microorganisms was established in Chapter 6. The objective of this thesis is foremost to determine if prescription antidepressant and antipsychotic drugs may undergo degradation in post-mortem specimens. Therefore, it was necessary to identify any degradation products of LURA and determine if these may also be present in authentic post-mortem specimens. The detection of degradation products would also determine whether they should be included in screening and quantification methods for future casework analyses as a marker of LURA administration.

Chemicals, materials, and instrumentation were used as listed in Chapter 3.

8.2 Identification of degradation products

The degradation of LURA as quantified by LC-DAD analysis (6.3.4 and 6.3.5) was not accompanied by the appearance of any additional chromatographic peaks that could be attributed to a LURA degradation product. (Note: additional peaks were observed, but they had UV-Vis spectra similar to peaks observed previously in stability experiments involving ZIPR [223]. Their identity is discussed in Chapter 9). The lack of detected peaks in the LC-DAD chromatograms that may correspond to a LURA degradant suggested the possible conversion of LURA to a compound or compounds no longer containing chromophores that absorbed in the specific wavelengths monitored during chromatography or that were sufficiently polar that they eluted in the solvent front. The LC-QTOF-MS screen (7.2.1) indicated degradation products may be present. Therefore, all subsequent efforts to identify LURA degradation products utilised mass spectrometry as the detection technique.

8.2.1 Experimental

An Agilent 1200 Series HPLC and Agilent 6520 Series LC-QTOF-MS was used as detailed in 3.3.2. All experimental extracts, including representative calibrator, QC, and blank samples, were screened using the LC-QTOF-MS method as outlined in 7.2.1.

8.2.1.1 MS data analysis

EICs were obtained for LURA from the known mass/charge ratio of its precursor ion (493.2631 m/z). Potential degradation products were screened using MDF set to a tolerance of ± 100 mDa.

Mass spectra presented are those following MFE. MDF and MFE are previously described in 7.2.1.1 and 5.5.1, respectively.

The relative response of the precursor ions for LURA (493.2631 m/z) and the possible degradation products (precursor ions: 360.2643, 388.2603, 402.2755, 430.3064, and 460.2814 m/z) were determined over time in each extract of the blood specimens. “Relative responses” were relative to AMIT for experiment WBI and WB2, to account for inter-aliquot variation. Due to apparent degradation of AMIT over time to NORT in experiment YB (as discussed in Chapter 7), relative responses were relative to LORA for experiment YB.

To assess if the detected possible degradation products may be present in the LURA powder standard used to prepare the working solution a small aliquot of the working solution was diluted using ethanol for direct analysis by LC-QTOF-MS. The QC solution was also diluted and analysed in the same manner.

8.2.1.2 MS/MS data analysis

MS/MS spectra were acquired for LURA (precursor ion: 493.2631 m/z) and the possible degradation products (precursor ions: 360.2643, 388.2603, 402.2755, 430.3064, and 460.2814 m/z) between collision energies of 20-40 eV.

To provide more evidence as to the chemical structure of the degradation products, GMF and calculated accurate masses were determined for the product ions of LURA and the degradation products. The MS/MS spectrum of LURA, as published by Kumar Talluri *et al.*, was also consulted [432].

8.2.1.3 Acetylation

Acetylation was performed as described in 7.2.1.4 on specimens containing the degradation product to determine if nucleophilic functionalities such as alcohols, thiols, or amines were present.

8.2.1.4 Standard comparison

An attempt to confirm the identity of the major degradation product postulated to be forming (identified by its abundant response at 360.265 m/z, see 7.2.2) by synthesis was carried out. One way to yield the degradant directly from LURA could be reductive cleavage of the N-S bond in the 1,2-benzisothiazole moiety [460]. However, possible side reactions and the expense of the starting material hindered this approach. Instead, methods used to synthesise LURA, outlined by Ganesh *et al.* [461] and Ae & Fujiwara [462], were modified in an attempt to produce

the proposed degradation product, N-debenzothiazole-lurasidone (ND-LURA) (Figure 8-1); major modifications from their published method included: not resolving the enantiomeric intermediate, as the LC-QTOF-MS method would not resolve the enantiomeric degradant product, and reacting the mesylated intermediate with a piperazine or a mono-Boc protected piperazine (with subsequent deprotection) instead of a 1,2-benziothiazole-substituted piperazine. An attempt to produce the *cis* analogue of ND-LURA was carried out separately (Figure 8-1) simply by omitting the step that involved epimerization of the *cis*-dimethylester to the *trans*-dimethylester (second step in Figure 8-2). Tristan Fraser carried out all synthetic work and synthetic products were characterised using accurate mass MS and high-field nuclear magnetic resonance spectrometry (NMR) [1]. X-ray crystallography confirmed the identity of the *trans* isomer.

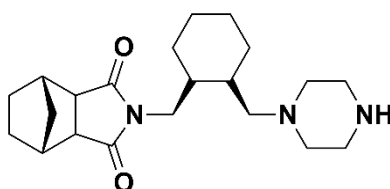


Figure 8-1: Structure of *cis*-N-debenzothiazole lurasidone.

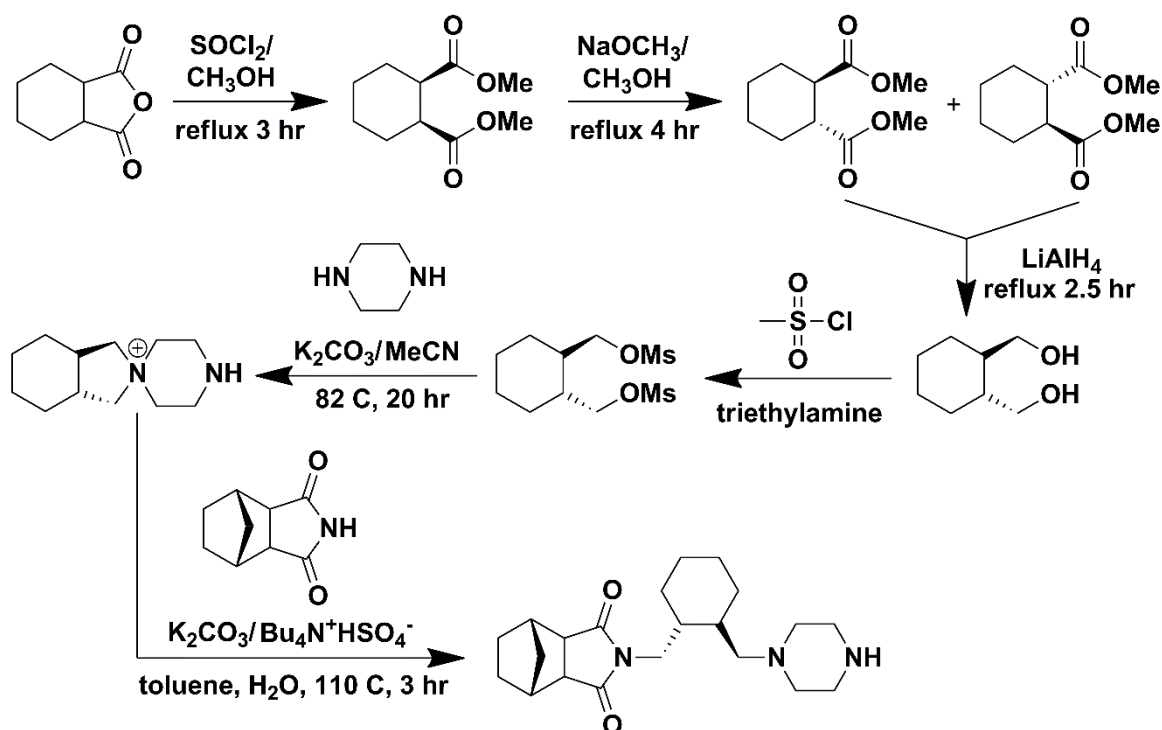


Figure 8-2: Synthetic scheme for N-debenzothiazole lurasidone.
Synthetic method used by Fraser to synthesise N-debenzothiazole lurasidone [1].

The synthesised compounds (*trans*-ND-LURA produced from mono-Boc piperazine, *trans*-ND-LURA produced from piperazine, and *cis*-ND-LURA produced from mono-Boc piperazine) were analysed in ethanolic solutions using LC-QTOF-MS concurrently with experimental extracts from the WBI experiment. The *trans*-ND-LURA product was also: 1) subjected to n-BuCl and the N₂ dry down step of the extraction method used when extracting analytes from blood specimens, followed by ethanol reconstitution (4.2.2); and 2) reconstituted in blood, before then being extracted as with experimental blood specimens (4.2.2).

8.2.2 Results

8.2.2.1 MS data analysis

Using MDF, three compounds were detected in Day 7 extracts of the week experiments that were considered potential LURA degradants. The most abundant of these was a compound with a precursor ion of 360.2643 m/z, followed by a compound with a precursor ion of 388.2603 m/z, and lastly a compound with a precursor ion of 402.2755 m/z. Except for the 402.2755 m/z compound, these ions were detected in extracts of all types of experimental blood specimens with drugs present (other than initial time-point extracts). The response for these degradants was greatest in inoculated, unpreserved blood specimens. These compounds were not detected in extracts of the calibrators or QCs.

In the seven-month experiment (YB, see 6.2), additional suspected LURA degradation products were also detected with precursor ions of 430.3064 and 460.2814 m/z. The EICs for these possible LURA degradants are shown in Figure 8-3.

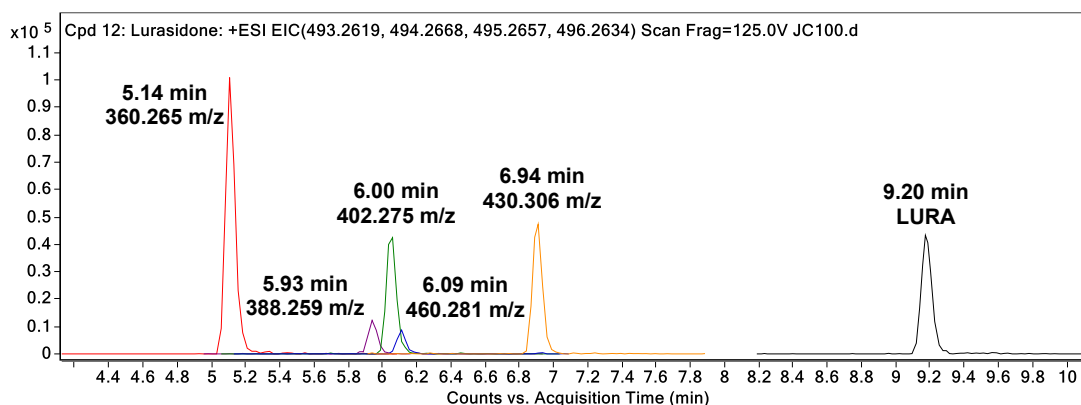


Figure 8-3: Extracted ion chromatograms of LURA and possible degradation products in an seven month extract of an inoculated, unpreserved room temperature blood specimen.

For the two week-long experiments (WBI and WB2, see 6.2), as the relative response of LURA decreased over time that of the potential 360.265 m/z degradation product increased in inoculated, unpreserved blood extracts (Figure 8-4).

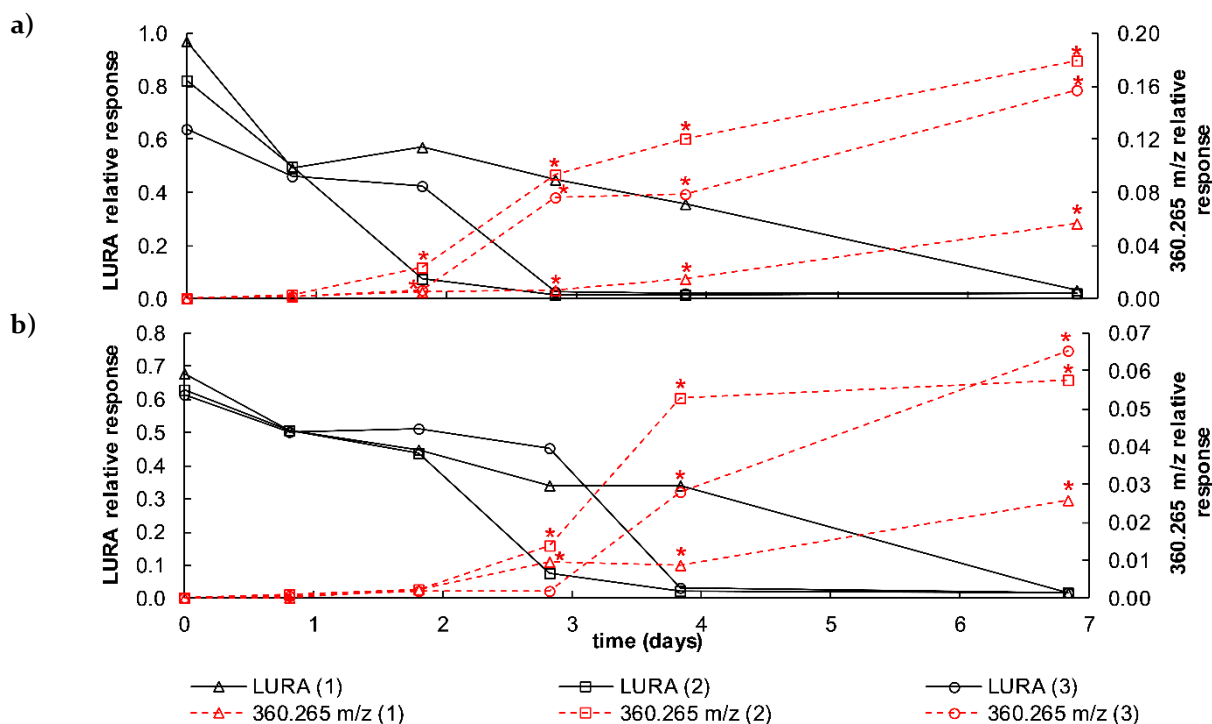


Figure 8-4: Relative response of LURA and 360.265 m/z degradation product over time in inoculated, unpreserved blood specimens for a) week experiment B1 and b) week experiment B2.

Asterisks indicate the acquisition of MS/MS spectra for the 360.265 m/z degradation product.

In non-inoculated, unpreserved and preserved blood extracts, and in inoculated, preserved blood extracts, there was also an increase in the response of the 360.265 m/z degradation product as the experiment progressed (Figure 8-5). This was not accompanied by significant decreases in LURA concentrations (6.3.4). The relative response of the 360.265 m/z degradation product in these extracts was after seven days 2-3-fold lesser than its relative response in extracts of the inoculated, unpreserved blood specimens. Auto-MS-MS spectra were not acquired for the 360.265 m/z degradant in extracts of non-inoculated, preserved blood specimens in experiment WB2. Clearly, the most rapid formation of the 360.265 m/z compound is in inoculated, unpreserved blood specimens, suggesting that microbial activity may be primarily responsible for the conversion of LURA to the 360.265 m/z degradant or that microorganisms may convert LURA to 360.265 m/z at a far greater rate than any endogenous blood components.

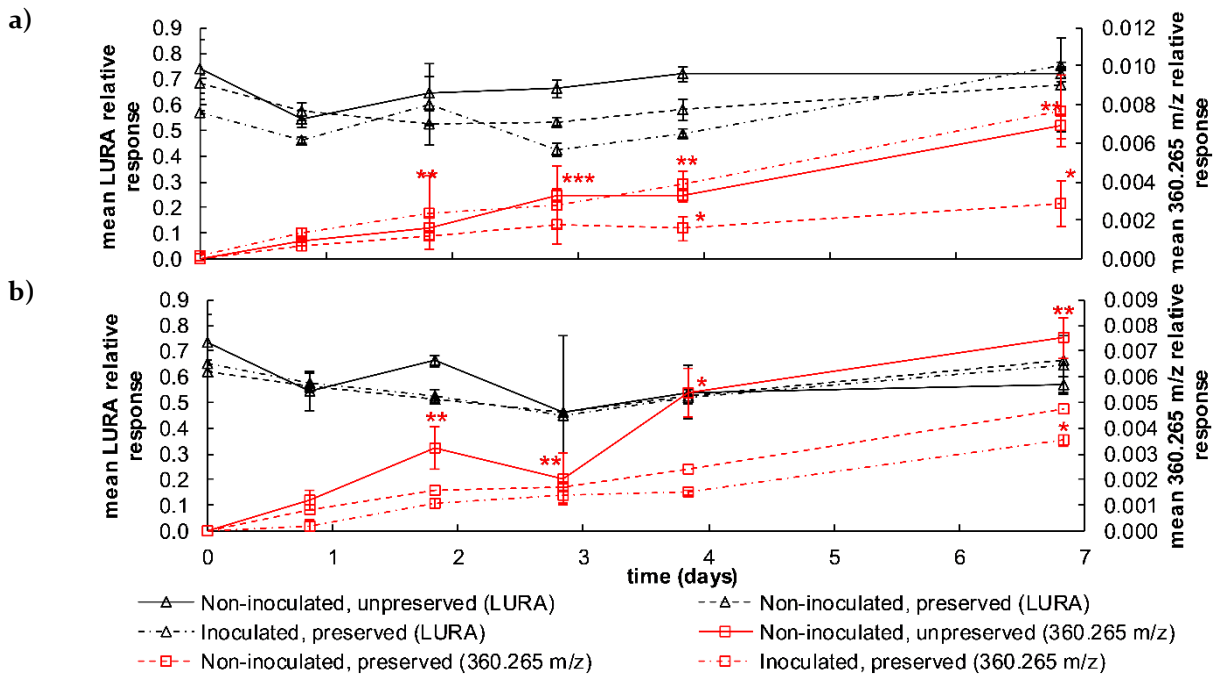


Figure 8-5: Relative response of LURA and 360.265 m/z degradation product over time in preserved and unpreserved, non-inoculated blood specimens and preserved, inoculated blood specimens for a) week experiment B1 and b) week experiment B2.

Asterisks indicate the acquisition of MS/MS spectra for the 360.265 m/z degradation product in: * one specimen type; ** two specimen type; *** all three specimen types. Error bars are \pm S.D., $n = 3$, except for non-inoculated, preserved specimens in experiment B2 where $n = 1$.

The 388.259 m/z and 402.275 m/z degradants had a much lower response on the LC-QTOF-MS. Thus, auto-MS/MS spectra were only acquired over time throughout the experimental extracts for inoculated, unpreserved blood specimens for 388.259 m/z in both experiments, and for 402.275 m/z in the initial week experiment (B1). The low signal intensities of these degradants in the other blood specimens may be due to their formation being accelerated by microbial activity as appeared to be the case for the 360.265 m/z degradant. Similar to the 360.265 m/z degradant, the 388.259 m/z compound appeared to be increasing in concentration in the blood specimens over time by extrapolation of the increased relative response of 388.259 m/z as the experiments progressed (Figure 8-6). After seven days, the relative response of the 388.259 m/z degradant did not exceed 0.006 in any replicate, up to 33-fold lesser than the relative response of the 360.265 m/z degradant. The relative response of the 402.275 m/z degradant was more variable over time, with auto-MS/MS spectra sporadically acquired (Figure 8-7).

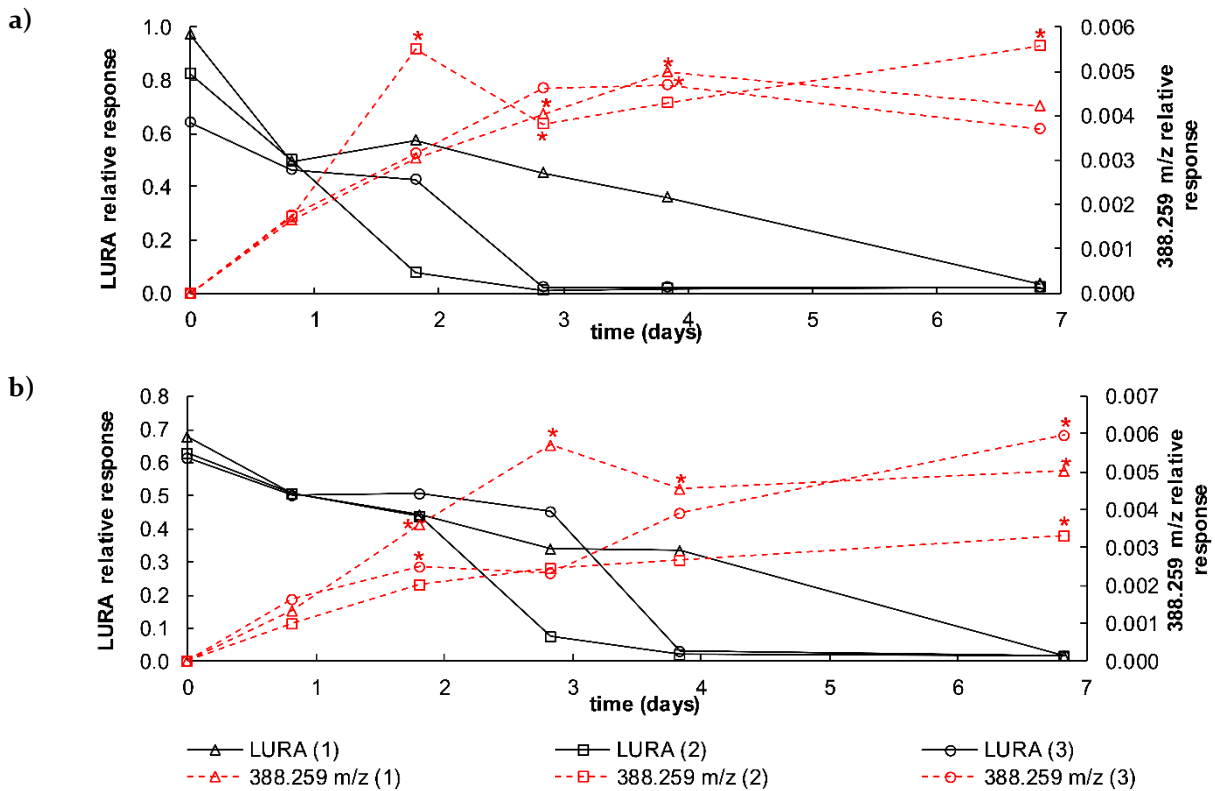


Figure 8-6: Relative response of LURA and 388.259 m/z degradation product over time in inoculated, unpreserved blood specimens for a) week experiment B1 and b) week experiment B2.

Asterisks indicate the acquisition of MS/MS spectra for the 388.259 m/z degradation product.

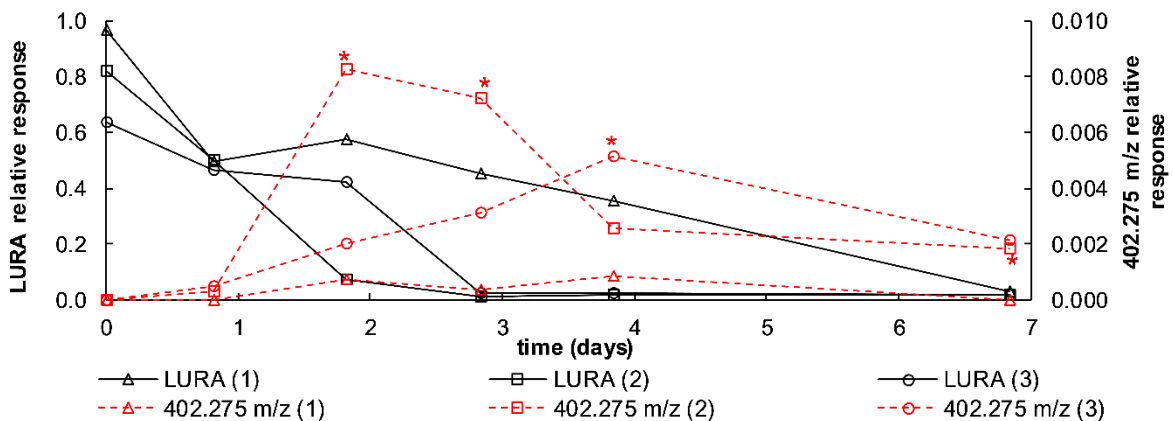


Figure 8-7: Relative response of LURA and 402.275 m/z degradation product over time in inoculated, unpreserved blood specimens for week experiment B1.

Asterisks indicate the acquisition of MS/MS spectra for the 402.275 m/z degradation product.

In the seven-month experiment the degradation product of m/z 360.265 was detected in extracts of all blood specimens except non-inoculated, unpreserved blood specimens stored at -20°C (Figure 8-8). Greatest relative responses of the degradant were observed in extracts of inoculated, unpreserved room temperature specimens. There was an up to 20-fold difference in relative response between inoculated and non-inoculated unpreserved room temperature specimens.

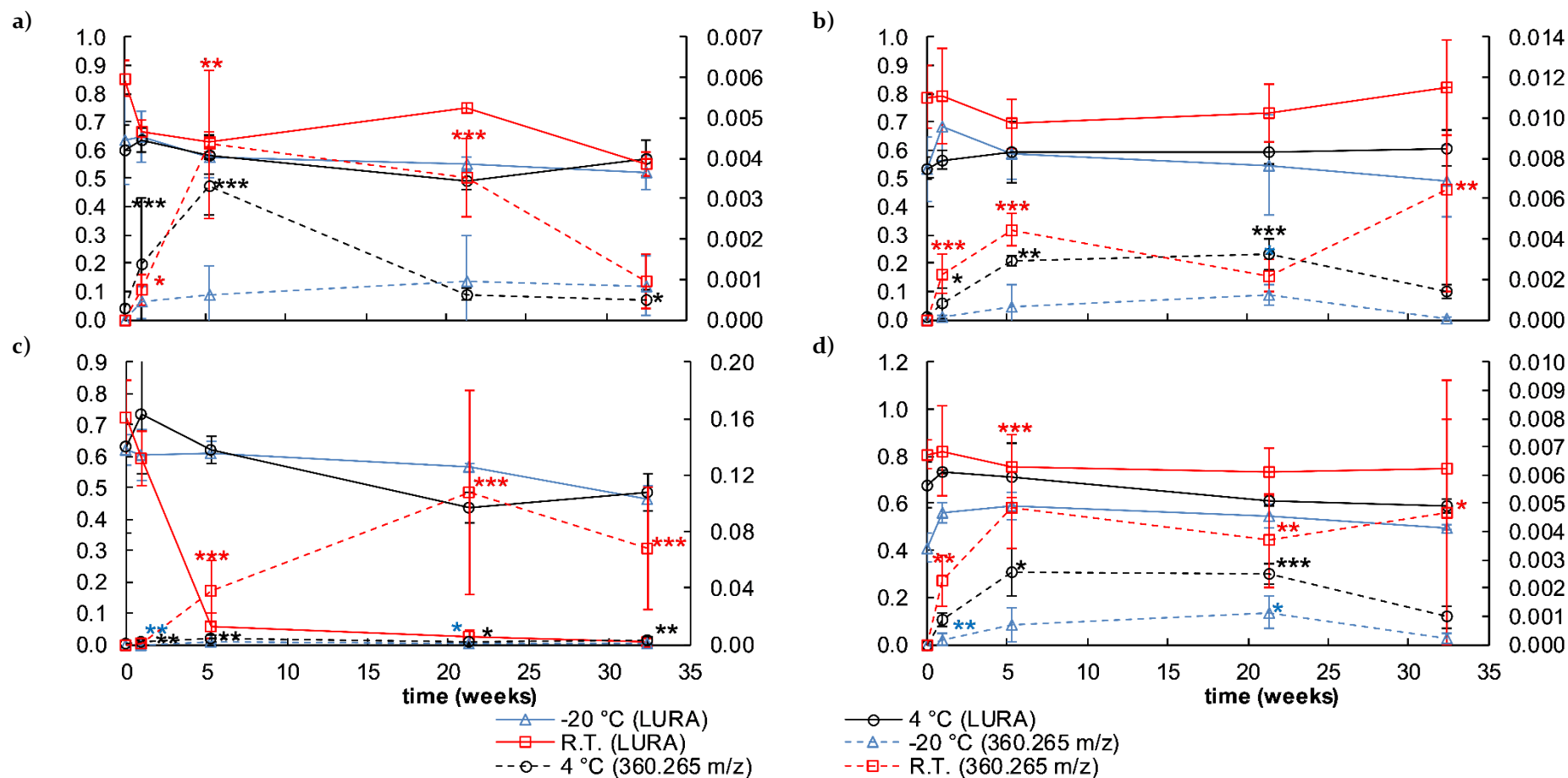


Figure 8-8: Relative response of LURA and 360.265 m/z degradation product over time in seven-month experiment in a) non-inoculated, unpreserved specimens, b) non-inoculated, preserved specimens, c) inoculated, unpreserved specimens, and d) inoculated, preserved specimens.

Primary Y-axis is mean LURA relative response. Secondary Y-axis is mean 360.265 m/z degradation product relative response. Asterisks indicate the acquisition of MS/MS spectra for 360.265 m/z degradation product in: * one replicate; ** two replicates; *** all three replicates. Error bars are \pm S.D., n = 3.

The 388.259 m/z degradant was only detected with auto-MS/MS spectra acquired in inoculated room temperature blood specimens. In preserved specimens, this occurred only after seven months, with a relative response around 0.0008. In unpreserved specimens, after ~21 weeks this degradant was detected (Figure 8-9). No auto-MS/MS spectra were acquired for this degradant in other specimens, consistent with the week experiments.

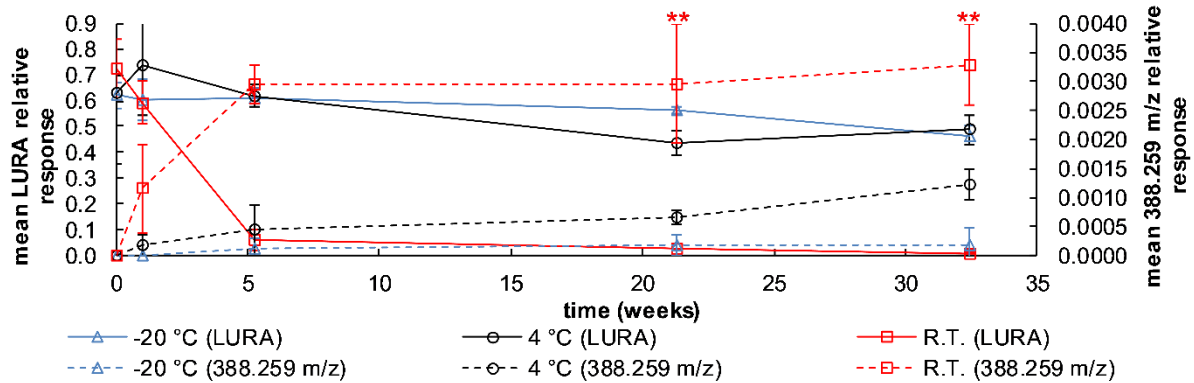


Figure 8-9: Relative response of LURA and 388.259 m/z degradation product over time in seven-month experiment in inoculated, unpreserved specimens.

Asterisks indicate the acquisition of MS/MS spectra for 388.259 m/z degradant in: * one replicate; ** two replicates; *** all three replicates. Error bars are \pm S.D., $n = 3$.

The 460.281 m/z degradant was only detected with acquired auto-MS/MS spectra in a sole inoculated, unpreserved room temperature specimen from ~21 weeks onward (Figure 8-10).

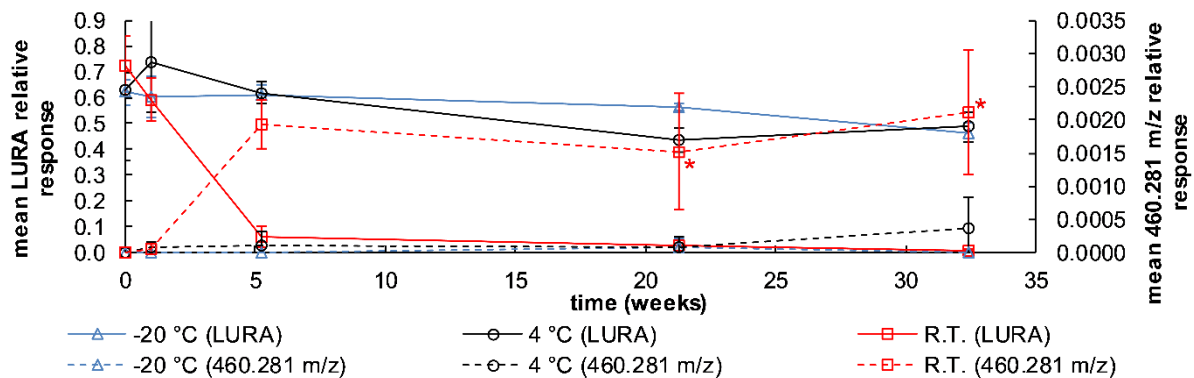


Figure 8-10: Relative response of LURA and 460.281 m/z degradation product over time in seven-month experiment in inoculated, unpreserved specimens.

Asterisks indicate the acquisition of MS/MS spectra for 460.281 m/z degradant in: * one replicate; ** two replicates; *** all three replicates. Error bars are \pm S.D., $n = 3$.

The 402.275 m/z degradation product was often detected in all blood specimens of the seven-month experiment that were stored at 4 °C and room temperature from ~21 weeks onward (Figure 8-11). This contrasted with its sporadic detection in inoculated, unpreserved blood specimens in the initial week experiment. In specimens of the seven-month experiment, it appeared that the response of 402.275 m/z increased over time. The 430.306 m/z degradant behaved similarly (Figure 8-12).

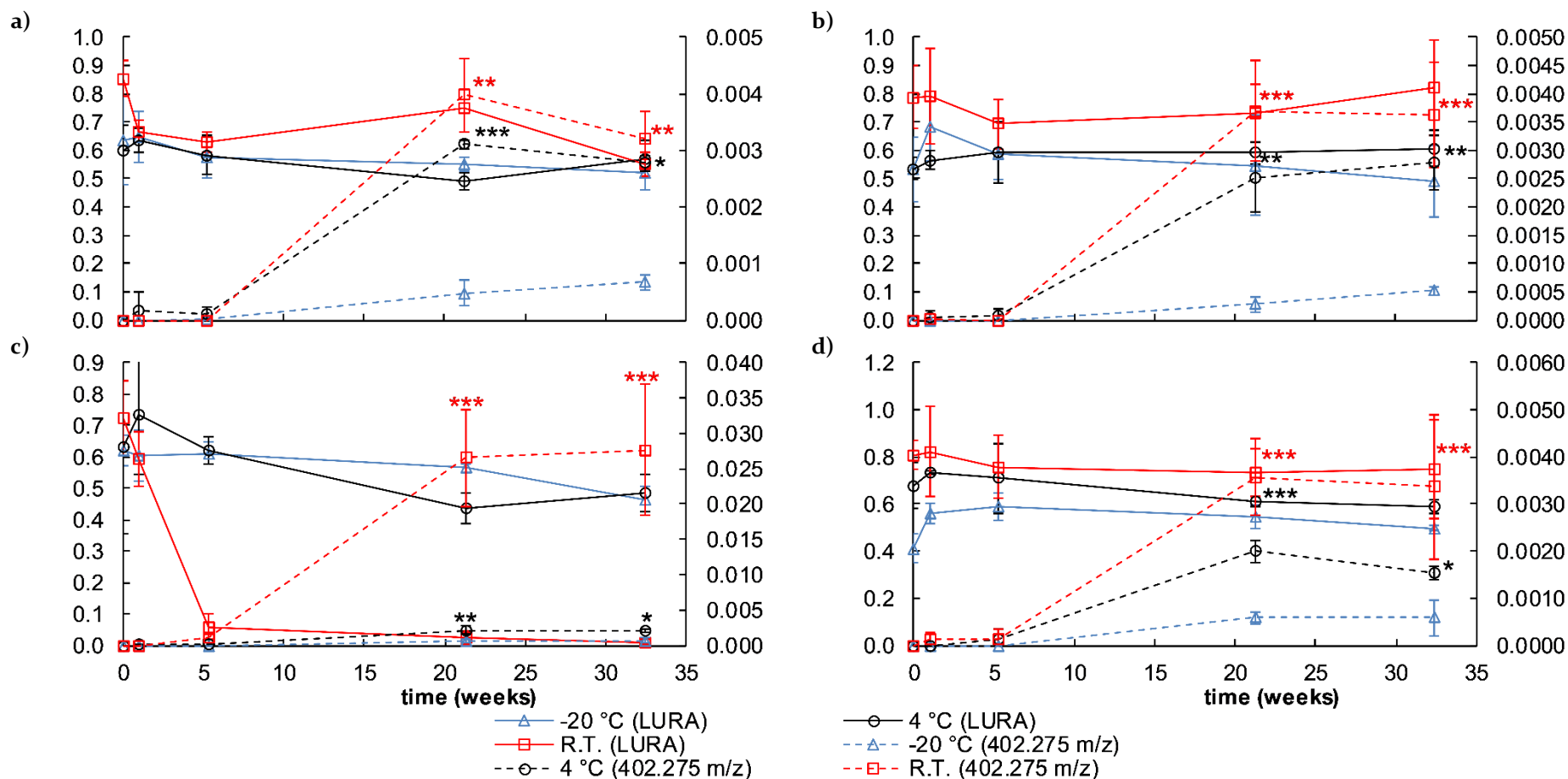


Figure 8-II: Relative response of LURA and 402.275 m/z degradation product over time in seven-month experiment in a) non-inoculated, unpreserved specimens, b) non-inoculated, preserved specimens, c) inoculated, unpreserved specimens, and d) inoculated, preserved specimens.

Primary Y-axis is mean LURA relative response. Secondary Y-axis is mean 402.275 m/z degradation product relative response. Asterisks indicate the acquisition of MS/MS spectra for 402.275 m/z degradation product in: * one replicate; ** two replicates; *** all three replicates. Error bars are ± S.D., n = 3.

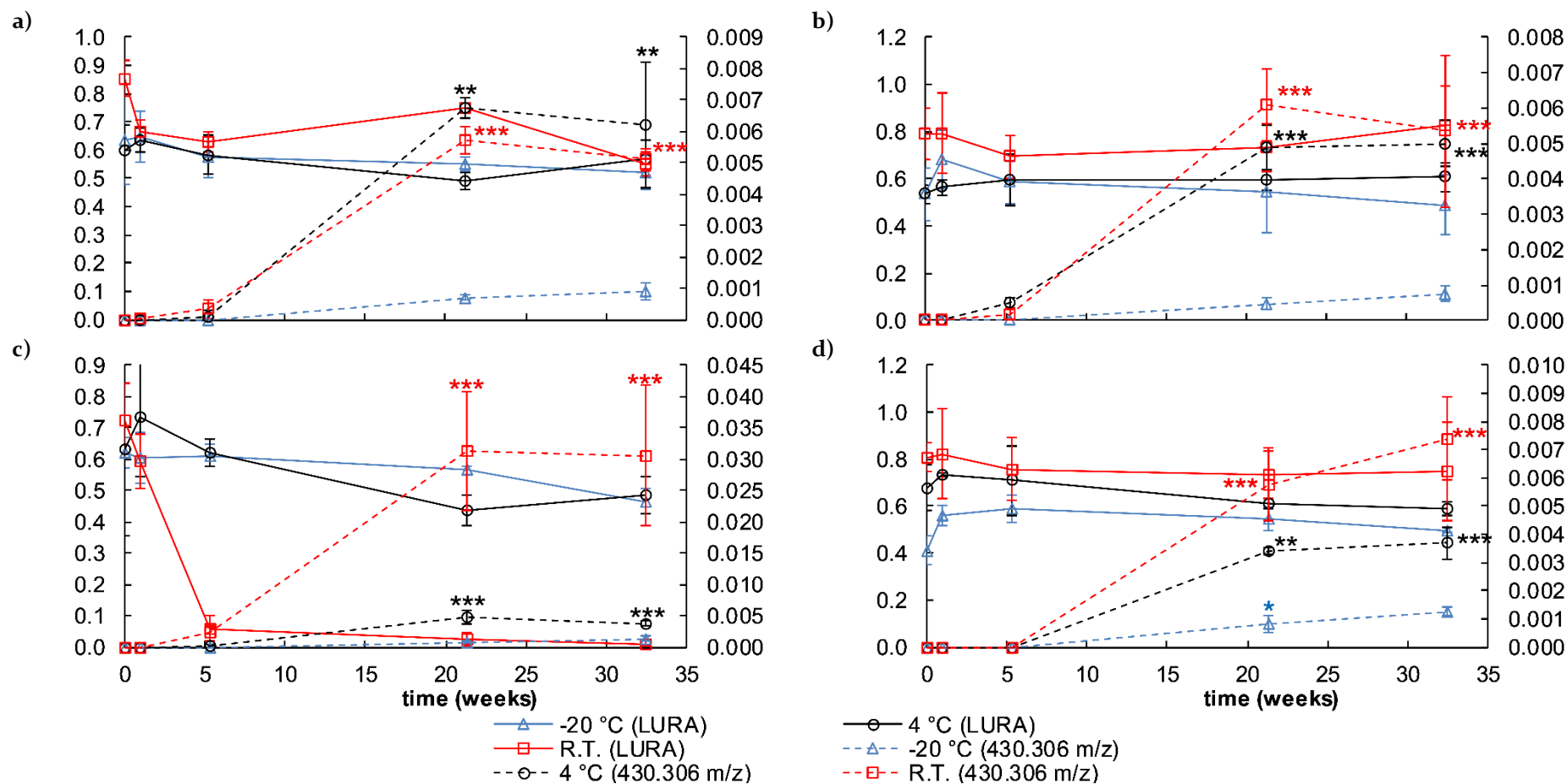


Figure 8-12: Relative response of LURA and 430.306 m/z degradation product over time in seven-month experiment in a) non-inoculated, unpreserved specimens, b) non-inoculated, preserved specimens, c) inoculated, unpreserved specimens, and d) inoculated, preserved specimens.

Primary Y-axis is mean LURA relative response. Secondary Y-axis is mean 430.306 m/z degradation product relative response. Asterisks indicate the acquisition of MS/MS spectra for 430.306 m/z degradation product in: * one replicate; ** two replicates; *** all three replicates. Error bars are \pm S.D., $n = 3$.

For all degradants, greatest absolute responses were obtained in inoculated, unpreserved specimens.

GMF for the possible LURA degradation products produced predicted isotope ratios similar to the observed isotope ratios for the precursor ions (Figure 8-13 and Figure 8-14). Based on the integer of the degradant masses, it appeared that there may be common structural modifications between the degradants. However, the high-resolution mass accuracy of the LC-QTOF-MS enabled it to be established that the mass differences between the degradants could not be due to the same structural modifications. The difference of 27.9960 mass units between the 360.265 m/z and 388.259 m/z degradants was similar to the mass of CO (calculated mass: 27.9949 Da, $\delta = -39.3$ ppm (-1.1 mDa)); the difference of 28.0309 mass units between the 402.275 m/z and 430.306 m/z degradants was similar to the mass of C₂H₄ (calculated mass: 28.0313 Da, $\delta = 14.3$ ppm (0.4 mDa)); the difference of 42.0112 mass units between the 360.265 m/z and 402.275 m/z degradants was similar to the mass of C₂H₂O (calculated mass: 42.0106 Da, $\delta = -14.3$ ppm (-0.6 mDa)); and the difference of 42.0461 mass units between the 388.259 m/z and 430.306 m/z degradants was similar to the mass of C₃H₆ (calculated mass: 42.0470 Da, $\delta = 1.3$ ppm (0.6 mDa)). These differences are reflected in the GMF for the precursor ions (Table 8-1).

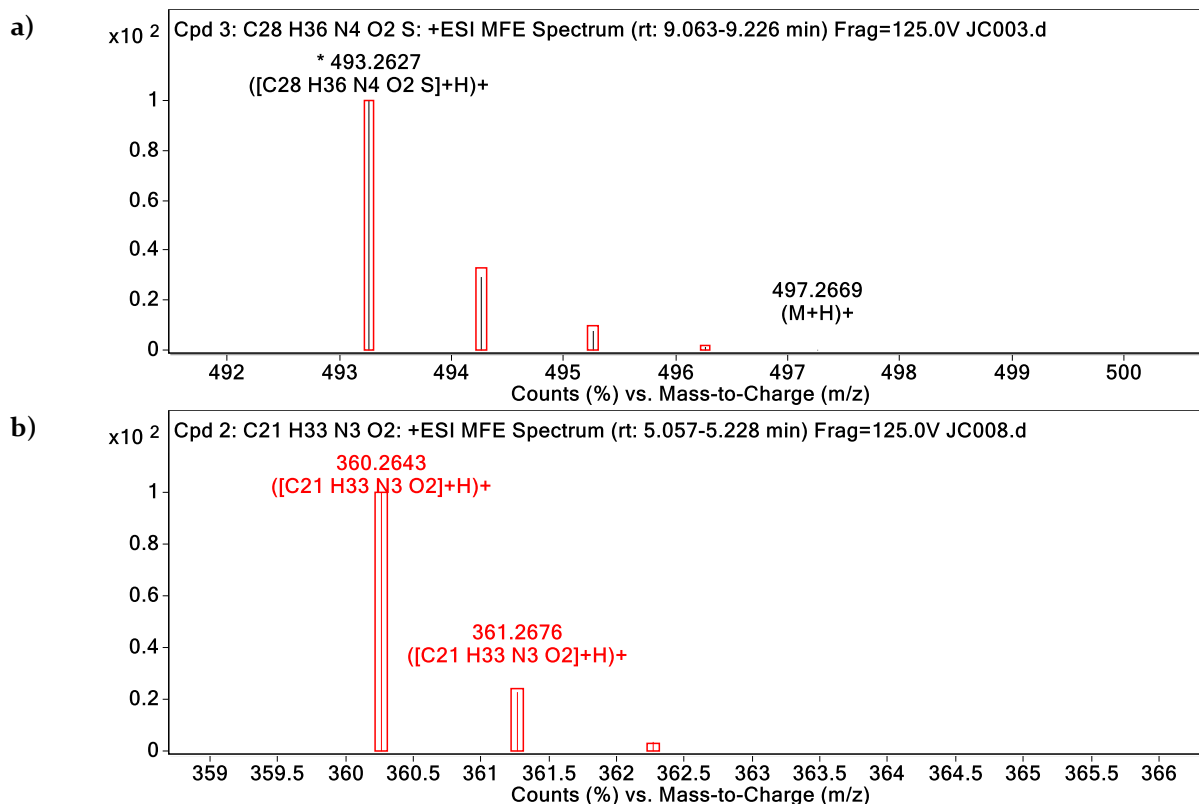


Figure 8-13: MS spectra with generated molecular formula showing predicted isotope ratios in red for: a) LURA and the major 360.265 m/z degradation product. Observed ion signal intensities are shown as lines within the boxes.

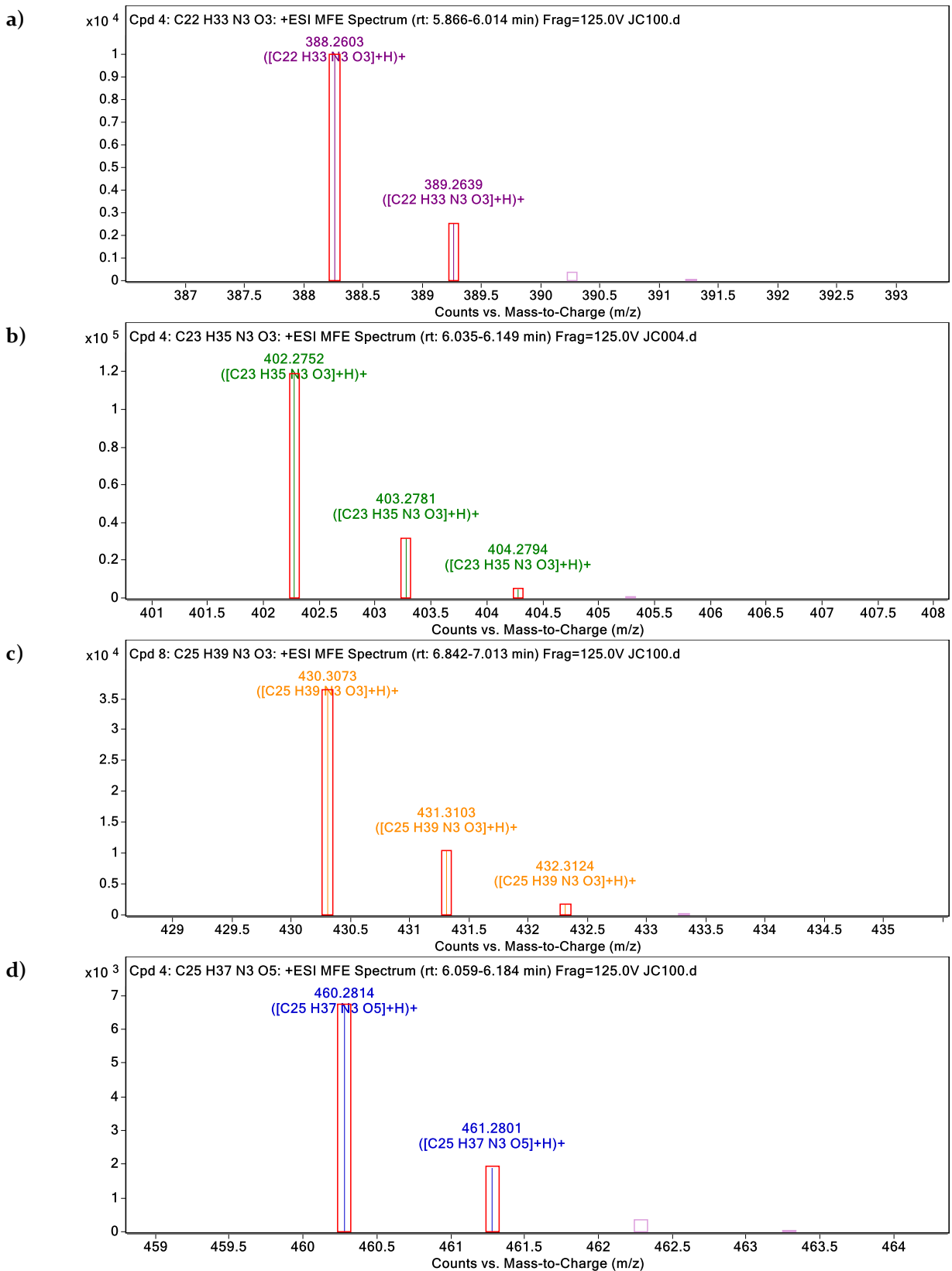


Figure 8-14: MS spectra with generated molecular formula showing predicted isotope ratios in red for degradation products with m/z of a) 388.259, and b) 402.275 c) 430.306 and d) 460.281.

Observed ion signal intensities are shown as lines within the boxes.

Traces of lurasidone-sulfoxide (LURA-SO) were also thought to be detected in both the experiments and calibrators and QCs, based on an observed precursor ion 15.9954 mass units greater than LURA (calculated accurate mass of an oxygen atom: 15.9949 Da, $\delta = -31.3$ ppm (-0.5 mDa)) (Figure 8-15). This presumptive identification was supported by MS/MS spectral similarities with a degradant reported by Kumar Talluri *et al.* that was detected following oxidative degradation of LURA with 10 % hydrogen peroxide (see 8.2.2.2) [432]. Furthermore, a degradant with a precursor ion of 551.2687 m/z was not detected in the acetylated extracts, as would be expected if the compound suspected to be LURA-SO was instead a hydroxylated product.

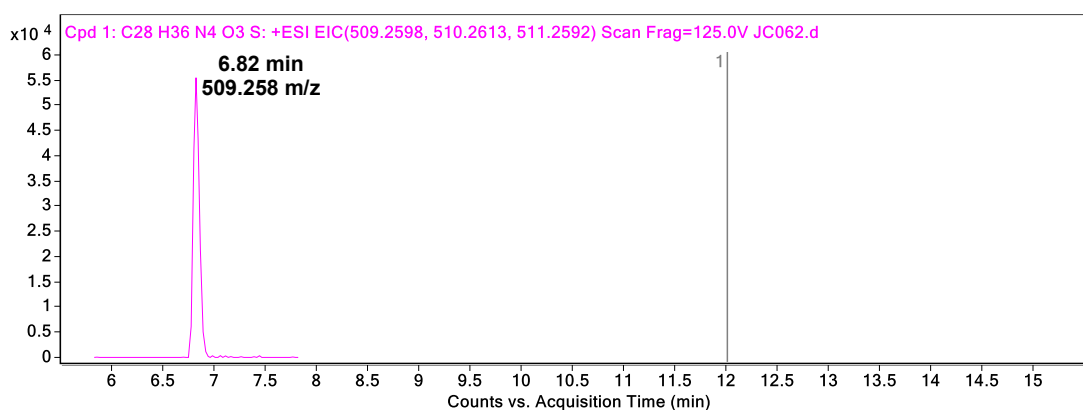


Figure 8-15: Extracted ion chromatogram of LURA-SO.

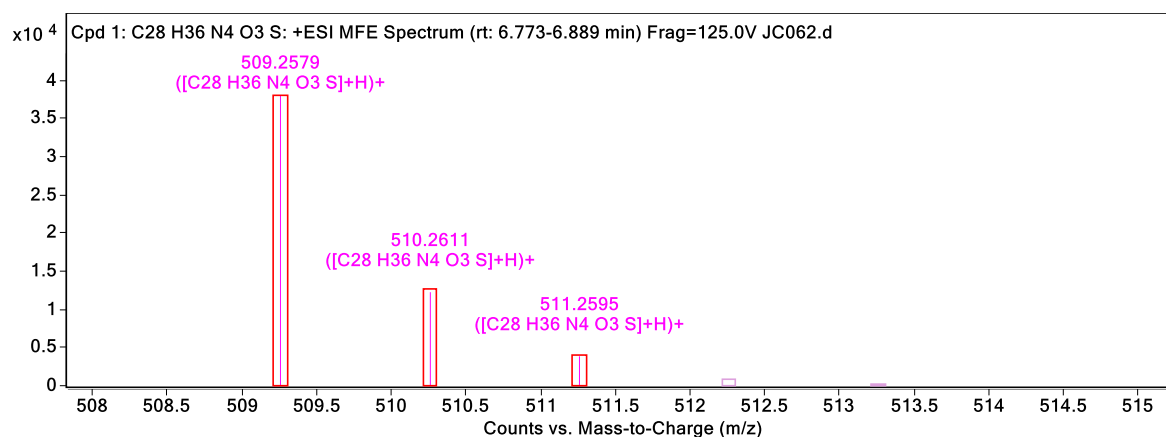


Figure 8-16: MS spectra with generated molecular formula showing predicted isotope ratios in red boxes for LURA-SO.

Observed ion signal intensities are shown as lines within the boxes.

The same trend as with CHLO-SO and PROC-SO (see 6.3.6.1) was observed for the formation and signal intensity of LURA-SO over time in the seven-month blood experiment specimens stored at -20 °C, 4 °C, and at room temperature. That is, greater LURA-SO appeared to evolve in blood specimens stored at -20 °C and room temperature, compared to those at 4 °C (Figure 8-17). The difference in final time-point mean relative responses between -20 °C and 4 °C

specimens and between room temperature and 4 °C specimens was significant (Welch's t-test: $p < 0.05$) for all inoculated specimens, and non-inoculated, unpreserved specimens. For non-inoculated, preserved specimens there was no significant difference between room temperature and 4 °C relative responses. As with CHLO-SO and PROC-SO, inoculated, unpreserved blood specimens presented an exception to this behaviour. In these specimens there were greater relative responses of LURA-SO for those stored at -20 °C and 4 °C and decreasing relative responses until LURA-SO become undetectable in those stored at room temperature (Figure 8-17 (c)). LURA-SO relative responses did not increase in the week experiments (data not shown), contrary to the behaviour of CHLO-SO and PROC-SO (6.3.6.1).

Table 8-1: MS data for LURA and degradation products.

Analyte	Measured [M+H] ⁺ (m/z)	Calculated [M+H] ⁺ (m/z)	GMF precursor ions	Mass accuracy (δ) (ppm)	Mass accuracy (δ) (mDa)
LURA	493.2627	493.2632	[C ₂₈ H ₃₆ N ₄ O ₂ S]H ⁺	1.0	0.5
360.265 m/z	360.2643	360.2646	[C ₂₁ H ₃₃ N ₃ O ₂]H ⁺	0.8	0.3
388.259 m/z	388.2603	388.2595	[C ₂₂ H ₃₃ N ₃ O ₃]H ⁺	-2.1	-0.8
402.275 m/z	402.2755	402.2751	[C ₂₃ H ₃₅ N ₃ O ₃]H ⁺	-1.0	-0.4
430.306 m/z	430.3064	430.3064	[C ₂₅ H ₃₉ N ₃ O ₃]H ⁺	0.0	0.0
460.281 m/z	460.2814	460.2806	[C ₂₅ H ₃₇ N ₃ O ₅]H ⁺	-1.7	-0.8
LURA-SO	509.2581	509.2579	[C ₂₈ H ₃₆ N ₄ O ₃ S]H ⁺	0.4	0.2

GMF = generated molecular formulae. Mass accuracies determined from single injection.

None of the degradation products were detected in the diluted aliquots of the QC and working solution nor in extracted calibrators or QCs.

Alkaline LURA degradation products previously reported in the literature by Kumar Talluri *et al.* were not detected [432]. Alkaline degradation products reported were those following hydrolysis of the amide carbonyl to produce DPI-DP3 (Figure 8-18). To identify these alkaline degradation products the authors first neutralised extracts before dilution in an aqueous mobile phase. In this thesis, analytes were extracted during the blood experiments using an unbuffered LLE method and organic solvent. The primary amine and carboxylic acid functionalities of DPI and DP2-3, respectively, may have limited the extent of their extraction, but to what extent is unknown. The limitation of only collecting neutral extracts to identify LURA degradation products from the week-long blood experiments was addressed in a subsequent qualitative experiment (see 8.3).

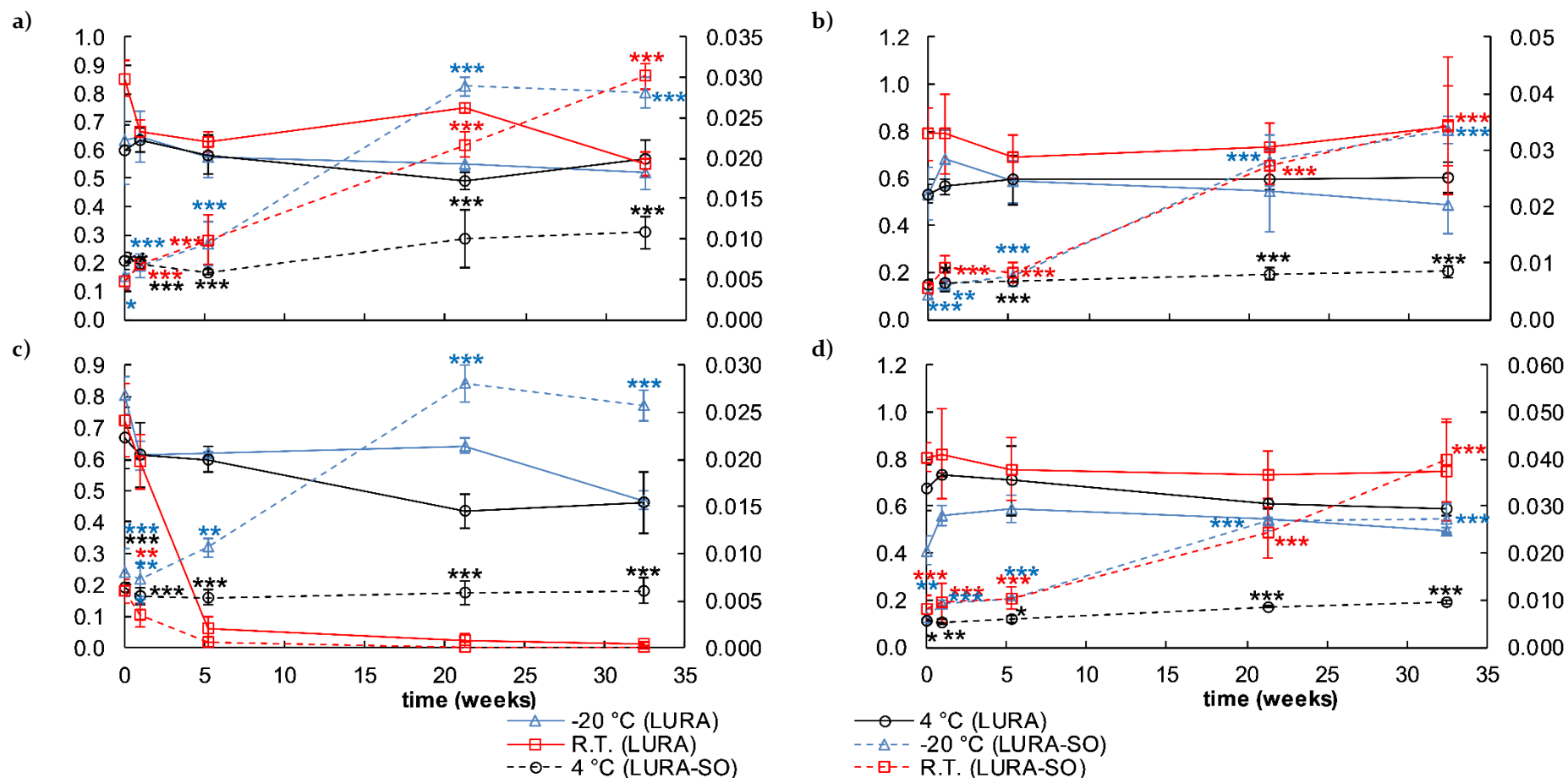


Figure 8-17: Relative response of LURA and LURA-SO over time in seven-month experiment in a) non-inoculated, unpreserved specimens, b) non-inoculated, preserved specimens, c) inoculated, unpreserved specimens, and d) inoculated, preserved specimens. Primary Y-axis is mean LURA relative response. Secondary Y-axis is mean LURA-SO relative response. Asterisks indicate the acquisition of MS/MS spectra for LURA-SO m/z degradation product in: * one replicate; ** two replicates; *** all three replicates. Error bars are \pm S.D., n = 3.

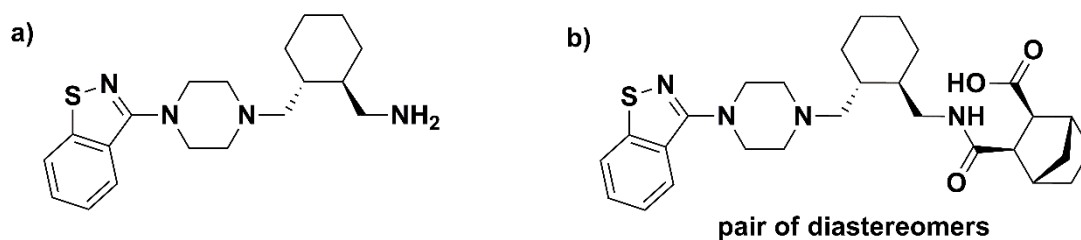


Figure 8-18: Chemical structure of a) DPI and b) DP2 and DP3 as postulated by Kumar Talluri *et al.* [432].

8.2.2.2 MS/MS data analysis

Optimum MS/MS spectra for LURA and the degradation products were those obtained at collision energy of 40 eV, with lower collision energies resulting in low intensity product ions (see Figure 8-19 and Figure 8-20). The 509.285 m/z degradant shared the major product ions of m/z 99.0917 and 358.2489 with the compound identified as LURA-SO by Kumar Talluri *et al.* (Figure 8-20 (c)) [432]. Therefore, this degradant was presumptively identified as LURA-SO.

The major degradation product (360.265 m/z) and LURA have common fragments at 67.054, 109.101, 120.081, and 166.086 m/z (Figure 8-19). These product ions in LURA correspond to those containing the 1,2 disubstituted cyclohexyl and [2.2.1]-bicycloheptyl-fused succinimide moieties (Figure 8-21). The 177.048 and 220.090 m/z product ions in the MS/MS spectrum of LURA are absent in the spectrum for the 360.265 m/z degradation product, with postulated structures for these fragments involving the 1,2-benzisothiazole moiety (Figure 8-21). Given also the mass difference of 132.9984 mass units between the degradation product and LURA it is therefore indicated that the 1,2-benzisothiazole moiety in LURA is not present in the degradation product (calculated mass of C₇H₃NS: 132.9986 Da, $\delta = 1.5$ ppm (0.2 mDa)) (Figure 8-21). This is provided the absence of the 1,2-benzisothiazole moiety in the degradation product is associated with the addition of a proton to form a secondary amine on the terminal end of the substituted piperazine. Formation of a secondary amine at this site is supported by the 87.092 and 195.186 m/z product ions unique to the 360.265 m/z degradation product (Figure 8-21). As the degradation product was not detected by UV-Vis (detection at 245, 254, 275, and 320 nm) the hypothesis that it is a compound that does not contain the 1,2-benzisothiazole moiety is consistent with the loss of the LURA chromophore. Based on the discussed MS/MS spectral similarities and differences between LURA and the degradant, the degradant was presumptively identified as N-debenzothiazole lurasidone (ND-LURA).

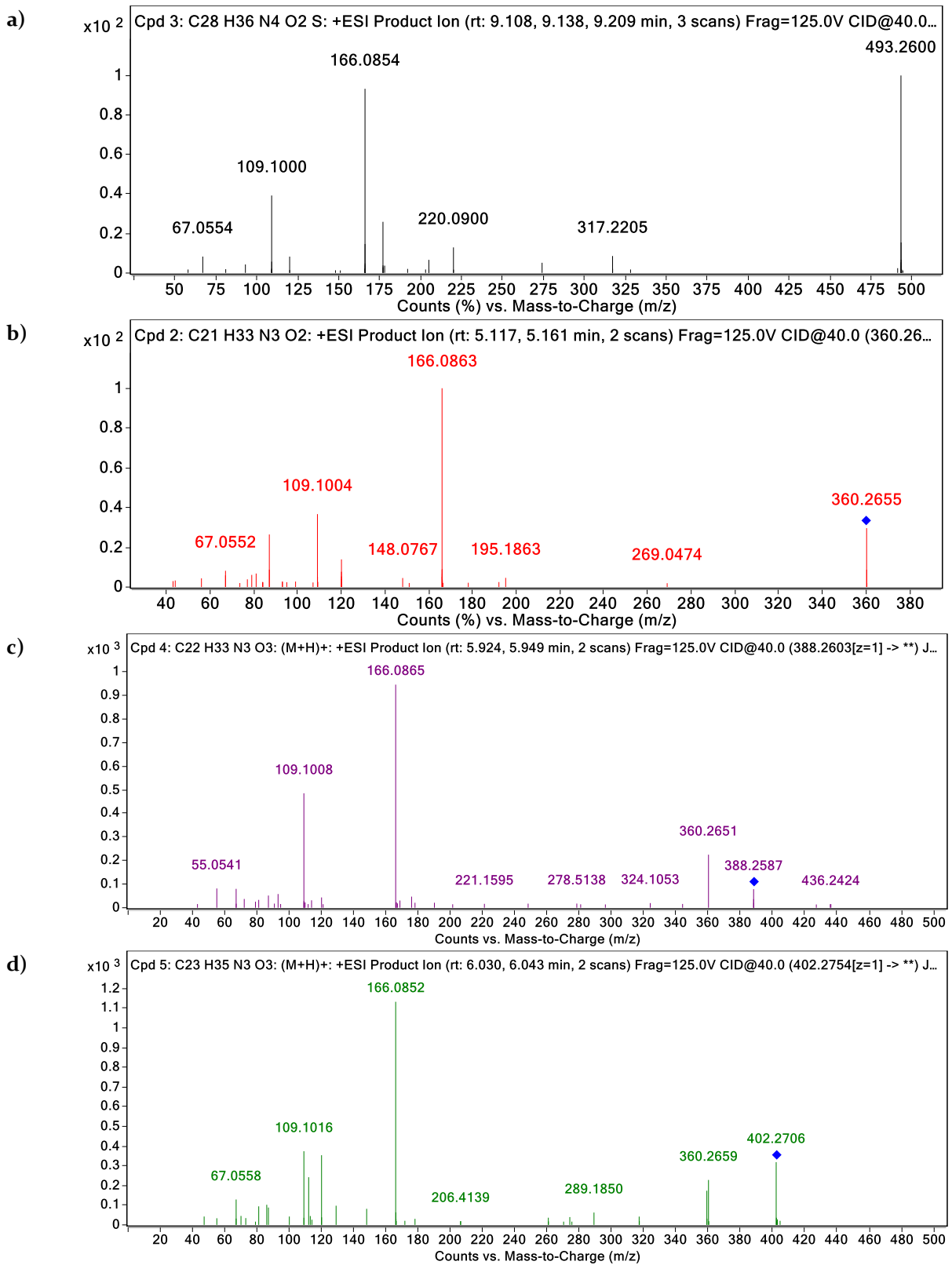


Figure 8-19: MS/MS spectra for: a) LURA; and degradation products with m/z of b) 360.265, c) 388.259, and d) 402.275. Collision energy = 40 eV.

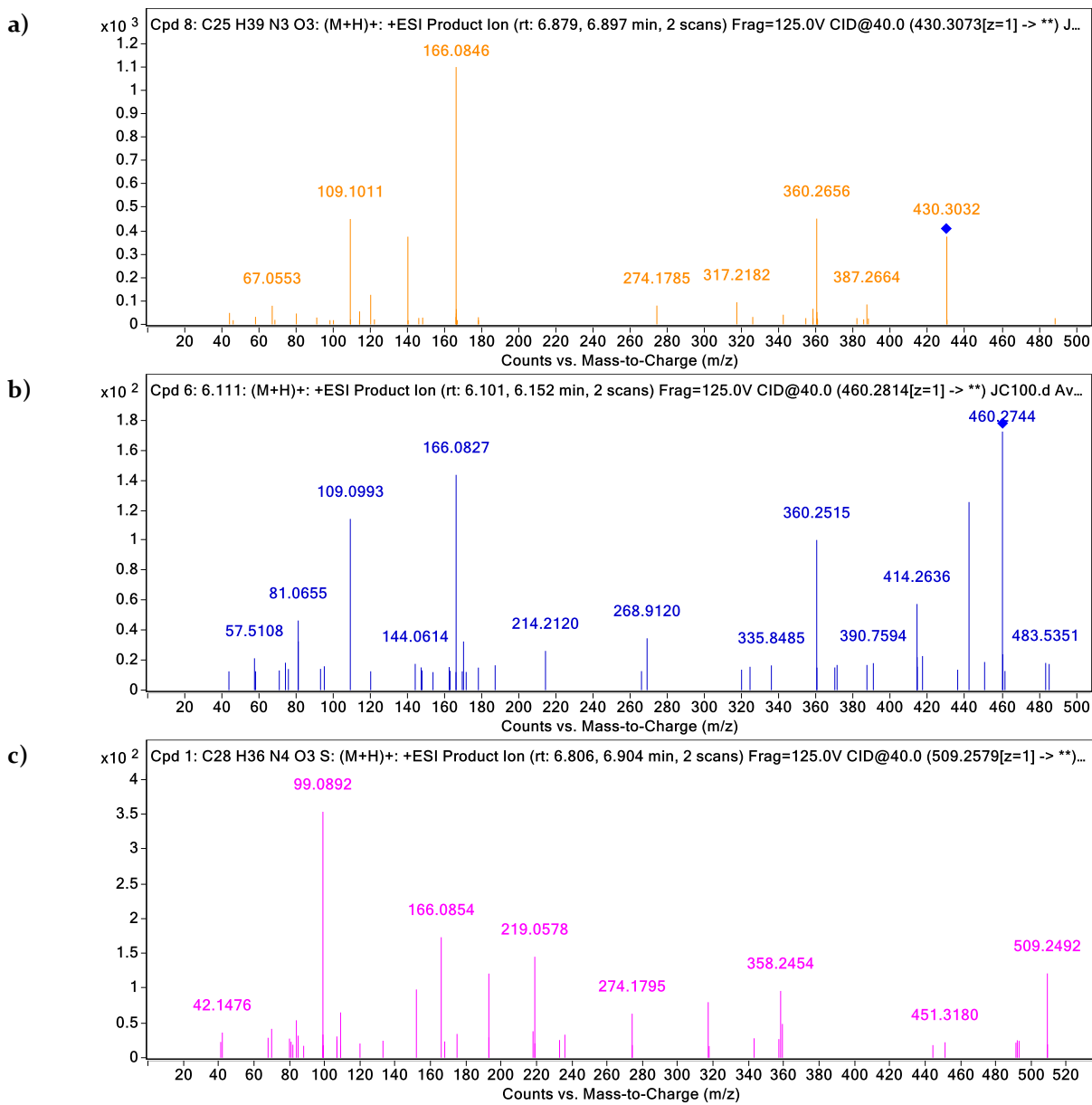


Figure 8-20: MS/MS spectra for: a) 430.306 m/z degradation product, b) 460.281 m/z degradation product, and c) LURA-SO. Collision energy = 40 eV.

Table 8-2: MS/MS data for LURA, LURA-SO and degradation products.

Analyte	Precursor ion (m/z)	Product ions (m/z)	GMF product ions	Calculated accurate mass (m/z)	Mass accuracy (δ) (ppm)	Mass accuracy (δ) (mDa)
LURA	493.2627	67.0554	C ₅ H ₇	67.0542	-17.9	-1.2
		109.1000	C ₈ H ₁₃	109.1012	11.0	1.2
		120.0796	C ₈ H ₁₀ N	120.0808	10.0	1.2
		166.0854	C ₉ H ₁₂ NO ₂	166.0863	5.4	0.9
		177.0471	C ₉ H ₉ N ₂ S	177.0481	5.6	1.0
		220.0900	C ₁₁ H ₁₄ N ₃ S	220.0903	1.4	0.3
		274.1825	C ₁₇ H ₂₄ NO ₂	274.1802	-8.4	-2.3
		317.2205	C ₁₉ H ₂₉ N ₂ O ₂	317.2224	6.0	1.9
	493.2600	[C ₂₈ H ₃₆ N ₄ O ₂ S]H ⁺	493.2632	6.5	3.2	
LURA-SO	509.2579	99.0892	C ₅ H ₁₁ N ₂	99.0917	25.2	2.5
		166.0854	C ₉ H ₁₂ NO ₂	166.0863	5.4	0.9
		358.2454	C ₂₁ H ₃₂ N ₃ O ₂	358.2489	9.8	3.5
360.265 m/z	360.2643	67.0552	C ₅ H ₇	67.0542	-14.9	-1.0
		87.0927	C ₄ H ₁₁ N ₂	87.0917	-11.5	-1.0
		109.1004	C ₈ H ₁₃	109.1012	7.3	0.8
		120.0842	C ₈ H ₁₀ N	120.0808	-28.3	-3.4
		166.0863	C ₉ H ₁₂ NO ₂	166.0863	0.0	0.0
		195.1863	C ₁₂ H ₂₃ N ₂	195.1856	-3.6	-0.7
		360.2655	[C ₂₁ H ₃₃ N ₃ O ₂]H ⁺	360.2646	-2.5	-0.9
388.259 m/z	388.2603	67.0531	C ₅ H ₇	67.0542	16.4	1.1
		87.0909	C ₄ H ₁₁ N ₂	87.0917	9.2	0.8
		109.1010	C ₈ H ₁₃	109.1012	1.8	0.2
		120.0807	C ₈ H ₁₀ N	120.0808	0.8	0.1
		166.0856	C ₉ H ₁₂ NO ₂	166.0863	4.2	0.7
		360.2631	C ₂₁ H ₃₄ N ₃ O ₂	360.2646	4.2	1.5
		388.2527	[C ₂₂ H ₃₃ N ₃ O ₃]H ⁺	388.2595	17.5	6.8
402.275 m/z	402.2755	67.0558	C ₅ H ₇	67.0542	-23.9	-1.6
		86.0586	C ₄ H ₈ NO	86.0600	16.3	1.4
		109.0986	C ₈ H ₁₃	109.1012	23.8	2.6
		112.0735	C ₆ H ₁₀ NO	112.0757	19.6	2.2
		120.0796	C ₈ H ₁₀ N	120.0808	10.0	1.2
		129.1024	C ₆ H ₁₃ N ₂ O	129.1022	-1.5	-0.2
		166.0873	C ₉ H ₁₂ NO ₂	166.0863	-6.0	-1.0
		360.2659	C ₂₁ H ₃₄ N ₃ O ₂	360.2646	-3.6	-1.3
		402.2736	[C ₂₃ H ₃₅ N ₃ O ₃]H ⁺	402.2751	3.7	1.5
430.306 m/z	430.3064	109.1021	C ₈ H ₁₃	109.1012	-8.2	-0.9
		120.0805	C ₈ H ₁₀ N	120.0808	2.5	0.3
		166.0846	C ₉ H ₁₂ NO ₂	166.0863	10.2	1.7
		360.2657	C ₂₁ H ₃₄ N ₃ O ₂	360.2646	-3.1	-1.1
		430.3020	[C ₂₅ H ₃₉ N ₃ O ₃]H ⁺	430.3064	10.2	4.4
460.281 m/z	460.2814	109.0993	C ₈ H ₁₃	109.1012	17.4	1.9
		166.0827	C ₉ H ₁₂ NO ₂	166.0863	21.7	3.6
		360.2515	C ₂₁ H ₃₄ N ₃ O ₂	360.2646	36.4	13.1

Ions unique to each degradation product compared to LURA are indicated in bold. GMF = generated molecular formula. Mass accuracies determined from single injection.

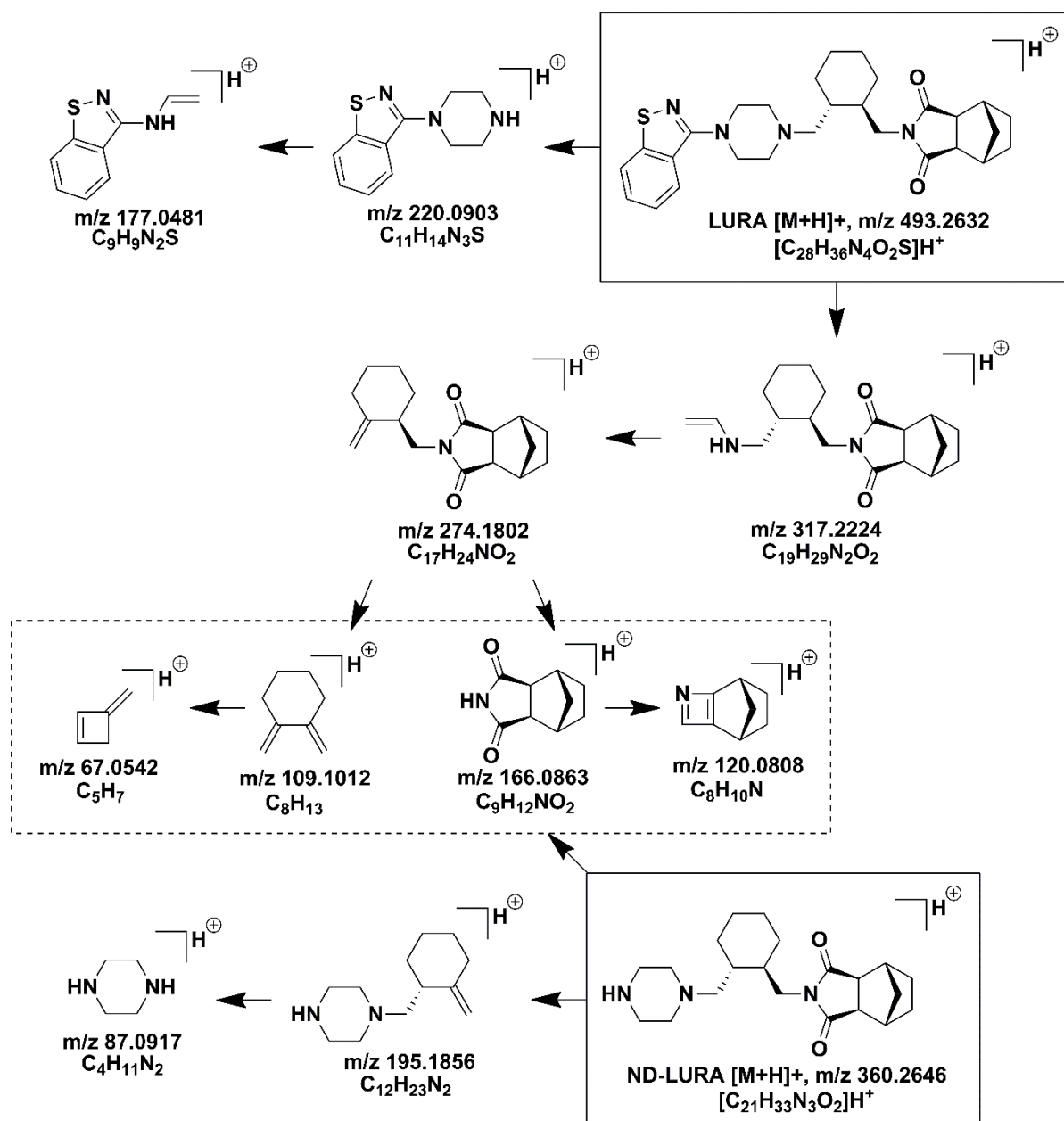


Figure 8-21: Proposed MS/MS fragmentation pathway for LURA and ND-LURA.

LURA MS/MS product ions with m/z of 67.054, 109.101, 120.081, 166.086, and 220.090 previously reported with postulated structures by Kumar Talluri *et al.* [432]. Fragments in common between LURA and the 360.265 m/z degradation product are indicated by the dotted-line box; m/z are calculated accurate mass/charge values.

One mechanism of degradation of LURA that can account for the loss of the 1,2-benzisothiazole moiety to produce the postulated ND-LURA degradation product was reductive cleavage (Figure 8-22 (a)) followed by hydrolysis of the reduced amidine group (Figure 8-22 (b)) to afford ND-LURA as depicted. This mechanism is similar to that postulated for zonisamide and RISP, where it is the isosteric 1,2-benzisoxazole moieties that undergo reductive cleavage to form a hydrolysable imine intermediate [223, 409]. The reductively-cleaved amidine intermediate of LURA was not detected in any sample extracts, non-inoculated controls, calibrators, or QCs analysed by LC-QTOF-MS. An amide intermediate was also not detected which may indicate: poor extraction by the unbuffered LLE method; that if it forms it is rapidly hydrolysed to ND-LURA; or that amidine hydrolysis exclusively proceeds by the alternate resonance structure as shown in Figure 8-22 (b).

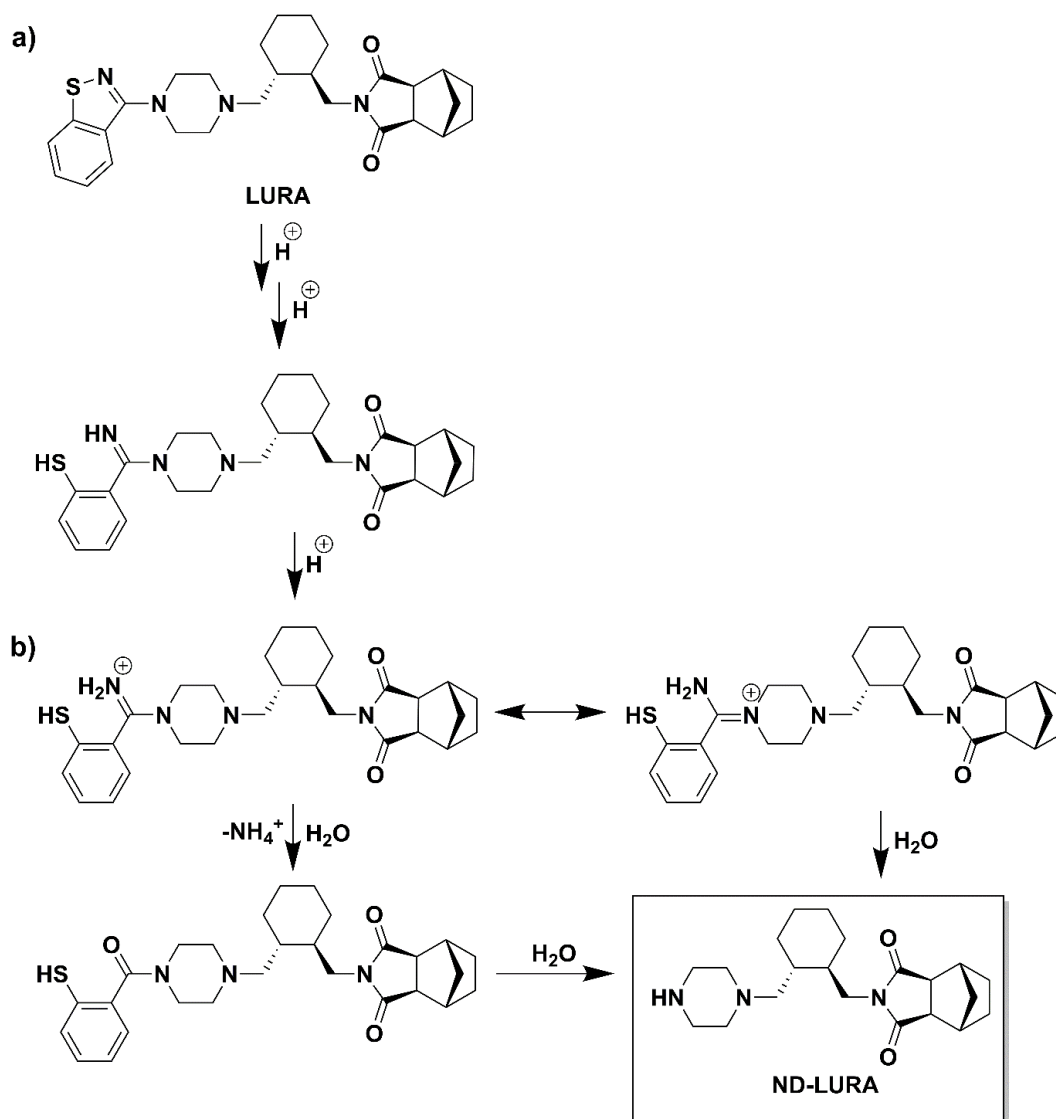


Figure 8-22: Proposed degradation of LURA via a) 1,2-benzisothiazole reduction and subsequent b) amidine hydrolysis of reductively cleaved LURA to yield the degradation product ND-LURA.

It may have also been the case that LURA was simply hydrolysed to ND-LURA without prior reductive cleavage. The antipsychotic drug ZIPR, containing the same 1,2-benzisothiazole moiety that is present in LURA (Figure 8-23 (a)), has been proposed by Prakash *et al.* to undergo degradation in this manner, although the authors also proposed that sulfur oxidation prior to hydrolysis was likely occurring [463]. The detected degradation product of ziprasidone (ZIPR), termed M4A by Prakash *et al.* [463] (Figure 8-23 (b)), is what would be expected if ZIPR were to also undergo reductive cleavage followed by amidine hydrolysis. The detection of M4A in ante-mortem urine and serum specimens also suggests that LURA may hydrolyse given the right pH conditions, as both specimens are usually sterile. However, ND-LURA was not detected in aqueous stability experiments carried out in this thesis at pH = 3, 7, or 11 (see Chapter 5), with pH 3 and 11 beyond the normal pH range of urine (5.5 to 7.0 [239]) (see 5.4).

Hemiaminal intermediates, that form during amide or amidine hydrolysis, were not detected in the analysis of any LC-QTOF-MS samples. Hemiaminal intermediates are known to be unstable as intermediates for N-dealkylation transformations that occur as part of Phase I metabolism [464]. Furthermore, hemiaminal intermediates for the N-dealkylation degradation products detailed in Chapter 7 were also not detected.

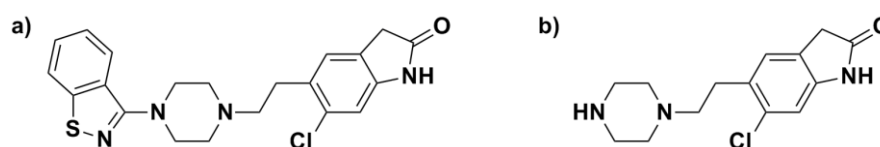


Figure 8-23: Structure of a) ziprasidone and b) ziprasidone metabolite M4A.

Given the mass difference between the 360.265 m/z and 402.275 m/z degradation products may correspond to C₂H₂O (see 8.2.2.1) it follows that the 402.275 m/z degradant may be an acetylated-derivative of the 360.265 m/z degradation product. Cleavage of the substituted piperazine moiety from the trans-1,2-disubstituted cyclohexyl moiety of LURA *via* an elimination reaction was postulated to produce the product ion of 220.0900 m/z (Figure 8-21). Similarly, this cleavage resulted in the product ion of 87.0927 m/z in the 360.265 m/z degradant (Figure 8-21). A similar elimination may also occur in the 402.275 m/z degradation product, leading to the product ion of 129.1024 m/z. Subsequent elimination reactions involving this product ion may then form the product ions at 86.0586 and 112.0735 m/z, which are also unique to the 402.275 m/z degradant. GMF and accurate mass data for these ions are consistent with the presence of an acetylated secondary amine (Table 8-2).

The 388.259, 430.306, and 460.281 m/z degradants have not yet been identified and further research would be required. Given the greater relative response of the 360.265 m/z product compared to these other degradants it was considered of greater forensic relevance.

8.2.2.3 Acetylation

Following treatment of extracts from the week and seven-month experiments with acetic anhydride the 360.265 m/z degradation product was not detected. For the week experiments, auto-MS/MS spectra were acquired for the 402.275 m/z degradant in inoculated, unpreserved blood specimens where MS/MS spectra were not previously acquired in non-acetylated extracts due to increased responses. 360.265 m/z becoming undetectable, and the acquisition of MS/MS spectra of 402.275 m/z in all inoculated, unpreserved blood specimens treated with acetic anhydride, likely indicates that the 402.275 m/z degradation product is a mono-acetyl derivative of the 360.265 m/z degradant. No poly-acetylated products of the 360.265 m/z degradation product were detected. This supported the hypothesis that the 360.265 m/z degradation product is ND-LURA (see 8.2.2.2) and its acetylation product possessed no nucleophilic moieties that may be further acetylated.

The 402.275 m/z degradation product was, in the case of the seven-month experiments, detected in extracts that were not treated with acetic anhydride and those treated with acetic anhydride. As with the acetylated extracts for the week experiments, no product ions consistent with acetylation of the 402.275 m/z degradation product were detected.

After acetylation, auto-MS/MS spectra were still acquired for the other suspected LURA degradation products of m/z 388.259 and 430.306 (in the week experiments only 388.259 m/z was detected). No precursor ion was acquired at 430.2715 m/z or 472.3178 m/z, which would correspond to mono-acetyl derivatives of the 388.259 m/z and 430.306 m/z degradants. This, combined with the finding that these degradants did not react with acetic anhydride, indicates that they do not contain functional groups that may be acetylated.

8.2.2.4 Standard comparison

The major 360.265 m/z degradation product produced similar MS/MS spectra to the synthesised *trans*-ND-LURA (and *cis*-ND-LURA, data not shown) (Figure 8-24 and Table 8-3).

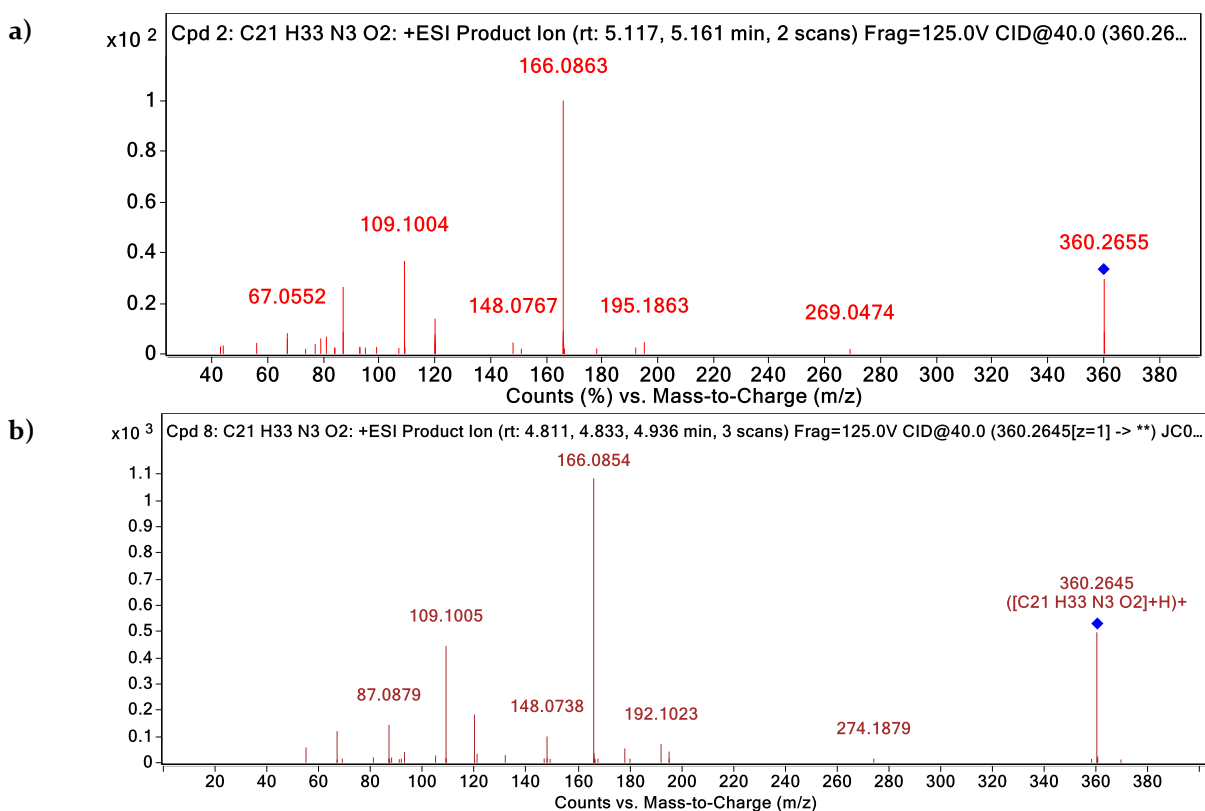


Figure 8-24: MS/MS spectra for a) the 360.265 m/z degradation product and b) *trans*-ND-LURA. Collision energy = 40 eV.

Table 8-3: MS/MS data for synthesised ND-LURA and major 360.265 m/z degradation product detected in blood experiments.

Analyte	Precursor ion (m/z)	Product ions (m/z)	GMF product ions	Calculated accurate mass (m/z)	Mass accuracy (δ) (ppm)	Mass accuracy (δ) (mDa)
<i>cis</i> -ND-LURA	360.2649	67.0550	C ₅ H ₇	67.0542	-11.9	-0.8
		87.0913	C ₄ H ₁₁ N ₂	87.0917	4.6	0.4
		109.1003	C ₈ H ₁₃	109.1012	8.2	0.9
		120.0801	C ₈ H ₁₀ N	120.0808	5.8	0.7
		166.0865	C ₉ H ₁₂ NO ₂	166.0863	-1.2	-0.2
		360.2645	[C ₂₁ H ₃₃ N ₃ O ₂] ⁺ H ⁺	360.2646	0.3	0.1
<i>trans</i> -ND-LURA	360.2647	67.0549	C ₅ H ₇	67.0542	-10.4	-0.7
		87.0920	C ₄ H ₁₁ N ₂	87.0917	-3.4	-0.3
		109.1012	C ₈ H ₁₃	109.1012	0.0	0.0
		120.0806	C ₈ H ₁₀ N	120.0808	1.7	0.2
		166.0861	C ₉ H ₁₂ NO ₂	166.0863	1.2	0.2
		360.2653	[C ₂₁ H ₃₃ N ₃ O ₂] ⁺ H ⁺	360.2646	-1.9	-0.7
360.265 m/z	360.2643	67.0552	C ₅ H ₇	67.0542	-14.9	-1.0
		87.0927	C ₄ H ₁₁ N ₂	87.0917	-11.5	-1.0
		109.1004	C ₈ H ₁₃	109.1012	7.3	0.8
		120.0842	C ₈ H ₁₀ N	120.0808	-28.3	-3.4
		166.0863	C ₉ H ₁₂ NO ₂	166.0863	0.0	0.0
		360.2655	[C ₂₁ H ₃₃ N ₃ O ₂] ⁺ H ⁺	360.2646	-2.5	-0.9

GMF = generated molecular formulae. Mass accuracies determined from single injection.

However, neither isomer of ND-LURA eluted with the same retention time as the 360.265 m/z degradation product (Figure 8-25 and Table 8-4), indicating that the identity of the major 360.265 m/z degradation product of LURA could not be ND-LURA. Despite this, all compounds afforded precursor ions with excellent mass accuracies for the GMF of ND-LURA, C₂₁H₃₃N₃O₂ (Table 8-4). These results indicate that the 360.265 m/z degradant likely possesses a similar structure to ND-LURA for the same major product ions to be detected (Table 8-3). It may be that the 360.265 m/z degradant is a structural isomer of C₂₁H₃₃N₃O₂ or is a compound of higher molecular weight that fragments in the MS source to yield an ion at 360.265 m/z, possibly with the structure assigned to the ND-LURA [M+H]⁺ precursor ion, and further product ions therefrom.

Table 8-4: LC-QTOF-MS data for synthesised ND-LURA and major 360.265 m/z degradation product detected in blood experiments.

Analyte	Retention time (min)	Measured [M+H] ⁺ (m/z)	Mass accuracy (δ) (ppm)*	Mass accuracy (δ) (mDa)
<i>cis</i> -ND-LURA	4.66	360.2649	-0.8	-0.3
<i>trans</i> -ND-LURA	4.83	360.2647	-0.3	-0.1
360.265 m/z	5.17	360.2643	0.8	0.3

*For all compounds a calculated [M+H]⁺ of 360.2646 m/z was obtained for the generated molecular formula of C₂₁H₃₃N₃O₂. Mass accuracies determined from single injection.

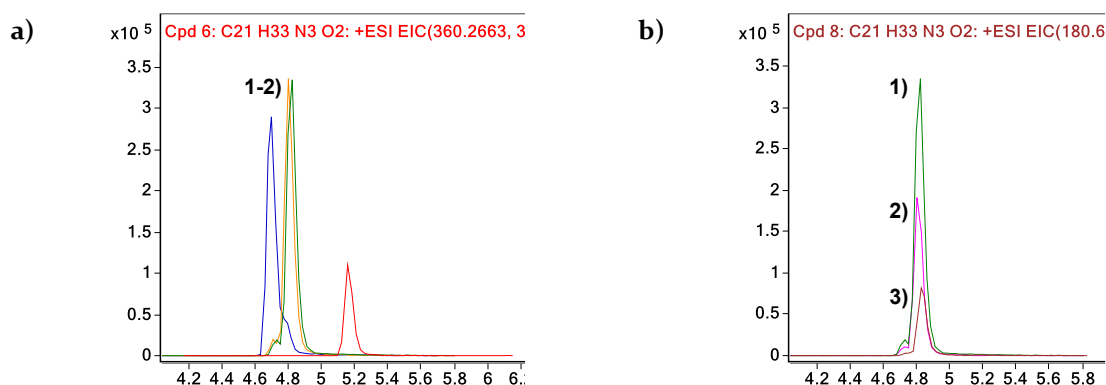


Figure 8-25: Extracted ion chromatograms of synthesised ND-LURA and 360.265 m/z degradation product.

a) *cis*-ND-LURA (4.66 min), *trans*-ND-LURA (4.83 min) (synthesised from 1) mono-Boc piperazine and 2) from unprotected piperazine), and the 360.265 m/z degradation product (5.17 min) detected in the blood experiments; and b) *trans*-ND-LURA in 1) ethanol, 2) following reconstitution in n-BuCl and N₂ dry down and subsequent ethanol reconstitution, and 3) following reconstitution in blood and subsequent extraction as with experimental blood specimens. Y-axis is counts. X-axis is acquisition time (min).

X-ray crystallography confirmed the identity of the synthesised *trans*-ND-LURA product, indicating that the degradation product observed in the blood experiments is not ND-LURA.

If the degradant is instead a structural isomer of $C_{21}H_{33}N_3O_2$ there are a few possibilities that may yield the MS/MS fragmentation observed for the 360.265 m/z degradation product. If reductive cleavage of LURA to produce the amidine intermediate shown in Figure 8-22 (b) is occurring, elimination of a proton to form an alkene followed by subsequent charge annihilation on the quaternary nitrogen is possible. Subsequent hydrolysis of the amidine would then yield the degradant shown in Figure 8-26 (a). Alternatively, the 360.265 m/z degradant may be a stereoisomer of ND-LURA in which the succinimide ring is *trans* to the methylene bridge of the [2.2.1]-bicycloheptyl moiety (Figure 8-26 (b)) (or a similar isomer of the compound shown in Figure 8-26 (a)). This conversion would require the unlikely inversion of the methylene carbons, which must proceed *via* strained intermediates, and would appear to have occurred completely as only one compound yielding an ion of m/z 360.265 was detected.

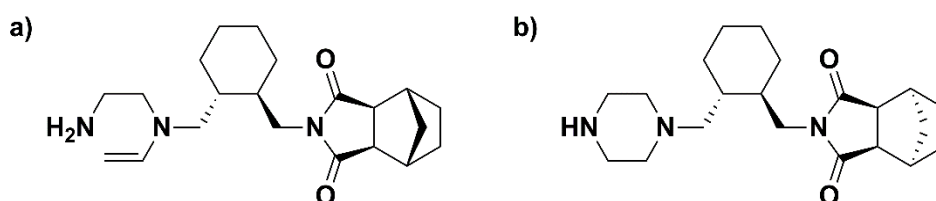


Figure 8-26: Structural isomers of $C_{21}H_{33}N_3O_2$.

8.3 Qualitative blood experiment

LC-QTOF-MS analysis of the experimental extracts of the blood experiments performed in Chapter 6 enabled the discovery of numerous suspected LURA degradation products (see 7.2). However, from these analyses alone their identity was unclear. Furthermore, the extraction method used on the blood specimens did not adjust specimen pH and thus did not target compounds with acidic (e.g. carboxylic acid) or alkaline (e.g. primary amine) functionalities. Such functionalities due to their pKas may require pH adjustments during extraction into organic solvents to enable their recovery above limits of detection.

A qualitative experiment using blood specimens was therefore carried out, with acidic, unbuffered, alkaline, and PPT extraction methods utilised for a more comprehensive screening of potential degradation products. The experimental design was as indicated in Table 6-1.

ZIPR, which was also found to degrade in the blood experiments (see Chapter 6), and buspirone (BUSP) were the other drugs spiked into blood for this experiment. BUSP was included due to numerous structural similarities with LURA (a disubstituted piperazine terminating in an amidine, and a succinimide) (Figure 8-27). AMIT and RISP were not spiked in these experiments.

The degradation of LURA in inoculated, unpreserved specimens was considered evidence of successful microorganism inoculation and respiration.

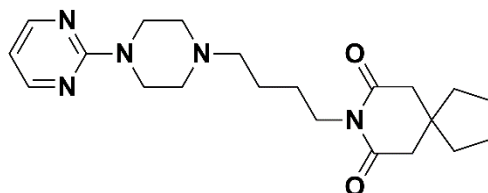


Figure 8-27: Chemical structure of buspirone.

8.3.1 Experimental

Ante-mortem blood (1 mL) was aliquoted into 5 mL sterile polystyrene Sarstedt tubes using a sterile plastic syringe. Drugs were spiked by removing organic solvent from ~45 µg/mL stocks under N₂ at 40 °C followed by reconstitution in ethanol (1.5 mL). Reconstituted drugs were then aliquoted (100 µL) using Luer-Slip plastic syringes with 0.2 µm filters into the sterile tubes. For preserved specimens, sodium fluoride (20 mg) was first weighed into tubes before the addition of blood.

Microorganisms were inoculated into specimens #2-3 and #6-7 (Table 6-1). This was achieved by diluting FMT specimens with water (3 mL) filter-sterilised using Luer-Slip plastic syringes with 0.2 µm filters. Diluted FMT specimens were vortexed to mix and aliquoted (50 µL) into relevant specimen tubes.

Prepared blood specimens were then vortexed, rolled, vortexed, and initial extracts collected (4.2.2). Wide-bore sterilised pipette tips with filters were used to collect sub-samples. Immediately following sub-sampling, specimens were incubated at 37 °C. Initial extracts were analysed by LC-DAD to confirm successful drug spiking.

After ~5 days, sub-samples from the specimen tubes were collected by placing the specimens on a mechanical roller (30 minutes at 25 rpm) followed by vortexing each specimen prior to collecting aliquots (100 µL) for analysis. Blood was aliquoted into borosilicate screw-cap extraction tubes. For the unbuffered LLE method, the extraction was performed as described in 4.2.2. Alkaline LLE was performed as described in 4.3.2.1 except for reconstitution. The acidic LLE proceeded by adding the aliquoted blood to water (400 µL), adding 1M potassium dihydrogen phosphate buffer (pH = 4) (200 µL), vortexing (5 sec), then adding ethyl acetate (5 mL). The tubes were capped then placed on a mechanical roller (15 minutes at 20 rpm). PPT

proceeded by adding acetonitrile (1 mL) dropwise to the aliquoted blood while vortexing. Sub-samples extracted by PPT were inverted following acetonitrile addition and capping.

For all extraction methods, the tubes were centrifuged (10 minutes at 1409 x *g*) and after centrifugation the organic layer transferred to a disposable borosilicate test tube for evaporation under N₂ at 40 °C. Extracts were reconstituted in ethanol (50 µL).

Final and initial extracts were analysed by LC-DAD method B (4.2.3) and the LC-QTOF-MS method previously described (3.3.2).

8.3.2 Results

By LC-DAD analysis, LURA degraded until below the LOD of the method in inoculated, unpreserved specimens after five days. ZIPR degraded until below the LOD of the method in all blood specimens after five days. These results were comparable to most replicates in the week experiment B1 and B2 blood experiments (Chapter 6). BUSP remained detected (and was not quantified).

No suspected LURA degradation products were detected in extracts from acidic LLE, alkaline LLE, and PPT extraction methods that were not previously detected in the unbuffered LLE extracts by LC-QTOF-MS analysis. Alkaline LURA degradation products previously reported in the literature by Kumar Talluri *et al.* were not detected (Figure 8-18) [432]. No degradation products deriving from BUSP were discovered, indicating the succinimide moiety in LURA was not expected to be a site of degradation in human whole blood, microbial or otherwise.

8.4 Hydrolysis of lurasidone in ante-mortem blood

Alkaline LLE was performed on non-inoculated blood specimens containing LURA after five weeks at room temperature (using the method described in 4.3.2.1, except for reconstitution in ethanol (50 µL)). Subsequent analysis by LC-QTOF-MS (using the method detailed in 3.3.2) revealed the presence of the 360.265 *m/z* degradant, through comparison with precursor and product MS/MS ions previously reported (see Figure 8-19). The ratio of the response of the 360.265 *m/z* degradation product to LURA was considerably lower than the ratios observed for extracts of inoculated, unpreserved blood specimens after 2-4 days at 37 °C, where ratios ranged from 0.012 to 6.84 (Table 8-5).

Table 8-5: Response ratio of 360.265 m/z compound to LURA in non-inoculated controls after five weeks at room temperature following alkaline LLE.

Condition	Replicate	LURA area	360.265 m/z area	Response ratio (360.265 m/z/LURA)	MS/MS of 360.265 m/z acquired
Unpreserved	1	2503182	34342	0.014	Y
	2	2921041	58618	0.020	Y
	3	3746700	65684	0.018	Y
Preserved	1	5047219	74599	0.015	Y
	2	6386651	67533	0.011	Y
	3	3547795	0	0	N

It was hypothesised that the source of 360.265 m/z in the non-inoculated controls could be due to alkaline hydrolysis of LURA during the alkaline LLE.

8.4.1 Experimental

To determine if the degradants may be forming during an alkaline LLE method immediate extractions, two-hour delayed extractions, and 24-hr delayed extractions from whole blood were carried out in hexuplicate. The method described in 4.3.2.1 was used, except for reconstitution of samples with ethanol (425 µL) following evaporation of the extraction solvent. Analysis proceeded by LC-QTOF-MS as previously specified (7.2.1). Neutral extracts of the non-inoculated blood specimens and inoculated blood specimens were also analysed by LC-QTOF-MS following extract dilution. The degradants were considered present if precursor and product ions were in agreement with those previously reported (see Table 8-1 and Table 8-2).

8.4.2 Results

None of the degradants were detected following the alkaline LLEs. Alkaline degradation products previously reported in the literature by Kumar Talluri *et al.* were also not detected [432]. Therefore, if detected, the presence of these degradants in alkaline LLE extracts could not be considered an analytical artefact due to alkaline hydrolysis.

As with the alkaline LLE blood extracts, the 360.265 m/z degradant was detected in unbuffered LLE extracts of both the non-inoculated blood specimens and inoculated blood specimens. However, the ratio of the 360.265 m/z degradation product to LURA was between 57 to 661 times less in extracts of the non-inoculated blood specimens compared to the inoculated blood specimens, with variation attributable due to replicate variations as discussed in Chapter 6 (Table 8-6 and Table 8-7).

Table 8-6: Ratio response of 360.265 m/z degradation product to LURA in non-inoculated blood specimens after five weeks at room temperature following unbuffered LLE.

Condition	Replicate	LURA area	360.265 m/z area	Ratio (360.265 m/z/LURA)	MS/MS of 360.265 m/z acquired
Unpreserved	1	2020636	18393	0.009	Y
	2	1830532	13259	0.007	N
	3	1681813	6787	0.004	Y
Preserved	1	3964109	28234	0.007	Y
	2	1651852	10290	0.006	Y
	3	2517380	14929	0.006	Y

Table 8-7: Ratio response of 360.265 m/z degradation product to LURA in inoculated blood specimens after five weeks at room temperature following unbuffered LLE.

Condition	Replicate	LURA area	360.265 m/z area	Ratio (360.265 m/z/LURA)	MS/MS of 360.265 m/z acquired
Unpreserved	1	170225	39292	0.231	Y
	2	200460	141590	0.706	Y
	3	33889	89649	2.645	Y
Preserved	1	2611348	16521	0.006	Y
	2	3079165	21976	0.007	Y
	3	1530111	8415	0.005	Y

Note the variation in ratio responses in unpreserved specimens.

For one replicate an MS peak having an accurate mass and retention time consistent with the 360.265 m/z compound was detected, however, no MS/MS spectra were obtained and thus the presence of this degradant could not be confirmed. This does not indicate that the degradant is absent in those samples, however, just that it is not present in an amount that triggers the acquisition of MS/MS data (5000 counts or greater).

8.5 Post-mortem casework analysis

The use of post-mortem specimens for research purposes is not legal in South Australia unless the deceased has not objected to research during life and consent is obtained from all people deemed senior available next of kin [237]. For this reason, instrument data obtained from post-mortem casework samples was instead analysed. Approval to re-analyse data files of cases where LURA was reported as present by staff at FSSA was obtained as previously indicated (1.7.3) to determine if the degradation products of LURA discovered in this thesis were present.

8.5.1 Data analysis

FSSA staff de-identified data files from LC-QTOF-MS analyses and supplied relevant autopsy and toxicology details for cases from 2016-2018 where LURA was reported. The non-refrigerated

interval (NRI) between the date of death and body refrigeration at the mortuary was determined for case comparison purposes due to the enhanced stability of LURA in inoculated, unpreserved blood specimens stored at 4°C (see 6.3.5).

At the time of initial analysis, drug screening was performed for the casework samples by extracting analytes from blood using an alkaline LLE followed by analysis using an Agilent 6545 LC-QTOF-MS in auto-MS/MS mode, which uses default collision energy of 20 eV [208]. To confirm that the possible LURA degradants would not be present due to degradation of LURA during the alkaline extraction procedure stability experiments (as per section 8.4.1) were performed. The results of this experiment indicated that the presence of the degradation products in re-analysed casework samples should not be due to an alkaline LLE method.

To assess the extent of drug degradation in each case the ratio of the MS peak area of each detected degradation product to LURA was calculated. Due to the absence of commercially available standards, degradation products were considered present in casework samples if precursor and product MS/MS ions were in agreement with those previously reported (see Table 8-1 and Table 8-2).

8.5.2 Results and discussion

Eleven cases were identified from 2016-2018 in which LURA was reported. Of these, three were considered by the pathologist to be decomposing, five had putrefactive amines detected by the toxicology analysis, and six did not have putrefactive amines detected by the toxicology analysis. In all eleven cases re-analysed, LURA remained detectable and gave a greater response than its degradation product (see Table 8-8 and Figure 8-28).

In nine out of eleven cases the 360.265 m/z degradation product was identified by comparison to retention time and MS/MS spectral data of the 360.265 m/z degradant in the blood experiments. Possible degradation of LURA during the alkaline extraction method used by FSSA was excluded based on previous findings (see section 8.4). Thus, the presence of the 360.265 m/z degradation product in casework specimens cannot be attributed to a known analytical artefact. Both cases where 360.265 m/z was not detected (Case C) or where its identity could not be confirmed due to no auto-MS/MS spectra acquisition (Case A) showed no signs of putrefaction. The individual in case A died in hospital and it is likely that the deceased was refrigerated immediately and thus an NRI of 0 was assigned. Other suspected LURA degradants were not detected other than the 430.306 m/z degradant, whose detection in Case J is based on retention time and precursor ion m/z alone, as no auto-MS/MS spectra were acquired.

Table 8-8: Case details for post-mortem cases with LURA detected.

Case	NRI* (days)	Putrefaction?	LURA area	360.265 m/z area	Ratio (360.265 m/z/LURA)	MS/MS of 360.265 m/z acquired
A	0 ⁺	No evidence	227515	10388	0.05	N
B	0	No evidence	179135	7946	0.04	Y
C	~1	No evidence	135437	0	N/A	N
D	1	Trace PEA	781953	142640	0.18	Y
E	1	Yes – PEA detected	390607	93669	0.24	Y
F	1	PEA	1043447	141553	0.14	Y
G	2	No evidence	336387	65974	0.2	Y
H	~2	Yes – PEA detected	296681	93669	0.32	Y
I	2	No evidence	435671	65974	0.15	Y
J	3	No evidence	736904	100400	0.14	Y
K	6	Yes – PEA detected	488775	88100	0.18	Y

*Non-refrigerated interval (time between death and body refrigeration at mortuary); ~exact date of death unknown, estimated NRI; ⁺died in hospital, body likely refrigerated promptly. PEA = phenylethylamine. The minimum area for detection was 5000 counts.

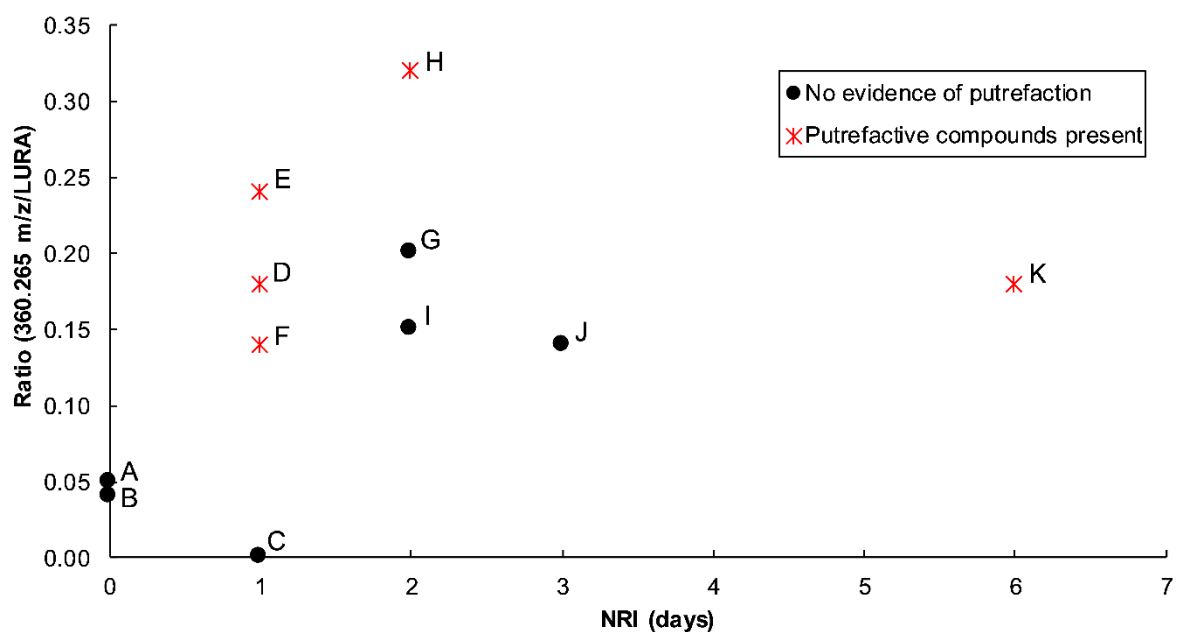


Figure 8-28: Non-refrigerated interval (NRI) and ratio of 360.265 m/z degradation product to LURA data for post-mortem cases.

Letters beside data points indicate Case. No auto-MS/MS spectra were acquired for 360.265 m/z for case A. NRI = non-refrigerated interval (time between death and body refrigeration at mortuary).

Overall, the reported 360.265 m/z to LURA ratio for non-decomposed cases ranged from 0-0.2 over an NRI of 0-3 days (n = 6) and for decomposed cases ranged from 0.14-0.32 over an NRI of 1-6 days (n = 5); most cases had an NRI of 1 or 2 days. Ratios for an NRI of 1 day ranged from 0-0.24 (n = 4) and for an NRI of 2 days ranged from 0.2-0.32 (n = 3). The cases with the greatest ratio of 360.265 m/z to LURA for reported NRIs of 1 and 2 days were those containing putrefactive amines (Cases D, E, F and H, see Figure 8-28). For cases E, H, and K, the pathologist also noted decomposition at autopsy. In comparison, case C, with a similar NRI to D, E, and F, was not reported to have any evidence of putrefaction and the 360.265 m/z degradant was not detected. For cases G and I, with a similar NRI to H, there was no reported evidence of putrefaction and the ratios of 360.265 m/z to LURA were less than 65 % that of case H.

Case D and G, and F and I, were found to have similar ratios for 360.265 m/z to LURA, despite an NRI difference of one day and the absence of putrefactive amines in the cases with greater NRIs (Figure 8-28). This suggests that the 360.265 m/z degradant may also be forming during autolysis or that the microorganisms responsible for LURA degradation to 360.265 m/z are not necessarily the same as those that lead to putrefactive amine formation.

Only one case each with an NRI of 3 and 7 days were analysed during the time period of the re-analysed casework data. The 3-day NRI case (Case J) was reported to show no evidence of putrefaction, whereas putrefactive compounds were present in the 7-day NRI case (Case K). Both cases had similar 360.265 m/z/LURA ratios as those cases with NRIs of 1-2 days. Based on the greater ratio found for Case H over Cases D-F it may be expected that K should have an even greater ratio still. However, it is not known what condition the bodies were in and the environment they were subject to after death and prior to mortuary admission.

It is not possible to reach any conclusion regarding whether the state of putrefaction and LURA degradation to 360.265 m/z may correlate due to the absence of contextual information concerning individual health and the environment and climate in which the bodies were discovered (see 1.2), and the small sample size at each NRI (n = 1-4). Furthermore, cases were only re-analysed in which LURA was reported as detected. Therefore, it is still unknown if 360.265 m/z may serve as a marker for LURA ingestion in the absence of LURA. The inclusion of 360.265 m/z as part of the screening library at FSSA may elucidate this in future. The future analysis of casework for this LURA degradant may also reveal a clearer trend between the extent of putrefaction and its formation.

8.6 Conclusions

Five hitherto unreported degradation products of LURA were discovered to form in inoculated, unpreserved specimens of the blood experiments performed in Chapter 6. No *in vitro* or *in vivo* pharmacokinetic studies have reported these degradation products to be metabolites [465] and forced degradation studies by Kumar Talluri *et al.* found that neither acidic hydrolysis, alkaline hydrolysis, neutral hydrolysis, oxidation, photolysis, or treatment at 80 °C resulted in the degradation of LURA to these degradants [432]. An experiment performed to assess the stability of LURA during alkaline extraction from whole blood also found that the detection of these degradation products in blood specimens was not an artefact of the analytical method and they were not detected in the hydrolysis experiments performed in this thesis (Chapter 5). These degradation products were also present in lesser quantities in non-inoculated blood, indicating that they may form in blood independent of microbial activity, but that microbial activity greatly enhances their formation.

The possible LURA degradation products were not detected by prior LC-DAD analysis, and thus their identities were hypothesised exclusively from liquid chromatography and tandem mass spectrometric analyses. Accurate mass data, mass fragmentation data, and acetylation derivatisation reactions supported the presumptive identification of the major degradation product of LURA, with a m/z of 360.265, to be an N-debenzothiazole derivative, ND-LURA. No acetyl derivatives were detected for the other suspected LURA degradants, 388.259 m/z , 430.306 m/z , and 460.281 m/z , indicating that they do not contain functionalities that may undergo acetylation. Despite the evidence in favour of the identity of the major 360.265 m/z degradant as ND-LURA, synthesised standards yielded dissimilar retention times; mass spectral data and GMF for precursor and product ions between the 360.265 m/z degradation product and the synthesised ND-LURA standards were similar, indicating the 360.265 m/z degradant may be a structural isomer of ND-LURA possessing a disubstituted cyclohexyl ring, a piperazine moiety, and the [2.2.1]-bicycloheptyl-fused succinimide moiety. The exact identity of these possible LURA degradants remains unknown.

The detection of the major LURA degradation product discovered in the blood experiments performed in Chapter 6 in authentic post-mortem cases confirms that the experiments suitably simulated the post-mortem environment. The major 360.265 m/z degradation product was detected in nine out of eleven post-mortem cases whose data was retrospectively analysed. In cases showing signs of putrefaction a greater response of the 360.265 m/z degradation product to LURA was revealed compared to those showing no evidence of putrefaction given the same

NRI. However, the 360.265 m/z degradant was also detected in four cases found to have no evidence of putrefaction, indicating that analytical and macroscopic signs of putrefaction alone may not indicate the partial degradation of LURA to the 360.265 m/z degradant. This retrospective data analysis of casework samples was limited chiefly by a small sample size and the uncertainties associated with casework specimens.

Several case studies have reported the complete degradation of RISP to HB-RISP following extended NRIs greater than four days [2, 3]. Partial conversion of RISP to HB-RISP has also been observed with NRIs ranging from 0-4 days [223]. Therefore, the apparent similar degradation rate of LURA to RISP as observed in the blood experiments (see Chapter 6) warrants the routine analysis of casework for the presence of the 360.265 m/z degradant. In the event that LURA is not detected in future cases this will identify cases where LURA quantification may produce falsely low concentrations.

As a result of this work, the newly discovered degradation product of LURA, 360.265 m/z, has been added to the FSSA LC-QTOF-MS drug screen to enable its detection in the future drug screening of post-mortem specimens. This will allow FSSA to highlight cases where quantification of this drug may be unreliable and enable prior drug administration to be determined even in cases where the parent drug has been completely degraded.

CHAPTER 9 - ZIPRASIDONE DEGRADATION PRODUCTS

9.1 Outline

In the experiments described in Chapter 6 ZIPR was found to be unstable in all blood specimens. This chapter details the investigation of numerous transient degradation products of ZIPR. Characterisation of degradation products was achieved using LC-QTOF-MS with MS/MS, which led to a hypothesis regarding their identity that was tested with deuterated ethanol and solvent stability experiments. The presence of ZIPR degradants in all blood extracts, regardless of preservative or microbial enrichment, also led to a retrospective analysis of casework data to establish if any of the identified products may be detected in authentic post-mortem blood specimens.

Chemicals, materials, and instrumentation were used as listed in Chapter 3.

9.2 LC-DAD and LC-QTOF-MS analyses of blood experiment extracts

9.2.1 Background

During the blood experiments described in Chapter 6, additional peaks were detected with retention times slightly earlier and later than that for AMIT. The UV-Vis absorbance spectra for these peaks appear similar (Figure 8-2) but with a slight shift in the λ_{\max} . This suggests that they may share a similar chromophore and that they could be produced via the same degradation pathway.

Butzbach previously reported the presence of these peaks when testing the stability of ZIPR and other antipsychotic drugs during an alkaline LLE, where it was hypothesised that their presence resulted from ZIPR degradation [223]. However, these peaks were never observed in the aqueous stability experiments detailed in Chapter 5, which indicates that they were formed by mechanisms other than chemical hydrolysis.

It was also suspected that the degradants were not produced by microbial degradation, as these peaks were detected in all extracts of experimental blood specimens containing ZIPR, regardless of preservative or inoculation status (Chapter 6). Furthermore, these peaks were often only detected in one of three inoculated, unpreserved blood extracts at any time point in the first week-long blood experiment of the set B drugs and not detected in any replicates after ~7 days, possibly due to their presence < LOD. This indicated possible formation and subsequent

degradation of these compounds in inoculated, unpreserved specimens. In comparison, detection was consistent and with an increasing relative response to LORA (IS) over time in all other blood extracts of this experiment (Figure 9-2), indicating an increase in concentration as the experiment progressed.

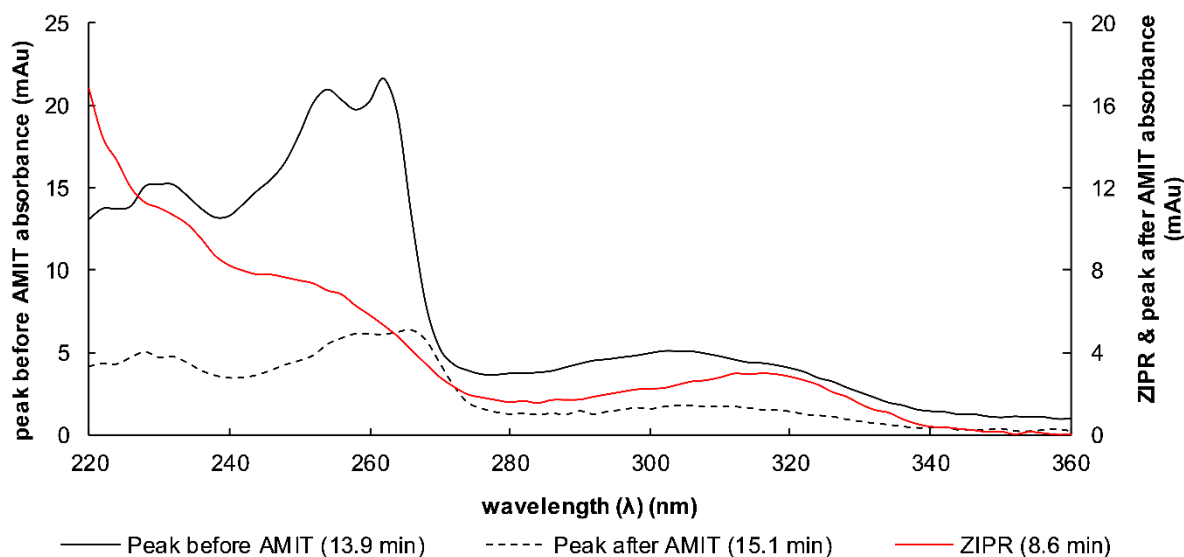


Figure 9-1: UV-Vis absorbance spectra of ZIPR and suspected ZIPR degradants in blood experiments.

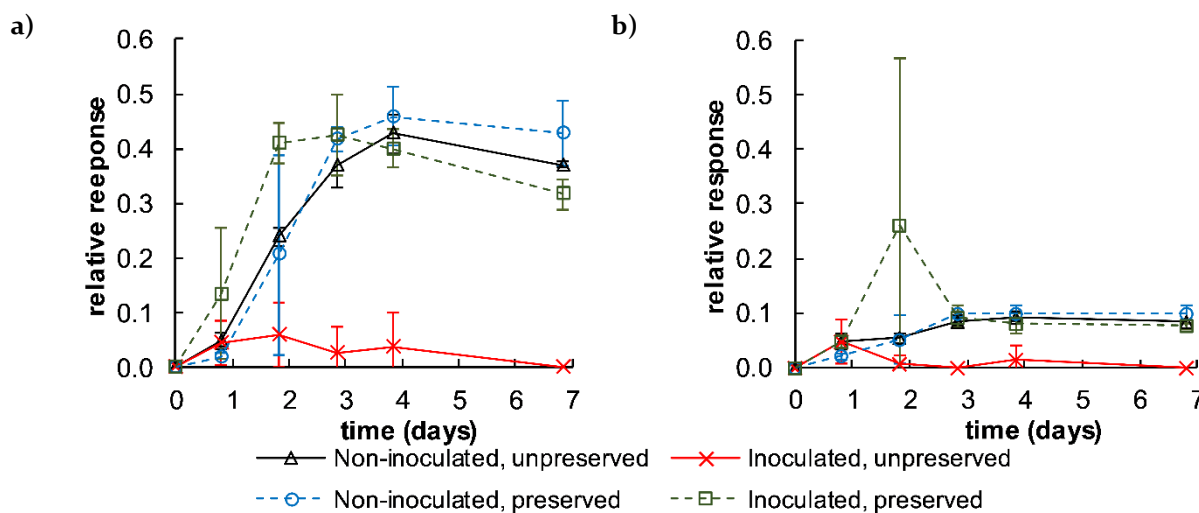


Figure 9-2: Relative response of unknown peaks eluting near AMIT in first week-long blood experiment (WBI) using B drugs: a) before AMIT, and b) after AMIT.

Responses are relative to LORA. Error bars are \pm S.D., $n = 3$.

As the LC-DAD method used reverse-phase chromatography, the retention times indicate that the suspected ZIPR degradants are more non-polar than ZIPR as they elute after ZIPR (see Figure 4-3). This observation also suggested the degradants may not result from the microbial degradation of ZIPR as metabolites are usually more polar than their parent drugs – during

metabolism polar functionalities are typically added to xenobiotics to aid in their elimination from the body.

Considering these factors, it was hypothesised that an unknown component in blood may be necessary for their formation.

9.2.2 Experimental

LC-QTOF-MS screening of experimental extracts (previously described in 7.2.1) was performed to identify potential ZIPR degradation products. Extracts from the qualitative blood experiment described in 8.3 were also screened by LC-QTOF-MS. The fractions of the LC-DAD eluent of extracted experimental blood specimens corresponding to the observed peaks either side of AMIT (Figure 9-2) were also manually collected. This was performed as previously described in section 5.5.2.

Diluted drug stocks, experimental extracts, and manually collected LC-DAD fractions were analysed using an Agilent 1200 Series HPLC with Agilent 6520 Series LC-QTOF-MS in auto-MS/MS mode, configured as described in section 3.3.2.

9.2.2.1 MS data analysis

The known mass of ZIPR was used to obtain EICs (Table 5-7). MDF, set to a tolerance of ± 100 mDa, was initially used to screen for potential degradation products. Upon discovering potential degradation products, MDF of the degradation product mass was then performed to screen for subsequent degradants. This process was repeated when further degradation products were discovered. Mass spectra presented are those following MFE. MDF and MFE are previously described in 7.2.1 and 5.5.1.

ZIPR possesses the 1,2-benzisothiazole moiety that is also present in LURA, which was thought to degrade and yield ND-LURA (see Chapter 8). Therefore, as ZIPR could theoretically degrade in a similar manner, the theoretical mass for the analogous ZIPR degradant (M4A (GMF for precursor ion of $[C_{14}H_{18}ClN_3O]H^+$, calculated 280.1211 m/z) (Figure 8-23 (b)) was targeted during mining of the LC-QTOF-MS data. Previously reported degradation products for ZIPR were screened for based on their calculated $[M+H]^+$ precursor ions [466, 467].

The response of the precursor ion for ZIPR (413.1190 m/z) and possible ZIPR degradation products (precursor ions: 439.1352, 439.1369, 441.1518, and 455.1317 m/z) and the ratio of each degradation product to ZIPR were determined over time in all blood experiment extracts and representative calibrators and QCs. For week experiments, response is reported as relative to

AMIT, to account for inter-aliquot variation. However, for the longer experiment (YB), response is reported relative to LORA, due to apparent degradation of AMIT over time to NORT in inoculated, unpreserved specimens as discussed in Chapter 7.

9.2.2.2 MS/MS data analysis

MS/MS spectra were collected for ZIPR (precursor ion: 413.1190 m/z) and the possible degradation products (precursor ions: 439.1352, 439.1369, 441.1518, and 455.1317 m/z) at collision energies of 20, 30, and 40 eV.

GMF and calculated accurate masses were determined for the product ions of ZIPR and all possible degradation products. From these data, potential chemical structures for the degradants were hypothesised. Comparison to the published MS/MS spectrum of ZIPR assisted in product ion identification [467].

9.2.3 Results

9.2.3.1 MS data analysis

MDF initially resulted in the detection of three compounds as potential ZIPR degradants (precursor ions: 439.1352, 439.1369, and 455.1317 m/z) in Day 7 extracts of the week experiments of all blood specimens except the inoculated, unpreserved blood specimens. The precursor ions 439.135 m/z and 439.137 m/z are referred to collectively as 439.135 m/z henceforth. The response for 455.132 m/z was detected as three resolved peaks in some instances, with the most intense peak at 7.55 min. Auto-MS/MS spectra were not acquired for the surrounding minor peaks. In comparison to ZIPR, the degradants were retained longer by the stationary phase (Figure 9-9). Interestingly, the two 439.135 m/z ions were also detected in calibrator and QC extracts, making them appear to be ZIPR impurities rather than degradants. However, they were not detected in diluted methanol drug stocks of ZIPR that were analysed by LC-QTOF-MS as would be expected were they impurities of ZIPR. Furthermore, a literature search of known ZIPR impurities did not yield any compounds that would be consistent with the degradants detected. It seemed probable that the compounds were forming rapidly in blood during the extraction and may be forming in blood over time in the specimens incubated at 37 °C. If this hypothesis were true, greater responses would be expected in Day 7 extracts of the week experiments compared to the calibrators and QCs. The sum of the response of 439.135 m/z was therefore analysed over time in all extracts, including extracts of the inoculated, unpreserved blood specimens where auto-MS/MS spectra was not acquired in final week extracts.

The ratio of the response between 439.135 m/z to AMIT, were greater in all experimental blood extracts compared to the high calibrators and QCs (Table 9-1), indicating that 439.135 m/z was present at greater concentrations in the experimental blood specimens than in the calibrators and QCs. This confirmed that the 439.135 m/z compounds were not ZIPR impurities.

Table 9-1: 439.135 m/z relative response and 439.135 m/z/ZIPR ratios observed in experimental blood extracts during the first week experiment compared to the mean observed in calibrators and QCs.

Sample	439.135 m/z relative response to AMIT	439.135 m/z/ZIPR ratio
Calibrator	Mean = 0.007	Mean = 0.016
QC	Mean = 0.005	Mean = 0.009
Experimental extracts	0.069-0.244	2.20-11.35

From the analysis of the 439.135 m/z compounds over time in inoculated, unpreserved blood extracts it was found that their response first increased before subsequently decreasing until auto-MS/MS spectra were no longer acquired. This contrasted with their behaviour in all other experimental blood extracts, where no decline in response was observed following an initial increase (Figure 9-3 and Figure 9-4). For these other conditions, the response of the 439.135 m/z degradants exceeds the maximum responses observed in the inoculated, unpreserved specimens.

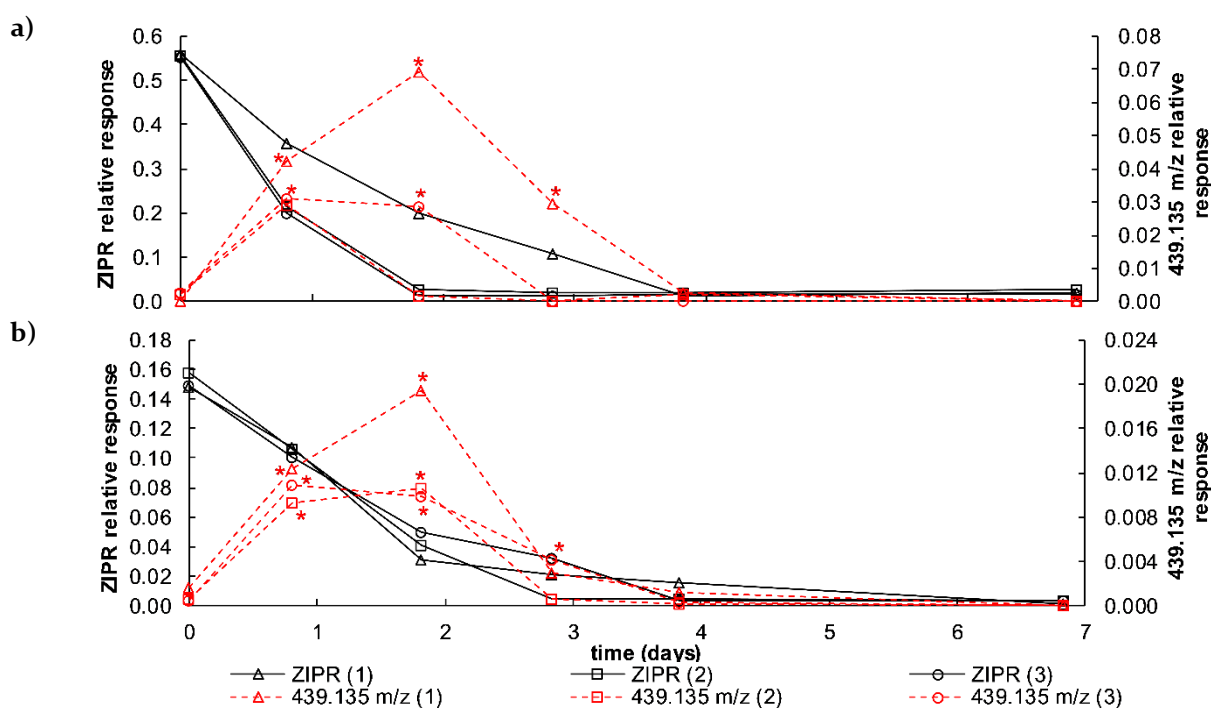


Figure 9-3: Relative response of ZIPR and 439.135 m/z degradation products over time in inoculated, unpreserved blood specimens for a) week experiment B1 and b) week experiment B2.

Asterisks indicate the acquisition of MS/MS spectra for the 439.135 m/z degradation products.

The precursor ion 455.132 m/z was not detected in calibrators and QCs. Integration of its response relative to AMIT over time in all extracts, determined from the sum of adjacent 455.132 m/z peaks detected (one to three), found that it behaved similarly to the 439.135 m/z degradants (Figure 9-4 (c-d)). However, unlike the 439.135 m/z degradation products, its MS/MS spectra was never obtained in extracts of inoculated, unpreserved blood specimens. While a peak was occasionally detected in extracts for these specimens with the same mass and retention time, ion counts were below the threshold of 5000 required to trigger auto-MS/MS acquisition.

The behaviour of the 439.135 m/z degradation products in inoculated, unpreserved specimens warranted further investigation. As it appeared to be a transient degradant in these specimens, its mass was used in a subsequent MDF search (i.e. 0.1352 ± 200 mDa) to screen for compounds it may subsequently degrade to. This search was applied to all blood specimens leading to the discovery of a precursor ion of 441.1518 m/z, eluting at 7.65 min.

Assessment of the response of the 441.152 m/z degradant over the 7 days of the week-long experiments in extracts revealed that in inoculated, unpreserved blood specimen extracts, the decrease in relative response of the 439.135 m/z precursor ions is accompanied by an increasing relative response for 441.152 m/z (Figure 9-5).

This may indicate that in inoculated unpreserved blood specimens, ZIPR first degrades to form the 439.135 m/z degradants and that these subsequently degrade to form the 441.152 m/z degradant, indicating likely microbial degradation of the 439.135 m/z degradants is occurring. In the 37 °C week-long experiments this precursor ion was primarily detected in inoculated, unpreserved blood extracts only. The one exception was its detection, with acquired MS/MS spectra, in one replicate of the final ~7th day extract for inoculated, preserved specimens in the second 37 °C week-long experiment with a relative response to AMIT of 0.0134.

From the extended seven-month experiment the 439.135 m/z degradants were gradually formed and degraded in all blood specimens at room temperature, but the rate of both processes was quickest in inoculated, unpreserved specimens (Figure 9-6). No MS/MS spectra of the 439.135 m/z degradants were acquired from extracts of inoculated, unpreserved specimens after ~21 weeks (Figure 9-6 (c)). At 4 °C in all blood specimens, an increasing relative response of the 439.135 m/z compounds can be observed over time (Figure 9-6). Trace amounts of 439.135 m/z were consistently detected in extracts of all blood specimens incubated at -20 °C. However, in the inoculated, unpreserved specimens it appears that over time increasing amounts of this degradant formed (Figure 9-6 (c)).

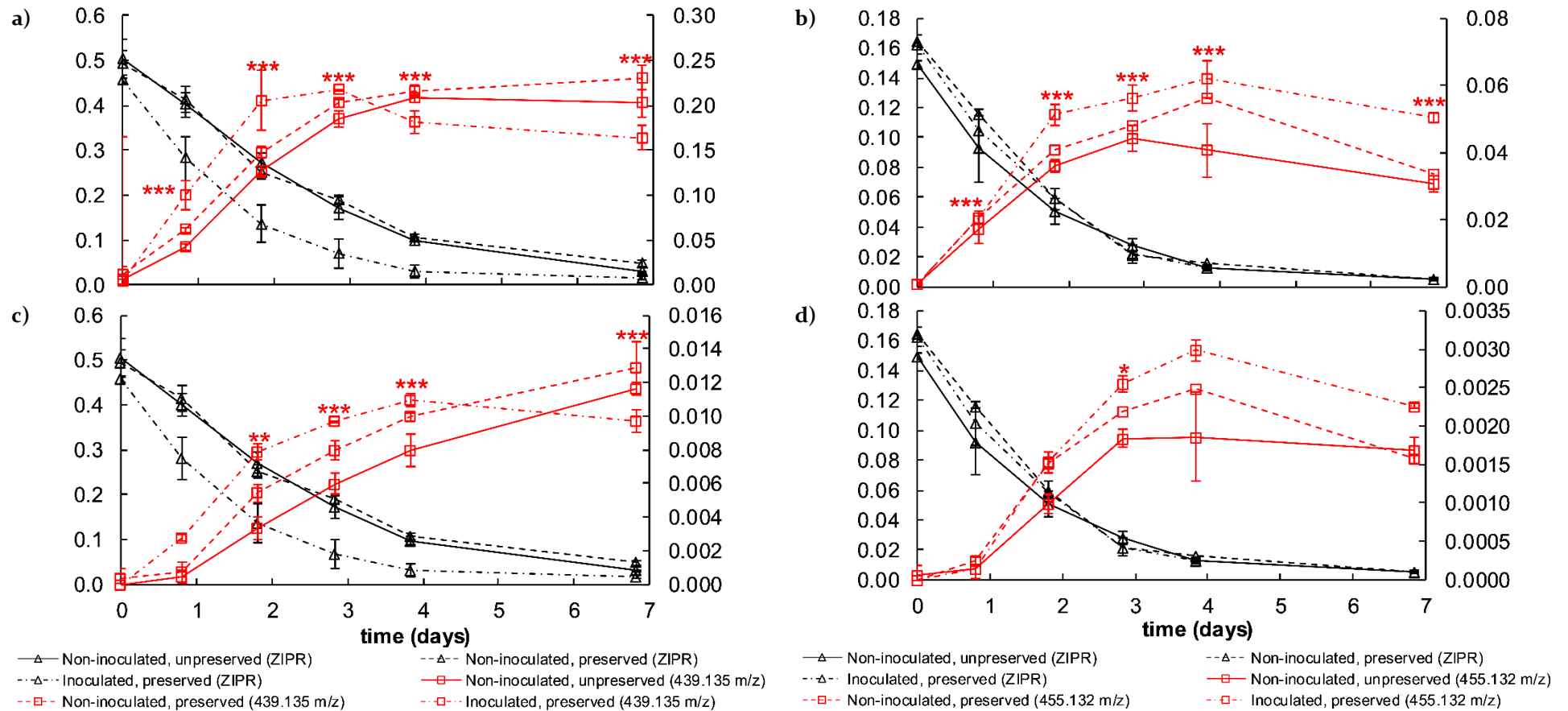


Figure 9-4: Relative response of ZIPR and a-b) 439.135 m/z and c-d) 455.132 m/z degradation products over time in preserved and unpreserved, non-inoculated blood specimens and preserved, inoculated blood specimens for a,c) week experiment B1 and b,d) week experiment B2.

Primary Y-axis is mean ZIPR relative response. Secondary Y-axis is a-b) mean 439.135 m/z degradation product relative response and c-d) mean 455.132 m/z degradation product relative response. Asterisks indicate the acquisition of MS/MS spectra in for degradation products in: * one specimen type; ** two specimen type; *** all three specimen types. Error bars are \pm S.D., $n = 3$, except for inoculated, preserved specimens in experiment B1 where $n = 2$ and non-inoculated, preserved specimens in experiment B2 where $n = 1$.

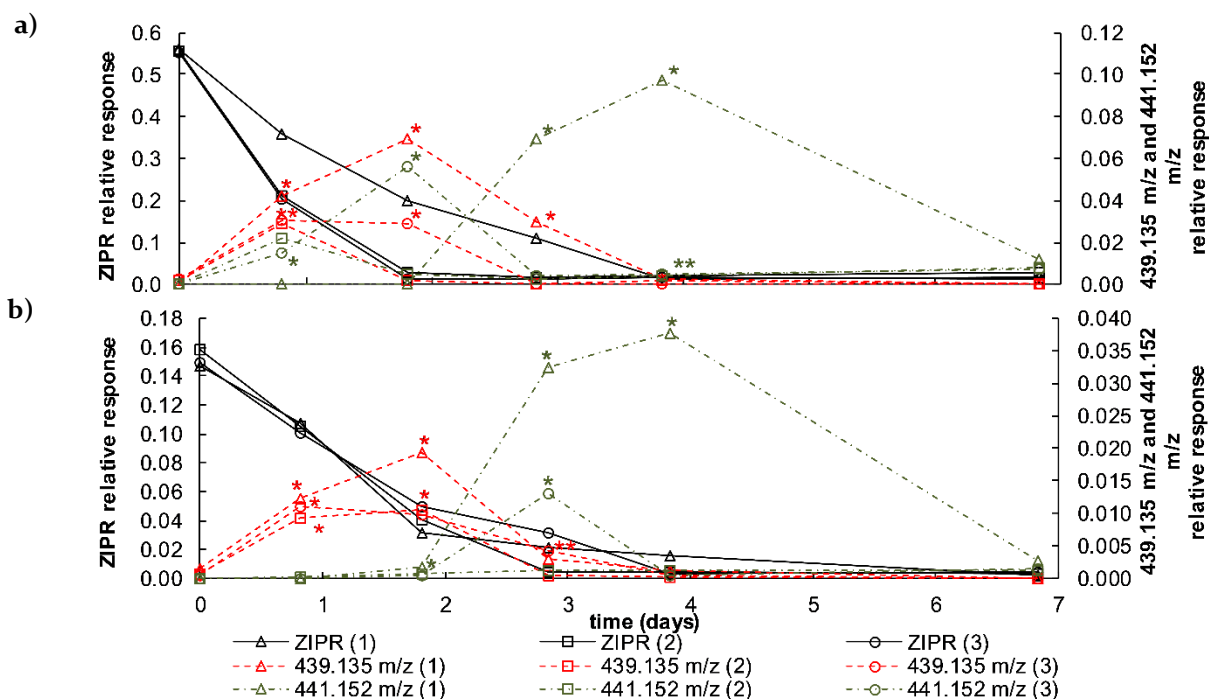


Figure 9-5: Relative response of ZIPR and the suspected ZIPR degradation products 439.135 m/z and 441.152 m/z over time in inoculated, unpreserved blood specimens for a) week experiment BI and b) week experiment B2.

Asterisks indicate the acquisition of MS/MS spectra for 439.135 m/z and 441.152 m/z degradation products in: * one replicate; ** two replicates; ***all three replicates.

At the conclusion of the seven-month experiment, the 441.152 m/z degradant was detected in extracts of all blood specimens stored at room temperature, excluding the non-inoculated, unpreserved specimens (Figure 9-7). In two non-inoculated, preserved specimens detection occurred after ~32 weeks (Figure 9-7 (a)). Detection occurred sooner in inoculated, preserved specimens at ~21 weeks (Figure 9-7 (c)), and quickest in inoculated, unpreserved specimens at ~1 week (Figure 9-7 (b)). It is unknown if this degradant may have been detected earlier in inoculated, preserved specimens if specimens were more frequently analysed. The only extracts where the 441.152 m/z degradation product was detected in specimens stored at 4 °C were from inoculated, unpreserved specimens at ~32 weeks (Figure 9-7 (c)). The 441.152 m/z precursor ion was not detected in extracts from specimens stored at -20 °C.

The 455.132 m/z degradants were not detected with MS/MS spectra acquired in extracts of inoculated, unpreserved specimens at any temperature in the seven-month experiment. The trend for all other blood specimens was formation followed by degradation (Figure 9-8). At -20 °C, 455.132 m/z precursor ions were not detected in any specimen.

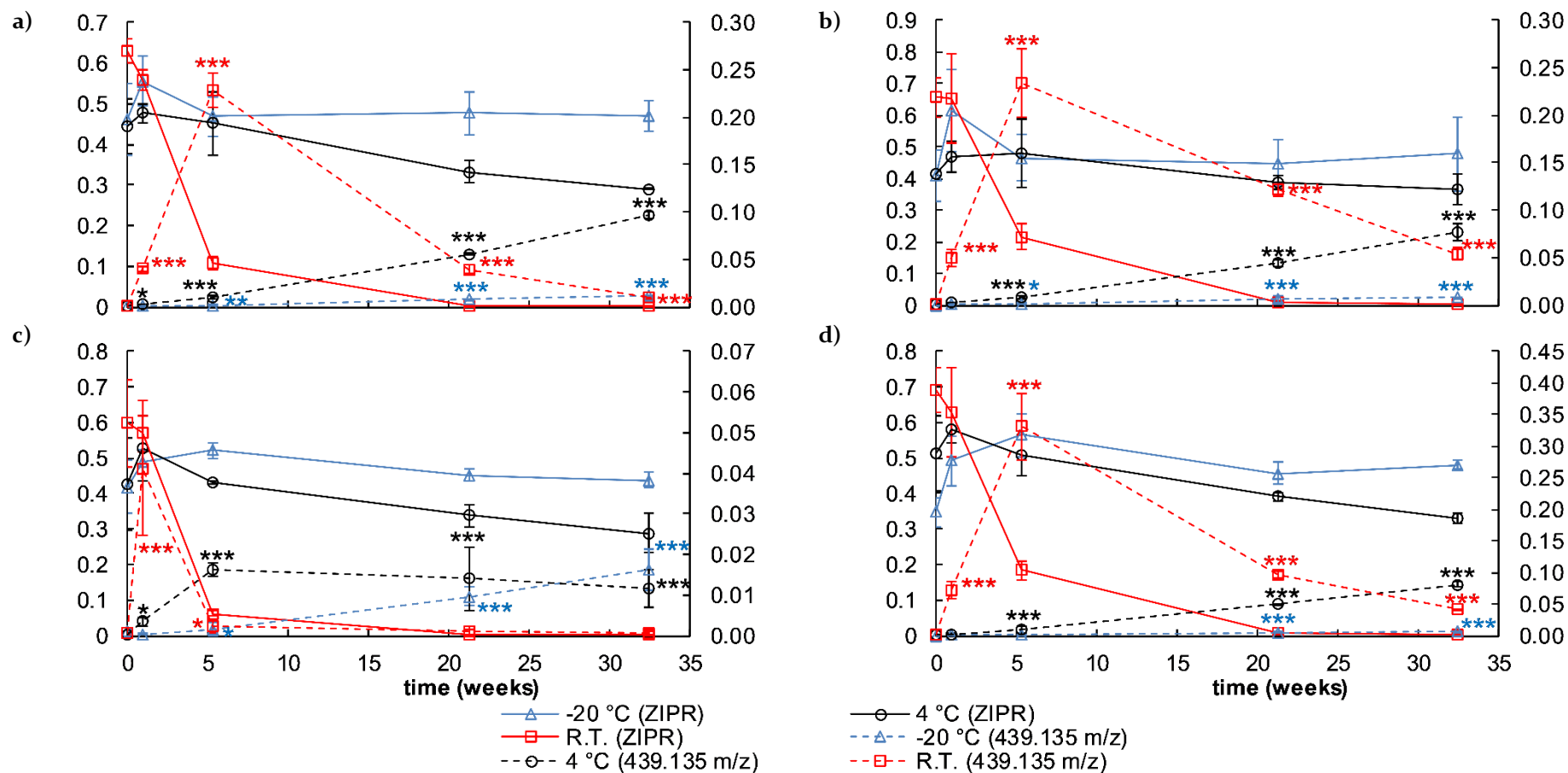


Figure 9-6: Relative response of ZIPR and 439.135 m/z degradation product over time in seven-month experiment in a) non-inoculated, unpreserved specimens, b) non-inoculated, preserved specimens, c) inoculated, unpreserved specimens, and d) inoculated, preserved specimens.

Primary Y-axis is mean ZIPR relative response. Secondary Y-axis is mean 439.135 m/z degradation product relative response. Asterisks indicate the acquisition of MS/MS spectra for 439.135 m/z degradation product in: * one replicate; ** two replicates; *** all three replicates. Error bars are \pm S.D., n = 3.

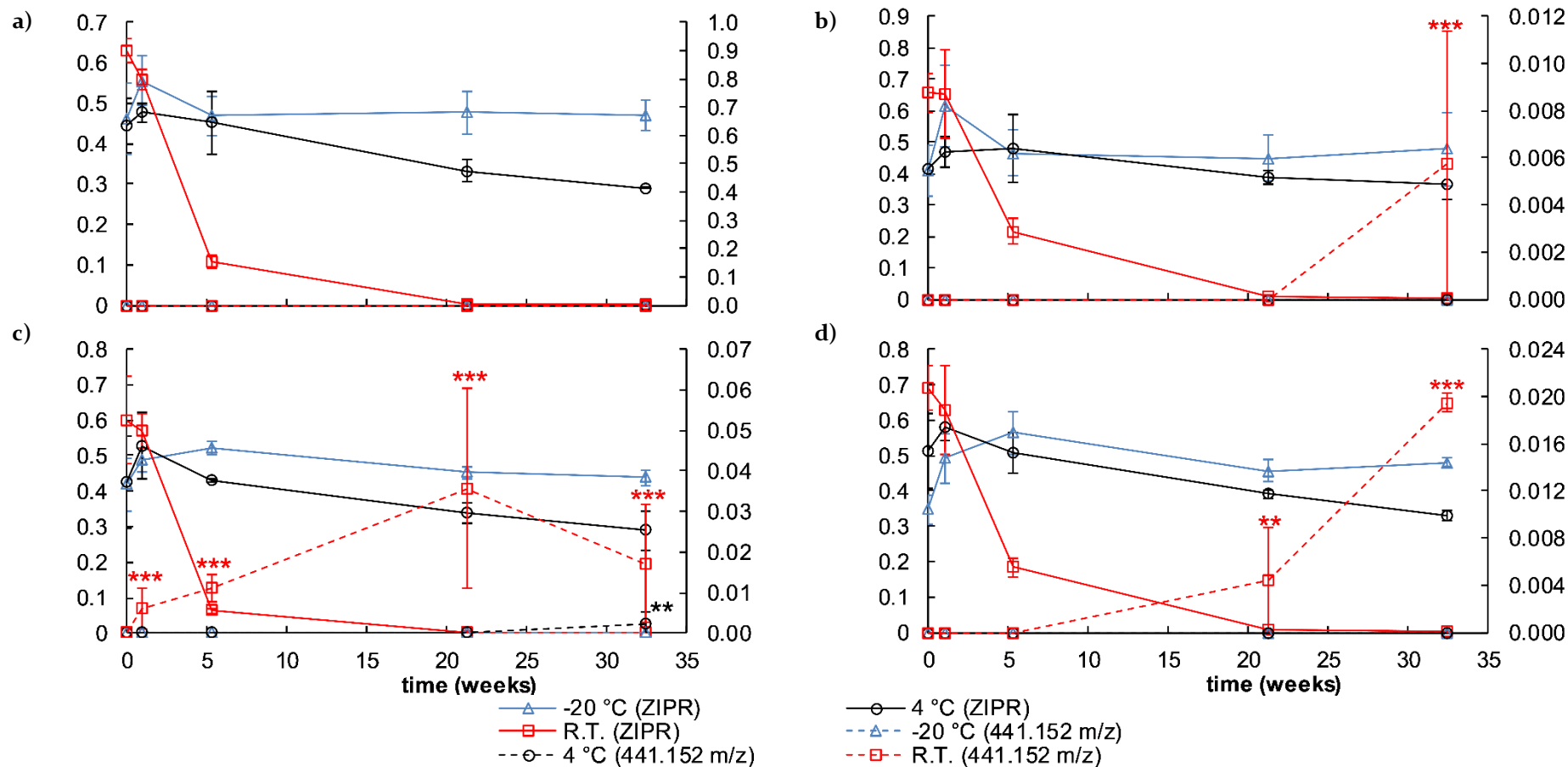


Figure 9-7: Relative response of ZIPR and 441.152 m/z degradation product over time in seven-month experiment in a) non-inoculated, unpreserved specimens, b) non-inoculated, preserved specimens, c) inoculated, unpreserved specimens, and d) inoculated, preserved specimens.

Primary Y-axis is mean ZIPR relative response. Secondary Y-axis is mean 441.152 m/z degradation product relative response. Asterisks indicate the acquisition of MS/MS spectra for 441.152 m/z degradation product in: * one replicate; ** two replicates; *** all three replicates. Error bars are \pm S.D., n = 3.

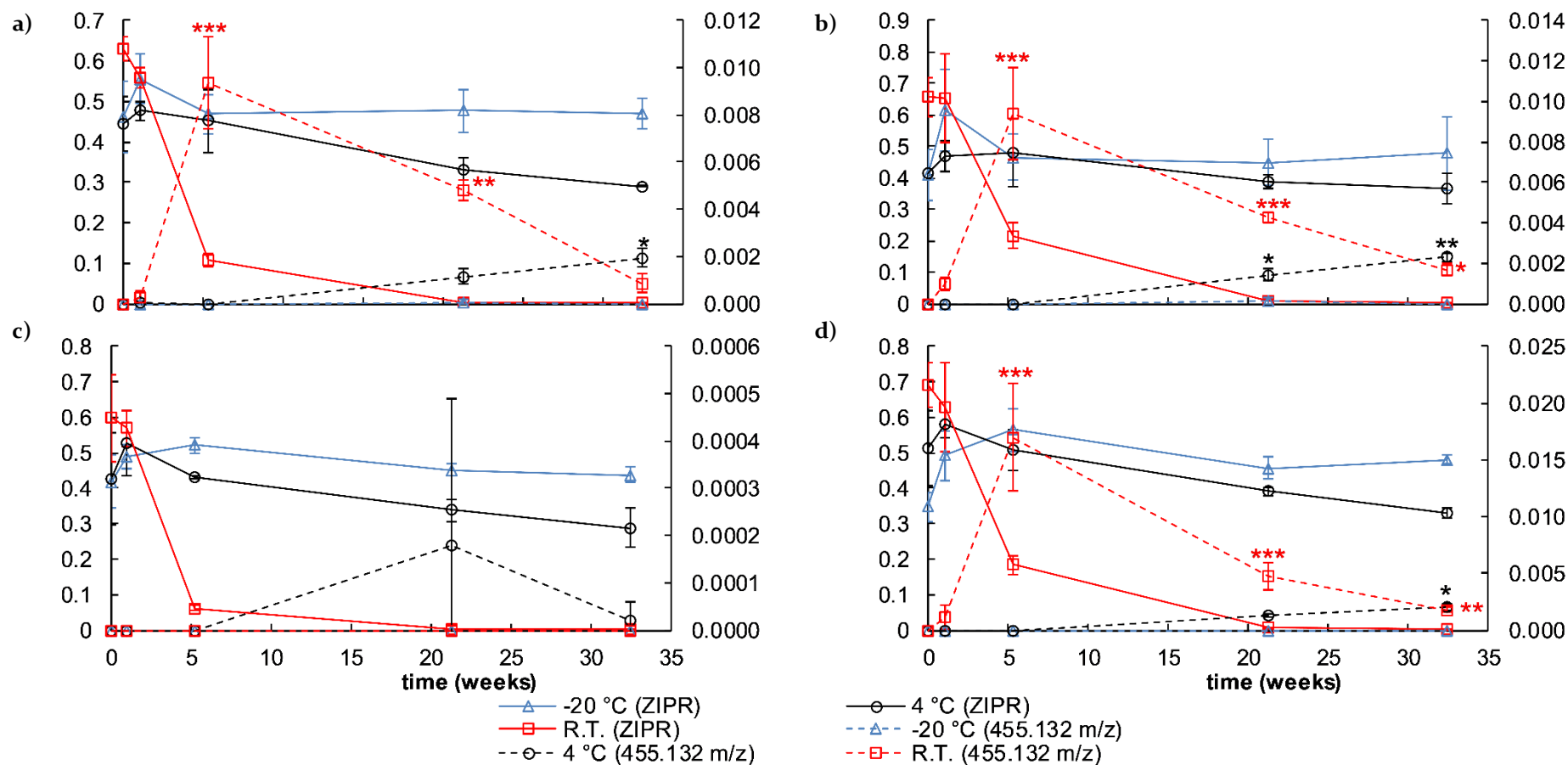


Figure 9-8: Relative response of ZIPR and 455.132 m/z degradation product over time in seven-month experiment in a) non-inoculated, unpreserved specimens, b) non-inoculated, preserved specimens, c) inoculated, unpreserved specimens, and d) inoculated, preserved specimens.

Primary Y-axis is mean ZIPR relative response. Secondary Y-axis is mean 455.132 m/z degradation product relative response. Asterisks indicate the acquisition of MS/MS spectra for 455.132 m/z degradation product in: * one replicate; ** two replicates; *** all three replicates. Error bars are ± S.D., n = 3.

The N-debenzothiazole derivative of ZIPR, termed M4A by Prakash *et al.* [463] (Figure 8-23 (b)), was not detected in any of the extracts, calibrators, or QCs analysed. Nor were any of the photodegradation products or ZIPR impurities reported by Raj *et al.* [466] or Skibiński [467]. Some of these reported compounds are oxindole ring-opened products with aryl primary amine functionality. In these compounds, delocalisation of the lone pair of electrons of the nitrogen of the arylamines is possible, and so the unbuffered LLE was expected to successfully extract them. These degradation products were also not detected in the acidic LLE, alkaline LLE, or protein precipitation extracts following the qualitative blood experiment (see 8.3).

EICs of all the possible ZIPR degradation products are shown in (Figure 9-9), alongside ZIPR. These compounds gave precursor ions in good agreement with GMF (Table 9-2) and predicted isotope ratios (Figure 9-11).

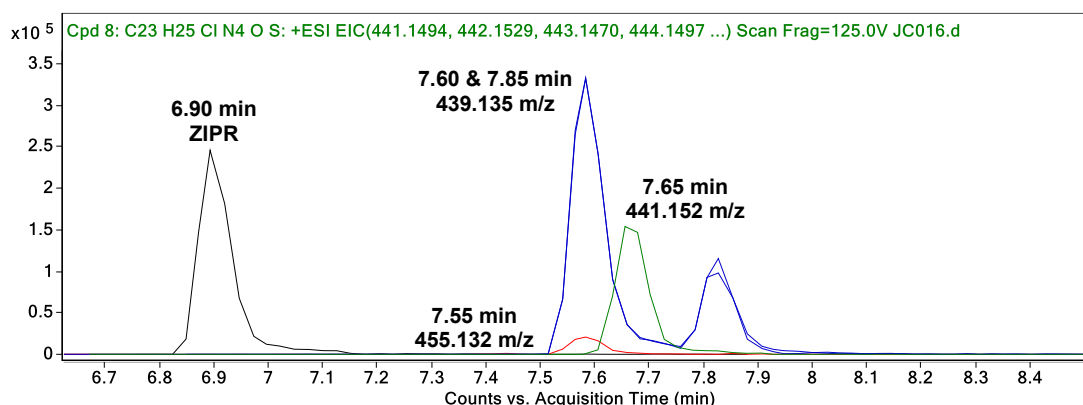


Figure 9-9: Extracted ion chromatograms of ZIPR and suspected degradation products. Compounds are overlaid from different extracts.

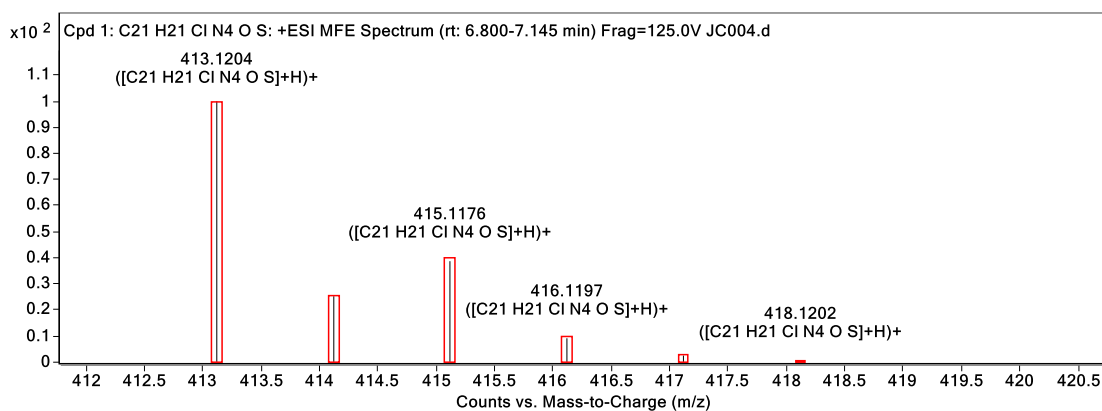


Figure 9-10: MS spectra with generated molecular formula showing predicted isotope ratios in red boxes for ZIPR.

Observed ion signal intensities are shown as lines within the boxes.

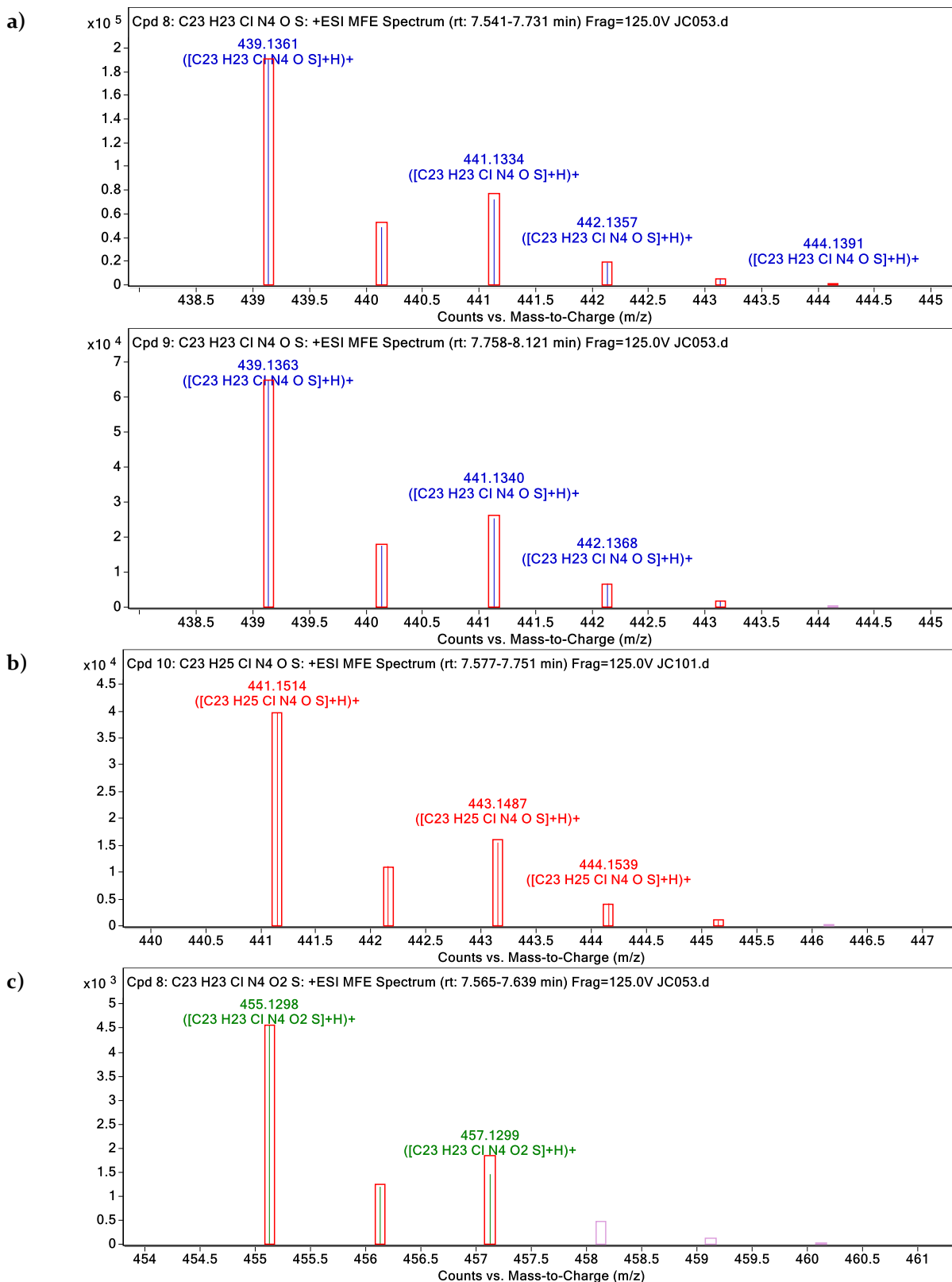


Figure 9-II: MS spectra with generated molecular formula showing predicted isotope ratios in red boxes for the suspected ZIPR degradants of m/z: a) 439.135, b) 441.152, and c) 455.132.

Observed ion signal intensities are shown as lines within the boxes.

Traces of what was thought may be ziprasidone-sulfoxide (ZIPR-SO), with a precursor ion of 429.1153 m/z, were also detected in the experiments. This precursor ion is 15.9963 mass units greater than that observed for ZIPR (calculated accurate mass of an oxygen atom: 15.9949 Da, $\delta = -87.5$ ppm (-1.4 mDa)) (Figure 9-13). As the same GMF may result from the hydroxylation of ziprasidone, or N-oxidation, the identity of this compound was not unambiguous.

In the week experiments, the 429.115 m/z degradant was only detected with MS/MS spectra acquired in extracts of two replicates of inoculated, unpreserved specimens after around 1 day. In the seven-month experiment, auto-MS/MS spectra were not acquired for 429.155 m/z at any time in extracts from room temperature blood specimens, other than in one replicate of non-inoculated, preserved specimens. Greatest responses were observed in extracts of -20 °C specimens (Figure 9-14). This differs from the trend observed for the suspected sulfoxide TRIF-SO in the same blood specimens in which greatest responses were observed in room temperature specimens (see Chapter 7).

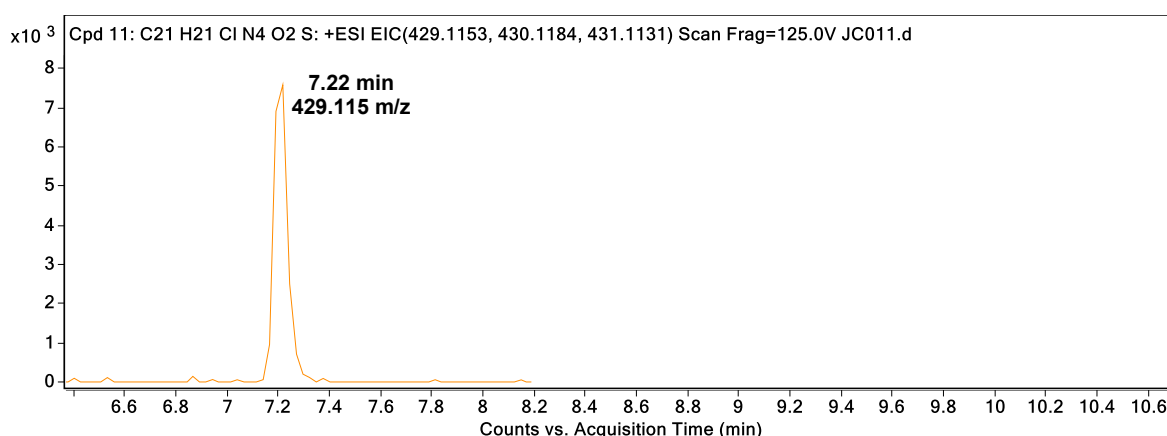


Figure 9-12: Extracted ion chromatogram of 429.115 m/z degradant.

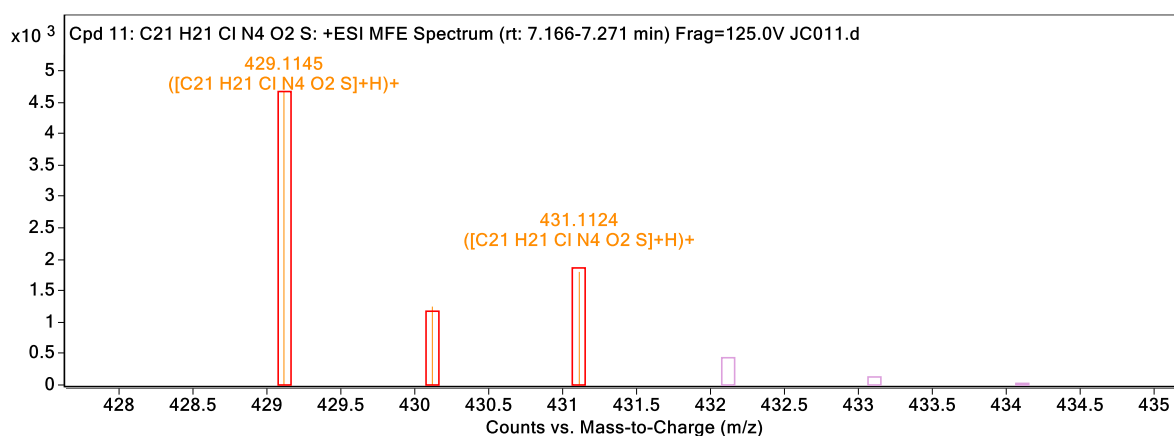


Figure 9-13: MS spectrum with generated molecular formula showing predicted isotope ratios in red boxes for 429.115 m/z degradant.

Observed ion signal intensities are shown as lines within the boxes.

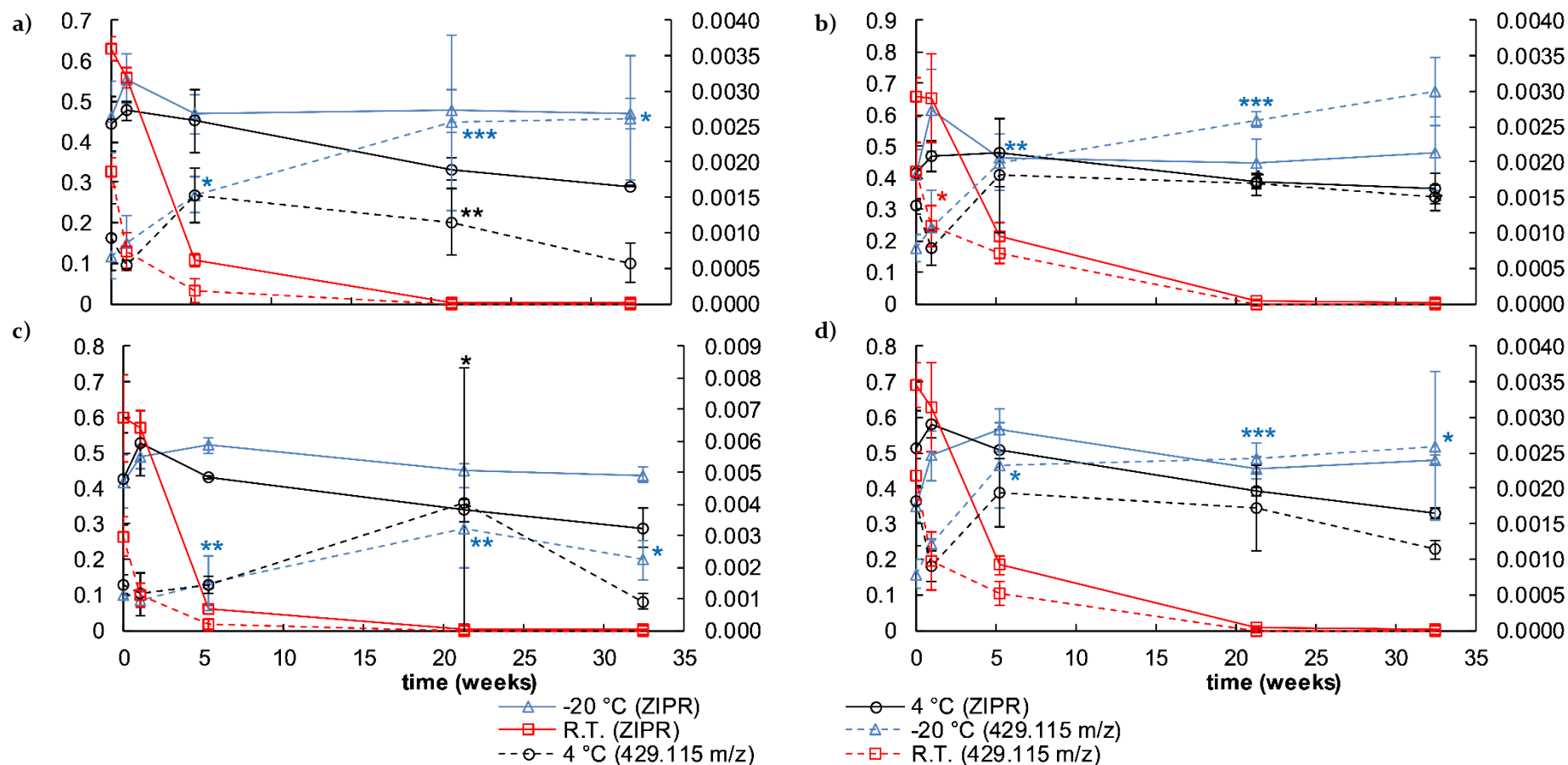


Figure 9-14: Relative response of ZIPR and 429.115 m/z degradation product over time in seven-month experiment in a) non-inoculated, unpreserved specimens, b) non-inoculated, preserved specimens, c) inoculated, unpreserved specimens, and d) inoculated, preserved specimens.

Primary Y-axis is mean ZIPR relative response. Secondary Y-axis is mean 429.115 m/z degradant relative response. Asterisks indicate the acquisition of MS/MS spectra for 429.115 m/z degradation product in: * one replicate; ** two replicates; *** all three replicates. Error bars are ± S.D., n = 3.

Table 9-2: MS data for ZIPR and possible ZIPR degradants.

Analyte	Measured [M+H] ⁺ (m/z)	Calculated [M+H] ⁺ (m/z)	GMF precursor ion	Mass accuracy (δ) (ppm)	Mass accuracy (δ) (mDa)
ZIPR	413.1190	413.1197	[C ₂₁ H ₂₁ ClN ₄ OS]H ⁺	1.7	0.7
439.135 at 7.60 min	439.1352	439.1354	[C ₂₃ H ₂₃ ClN ₄ OS]H ⁺	0.5	0.2
439.137 at 7.85 min	439.1369	439.1354	[C ₂₃ H ₂₃ ClN ₄ OS]H ⁺	-3.4	-1.5
441.152	441.1518	441.1510	[C ₂₃ H ₂₅ ClN ₄ OS]H ⁺	-1.8	-0.8
455.132	455.1317	455.1303	[C ₂₃ H ₂₃ ClN ₄ O ₂ S]H ⁺	-3.1	-1.4
429.115	429.1153	429.1147	[C ₂₁ H ₂₁ ClN ₄ O ₂ S]H ⁺	-1.4	-0.6

GMF = generated molecular formulae. Mass accuracies determined from single injection.

9.2.3.2 MS/MS data analysis

MS/MS spectra collected at 20 eV and 30 eV did not produce sufficient MS/MS ions to assist with structural determination of the degradants. More structural information was obtained from the MS/MS spectra of ZIPR and its suspected degradants at a collision energy of 40 eV (Figure 9-15 and Figure 9-16).

The MS/MS spectra of three of the precursor ions (439.135, 439.137 and 441.152 m/z) were found to have four commonalities with the MS/MS spectrum for ZIPR: i) precursor and major product ion masses have a similar neutral loss of 219.0827-219.0857 m/z; ii) a product ion at 177.0481 m/z, previously postulated to be a ion characteristic of the 1,2-benzisothiazole moiety present in both LURA and ZIPR (see Figure 8-21); iii) a difference of 34.9686-34.9716 m/z units between two product ions (194.0352 and 159.0666 m/z in ZIPR; 220.0515/220.0525 and 185.0829/185.0827 m/z in the 439.135 and 439.137 m/z ions; 222.0680 and 187.0964 m/z in the 441.152 m/z ion), suggesting fragment loss of a chlorine atom (calculated mass for Cl: 34.9694 Da, δ = -62.9 – 22.9 ppm (-2.2 – 0.8 mDa)); and supporting the characteristic MS product ion ratio pattern of chlorine (Figure 9-11); and iv) a difference of 27.9919-27.9983 m/z between two product ions (194.0352 and 166.0410 m/z in ZIPR; 220.0515/220.0525 and 192.0532/192.0606 m/z in the 439.1352 and 439.1369 m/z ions; 222.0680 and 194.0748 m/z in the 441.1518 m/z ion), suggesting fragment loss of carbon monoxide (calculated mass for CO: 27.9949 Da, δ = -121.5 – 107.2 ppm (-3.4 – 3.0 mDa)) and thus the presence of carbonyl functionality. These four similarities between the four MS/MS spectra supported the hypothesis of these detected ions as ZIPR degradants. The MS/MS spectra obtained for 455.132 m/z were noisy due to being lower in intensity, and therefore harder to interpret. Nevertheless, the 455.132 m/z degradant shares with ZIPR features i) and ii) as described above.

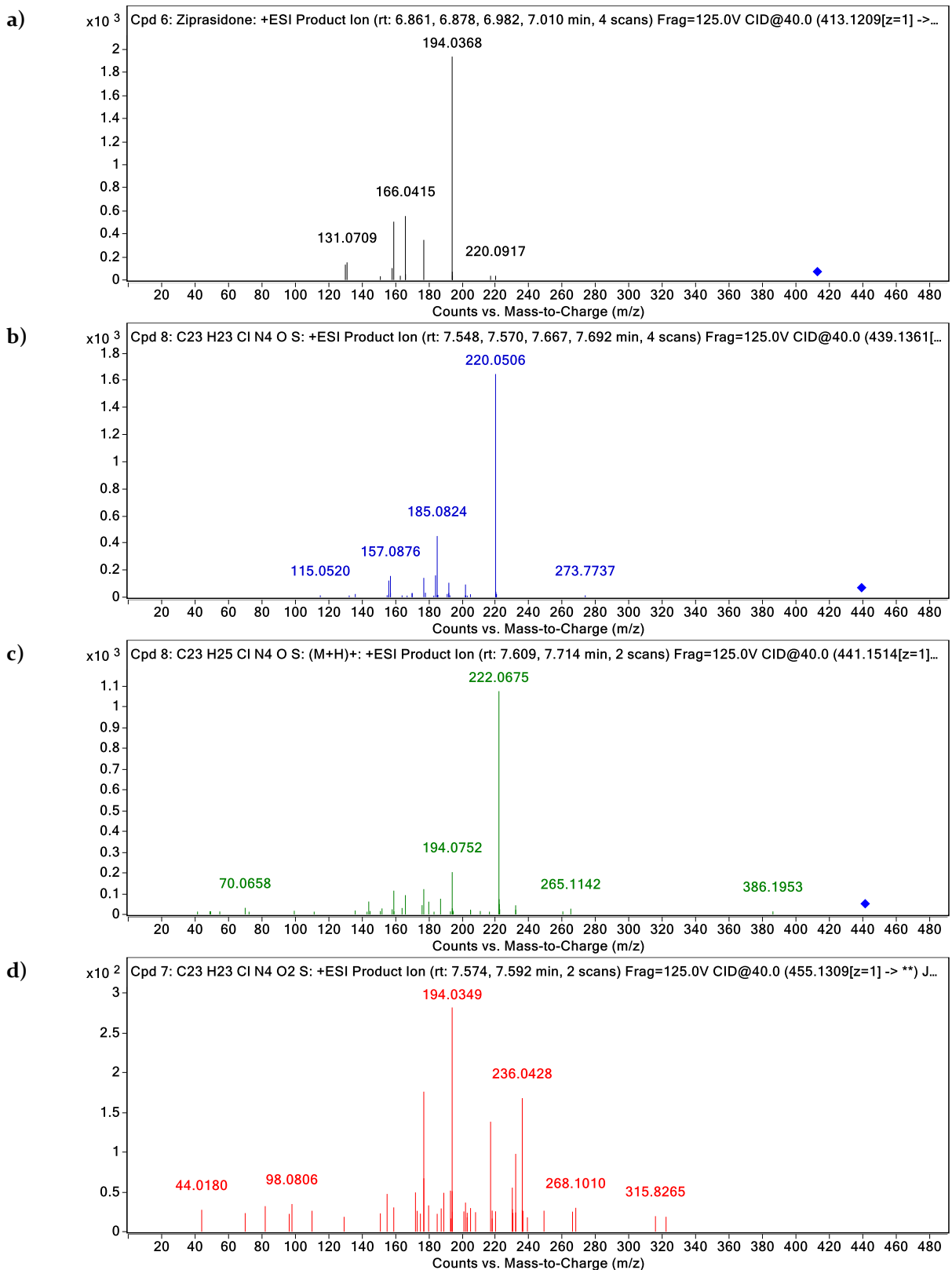


Figure 9-15: MS/MS spectra for a) ZIPR and the suspected degradants of m/z: b) 439.135, c) 441.152, and d) 455.132. Collision energy = 40 eV.

Overall, the MS/MS spectra indicated for these degradants, that the 1,2-benzisothiazole moiety was still intact and that it was lost as a neutral fragment with a mass of 219.083 Da (3-(1-piperazinyl)-1,2-benisothiazole) when forming the ions at 194.0352, 220.0515/220.0525, 222.0680, and 236.0456 m/z, in ZIPR, and the degradants of m/z 439.135, 441.152, and 455.132, respectively (calculated mass: 219.0830 Da, $\delta = -12.3 - 1.4$ ppm (-2.7 - 0.3 mDa)) (Table 9-3).

For the 439.135 m/z and 441.152 m/z degradants, it also appeared that the aryl chlorine and oxindole carbonyl moiety were still present. Therefore, it was hypothesised that the degradation of ZIPR was occurring at the oxindole moiety, with no net gain or loss of carbonyl functionality. Given the similar elution times of the 439.135 m/z precursor ions in both the LC-DAD and LC-QTOF-MS methods, and their similar UV-Vis and MS/MS spectra, it was hypothesised that they may be cis-trans isomers. Production of the 441.152 m/z degradation product (see Figure 9-5) could then be due to hydrogenation.

The major product ion of the 429.115 m/z degradant was 194.0336 m/z (Figure 9-16), indicating a neutral loss of 235.0802 Da. This is 15.9980 Da greater than the mass difference between the major product ion of ZIPR (194.0368 m/z) and ZIPR's precursor ion (413.1190 m/z). This is consistent with the identity of 429.115 m/z as a sulfoxide (calculated mass for $C_{11}H_{13}N_3OS$: 235.0779 Da, $\delta = -9.8$ ppm (-2.3 mDa)) if the neutral loss corresponds to an S-oxide 1,2-benzisothiazolepiperazine.

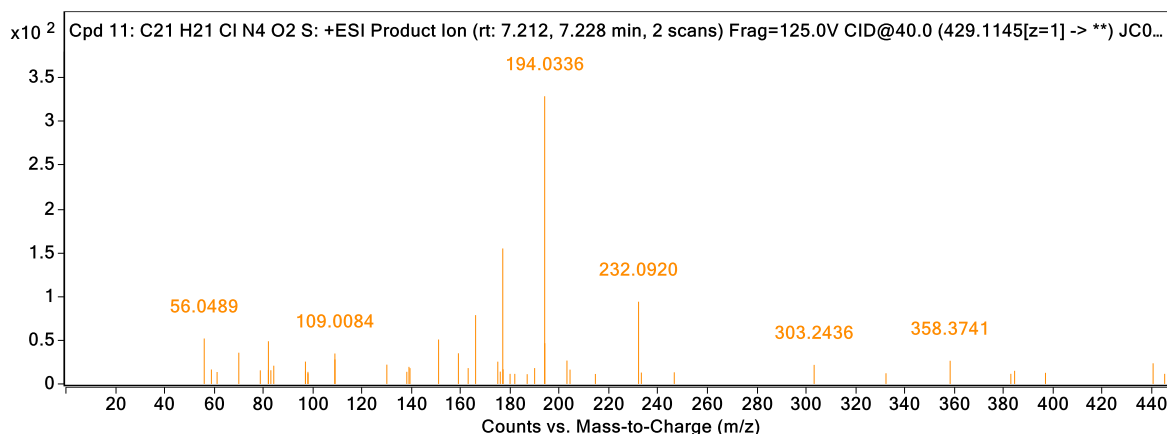


Figure 9-16: MS/MS spectra for 429.115 m/z degradant. Collision energy = 40 eV.

A review of the literature found support for the hypothesis that the degradation of ZIPR was occurring at the oxindole moiety to produce cis-trans isomers. Oxindoles are reported to undergo aldol condensation with aldehydes and ketones at the methylene adjacent to the carbonyl [468, 469]. This can occur in the presence of either acid or base, to produce a mixture of *E/Z* isomers of 3-alkenyl-oxindoles [470]. During the synthesis of ZIPR, the oxindole moiety

has been reported to react with methyl isobutyl ketone in an aldol condensation reaction, leading to reduced product yields [471]. Oxindoles may also undergo nucleophilic N-alkylation and methylene-alkylation [470]. Inter- or intra-molecular alkylation can follow [470].

Table 9-3: MS/MS data for ZIPR and suspected degradants.

Analyte	Precursor ion (m/z)	Product ions (m/z)	GMF ions	product	Calculated accurate mass (m/z)	Mass accuracy (δ) (ppm)	Mass accuracy (δ) (mDa)
ZIPR	413.1190	159.0666	C ₁₀ H ₉ NO		159.0679	8.2	1.3
		166.0410	C ₉ H ₉ ClN		166.0418	4.8	0.8
		177.0453	C ₉ H ₉ N ₂ S		177.0481	15.8	2.8
		194.0352	C ₁₀ H ₉ ClNO		194.0367	7.7	1.5
		413.1209	[C ₂₁ H ₂₁ ClN ₄ OS]H ⁺		413.1197	-2.9	-1.2
439.135 m/z at 7.60 min	439.1352	157.0855	C ₁₁ H ₁₁ N		157.0886	19.7	3.1
		177.0477	C ₉ H ₉ N ₂ S		177.0481	2.3	0.4
		185.0827	C ₁₂ H ₁₁ NO		185.0835	4.3	0.8
		192.0606	C ₁₁ H ₁₁ ClN		192.0575	-16.1	-3.1
		220.0525	C ₁₂ H ₁₁ ClNO		220.0524	-0.6	-0.1
439.1345	[C ₂₃ H ₂₃ ClN ₄ OS]H ⁺		439.1354	2.0	0.9		
439.137 m/z at 7.85 min	439.1369	157.0855	C ₁₁ H ₁₁ N		157.0886	19.7	3.1
		177.0445	C ₉ H ₉ N ₂ S		177.0481	20.3	3.6
		185.0829	C ₁₂ H ₁₁ NO		185.0835	3.2	0.6
		192.0532	C ₁₁ H ₁₁ ClN		192.0575	22.4	4.3
		220.0515	C ₁₂ H ₁₁ ClNO		220.0524	4.1	0.9
439.1354	[C ₂₃ H ₂₃ ClN ₄ OS]H ⁺		439.1354	0.0	0.0		
441.152 m/z	441.1518	166.0409	C ₉ H ₉ ClN		166.0418	5.4	0.9
		177.0437	C ₉ H ₉ N ₂ S		177.0481	24.9	4.4
		187.0964	C ₁₂ H ₁₃ NO		187.0992	15.0	2.8
		194.0748	C ₁₁ H ₁₃ ClN		194.0731	-8.8	-1.7
		222.0680	C ₁₂ H ₁₃ ClNO		222.0680	0.0	0.0
441.1499	[C ₂₃ H ₂₅ ClN ₄ OS]H ⁺		441.1510	2.5	1.1		
455.132 m/z	455.1317	177.0536	C ₉ H ₉ N ₂ S		177.0481	-31.1	-5.5
		194.0375	C ₁₀ H ₉ ClNO		194.0367	-4.1	-0.8
		236.0456	C ₁₂ H ₁₁ ClNO ₂		236.0473	7.2	1.7
		455.1257	[C ₂₃ H ₂₃ ClN ₄ O ₂ S]H ⁺		455.1303	10.1	4.6
429.115 m/z	429.1145	166.0415	C ₉ H ₉ ClN		166.0418	1.8	0.3
		177.0482	C ₉ H ₉ N ₂ S		177.0481	-0.6	-0.1
		194.0336	C ₁₀ H ₉ ClNO		194.0367	16.0	3.1

Ions shared between each compound are indicated in bold. GMF = generated molecular formulae. Mass accuracies determined from single injection.

Four structural isomers were postulated (Figure 9-17), based on the prior discussion and the GMF obtained for the precursor and product ions (Figure 9-17 and Table 9-3). 1-vinyl-ziprasidone (Figure 9-17 (a)) was not suspected of forming, as no stereocentre is present which is inconsistent with the observed closely eluting 439.135 m/z precursor ions. An alkylation reaction to produce 3-vinyl-ziprasidone (Figure 9-17 (b)) creates a stereocentre at the methylene carbon. However, the pair of 3-vinyl-ziprasidone compounds produced would be enantiomeric

and would not have separated by the LC-DAD method employed to yield the two resolved peaks that were observed (see Figure 8-2). If the identity of the 439.135 m/z degradants is that of an alkylated diastereomeric pair it is of note that the dialkylated product (GMF for precursor ion of $[C_{25}H_{25}ClN_4OS]H^+$, calculated 465.1510 m/z) was not detected, although it is possible that a second alkylation could not proceed due to steric hinderance. Mono-alkylation followed by cyclization of the intermediate to yield spiro[cyclopropane-1,3']-ziprasidone could explain non-detection of a dialkylated product (Figure 9-17 (c)), however, no manner of subsequent degradation of spiro[cyclopropane-1,3']-ziprasidone could be proposed that would produce a precursor ion of 441.152 m/z. If only one structural isomer is responsible for the two 439.135 m/z degradants detected then the most probable identity is 3-ethylidene-ziprasidone (3E-ZIPR) (Figure 9-17 (d)), with clear cis-trans stereochemistry possible.

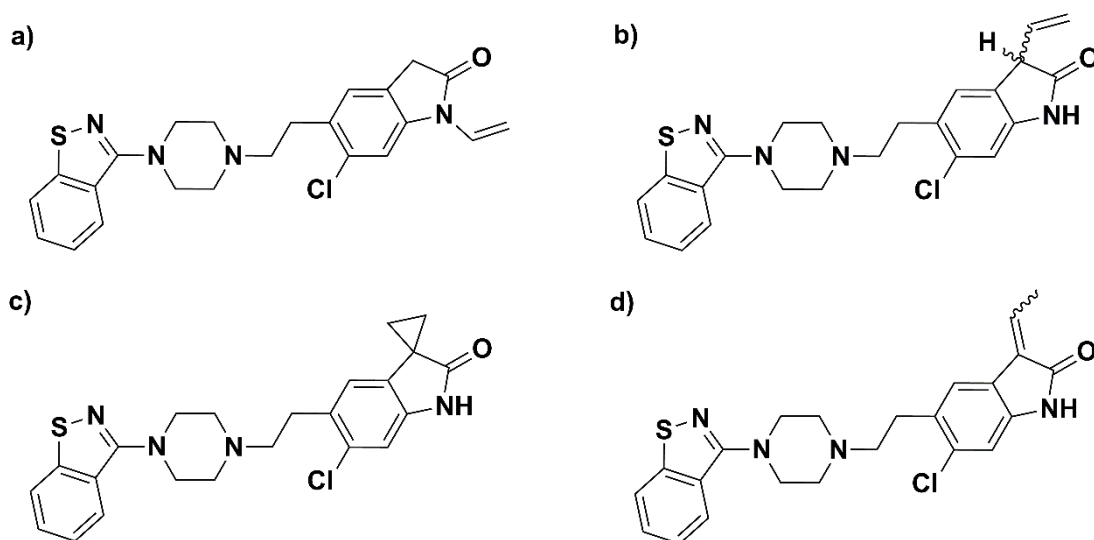


Figure 9-17: Structural isomers of $C_{23}H_{23}ClN_4OS$: a) 1-vinyl-ziprasidone, b) 3-vinyl-ziprasidone, c) spiro[cyclopropane-1,3']-ziprasidone, and d) 3-ethylidene-ziprasidone.

It was not considered likely that a mixture of differently substituted isomers of $C_{23}H_{23}ClN_4OS$ were forming in the blood specimens due to the similar retention time and UV-Vis spectra of both 439.135 m/z degradants and their red shifted UV-Vis spectra compared to ZIPR (Figure 8-2). If 1-vinyl-ziprasidone were to be forming in combination with any of the other proposed structural isomers greater chromatographic separation would have been expected, as 1-vinyl-ziprasidone does not possess a secondary amine able to undergo hydrogen bonding with the mobile phase of the LC-DAD and LC-QTOF-MS methods. If 3-vinyl-ziprasidone or spiro[cyclopropane-1,3']-ziprasidone were forming the red shifts in the UV-Vis spectra of the 439.135 m/z degradants would not be expected as there is no greater conjugation in these

compounds compared to ZIPR [204, 472]. In forming 3E-ZIPR, the methylene carbon of ZIPR changes hybridisation from sp^3 to sp^2 . This converts the oxindole moiety into a π -conjugated system. This could explain the significant change in the UV-Vis absorbance spectra between ZIPR and the two 439.135 m/z degradants and the red shift could be attributed to the greater conjugation of 3E-ZIPR (Figure 8-2) [204, 472]. If the hypothesised identity of the 439.135 m/z pair of degradation products is correct, their fragmentation pathway in the LC-QTOF-MS method may be as shown (Figure 9-18).

The simplest explanation for the formation of the *E*- and *Z*- isomers of 3E-ZIPR is the aldol condensation of ZIPR and acetaldehyde. The reaction between oxindole and acetaldehyde under base catalysis to produce *E/Z* 3-ethylidene isomers has been reported in literature [473]. Acetaldehyde may be present endogenously in the ante-mortem whole blood sourced for the experiments [474]. It may also form from the oxidation of the ethanol used to dissolve and spike the drugs into blood [475, 476]. Alternatively, ZIPR may be coupling with another carbonyl that then fragments to form the 3-ethylidene adduct.

Identification of the 439.135 m/z degradant as 3E-ZIPR is consistent with 441.152 m/z being a product that forms following the hydrogenation 3E-ZIPR (i.e. 3-ethyl-ziprasidone (3A-ZIPR)). This would explain the correlation in 439.135 m/z response reduction with 441.152 m/z response gain (Figure 9-5). The reduction of 3-alkylidene oxindoles has been reported following treatment with *Saccharomyces cerevisiae*, glucose, and water to produce a racemic mixture of enantiomeric 3-alkyl oxindoles [477]. In the week-long blood experiments, *Clostridium perfringens* was the dominant microorganism present in the inoculated, unpreserved blood specimens (see Chapter 6). Importantly, *C. perfringens* was reported to reduce the alkene of caffeic acid to dihydrocaffeic acid under anaerobic conditions at 37 °C [262]. This information lends further support to the hypothesis that the 441.152 m/z degradant is the hydrogenated product of 3E-ZIPR. GMF are consistent with the proposed MS/MS fragmentation of 3A-ZIPR (Figure 9-19 and Table 9-3). 3-alkyl oxindoles are also known to epimerise [477], and therefore, the 3A-ZIPR product is expected to exist as a mixture of its enantiomers in the blood specimens, regardless of whether it may or may not be formed enantioselectively by a microbial enzyme.

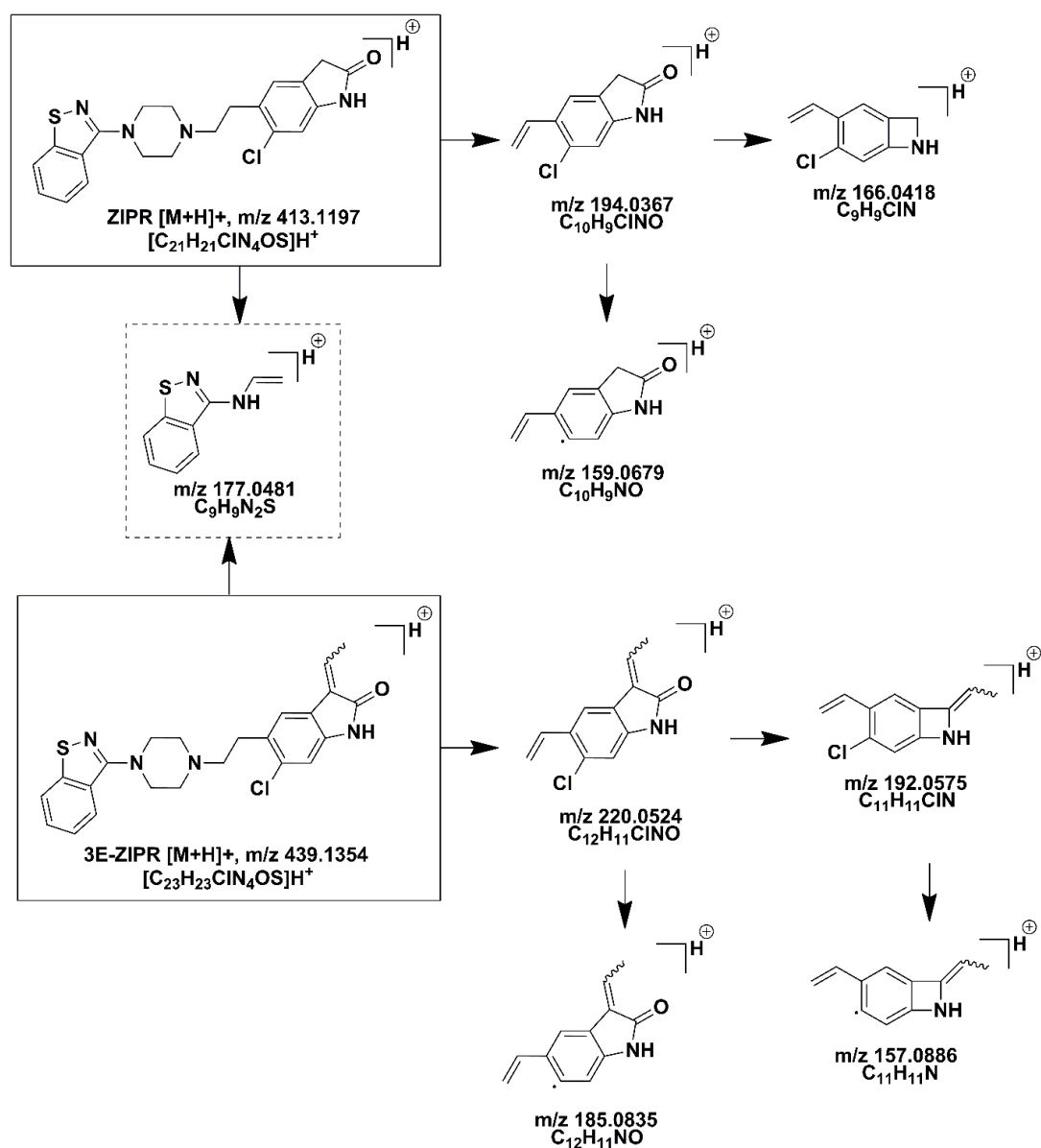


Figure 9-18: Proposed MS/MS fragmentation pathway for ZIPR and the 439.135 m/z (3E-ZIPR) degradation products.

Fragment in common between ZIPR and the 439.135 m/z (3E-ZIPR) degradation products is indicated by the dotted-line box; m/z are calculated accurate mass/charge values.

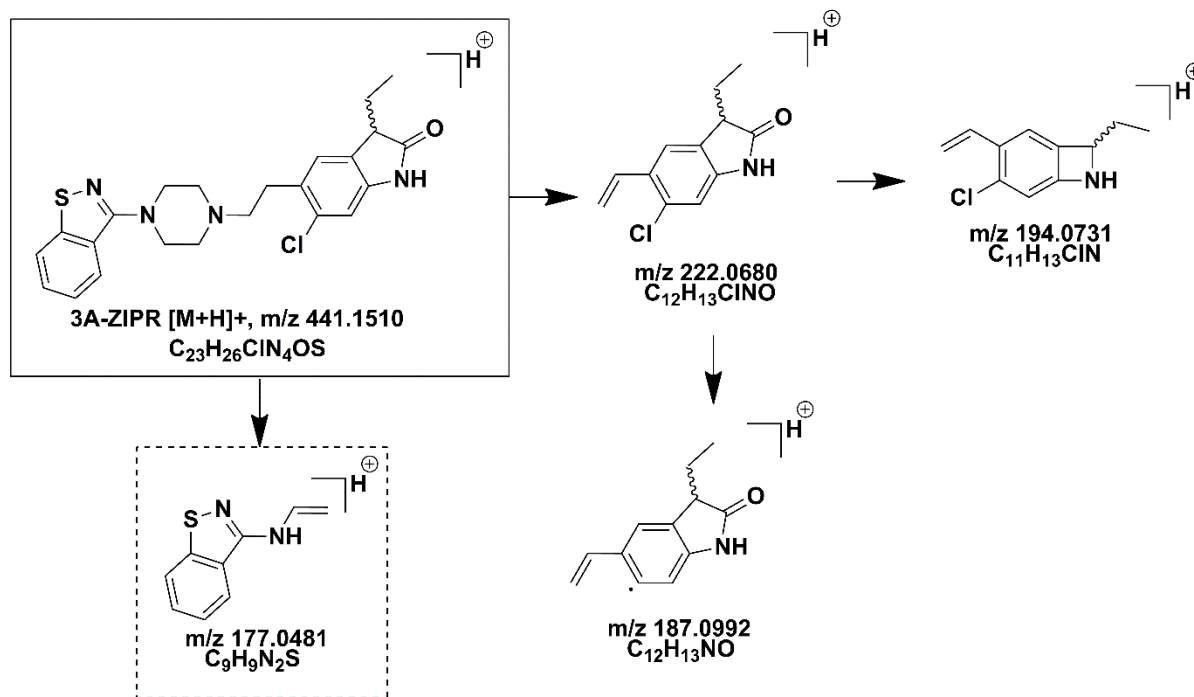


Figure 9-19: Proposed MS/MS fragmentation pathway for 441.152 m/z (3A-ZIPR degradation product).

Fragment in common between ZIPR and the 441.152 m/z (3A-ZIPR) degradation product is indicated by the dotted-line box; m/z are calculated accurate mass/charge values.

The low response for the 455.132 m/z degradation product made it more challenging to deduce its identity. Nevertheless, the GMF for the MS precursor ion had a mass accuracy of -3.1 ppm (-1.4 mDa) (Table 9-2). Based on this molecular formula numerous structural isomers were proposed. The observed 455.1317 m/z precursor ion 15.9948-15.9965 m/z greater than the two 439 m/z precursor ions and therefore it may be that the 455.132 m/z degradant is the sulfoxide or N-oxide of 3E-ZIPR (calculated mass for O: 15.9949 Da, $\delta = -100.0 - 6.3$ ppm (-1.6 - 0.1 mDa)) (Figure 9-20 (a)). The absence of the 232.0920 m/z product ion peak in the MS/MS spectra, present in what is presumed to be ZIPR-SO (the 429.115 m/z degradant) (Figure 9-16), suggests this may not be the case. Furthermore, the only product ion in common with 3E-ZIPR was 177.0481 m/z, corresponding to the 1,2-benzisothiazole moiety. Major product ions attributed to the 3-substituted oxindole moiety of 3E-ZIPR (see Figure 9-18) were not dominant in the MS/MS spectra of the 455.132 m/z degradant (Figure 9-15 (d)). The mass increase of 42.0127 Da from ZIPR could also result from acetylation at the oxindole (calculated mass of C₂H₂O: 42.0106 Da, $\delta = -2.4$ ppm (-0.1 mDa)). Theoretically, this could occur at the nitrogen, the methylene carbon, or the oxygen [470] and up to three different ions with the same m/z were detected for this degradation product (Figure 9-20 (b-d)). Precursor ions consistent with the combination of different acetylation reactions across the oxindole were not detected (GMF for precursor ions

of $[C_{25}H_{25}ClN_4O_3S]H^+$ and $[C_{27}H_{27}ClN_4O_3S]H^+$, calculated 497.1409 m/z and 539.1514 m/z, respectively), discrediting this possibility.

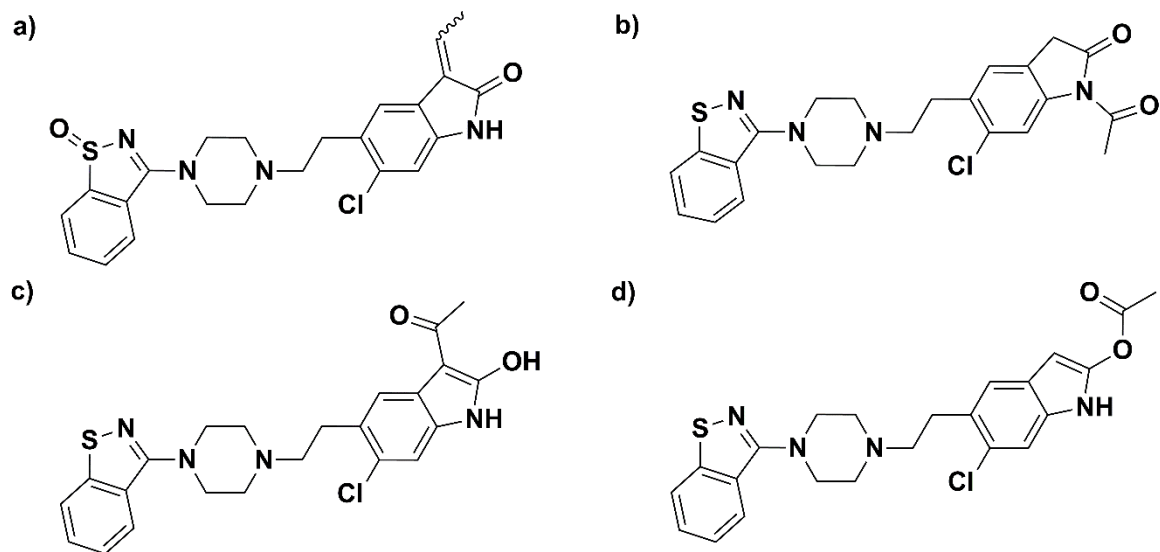


Figure 9-20: Structural isomers of $C_{23}H_{23}ClN_4O_2S$: a) 3-ethylidene ziprasidone sulfoxide, b) 1-acetyl-ziprasidone, c) 3-acetyl-ziprasidone, and d) 2-acetyl-ziprasidone.

If the product ion of 177.0481 m/z present in all degradants is indeed the 1,2-benzisothiazole moiety of ZIPR this would indicate this moiety is not degraded in ZIPR as it was hypothesised to be in the case of LURA degradation in the same blood experiments (Chapter 8). N-debenzothiazole derivatives of 3E-ZIPR (GMF for precursor ion of $[C_{16}H_{20}ClN_3O]H^+$, calculated 306.1368 m/z) and 3A-ZIPR (GMF for precursor ion of $[C_{16}H_{22}ClN_3O]H^+$, calculated 308.1524 m/z) were also not detected (Figure 9-21).

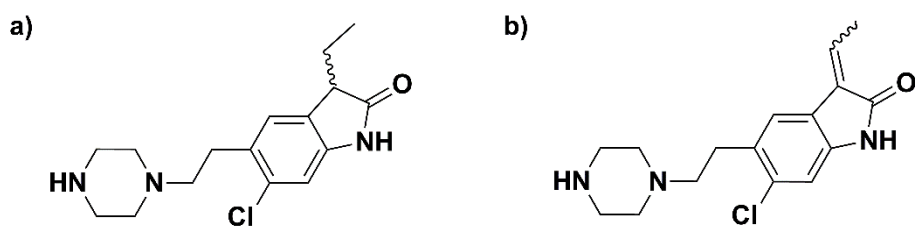


Figure 9-21: Chemical structure of unobserved theoretical degradants a) N-debenzothiazole-3-ethyl-ziprasidone and b) N-debenzothiazole-3-ethylidene-ziprasidone.

ZIPR oxidised at the methylene carbon to form an isatin has been reported to undergo an aldol condensation with ZIPR to produce a dimer [478]. The possibility that ZIPR was oxidising in blood to produce a dimer was considered, as haemoglobin in blood has been postulated to cause

phenothiazines to oxidise [427, 428], and a proposed intermediate between oxyhaemoglobin and methemoglobin is purported to oxidise ethanol to acetaldehyde [476]. In this thesis, an increase in sulfoxide products was observed during experiments (6.3.6) and a sulfoxide was observed following extraction of a phenothiazine from blood that was not otherwise detected in neat standard analysis (4.3.4). It follows that if ZIPR is oxidised to form the isatin in blood that subsequent condensation between the isatin and other carbonyl compounds may be occurring. Ziprasidone-isatin (GMF for precursor ion of $[C_{21}H_{19}ClN_4O_2S]H^+$, calculated 427.0990 m/z), the dimer (GMF for precursor ion of $[C_{42}H_{38}Cl_2N_8O_2S_2]H^+$, calculated 821.2009 m/z, 411.1041 m/z for the $[M+2H]^{2+}$ ion), and a hypothesised N-debenzothiazole derivative of the dimer (GMF for precursor ion of $[C_{28}H_{32}Cl_2N_6O_2]H^+$, calculated 555.2037 m/z, 278.1055 m/z for the $[M+2H]^{2+}$ ion) were not detected in the blood experiments (Figure 9-22). None of the alkaline degradation products detected in the experiments in Chapter 5 were detected in any of the extracts of the blood specimens using the same LC-QTOF-MS analysis method.

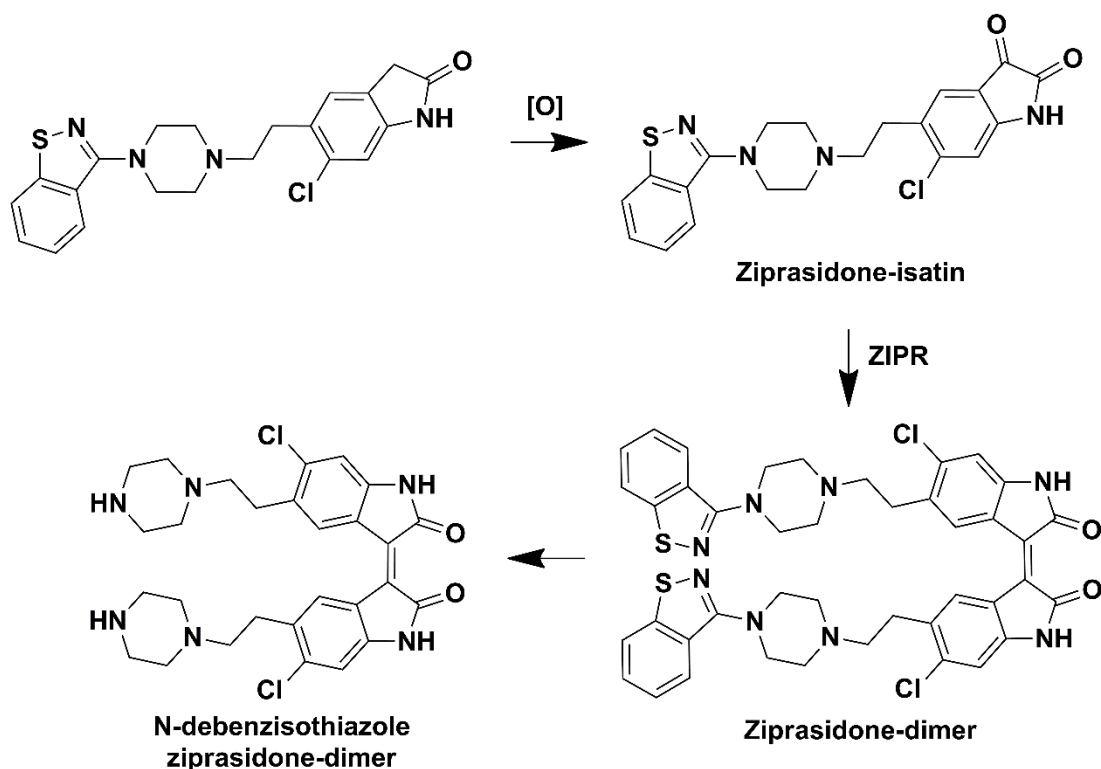


Figure 9-22: Structure and pathway of formation of hypothetical ZIPR species.

9.2.3.3 Fraction collection and LC-QTOF-MS analysis

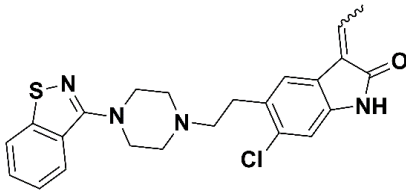
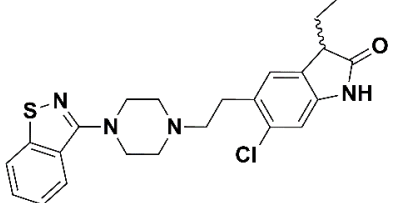
Manual fraction collection followed by LC-QTOF-MS analysis confirmed that the compounds responsible for the peaks appearing before and after AMIT in the LC-DAD method were those relating to the 439.135 m/z degradants described in 9.2.3.2.

9.2.4 Summary

Five ZIPR degradants were detected by LC-QTOF-MS analysis, two of which were also detected by LC-DAD analysis and hypothesised to be geometric isomers. These two degradants were previously regarded as possible ZIPR degradation products [223].

Based on relative responses, and detection by the LC-DAD method, the degradants of m/z 439.135 and 441.152 m/z were indicated to be the major ZIPR degradants. The degradation and formation of these degradants appear to be related processes. It was hypothesised that an aldol condensation between ZIPR and a carbonyl compound was catalysed in blood to produce 3E-ZIPR and that subsequent hydrogenation, seemingly caused by inoculated microorganisms, yielded 3A-ZIPR (Table 9-4). Accurate mass data, mass fragmentation data, and UV-Vis spectra supported the presumptive identification of the 439.135 m/z degradants as 3E-ZIPR isomers.

Table 9-4: Hypothesised ZIPR degradation products chemical information.

Name	Structure	Molecular formula	Exact mass (Da)
(E/Z) 3-ethylidene-ziprasidone (3E-ZIPR)		$C_{23}H_{23}ClN_4OS$	438.13
3-ethyl-ziprasidone (3A-ZIPR)		$C_{23}H_{25}ClN_4OS$	440.14

No precursor ions were detected that may have corresponded to degradants that 3E-ZIPR or 3A-ZIPR subsequently degraded to.

To test the hypothesised degradation product identities the experiments detailed in 9.3 and 9.4 were performed.

9.3 Deuterated ethanol experiment

In section 9.2 it was proposed that ZIPR was degrading in blood specimens by a reaction with acetaldehyde and that the acetaldehyde likely originated from oxidised ethanol used to spike the drugs. To test this hypothesis, a similar experiment to those in Chapter 6 was performed.

The critical difference was that, in place of ethanol, ethanol-d₆ was used to reconstitute the two drugs, ZIPR, and AMIT.

If ZIPR did degrade in the manner proposed it was expected that deuterated analogues of 3E-ZIPR would be detected. Assuming no hydrogen-deuterium exchanges, and the reaction of oxidised ethanol with ZIPR, a tetra-deuterated analogue would be the dominant species detected. However, acetaldehyde contains acidic hydrogens adjacent to the carbonyl which prior to reaction with ZIPR may undergo hydrogen-deuterium exchanges. This leads to the possibilities of forming mono- di- or tri-deuterated analogues (Table 9-5).

Table 9-5: Calculated molecular formulae and precursor ions for predicted deuterated analogues of 3-ethylidene-ziprasidone.

No. of deuterium	GMF precursor ion	Calculated [M+H] ⁺ (m/z)	Predicted fragments (m/z)
1	[C ₂₃ H ₂₂ DCIN ₄ OS]H ⁺	440.1417	158, 177 , 186, 193, 221
2	[C ₂₃ H ₂₁ D ₂ CIN ₄ OS]H ⁺	441.1479	159, 177 , 187, 194, 222
3	[C ₂₃ H ₂₀ D ₃ CIN ₄ OS]H ⁺	442.1542	160, 177 , 188, 195, 223
4	[C ₂₃ H ₁₉ D ₄ CIN ₄ OS]H ⁺	443.1605	161, 177 , 189, 196, 224

Ions in common across all structural isomers indicated in bold. GMF = generated molecular formulae.

The detection of deuterated degradation products would also provide information as to whether the degradants contain functionalities that may undergo hydrogen-deuterium exchanges with any deuterium introduced by ethanol-d₆ and, if oxidising, acetaldehyde-d₄.

9.3.1 Experimental

A mixed ZIPR and AMIT working solution was prepared at concentrations equivalent to those used in the Chapter 6 experiments (i.e. ZIPR: ~75µg/mL; AMIT: ~50µg/mL). Sodium fluoride (100 mg) was weighed into three of the six 5 mL sterile polystyrene Sarstedt tubes (Table 9-6). Ca. 5 mL of ante-mortem human whole blood (3.2.2.1) was then aliquoted into all tubes, using a sterile 20 mL Luer-Slip plastic syringe. Organic solvent was evaporated from the stock (4.5 mL) of ZIPR and AMIT under N₂ at 40 °C followed by reconstitution in ethanol-d₆ (750 µL). Drugs were spiked into the blood specimens using Luer-Slip plastic syringes with sterile 0.2 µm filters (100 µL). No microorganisms were inoculated into any blood specimens. Specimens were then vortexed, rolled on a mechanical roller (30 minutes at 25 rpm), and initial sub-samples collected and extracted as per the unbuffered LLE method (4.2.2). After extraction specimens were incubated at 37 °C in the dark.

Sub-samples were collected and extracted from specimens every day for four days, and then once more after the 7th day of incubation at 37 °C. Prior to sub-sampling specimens were rolled

on a mechanical roller (30 minutes at 25 rpm). After each sub-sampling specimens were once more incubated at 37 °C. Extracts were qualitatively analysed using an Agilent 1100 Series HPLC-DAD with instrumentation as detailed in 3.3.1 and conditions as detailed in 4.2.3, using the method B gradient program (Table 4-2). Extracts were diluted with 375 µL of ethanol prior to Agilent 6520 Series LC-QTOF-MS analysis (see 3.3.2 for instrument and condition details).

Table 9-6: Deuterated ethanol experiment design.

Sample type	Blood matrix	Sterile drugs				
Sample #	1	2	3	4	5	6
Preservatives				✓	✓	✓
Drugs		✓	✓	✓	✓	✓

MDF, set to a tolerance of ± 300 mDa, was used to screen for compounds in the LC-QTOF-MS data. MDF and MFE were previously described in 7.2.1.1 and 5.5.1, respectively. The response of the precursor ion for ZIPR (413.1190 m/z) and possible ZIPR deuterated degradation products (precursor ions: 440.1417, 440.1416, 443.1455, 443.1413, and 456.1367 m/z) were determined over time in all extracts, relative to the response of AMIT. MS/MS spectra were acquired for the precursor ions, where possible, at collision energies of 20, 30, and 40 eV. GMF and calculated accurate masses were determined for product ions.

9.3.2 Results

In the LC-DAD chromatograms, peaks were detected over time in extracts of the unpreserved blood specimens with striking similarity to the peaks corresponding to the 439.135 m/z degradants (Figure 9-23). The lower response obtained for the deuterated compounds may have impacted absorbance at the lower wavelengths.

Three compounds were detected by MDF of the LC-QTOF-MS data. Precursor ions for each compound were: 440.1417, 440.1416, and 456.1367 m/z. It can be seen that the 440.142 m/z ions eluted at the same time as the 439.135 m/z ions in the non-deuterated experiment, and the major 456.137 m/z ion at the same time as the major 455.132 m/z ion in the non-deuterated experiment (Figure 9-9 and Figure 9-24). In the non-deuterated experiment, 455.132 m/z was noted to appear as up to three resolved peaks. The detected compound in the deuterated experiment, 456.137 m/z, had similar minor peaks either side of the major peak. GMF were consistent with the identity of the 440.142 m/z and 456.137 m/z ions as monodeuterated analogues of 439.135 m/z and 455.132 m/z (Table 9-7). Predicted isotope ratios for these precursor ions are shown in Figure 9-25.

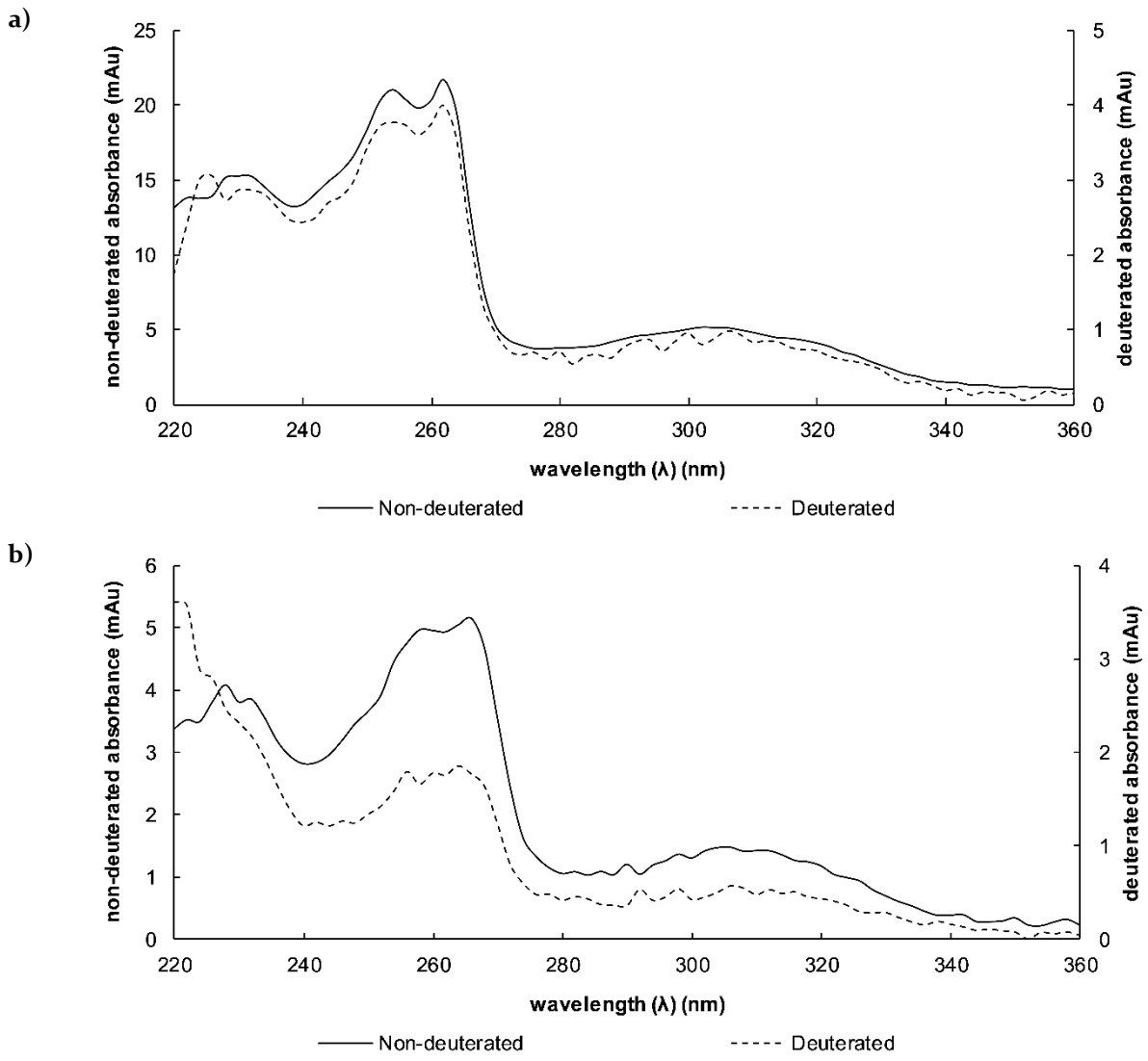


Figure 9-23: UV-Vis absorbance spectra of additional peaks observed in deuterated experiment compared to a) early eluting 439.135 m/z peak and b) later eluting 439.135 m/z peak observed in non-deuterated experiments.

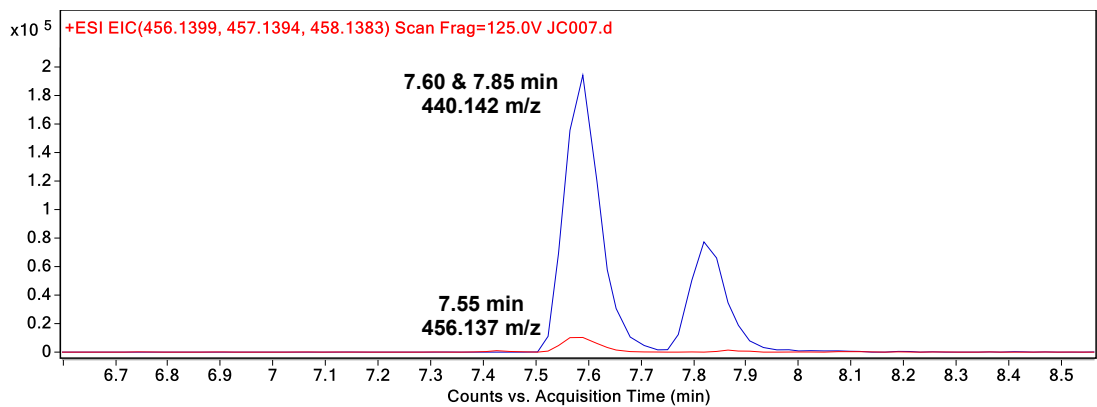


Figure 9-24: Extracted ion chromatograms of suspected deuterated degradants of ZIPR.

Table 9-7: MS data for deuterated degradants of ZIPR.

Analyte	Measured [M+H] ⁺ (m/z)	Calculated [M+H] ⁺ (m/z)	GMF precursor ions	Mass accuracy (δ) (ppm)	Mass accuracy (δ) (mDa)
440.142 m/z at 7.60 min	440.1417	440.1417	[C ₂₃ H ₂₂ DCIN ₄ OS]H ⁺	0	0
440.142 m/z at 7.85 min	440.1428	440.1417	[C ₂₃ H ₂₂ DCIN ₄ OS]H ⁺	-2.5	-1.1
456.137 m/z	456.1373	456.1366	[C ₂₃ H ₂₂ DCIN ₄ O ₂ S]H ⁺	-1.5	-0.7

GMF = generated molecular formulae. Mass accuracies determined from single injection.

As with the 439.135 m/z and 455.132 m/z degradants, it appears that in the deuterated experiments 440.142 m/z and 456.137 m/z formed as ZIPR degraded and then themselves subsequently degraded (Figure 9-26). An MS peak with accurate mass and retention time consistent with 439.135 m/z and 455.132 m/z was detected, however, no auto-MS/MS spectra were acquired from any of the extracts.

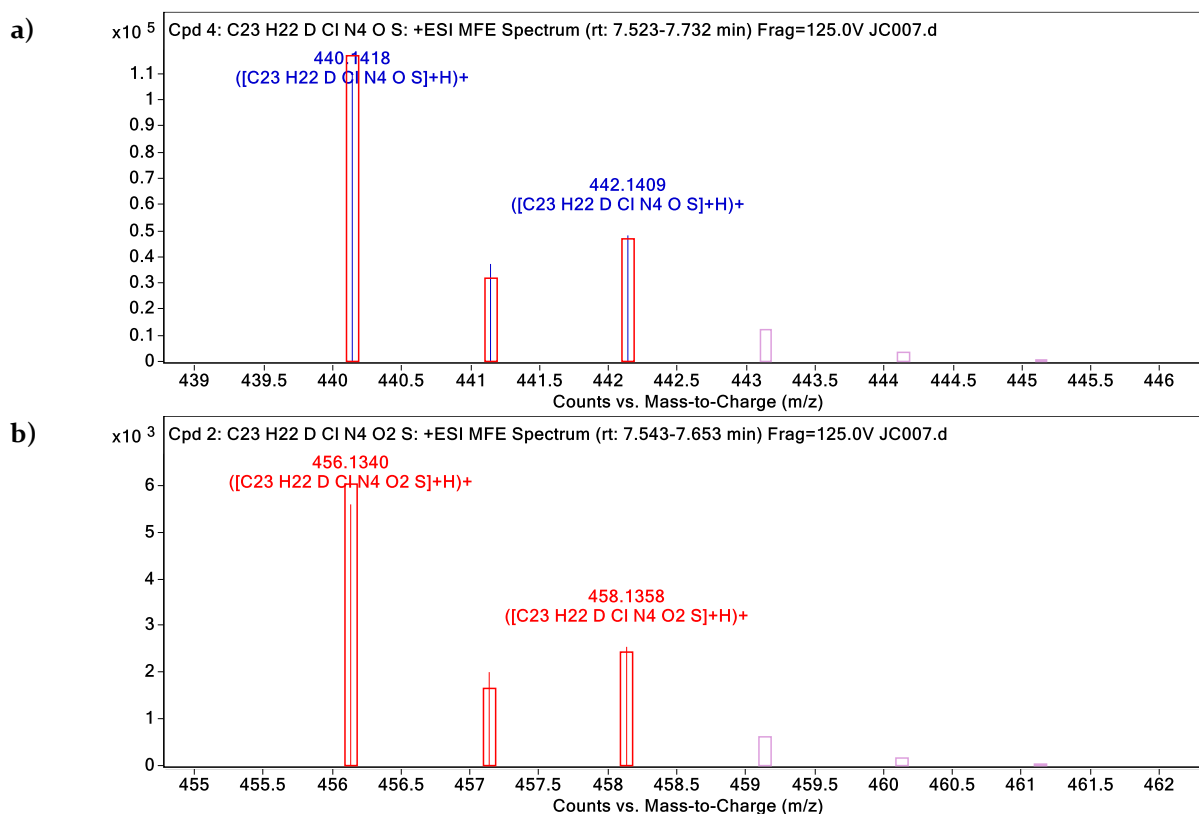


Figure 9-25: MS spectra with generated molecular formula showing predicted isotope ratios in red boxes for degradants of m/z a) 440.142 and b) 456.137.

Observed ion responses are shown as lines within the boxes.

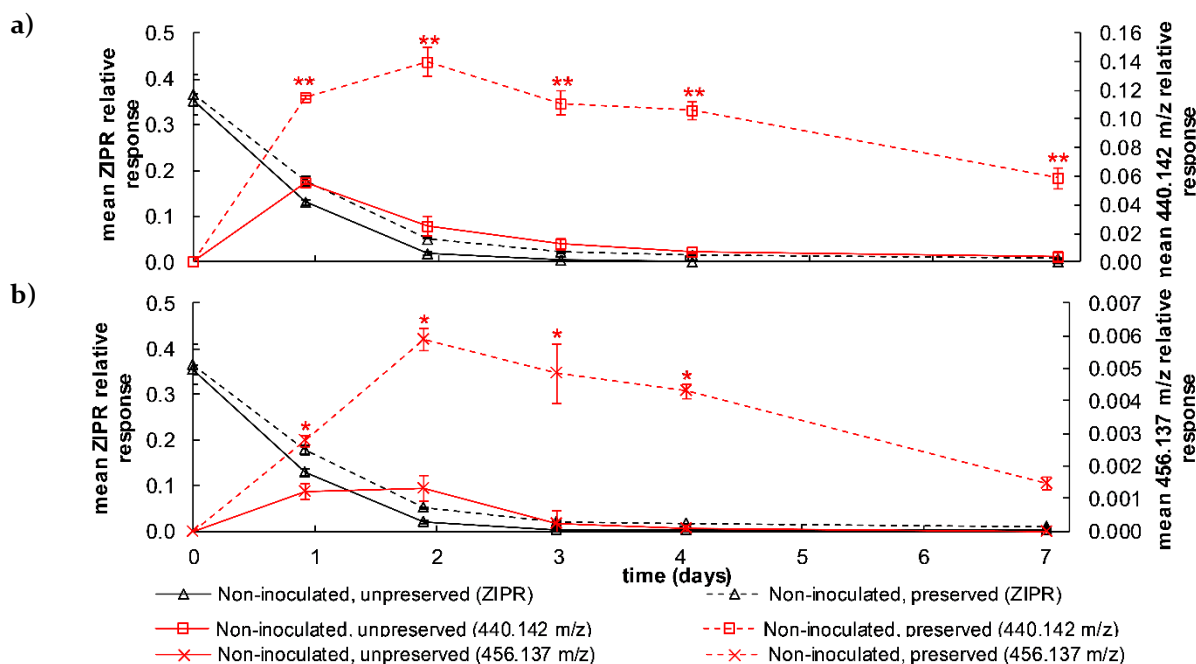


Figure 9-26: Relative response of ZIPR and degradants of m/z a) 440.142 and b) 456.137 over time in preserved and unpreserved, non-inoculated blood specimens for deuterated experiment.

Asterisks indicate the acquisition of MS/MS spectra for degradation products. Error bars are \pm S.D., $n = 2$ for unpreserved and $n = 3$ for preserved specimens.

The product ion at 177.0481 m/z was common amongst all ZIPR degradants (Table 9-3) and all deuterated degradants, as predicted (Figure 9-27). GMF for fragment ions produced acceptable mass accuracies as deuterated analogues of the 439.135 m/z fragments (Table 9-8). The measured mass difference between the 439.135 m/z and 440.142 m/z degradants and the 455.132 m/z and 456.137 m/z degradants ranged from 1.0023-1.0065 Da, affording a mass accuracy of -0.2 – 4.0 mDa if the difference is attributable to a deuterium atom (calculated mass difference between H and D of: 1.0063 Da). This supported the identity of the 440.142 m/z and 456.137 m/z degradants in the deuterated experiments as deuterated analogues of the 439.135 m/z and 455.132 m/z degradants. The mass difference between the product ions of the 439.135 m/z (220, 192, 185, 157 m/z) and 440.142 m/z (221, 193, 186, and 158 m/z) degradation products ranged from 1.0010-1.0100 Da (mass difference compared to a calculated mass of 1.0063 = -3.7 – 5.3 mDa). The mass difference between the product ions of the 455.132 m/z (236 and 194 m/z) and 456.137 m/z (237 and 195 m/z) degradation products ranged from 0.9953-1.0134 Da (mass difference compared to a calculated mass of 1.0063 = -7.1 – 11.0 mDa). These results indicate that deuteration is occurring on the oxindole moiety of the ZIPR degradation products. However, product ion mass accuracies were poor for the 456.137 m/z compound, possibly due to the low intensity of the ions.

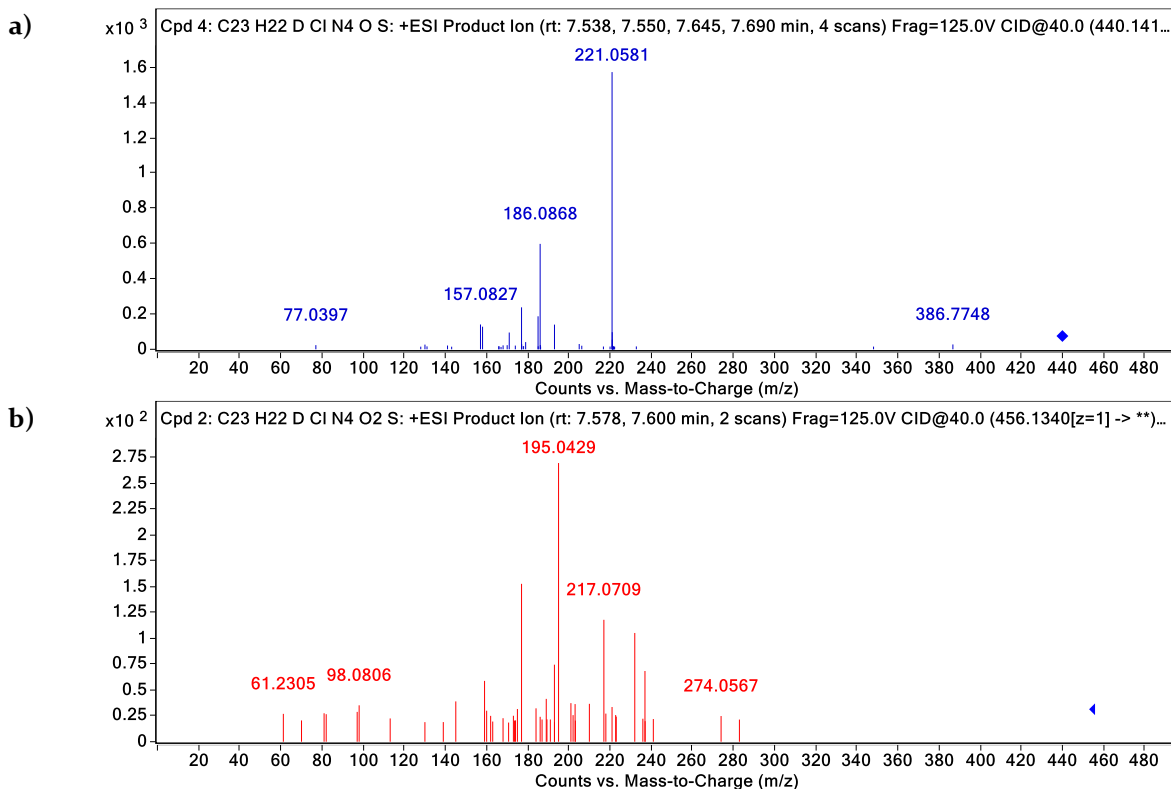


Figure 9-27: MS/MS spectra for degradants of m/z a) 440.142 and b) 456.137. Collision energy = 40 eV.

Table 9-8: MS/MS data for deuterated degradants of ZIPR.

Analyte	Precursor ion (m/z)	Product ions (m/z)	GMF product ions	Calculated accurate mass (m/z)	Mass accuracy (δ) (ppm)	Mass accuracy (δ) (mDa)
440.142 m/z at 7.60 min	440.1417	158.0933	C ₁₁ H ₁₀ DN	158.0949	10.1	1.6
		177.0467	C ₉ H ₉ N ₂ S	177.0481	7.9	1.4
		186.0885	C ₁₂ H ₁₀ DNO	186.0898	7.0	1.3
		193.0616	C ₁₁ H ₁₀ DCIN	193.0637	10.9	2.1
		221.0584	C ₁₂ H ₁₀ DCINO	221.0586	0.9	0.2
		440.1405	[C ₂₃ H ₂₃ DCIN ₄ OS]H ⁺	440.1417	2.7	1.2
440.142 m/z at 7.85 min	440.1416	158.0921	C ₁₁ H ₁₀ DN	158.0949	17.7	2.8
		177.0461	C ₉ H ₉ N ₂ S	177.0481	11.3	2.0
		186.0889	C ₁₂ H ₁₀ DNO	186.0898	4.8	0.9
		193.0632	C ₁₁ H ₁₀ DCIN	193.0637	2.6	0.5
		221.0578	C ₁₂ H ₁₀ DCINO	221.0586	3.6	0.8
		440.1401	[C ₂₃ H ₂₃ DCIN ₄ OS]H ⁺	440.1417	3.6	1.6
456.137 m/z	456.1340	177.0464	C ₉ H ₉ N ₂ S	177.0481	9.6	1.7
		195.0429	C ₁₀ H ₈ DCINO	195.0430	0.5	0.1
		237.0590	C ₁₂ H ₁₀ DCINO ₂	237.0536	-22.8	-5.4
		456.1277	[C ₂₃ H ₂₃ DCIN ₄ O ₂ S]H ⁺	456.1366	19.5	8.9

Ions shared between each compound are indicated in bold. GMF = generated molecular formula. Mass accuracies determined from single injection.

In ZIPR, the only hydrogens readily exchangeable with deuterium are the two acidic hydrogens on the methylene carbon adjacent to carbonyl in the oxindole moiety [479]. In theory, the hydrogen of the amide is also able to undergo H-D exchange, as this proton reportedly also has a similar pKa value of ~18 [469, 470]. In practice, treatment of a ZIPR precursor containing the oxindole moiety with D₂SO₄ and D₂O results in exchange only at the acidic hydrogens adjacent to the carbonyl [479]. Czarnik also claimed that while the amide hydrogen may exchange with deuterium under physiological conditions it is also expected to readily exchange back [479]. Supporting this, deuterated analogues of ZIPR (d₁ and d₂) (GMF for precursor ions of [C₂₁H₂₀DCIN₄OS]H⁺ and [C₂₁H₁₉D₂CIN₄OS]H⁺, with respective calculated precursor ions of 414.1260 and 415.1323 m/z), were not detected in initial extracts in the deuterated experiment.

In light of this, there are only two ways a mono-deuterated product may be produced: i) a deuterium-enriched species has reacted with ZIPR and resulted in elimination of both acidic hydrogens at the methylene group; or ii) a species has reacted with ZIPR and eliminated one acidic hydrogen at the methylene group (e.g. by an alkylation reaction), leaving the other able to exchange with deuterium. The latter possibility was considered when postulating structures for the 439.135 m/z degradants (3-vinyl-ziprasidone: Figure 9-17 (b)). However, no precursor ions indicative of dialkylated products were detected and UV-Vis spectra indicated the 439.135 m/z degradants had a more extensive system of π-conjugated bonds compared to ZIPR.

If the 439.135 m/z degradants are formed between the reaction of acetaldehyde and ZIPR and if it is 3E-ZIPR then exogenous acetaldehyde derived from ethanol-d₆ could be the source, provided hydrogen-deuterium exchange of all acidic hydrogens in acetaldehyde occurs prior to reaction (i.e. acetaldehyde-d would be the reactive species). If the degradation of ZIPR does not involve acetaldehyde, and 3E-ZIPR is the correct identity of the 439.135 m/z degradants, then degradation must involve an adduct which exchanges with deuterium before a fragment elimination from ZIPR.

Of the proposed structures for the identity of the 455.132 m/z degradant (Figure 9-20) 3-acetyl-ziprasidone or 3E-ZIPR sulfoxide are most probable given the detection of a mono-deuterated analogue. In the former structure the hydrogen of the alcohol would be able to exchange with deuterium in the blood matrix and in the latter the deuterium would have been incorporated in the prior formation of 3E-ZIPR-d.

9.4 Solvent reactivity

In section 9.3 it was proposed that acetaldehyde may react with ZIPR to produce 3E-ZIPR. One proposed identity for a degradant giving a mass of 455.132 m/z was also ZIPR acetylated at the oxindole moiety. To test these hypotheses, the reactivity of ZIPR toward solvents was qualitatively assessed using both the LC-DAD and LC-QTOF-MS methods. ZIPR was tested for reactivity with absolute ethanol, acetaldehyde, glacial acetic acid, and acetone. The first three are related in series by oxidation of ethanol. Acetone was also tested as its mechanism of reaction with ZIPR was expected to be the same as acetaldehyde. If so, a 3-(propan-2-ylidene)-ziprasidone degradant would be detected (calculated precursor ion of 453.1510 m/z from GMF of $C_{24}H_{25}ClN_4OS$) (Figure 9-28). This compound is also an impurity of ZIPR [480] but was not detected in analyses of diluted drug stocks in this thesis.

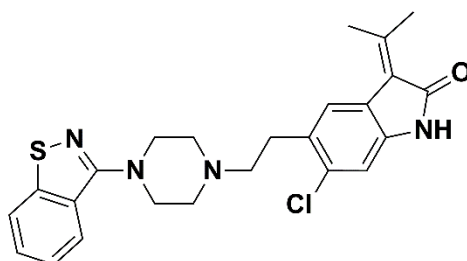


Figure 9-28: Hypothesised product following the reaction of ZIPR with acetone (3-(propan-2-ylidene)-ziprasidone).

To preclude cross reactions the LORA IS was not included in these experiments. Therefore, although retention times of any detected degradation products were noted other information such as UV-Vis spectra and MS/MS data were used for identification purposes.

9.4.1 Experimental

9.4.1.1 Week experiment

In triplicate, methanol working solution of ZIPR was spiked into clear autosampler vials and solvent (500 μ L) added to give a final concentration for ZIPR of ~ 5 μ g/mL. Vials were then placed in the dark at room temperature for seven days before analysis using an Agilent 1100 Series HPLC-DAD with instrumentation as detailed in 3.3.1 and conditions as detailed in 4.2.3, using the method B gradient program (Table 4-2). Concurrently, aliquots were diluted 5-fold with solvent prior to Agilent 6520 Series LC-QTOF-MS analysis (see 3.3.2 for instrument details).

9.4.1.2 Short acetaldehyde experiment

The reaction of acetaldehyde with ZIPR was also monitored over a shorter time. In this experiment, methanol working solution of ZIPR was spiked into three clear autosampler vials

and acetaldehyde (500 μL) added to each to give a final concentration for ZIPR of $\sim 10 \mu\text{g/mL}$. From these solutions, an 8-fold dilution in acetaldehyde was performed to prepare a triplicate set of ZIPR solutions at $\sim 1.1 \mu\text{g/mL}$. The more concentrated ZIPR solutions were analysed by the LC-DAD method detailed above, and the lesser concentrated solutions by the LC-QTOF-MS method. Solutions were injected repeatedly over a period of 23 hours for LC-DAD analysis and 40 hrs for LC-QTOF-MS analysis.

9.4.2 Results

9.4.2.1 Week experiment

After seven days, ZIPR was detected in all solutions by LC-DAD analysis, except for those in which acetaldehyde was present. In the acetaldehyde solutions, a small peak eluting 1.3 min after the second 439.135 m/z degradant peak in blood specimens was detected. The absorbance spectra of the tentatively identified degradant and product between ZIPR and acetaldehyde were similar, with two λ_{max} around 255 and 265 nm, suggesting a similar chromophore may be present (Figure 9-29). No other products were detected by LC-DAD analysis in any other solutions.

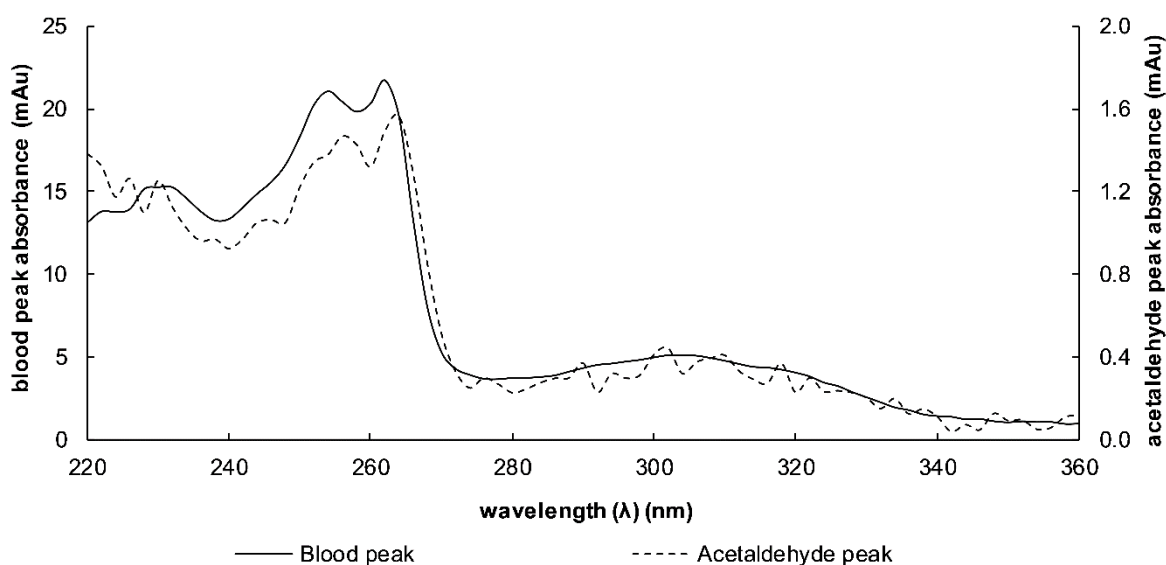


Figure 9-29: UV-Vis absorbance spectra of 439.135 m/z peak in blood and peak detected in week-long acetaldehyde experiment.

Ethanol solutions were analysed using LC-QTOF-MS. Auto-MS/MS spectra were acquired for a precursor ion of 439.1353 m/z. Retention time and MS/MS spectra matched the 439.135 m/z degradants hypothesised to be 3E-ZIPR (Figure 9-15 (b)). The mean ratio of 439.135 m/z to ZIPR

was determined to be 0.02 ± 0.004 . This was comparable to the 439.135 m/z/ZIPR ratios observed in the calibrators and QCs and considerably less than the maximum observed in the blood specimens during the first week experiment (Table 9-1).

ZIPR was not detected in acetaldehyde solutions, nor was a precursor ion of 439.135 m/z (at any retention time). A variety of possible ZIPR degradation products were detected (see 9.4.2.3).

The hypothesised degradant (Figure 9-28) from the aldol condensation of ZIPR and acetone was not detected in acetone solutions. Instead, a different set of ZIPR-derived compounds were detected (see 9.4.2.4).

9.4.2.2 Short acetaldehyde experiment

A summary of peaks observed in the LC-DAD data and their UV-Vis spectra is provided (Table 9-9 and Figure 9-30).

Table 9-9: Summary of LC-DAD chromatogram data in short acetaldehyde experiment.

Time since ZIPR spiked	Peaks first detected (min)	UV-Vis spectra observations
Initial analysis	10.9	Similar λ_{\max} to ZIPR
	16.4	λ_{\max} around 330-340 nm
2 hours	14.0	Similar λ_{\max} to ZIPR
	19.0	λ_{\max} around 330-340 nm
6 hours	15.7	Similar λ_{\max} to ZIPR
8 hours	1.5	λ_{\max} around 220 nm
	19.8	

ZIPR was only detected in the initial analysis by LC-DAD, indicating degradation below the LOD within 2 hours. The two 439.135 m/z degradants were found to have retention times in the LC-DAD method of 13.9 and 15.1 min and λ_{\max} at 250-270 nm (see Figure 8-2 for UV-Vis spectra). Based on UV-Vis spectra, no peaks between the short acetaldehyde experiment and the blood experiment were in common.

For the LC-QTOF-MS analyses, no MS/MS spectra were acquired for ZIPR ~80 minutes after spiking ZIPR into acetaldehyde. The 429.115 m/z degradant suspected to be ZIPR-SO was detected from the first analysis until ~9 hours. After ~3 hours, two suspected ZIPR-derived compounds were detected (see 9.4.2.3) but a compound with $[M+H]^+=439.135$ m/z was not detected at any retention time.

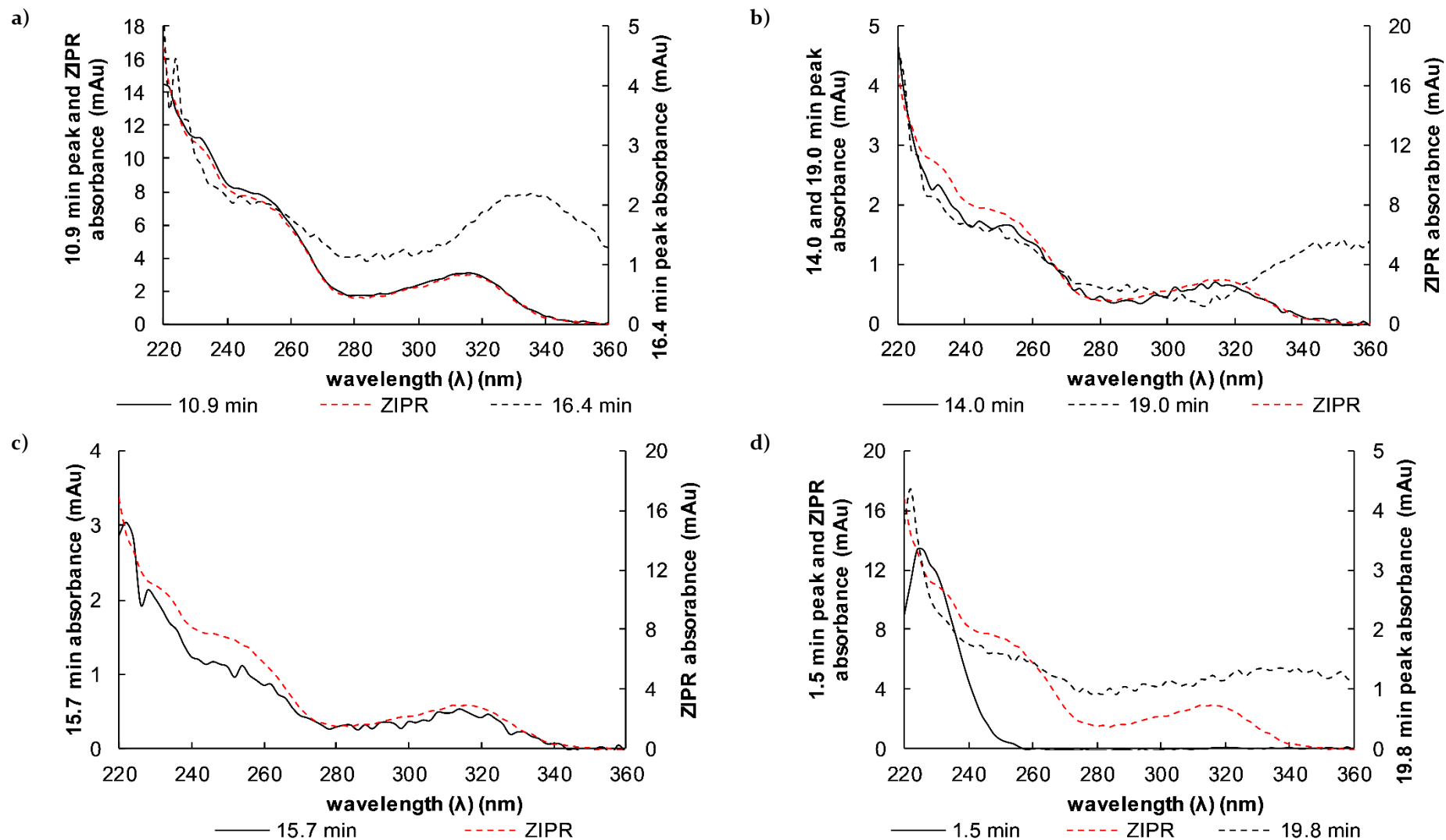


Figure 9-30: UV-Vis absorbance spectra of peaks detected during a) initial analyses, b) after two hours, c) after six hours, and d) from ten hours. ZIPR shown for comparison only.

9.4.2.3 Acetaldehyde reaction products

In the short experiment, precursor ions 473.1396 and 517.1660 m/z were detected three hours into the experiment and remained detected until ~37 hours. In the week-long experiment, precursor ions 561.1902 and 605.2191 m/z were detected in two and one replicate (out of a total of three replicates), respectively. All compounds eluted after ZIPR (Table 9-10).

GMF indicate that successive additions of C₂H₄O (calculated accurate mass of 44.0262 Da) occurred (Table 9-10). This corresponds to the molecular formula of acetaldehyde and therefore it appears acetaldehyde forms an adduct or adducts with ZIPR. These compounds were not detected in any extracts of the blood specimens from the Chapter 6 experiments.

All acetaldehyde-derived compounds were observed to have a major product ion at ~232.0900 m/z (data not shown). This is in common with the 429.115 m/z degradant thought to be ZIPR-SO (Figure 9-16) and therefore it may be that the sulfoxide is formed prior to reaction with acetaldehyde.

Table 9-10: LC-QTOF-MS data for acetaldehyde degradants of ZIPR.

Analyte m/z	Retention time (min)	Measured [M+H] ⁺ (m/z)	Calculated [M+H] ⁺ (m/z)	GMF precursor ion	Mass accuracy (δ) (ppm)	Mass accuracy (δ) (mDa)
473.140 m/z	7.55	473.1396	473.1409	[C ₂₃ H ₂₅ ClN ₄ O ₃ S]H ⁺	2.7	1.3
517.166 m/z	7.80	517.1664	517.1671	[C ₂₅ H ₂₉ ClN ₄ O ₄ S]H ⁺	1.4	0.7
561.190 m/z	7.45	561.1902	561.1933	[C ₂₇ H ₃₃ ClN ₄ O ₅ S]H ⁺	5.5	3.1
605.219 m/z	7.60	605.2191	605.2195	[C ₂₉ H ₃₇ ClN ₄ O ₆ S]H ⁺	0.7	0.4

GMF = generated molecular formulae. Mass accuracies determined from single injection.

9.4.2.4 Acetone reaction products

In the week-long experiment, the precursor ion 471.1614 m/z was detected in all three replicates. In one replicate, the precursor ions 443.1302 and 457.1455 m/z were also detected. The hypothesised 3-(propan-2-ylidene)-ziprasidone degradant (Figure 9-28) was not detected.

The mass differences between the ZIPR-derived acetone degradant precursor ions were 14.0153 and 14.0159 Da. This corresponds to a methylene group (calculated accurate mass of 14.0157 Da, δ = -0.2 – 0.4 mDa). GMF indicated this also (Table 9-11).

Table 9-11: MS data for acetone degradants of ZIPR.

Analyte m/z	Retention time (min)	Measured [M+H] ⁺ (m/z)	Calculated [M+H] ⁺ (m/z)	GMF precursor ion	Mass accuracy (δ) (ppm)	Mass accuracy (δ) (mDa)
443.130 m/z	6.88	443.1302	443.1303	[C ₂₂ H ₂₃ ClN ₄ O ₂ S]H ⁺	0.2	0.1
457.147 m/z	7.17	457.1455	457.1460	[C ₂₃ H ₂₅ ClN ₄ O ₂ S]H ⁺	1.1	0.5
471.162 m/z	7.35	471.1614	471.1616	[C ₂₄ H ₂₇ ClN ₄ O ₂ S]H ⁺	0.4	0.2

GMF = generated molecular formulae. Mass accuracies determined from single injection.

9.4.3 Summary

The detection of the 439.135 m/z degradants in ethanol solutions of ZIPR and the non-detection of them in acetaldehyde solutions does not support the hypothesis put forth that the proposed identity of 439.135 m/z is 3E-ZIPR and that this degradant forms from the reaction between acetaldehyde and ZIPR. The only way this hypothesis holds is if trace levels of acetaldehyde in ethanol react with ZIPR in a different manner to neat acetaldehyde. Similarly, the expected analogous reaction between ZIPR and acetone to form 3-(propan-2-ylidene)-ziprasidone (Figure 9-28), has not taken place in neat acetone.

Table 9-12: Overview of ZIPR and solvent reactivity.

Solvent	LC-DAD analysis	LC-QTOF-MS analysis	
	ZIPR detected?	ZIPR detected?	Degradants?
Ethanol	✓	✓	439.135 m/z detected
Acetaldehyde	✗	Undetected after ~80 minutes	439.135 m/z not detected Other degradants detected
Acetic acid	✓	✓	439.135 m/z not detected
Acetone	✓	✓	439.135 m/z not detected Other degradants detected

Extracts from blood experiments are reconstituted in ethanol before analysis. Therefore, it is possible that some degree of pre-analytical transformation of ZIPR to the 439.135 m/z degradants may be occurring. This may explain the presence of trace amounts of 439.135 m/z degradation products in calibrators and QCs and in -20 °C blood specimen extracts (Figure 7-3).

Both acetone and acetaldehyde were found to react with ZIPR by what appears to be multi-step reactions imparting the same increase in mass. The identity of these products is unknown and further work is outside the scope of this project.

9.5 Post-mortem casework analysis

Approval to re-analyse data files of cases where ZIPR was reported as present by staff at FSSA was obtained as previously described (see 1.7.3).

9.5.1 Data analysis

De-identified autopsy and toxicology details were supplied for cases from 2016-2018 analysed at FSSA where ZIPR was reported. The non-refrigerated interval (NRI) between the date of death and body storage in 4 °C fridges at the mortuary was determined and any toxicology or pathology comments regarding putrefaction noted.

An alkaline LLE followed by analysis using an Agilent 6545 LC-QTOF-MS in auto-MS/MS mode was employed for the initial analysis of these cases. Due to the absence of commercially available standards, ZIPR degradation products were considered present in casework samples if precursor and product MS/MS ions agreed with those previously reported (see Table 9-3). The ratio of the MS peak area of each detected degradation product to ZIPR was calculated.

9.5.2 Results and discussion

Two cases were identified from 2016-2018 in which ZIPR was reported (Table 9-13). Both cases had NRIs greater than 3 days. However, the only ZIPR degradant detected was one peak of the 439.135 m/z degradant, and only in one case (Case B). This identification was made based on retention time and precursor ion alone, as no auto-MS/MS spectra were acquired to verify if the detected 439.135 m/z ion was the 3E-ZIPR degradation product postulated. Case B showed signs of putrefaction, and, perhaps because of this, 439.135 m/z may have already degraded to the 441.152 m/z degradant when analysed. However, no ion at 441.152 m/z was detected. An approximately ten-fold lower concentration of ZIPR was reported in Case B compared to Case A, which may be indicative of greater post-mortem degradation in Case B. However, many other variables may be the cause of low ZIPR concentrations and any comparison between the cases is flawed without detailed knowledge of case circumstances.

Among the two cases retrospectively analysed, Case B was noted to have ethanol present at a level of 0.08 mg/dL, whereas ethanol was not detected in Case A. Given the hypothesised mechanism of formation of the 439.135 m/z degradants involves ethanol oxidising to

acetaldehyde which then reacts with ZIPR it would be of interest to determine if ethanol ingestion is correlated with 439.135 m/z detection in future cases analysed.

Table 9-13: Case details for post-mortem cases with ZIPR detected.

Case	NRI* (days)	Putrefaction?	ZIPR area	439.135 m/z area	Ratio (439.135 m/z/ZIPR)	MS/MS of 439.135 m/z acquired
A	3	No	127894	0	N/A	N
B	7	Yes - PEA detected	26966	5145	0.19	N

*Non-refrigerated interval (time between death and body refrigeration at mortuary). PEA = phenylethylamine. The minimum area for detection was 5000 counts.

9.6 Conclusions

Five ZIPR degradation product candidates were detected in the blood experiments. Most were observed to be transient, initially increasing in response before then decreasing over time (see 9.2.2.1). None were observed in prior aqueous stability experiments involving ZIPR (Chapter 5). Except for the 429.115 m/z degradant, which was presumptively identified as ZIPR-SO, no publications have before reported these compounds.

The results suggest that ZIPR is transformed at the oxindole moiety. From the deuterated ethanol experiment it was established that the 439.135 m/z and 455.132 m/z ZIPR degradation products were enriched with one deuterium atom during formation. The possibility that H-D exchange was occurring following formation was considered but was not consistent with the structural possibilities for the 439.135 m/z degradants based on their GMF and UV-Vis spectra. The hypothesis that *E/Z* isomers of 3E-ZIPR are formed from exogenous acetaldehyde in the blood experiments following ethanol oxidation was supported, although an aldol reaction with a larger carbonyl that fragments was not decisively excluded. It appears that the identity of the 455.132 m/z degradation product may be either 3-acetyl-ziprasidone or a sulfoxide of 3E-ZIPR.

3E-ZIPR also appears to be present as an artefact of the analytical method, due to either reconstitution of extracts in ethanol, the use of ethanol to spike drugs into blood specimens, or a combination of both. However, an ethanolic solution of ZIPR prepared one week before LC-QTOF-MS analysis only detected traces of 3E-ZIPR compared to the quantity present in the experimental blood specimens. Solutions of ZIPR and acetaldehyde were also monitored over time by LC-DAD and LC-QTOF-MS and the 439.135 m/z degradation products were not detected. From this, it was postulated that in neat acetaldehyde a different pathway of degradation occurs. The demonstrated reactivity of ZIPR with simple carbonyl compounds

highlights the possibility of its instability in formalin solutions and therefore the detection of ZIPR in embalmed cases may also be compromised.

Based on $[M+H]^+$ precursor ion and MS/MS product ion shifts it appears that 3E-ZIPR is hydrogenated to yield 3A-ZIPR. 3E-ZIPR, 3A-ZIPR, and the 455.132 m/z degradation product all degrade further in an unknown manner. Both 3E-ZIPR and 3A-ZIPR formation and degradation proceeded at a significantly greater rate in inoculated, unpreserved specimens. It could also be that 455.132 m/z formation and degradation is similarly rapid in inoculated, unpreserved specimens compared to other blood specimens. This would explain the absence of acquired MS/MS spectra for the 455.132 m/z degradant in extracts of those specimens. However, it is also not possible to exclude that the environment in inoculated, unpreserved specimens may be non-conducive toward the degradation of ZIPR to the 455.132 m/z product as detection of 455.132 m/z was not supported by MS/MS data. Another possibility is that the presence of coeluting matrix compounds in the inoculated, unpreserved specimens is lowering the response of the 455.132 m/z ion due to ion suppression.

The greater rates of 3E-ZIPR and 3A-ZIPR formation and degradation observed in inoculated, unpreserved blood specimens may be partially attributed to microbial activity. There is evidence that 3-alkylideneoxindoles may be hydrogenated by yeast [477], and furthermore, the dominant microorganism in the blood specimens during the week-long experiments, *C. perfringens*, is known to hydrogenate alkenes [262]. This microorganism is also known to synthesis ethanol [22], which appears to contribute to 3E-ZIPR formation.

The seven-month experiment in this thesis found almost complete degradation of ZIPR after ~21 weeks. This is similar to the results of Saar *et al.*, who tested ZIPR stability in unpreserved ante-mortem human whole blood [291]. Saar *et al.* used methanol to spike drugs into blood. Therefore, absent external ethanol in blood, ZIPR still degrades. However, no details were provided by Saar *et al.* regarding attempts to identify any ZIPR degradation products.

ZIPR does not appear to degrade in blood to produce a compound with mass differences between parent and degradant similar to LURA and ND-LURA. This was true even in inoculated, unpreserved specimens, where the production of the suspected ND-LURA degradation product was greatest (Chapter 8).

ZIPR was infrequently reported in casework analysed at FSSA over the period in which ethics approval was obtained for retrospective data analysis. A precursor ion of 439.135 m/z was detected in only one of two cases, and without auto-MS/MS spectra acquisition to support its

identity as the proposed 3E-ZIPR degradant. Therefore, due to limited data from casework, the significance of the discovered ZIPR degradation products remains unclear.

CHAPTER 10 - CONCLUSIONS AND FUTURE WORK

10.1 Conclusions

This thesis examined the stability of 17 prescription psychoactive drugs in human whole blood spiked with human faecal microbiota transplant (FMT) slurries, modelling the post-mortem environment of blood. Analytical methods using LC-DAD were developed and validated to be fit for purpose (Chapter 4), allowing for quantification of the drugs in human whole blood and assessment of their susceptibility to microbial degradation (Chapter 6). LC-QTOF-MS was used to analyse experimental extracts qualitatively and identify potential degradation products that may be forming for any drugs found to degrade. The identity of potential hydrolytic degradation products of these drugs was established to determine if drugs may be hydrolysing in the blood specimens, rather than microbially degrading (Chapter 5). Additionally, control specimens were also prepared without the FMT spiked, to determine whether observed degradation in inoculated specimens may be primarily attributed to microbial activity.

Lurasidone and risperidone were found to be unstable to numerous freeze-thaw cycles (from storage at -20 °C) during method validation. Therefore, for laboratories testing for these drugs it is advised that specimens are not stored at -20 °C. If this is unavoidable (*e.g.* due to instability risks at higher temperatures for other drugs) then paired specimens should be collected, with one used for screening and the other for quantification, to minimise the number of freeze-thaw cycles LURA experiences.

The dominant species detected by 16S rRNA sequencing in specimens unpreserved and incubated at 37 °C were consistent with species that have been detected in post-mortem blood, supporting the suitability of the method. Further support for this experimental approach was achieved by including a drug known to microbially degrade in post-mortem specimens as a control, with its bacterial degradation product detected by the LC-DAD and LC-QTOF-MS methods utilised.

Overall, the experiments performed in this thesis established that for aripiprazole, asenapine, chlorpromazine, clomipramine, clozapine, dothiepin, flupentixol, fluphenazine, haloperidol, mirtazapine, moclobemide, periciazine, prochlorperazine, quetiapine and trifluoperazine no degradation products are required to be screened for their analysis in post-mortem blood as

they did not significantly degrade in the post-mortem blood model (Chapter 6). However, there is evidence that post-mortem redistribution may affect post-mortem femoral blood concentrations of chlorpromazine and clozapine [78], flupentixol [80], and mirtazapine [79]. Therefore, while they are not expected to degrade to undetectable levels in post-mortem blood, any quantitative results may not be representative of those peri-mortem. For drugs such as haloperidol and quetiapine, where post-mortem redistribution does not appear to influence post-mortem femoral blood concentrations [78], it is expected they will have comparable stability to that observed for them in the blood experiments, unless any conjugated metabolites (such as haloperidol glucuronide [481]) convert back to elevate parent drug concentrations.

Interestingly, the storage of blood specimens at 4 °C appeared to reduce rates of N-dealkylation degradation product and oxidative degradant formation and chlorpromazine, fluphenazine, prochlorperazine, and flupentixol degradation (Chapter 7). However, it cannot be advised that blood specimens be stored at 4 °C in preference to -20 °C as that may compromise the stability of other analytes.

The potential for the antipsychotic lurasidone (LURA) to degrade by microbial activity was strongly supported by its degradation in the same blood specimens in which the microbial control drug, risperidone, was found to degrade to its bacterial degradation product.

High resolution mass spectrometry of lurasidone's major degradation product ($[M+H]^+ = 360.265$ m/z) indicated that the 1,2-benzisothiazole moiety, as expected if degradation followed the same pathway as risperidone, was not present in the degradation product. However, LC-QTOF-MS retention time comparisons to synthesised standards of *E/Z*-N-debenzisothiazole-lurasidone revealed that this degradant was not N-debenzisothiazole-lurasidone. Nevertheless, the unknown degradant was detected in retrospectively analysed case instrument data of authentic post-mortem casework specimens for cases both with and without signs of putrefaction, further supporting the environment of the experimental blood specimens as suitably simulating the post-mortem environment (Chapter 8). Greater ratios of the degradation product to LURA were evident in putrefied cases compared to cases without putrefaction with the same non-refrigerated intervals. This provided limited evidence that microorganisms in the specimens may be responsible for the degradation of LURA to the degradation product. However, the sample size of cases where LURA was detected at FSSA was small.

The rate of LURA degradation was comparable to risperidone in the same experiments, with degradation to undetectable levels observed in room temperature and 37 °C inoculated, unpreserved blood specimens. Risperidone can degrade to undetectable levels in authentic post-mortem blood specimens [2, 3], requiring the inclusion of its bacterial metabolite in post-mortem toxicology screening methods. Given this, it is recommended that the major 360.265 m/z degradation product of LURA is included in post-mortem toxicology screening methods for LURA. This degradation product has now been included in the drug screening method at FSSA to indicate post-mortem LURA degradation and thus highlight cases where LURA quantification may not represent concentrations present at time of death. Lowered concentrations caused by post-mortem processes could result in interpretative issues when determining cause/manner of death, which is a particular concern for multi-drug toxicities involving LURA where multiple other drugs may also be present at lower concentrations. The inclusion of this degradant in the drug screening method will also enable its use as a marker for LURA administration if any cases present where LURA is completely degraded by microorganisms. Establishing that LURA is present in post-mortem samples is also necessary for determining medication adherence. Complete degradation of LURA was not demonstrated in any of the cases whose data was retrospectively analysed in this thesis. The future screening of casework may establish whether complete degradation of LURA may occur given extended non-refrigerated intervals, as has been demonstrated for risperidone.

The antipsychotic ziprasidone (ZIPR) was found to degrade in all human whole blood matrices stored at 37 °C for a week and at room temperature for ~21 weeks, regardless of preservative or inoculation status. Greater than 20 % losses were also observed in unpreserved specimens incubated at 4 °C after seven months.

It was hypothesised that ZIPR may degrade in blood samples by reaction with acetaldehyde to produce alkene degradants (3-ethylidene-ziprasidone (3E-ZIPR)) as geometric isomers (Chapter 9). Evidence suggests that 3E-ZIPR is then hydrogenated by microbial activity to yield enantiomeric alkane products (3-ethyl-ziprasidone (3A-ZIPR)) unresolved by the analytical methods employed in this research. Another degradant was also produced in non-inoculated specimens whose identity was not clearly established. These degradants were themselves subsequently degraded into compounds that were not identified in this thesis. Deuteration experiments indicated that the source of the acetaldehyde in the blood experiments carried out in this thesis is most probably from the oxidation of ethanol in stored blood specimens, calibrators and QCs. This may indicate that these degradation products are artefacts of the

experimental protocol used, due to the introduction of ethanol into the blood specimens when spiking the drugs.

ZIPR was infrequently detected in casework from 2016-2018 retrospectively analysed at FSSA. As a result of this, it is unknown whether the degradants detected in the blood experiments (tentatively identified as 3E-ZIPR and 3A-ZIPR) may be useful to include in post-mortem toxicology screening methods as markers of ZIPR. It may be that they could be particularly relevant for cases involving co-ingestion of ZIPR and ethanol, as greater acetaldehyde blood levels may produce greater 3E-ZIPR and 3A-ZIPR concentrations.

Overall, it has been established that the concentrations of LURA and ZIPR in decomposed post-mortem blood may not reliably correlate to peri-mortem concentrations. The post-mortem redistribution behaviour of these drugs at the time of this thesis remains unknown.

10.2 Future work

This thesis forms part of a body of work that must be continually undertaken by forensic toxicologists. There are drugs and metabolites in use for which post-mortem drug stability has not yet been investigated. As drugs are developed and released there is a continuing need to investigate drug redistribution and degradation in the post-mortem environment to ensure appropriate screening methods and result interpretation in forensic toxicology.

LC-DAD methods were used to analyse the antidepressant and antipsychotic drugs investigated in this thesis due to the thermal instability of some analytes precluding GC-MS and the known issue of unpredictable matrix effects that are encountered with decomposing blood impacting quantification using LC-QTOF-MS. Such matrix effects may have produced artefactual changes in drug signals over time that could be wrongly interpreted as due to drug degradation [223]. However, there were issues associated with the use of LC-DAD. Foremost, the use of LC-DAD alone was not sufficient for demonstrating the formation of a degradation product from LURA. That is, the chromatographic peaks observed to appear as LURA degraded were identified by manual fraction collection and LC-QTOF-MS analysis as products that may arise from ZIPR degradation, as the two drugs were in the same mixture. No other chromatographic peaks were produced. Conversely, however, this was informative toward the structure of the LURA degradation product as likely having no chromophore present. The UV-Vis spectral data obtained for the ZIPR degradation products, along with subsequent mass spectral data obtained following fraction collection, also assisted in identifying them as degradants with more extended conjugation than the parent drug. Of greater consequence was that as experiments

progressed, degradation products were found to coelute on the shoulder of analytes. This resulted in a necessary re-validation of the analytical method for those particular analytes with quantification achieved using peak height rather than peak area. Although not ideal, this post hoc validation was successful. However, there were issues analysing ASEN and MIRT past certain time points in the experiment due to coelution with degradants in the LC-DAD method. Nevertheless, it was clear that ASEN and MIRT were co-eluting with degradants due to analysis of UV-Vis spectra across their peaks.

The use of an unbuffered LLE method is not recommended for future research in this field as pH shifts throughout the experiments may have been a contributing factor regarding the variable extraction recoveries of AMIT observed. Instead, if a neutral LLE method is desired, the use of a buffer with a pH similar to blood is advised.

It is recommended that future studies exploring drug degradation utilise LC-MS/MS techniques in combination with isotopically labelled IS analogues of the drugs under investigation. This approach, though more costly if the standards are available, would enable matrix effects to be corrected for, but only if the IS has the same retention time as the drug [222]. Analysing fewer analytes or one analyte in experiments only may also prevent the saturation or inhibition of any microbial enzymes that may effectuate degradation, which may have been the reason for the observed slow dealkylation of many of the drugs in the blood experiments of this thesis. To prevent enzyme saturation, the use of LC-MS/MS techniques is favoured due to greater sensitivity in comparison to LC-DAD, as drug concentrations in blood would not need to be as great. If the use of LC-MS/MS is unfeasible, it is recommended that studies of this nature utilising LC-DAD examine fewer analytes per sample also to reduce the possibility of coelution with degradants.

Although not used in this work, GC-MS (or GC-MS/MS) techniques would be suitable for the analysis of more volatile drugs, provided they and their degradants are also thermally stable. In this case, risperidone or lurasidone would not be able to be used as markers for successful microbial inoculation and metabolism in specimens. A drug such as nitrazepam, which degrades to its 7-amino metabolite at a greater rate in bacterially inoculated samples, could instead be used.

In this thesis, comparisons of the stability of drugs between non-inoculated and inoculated specimens was used to infer if any drug degradation may be attributable to microbial activity. It was not established if the dominant microorganisms in the inoculated specimens were

responsible for the degradation observed. Future work could investigate the stability of LURA and ZIPR when exposed to specific microbial species in culture media, or specific species in sterilised whole blood to determine the organisms responsible for biotransformation. Key microorganisms to include in such studies would be *Clostridium* spp. (in particular, *C. perfringens*), *Enterococcus* spp. and *Bacteroides* spp. (in particular, *B. fragilis*), due to their presence in the specimens in the unpreserved blood specimens in this thesis and in authentic post-mortem specimens.

The approach to investigate post-mortem drug degradation utilised in this thesis, whereby casework was retrospectively analysed following degradant detection in *in vitro* experiments, is recommended for future experiments in this field. Other interesting approaches could have been to incubate specimens at body temperature at first and slowly decrease the temperature, as is likely to occur during the post-mortem interval, or to preserve specimens following a period of their unpreserved incubation. However, both approaches require the control of more variables than were present in the thesis experimental. A variety of incubation times, final storage temperatures, and rate of temperature decreases would need to be studied for these approaches. Such a comprehensive experiment supports the use of these methods only to explore how drugs known to degrade may behave in authentic casework, however the environmental conditions that human remains are in during the post-mortem interval are not always known, nor would they be the same for each case.

There is an impetus to determine if other drugs possessing the same moieties as those proposed to degrade in LURA and ZIPR may behave similarly in post-mortem specimens or *in vitro* surrogates. Perospirone, an antipsychotic that is currently only available for therapeutic use in China and Japan, also contains the 1,2-benzisothiazole moiety present in both LURA and ZIPR (Figure 10-1 (a)). As is the case with LURA, reductively cleaved metabolites but no metabolites similar to N-debenzothiazole-lurasidone (ND-LURA) or N-debenzothiazole-ziprasidone have been reported [465, 482]. No English-language literature is available concerning the aqueous stability of perospirone. Given the structural similarity between perospirone and LURA it is hypothesised that it may degrade microbially to a product similar to ND-LURA (Figure 10-1 (b)). Experiments on the stability of perospirone may also assist in further elucidating the identity of the major microbial metabolite of LURA detected in this thesis.

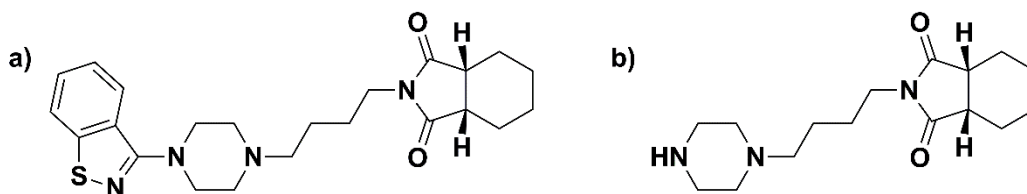


Figure 10-1: Structure of a) perospirone and b) postulated microbial degradation product of perospirone.

Ropinirole is a drug used to treat Parkinson's disease and restless legs syndrome, with the potential to effectuate cardiotoxicity [483]. In common with ZIPR, it contains an oxindole moiety (Figure 10-2 (a)). It is therefore hypothesised that it may degrade in a similar manner as was observed with ZIPR in this thesis. If so, its reaction with acetaldehyde may be expected to produce an analogous degradant with an alkene moiety in ante-mortem blood or preserved, post-mortem blood (Figure 10-2 (b)) and an analogous degradant with an alkane moiety in unpreserved, post-mortem blood due to subsequent alkene reduction by microorganisms (Figure 10-2 (c)). *In vitro* experiments are required to establish the reactivity of ropinirole to acetaldehyde and its stability in blood.

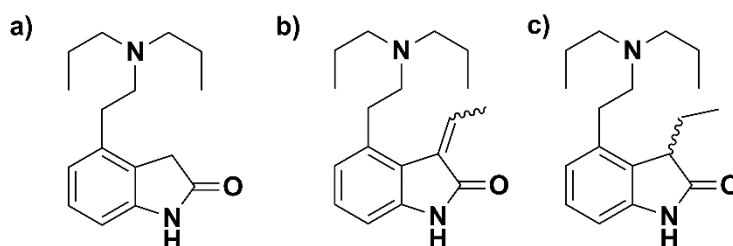


Figure 10-2: Structure of a) ropinirole and b-c) postulated degradation products of ropinirole.

The drug roluperidone, which is currently undergoing Phase III clinical trials for treatment of schizophrenia, contains an N-substituted oxindole (Figure 10-3 (a)) [484]. If successfully marketed it would also be important to establish if this drug degrades in a manner similar to that proposed for ZIPR (Figure 10-3 (b-c)).

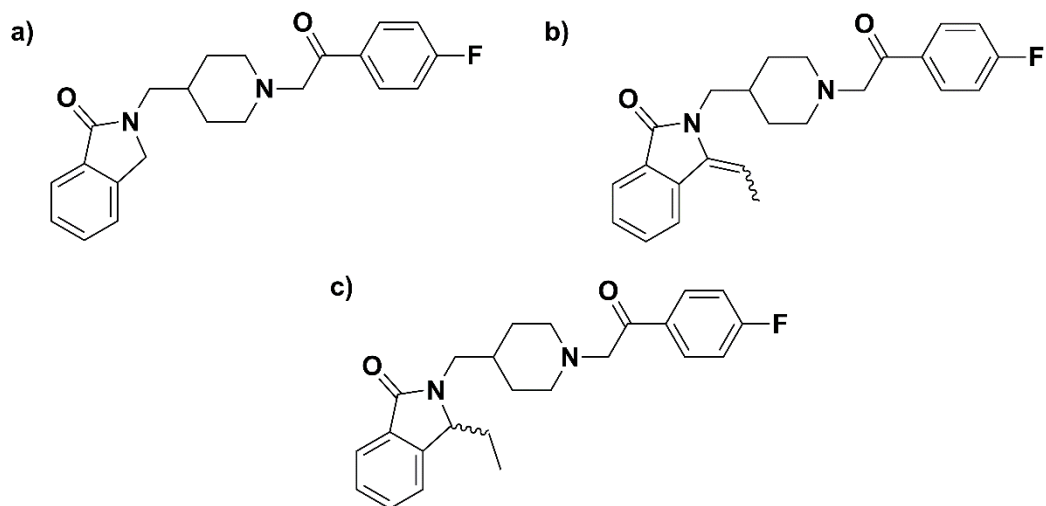


Figure 10-3: Structure of a) roluperidone and b-c) postulated degradation products of roluperidone.

This study did not set out to determine the stability of the active metabolites of any of the drugs investigated and this is also a clear avenue for further research. However, NORT and NOR-QUET are active metabolites of their parent drugs [153], and these compounds were observed to be increasing over time in the blood experiments. NOR-CHLO, which is also an active metabolite [153], was also presumptively identified and was produced similarly to NORT and NOR-QUET. Therefore, in authentic post-mortem blood specimens concentrations of N-dealkylated metabolites may increase over time due to parent drug degradation. Given the temperatures and time period required for conversion are significant these transformations are not expected to alter the interpretation of toxicology results, unless the microbial communities in the room temperature experiments are responsible and active earlier in authentic specimens. Similarly, it may be the case that sulfoxide metabolites increase over time from parent drug degradation. However, it is not known whether sulfoxide metabolites may be reduced back to the parent drug. Such a mechanism would explain increases of thioridazine in preserved femoral post-mortem blood that have been reported after a year of storage at $-20\text{ }^{\circ}\text{C}$ [313]. In the experiments in this thesis there was no indication that N-dealkylation products or sulfoxide metabolites further degraded. Determining if the conjugated metabolites of these drugs may convert back to the parent drug is also necessary in future work. The stability of any glucuronide metabolites in particular should be investigated, given the ability of other drugs to increase in concentration from hydrolysis of their glucuronides in stored blood specimens [256, 257, 394].

APPENDIX A - IDENTIFICATION OF PROCHLORPERAZINE STOCK IMPURITY

A.1 Identification of prochlorperazine stock impurity

The IS for most analytes was initially TRIM but was later changed due to an impurity of PROC present in a later stock solution co-eluting with TRIM. The UV-Vis spectrum of the PROC impurity was similar to the parent drug (Figure A-1) with a slight red shift in the λ_{\max} . To determine its identity, manual fraction collection followed by LC-QTOF-MS analysis was carried out (see 5.5.2).

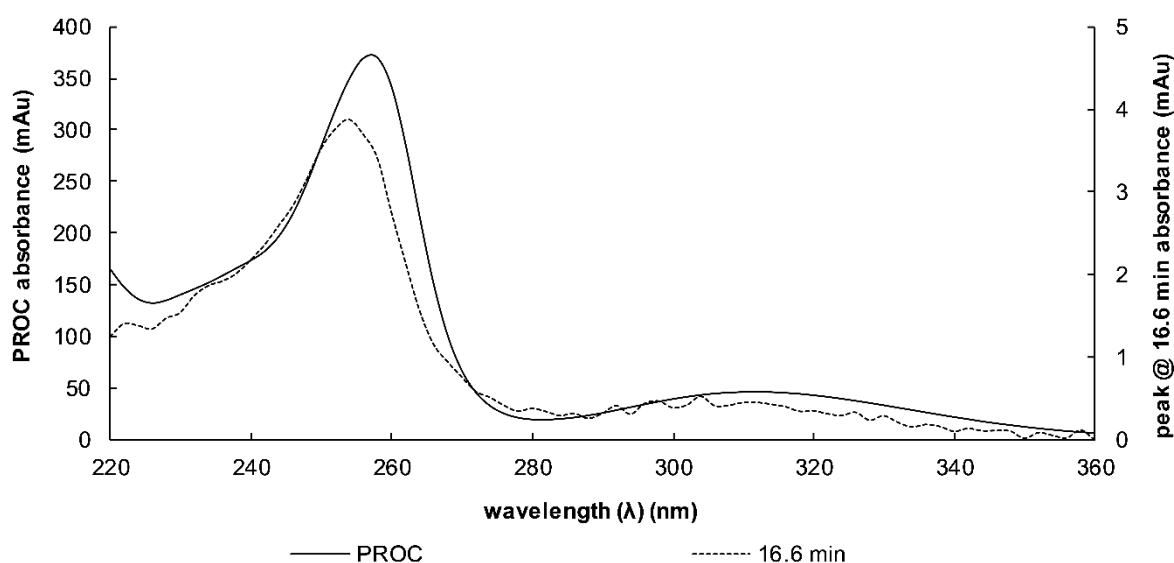


Figure A-1: UV-Vis absorbance spectra of PROC (solid line) and impurity at RT=16.6 min (dotted line).

A.1.1 Experimental

Manual fraction collection was performed on an extracted HIGH QC (9.1 $\mu\text{g}/\text{mL}$) prepared during method validation accuracy and precision experiments (see 4.4.1.4) using the LC-DAD method as indicated in 4.2.3. An Agilent 1200 Series HPLC and Agilent 6520 Series LC-QTOF-MS were used in tandem to analyse the collected fraction as described in 3.3. Diluted PROC stock solution was also analysed by LC-QTOF-MS.

BPCs were first examined for both PROC and the manually collected fraction. PROC was identified from its known precursor ion and retention time of the method (Table 5-7). Mass spectra were obtained for PROC and the peak in the collected fraction using MFE. Mass spectra

presented below are those following MFE. Agilent MassHunter software was used to generate molecular formulae for precursor and product ions.

A.1.2 Results

Analysis of the MS and MS/MS data of the collected fraction lead to the tentative identification of this impurity as PERA, a dechlorinated photo-degradation product of PROC [485]. Identification of the impurity as PERA was supported by: the isotope ratios of the impurity (Figure A-2 (b)), which indicates the impurity does not possess any chlorine atoms [205]; common product ion fragments between PROC and PERA at 70.0657, 113.1073, and 141.1386 m/z (Figure A-3 and Figure A-4); a mass difference between PROC and PERA of 34 mass units (indicative of the loss of a chlorine atom and addition of a hydrogen atom) (Table A-1); and GMF and calculated accurate masses of the precursor and product ions (Table A-1 and Table A-2). The phenothiazine moiety, whether chlorinated or dechlorinated, appears to be lost as a neutral fragment when forming the ion at 141.139 m/z.

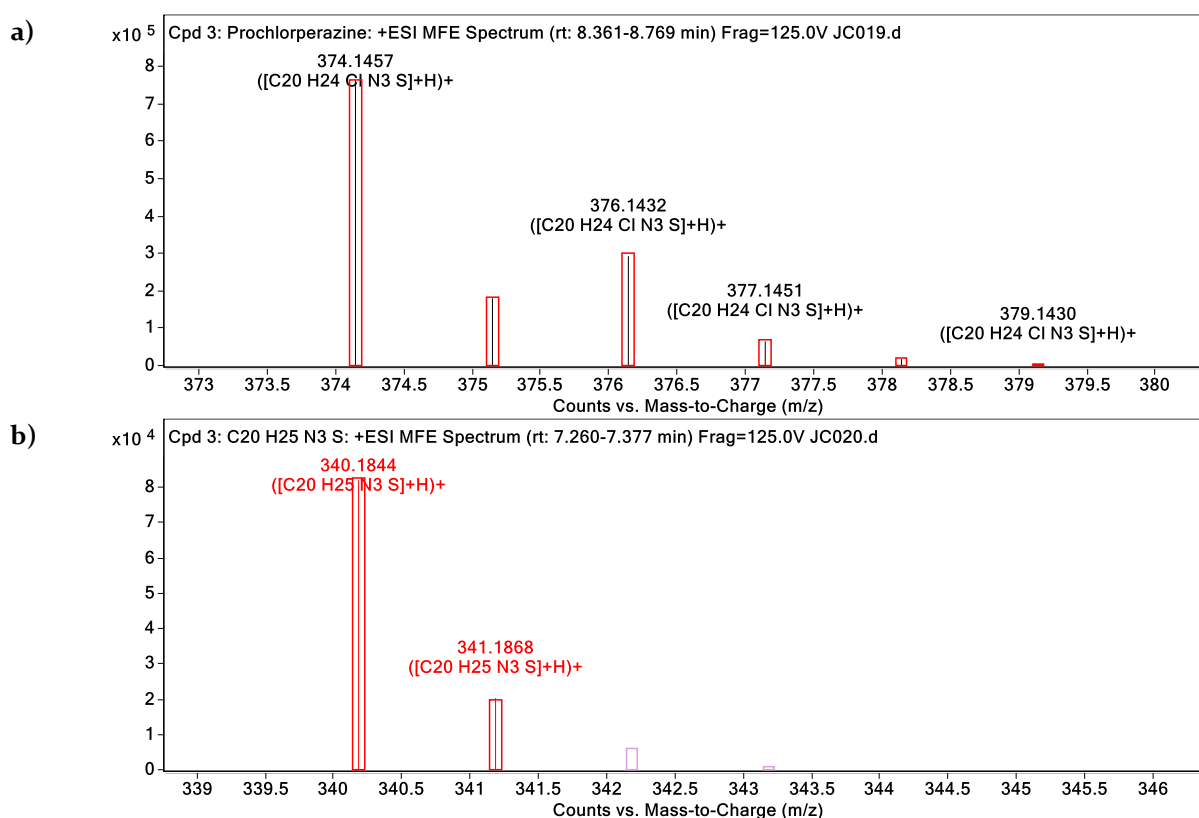


Figure A-2: MS spectra with generated molecular formula showing predicted isotope ratios as red boxes for a) PROC and b) PERA. Observed ion signal intensities are shown as lines within the boxes.

Table A-1: MS data for PROC and PERA.

Analyte	Retention time (min)	Measured [M+H] ⁺ (m/z)	Calculated [M+H] ⁺ (m/z)	GMF precursor ion	Mass accuracy (δ) (ppm)	Mass accuracy (δ) (mDa)
PROC	8.51	374.1457	374.1452	[C ₂₀ H ₂₄ ClN ₃ S]H ⁺	-1.3	-0.5
PERA	7.30	340.1844	340.1842	[C ₂₀ H ₂₅ N ₃ S]H ⁺	-0.6	-0.2

GMF = generated molecular formulae. Mass accuracies determined from single injection.

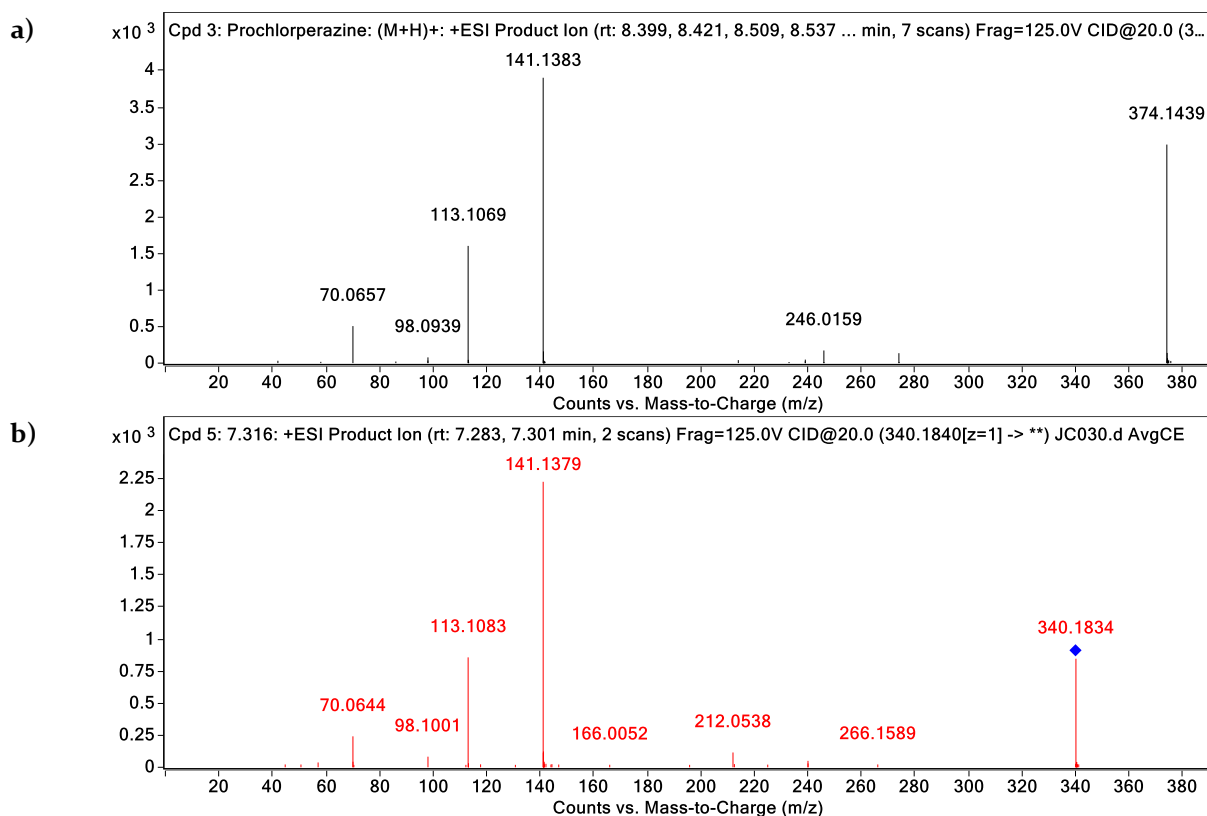


Figure A-3: MS/MS spectra for a) PROC and b) PERA. Collision energy = 20 eV.

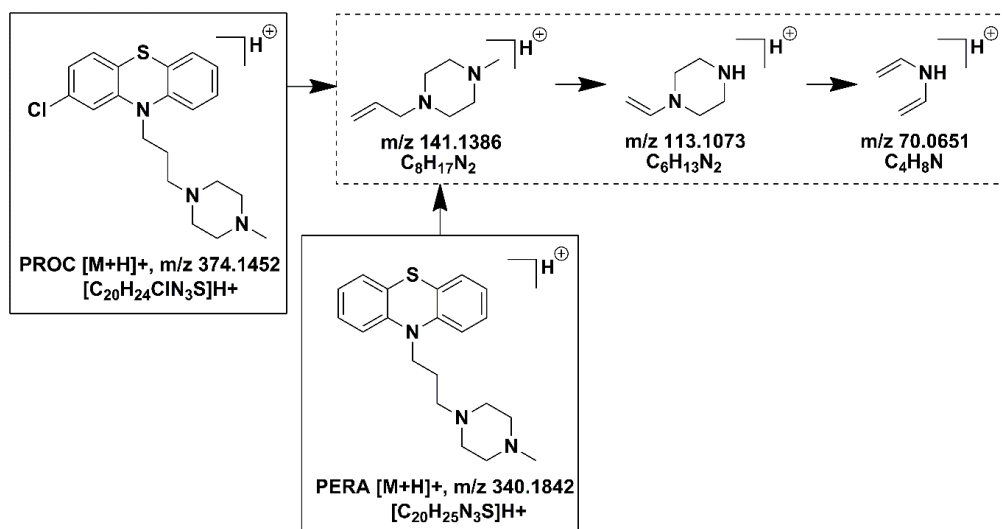


Figure A-4: Possible fragmentation pathway of PROC and PERA.

Fragments in common are indicated by the dotted-line box; m/z are calculated accurate mass/charge values.

Table A-2: MS/MS data at 20 eV for PROC and PERA.

Analyte	Precursor ion (m/z)	Product ions (m/z)	GMF product ions	Calculated accurate mass (m/z)	Mass accuracy (δ) (ppm)	Mass accuracy (δ) (mDa)
PROC	374.1457	70.0657	C ₄ H ₈ N	70.0651	-8.6	-0.6
		113.1069	C ₆ H ₁₃ N ₂	113.1073	3.5	0.4
		141.1383	C ₈ H ₁₇ N ₂	141.1386	2.1	0.3
		374.1439	[C ₂₀ H ₂₄ ClN ₃ S]H ⁺	374.1452	3.5	1.3
PERA	340.1844	70.0644	C ₄ H ₈ N	70.0651	10.0	0.7
		113.1083	C ₆ H ₁₃ N ₂	113.1073	-8.8	-1.0
		141.1379	C ₈ H ₁₇ N ₂	141.1386	5.0	0.7
		340.1834	[C ₂₀ H ₂₅ N ₃ S]H ⁺	340.1842	2.4	0.8

GMF = generated molecular formulae. Mass accuracies determined from single injection.

A.1.3 Conclusions

The presence of PERA as an impurity in the stock solution of PROC that co-extracts in the unbuffered LLE method was hypothesised, and this is supported by accurate mass data, mass fragmentation data, and observed and predicted isotope ratios.

Some microorganisms, such as *Escherichia coli*, present in the human gastrointestinal tract [31], have been implicated in the de-chlorination of xenobiotics [271]. Therefore, although the signal for PERA was low relative to the IS, it coeluted with TRIM. Therefore, there existed the potential for considerable interference if PERA were to form from microbial degradation of PROC. Consequently, the response of PERA over time was also monitored in the experimental work described in Chapter 6 and TRIM was not used as an IS for this work.

It is possible that other aryl chlorides may also degrade in a similar manner. For example, such degradation is reported to be the case for CHLO, which forms PROM in anaerobic conditions [486, 487], and ZIPR [467], which is photolytically dechlorinated. These hypothesised degradants were actively searched for in LC-QTOF-MS data of blood extracts for the experiments in Chapter 6.

For experiments performed in Chapter 6 an IS that eluted after the analytes, rather than part-way through the chromatographic run, was chosen to mitigate the potential future issue of an IS co-eluting with degradation products. For this reason, as well as its similar chemical structure to most of the other analytes, LORA, was chosen as the preferred IS.

APPENDIX B - BLOOD EXPERIMENTS DATA

B.1 Data normalisation

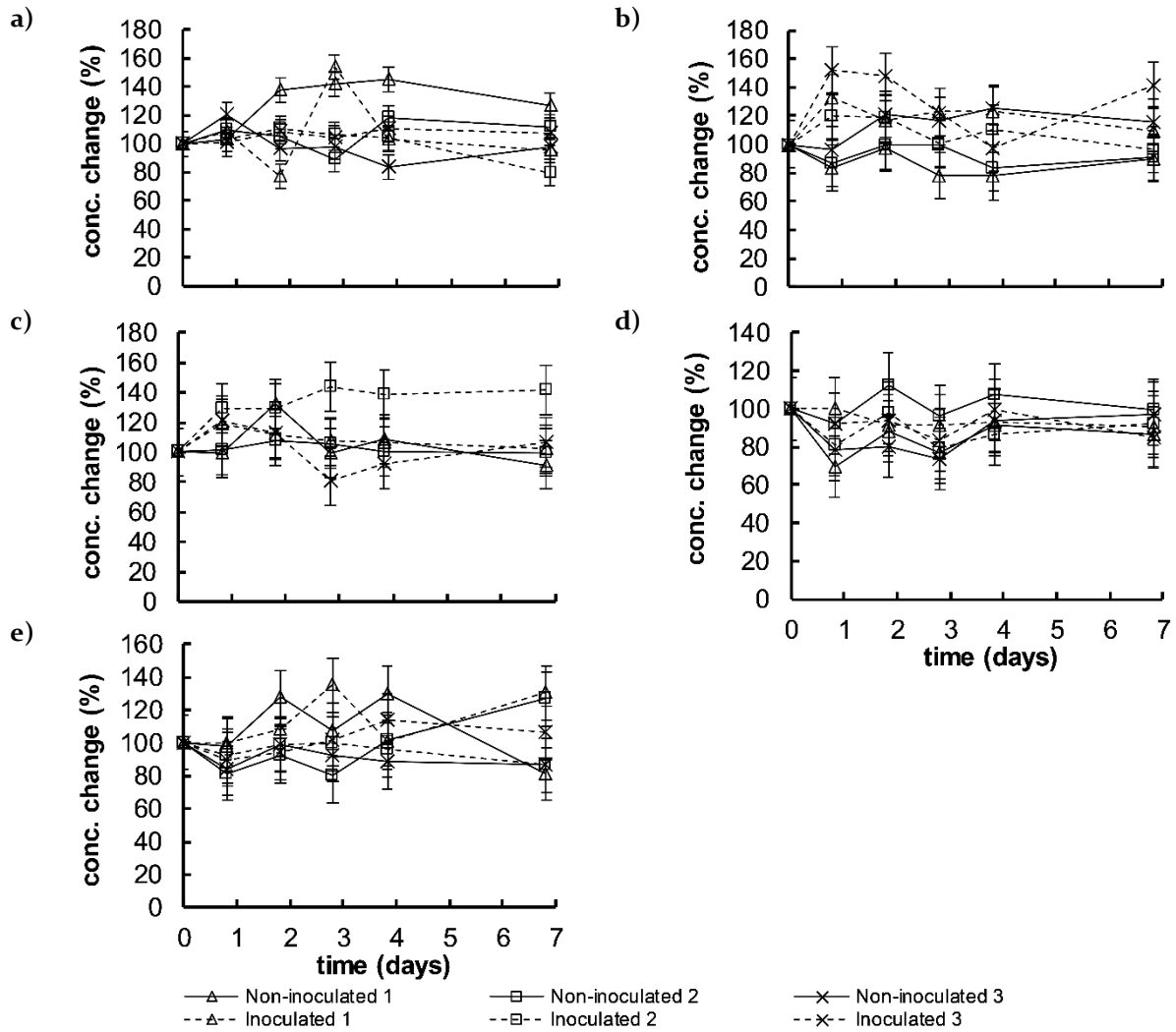


Figure B-1: Concentration change (%) of AMIT in a,c,e) preserved and b,d) unpreserved blood specimens incubated at 37 °C for 7 days in a) experiment WA, b-c) experiment WBI, and d-e) experiment WB2.

Error bars are ± uncertainty (6.2.3.3).

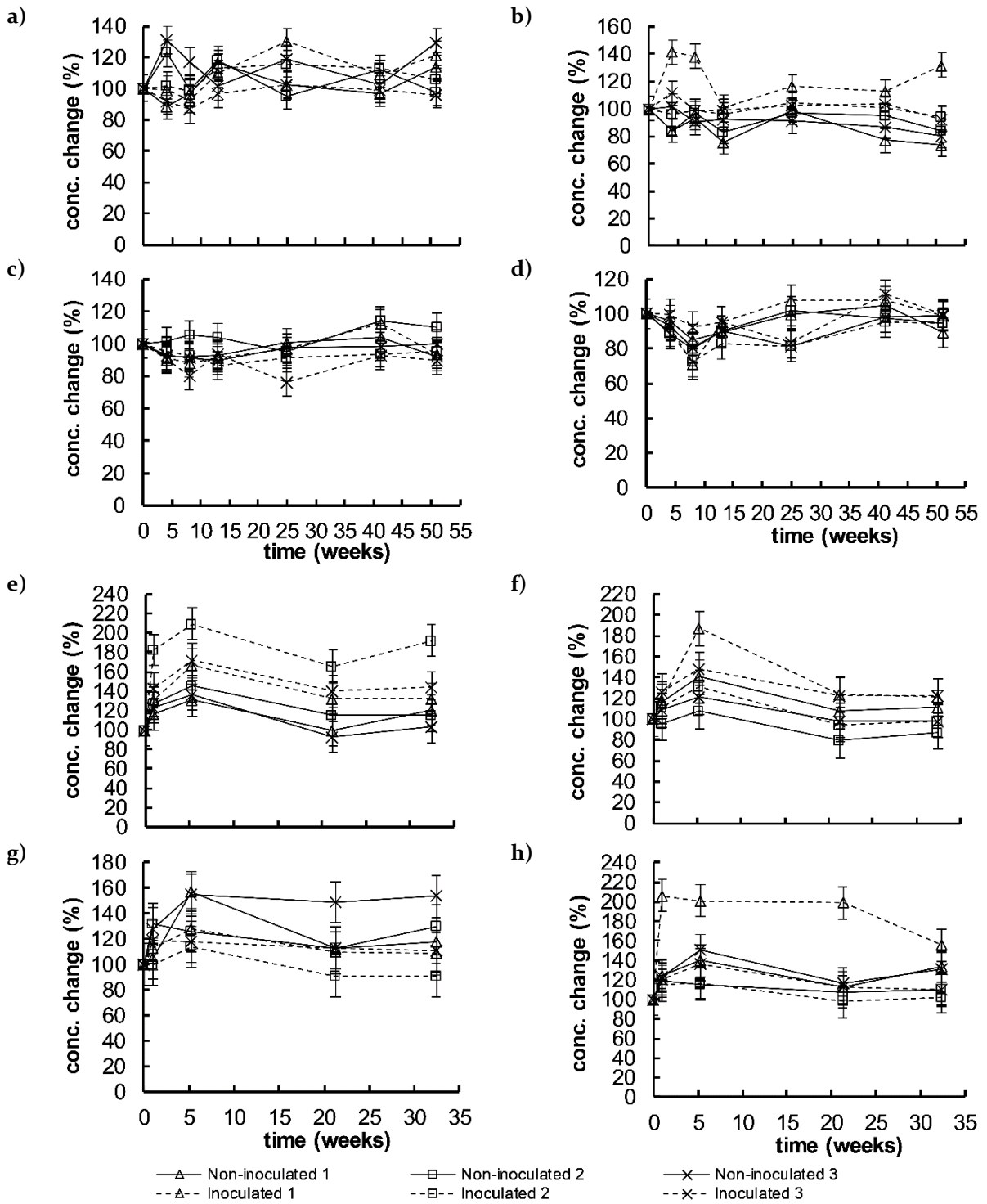


Figure B-2: Concentration change (%) of AMIT in a,c,e,g) preserved and b,d,f,h) unpreserved blood specimens incubated for 12 months a-b) at -20 °C and c-d) 4 °C in experiment YA and incubated for 7 months e-f) at -20 °C and g-h) 4 °C in experiment YB. Error bars are ± uncertainty (6.2.3.3).

B.2 Risperidone degradation

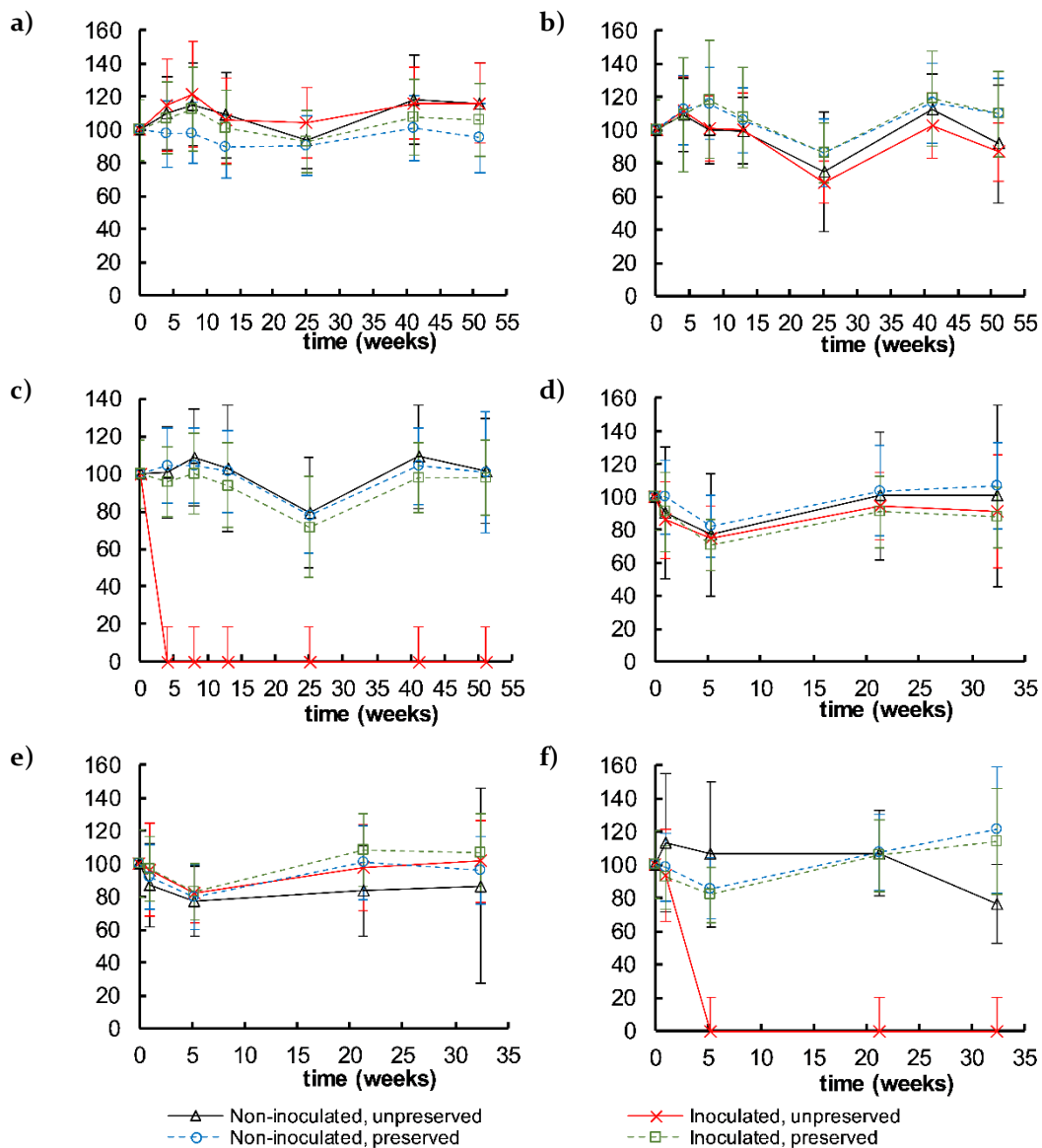


Figure B-3: Relative concentration change (%) of RISP in blood specimens incubated at a) -20 °C, b) 4 °C, and c) room temperature for 12 months in experiment YA and at d) -20 °C, e) 4 °C, and f) room temperature for 7 months in experiment YB.

Y-axis is concentration change (%) for inoculated, unpreserved, room temperature specimens in experiment YA and YB and non-inoculated unpreserved, room temperature specimens in experiment YB, and relative concentration change (%) for all other specimens. Error bars are \pm uncertainty (6.2.3.3).

B.3 Drug degradation in the week experiments

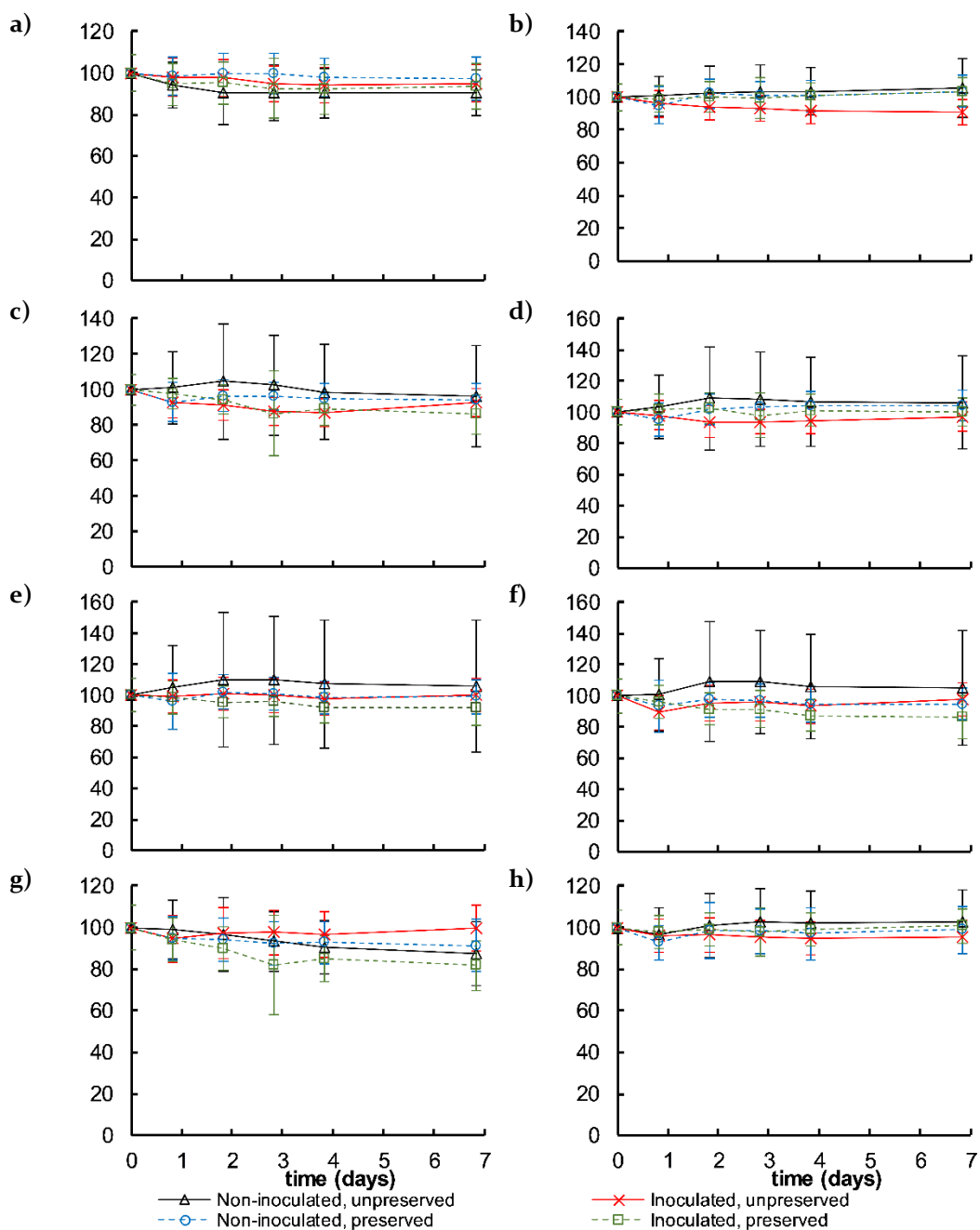


Figure B-4: Relative concentration change (%) of a) ASEN, b) CLOZ, c) FLPH, d) FLTX, e) HALO, f) PERI, g) PROC, and h) QUET in blood specimens incubated at 37 °C for 7 days in experiment WA.

Y-axis is relative concentration change (%). Error bars are \pm uncertainty (6.2.3.3).

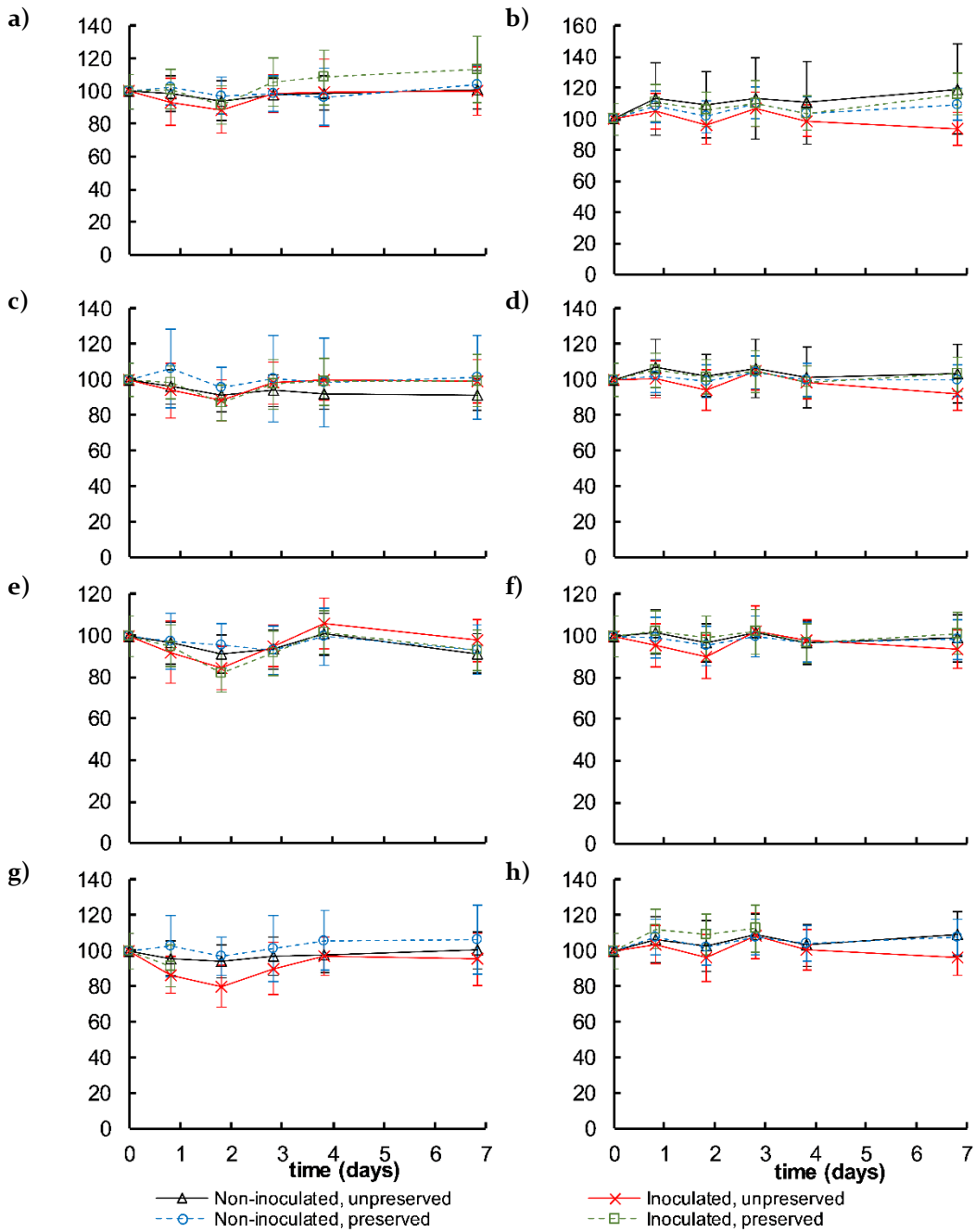


Figure B-5: Relative concentration change (%) of a-b) ARIP, c-d) CLOM, and e-f) DOTH, and g-h) MIRT in blood specimens incubated at 37 °C for 7 days in a,c,e,g) experiment WB1 and b,d,f,h) experiment WB2.

Y-axis is relative concentration change (%). MIRT relative concentration changes reported up to 1 day and 3 days in inoculated, preserved specimens in WB1 and WB2, respectively. Error bars are ± uncertainty (6.2.3.3).

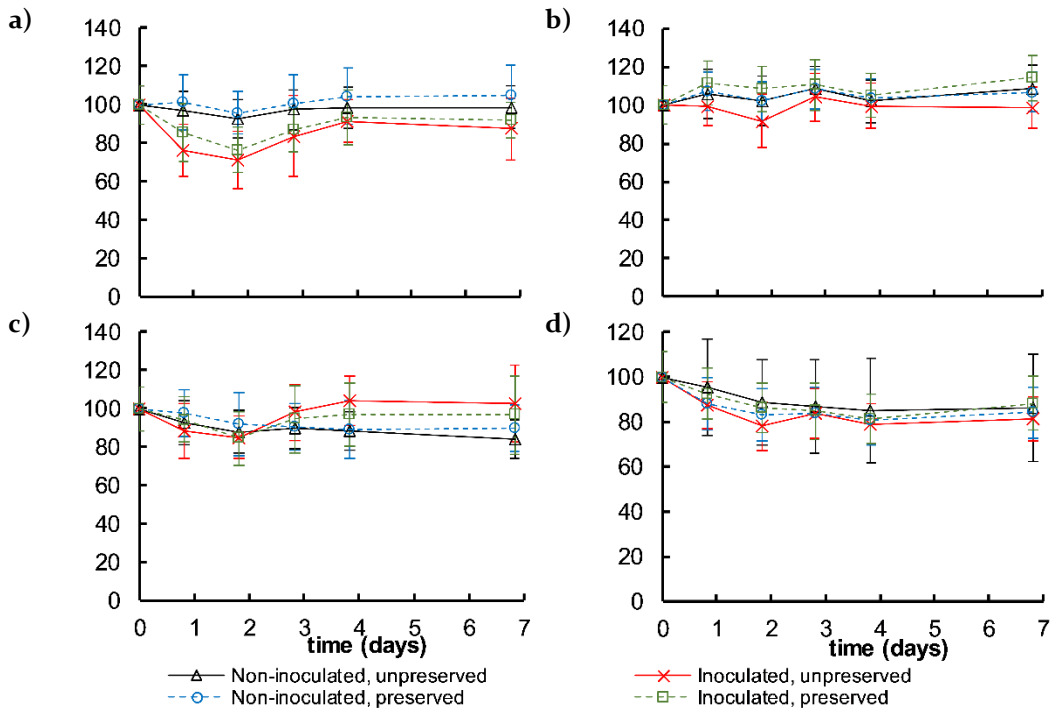


Figure B-6: Relative concentration change (%) of a-b) MOCL and c-d) TRIF in blood specimens incubated at 37 °C for 7 days in a,c) experiment WB1 and b,d) experiment WB2. Y-axis is relative concentration change (%). Error bars are \pm uncertainty (6.2.3.3).

B.4 Drug degradation in the longer-term experiments

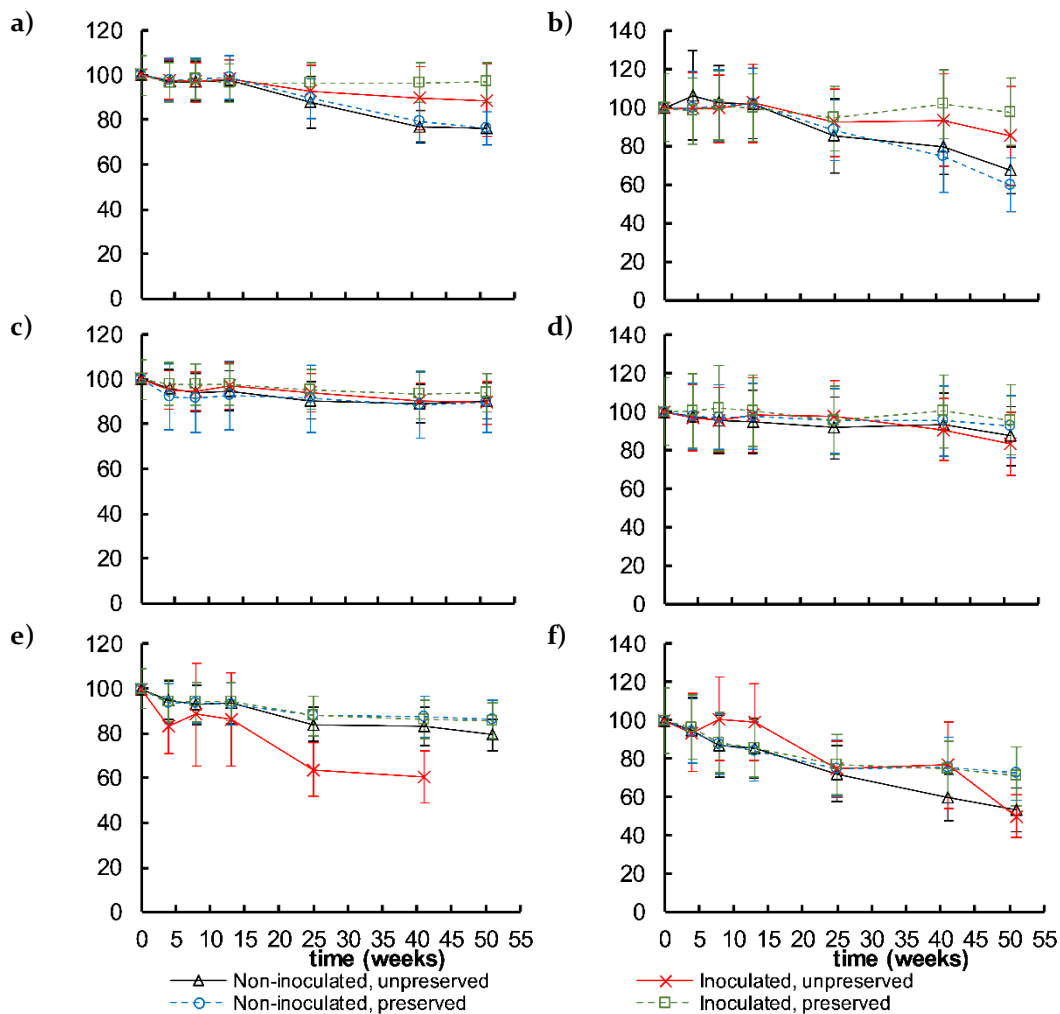


Figure B-7: Relative concentration change (%) of a,c,e) ASEN and b,d,f) CHLO in blood specimens incubated at a,b) -20 °C, c,d) 4 °C, and e,f) room temperature for 12 months in experiment YA.

Y-axis is concentration change (%) for inoculated, unpreserved, room temperature specimens and relative concentration change (%) for all other specimens. ASEN concentration changes only reported up to ~41 weeks in inoculated, unpreserved specimens stored at room temperature. Error bars are \pm uncertainty (6.2.3.3).

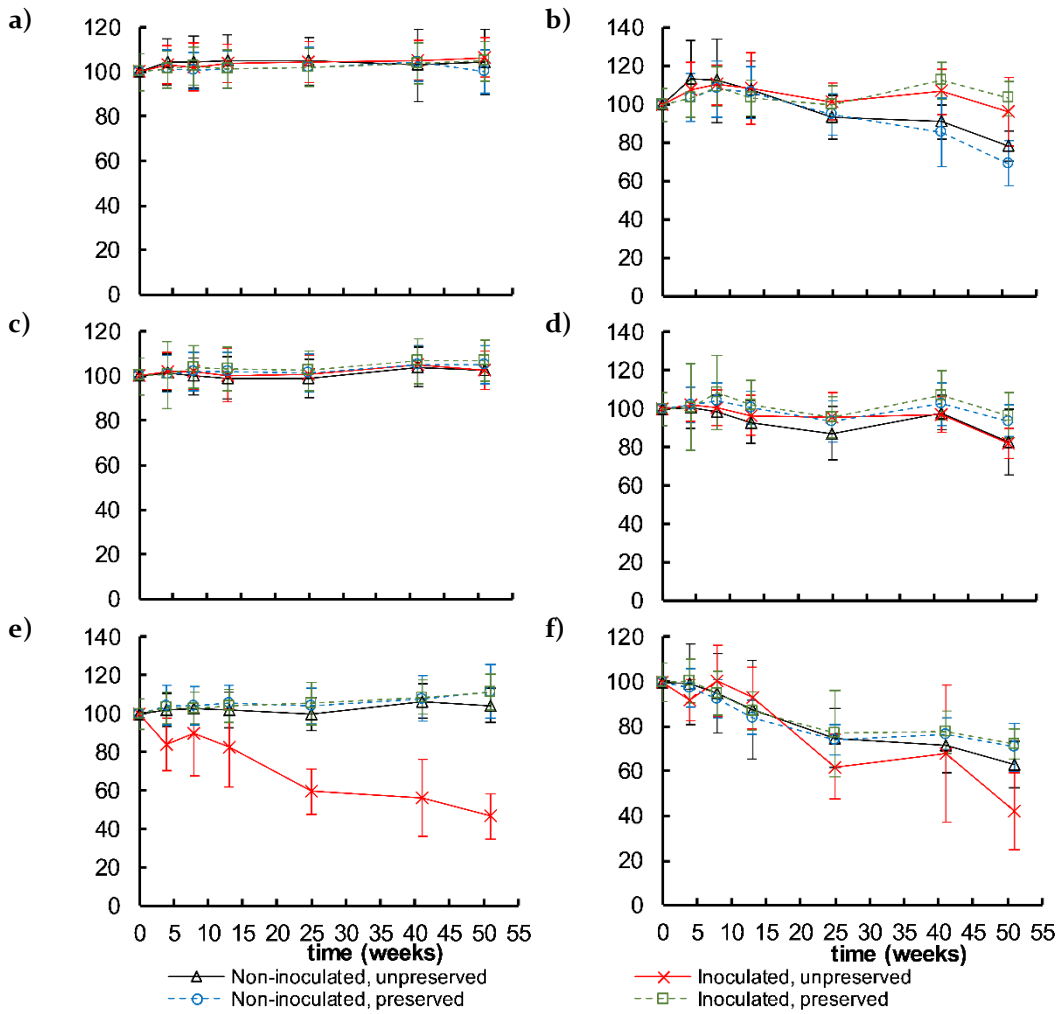


Figure B-8: Relative concentration change (%) of a,c,e) CLOZ and b,d,f) FLPH in blood specimens incubated at a,b) -20 °C, c,d) 4 °C, and e,f) room temperature for 12 months in experiment YA.

Y-axis is concentration change (%) for inoculated, unpreserved, room temperature specimens and relative concentration change (%) for all other specimens. Error bars are ± uncertainty (6.2.3.3).

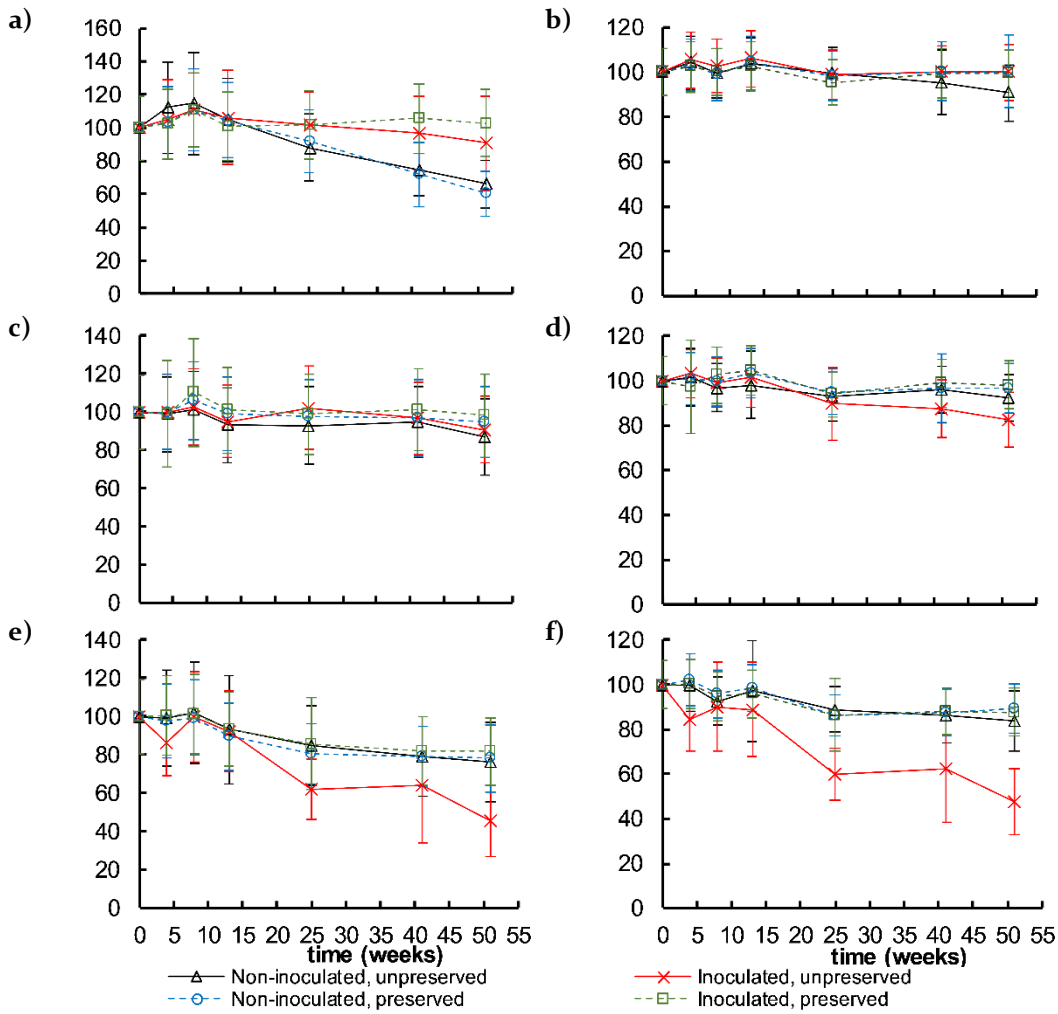


Figure B-9: Relative concentration change (%) of a,c,e) FLTX and b,d,f) HALO in blood specimens incubated at a,b) -20 °C, c,d) 4 °C, and e,f) room temperature for 12 months in experiment YA.

Y-axis is concentration change (%) for inoculated, unpreserved, room temperature specimens and relative concentration change (%) for all other specimens. Error bars are ± uncertainty (6.2.3.3).

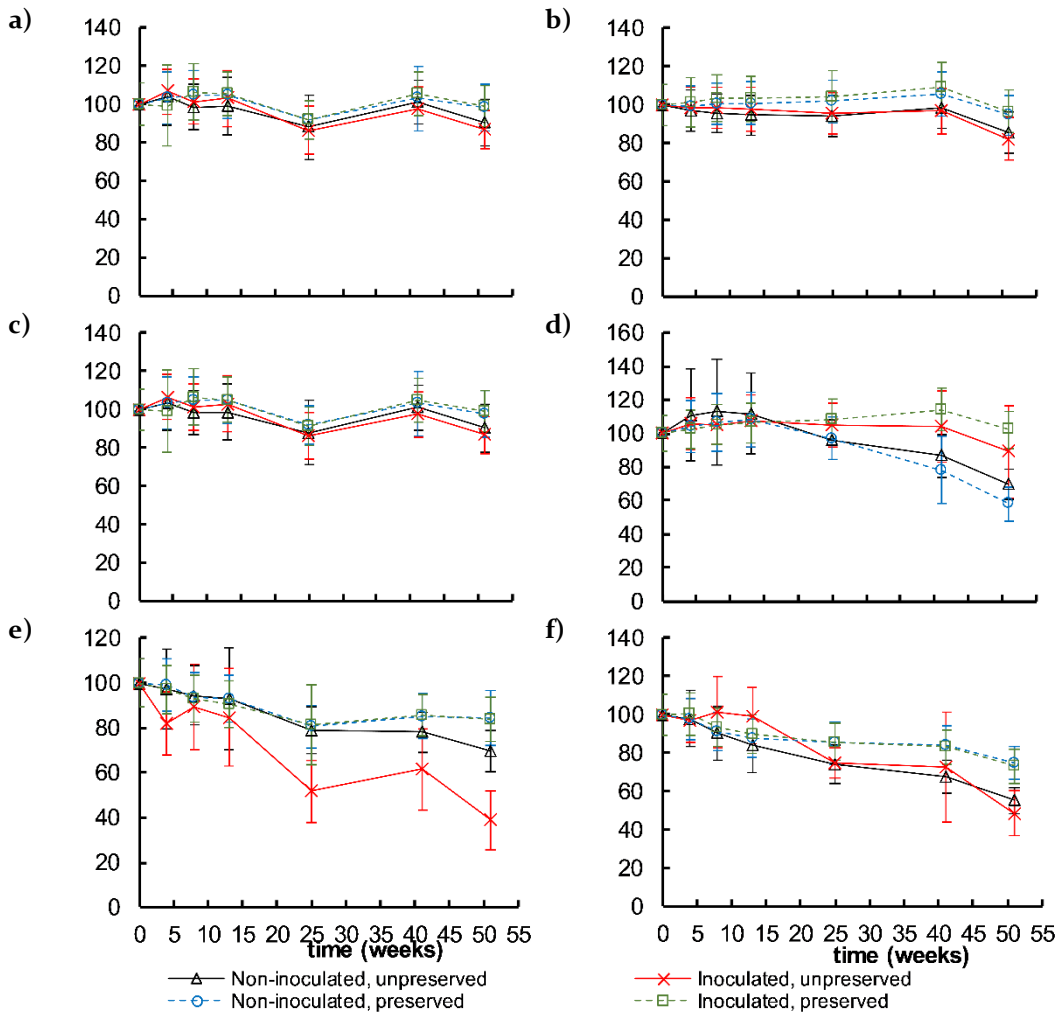


Figure B-10: Relative concentration change (%) of a,c,e) PERI and b,d,f) PROC in blood specimens incubated at a,b) -20 °C, c,d) 4 °C, and e,f) room temperature for 12 months in experiment YA.

Y-axis is concentration change (%) for inoculated, unpreserved, room temperature specimens and relative concentration change (%) for all other specimens. Error bars are \pm uncertainty (6.2.3.3).

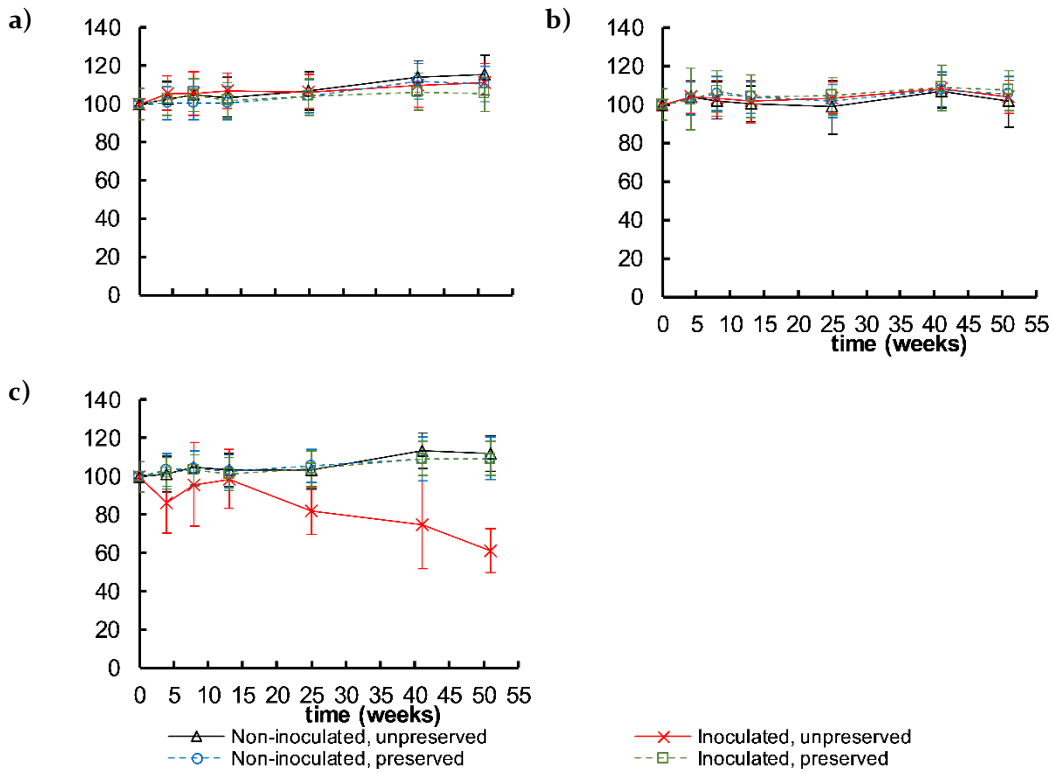


Figure B-II: Relative concentration change (%) of QUET in blood specimens incubated at a) -20 °C, b) 4 °C, and c) room temperature for 12 months in experiment YA.

Y-axis is concentration change (%) for inoculated, unpreserved, room temperature specimens and relative concentration change (%) for all other specimens. Error bars are \pm uncertainty (6.2.3.3).

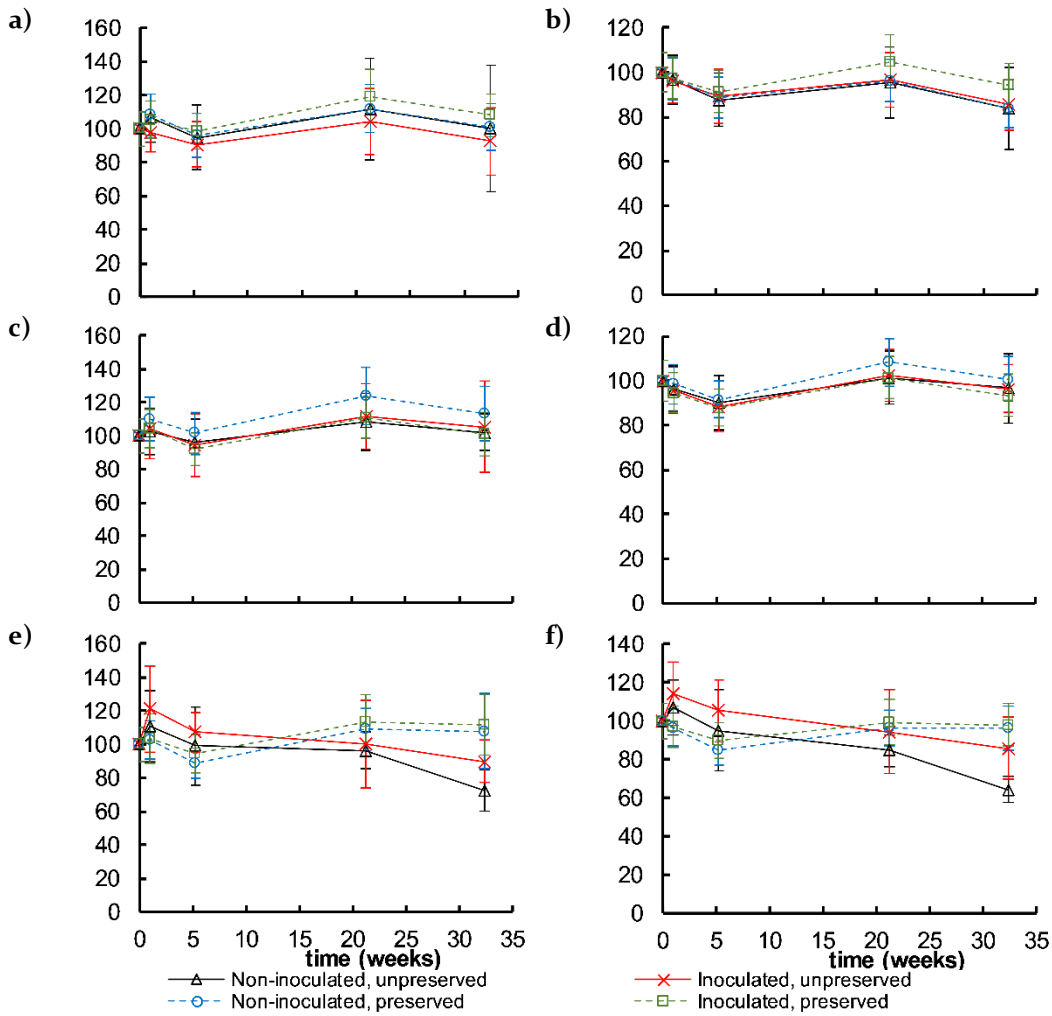


Figure B-12: Relative concentration change (%) of a,c,e) ARIP and b,d,f) CLOM in blood specimens incubated at a,b) -20 °C, c,d) 4 °C, and e,f) room temperature for 7 months in experiment YB.

Y-axis is concentration change (%) for non-inoculated and inoculated, unpreserved, room temperature specimens and relative concentration change for all other specimens. Error bars are ± uncertainty (6.2.3.3).

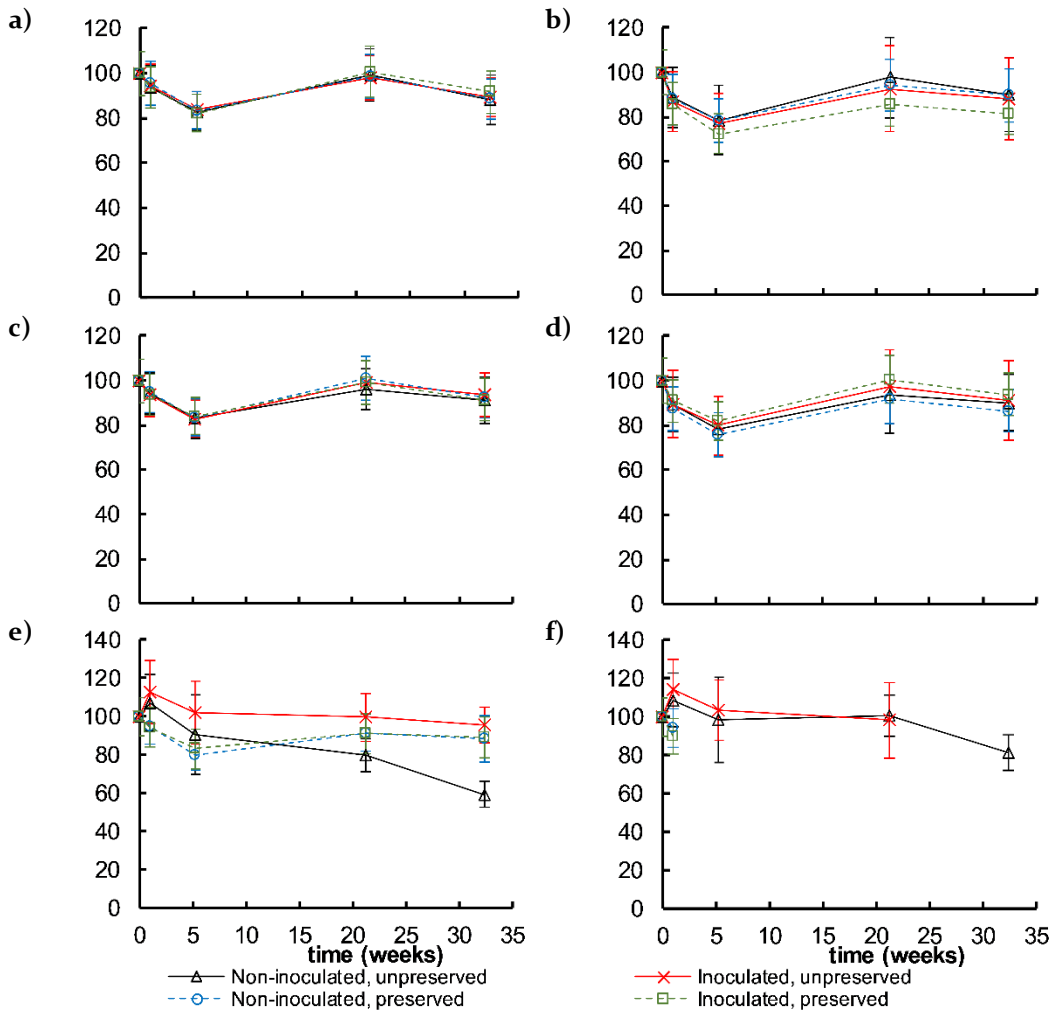


Figure B-13: Relative concentration change (%) of a,c,e) DOTH and b,d,f) MIRT in blood specimens incubated at a,b) -20 °C, c,d) 4 °C, and e,f) room temperature for 7 months in experiment YB.

Y-axis is concentration change (%) for non-inoculated and inoculated, unpreserved, room temperature specimens and relative concentration change for all other specimens. MIRT concentration changes only reported up to ~1 week for preserved specimens stored at room temperature and up to ~32 weeks in inoculated, unpreserved specimens. Error bars are \pm uncertainty (6.2.3.3).

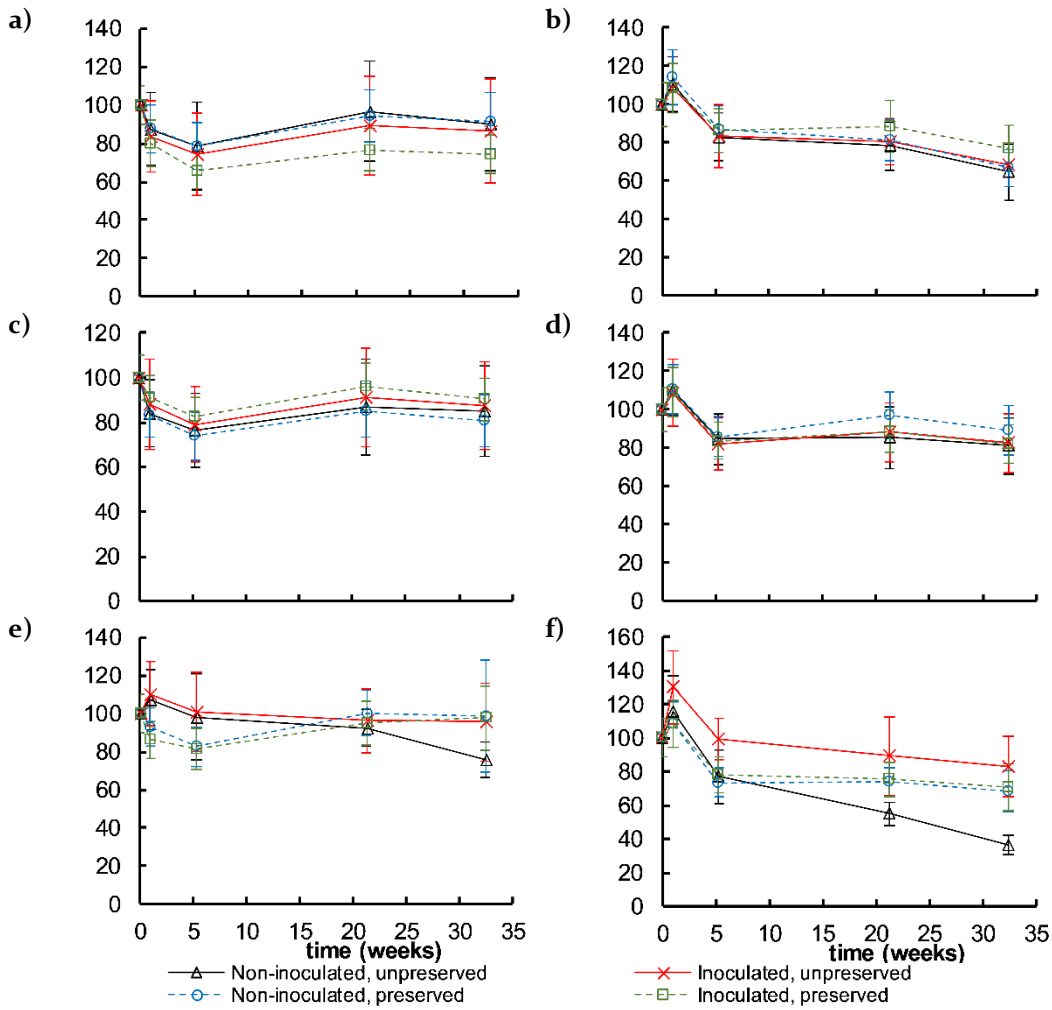


Figure B-14: Relative concentration change (%) of a,c,e) MOCL and b,d,f) TRIF in blood specimens incubated at a,b) -20 °C, c,d) 4 °C, and e,f) room temperature for 7 months in experiment YB.

Y-axis is concentration change (%) for non-inoculated and inoculated, unpreserved, room temperature specimens and relative concentration change for all other specimens. Error bars are ± uncertainty (6.2.3.3).

APPENDIX C - MICROBIAL COMMUNITIES

C.1 Sequencing results

Table C-1: DNA sequencing details.

Sample	Raw sequences	Clean sequences	Sample	Raw sequences	Clean sequences
WA_I1	21,966	21,353	YA_6-SUN2	43,038	42,790
WA_I2	19,007	18,452	YA_6-SUN3	74,593	74,403
WA_CUN	81,699	81,317	YA_6-SPI	56,857	56,056
WA_CP	98,686	98,426	YA_6-SP2	149,738	149,100
WA_SUN1	68,871	68,584	YA_6-SP3	59,635	59,058
WA_SUN2	64,999	64,707	YA_I2-CUN	90,820	90,543
WA_SUN3	99,565	99,257	YA_I2-CP	80,484	80,131
WA_SPI	97,249	96,545	YA_I2-SUN1	72,656	72,433
WA_SP2	131,242	130,993	YA_I2-SUN2	126,618	126,462
WB_I1	76,574	75,507	YA_I2-SUN3	65,133	65,007
WB_I2	92,962	92,014	YA_I2-SPI	14,015	13,967
WB_CUN2	59,537	59,383	YA_I2-SP2	11,430	11,327
WB_CUN3	106,872	106,799	YA_I2-SP3	119,861	119,528
WB_CPI	76,866	76,782	YB_I1	46,657	45,780
WB_SUN1	79,942	79,847	YB_I2	175,892	174,810
WB_SUN2	66,006	65,733	YB_7-CUN1	132,988	132,872
WB_SUN3	67,709	67,511	YB_7-CUN2	98,065	98,025
YA_I1	23,946	23,242	YB_7-CUN3	36,115	36,025
YA_I2	30,069	29,384	YB_7-CPI	30,816	30,777
YA_3-CUN	47,950	47,723	YB_7-CP2	46,608	46,376
YA_3-CP	49,657	49,246	YB_7-CP3	15,628	15,578
YA_3-SUN1	46,566	46,360	YB_7-SUN1	90,348	90,298
YA_3-SUN2	57,096	56,891	YB_7-SUN2	117,045	116,961
YA_3-SUN3	52,167	52,007	YB_7-SUN3	106,041	105,983
YA_6-CUN	70,466	70,182	YB_7-SPI	26,158	26,042
YA_6-CP	77,717	77,396	YB_7-SP2	24,270	24,065
YA_6-SUN1	47,314	47,076	YB_7-SP3	34,089	33,996

C.2 Community comparisons

Table C-2: Two-way PERMANOVA results for microbial community analyses.

Source	df	SS	MS	Pseudo-F	p
FMT and blood specimens					
Specimen	1	1.1532	1.1532	6.9847	0.0001
Preservative	1	2.1798	2.1798	13.2030	0.0001
Interaction	1	-2.3516	-2.3516	-14.2430	0.0001
Residual	50	8.2549	0.1651		
Total	53	9.2362			
Blood specimens					
Temperature	1	0.4860	0.4860	4.5421	0.0028
Preservative	1	3.4368	3.4368	32.1190	0.0001
Interaction	1	-0.5296	-0.5296	-4.9493	0.0012
Residual	42	4.4941	0.1070		
Total	45	7.8873			
Temperature	1	0.4860	0.4860	0.9909	0.0429
Time	4	1.2870	0.3218	0.6560	0.0422
Interaction	4	-11.5430	-2.8857	-5.8835	0.9924
Residual	36	17.6570	0.4905		
Total	45	7.8873			
Temperature	1	0.4860	0.4860	1.9257	0.0367
Drug Set	2	0.2397	0.1199	0.4749	0.6274
Interaction	2	-2.9340	-1.4670	-5.8124	0.3764
Residual	40	10.0960	0.2524		
Total	45	7.8873			
Preservative	1	3.4368	3.4368	32.9660	0.0001
Time	4	1.2870	0.3218	3.0862	0.0001
Interaction	4	-0.5896	-0.1474	-1.4138	0.0533
Residual	36	3.7531	0.1043		
Total	45	7.8873			
Preservative	1	3.4368	3.4368	28.0080	0.0001
Drug Set	2	0.2397	0.1199	0.9769	0.2599
Interaction	2	-0.6975	-0.3488	-2.8421	0.1988
Residual	40	4.9083	0.1227		
Total	45	7.8873			
Time	4	1.2870	0.3218	0.9246	0.0633
Drug Set	2	0.2397	0.1199	0.3445	0.6866
Interaction	8	-4.4265	-0.5533	-1.5901	0.9969
Residual	31	10.7870	0.3480		
Total	45	7.8873			

FMT: faecal microbiota transplant; df: degrees of freedom; SS: sum of squares; MS: mean squares; p: significance. Permutations: 9999. Lowest possible p-value: 0.0001. Significant factors ($p < 0.05$) indicated in bold.

C.3 Taxa relative abundance

C.3.1 Phyla

The most abundant phyla present in DNA extracts of the faecal specimens prior to experiment inoculations was Firmicutes (Figure C-1). Actinobacteria, Bacteroidetes, and Euryarchaeota species were next most abundant. Past studies performed to assess microbial diversity in the human gut have reported greatest abundances of Bacteroidetes and Firmicutes [488, 489]. The greater dominance of Firmicutes and Actinobacteria in the initial faecal samples in contrast to Bacteroidetes may be attributed to the spore-forming ability of species of the former two phyla which could have enhanced their survival during freezing and thawing of the faeces [490].

Firmicutes, Bacteroidetes, Actinobacteria, and Proteobacteria were the dominant phyla detected in all blood specimens. Cyanobacteria, Euryarchaeota, Tenericutes, and Verrucomicrobia taxa were generally undetected in unpreserved blood specimens of all experiments, except for one specimen (WA_SUN2) where a *Methanobrevibacter* sp. was detected. Euryarchaeota, Tenericutes, and Verrucomicrobia taxa were generally detected in all preserved blood specimens of all experiments, except for one specimen (YA_12-SPI) where no Tenericutes reads were obtained.

Firmicutes was the dominant phylum in most preserved blood specimens. However, in preserved microbial matrix specimens in experiment YA (YA_3-CP, YA_6-CP, and YA_12-CP) Bacteroidetes taxa dominated (Figure C-1). For both week experiments, the abundance of Bacteroidetes was greater in unpreserved blood specimens compared to the faecal specimens prior to each experiment. In some specimens of experiment WBI, the abundance of Bacteroidetes taxa increased to surpass Firmicutes taxa. For this experiment, Proteobacteria were also more greatly abundant in some unpreserved blood specimens (WB_CUN2, WB_SUN1, WB_SUN2, and WB_SUN3). The relative abundance of Actinobacteria were generally lower in unpreserved experimental blood specimens, excluding WA-CUN. However, Firmicutes were generally the dominant taxa detected in week experiment specimens other than WB_CUN3 and WB_SUN1.

In experiment YA, Bacteroidetes taxa dominated in all specimens. Extracts collected after 6 and 12 months showed that Bacteroidetes remained dominant in the microbial matrix specimens but Firmicutes once more dominated the drug specimens (Figure C-1). Abundance of Proteobacteria were also greater in YA_3-SUN2 and YA_6-SUN2 compared to initial faecal extracts. Actinobacteria abundance sporadically was greater in blood specimens.

In experiment YB, Actinobacteria and Bacteroidetes taxa were generally more abundant in blood specimens than in the initial faecal specimens (Figure C-1). In two unpreserved specimens Proteobacteria taxa were also more dominant (YB_7-CUN1 and YB_7-SUN2).

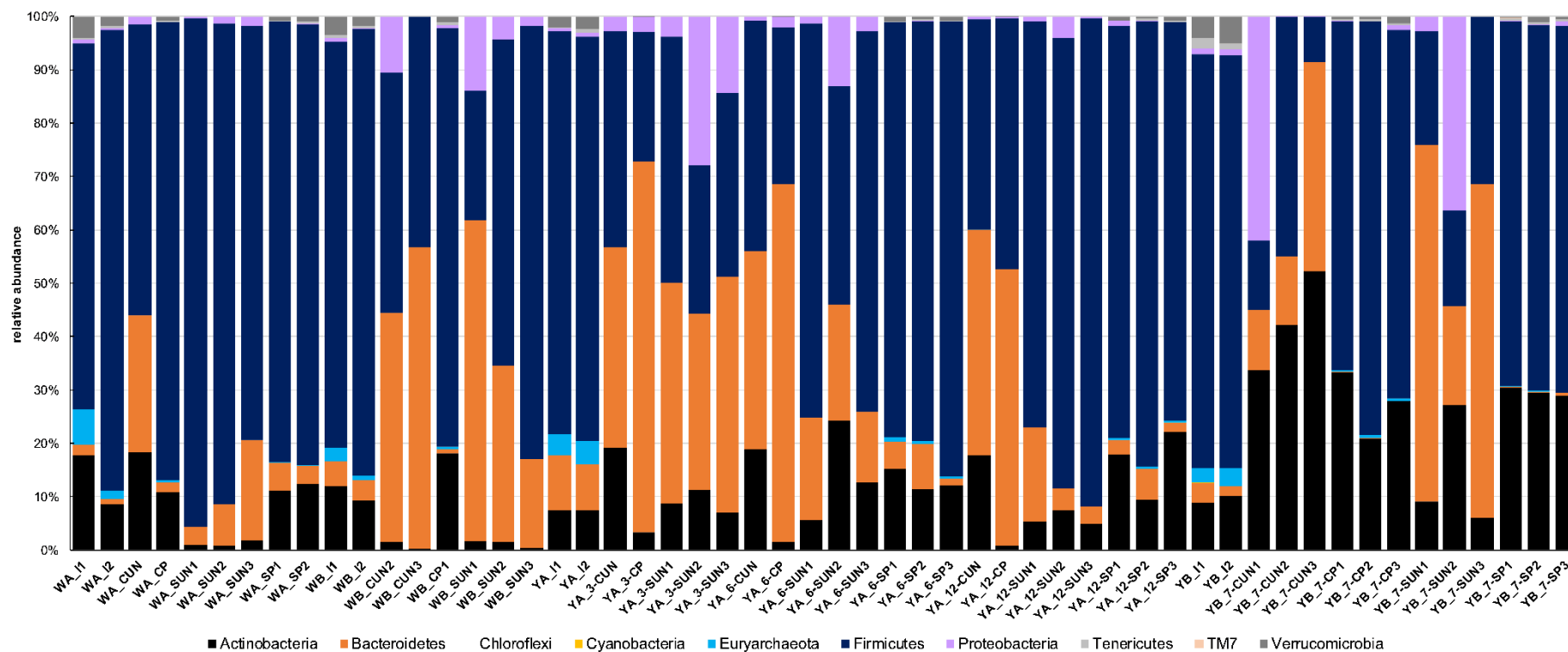


Figure C-1: Relative abundance of prokaryotic phyla in experiment specimens.
See Table 6-4 for sample ID nomenclature.

C.3.2 Firmicutes

For most specimens, the most abundant order detected for the phylum Firmicutes was Clostridiales of class Clostridia (Figure C-2). In blood specimens stored at room temperature for three months and seven months there was a dominance of, or shared dominance with, Lactobacillales of class Bacilli. YA_12-CP and YA_7-CUN3 were the only two samples where a Bacillales OTU (an undefined Bacillaceae and *Bacillus cereus*, respectively) were present with greater than 20 % of relative abundance. Bacilli and Clostridia species are spore-forming [490].

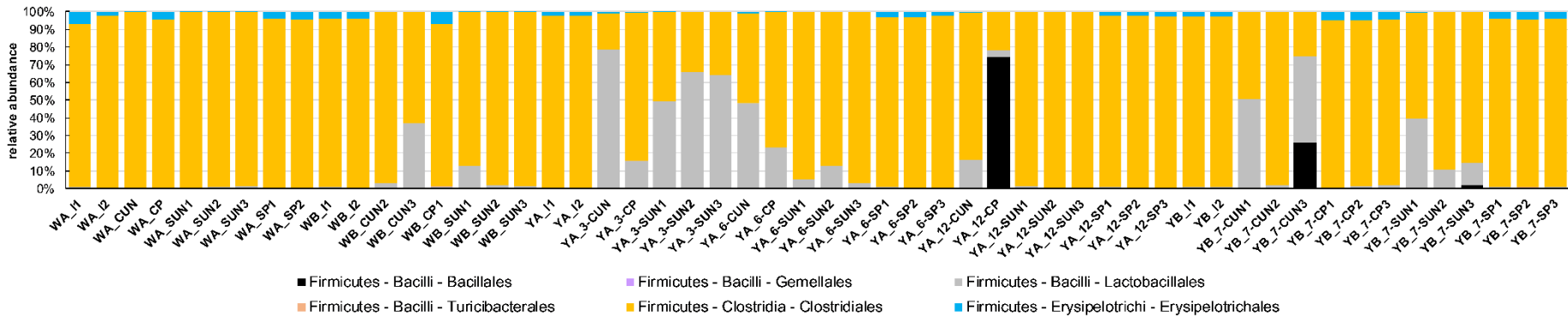


Figure C-2: Order abundance of phylum Firmicutes in specimens.

See Table 6-4 for sample ID nomenclature.

C.3.2.1 Clostridia

In preserved blood specimens and the FMT specimens Lachnospiraceae and Ruminococcaceae taxa were dominant (Figure C-3). In unpreserved blood specimens from the week experiments, where specimens were incubated at 37 °C, Clostridiaceae and Tissierellaceae taxa dominated. In unpreserved blood specimens stored at room temperature Eubacteriaceae (identified at the genus level as *Pseudoramibacter_Eubacterium*) and Ruminococcaceae taxa were co-dominant with Tissierellaceae taxa at the three-month point, with increasing dominance of Tissierellaceae over time.

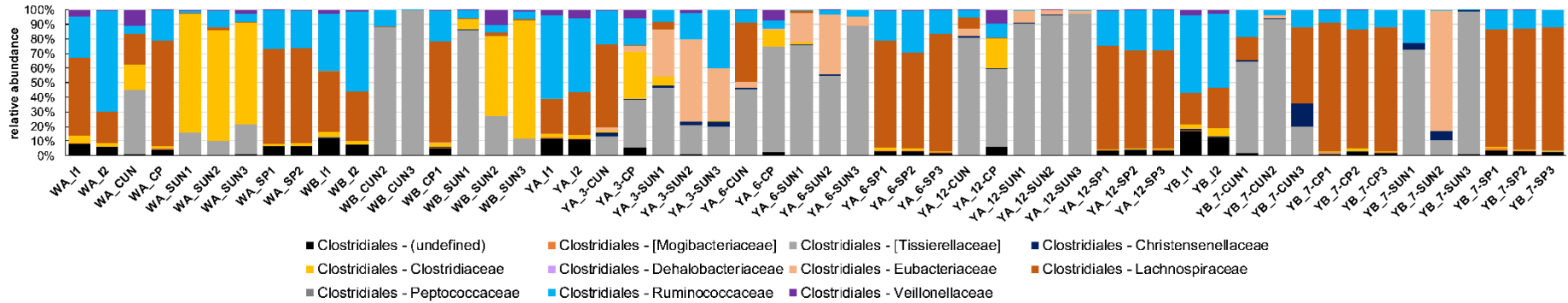


Figure C-3: Family abundance of order Clostridiales (of phylum Firmicutes) in specimens.

See Table 6-4 for sample ID nomenclature.

C. perfringens was the only species of the Clostridiaceae family conclusively identified by AGRF sequencing and bioinformatics analyses (Figure C-4). This species was the dominant *Clostridium* species detected in unpreserved blood specimens incubated at 37 °C (WA and WB). In preserved and unpreserved room temperature specimens stored at room temperature (YA and YB) numerous undefined Clostridiaceae and *Clostridium* taxa were detected. For some unpreserved specimens, no reads were obtained for any Clostridiaceae taxa.

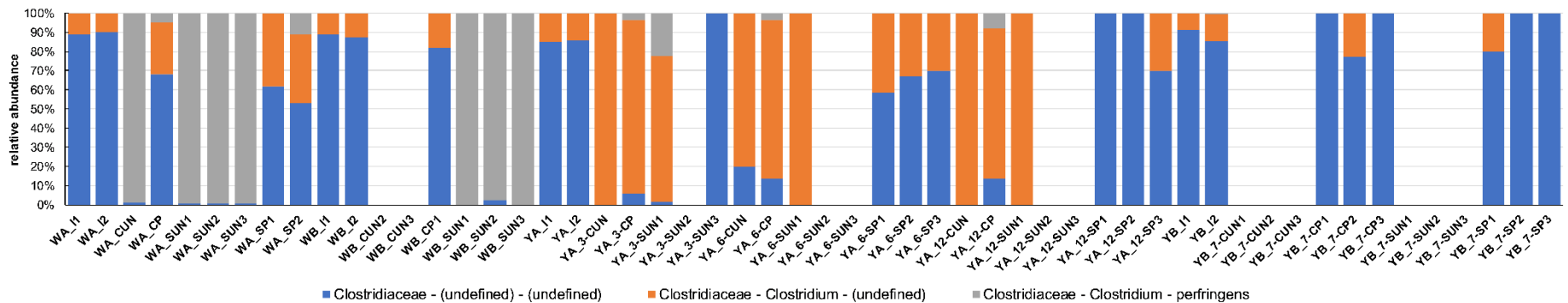


Figure C-4: Species abundance of family Clostridiaceae (of order Clostridiales of class Clostridia of phylum Firmicutes) in specimens.

See Table 6-4 for sample ID nomenclature.

The taxa identified of the family Lachnospiraceae were similar in all FMT and preserved blood specimens. For these specimens, undefined *Blautia* spp. co-dominated with numerous undefined Lachnospiraceae taxa (Figure C-5). In unpreserved specimens in experiment WA there were more taxa defined at the genus level and for these specimens in experiment WB there was a greater dominance of either *Ruminococcus gnavus* or *Blautia* spp. Reads were generally not obtained for Lachnospiraceae taxa for unpreserved specimens spiked with drugs in the longer experiments.

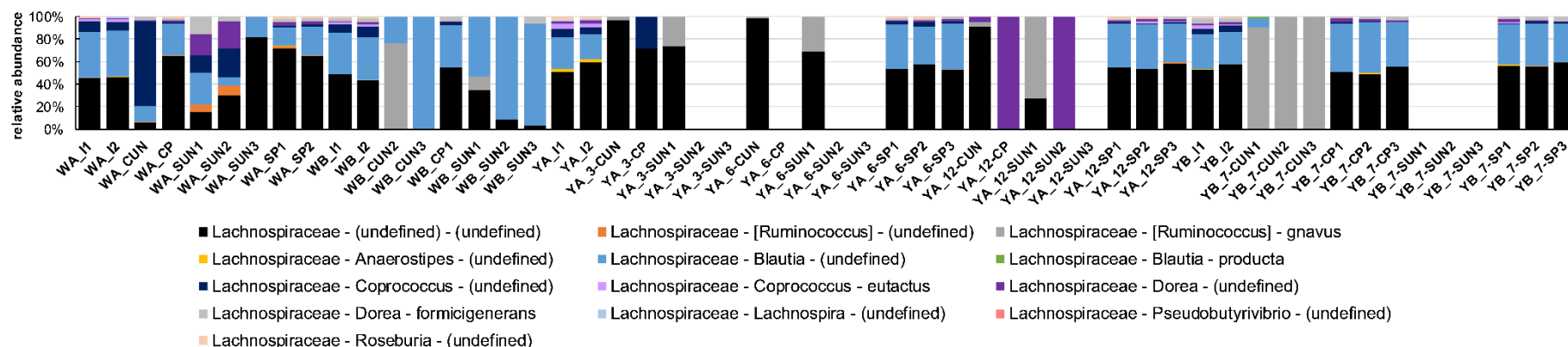


Figure C-5: Species abundance of family Lachnospiraceae (of order Clostridiales of class Clostridia of phylum Firmicutes) in specimens. See Table 6-4 for sample ID nomenclature.

For most FMT specimens no reads were obtained for any Tissierellaceae taxa. Therefore, it is thought these species were present in such minor numbers in comparison to other taxa that the depth bias of 16S rRNA sequencing impeded their detection. For blood specimens, and particularly for unpreserved blood specimens, they were more abundant. No taxa were defined at the species level and there was no apparent trend of dominance (Figure C-6).

For most specimens, undefined Ruminococcaceae taxa were dominant amongst Ruminococcaceae taxa (Figure C-7). In some unpreserved blood specimens *Oscillospira* spp. were also identified.

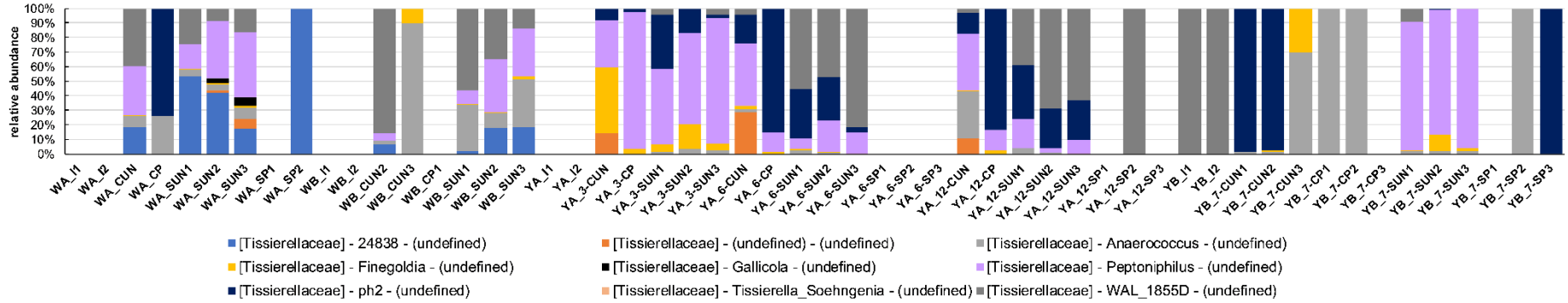


Figure C-6: Species abundance of family Tissierellaceae (of order Clostridiales of class Clostridia of phylum Firmicutes) in specimens.
See Table 6-4 for sample ID nomenclature.

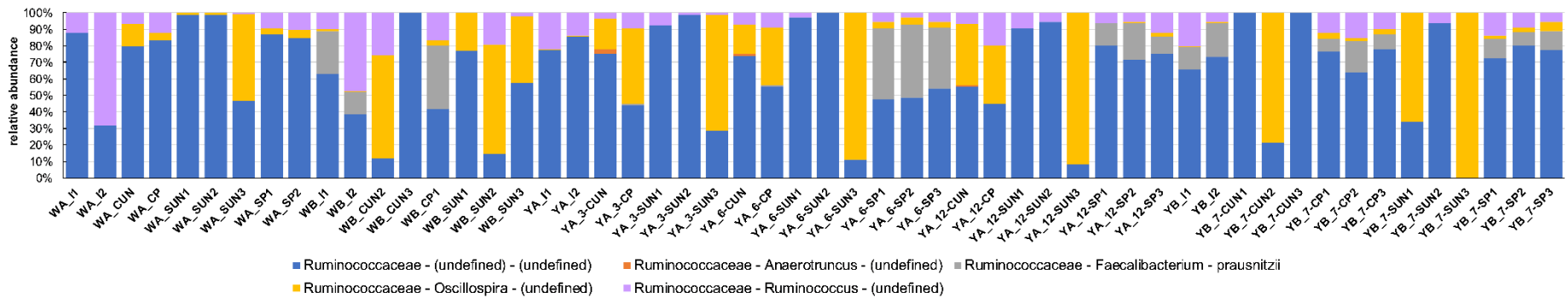


Figure C-7: Species abundance of family Ruminococcaceae (of order Clostridiales of class Clostridia of phylum Firmicutes) in specimens.
See Table 6-4 for sample ID nomenclature.

For low abundance Clostridiales taxa: Mogibacteriaceae were undefined at the genus level, and not detected in unpreserved blood specimens stored at room temperature; no trend was apparent for the abundance and presence of Christensenellaceae, Dehalobacteriaceae, Peptococcaceae, and Veillonellaceae taxa.

C.3.2.2 Bacilli

The most abundant Bacilli taxa were of the order Lactobacillales (Figure C-8). In unpreserved blood specimens, *Enterococcus* taxa were dominant. In the unpreserved blood specimens incubated at 37 °C an undefined *Facklamia* species was often detected. Preserved blood specimens and the FMT specimens were generally dominated by undefined *Streptococcus* spp.

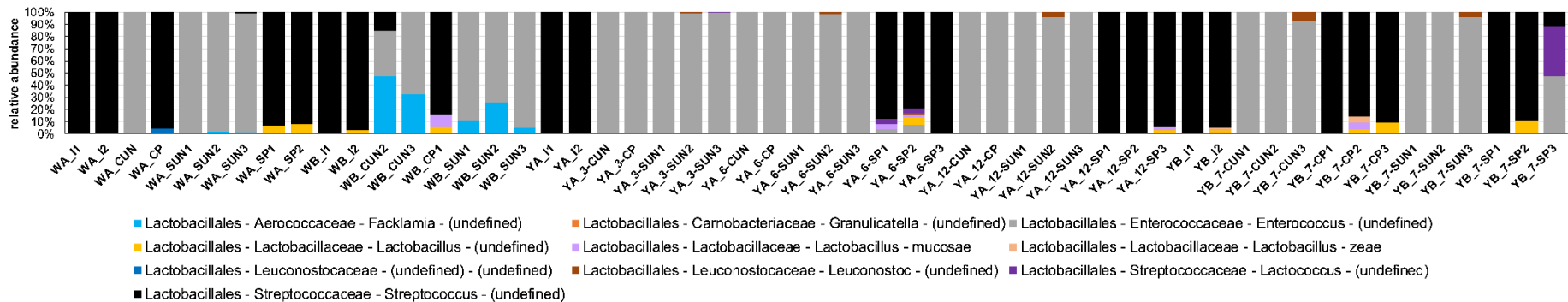


Figure C-8: Species abundance of order Lactobacillales (of class Bacilli of phylum Firmicutes) in specimens.

See Table 6-4 for sample ID nomenclature.

Various Bacillales taxa were identified at the species level in blood specimens. *Bacillus cereus* was uniquely detected in YB_UN specimens, and *Staphylococcus aureus*, *Staphylococcus epidermidis*, and an undefined *Listeria* sp. only detected in preserved blood specimens. However, these taxa were not consistently detected across specimens with the same environmental conditions.

Taxa of the Erysipelotrichi class were generally less abundant or not detected in unpreserved blood specimens. Amongst this class the dominant taxa detected were *Eubacterium bifforme* and an undefined *Catenibacterium* species, which was only present in preserved blood specimens and FMT specimens.

C.3.3 Bacteroidetes

The most abundant family amongst Bacteroidetes families was almost invariably Bacteroidaceae in the FMT specimens and blood specimens incubated at 37 °C (Figure C-9). In the WB_SUN2 and WB_SUN3 specimens, Porphyromonadaceae taxa co-dominated with Bacteroidaceae. Porphyromonadaceae taxa were predominantly undefined *Porphyromonas* spp. in unpreserved blood specimens incubated at 37 °C and Parabacteroides spp. in other specimens. In the blood specimens stored at room temperature there was generally a greater abundance of Odoribacteraceae detected than in other specimens. Odoribacteraceae taxa were identified as undefined *Butyricimonas* and *Odoribacter* spp..

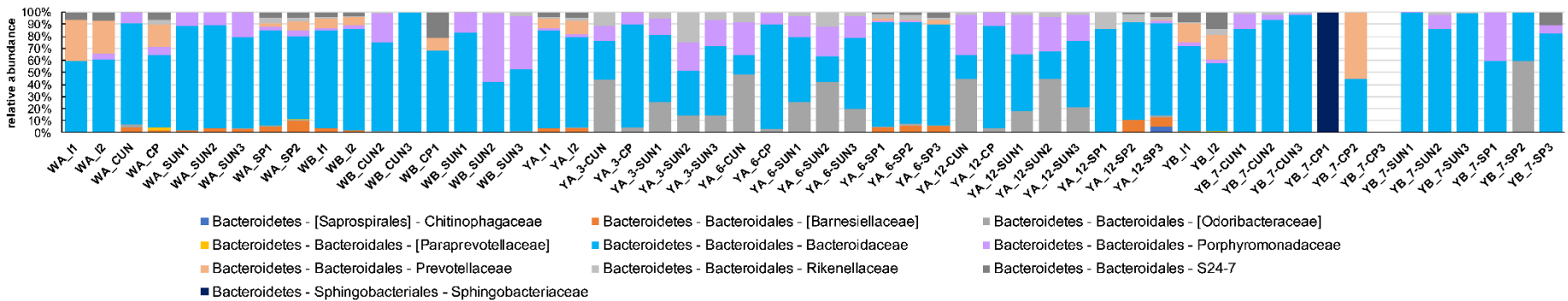


Figure C-9: Family abundance of phylum Bacteroidetes in specimens.

See Table 6-4 for sample ID nomenclature.

The dominant *Bacteroides* taxa identified at the species level were *Bacteroides fragilis*, *Bacteroides ovatus*, and undefined *Bacteroides* (Figure C-10). For all three species there was no general trend associated with their detection, however, *B. fragilis* was generally more abundant in unpreserved blood specimens than other specimens.

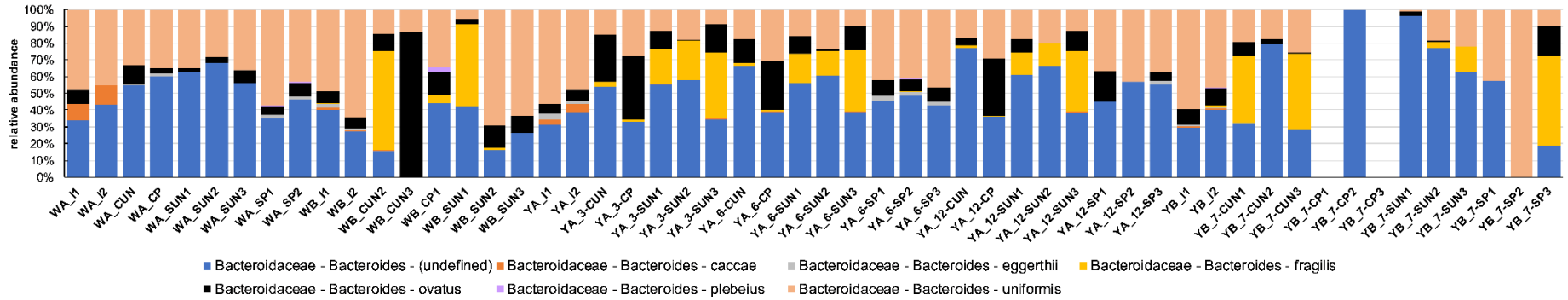


Figure C-10: Species abundance of family Bacteroidaceae (of order Bacteroidales of class Bacteroidia of phylum Bacteroidetes) in specimens.
 See Table 6-4 for sample ID nomenclature.

For low abundance Bacteroidetes taxa: Barnesiellaceae were not detected in YB specimens and YA_UN specimens; *Prevotella copri* was the dominant Prevotellaceae taxon, detected predominantly in FMT specimens and some preserved blood specimens; Rikenellaceae were not detected in YB_P specimens; and S24-7 were not detected in unpreserved blood specimens.

C.3.4 Actinobacteria

Coriobacteriales was the most abundant order of the Actinobacteria phylum detected in all specimens (Figure C-II). In unpreserved blood specimens, Coriobacteriales was more dominant and Bifidobacteriales less dominant compared to their general abundances in FMT specimens and preserved blood specimens. No Bifidobacteriales taxa were detected in unpreserved blood specimens stored at room temperature. The poorly abundant Acidimicrobiales and Actinomycetales taxa were not detected in any unpreserved blood specimens stored at room temperature.

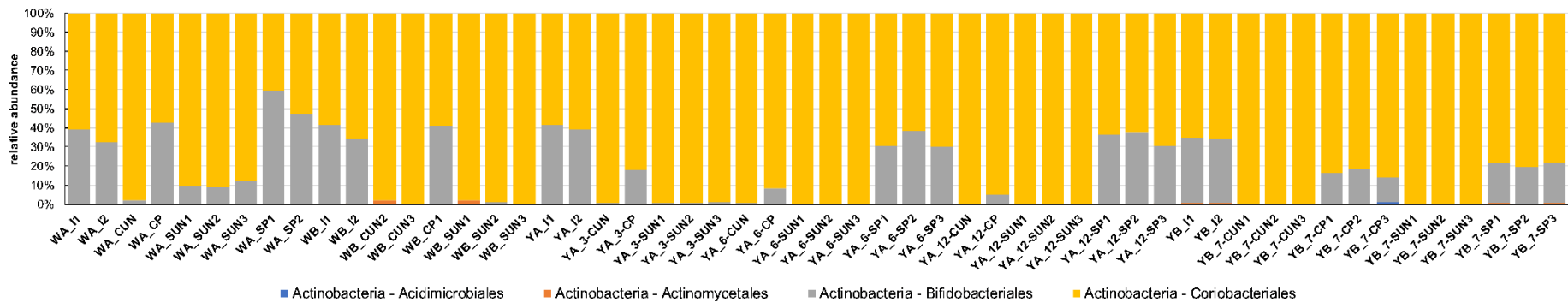


Figure C-II: Order abundance of phylum Actinobacteria in specimens.

See Table 6-4 for sample ID nomenclature.

Amongst Coriobacteriales taxa, *Eggerthella lenta* dominated most unpreserved blood specimens, whereas *Collinsella aerofaciens* dominated most preserved blood specimens and FMT specimens (Figure C-12). Both are obligate anaerobes. Exceptions to these generalisations were: YA_CP specimens, where *Eggerthella lenta* dominated: WA_UN specimens, where *Collinsella aerofaciens* and an undefined *Slackia* sp. were also highly abundant: and WB_CUN specimens. *Adlercreutzia* spp. were generally only detected in preserved blood specimens and FMT specimens, however, were also identified in WB_CUN3.

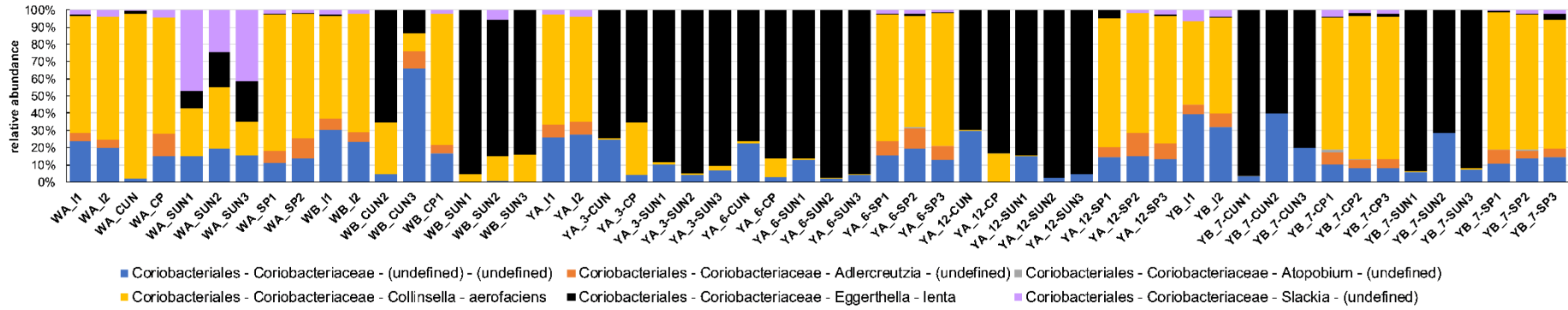


Figure C-12: Species abundance of order Coriobacteriales (of phylum Actinobacteria) in specimens.
See Table 6-4 for sample ID nomenclature.

Bifidobacterium adolescentis was the dominant Bifidobacteriales taxon present in FMT, WA_SP, and YB_SP specimens (Figure C-13). *Bifidobacterium longum* was generally more abundant in WA_UN and YA_3-month specimens than other specimens. *Bifidobacterium pseudolongum* was only identified in FMT specimens and preserved blood specimens stored at room temperature.

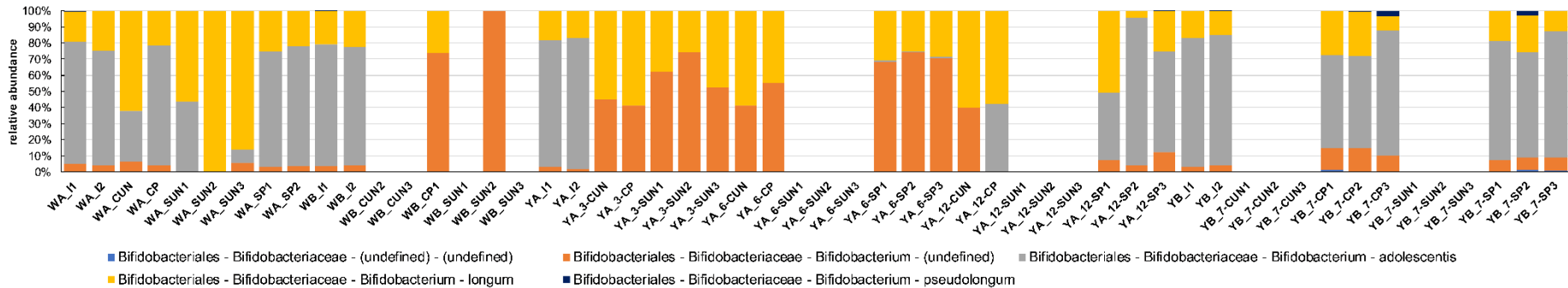


Figure C-13: Species abundance of order Bifidobacteriales (of phylum Actinobacteria) in specimens.
See Table 6-4 for sample ID nomenclature.

C.3.5 Proteobacteria

No Proteobacteria taxa were detected in the WB_CUN3 and YA_7-SUN3 specimens. For most other specimens, Proteobacteria taxa were dominated by taxa of the family Enterobacteriales (Figure C-14). Exceptions to this included: WA_SP specimens, where Burkholderiales and Desulfovibrionales taxa were dominant; WB_CPI, where Pseudomonadales was most dominant; some preserved specimens incubated at room temperature, which saw a greater dominance of Rhizobiales; and the YB_7-CUN2 and YB_7-CUN3 specimens, in which Burkholderiales dominated.

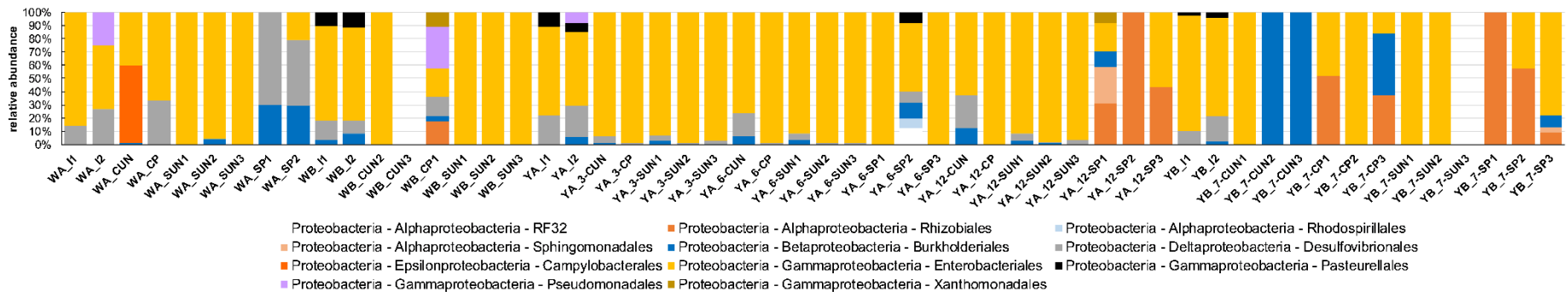


Figure C-14: Order abundance of phylum Proteobacteria in specimens.

See Table 6-4 for sample ID nomenclature.

Amongst the most dominant taxa: Enterobacteriales were only identified to the genus level in YB_I2, where an undefined *Serratia* sp. was detected. An undefined *Oxalobacter* sp. was the most common Burkholderiales taxon detected in both unpreserved blood specimens stored at room temperature and FMT specimens. Desulfovibrionales taxa were not detected in WA_UN, WB_UN, and YB blood specimens. Undefined *Desulfovibrio* spp. were detected in varying proportions in most other specimens. *Bilophila* sp. were detected sporadically. An undefined *Campylobacter* sp. (of order Campylobacterales) was detected in WA_CUN only.

Undefined *Pseudomonas* sp. (of order Pseudomonadales) was detected in the FMT specimens, WA_I2 and YA_I2, and the blood specimen WB_CPI. In WB_CPI an undefined *Acinetobacter* sp. was also detected. The Rhizobiales taxa were identified to the family level as undefined Bradyrhizobiaceae and Methylocystaceae, and to the genus level as an undefined *Methylobacterium* sp.. Bradyrhizobiaceae were exclusively detected in preserved blood specimens stored at room temperature for 7 and 12 months, and Methylocystaceae detected exclusively in WB_CPI. The *Methylobacterium* sp. was detected in WB_CPI, YA_I2-SP1, YA_I2-SP3, and YB_7-CP3.

APPENDIX D - DEGRADATION PRODUCTS

D.1 N-dealkylation degradation products

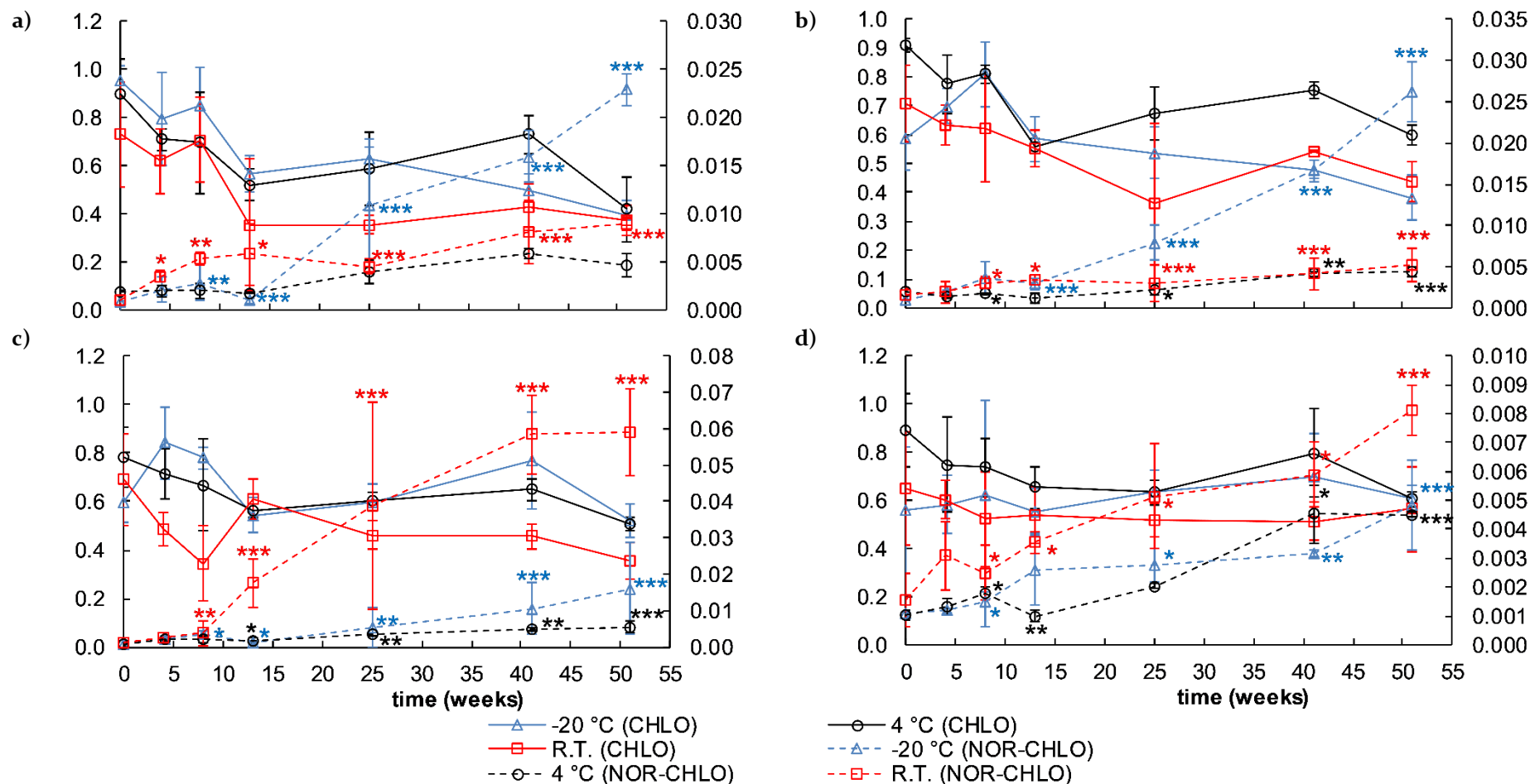


Figure D-1: Relative response of CHLO and NOR-CHLO over time in year experiment in a) non-inoculated, unpreserved specimens, b) non-inoculated, preserved specimens, c) inoculated, unpreserved specimens, and d) inoculated, preserved specimens.

Primary Y-axis is mean CHLO relative response. Secondary Y-axis is mean NOR-CHLO relative response. Asterisks indicate the acquisition of MS/MS spectra for NOR-CHLO in: * one replicate; ** two replicates; *** all three replicates. Error bars are \pm S.D., $n = 3$.

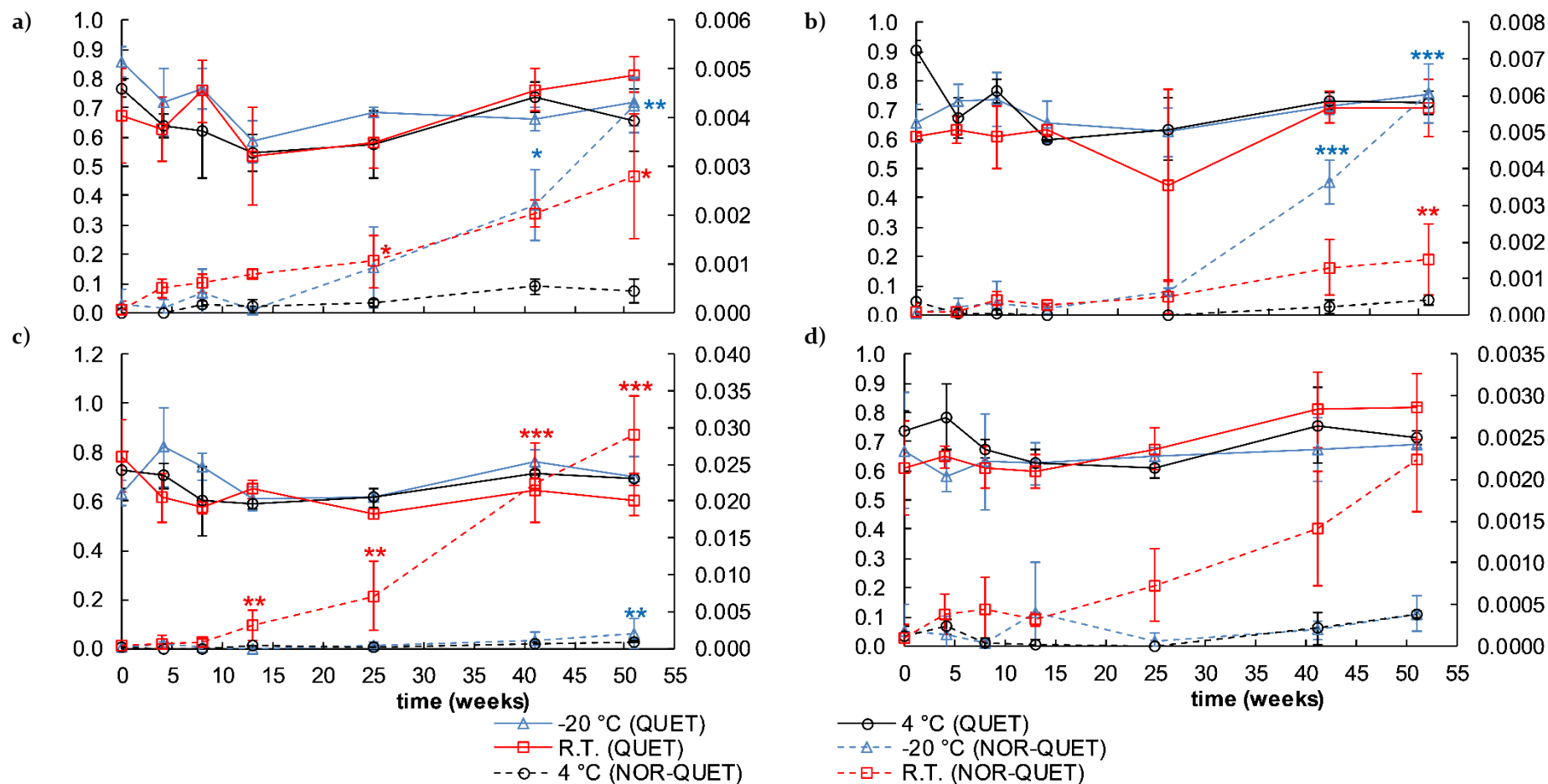


Figure D-2: Relative response of QUET and NOR-QUET over time in year experiment in a) non-inoculated, unpreserved specimens, b) non-inoculated, preserved specimens, c) inoculated, unpreserved specimens, and d) inoculated, preserved specimens.

Primary Y-axis is mean QUET relative response. Secondary Y-axis is mean NOR-QUET relative response. Asterisks indicate the acquisition of MS/MS spectra for NOR-QUET in: * one replicate; ** two replicates; *** all three replicates. Error bars are \pm S.D., n = 3.

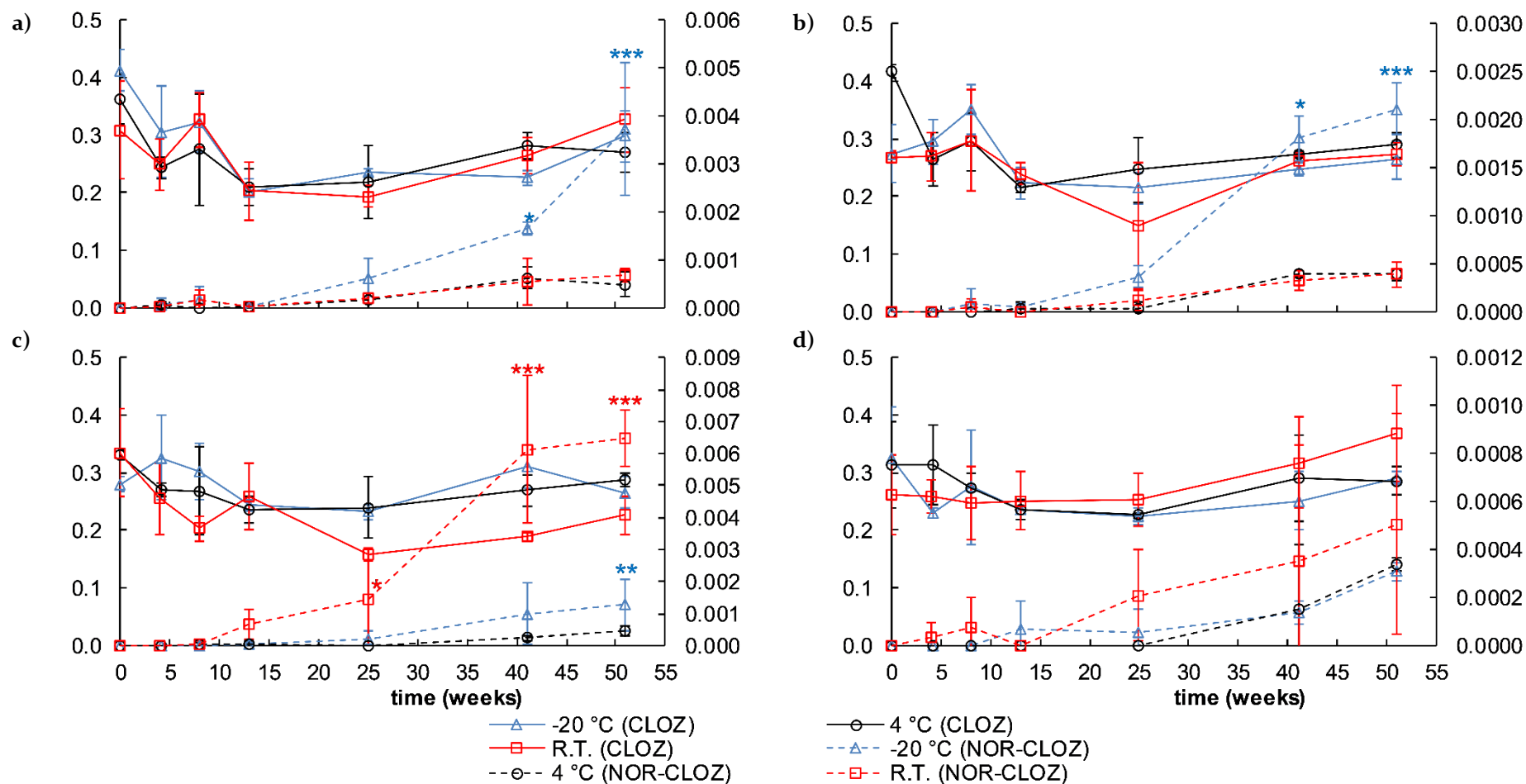


Figure D-3: Relative response of CLOZ and NOR-CLOZ over time in year experiment in a) non-inoculated, unpreserved specimens, b) non-inoculated, preserved specimens, c) inoculated, unpreserved specimens, and d) inoculated, preserved specimens.

Primary Y-axis is mean CLOZ relative response. Secondary Y-axis is mean NOR-CLOZ relative response. Asterisks indicate the acquisition of MS/MS spectra for NOR-CLOZ in: * one replicate; ** two replicates; *** all three replicates. Error bars are ± S.D., n = 3.

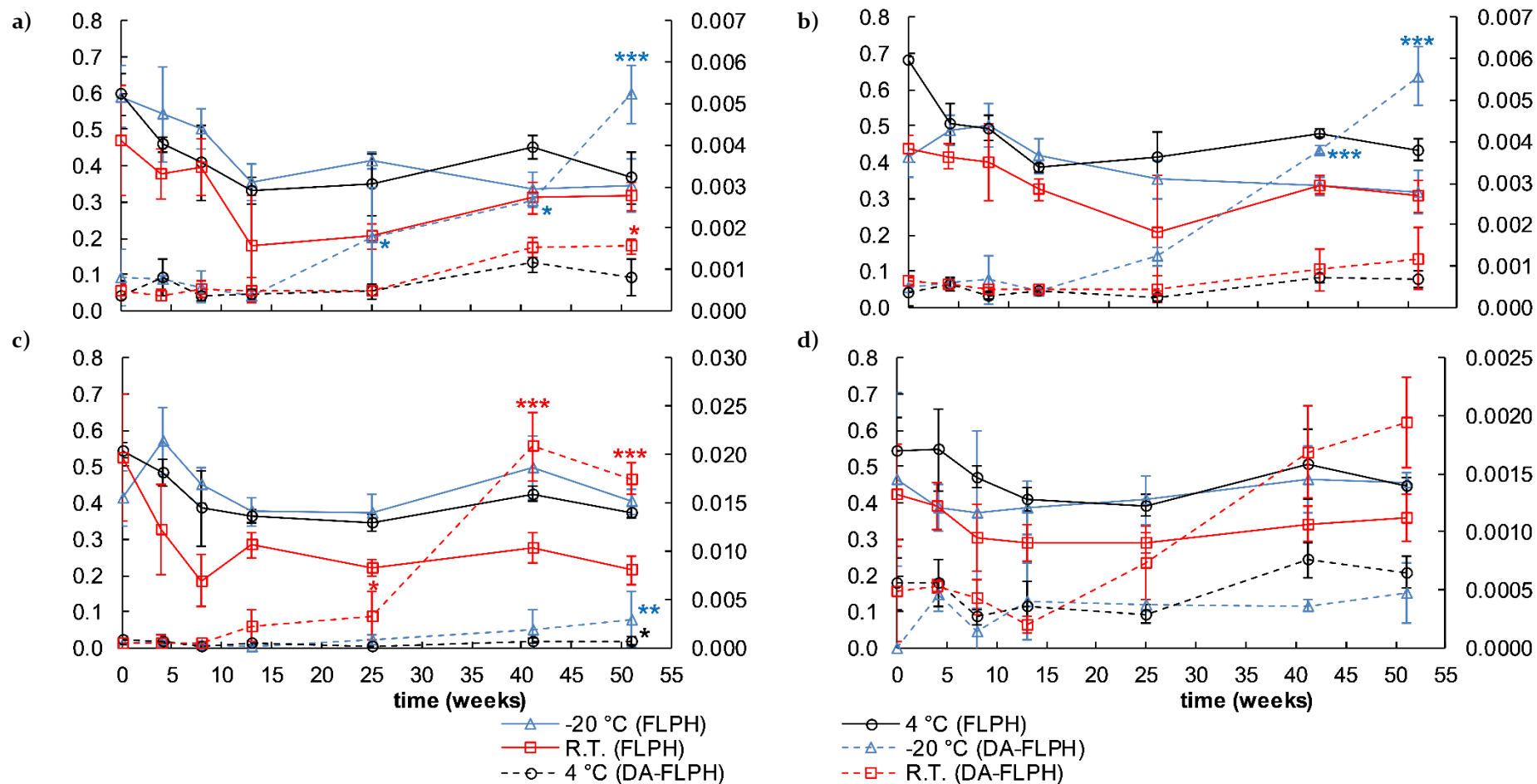


Figure D-4: Relative response of FLPH and DA-FLPH over time in year experiment in a) non-inoculated, unpreserved specimens, b) non-inoculated, preserved specimens, c) inoculated, unpreserved specimens, and d) inoculated, preserved specimens.

Primary Y-axis is mean FLPH relative response. Secondary Y-axis is mean DA-FLPH relative response. Asterisks indicate the acquisition of MS/MS spectra for DA-FLPH in: * one replicate; ** two replicates; *** all three replicates. Error bars are ± S.D., n = 3.

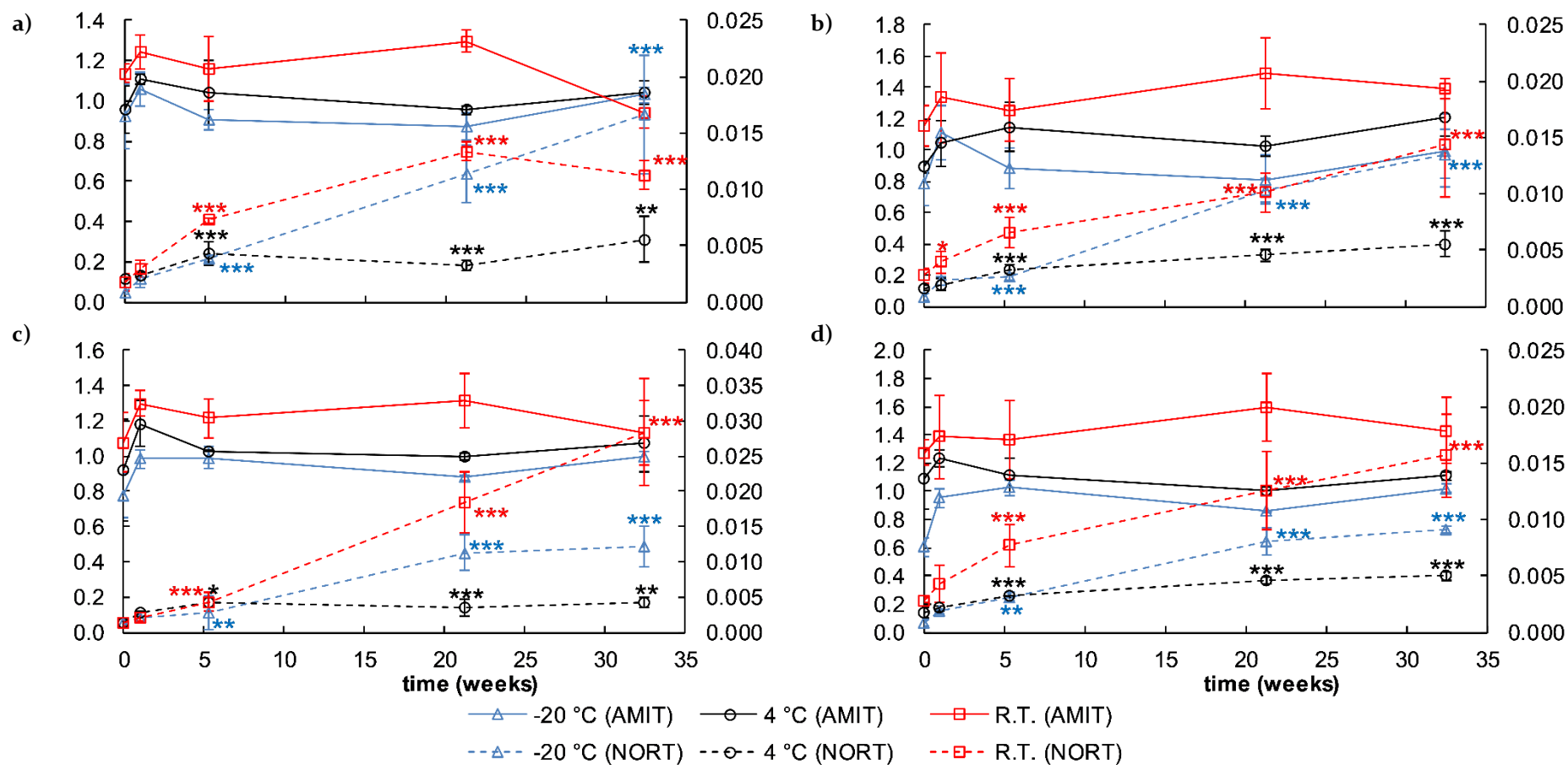


Figure D-5: Relative response of AMIT and NORT over time in experiment YB in a) non-inoculated, unpreserved specimens, b) non-inoculated, preserved specimens, c) inoculated, unpreserved specimens, and d) inoculated, preserved specimens.

Primary Y-axis is mean AMIT relative response. Secondary Y-axis is mean NORT relative response. Asterisks indicate the acquisition of MS/MS spectra for NORT in: * one replicate; ** two replicates; *** all three replicates. Error bars are \pm S.D., $n = 3$.

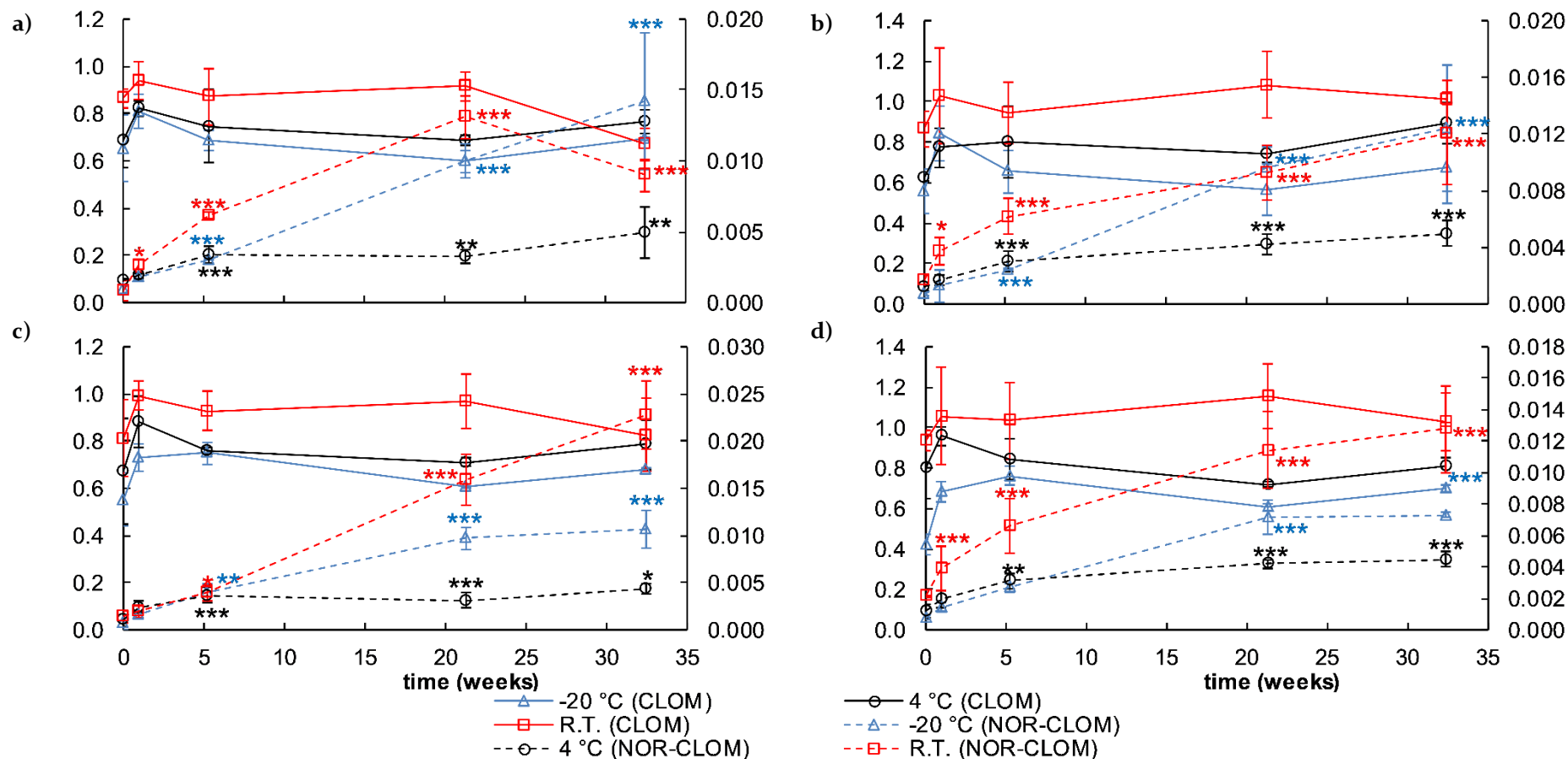


Figure D-6: Relative response of CLOM and NOR-CLOM over time in seven-month experiment in a) non-inoculated, unpreserved specimens, b) non-inoculated, preserved specimens, c) inoculated, unpreserved specimens, and d) inoculated, preserved specimens. Primary Y-axis is mean CLOM relative response. Secondary Y-axis is mean NOR-CLOM relative response. Asterisks indicate the acquisition of MS/MS spectra for NOR-CLOM in: * one replicate; ** two replicates; *** all three replicates. Error bars are \pm S.D., n = 3.

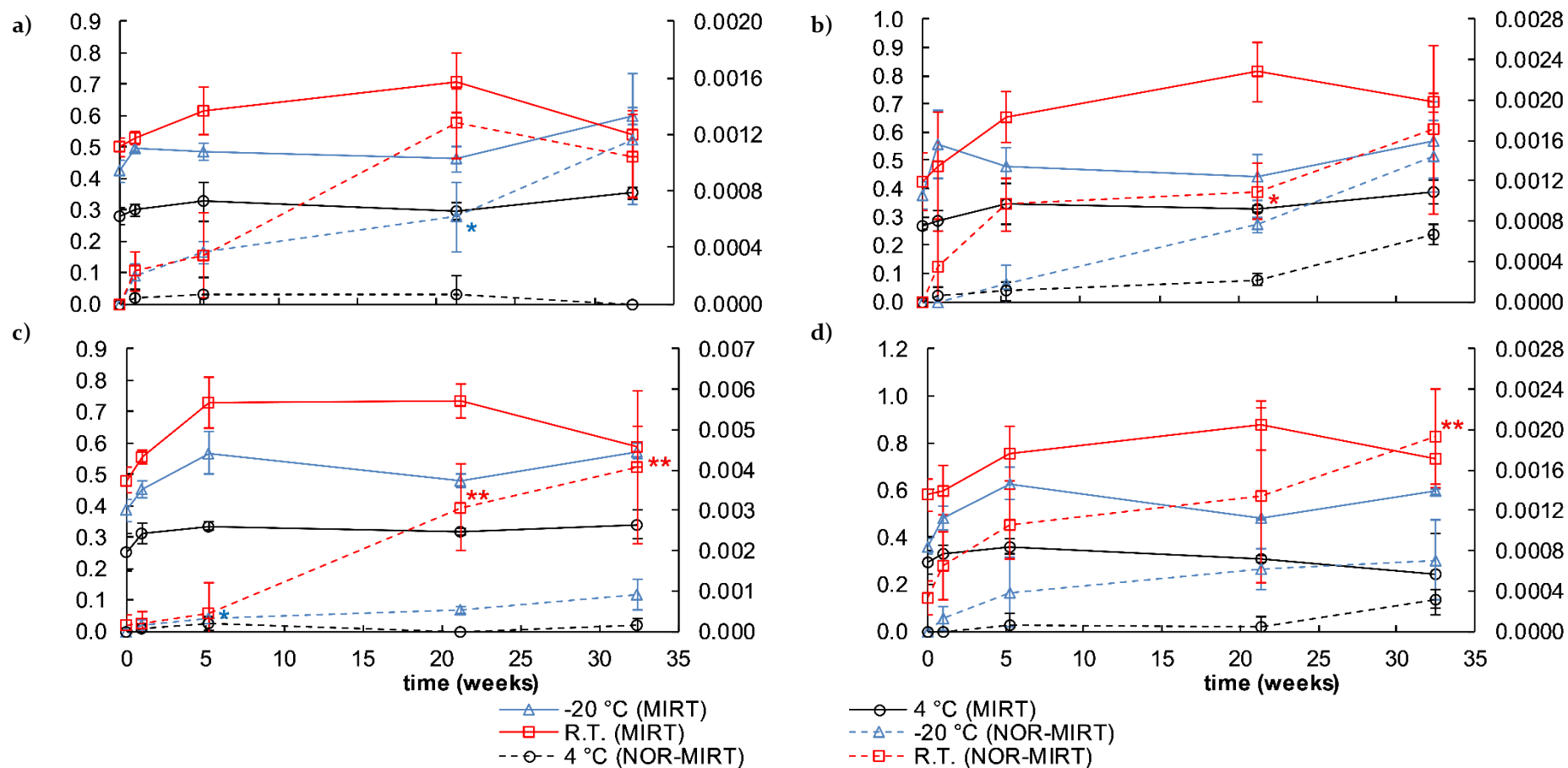


Figure D-7: Relative response of MIRT and NOR-MIRT over time in seven-month experiment in a) non-inoculated, unpreserved specimens, b) non-inoculated, preserved specimens, c) inoculated, unpreserved specimens, and d) inoculated, preserved specimens. Primary Y-axis is mean MIRT relative response. Secondary Y-axis is mean NOR-MIRT relative response. Asterisks indicate the acquisition of MS/MS spectra for NOR-MIRT in: * one replicate; ** two replicates; *** all three replicates. Error bars are \pm S.D., n = 3.

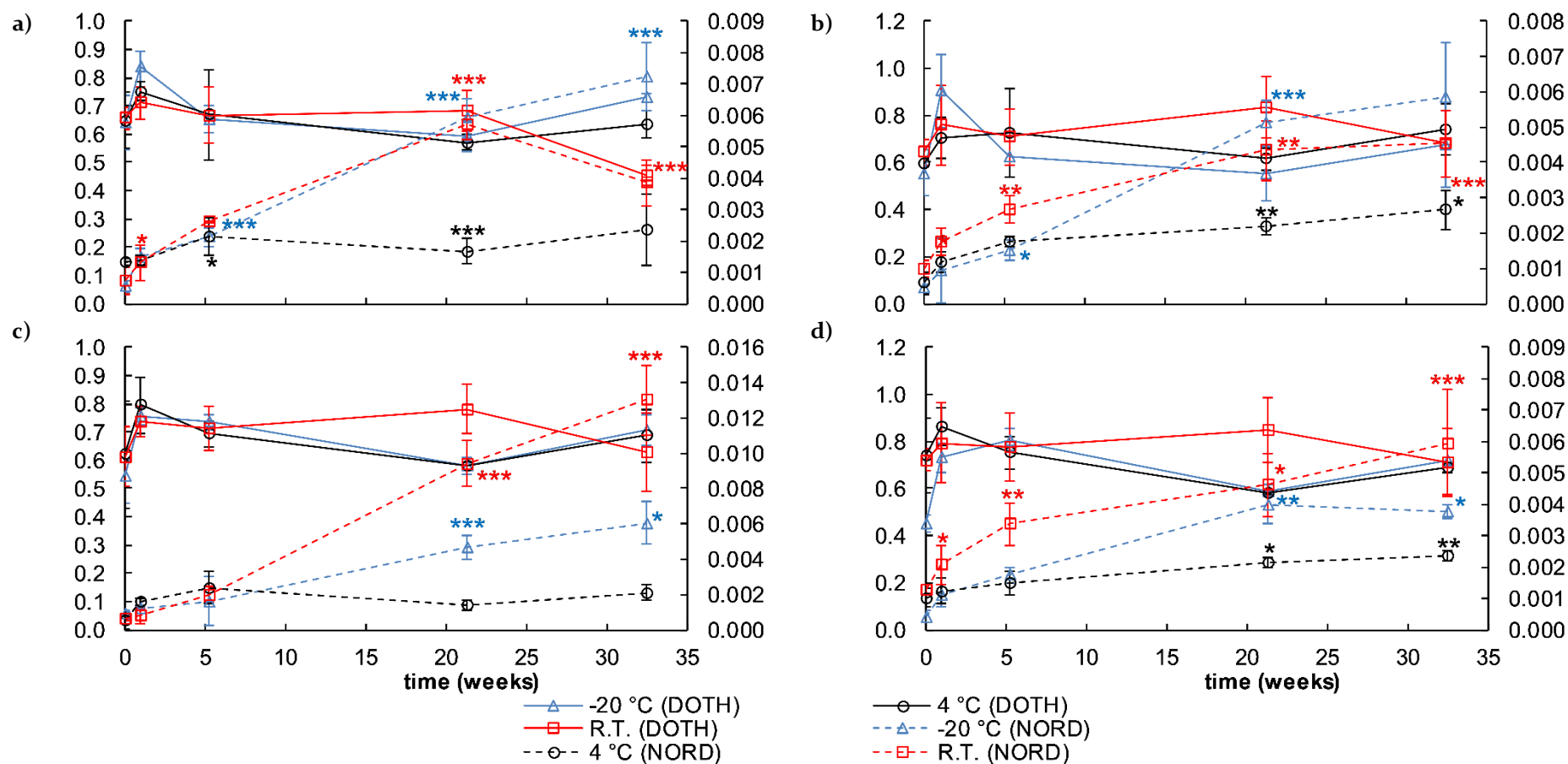


Figure D-8: Relative response of DOTH and NORD over time in seven-month experiment in a) non-inoculated, unpreserved specimens, b) non-inoculated, preserved specimens, c) inoculated, unpreserved specimens, and d) inoculated, preserved specimens.

Primary Y-axis is mean DOTH relative response. Secondary Y-axis is mean NORD relative response. Asterisks indicate the acquisition of MS/MS spectra for NORD in: * one replicate; ** two replicates; *** all three replicates. Error bars are \pm S.D., n = 3.

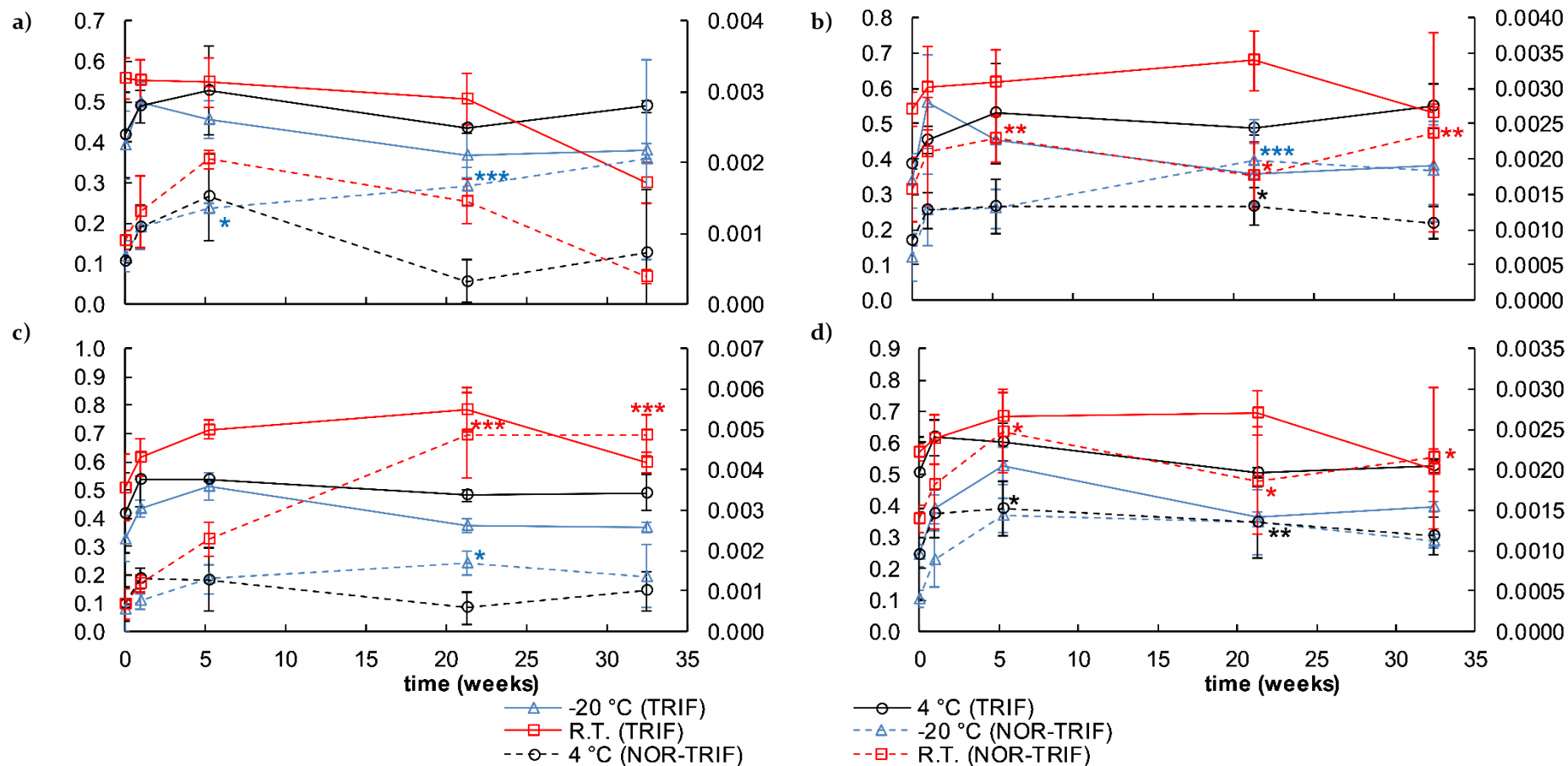


Figure D-9: Relative response of TRIF and NOR-TRIF over time in seven-month experiment in a) non-inoculated, unpreserved specimens, b) non-inoculated, preserved specimens, c) inoculated, unpreserved specimens, and d) inoculated, preserved specimens. Primary Y-axis is mean TRIF relative response. Secondary Y-axis is mean NOR-TRIF relative response. Asterisks indicate the acquisition of MS/MS spectra for NOR-TRIF in: * one replicate; ** two replicates; *** all three replicates. Error bars are \pm S.D., n = 3.

D.2 Sulfoxide degradation products

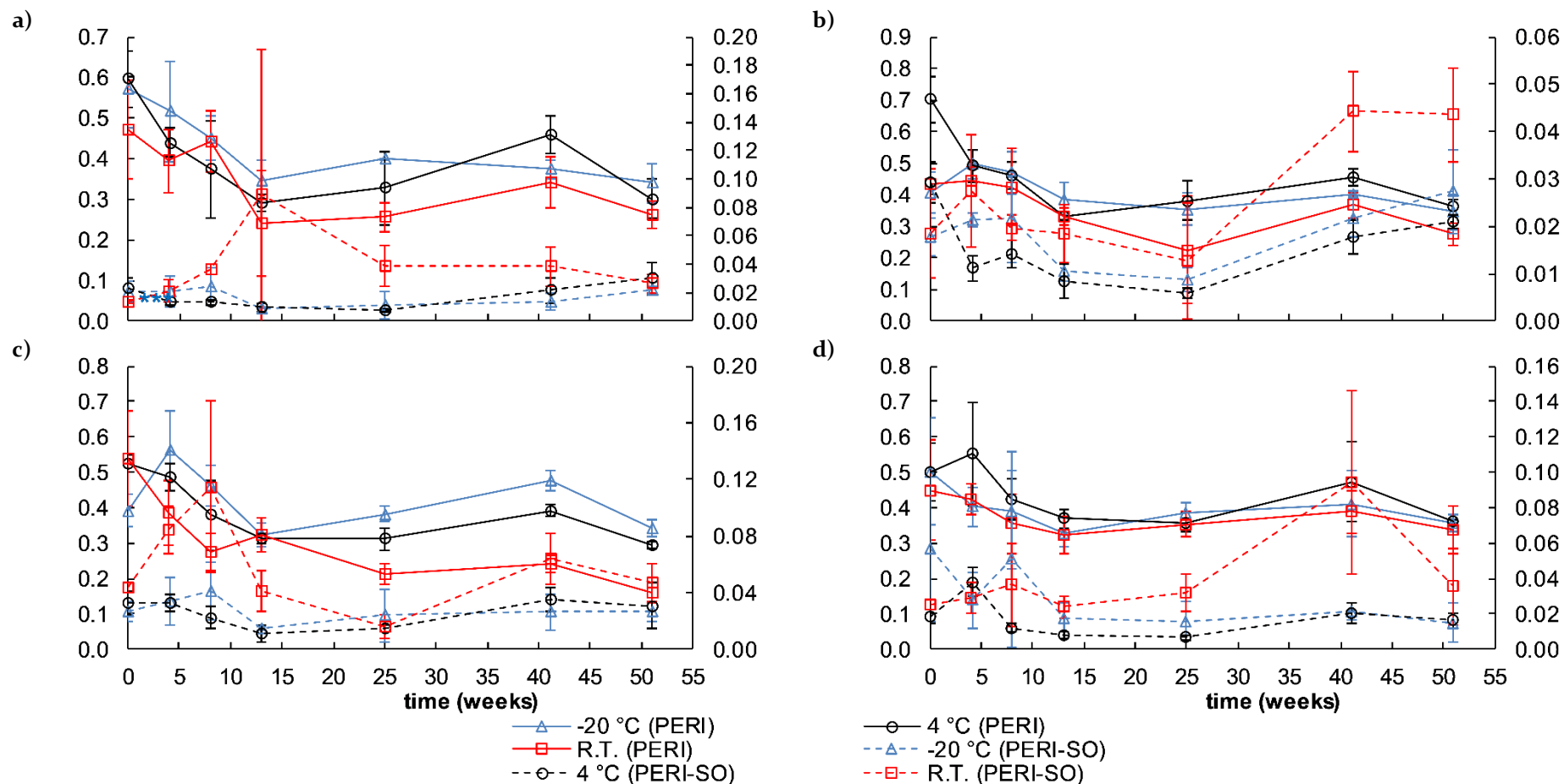


Figure D-10: Relative response of PERI and PERI-SO over time in seven-month experiment in a) non-inoculated, unpreserved specimens, b) non-inoculated, preserved specimens, c) inoculated, unpreserved specimens, and d) inoculated, preserved specimens.

Primary Y-axis is mean PERI relative response. Secondary Y-axis is mean PERI-SO relative response. Auto-MS/MS spectra acquired for PERI-SO in all specimens and replicates. Error bars are \pm S.D., n = 3.

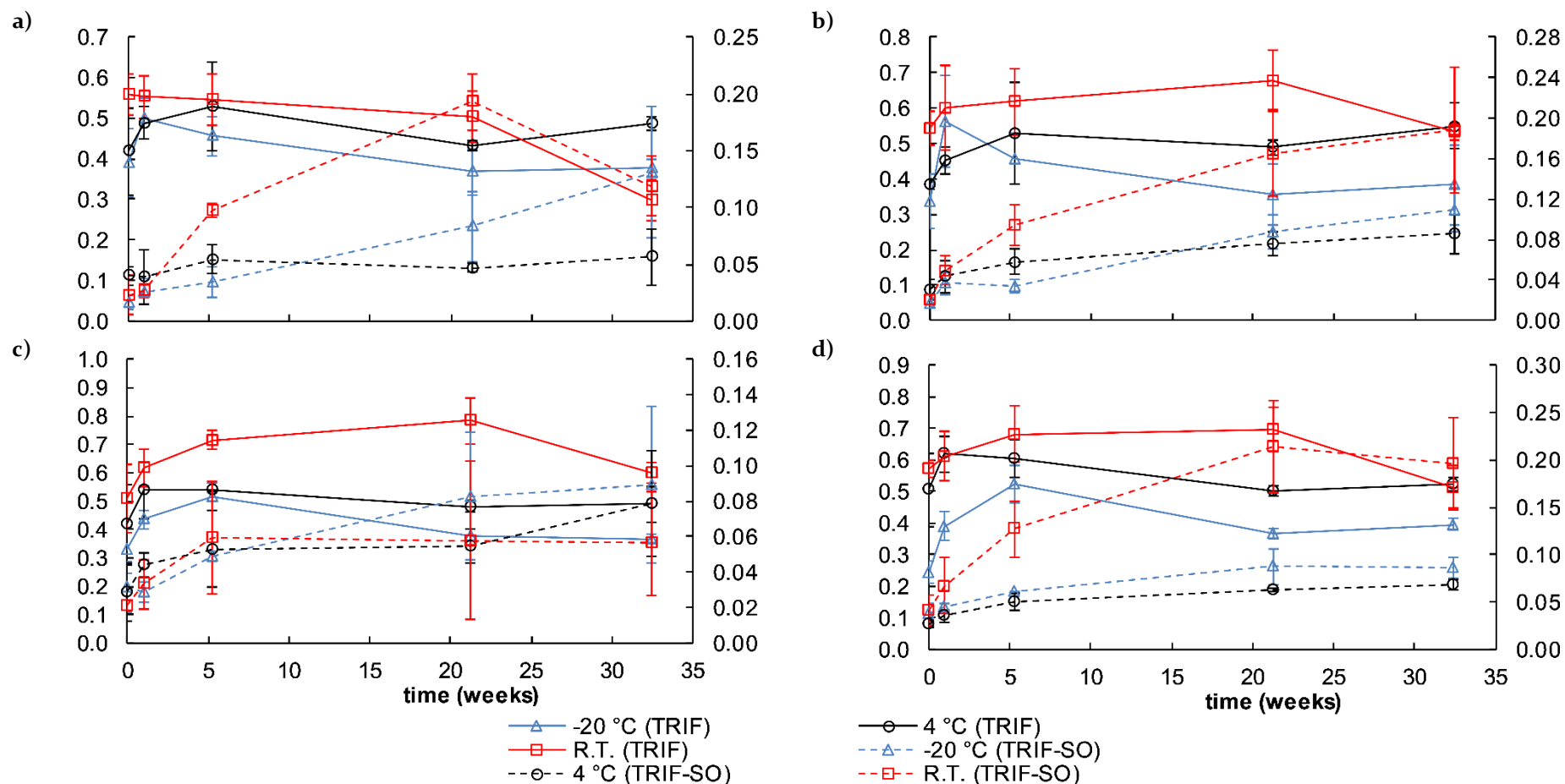


Figure D-II: Relative response of TRIF and TRIF-SO over time in seven-month experiment in a) non-inoculated, unpreserved specimens, b) non-inoculated, preserved specimens, c) inoculated, unpreserved specimens, and d) inoculated, preserved specimens.

Primary Y-axis is mean TRIF relative response. Secondary Y-axis is mean TRIF-SO relative response. Auto-MS/MS spectra acquired for TRIF-SO in all specimens except for: a T0 4 °C, non-inoculated, unpreserved specimen and a ~5 week -20 °C, inoculated, unpreserved specimen. Error bars are \pm S.D., n = 3.

REFERENCES

1. Fraser, T., *Confirming the Identity of the Microbial Degradation Product of Lurasidone*, in College of Science and Engineering, Flinders University. 2018. Bachelor of Science (Forensic and Analytical Science) (Honours).
2. Butzbach, D.M., *et al.*, *Bacterial Degradation of Risperidone and Paliperidone in Decomposing Blood*. *Journal of Forensic Sciences*, 2013. **58**(1): p. 90-100.
3. Taylor, K. and S. Elliott, *An unusual case of risperidone instability in a fatality presenting an analytical and interpretative challenge*. *Drug Testing and Analysis*, 2013. **5**(9-10): p. 748-752.
4. Rao, R.B. and M.A. Flomenbaum, *Postmortem Toxicology*, in *Goldfrank's Toxicologic Emergencies. Ninth edition*. L.S. Nelson, *et al.*, Editors. 2011, New York, USA: McGraw-Hill Companies, Inc. p. 471-478.
5. Langlois, N.E.I., *et al.*, *An audit of the toxicology findings in 555 medico-legal autopsies finds manner of death changed in 5 cases*. *Forensic Science, Medicine, and Pathology*, 2013. **9**(1): p. 44-47.
6. Gruszecki, A.C., J. Booth, and G.G. Davis, *The Predictive Value of History and Scene Investigation for Toxicology Results in a Medical Examiner Population*. *The American Journal of Forensic Medicine and Pathology*, 2007. **28**(2): p. 103-106.
7. Pilgrim, J.L., D. Gerostamoulos, and O.H. Drummer, *The role of toxicology interpretations in prevention of sudden death*. *Forensic science, medicine, and pathology*, 2012. **8**(3): p. 263-269.
8. Gill, J.R. and I.A. Scordi-Bello, *Natural, Unexpected Deaths: Reliability of a Presumptive Diagnosis*. *Journal of Forensic Sciences*, 2010. **55**(1): p. 77-81.
9. Nelson, D.L., A.L. Lehninger, and M.M. Cox, *Lehninger Principles of Biochemistry. Fifth edition*. 2008, New York, USA: Macmillan.
10. Evans, W.E.D., *The chemistry of death*. 1963, Springfield, USA: Charles C Thomas Pub Ltd.
11. Janaway, R.C., S.L. Percival, and A.S. Wilson, *Decomposition of Human Remains*, in *Microbiology and Aging*. S.L. Percival, Editor. 2009, Towata, USA: Humana Press. p. 313-334.
12. Donaldson, A.E. and I.L. Lamont, *Biochemistry Changes That Occur after Death: Potential Markers for Determining Post-Mortem Interval*. *PLoS ONE*, 2013. **8**(11): p. e82011.
13. Willey, J.M., L.M. Sherwood, and C.J. Woolverton, *Prescott's Microbiology. Ninth edition*. 2014, New York, USA: McGraw-Hill.
14. Janaway, R.C., *The decay of buried human remains and their associated materials*, in *Studies in Crime: An Introduction to Forensic Archaeology*. J. Hunter, C. Roberts, and A. Martin, Editors. 1996, London, UK: Psychology Press. p. 58-85.
15. Mesli, V., C. Neut, and V. Hedouin, *Postmortem bacterial translocation*, in *Forensic Microbiology*. D.O. Carter, *et al.*, Editors. 2017, Hoboken, USA: John Wiley & Sons, Ltd. p. 192-211.
16. Kellerman, G.D., N.G. Waterman, and L.F. Scharefenberger, *Demonstration in vitro of postmortem bacterial transmigration*. *American Journal of Clinical Pathology*, 1976. **66**(5): p. 911-915.
17. Melvin Jr, J.R., *et al.*, *Bacterial transmigration as an indicator of time of death*. *Journal of Forensic Sciences*, 1984. **29**(2): p. 412-417.
18. Myrvik, Q.N. and R.S. Weiser, *Fundamentals of medical bacteriology and mycology. Second edition*. 1988, Philadelphia, USA: Lea & Febiger.
19. Morris, J.A., L.M. Harrison, and S.M. Partridge, *Practical and theoretical aspects of postmortem bacteriology*. *Current Diagnostic Pathology*, 2007. **13**(1): p. 65-74.
20. Hyde, E.R., *et al.*, *The living dead: bacterial community structure of a cadaver at the onset and end of the bloat stage of decomposition*. *PLoS ONE*, 2013. **8**(10): p. e77733.

21. Tuomisto, S., P.J. Karhunen, and T. Pessi, *Time-dependent post mortem changes in the composition of intestinal bacteria using real-time quantitative PCR*. *Gut Pathogens*, 2013. **5**(35): p. 1-5.
22. Corry, J.E., *Possible Sources of Ethanol Ante- and Post-mortem: its Relationship to the Biochemistry and Microbiology of Decomposition*. *Journal of Applied Bacteriology*, 1978. **44**(1): p. 1-56.
23. Metcalf, J.L., *et al.*, *A microbial clock provides an accurate estimate of the postmortem interval in a mouse model system*. *eLIFE*, 2013. **2**: p. e01104.
24. Hyde, E.R., *et al.*, *Microbial communities associated with decomposing corpses*, in *Forensic Microbiology*. D.O. Carter, *et al.*, Editors. 2017, Hoboken, USA: John Wiley & Sons, Ltd. p. 245-273.
25. Javan, G.T., *et al.*, *Cadaver Thanatobiome Signatures: The Ubiquitous Nature of Clostridium Species in Human Decomposition*. *Frontiers in Microbiology*, 2017. **8**: p. 2096.
26. Paczkowski, S. and S. Schütz, *Post-mortem volatiles of vertebrate tissue*. *Applied Microbiology and Biotechnology*, 2011. **91**(4): p. 917-35.
27. Schoenen, D. and H. Schoenen, *Adipocere formation—The result of insufficient microbial degradation*. *Forensic Science International*, 2013. **226**(1-3): p. 301.e1-301.e6.
28. Zhou, C. and R.W. Byard, *Factors and processes causing accelerated decomposition in human cadavers – An overview*. *Journal of Forensic and Legal Medicine*, 2011. **18**(1): p. 6-9.
29. Ferreira, M.T. and E. Cunha, *Can we infer post mortem interval on the basis of decomposition rate? A case from a Portuguese cemetery*. *Forensic Science International*, 2013. **226**(1-3): p. 298.e1-298.e6.
30. Qin, J., *et al.*, *A human gut microbial gene catalogue established by metagenomic sequencing*. *Nature*, 2010. **464**(7285): p. 59-65.
31. Rajilić-Stojanović, M. and W.M. de Vos, *The first 1000 cultured species of the human gastrointestinal microbiota*. *FEMS Microbiology Reviews*, 2014. **38**(5): p. 996-1047.
32. Lagier, J.-C., *et al.*, *Culture of previously uncultured members of the human gut microbiota by culturomics*. *Nature Microbiology*, 2016. **1**(12): p. 16203.
33. Yatsunenko, T., *et al.*, *Human gut microbiome viewed across age and geography*. *Nature*, 2012. **486**(7402): p. 222-227.
34. Wagner Mackenzie, B., D.W. Waite, and M.W. Taylor, *Evaluating variation in human gut microbiota profiles due to DNA extraction method and inter-subject differences*. *Frontiers in Microbiology*, 2015. **6**: p. 130.
35. Ley, R.E., *et al.*, *Obesity alters gut microbial ecology*. *Proceedings of the National Academy of Sciences of the United States of America*, 2005. **102**(31): p. 11070-11075.
36. Rodríguez, M.M., *et al.*, *Obesity changes the human gut mycobiome*. *Scientific Reports*, 2015. **5**: p. 14600.
37. Scheperjans, F., *et al.*, *Gut microbiota are related to Parkinson's disease and clinical phenotype*. *Movement Disorders*, 2015. **30**(3): p. 350-358.
38. Larsen, N., *et al.*, *Gut Microbiota in Human Adults with Type 2 Diabetes Differs from Non-Diabetic Adults*. *PLoS ONE*, 2010. **5**(2): p. e9085.
39. De Filippo, C., *et al.*, *Impact of diet in shaping gut microbiota revealed by a comparative study in children from Europe and rural Africa*. *Proceedings of the National Academy of Sciences*, 2010. **107**(33): p. 14691-14696.
40. Bahr, S.M., *et al.*, *Use of the second-generation antipsychotic, risperidone, and secondary weight gain are associated with an altered gut microbiota in children*. *Translational Psychiatry*, 2015. **5**(10): p. e652.

41. Christoffersen, S., *The importance of microbiological testing for establishing cause of death in 42 forensic autopsies*. *Forensic Science International*, 2015. **250**: p. 27-32.
42. Martínez-Ramírez, J.A., *et al.*, *Studies on drug metabolism by fungi colonizing decomposing human cadavers. Part I: DNA sequence-based identification of fungi isolated from postmortem material*. *Analytical and Bioanalytical Chemistry*, 2013. **405**(26): p. 8443-8450.
43. Schwarz, P., *et al.*, *Molecular identification of fungi found on decomposed human bodies in forensic autopsy cases*. *International Journal of Legal Medicine*, 2015. **129**(4): p. 785-791.
44. Tibbett, M. and D.O. Carter, *Mushrooms and taphonomy: The fungi that mark woodland graves*. *Mycologist*, 2003. **17**(1): p. 20-24.
45. Tranchida, M.C., N.D. Centeno, and M.N. Cabello, *Soil fungi: Their potential use as a forensic tool*. *Journal of Forensic Sciences*, 2014. **59**(3): p. 785-789.
46. Ishii, K., *et al.*, *Analysis of fungi detected in human cadavers*. *Legal Medicine*, 2006. **8**(3): p. 188-190.
47. Carter, D.O. and M. Tibbett, *Taphonomic mycota: Fungi with forensic potential*. *Journal of Forensic Sciences*, 2003. **48**(1): p. 168-171.
48. Rose, G.W. and R.N. Hockett, *The microbiologic evaluation and enumeration of postmortem specimens from human remains*. *Health Laboratory Science*, 1971. **8**(2): p. 75.
49. Morris, J.A., L.M. Harrison, and S.M. Partridge, *Postmortem bacteriology: a re-evaluation*. *Journal of Clinical Pathology*, 2006. **59**(1): p. 1-9.
50. Sidrim, J.J.C., *et al.*, *Fungal microbiota dynamics as a postmortem investigation tool: Focus on Aspergillus, Penicillium and Candida species*. *Journal of Applied Microbiology*, 2010. **108**(5): p. 1751-1756.
51. Javan, G.T., *et al.*, *Human thanatomicrobiome succession and time since death*. *Scientific Reports*, 2016. **6**: p. 29598.
52. Handke, J., *et al.*, *Successive bacterial colonisation of pork and its implications for forensic investigations*. *Forensic Science International*, 2017. **281**: p. 1-8.
53. Dolan, C.T., A.L. Brown Jr, and R.E. Ritts Jr, *Microbiological examination of postmortem tissues*. *Archives of Pathology*, 1971. **92**(3): p. 206-211.
54. Lawson, A.J., D. Linton, and J. Stanley, *16S rRNA gene sequences of 'Candidatus Campylobacter hominis', a novel uncultivated species, are found in the gastrointestinal tract of healthy humans*. *Microbiology*, 1998. **144**(8): p. 2063-2071.
55. Lagier, J.-C., *et al.*, *Culturing the human microbiota and culturomics*. *Nature Reviews Microbiology*, 2018. **16**(9): p. 540.
56. Suau, A., *et al.*, *Direct Analysis of Genes Encoding 16S rRNA from Complex Communities Reveals Many Novel Molecular Species within the Human Gut*. *Applied and Environmental Microbiology*, 1999. **65**(11): p. 4799-4807.
57. Breitbart, M., *et al.*, *Metagenomic Analyses of an Uncultured Viral Community from Human Feces*. *Journal of Bacteriology*, 2003. **185**(20): p. 6220-6223.
58. Gouba, N., D. Raoult, and M. Drancourt, *Eukaryote Culturomics of the Gut Reveals New Species*. *PLoS ONE*, 2014. **9**(9): p. e106994.
59. Pechal, J.L., *et al.*, *The potential use of bacterial community succession in forensics as described by high throughput metagenomic sequencing*. *International Journal of Legal Medicine*, 2014. **128**(1): p. 193-205.
60. Carter, D.O., *et al.*, *Seasonal variation of postmortem microbial communities*. *Forensic Science, Medicine, and Pathology*, 2015. **11**(2): p. 202-207.
61. Finley, S.J., M.E. Benbow, and G.T. Javan, *Microbial communities associated with human decomposition and their potential use as postmortem clocks*. *International Journal of Legal Medicine*, 2015. **129**(3): p. 623-632.

62. Damann, F.E., D.E. Williams, and A.C. Layton, *Potential Use of Bacterial Community Succession in Decaying Human Bone for Estimating Postmortem Interval*. *Journal of Forensic Sciences*, 2015. **60**(4): p. 844-850.
63. Pechal, J.L., *et al.*, *Microbial Community Functional Change during Vertebrate Carrion Decomposition*. *PLoS ONE*, 2013. **8**(11): p. e79035.
64. Hyde, E.R., *et al.*, *Initial insights into bacterial succession during human decomposition*. *International Journal of Legal Medicine*, 2015. **129**(3): p. 661-671.
65. Benbow, M.E., *et al.*, *The Potential of High-throughput Metagenomic Sequencing of Aquatic Bacterial Communities to Estimate the Postmortem Submersion Interval*. *Journal of Forensic Sciences*, 2015. **60**(6): p. 1500-1510.
66. Suhr, M.J. and H.E. Hallen-Adams, *The human gut mycobiome: pitfalls and potentials—a mycologist's perspective*. *Mycologia*, 2015. **107**(6): p. 1057-1073.
67. Jones, G.R., *Postmortem toxicology*, in *Clarke's Analytical Forensic Toxicology. Second edition*. A. Negrusz and G. Cooper, Editors. 2013, London, UK: Pharmaceutical Press. p. 189-214.
68. Pounder, D.J. and G.R. Jones, *Post-mortem drug redistribution — A toxicological nightmare*. *Forensic Science International*, 1990. **45**(3): p. 253-263.
69. Prouty, R.W. and W.H. Anderson, *The forensic science implications of site and temporal influences on postmortem blood-drug concentrations*. *Journal of Forensic Sciences*, 1990. **35**(2): p. 243-270.
70. Sastre, C., *et al.*, *Post mortem redistribution of drugs: current state of knowledge*. *Current Pharmaceutical Design*, 2017. **23**(36): p. 5530-5541.
71. Drummer, O.H. and S.H.Y. Wong, *Pharmacokinetics and Metabolism*, in *Clarke's Analytical Forensic Toxicology. Second edition*. A. Negrusz and G. Cooper, Editors. 2013, London, UK: Pharmaceutical Press. p. 11-38.
72. McIntyre, I.M., *Liver and peripheral blood concentration ratio (L/P) as a marker of postmortem drug redistribution: a literature review*. *Forensic Science, Medicine, and Pathology*, 2014. **10**(1): p. 91-96.
73. Apple, F.S. and C.M. Bandt, *Liver and blood postmortem tricyclic antidepressant concentrations*. *American Journal of Clinical Pathology*, 1988. **89**(6): p. 794-796.
74. Pounder, D.J., *et al.*, *Site to site variability of postmortem drug concentrations in liver and lung*. *Journal of Forensic Sciences*, 1996. **41**(6): p. 927-932.
75. Robertson, M.D. and O.H. Drummer, *Postmortem distribution and redistribution of nitrobenzodiazepines in man*. *Journal of Forensic Sciences*, 1998. **43**(1): p. 9-13.
76. Molina, D.K., *Handbook of Forensic Toxicology for Medical Examiners*. 2009, Boca Raton, USA: CRC Press.
77. Han, E., *et al.*, *Evaluation of postmortem redistribution phenomena for commonly encountered drugs*. *Forensic Science International*, 2012. **219**(1-3): p. 265-271.
78. Saar, E., *et al.*, *The time-dependant post-mortem redistribution of antipsychotic drugs*. *Forensic Science International*, 2012. **222**(1-3): p. 223-227.
79. Gerostamoulos, D., *et al.*, *The effect of the postmortem interval on the redistribution of drugs: a comparison of mortuary admission and autopsy blood specimens*. *Forensic Science, Medicine, and Pathology*, 2012. **8**(4): p. 373-379.
80. Staeheli, S.N., *et al.*, *Development of CT-guided biopsy sampling for time-dependent postmortem redistribution investigations in blood and alternative matrices—proof of concept and application on two cases*. *Analytical and Bioanalytical Chemistry*, 2016. **408**(4): p. 1249-1258.
81. Brockbals, L., *et al.*, *Fatal poisoning involving cyclopropylfentanyl — Investigation of time-dependent postmortem redistribution*. *Forensic Science International*, 2019. **294**: p. 80-85.

82. Palamalai, V., *et al.*, *Superiority of postmortem liver fentanyl concentrations over peripheral blood influenced by postmortem interval for determination of fentanyl toxicity*. *Clinical Biochemistry*, 2013. **46**(7-8): p. 598-602.
83. Apple, F.S., *A better understanding of the interpretation of postmortem blood drug concentrations*. *Journal of Analytical Toxicology*, 2011. **35**(6): p. 381-383.
84. Butzbach, D.M., *et al.*, *Stability of Serotonin-Selective Antidepressants in Sterile and Decomposing Liver Tissue*. *Journal of Forensic Sciences*, 2013. **58**: p. S117-S125.
85. Tuomisto, S., *et al.*, *Evaluation of Postmortem Bacterial Migration Using Culturing and Real-Time Quantitative PCR*. *Journal of Forensic Sciences*, 2013. **58**(4): p. 910-916.
86. Rohrig, T.P. and C.A. Hicks, *Brain Tissue: A Viable Postmortem Toxicological Specimen*. *Journal of Analytical Toxicology*, 2015. **39**(2): p. 137-139.
87. Rodda, K.E., *et al.*, *Brain distribution of selected antipsychotics in schizophrenia*. *Forensic Science International*, 2006. **157**(2-3): p. 121-130.
88. Vanbinst, R., *et al.*, *Bile analysis of drugs in postmortem cases*. *Forensic Science International*, 2002. **128**(1-2): p. 35-40.
89. Maublanc, J., *et al.*, *Identification and quantification of 35 psychotropic drugs and metabolites in hair by LC-MS/MS: application in forensic toxicology*. *International Journal of Legal Medicine*, 2015. **129**(2): p. 259-268.
90. Cappelle, D., *et al.*, *Nail analysis for the detection of drugs of abuse and pharmaceuticals: a review*. *Forensic Toxicology*, 2015. **33**(1): p. 12-36.
91. Druid, H. and P. Holmgren, *A compilation of fatal and control concentrations of drugs in postmortem femoral blood*. *Journal of Forensic Sciences*, 1997. **42**(1): p. 79-87.
92. Launiainen, T. and I. Ojanperä, *Drug concentrations in post-mortem femoral blood compared with therapeutic concentrations in plasma*. *Drug Testing and Analysis*, 2014. **6**(4): p. 308-316.
93. Jones, A.W. and A. Holmgren, *Concentration distributions of the drugs most frequently identified in post-mortem femoral blood representing all causes of death*. *Medicine, Science and the Law*, 2009. **49**(4): p. 257-273.
94. Reis, M., *et al.*, *Reference concentrations of antidepressants. A compilation of postmortem and therapeutic levels*. *Journal of Analytical Toxicology*, 2007. **31**(5): p. 254-264.
95. Byard, R.W. and D.M. Butzbach, *Issues in the interpretation of postmortem toxicology*. *Forensic Science, Medicine, and Pathology*, 2012. **8**(3): p. 205-207.
96. Byard, R.W., *Post mortem toxicology in the elderly*. *Forensic Science, Medicine, and Pathology*, 2013. **9**(2): p. 254-255.
97. Drummer, O.H., *Post-mortem toxicology in the elderly*. *Forensic Science, Medicine, and Pathology*, 2013. **9**(2): p. 258-259.
98. Gasche, Y., *et al.*, *Codeine intoxication associated with ultrarapid CYP2D6 metabolism*. *The New England Journal of Medicine*, 2004. **351**(27): p. 2827-2831.
99. Stanworth, D., N.C.A. Hunt, and R.J. Flanagan, *Clozapine—A dangerous drug in a clozapine-naïve subject*. *Forensic Science International*, 2012. **214**(1-3): p. e23-e25.
100. Edward, K.-L. and C. Alderman, *Psychopharmacology: Practice and Contexts*. 2013, Sydney, Australia: Oxford University Press.
101. Preston, C.L., *Stockley's Drug Interactions. Eleventh edition*. 2016, London, UK: Pharmaceutical Press.
102. Jusic, N. and M. Lader, *Post-mortem antipsychotic drug concentrations and unexplained deaths*. *The British Journal of Psychiatry*, 1994. **165**(6): p. 787-791.
103. Gronewold, A., *et al.*, *Doxepin and nordoxepin concentrations in body fluids and tissues in doxepin associated deaths*. *Forensic Science International*, 2009. **190**(1): p. 74-79.

104. Apple, F.S., *Postmortem Tricyclic Antidepressant Concentrations: Assessing Cause of Death Using Parent Drug to Metabolite Ratio*. Journal of Analytical Toxicology, 1989. **13**(4): p. 197-198.
105. Hiroeh, U., *et al.*, *Death by homicide, suicide, and other unnatural causes in people with mental illness: a population-based study*. Lancet, 2001. **358**(9299): p. 2110-2112.
106. Joiner Jr, T.E., J.S. Brown, and L.R. Wingate, *The psychology and neurobiology of suicidal behavior*. Annual Review of Psychology, 2005. **56**: p. 287-314.
107. Pilgrim, J.L., D. Gerostamoulos, and O.H. Drummer, *Deaths involving contraindicated and inappropriate combinations of serotonergic drugs*. International Journal of Legal Medicine, 2011. **125**(6): p. 803-15.
108. Ray, W.A., *et al.*, *Atypical antipsychotic drugs and the risk of sudden cardiac death*. The New England Journal of Medicine, 2009. **360**(3): p. 225-235.
109. Gillman, P.K., *Tricyclic antidepressant pharmacology and therapeutic drug interactions updated*. British Journal of Pharmacology, 2007. **151**(6): p. 737-748.
110. Morey, S., *et al.*, *The importance of toxicology in death investigations*, in Forensic and Clinical Toxicology Association (FACTA) annual meeting. 2019. Adelaide, Australia.
111. Du Mont, J., *et al.*, *Drug-facilitated sexual assault in Ontario, Canada: toxicological and DNA findings*. Journal of Forensic and Legal Medicine, 2010. **17**(6): p. 333-338.
112. Johansen, S.S., *Detection of the antipsychotic drug quetiapine in the blood, urine and hair samples of the victim of a drug-facilitated sexual assault*. Forensic Science International, 2017. **270**: p. e12-e15.
113. *Melbourne man accused of shooting partner in face with speargun, dosing drinks and rape*. The Age, 2018: Australia.
114. Gravensteen, I.K., *et al.*, *Psychoactive substances in natural and unnatural deaths in Norway and Sweden—a study on victims of suicide and accidents compared with natural deaths in psychiatric patients*. BMC Psychiatry, 2019. **19**(1): p. 33.
115. Darke, S., J. Duflou, and M. Torok, *Toxicology and circumstances of completed suicide by means other than overdose*. Journal of Forensic Sciences, 2009. **54**(2): p. 490-494.
116. Methling, M., *et al.*, *Toxicological findings in suicides – frequency of antidepressant and antipsychotic substances*. Forensic Science, Medicine and Pathology, 2018. **15**(1): p. 23-30.
117. Smart, C., I.M. Anderson, and R.H. McAllister-Williams, *Antidepressants and electroconvulsive therapy*, in *Fundamentals of Clinical Psychopharmacology. Fourth edition*. I.M. Anderson and R.H. McAllister-Williams, Editors. 2015, Portland, USA: CRC Press. p. 67-85.
118. Cesura, A.M. and A. Pletscher, *The new generation of monoamine oxidase inhibitors*. Progress in Drug Research, 1992. **38**: p. 171-297.
119. Fava, M., *et al.*, *15 Years of Clinical Experience With Bupropion HCl: From Bupropion to Bupropion SR to Bupropion XL*. Primary Care Companion to The Journal of Clinical Psychiatry, 2005. **7**(3): p. 106-113.
120. Therapeutic Goods Administration, *ZYBAN® SR bupropion hydrochloride 150 mg tablets – Product Information*. 2017: Australia.
121. Gillman, P.K., *A systematic review of the serotonergic effects of mirtazapine in humans: implications for its dual action status*. Human Psychopharmacology: Clinical and Experimental, 2006. **21**(2): p. 117-125.
122. Millan, M.J., *et al.*, *Mirtazapine enhances frontocortical dopaminergic and corticolimbic adrenergic, but not serotonergic, transmission by blockade of α_2 - adrenergic and serotonin_{2C} receptors: a comparison with citalopram*. European Journal of Neuroscience, 2000. **12**(3): p. 1079-1095.
123. Hoes, M.J. and Z.J. H, *Mirtazapine as treatment for serotonin syndrome*. Pharmacopsychiatry, 1996. **29**(2): p. 81-81.

124. Mabbott, V. and P. Storey, *Australian Statistics on Medicines 2015*. Department of Health. 2016, Australia: Commonwealth of Australia.
125. Wang, S.-M., *et al.*, *Addressing the Side Effects of Contemporary Antidepressant Drugs: A Comprehensive Review*. Chonnam Medical Journal, 2018. **54**(2): p. 101-112.
126. Masand, P.S. and S. Gupta, *Long-term side effects of newer-generation antidepressants: SSRIS, venlafaxine, nefazodone, bupropion, and mirtazapine*. Annals of Clinical Psychiatry, 2002. **14**(3): p. 175-182.
127. Pacher, P. and V. Kecskemeti, *Cardiovascular Side Effects of New Antidepressants and Antipsychotics: New Drugs, old Concerns?* Current Pharmaceutical Design, 2004. **10**(20): p. 2463-2475.
128. Gillman, P.K., *Monoamine oxidase inhibitors, opioid analgesics and serotonin toxicity*. British Journal of Anaesthesia, 2005. **95**(4): p. 434-441.
129. Goeringer, K.E., *et al.*, *Postmortem forensic toxicology of selective serotonin reuptake inhibitors: a review of pharmacology and report of 168 cases*. Journal of Forensic Sciences, 2000. **45**(3): p. 633-648.
130. Boyer, E.W. and M. Shannon *The Serotonin Syndrome*. The New England Journal of Medicine, 2005. **352**(11): p. 1112-1120.
131. Amsterdam, J.D., F. García - España, and M. Rosenzweig, *Clomipramine augmentation in treatment - resistant depression*. Depression and Anxiety, 1997. **5**(2): p. 84-90.
132. Harris, C.R., J. Gualtieri, and G. Stark, *Fatal Bupropion Overdose*. Journal of Toxicology: Clinical Toxicology, 1997. **35**(3): p. 321-324.
133. Balit, C.R., C.N. Lynch, and G.K. Isbister, *Bupropion poisoning: a case series*. Medical Journal of Australia, 2003. **178**(2): p. 61-64.
134. Berling, I. and G.K. Isbister, *Mirtazapine overdose is unlikely to cause major toxicity*. Clinical Toxicology, 2014. **52**(1): p. 20-24.
135. Stephen Waring, W., A.M. Good, and D. Nicholas Bateman, *Lack of significant toxicity after mirtazapine overdose: a five-year review of cases admitted to a regional toxicology unit*. Clinical Toxicology, 2007. **45**(1): p. 45-50.
136. Anderson, D.T., K.L. Fritz, and J.J. Muto, *Distribution of Mirtazapine (Remeron®) in Thirteen Postmortem Cases*. Journal of Analytical Toxicology, 1999. **23**(6): p. 544-548.
137. Kirkton, C. and I.M. McIntyre, *Therapeutic and toxic concentrations of mirtazapine*. Journal of Analytical Toxicology, 2006. **30**(9): p. 687-691.
138. Stahl, S.M., *Antipsychotics and mood stabilizers: Stahl's essential psychopharmacology. Third edition*. 2008, Cambridge, UK: Cambridge University Press.
139. Huthwaite, M., *et al.*, *Off label or on trend: a review of the use of quetiapine in New Zealand*. The New Zealand Medical Journal, 2018. **131**(1474): p. 45-50.
140. Lee, J., *et al.*, *Increasing rates of quetiapine overdose, misuse, and mortality in Victoria, Australia*. Drug and Alcohol Dependence, 2018. **187**: p. 95-99.
141. Maglione, M., *et al.*, *Off-label use of atypical antipsychotics: an update*. Comparative Effectiveness Reviews, 2011. **43**.
142. Tiller, J., *et al.*, *Antipsychotic use in the elderly: what doctors say they do, and what they do*. Australasian Journal on Ageing, 2008. **27**(3): p. 134-142.
143. Karlsson, A. and L. Burns, *Australian Drug Trends 2017. Findings from the Illicit Drug Reporting System (IDRS)*. National Drug and Alcohol Research Centre. 2018, Sydney, UNSW, Australia.
144. Stafford, J. and L. Burns, *Australian Drug Trends 2014. Findings from the Illicit Drug Reporting System (IDRS)*. National Drug and Alcohol Research Centre. 2015, Sydney, UNSW, Australia.

145. Malekshahi, T., *et al.*, *Misuse of atypical antipsychotics in conjunction with alcohol and other drugs of abuse*. *Journal of Substance Abuse Treatment*, 2015. **48**(1): p. 8-12.
146. Julien, R.M., C.D. Advokat, and J.E. Comaty, *A primer of drug action: a comprehensive guide to the actions, uses, and side effects of psychoactive drugs*. Eleventh edition. 2007, New York, USA: Worth Publishers.
147. Muench, J. and A.M. Hamer, *Adverse effects of antipsychotic medications*. *American Family Physician*, 2010. **81**(5): p. 617-622.
148. Lieberman, J.A., *et al.*, *Effectiveness of Antipsychotic Drugs in Patients with Chronic Schizophrenia*. *The New England Journal of Medicine*, 2005. **353**(12): p. 1209-23.
149. Leucht, S., *et al.*, *Second-generation versus first-generation antipsychotic drugs for schizophrenia: a meta-analysis*. *Lancet*, 2009. **373**(9657): p. 31-41.
150. Morgan, A.P., *et al.*, *The Antipsychotic Olanzapine Interacts with the Gut Microbiome to Cause Weight Gain in Mouse*. *PLoS ONE*, 2014. **9**(12).
151. Ely, S.F., A.R. Neitzel, and J.R. Gill, *Fatal Diabetic Ketoacidosis and Antipsychotic Medication*. *Journal of Forensic Sciences*, 2013. **58**(2): p. 398-403.
152. Stark, A. and J. Scott, *A review of the use of clozapine levels to guide treatment and determine cause of death*. *Australian & New Zealand Journal of Psychiatry*, 2012. **46**(9): p. 816-825.
153. Baselt, R.C., *Disposition of Toxic Drugs and Chemical in Man*. Tenth edition. 2014, Seal Beach, USA: Biomedical Publications.
154. Kilian, J.G., *et al.*, *Myocarditis and cardiomyopathy associated with clozapine*. *Lancet*, 1999. **354**(9193): p. 1841-1845.
155. Hibbard, K.R., *et al.*, *Fatalities Associated With Clozapine-Related Constipation and Bowel Obstruction: A Literature Review and Two Case Reports*. *Psychosomatics*, 2009. **50**(4): p. 416-419.
156. Purhonen, M., *et al.*, *Outcome of patients after market withdrawal of thioridazine: a retrospective analysis in a nationwide cohort*. *Pharmacoepidemiology and drug safety*, 2012. **21**(11): p. 1227-1231.
157. Gareri, P., *et al.*, *Use and safety of antipsychotics in behavioral disorders in elderly people with dementia*. *Journal of Clinical Psychopharmacology*, 2014. **34**(1): p. 109-123.
158. Gareri, P., *et al.*, *Use of atypical antipsychotics in the elderly: a clinical review*. *Clinical Interventions in Aging*, 2014. **9**: p. 1363-1373.
159. Lomax, P. and E. Schönbaum, *The effects of drugs on thermoregulation during exposure to hot environments*, in *Progress in Brain Research*. H.S. Sharma and J. Westman, Editors. 1998, Amsterdam, Netherlands: Elsevier. p. 193-204.
160. Clark, W.G. and J.M. Lipton, *Drug-related heatstroke*. *Pharmacology & Therapeutics*, 1984. **26**(3): p. 345-388.
161. Martin-Latry, K., *et al.*, *Psychotropic drugs use and risk of heat-related hospitalisation*. *European Psychiatry*, 2007. **22**(6): p. 335-338.
162. Herbst, J., *et al.*, *Heat-related deaths in Adelaide, South Australia: Review of the literature and case findings – An Australian perspective*. *Journal of Forensic and Legal Medicine*, 2014. **22**: p. 73-78.
163. Zonnenberg, C., *et al.*, *Hypothermia due to Antipsychotic Medication: A Systematic Review*. *Frontiers in Psychiatry*, 2017. **8**: p. 165.
164. Bouchama, A., *et al.*, *Prognostic factors in heat wave-related deaths: a meta-analysis*. *Archives of Internal Medicine*, 2007. **167**(20): p. 2170-2176.
165. Shiloh, R., *et al.*, *Abnormal thermoregulation in drug-free male schizophrenia patients*. *European Neuropsychopharmacology*, 2001. **11**(4): p. 285-288.
166. Therapeutic Goods Administration, *QUILONUM® SR - Product Information*. 2017: Australia.
167. Fakhoury, M., *Could cannabidiol be used as an alternative to antipsychotics?* *Journal of Psychiatric Research*, 2016. **80**: p. 14-21.

168. Gallego, J.A., *et al.*, *Prevalence and correlates of antipsychotic polypharmacy: A systematic review and meta-regression of global and regional trends from the 1970s to 2009*. *Schizophrenia Research*, 2012. **138**(1): p. 18-28.
169. Broekema, W.J., I.W. de Groot, and P.N. van Harten, *Simultaneous prescribing of atypical antipsychotics, conventional antipsychotics and anticholinergics-a European study*. *Pharmacy World & Science*, 2007. **29**(3): p. 126-30.
170. Fleischhacker, W.W. and H. Uchida, *Critical review of antipsychotic polypharmacy in the treatment of schizophrenia*. *International Journal of Neuropsychopharmacology*, 2014. **17**(7): p. 1083-1093.
171. Ellett, L.M.K., *et al.*, *Antipsychotic polypharmacy in older Australians*. *International Psychogeriatrics*, 2018. **30**(4): p. 539-546.
172. Schatzberg, A.F., *New approaches to managing psychotic depression*. *Journal of Clinical Psychiatry*, 2003. **64**(1): p. 19-23.
173. Drug Utilisation Sub-Committee, *Use of antipsychotics in the middle aged*. Department of Health. 2013, Canberra: Australian Government.
174. Drug Utilisation Sub-Committee, *Use of antipsychotics in children and adolescents*. Department of Health. 2013, Canberra: Australian Government.
175. Härtter, S., *et al.*, *Inhibition of antidepressant demethylation and hydroxylation by fluvoxamine in depressed patients*. *Psychopharmacology*, 1993. **110**(3): p. 302-308.
176. Jayasinghe, R. and P. Kovoor, *Drugs and the QTc interval*. *Australian Prescriber*, 2002. **25**(3): p. 63-65.
177. Daniel, W.A., *et al.*, *Pharmacokinetics and metabolism of thioridazine during co-administration of tricyclic antidepressants*. *British Journal of Pharmacology*, 2000. **131**(2): p. 287-295.
178. Duggal, H.S. and J. Fetchko, *Serotonin syndrome and atypical antipsychotics*. *American Journal of Psychiatry*, 2002. **159**(4): p. 672-a.
179. Karki, S.D. and G.-R. Masood, *Combination risperidone and SSRI-induced serotonin syndrome*. *Annals of Pharmacotherapy*, 2003. **37**(3): p. 388-391.
180. Hamilton, S. and K. Malone, *Serotonin syndrome during treatment with paroxetine and risperidone*. *Journal of Clinical Psychopharmacology*, 2000. **20**(1): p. 103-105.
181. Odagaki, Y., *Atypical neuroleptic malignant syndrome or serotonin toxicity associated with atypical antipsychotics?* *Current Drug Safety*, 2009. **4**(1): p. 84-93.
182. Marlowe, K. and D. Schirgel, *Quetiapine and citalopram: aetiological significances in serotonin syndrome*. *The New Zealand Medical Journal*, 2006. **119**(1237): p. U2058.
183. Rim, C.L. and M.J. Gitlin, *Ziprasidone, monoamine oxidase inhibitors, and the serotonin syndrome*. *Journal of Clinical Psychopharmacology*, 2010. **30**(4): p. 470-471.
184. Duggal, H.S. and J. Kithas, *Possible neuroleptic malignant syndrome with aripiprazole and fluoxetine*. *American Journal of Psychiatry*, 2005. **162**(2): p. 397-a.
185. Strawn, J.R., P.E. Keck Jr, and S.N. Caroff, *Neuroleptic malignant syndrome*. *The American Journal of Psychiatry*, 2007. **164**(6): p. 870-876.
186. Thorn, C.F., *et al.*, *PharmGKB summary: clozapine pathway, pharmacokinetics*. *Pharmacogenetics and Genomics*, 2018. **28**(9): p. 214-222.
187. Lemberger, L., *et al.*, *Fluoxetine: clinical pharmacology and physiologic disposition*. *The Journal of Clinical Psychiatry*, 1985. **46**(3 Pt 2): p. 14-19.
188. Gillman, K., *Drug interactions and fluoxetine: a commentary from a clinician's perspective*. *Expert Opinion on Drug Safety*, 2005. **4**(6): p. 965-968.
189. Leikin, J.B. and W.A. Watson, *Post-mortem Toxicology: What The Dead Can And Cannot Tell Us*. *Journal of Toxicology: Clinical Toxicology*, 2003. **41**(1): p. 47-56.

190. Giaginis, C., A. Tsantili-Kakoulidou, and S. Theocharis, *Quantitative structure–activity relationship (QSAR) methodology in forensic toxicology: Modeling postmortem redistribution of structurally diverse drugs using multivariate statistics*. *Forensic Science International*, 2009. **190**(1–3): p. 9-15.
191. Pounder, D.J., A.K. Hartley, and P.J. Watmough, *Postmortem Redistribution and Degradation of Dothiepin Human Case Studies and an Animal Model*. *The American Journal of Forensic Medicine and Pathology*, 1994. **15**(3): p. 231-235.
192. Skov, L., S.S. Johansen, and K. Linnet, *Postmortem Femoral Blood Reference Concentrations of Aripiprazole, Chlorprothixene, and Quetiapine*. *Journal of Analytical Toxicology*, 2015. **39**(1): p. 41-44.
193. Dalpe-Scott, M., *et al.*, *A comparison of drug concentrations in postmortem cardiac and peripheral blood in 320 cases*. *Canadian Society of Forensic Science Journal*, 1995. **28**(2): p. 113-121.
194. Moffatt, A., *et al.*, *Clarke's Analysis of Drugs and Poisons. Fourth edition*. 2011, London: Pharmaceutical Press.
195. Stevens, H.M., *The Stability of Some Drugs and Poisons in Putrefying Human Liver Tissues*. *Journal of the Forensic Science Society*, 1984. **24**(6): p. 577-589.
196. Government of South Australia, *Forensic Science SA: Toxicology manual*. Attorney-General's Department. 2018.
197. Stimpfl, T., *Extraction*, in *Clarke's Analytical Forensic Toxicology. Second edition*. A. Negrusz and G. Cooper, Editors. 2013, London, UK: Pharmaceutical Press. p. 357-370.
198. Tsujikawa, K., *et al.*, *Degradation pathways of 4-methylmethcathinone in alkaline solution and stability of methcathinone analogs in various pH solutions*. *Forensic Science International*, 2012. **220**(1–3): p. 103-110.
199. Flanagan, R.J., *et al.*, *Fundamentals of Analytical Toxicology*. 2007: John Wiley & Sons Ltd.
200. Drummer, O.H., *et al.*, *Capillary gas chromatographic drug screen for use in forensic toxicology*. *Journal of Analytical Toxicology*, 1994. **18**(3): p. 134-138.
201. Novák, P. and V. Havlíček, *Protein Extraction and Precipitation*, in *Proteomic Profiling and Analytical Chemistry. Second edition*. P. Ciborowski and J. Silberring, Editors. 2016, Boston, USA: Elsevier. p. 51-62.
202. Di Rago, M., *et al.*, *Fast targeted analysis of 132 acidic and neutral drugs and poisons in whole blood using LC–MS/MS*. *Forensic Science International*, 2014. **243**: p. 35-43.
203. Scientific Working Group for Forensic Toxicology, *Scientific Working Group for Forensic Toxicology (SWGTOX) Standard Practices for Method Validation in Forensic Toxicology*. *Journal of Analytical Toxicology*, 2013. **37**(7): p. 452-474.
204. Christian, G.D., *Analytical Chemistry. Sixth edition*. 2004, Hoboken, USA: John Wiley & Sons, Inc.
205. Watson, D., *et al.*, *Mass spectrometry*, in *Clarke's Analytical Forensic Toxicology. Second edition*. A. Negrusz and G. Cooper, Editors. 2013, London, UK: Pharmaceutical Press. p. 553-584.
206. Kostakis, C., P. Harpas, and P.C. Stockham, *Forensic toxicology in Liquid Chromatography. Second edition*. S. Fanali, *et al.*, Editors. 2017, Amsterdam, Netherlands: Elsevier. p. 301-358.
207. Springfield, A.C. and E. Bodiford, *An overdose of risperidone*. *Journal of Analytical Toxicology*, 1996. **20**(3): p. 202-203.
208. Partridge, E., *et al.*, *A Validated Method for the Screening of 320 Forensically Significant Compounds in Blood by LC/QTOF, with Simultaneous Quantification of Selected Compounds*. *Journal of Analytical Toxicology*, 2018. **42**(4): p. 220-231.
209. Di Rago, M., *et al.*, *An LC/MS-MS method for the rapid targeted semi-quantitation of 327 basic and neutral analytes in post-mortem whole blood and its application in the Victorian overnight toxicology service*, in *Forensic and Clinical Toxicology Association (FACTA) annual meeting*. 2017. Melbourne, Australia.

210. Trobbiani, S., P. Stockham, and T. Scott, *Increasing the linear dynamic range in LC-MS: is it valid to use a less abundant isotopologue?* Drug Testing and Analysis, 2017. **9**(10): p. 1630-1636.
211. Favretto, D., J.P. Pascali, and F. Tagliaro, *New challenges and innovation in forensic toxicology: Focus on the "New Psychoactive Substances"*. Journal of Chromatography A, 2013. **1287**: p. 84-95.
212. Kebarle, P. and U.H. Verkerk, *Electrospray: From ions in solution to ions in the gas phase, what we know now*. Mass Spectrometry Reviews, 2009. **28**(6): p. 898-917.
213. Agilent Technologies, *Agilent 6200 Series TOF and 6500 Series Q-TOF LC/MS System Concepts Guide: The Big Picture*. 2014: USA.
214. Partridge, E., et al., *A Case Study Involving U-47700, Diclazepam and Flubromazepam—Application of Retrospective Analysis of HRMS Data*. Journal of Analytical Toxicology, 2018. **42**(9): p. 655-660.
215. Kriikku, P., et al., *Toxic lifespan of the synthetic opioid U-47,700 in Finland verified by re-analysis of UPLC-TOF-MS data*. Forensic Science International, 2019. **300**: p. 85-88.
216. Brown, D.H., et al., *β - Methylphenylethylamines: common fragmentation pathways with amphetamines in electrospray ionization collision - induced dissociation*. Drug Testing and Analysis, 2016. **8**(3-4): p. 344-350.
217. Taylor, P.J., *Matrix effects: the Achilles heel of quantitative high-performance liquid chromatography-electrospray-tandem mass spectrometry*. Clinical Biochemistry, 2005. **38**(4): p. 328-334.
218. Peters, F.T., O.H. Drummer, and F. Musshoff, *Validation of new methods*. Forensic Science International, 2007. **165**(2-3): p. 216-224.
219. Saar, E., et al., *Comparison of extraction efficiencies and LC-MS-MS matrix effects using LLE and SPE methods for 19 antipsychotics in human blood*. Analytical and Bioanalytical Chemistry, 2009. **393**(2): p. 727-734.
220. Furey, A., et al., *Ion suppression; A critical review on causes, evaluation, prevention and applications*. Talanta, 2013. **115**: p. 104-122.
221. Matuszewski, B.K., M.L. Constanzer, and C.M. Chavez-Eng, *Strategies for the Assessment of Matrix Effect in Quantitative Bioanalytical Methods Based on HPLC-MS/MS*. Analytical Chemistry, 2003. **75**(13): p. 3019-3030.
222. Wang, S., M. Cyronak, and E. Yang, *Does a stable isotopically labeled internal standard always correct analyte response?: A matrix effect study on a LC/MS/MS method for the determination of carvedilol enantiomers in human plasma*. Journal of Pharmaceutical and Biomedical Analysis, 2007. **43**(2): p. 701-707.
223. Butzbach, D.M., *The stability of selected psychiatric medications during simulated post-mortem decomposition*, in School of Chemical and Physical Sciences, Flinders University. 2011. Doctor of Philosophy.
224. Kupiec, T., et al., *High-performance liquid chromatography*, in *Clarke's Analytical Forensic Toxicology. Second edition*. A. Negrusz and G. Cooper, Editors. 2013, London, UK: Pharmaceutical Press. p. 529-554.
225. Cohen, R., et al., *Fungal flora of the normal human small and large intestine*. New England Journal of Medicine, 1969. **280**(12): p. 638-641.
226. Kalser, M.H., et al., *Normal Viral and Bacterial Flora of the Human Small and Large Intestine*. New England Journal of Medicine, 1966. **274**(10): p. 558-563.
227. DeSantis, T.Z., et al., *Greengenes, a chimera-checked 16S rRNA gene database and workbench compatible with ARB*. Applied and Environmental Microbiology, 2006. **72**(7): p. 5069-5072.
228. Singh, B., T.L. Crippen, and J.K. Tomberlin, *An introduction to metagenomic data generation, analysis, visualization, and interpretation*, in *Forensic Microbiology*. D.O. Carter, et al., Editors. 2017, Hoboken, USA: John Wiley & Sons, Ltd. p. 94-126.

229. Pace, N.R., *et al.*, *The Analysis of Natural Microbial Populations by Ribosomal RNA Sequences*, in *Advances in Microbial Ecology*. K.C. Marshall, Editor. 1986, New York, USA: Springer US. p. 1-55.
230. Dale, J.W., M. Von Schantz, and N. Plant, *From genes to genomes: concepts and applications of DNA technology. Third edition*. 2012, West Sussex, UK: John Wiley & Sons.
231. Illumina, I., *Technology Spotlight: Illumina® Sequencing*. 2010.
232. Magurran, A.E., *Diversity indices and species abundance models*, in *Ecological diversity and its measurement*. 1988, Dordrecht, Netherlands: Springer. p. 7-45.
233. McMurdie, P.J. and S. Holmes, *Waste Not, Want Not: Why Rarefying Microbiome Data Is Inadmissible*. PLoS Computational Biology, 2014. **10**(4): p. e1003531.
234. Ramette, A., *Multivariate analyses in microbial ecology*. FEMS Microbiology Ecology, 2007. **62**(2): p. 142-160.
235. Goodrich, J.K., *et al.*, *Conducting a microbiome study*. Cell, 2014. **158**(2): p. 250-262.
236. Anderson, M.J., *Permutational multivariate analysis of variance (PERMANOVA)*. Wiley StatsRef: Statistics Reference Online, 2014: p. 1-15.
237. The Parliament of South Australia, *Transplantation and Anatomy Act 1983 (South Australia) Version 1.2.2014*. 2014.
238. Savage, D.C., *Microbial ecology of the gastrointestinal tract*. Annual Reviews in Microbiology, 1977. **31**(1): p. 107-133.
239. Rose, C., *et al.*, *The Characterization of Feces and Urine: A Review of the Literature to Inform Advanced Treatment Technology*. Critical Reviews in Environmental Science and Technology, 2015. **45**(17): p. 1827-1879.
240. Costello, E.K., *et al.*, *Bacterial Community Variation in Human Body Habitats Across Space and Time*. Science, 2009. **326**(5960): p. 1694-1697.
241. The Human Microbiome Project Consortium, *Structure, function and diversity of the healthy human microbiome*. Nature, 2012. **486**(7402): p. 207-214.
242. Walter, J. and R. Ley, *The Human Gut Microbiome: Ecology and Recent Evolutionary Changes*. Annual Review of Microbiology, 2011. **65**(1): p. 411-429.
243. Yu, Y., *et al.*, *Group-specific primer and probe sets to detect methanogenic communities using quantitative real-time polymerase chain reaction*. Biotechnology and Bioengineering, 2005. **89**(6): p. 670-679.
244. Laudadio, I., *et al.*, *Quantitative Assessment of Shotgun Metagenomics and 16S rDNA Amplicon Sequencing in the Study of Human Gut Microbiome*. Omics: A Journal of Integrative Biology, 2018. **22**(4): p. 248-254.
245. Burcham, Z.M. and H.R. Jordan, *History, current, and future use of microorganisms as physical evidence*, in *Forensic Microbiology*. D.O. Carter, *et al.*, Editors. 2017, Hoboken, USA: John Wiley & Sons, Ltd. p. 25-55.
246. Saukko, P. and B. Knight, *Knight's Forensic Pathology. Third edition*. 2004, London, UK: Arnold Publishers.
247. Musshoff, F., *et al.*, *Fatal blood and tissue concentrations of more than 200 drugs*. Forensic Science International, 2004. **142**(2-3): p. 161-210.
248. Schulz, M., *et al.*, *Therapeutic and toxic blood concentrations of nearly 1,000 drugs and other xenobiotics*. Critical Care, 2012. **16**(4): p. R136.
249. Skov, L., S.S. Johansen, and K. Linnet, *Postmortem Quetiapine Reference Concentrations in Brain and Blood*. Journal of Analytical Toxicology, 2015. **39**(7): p. 557-561.
250. Scheline, R.R., *Drug metabolism by intestinal microorganisms*. Journal of Pharmaceutical Sciences, 1968. **57**(12): p. 2021-2037.
251. Sousa, T., *et al.*, *The gastrointestinal microbiota as a site for the biotransformation of drugs*. International Journal of Pharmaceutics, 2008. **363**(1-2): p. 1-25.

252. Kang, M.J., *et al.*, *The effect of gut microbiota on drug metabolism*. Expert Opinion on Drug Metabolism and Toxicology, 2013. **9**(10): p. 1295-1308.
253. Abourashed, E.A., A.M. Clark, and C.D. Hufford, *Microbial models of mammalian metabolism of xenobiotics: an updated review*. Current Medicinal Chemistry, 1999. **6**(5): p. 359-374.
254. Asha, S. and M. Vidyavathi, *Cunninghamella – A microbial model for drug metabolism studies – A review*. Biotechnology Advances, 2009. **27**(1): p. 16-29.
255. Soleim, H.A. and R.R. Scheline, *Metabolism of xenobiotics by strains of intestinal bacteria*. Acta Pharmacologica et Toxicologica, 1972. **31**(5 - 7): p. 471-480.
256. Thai, K., *et al.*, *Post-mortem production of paracetamol via degradation of its metabolites*, in The 22nd International Symposium on the Forensic Sciences, Australian and New Zealand Forensic Science Society. 2014. Adelaide, Australia.
257. Scott, T., *et al.*, *Post-mortem production of paracetamol via degradation of its metabolites*, in The 53rd TIAFT meeting. 2015. Firenze, Italy.
258. Spatz, M., *et al.*, *Role of intestinal microorganisms in determining cycasin toxicity*. Experimental Biology and Medicine, 1967. **124**(3): p. 691-697.
259. Norman, A. and R. Grubb, *Hydrolysis of conjugated bile acids by clostridia and enterococci*. Acta Pathologica Microbiologica Scandinavica, 1955. **36**(6): p. 537-547.
260. Holt, R., *The bacterial degradation of chloramphenicol*. Lancet, 1967. **289**(7502): p. 1259-1260.
261. Grassi, H.C., E.D.J. Andrades, and F. Marquina, *Preliminary report on isolation and characterization of cocaine metabolizing fungi and their involvement in human mycoses*. Journal of Medical Mycology, 2006. **16**(1): p. 1-8.
262. Peppercorn, M.A. and P. Goldman, *Caffeic acid metabolism by bacteria of the human gastrointestinal tract*. Journal of Bacteriology, 1971. **108**(3): p. 996-1000.
263. Wadworth, A.N. and A. Fitton, *Olsalazine. A review of its pharmacodynamic and pharmacokinetic properties, and therapeutic potential in inflammatory bowel disease*. Drugs, 1991. **41**(4): p. 647-664.
264. Robertson, M.D. and O.H. Drummer, *Postmortem drug metabolism by bacteria*. Journal of Forensic Sciences, 1995. **40**(3): p. 382-382.
265. Basit, A.W., J.M. Newton, and L.F. Lacey, *Susceptibility of the H2-receptor antagonists cimetidine, famotidine and nizatidine, to metabolism by the gastrointestinal microflora*. International Journal of Pharmaceutics, 2002. **237**(1-2): p. 23-33.
266. Watanabe, K., *et al.*, *Metabolism of omeprazole by gut flora in rats*. Journal of Pharmaceutical Sciences, 1995. **84**(4): p. 516-517.
267. Rosenfeld, R.S., I. Paul, and T. Yamauchi, *Sterol esterification in feces*. Archives of Biochemistry and Biophysics, 1967. **122**(3): p. 653-657.
268. Dull, B.J., K. Salata, and P. Goldman, *Role of the intestinal flora in the acetylation of sulfasalazine metabolites*. Biochemical Pharmacology, 1987. **36**(21): p. 3772-3774.
269. Harris, B.E., *et al.*, *Conversion of 5-fluorocytosine to 5-fluorouracil by human intestinal microflora*. Antimicrobial Agents and Chemotherapy, 1986. **29**(1): p. 44-48.
270. Indahl, S.R. and R.R. Scheline, *Decarboxylation of 4-hydroxycinnamic acids by Bacillus strains isolated from rat intestine*. Applied Microbiology, 1968. **16**(4): p. 667.
271. Mendel, J.L. and M.S. Walton, *Conversion of p, p-DDT to p, p-DDD by Intestinal Flora of the Rat*. Science, 1966. **151**(3717): p. 1527-1528.
272. Goldin, B.R., M.A. Peppercorn, and P. Goldman, *Contributions of host and intestinal microflora in the metabolism of L-dopa by the rat*. Journal of Pharmacology and Experimental Therapeutics, 1973. **186**(1): p. 160-166.
273. Shamat, M.A., *The role of the gastrointestinal microflora in the metabolism of drugs*. International Journal of Pharmaceutics, 1993. **97**(1): p. 1-13.

274. Smith, G.E. and L.A. Griffiths, *Metabolism of N-acylated and O-alkylated drugs by the intestinal microflora during anaerobic incubation in vitro*. *Xenobiotica*, 1974. **4**(8): p. 477-487.
275. Caldwell, J. and G.M. Hawksworth, *The demethylation of methamphetamine by intestinal microflora*. *Journal of Pharmacy and Pharmacology*, 1973. **25**(5): p. 422-424.
276. Hamilton, I.R., *Biochemical Effects of Fluoride on Oral Bacteria*. *Journal of Dental Research*, 1990. **69**(2 suppl): p. 660-667.
277. Baselt, R.C., R.F. Shaw, and R. McEvilly, *Effect of sodium fluoride on cholinesterase activity in postmortem blood*. *Journal of Forensic Sciences*, 1985. **30**(4): p. 1206-1209.
278. Isenschmid, D.S., B.S. Levine, and Y.H. Caplan, *A Comprehensive Study of the Stability of Cocaine and Its Metabolites*. *Journal of Analytical Toxicology*, 1989. **13**(5): p. 250-256.
279. Moriya, F., Y. Hashimoto, and T.-t. Kuo, *Pitfalls When Determining Tissue Distributions of Organophosphorus Chemicals: Sodium Fluoride Accelerates Chemical Degradation*. *Journal of Analytical Toxicology*, 1999. **23**(3): p. 210-215.
280. Pannell, M., *et al.*, *Death due to malathion poisoning*. *Journal of Clinical Forensic Medicine*, 2001. **8**(3): p. 156-159.
281. Rositano, J., *et al.*, *Two suicides by mevinphos*, in *The 22nd International Symposium on the Forensic Sciences*, Australian and New Zealand Forensic Science Society. 2014. Adelaide, Australia.
282. Zaitso, K., *et al.*, *Long-term stability of various drugs and metabolites in urine, and preventive measures against their decomposition with special attention to filtration sterilization*. *Forensic Science International*, 2008. **174**(2): p. 189-196.
283. Megyesi, M.S., S.P. Nawrocki, and N.H. Haskell, *Using accumulated degree-days to estimate the postmortem interval from decomposed human remains*. *Journal of Forensic Sciences*, 2005. **50**(3): p. 618-26.
284. Maskell, P.D., *et al.*, *Postmortem redistribution of the heroin metabolites morphine and morphine-3-glucuronide in rabbits over 24 h*. *International Journal of Legal Medicine*, 2016. **130**(2): p. 519-531.
285. Bennett, J.R., *The organ retention furore: the need for consent*. *Clinical Medicine*, 2001. **1**(3): p. 167.
286. Madigan, M.T., *et al.*, *Brock Biology of Microorganisms*. 2014, London, UK: Pearson.
287. Martínez-Ramírez, J.A., G. Walther, and F.T. Peters, *Studies on drug metabolism by fungi colonizing decomposing human cadavers. Part II: biotransformation of five model drugs by fungi isolated from post-mortem material*. *Drug Testing and Analysis*, 2015. **7**(4): p. 265-279.
288. Li, B., *et al.*, *Butyrylcholinesterase, paraoxonase, and albumin esterase, but not carboxylesterase, are present in human plasma*. *Biochemical Pharmacology*, 2005. **70**(11): p. 1673-1684.
289. Ley, R.E., *et al.*, *Evolution of Mammals and Their Gut Microbes*. *Science*, 2008. **320**(5883): p. 1647-1651.
290. Furet, J.-P., *et al.*, *Comparative assessment of human and farm animal faecal microbiota using real-time quantitative PCR*. *FEMS Microbiology Ecology*, 2009. **68**(3): p. 351-362.
291. Saar, E., *et al.*, *Assessment of the stability of 30 antipsychotic drugs in stored blood specimens*. *Forensic Science International*, 2012. **215**(1-3): p. 152-158.
292. Lough, P.S. and R. Fehn, *Efficacy of 1% sodium fluoride as a preservative in urine samples containing glucose and Candida albicans*. *Journal of Forensic Sciences*, 1993. **38**(2): p. 266-271.
293. Yajima, D., *et al.*, *Ethanol production by Candida albicans in postmortem human blood samples: Effects of blood glucose level and dilution*. *Forensic Science International*, 2006. **164**(2-3): p. 116-121.
294. Martínez-Ramírez, J.A., K. Voigt, and F.T. Peters, *Studies on the metabolism of five model drugs by fungi colonizing cadavers using LC-ESI-MS/MS and GC-MS analysis*. *Analytical and Bioanalytical Chemistry*, 2012. **404**(5): p. 1339-1359.

295. Martínez-Ramírez, J.A., *et al.*, *Search for fungi-specific metabolites of four model drugs in postmortem blood as potential indicators of postmortem fungal metabolism*. *Forensic Science International*, 2016. **262**: p. 173-178.
296. Kugelberg, F.C. and A.W. Jones, *Interpreting results of ethanol analysis in postmortem specimens: A review of the literature*. *Forensic Science International*, 2007. **165**(1): p. 10-29.
297. Dick, G.L. and H.M. Stone, *Alcohol loss arising from microbial contamination of drivers' blood specimens*. *Forensic Science International*, 1987. **34**(1-2): p. 17-27.
298. Hunsaker, D.M. and J.C. Hunsaker III, *Alcohol: Blood and Body Fluid Analysis*, in *Encyclopedia of Forensic and Legal Medicine*. R.W. Byard, *et al.*, Editors. 2005, Amsterdam, Netherlands: Elsevier Science. p. 29-38.
299. Gilliland, M.G. and R.O. Bost, *Alcohol in decomposed bodies: postmortem synthesis and distribution*. *Journal of Forensic Sciences*, 1993. **38**(6): p. 1266-1274.
300. Lewis, R.J., *et al.*, *Ethanol formation in unadulterated postmortem tissues*. *Forensic Science International*, 2004. **146**(1): p. 17-24.
301. Høiseth, G., *et al.*, *Disappearance of ethyl glucuronide during heavy putrefaction*. *Forensic Science International*, 2008. **176**(2-3): p. 147-151.
302. Helander, A., I. Olsson, and H. Dahl, *Postcollection Synthesis of Ethyl Glucuronide by Bacteria in Urine May Cause False Identification of Alcohol Consumption*. *Clinical Chemistry*, 2007. **53**(10): p. 1855-1857.
303. Helander, A. and H. Dahl, *Urinary tract infection: a risk factor for false-negative urinary ethyl glucuronide but not ethyl sulfate in the detection of recent alcohol consumption*. *Clinical Chemistry*, 2005. **51**(9): p. 1728-1730.
304. Schloegl, H., *et al.*, *Stability of ethyl glucuronide in urine, post-mortem tissue and blood samples*. *International Journal of Legal Medicine*, 2006. **120**(2): p. 83-88.
305. Thierauf, A., *et al.*, *Ethyl sulphate and ethyl glucuronide in vitreous humor as postmortem evidence marker for ethanol consumption prior to death*. *Forensic Science International*, 2011. **210**(1): p. 63-68.
306. Halter, C.C., *et al.*, *Assessment of the stability of the ethanol metabolite ethyl sulfate in standardised degradation tests*. *Forensic Science International*, 2009. **186**(1-3): p. 52-55.
307. Baranowski, S., *et al.*, *In vitro study of bacterial degradation of ethyl glucuronide and ethyl sulphate*. *International Journal of Legal Medicine*, 2008. **122**(5): p. 389-93.
308. Hernández Redondo, A., *et al.*, *Inhibition of bacterial degradation of EtG by collection as dried urine spots (DUS)*. *Analytical and Bioanalytical Chemistry*, 2012. **402**(7): p. 2417-2424.
309. Høiseth, G., *et al.*, *Practical use of ethyl glucuronide and ethyl sulfate in postmortem cases as markers of antemortem alcohol ingestion*. *International Journal of Legal Medicine*, 2010. **124**(2): p. 143-148.
310. Helander, A., *et al.*, *Detection Times for Urinary Ethyl Glucuronide and Ethyl Sulfate in Heavy Drinkers during Alcohol Detoxification*. *Alcohol and Alcoholism*, 2009. **44**(1): p. 55-61.
311. Nagata, T., *et al.*, *Methamphetamine and amphetamine concentrations in postmortem rabbit tissues*. *Forensic Science International*, 1990. **48**(1): p. 39-47.
312. Giorgi, S.N. and J.E. Meeker, *A 5-Year Stability Study of Common Illicit Drugs in Blood*. *Journal of Analytical Toxicology*, 1995. **19**(6): p. 392-398.
313. Holmgren, P., *et al.*, *Stability of drugs in stored postmortem femoral blood and vitreous humor*. *Journal of Forensic Sciences*, 2004. **49**(4): p. 820-825.
314. Karinen, R., *et al.*, *Long-Term Storage of Authentic Postmortem Forensic Blood Samples at -20° C: Measured Concentrations of Benzodiazepines, Central Stimulants, Opioids and Certain Medicinal Drugs Before and After Storage for 16-18 Years*. *Journal of Analytical Toxicology*, 2014. **38**(9): p. 686-695.

315. Clauwaert, K.M., J.F. Van Boclaer, and A.P. De Leenheer, *Stability study of the designer drugs "MDA, MDMA and MDEA" in water, serum, whole blood, and urine under various storage temperatures*. *Forensic Science International*, 2001. **124**(1): p. 36-42.
316. Jiménez, C., *et al.*, *Stability studies of amphetamine and ephedrine derivatives in urine*. *Journal of Chromatography B*, 2006. **843**(1): p. 84-93.
317. Wenholz, D.S., *et al.*, *A study to model the post-mortem stability of 4-MMC, MDMA and BZP in putrefying remains*. *Forensic Science International*, 2016. **265**: p. 54-60.
318. Batziris, H.P., I.M. McIntyre, and O.H. Drummer, *The effect of sulfur-metabolising bacteria on sulfur-containing psychotropic drugs*. *International Biodeterioration & Biodegradation*, 1999. **44**(2-3): p. III-III6.
319. Lutfi, L.A., *Stability of drugs of forensic interest in post mortem blood*, in Department of Forensic Medicine and Science, University of Glasgow. 1998. Doctor of Philosophy.
320. Yonemitsu, K. and D.J. Pounder, *Postmortem changes in blood tranlycypromine concentration: Competing redistribution and degradation effects*. *Forensic Science International*, 1993. **59**(2): p. 177-184.
321. Sykutera, M., E. Pufal, and K. Sliwka, *The influence of temperature and time of storage on the stability of fluoxetine in biological material*. *Z Zagadnien Nauk Sadowych*, 2002. **50**: p. 5-16.
322. McIntyre, I.M., P. Mallett, and R. Stabley, *Postmortem distribution of trazodone concentrations*. *Forensic Science International*, 2015. **251**: p. 195-201.
323. Mannens, G., *et al.*, *Absorption, metabolism, and excretion of risperidone in humans*. *Drug Metabolism and Disposition*, 1993. **21**(6): p. 1134-1141.
324. Vermeir, M., *et al.*, *Absorption, Metabolism, and Excretion of Paliperidone, a New Monoaminergic Antagonist, in Humans*. *Drug Metabolism and Disposition*, 2008. **36**(4): p. 769-779.
325. McKay, G., J.K. Cooper, and K.K. Midha, *The effect of sample storage on the stability of chlorpromazine in plasma and whole blood*. *Journal of Pharmacological Methods*, 1984. **12**(3): p. 221-223.
326. Coutselinis, A., G. Dimopoulos, and C. Dritsas, *Fatal intoxication with chlorpromazine with special regard to the influence of putrefaction on its toxicological analysis*. *Forensic Science*, 1974. **4**: p. 191-194.
327. Duffort, G., *et al.*, *Étude de la stabilité in vitro de 21 antidépresseurs et de 16 neuroleptiques dans le sang total*. *Annales de Toxicologie Analytique*, 2005. **17**(3): p. 195-202.
328. Heller, S., *et al.*, *Assessment of storage and transport stability of new antidepressant and antipsychotic drugs for a nationwide TDM service*. *Therapeutic Drug Monitoring*, 2004. **26**(4): p. 459-461.
329. Karinen, R., *et al.*, *Comparison of the Stability of Stock Solutions of Drugs of Abuse and Other Drugs Stored in a Freezer, Refrigerator, and at Ambient Temperature for Up to One Year*. *Journal of Analytical Toxicology*, 2011. **35**(8): p. 583-590.
330. Robertson, M.D. and O.H. Drummer, *Stability of nitrobenzodiazepines in postmortem blood*. *Journal of Forensic Sciences*, 1998. **43**(1): p. 5-8.
331. Skopp, G., *et al.*, *A preliminary study on the stability of benzodiazepines in blood and plasma stored at 4°C*. *International Journal of Legal Medicine*, 1997. **111**(1): p. 1-5.
332. El Mahjoub, A. and C. Staub, *Stability of benzodiazepines in whole blood samples stored at varying temperatures*. *Journal of Pharmaceutical and Biomedical Analysis*, 2000. **23**(6): p. 1057-1063.
333. Pépin, G., N. Dubourvieux, and Y. Gaillard, *Difficulty of interpretation of rates concerning benzodiazepines and other anxiolytic molecules in post mortem blood taken during autopsy: Study of their degradation in vitro after 6-months storage at different temperatures*. *Journal de Medecine Legale Droit Medical*, 1998. **41**(5): p. 341-353.
334. Al-Hadidi, K.A. and J.S. Oliver, *Stability of temazepam in blood*. *Science & Justice*, 1995. **35**(2): p. 105-108.

335. Levine, B., R. Blanke, and J. Valentour, *Postmortem stability of benzodiazepines in blood and tissues*. Journal of Forensic Sciences, 1983. **28**(1): p. 102-115.
336. Melo, P., M.L. Bastos, and H.M. Teixeira, *Benzodiazepine Stability in Postmortem Samples Stored at Different Temperatures*. Journal of Analytical Toxicology, 2012. **36**(1): p. 52-60.
337. Entwistle, N., *et al.*, *The Occurrence of Chlordiazepoxide Degradation Products in Sudden Deaths Associated with Chlordiazepoxide Overdosage*. Journal of the Forensic Science Society, 1986. **26**(1): p. 45-54.
338. Alfazil, A.A., *Stability of drugs and pesticides of forensic toxicological interest and their metabolites in biological samples.*, in Department of Forensic Medicine and Science, University of Glasgow. 2009. Doctor of Philosophy.
339. Martindale, S.M., R.H. Powers, and S.C. Bell, *Production of human metabolites by gastrointestinal bacteria as a potential source of post-mortem alteration of antemortem drug/metabolite concentrations*. Drug Testing and Analysis, 2015. **7**(1): p. 75-82.
340. Johnson, J.R., *et al.*, *Stability of Δ^9 -Tetrahydrocannabinol (THC), 11-Hydroxy-THC, and 11-Nor-9-carboxy-THC in Blood and Plasma*. Journal of Analytical Toxicology, 1984. **8**(5): p. 202-204.
341. Skopp, G. and L. Pötsch, *An Investigation of the Stability of Free and Glucuronidated 11-Nor- Δ^9 -Tetrahydrocannabinol-9-carboxylic Acid in Authentic Urine Samples*. Journal of Analytical Toxicology, 2004. **28**(1): p. 35-40.
342. Scheidweiler, K.B., *et al.*, *In vitro stability of free and glucuronidated cannabinoids in blood and plasma collected in plastic gray-top sodium fluoride tubes following controlled smoked cannabis*. Forensic Toxicology, 2016. **34**(1): p. 179-185.
343. Larsen, N.A., *et al.*, *Crystal structure of a bacterial cocaine esterase*. Nature Structural & Molecular Biology, 2002. **9**(1): p. 17-21.
344. Stewart, D.J., *et al.*, *Hydrolysis of cocaine in human plasma by cholinesterase*. Life Sciences, 1977. **20**(9): p. 1557-1563.
345. Baselt, R.C., *et al.*, *Improved long-term stability of blood cocaine in evacuated collection tubes*. Journal of Forensic Sciences, 1993. **38**(4): p. 935-937.
346. Moriya, F. and Y. Hashimoto, *Postmortem stability of cocaine and cocaethylene in blood and tissues of humans and rabbits*. Journal of Forensic Sciences, 1996. **41**(4): p. 612-616.
347. Logan, B.K., *Ecgonine is an important marker for cocaine use in inadequately preserved specimens*. Journal of Analytical Toxicology, 2001. **25**: p. 219-220.
348. Castro, A.L., *et al.*, *Gamma-hydroxybutyric acid endogenous production and post-mortem behaviour – The importance of different biological matrices, cut-off reference values, sample collection and storage conditions*. Journal of Forensic and Legal Medicine, 2014. **27**: p. 17-24.
349. Moriya, F. and Y. Hashimoto, *Site-dependent production of γ -hydroxybutyric acid in the early postmortem period*. Forensic Science International, 2005. **148**(2): p. 139-142.
350. Kintz, P., *et al.*, *GHB in postmortem toxicology: Discrimination between endogenous production from exposure using multiple specimens*. Forensic Science International, 2004. **143**(2-3): p. 177-181.
351. Korb, A.-S. and G. Cooper, *Endogenous Concentrations of GHB in Postmortem Blood from Deaths Unrelated to GHB Use*. Journal of Analytical Toxicology, 2014. **38**(8): p. 582-588.
352. Elliott, S., *The Presence of Gamma-Hydroxybutyric Acid (GHB) in Postmortem Biological Fluids*. Journal of Analytical Toxicology, 2001. **25**(2): p. 152.
353. Zvosec, D.L., *et al.*, *Case series of 226 γ -hydroxybutyrate-associated deaths: lethal toxicity and trauma*. The American Journal of Emergency Medicine, 2011. **29**(3): p. 319-332.
354. Beránková, K., K. Mutnanská, and M. Balíková, *Gamma-hydroxybutyric acid stability and formation in blood and urine*. Forensic Science International, 2006. **161**(2): p. 158-162.

355. Fjeld, B., *et al.*, Long-term stability of GHB in post-mortem samples and samples from living persons, stored at -20°C, using fluoride preservatives. *Forensic Science International*, 2012. **222**(1): p. 47-51.
356. Jones, A.W., *et al.*, Stability of γ -Hydroxybutyrate in Blood Samples from Impaired Drivers after Storage at 4°C and Comparison of GC-FID-GBL and LC-MS-MS Methods of Analysis. *Journal of Analytical Toxicology*, 2015. **39**(4): p. 294-299.
357. Andresen-Streichert, H., *et al.*, Endogenous gamma-hydroxybutyric acid (GHB) concentrations in post-mortem specimens and further recommendation for interpretative cut-offs. *International Journal of Legal Medicine*, 2015. **129**(1): p. 57-68.
358. Petersen, I.N., *et al.*, Identification of a New Metabolite of GHB: Gamma-Hydroxybutyric Acid Glucuronide. *Journal of Analytical Toxicology*, 2013. **37**(5): p. 291-297.
359. Marinetti, L.J., *γ -Hydroxybutyric Acid and Its Analogs, γ -Butyrolactone and 1,4-Butanediol, in Benzodiazepines and GHB*. S.J. Salamone, Editor. 2001, Totowa, USA: Humana Press. p. 95-126.
360. Hanisch, S., N. Stachel, and G. Skopp, A potential new metabolite of gamma-hydroxybutyrate: sulfonated gamma-hydroxybutyric acid. *International Journal of Legal Medicine*, 2016. **130**(2): p. 411-414.
361. Høiseth, G., *et al.*, Long-term stability of morphine, codeine, and 6-acetylmorphine in real-life whole blood samples, stored at -20°C. *Forensic Science International*, 2014. **239**: p. 6-10.
362. Papoutsis, I., *et al.*, Stability of Morphine, Codeine, and 6-Acetylmorphine in Blood at Different Sampling and Storage Conditions. *Journal of Forensic Sciences*, 2014. **59**(2): p. 550-554.
363. Hadidi, K.A. and J.S. Oliver, Stability of morphine and buprenorphine in whole blood. *International Journal of Legal Medicine*, 1998. **III**(3): p. 165-167.
364. Lin, D.-L., H. Liu, and C.-Y. Chen, Storage Temperature Effect on the Stability of Morphine and Codeine in Urine. *Journal of Analytical Toxicology*, 1995. **19**(5): p. 275-280.
365. Moriya, F. and Y. Hashimoto, Distribution of free and conjugated morphine in body fluids and tissues in a fatal heroin overdose: is conjugated morphine stable in postmortem specimens? *Journal of Forensic Sciences*, 1997. **42**(4): p. 736-740.
366. Skopp, G., *et al.*, Stability of Morphine, Morphine-3-Glucuronide, and Morphine-6-Glucuronide in Fresh Blood and Plasma and Postmortem Blood Samples. *Journal of Analytical Toxicology*, 2001. **25**(1): p. 2-7.
367. Munro, G. and C. Wilkin, *New Psychoactive Drugs: No Easy Answer*. Australian Drug Foundation. 2014, Melbourne, Australia.
368. Goggin, L.S., N. Gately, and R.I. Bridle, Novel Psychoactive Substance and Other Drug Use by Young Adults in Western Australia. *Journal of Psychoactive Drugs*, 2015. **47**(2): p. 140-148.
369. Johnson, R.D. and S.R. Botch-Jones, The Stability of Four Designer Drugs: MDPV, Mephedrone, BZP and TFMPP in Three Biological Matrices under Various Storage Conditions. *Journal of Analytical Toxicology*, 2013. **37**(2): p. 51-55.
370. Busardò, F.P., *et al.*, Assessment of the stability of mephedrone in ante-mortem and post-mortem blood specimens. *Forensic Science International*, 2015. **256**: p. 28-37.
371. Couper, F.J. and O.H. Drummer, Postmortem stability and interpretation of beta 2-agonist concentrations. *Journal of Forensic Sciences*, 1999. **44**(3): p. 523-526.
372. Battah, A.H. and K.A. Hadidi, Stability of trihexyphenidyl in stored blood and urine specimens. *International Journal of Legal Medicine*, 1998. **III**(3): p. 111-114.
373. Kiencke, V., *et al.*, Quantitative determination of valproic acid in postmortem blood samples—evidence of strong matrix dependency and instability. *International Journal of Legal Medicine*, 2013. **127**(6): p. 1101-1107.
374. Nilsson, G.H., *et al.*, Quantitative Analysis of Zopiclone, N-desmethylzopiclone, Zopiclone N-oxide and 2-Amino-5-chloropyridine in Urine Using LC-MS-MS. *Journal of Analytical Toxicology*, 2014. **38**(6): p. 327-334.

375. Pounder, D.J. and J.I. Davies, *Zopiclone poisoning: tissue distribution and potential for postmortem diffusion*. *Forensic Science International*, 1994. **65**(3): p. 177-183.
376. Jantos, R., et al., *Degradation of zopiclone during storage of spiked and authentic whole blood and matching dried blood spots*. *International Journal of Legal Medicine*, 2013. **127**(1): p. 69-76.
377. Nilsson, G.H., et al., *Stability tests of zopiclone in whole blood*. *Forensic Science International*, 2010. **200**(1-3): p. 130-135.
378. Nilsson, G.H., et al., *Influence of pre-analytical conditions on the interpretation of zopiclone concentrations in whole blood*. *Forensic Science International*, 2011. **207**(1-3): p. 35-39.
379. Lokan, R.J., R.A. James, and R.B. Dymock, *Apparent post-mortem production of high levels of cyanide in blood*. *Journal of the Forensic Science Society*, 1987. **27**(4): p. 253-259.
380. McAllister, J.L., et al., *Stability of Cyanide in Cadavers and in Postmortem Stored Tissue Specimens: A Review*. *Journal of Analytical Toxicology*, 2008. **32**(8): p. 612-620.
381. McAllister, J.L., et al., *The effect of sodium fluoride on the stability of cyanide in postmortem blood samples from fire victims*. *Forensic Science International*, 2011. **209**(1-3): p. 29-33.
382. Gomes, R., R. Liteplo, and M. Meek, *Ethylene glycol: human health aspects*, in *Concise international chemical assessment document 45*. 2002, Geneva, Switzerland: World Health Organization.
383. Wurita, A., et al., *Sensitive determination of ethylene glycol, propylene glycol and diethylene glycol in human whole blood by isotope dilution gas chromatography-mass spectrometry, and the presence of appreciable amounts of the glycols in blood of healthy subjects*. *Forensic Toxicology*, 2013. **31**(2): p. 272-280.
384. Wurita, A., et al., *Occurrence of postmortem production of ethylene glycol and propylene glycol in human specimens*. *Forensic Toxicology*, 2014. **32**(1): p. 162-168.
385. Wurita, A., et al., *Presence of appreciable amounts of ethylene glycol, propylene glycol, and diethylene glycol in human urine of healthy subjects*. *Forensic Toxicology*, 2014. **32**(1): p. 39-44.
386. Rosano, T.G., et al., *Ethylene Glycol and Glycolic Acid in Postmortem Blood from Fatal Poisonings*. *Journal of Analytical Toxicology*, 2009. **33**(8): p. 508-513.
387. Toth-Manikowski, S.M., H. Menn-Josephy, and J. Bhatia, *A Case of Chronic Ethylene Glycol Intoxication Presenting without Classic Metabolic Derangements*. *Case Reports in Nephrology*, 2014. **2014**: p. 128145.
388. Viinamäki, J., A. Sajantila, and I. Ojanperä, *Ethylene Glycol and Metabolite Concentrations in Fatal Ethylene Glycol Poisonings*. *Journal of Analytical Toxicology*, 2015. **39**(6): p. 481-485.
389. Viinamäki, J., et al., *Elevated formic acid concentrations in putrefied post-mortem blood and urine samples*. *Forensic Science International*, 2011. **208**(1-3): p. 42-46.
390. Magnuson, B.A., et al., *Aspartame: a safety evaluation based on current use levels, regulations, and toxicological and epidemiological studies*. *Critical Reviews in Toxicology*, 2007. **37**(8): p. 629-727.
391. Jones, G.R., P.P. Singer, and K. Rittenbach, *The Relationship of Methanol and Formate Concentrations in Fatalities Where Methanol Is Detected*. *Journal of Forensic Sciences*, 2007. **52**(6): p. 1376-1382.
392. Wallage, H.R. and J.H. Watterson, *Formic acid and methanol concentrations in death investigations*. *Journal of Analytical Toxicology*, 2008. **32**(3): p. 241-247.
393. Schiwarra, H.W., H. Siegel, and A. Goebel, *Increase and decrease in formic acid concentration in urine samples stored at room temperature*. *European Journal of Clinical Chemistry and Clinical Biochemistry*, 1992. **30**(2): p. 75-79.
394. Carroll, F.T., et al., *Morphine-3-D glucuronide stability in postmortem specimens exposed to bacterial enzymatic hydrolysis*. *The American Journal of Forensic Medicine and Pathology*, 2000. **21**(4): p. 323-329.

395. Thai, K., *Investigation of paracetamol production in-vitro in biological samples via degradation of its three main metabolites*, in School of Chemical and Physical Sciences, Flinders University. 2013. Bachelor of Science (Forensic and Analytical Chemistry) (Honours).
396. Liu, Y., et al., *Stability of Ethyl Glucuronide, Ethyl Sulfate, Phosphatidylethanol and Fatty Acid Ethyl Esters in Postmortem Human Blood*. *Journal of Analytical Toxicology*, 2018. **42**(5): p. 346-352.
397. Piper, T., et al., *Potential of GHB phase-II-metabolites to complement current approaches in GHB post administration detection*. *Forensic Science International*, 2017. **279**: p. 157-164.
398. Mehling, L.-M., et al., *GHB-O- β -glucuronide in blood and urine is not a suitable tool for the extension of the detection window after GHB intake*. *Forensic Toxicology*, 2017. **35**(2): p. 263-274.
399. Tittarelli, R., et al., *Ultra-high-performance liquid chromatography tandem mass spectrometry determination of GHB, GHB-glucuronide in plasma and cerebrospinal fluid of narcoleptic patients under sodium oxybate treatment*. *Forensic Science International*, 2017. **274**: p. 70-74.
400. Watanabe, S., et al., *Biotransformation of synthetic cannabinoids JWH-018, JWH-073 and AM2201 by *Cunninghamella elegans**. *Forensic Science International*, 2016. **261**: p. 33-42.
401. Staeheli, S.N., et al., *Time-dependent postmortem redistribution of morphine and its metabolites in blood and alternative matrices—application of CT-guided biopsy sampling*. *International Journal of Legal Medicine*, 2017. **131**(2): p. 379-389.
402. Sørensen, L.K. and J.B. Hasselstrøm, *Ascorbic Acid Improves the Stability of Buprenorphine in Frozen Whole Blood Samples*. *Journal of Analytical Toxicology*, 2019. **43**(6): p. 482-488.
403. Saar, E., et al., *Identification of 2-hydroxymethyl-olanzapine as a novel degradation product of olanzapine*. *Forensic Science International*, 2012. **220**(1-3): p. 74-79.
404. Sørensen, L.K. and J.B. Hasselstrøm, *The effect of antioxidants on the long-term stability of THC and related cannabinoids in sampled whole blood*. *Drug Testing and Analysis*, 2018. **10**(2): p. 301-309.
405. Sørensen, L.K. and J.B. Hasselstrøm, *Stability of propofol in sampled antemortem blood*, in The 53rd TIAFT Meeting. 2015. Florence, Italy.
406. Glicksberg, L. and S. Kerrigan, *Stability of Synthetic Cathinones in Blood*. *Journal of Analytical Toxicology*, 2017. **41**(9): p. 711-719.
407. Adamowicz, P. and A. Malczyk, *Stability of synthetic cathinones in blood and urine*. *Forensic Science International*, 2019. **295**: p. 36-45.
408. Czerwinska, J., et al., *Stability of mephedrone and five of its phase I metabolites in human whole blood*. *Drug Testing and Analysis*, 2018. **11**(4): p. 586-594.
409. Kitamura, S., et al., *The role of mammalian intestinal bacteria in the reductive metabolism of zonisamide*. *Journal of Pharmacy and Pharmacology*, 1997. **49**(3): p. 253-256.
410. Mutlib, A.E., J.T. Strupczewski, and S.M. Chesson, *Application of hyphenated LC/NMR and LC/MS techniques in rapid identification of in vitro and in vivo metabolites of iloperidone*. *Drug Metabolism and Disposition*, 1995. **23**(9): p. 951-964.
411. Stiff, D.D., J.T. Robicheau, and M.A. Zemaitis, *Reductive metabolism of the anticonvulsant agent zonisamide, a 1, 2-benzisoxazole derivative*. *Xenobiotica*, 1992. **22**(1): p. 1-11.
412. Lane, D.J., *16S/23S rRNA sequencing*, in *Nucleic acid techniques in bacterial systematics*. E. Stackebrandt and M. Goodfellow, Editors. 1991, New York, USA: John Wiley and Sons. p. 115-175.
413. Osborn, A.M., E.R. Moore, and K.N. Timmis, *An evaluation of terminal-restriction fragment length polymorphism (T - RFLP) analysis for the study of microbial community structure and dynamics*. *Environmental Microbiology*, 2000. **2**(1): p. 39-50.
414. Benson, S., *I Need to Know What's In a Bag of Blood?* *Transfusion Fact Sheet*, 2011. **3**(9).
415. Peck, C.C., et al., *Adenine Blood Preservation*. *CRC Critical Reviews in Clinical Laboratory Sciences*, 1981. **13**(3): p. 173-212.

416. Frank Henderson, J., *Inhibition of microbial growth by naturally-occurring purine bases and ribonucleosides*. *Pharmacology & Therapeutics*, 1980. **8**(3): p. 605-627.
417. Costello, S.P., *et al.*, *Establishing a fecal microbiota transplant service for the treatment of Clostridium difficile infection*. *Clinical Infectious Diseases*, 2016. **62**(7): p. 908-914.
418. Junkins, E.N., E.R. Hyde, and D.O. Carter, *Culture and long-term storage of microorganisms for forensic science*, in *Forensic Microbiology*. D.O. Carter, *et al.*, Editors. 2017, Hoboken, USA: John Wiley & Sons, Ltd. p. 127-145.
419. Kraus, D., *Consolidated data analysis and presentation using an open-source add-in for the Microsoft Excel® spreadsheet software*. *Medical Writing*, 2014. **23**(1): p. 25-28.
420. Hammer, Ø., D.A. Harper, and P.D. Ryan, *PAST: paleontological statistics software package for education and data analysis*. *Palaeontologia Electronica*, 2001. **4**(1): p. 9.
421. Ruxton, G.D., *The unequal variance t-test is an underused alternative to Student's t-test and the Mann-Whitney U test*. *Behavioral Ecology*, 2006. **17**(4): p. 688-690.
422. Saar, E., *et al.*, *Identification and quantification of 30 antipsychotics in blood using LC - MS/MS*. *Journal of Mass Spectrometry*, 2010. **45**(8): p. 915-925.
423. Rop, P.P., *Concentrations of cis(Z)-Clopenthixol and trans(E)-Clopenthixol in a Lethal Case Involving Zuclopenthixol, Diazepam, and Cyamemazine*. *Journal of Analytical Toxicology*, 2001. **25**(5): p. 348-352.
424. Therapeutic Goods Administration, *CLOPIXOL® Film-Coated Tablets, Clopixol Acuphase Injection, Clopixol Depot Injection - Product Information*. 2013.
425. Hawes, E.M., *et al.*, *Therapeutic monitoring of chlorpromazine. III: Minimal interconversion between chlorpromazine and metabolites in human blood*. *Therapeutic Drug Monitoring*, 1986. **8**(1): p. 37-41.
426. McKay, G., *et al.*, *Therapeutic monitoring of chlorpromazine II: Pitfalls in whole blood analysis*. *Therapeutic Drug Monitoring*, 1985. **7**(4): p. 472-477.
427. Campbell, C., H. Cornthwaite, and J. Watterson, *Oxidation of Selected Phenothiazine Drugs During Sample Preparation: Effects of Varying Extraction Conditions on the Extent of Oxidation*. *Journal of Analytical Toxicology*, 2017. **42**(2): p. 99-114.
428. Traficante, L.J., *et al.*, *Rapid in vitro sulfoxidation of chlorpromazine by human blood: Inhibition by an endogenous plasma protein factor*. *Life Sciences*, 1979. **24**(4): p. 337-345.
429. Strong, H.A., *et al.*, *The reduction of sulphinpyrazone and sulindac by intestinal bacteria*. *Xenobiotica*, 1987. **17**(6): p. 685-696.
430. Eap, C.B., L. Koeb, and P. Baumann, *Artifacts in the analysis of thioridazine and other neuroleptics*. *Journal of Pharmaceutical and Biomedical Analysis*, 1993. **11**(6): p. 451-457.
431. Gu, H., *et al.*, *Selecting the Correct Weighting Factors for Linear and Quadratic Calibration Curves with Least-Squares Regression Algorithm in Bioanalytical LC-MS/MS Assays and Impacts of Using Incorrect Weighting Factors on Curve Stability, Data Quality, and Assay Performance*. *Analytical Chemistry*, 2014. **86**(18): p. 8959-8966.
432. Kumar Talluri, M.V.N., *et al.*, *Structural characterization of alkaline and oxidative stressed degradation products of lurasidone using LC/ESI/QTOF/MS/MS*. *Journal of Pharmaceutical and Biomedical Analysis*, 2015. **105**: p. 1-9.
433. Carter, D.O., *Personal communications*. 2016.
434. Shija, R., V. Bruce Sunderland, and C. McDonald, *Alkaline hydrolysis of methyl, ethyl and n-propyl 4-hydroxybenzoate esters in the liquid and frozen states*. *International Journal of Pharmaceutics*, 1992. **80**(1): p. 203-211.
435. Concannon, J., *et al.*, *Stability of aqueous solutions of amoxicillin sodium in the frozen and liquid states*. *American Journal of Hospital Pharmacy*, 1986. **43**(12): p. 3027-3030.

436. Mata, D.C., *Stability of 26 Sedative Hypnotics in Six Toxicological Matrices at Different Storage Conditions*. Journal of Analytical Toxicology, 2016. **40**(8): p. 663-668.
437. Wyman, J.F., *et al.*, *The Temporal Fate of Drugs in Decomposing Porcine Tissue*. Journal of Forensic Sciences, 2011. **56**(3): p. 694-699.
438. Joint Committee for Guides in Metrology, *JGCM 100: 2008 (GUM 1995 with minor corrections)*, in *Evaluation of measurement data-Guide to the expression of uncertainty in measurement*. 2008.
439. Sandven, P. and J. Lassen, *Importance of Selective Media for Recovery of Yeasts from Clinical Specimens*. Journal of Clinical Microbiology, 1999. **37**(11): p. 3731-3732.
440. Khelaifia, S., D. Raoult, and M. Drancourt, *A Versatile Medium for Cultivating Methanogenic Archaea*. PLoS ONE, 2013. **8**(4): p. e61563.
441. MoBio Laboratories, I., *PowerSoil® DNA Isolation Kit: Instruction Manual*. 2013.
442. Hart, M.L., *et al.*, *Comparative evaluation of DNA extraction methods from feces of multiple host species for downstream next-generation sequencing*. PLoS ONE, 2015. **10**(11): p. e0143334.
443. Lou, J., *Entropy and diversity*. Oikos, 2006. **113**(2): p. 363-375.
444. Anderson, M., R.N. Gorley, and R.K. Clarke, *Permanova+ for primer: Guide to software and statistical methods. First edition*. 2008: Primer-E Limited.
445. Bray, J.R. and J.T. Curtis, *An ordination of the upland forest communities of southern Wisconsin*. Ecological Monographs, 1957. **27**(4): p. 325-349.
446. Lagier, J.C., *et al.*, *Microbial culturomics: paradigm shift in the human gut microbiome study*. Clinical Microbiology and Infection, 2012. **18**(12): p. 1185-1193.
447. Beutler, E. and C. West, *Simplified determination of carboxyhemoglobin*. Clinical Chemistry, 1984. **30**(6): p. 871-874.
448. Høiseth, G., *et al.*, *In vitro formation of ethanol in autopsy samples containing fluoride ions*. International Journal of Legal Medicine, 2008. **122**(1): p. 63-66.
449. Jones, A.W., *et al.*, *Storage of specimens at 4 C or addition of sodium fluoride (1%) prevents formation of ethanol in urine inoculated with Candida albicans*. Journal of Analytical Toxicology, 1999. **23**(5): p. 333-336.
450. Labbe, R.G. and T.H. Huang, *Generation times and modeling of enterotoxin-positive and enterotoxin-negative strains of Clostridium perfringens in laboratory media and ground beef*. Journal of Food Protection, 1995. **58**(12): p. 1303-1306.
451. Rocha, E.R. and C.J. Smith, *Haem and Iron Metabolism in Bacteroides*, in *Iron uptake and homeostasis in microorganisms*. P. Cornelis and S.C. Andrews, Editors. 2010, Norfolk, UK: Horizon Scientific Press. p. 153-166.
452. Dayer, M.R., A.A. Moosavi-Movahedi, and M.S. Dayer, *Band assignment in hemoglobin porphyrin ring spectrum: Using four-orbital model of Gouterman*. Protein & Peptide Letters, 2010. **17**(4): p. 473-479.
453. Malinski, T., E. Kubaszewski, and F. Kiechle, *Electrochemical and Spectroscopic Methods of Nitric Oxide Detection*, in *Nitric Oxide Synthase, Characterization and Functional Analysis*. M.D. Maines, Editor. 1996, San Diego, USA: Academic Press. p. 14-33.
454. Russo, S.F. and R.B. Sorstokke, *Hemoglobin. Isolation and chemical properties*. Journal of Chemical Education, 1973. **50**(5): p. 347.
455. Haiying, Z., *et al.*, *Mass defect filter technique and its applications to drug metabolite identification by high - resolution mass spectrometry*. Journal of Mass Spectrometry, 2009. **44**(7): p. 999-1016.
456. Supelco Technical Service Department, *Acetic anhydride product specification*. 1997, Bellefonte, USA: Sigma-Aldrich.
457. Starke, D.W., K.S. Blisard, and J.J. Mieyal, *Substrate specificity of the monooxygenase activity of hemoglobin*. Molecular Pharmacology, 1984. **25**(3): p. 467-475.

458. Wandersman, C. and C. Simon, *Haem uptake and iron extraction by bacteria*, in *Iron Uptake and Homeostasis in Microorganisms*. P. Cornelis and S.C. Andrews, Editors. 2010, Norfolk, UK: Horizon Scientific Press. p. 17-31.
459. Blaiseau, P.L., *et al.*, *Iron uptake in yeasts*, in *Iron Uptake and Homeostasis in Microorganisms*. P. Cornelis and S.C. Andrews, Editors. 2010, Norfolk, UK: Horizon Scientific Press. p. 265-284.
460. Uno, H. and M. Kurokawa, *Studies on 3-substituted 1, 2-benzisoxazole derivatives. VII. Catalytic reduction of 3-sulfamoylmethyl-1, 2-benzisoxazole and reactions of the resulting products*. Chemical and Pharmaceutical Bulletin, 1982. **30**(1): p. 333-335.
461. Ravi Ganesh, K., *et al.*, *Enantioselective Synthesis of ((1 R, 2 R)-Cyclohexane-1, 2-diyl) bis (methylene) dimethanesulfonate, a Lurasidone Hydrochloride Intermediate*. Synthetic Communications, 2015. **45**(23): p. 2676-2682.
462. Ae, N. and Y. Fujiwara, *Process of preparing a quaternary ammonium salt using phosphate*. 2014, Google Patents.
463. Prakash, C., *et al.*, *Metabolism and Excretion of a New Antipsychotic Drug, Ziprasidone, in Humans*. Drug Metabolism and Disposition, 1997. **25**(7): p. 863-872.
464. Testa, B. and P. Jenner, *Novel drug metabolites produced by functionalization reactions: chemistry and toxicology*. Drug Metabolism Reviews, 1978. **7**(2): p. 325-369.
465. Tabacova, S., *Lurasidone pharmacology review*. 2009, Department of Health and Human Services, Public Health Service, Food and Drug Administration, Center for Drug Evaluation and Research.
466. Raj, S., *et al.*, *Development of a stability-indicating UPLC method for determining ziprasidone hydrochloride and its associated degradation products present in active pharmaceutical ingredients and pharmaceutical dosage forms*. Journal of Liquid Chromatography & Related Technologies, 2012. **36**(7): p. 968-982.
467. Skibiński, R., *Photostability study and identification of photodegradation products of ziprasidone by UHPLC-DAD/ESI-Q-TOF*. Journal of Liquid Chromatography & Related Technologies, 2012. **35**(15): p. 2097-2112.
468. Millemaggi, A. and R.J.K. Taylor, *3 - Alkenyl - oxindoles: Natural Products, Pharmaceuticals, and Recent Synthetic Advances in Tandem/Telescoped Approaches*. European Journal of Organic Chemistry, 2010. **2010**(24): p. 4527-4547.
469. Joule, J.A. and K. Mills, *Heterocyclic chemistry*. 2008, West Sussex, UK: John Wiley & Sons.
470. Bergman, J., *Oxindoles*, in *Advances in Heterocyclic Chemistry*. E.F.V. Scriven and C.A. Ramsden, Editors. 2015, New York, USA: Academic Press. p. 1-81.
471. Howard, H.R., *et al.*, *3-Benzisothiazolylpiperazine derivatives as potential atypical antipsychotic agents*. Journal of Medicinal Chemistry, 1996. **39**(1): p. 143-148.
472. Cordonnier, J. and J. Schaep, *Ultraviolet, visible and fluorescence spectrophotometry*, in *Clarke's Analytical Forensic Toxicology. Second edition*. A. Negrusz and G. Cooper, Editors. 2013, London, UK: Pharmaceutical Press. p. 425-452.
473. Nozoye, T., T. Nakai, and A. Kubo, *Reactions of Indole Related Compounds. III.(E) and (Z)-2-Oxindolin-3-ethylidenes*. Chemical and Pharmaceutical Bulletin, 1977. **25**(1): p. 196-198.
474. Peterson, C.M. and C.M. Polizzi, *Improved method for acetaldehyde in plasma and hemoglobin-associated acetaldehyde: Results in teetotalers and alcoholics reporting for treatment*. Alcohol, 1987. **4**(6): p. 477-480.
475. Chen, H.M., *et al.*, *Studies of the Oxidation of Ethanol to Acetaldehyde by Oxyhemoglobin Using Fluorogenic High - Performance Liquid Chromatography*. Alcoholism: Clinical and Experimental Research, 1994. **18**(5): p. 1202-1206.
476. Smalldon, K.W. and G.A. Brown, *The stability of ethanol in stored blood: Part II. The mechanism of ethanol oxidation*. Analytica Chimica Acta, 1973. **66**(2): p. 285-290.

477. Rossetti, A., *et al.*, *Biocatalysed olefin reduction of 3-alkylidene oxindoles by baker's yeast*. *Tetrahedron*, 2017. **73**(31): p. 4584-4590.
478. Hong, J., J.C. Shah, and M.D. McGonagle, *Effect of Cyclodextrin Derivation and Amorphous State of Complex on Accelerated Degradation of Ziprasidone*. *Journal of Pharmaceutical Sciences*, 2011. **100**(7): p. 2703-2716.
479. Czarnik, A.W., *Deuterium-enriched ziprasidone*. 2009, Google Patents.
480. Singh, A., *et al.*, *A Rapid Stability-Indicating LC Method for Ziprasidone Hydrochloride*. *Chromatographia*, 2007. **65**(3): p. 191-196.
481. M. Whirl-Carrillo, *et al.*, *Pharmacogenomics Knowledge for Personalized Medicine*. *Clinical Pharmacology & Therapeutics*, 2012. **92**(4): p. 414-417.
482. Caccia, S., *Pharmacokinetics and metabolism update for some recent antipsychotics*. *Expert Opinion on Drug Metabolism & Toxicology*, 2011. **7**(7): p. 829-846.
483. Duband, S., *et al.*, *A fatal intoxication case involving ropinirole*. *Journal of Forensic and Legal Medicine*, 2012. **19**(7): p. 422-425.
484. AdisInsight. *Drug Profile: Roluperidone - Minerva Neurosciences*. 2018 [cited 11 May 2019]; Available from: <https://adisinsight.springer.com/drugs/800029911>.
485. Lew, A., Q. Gao, and L.H. Takahashi, *Analysis and identification of prochlorperazine impurities and forced degradation products using a stability-indicating hplc method*. *Journal of Liquid Chromatography & Related Technologies*, 2011. **34**(8): p. 634-651.
486. Huang, C.L. and F.L. Sands, *Effect of ultraviolet irradiation on chlorpromazine II. Anaerobic condition*. *Journal of Pharmaceutical Sciences*, 1967. **56**(2): p. 259-264.
487. Trautwein, C. and K. Kümmerer, *Degradation of the tricyclic antipsychotic drug chlorpromazine under environmental conditions, identification of its main aquatic biotic and abiotic transformation products by LC-MSn and their effects on environmental bacteria*. *Journal of Chromatography B*, 2012. **889-890**: p. 24-38.
488. Ley, R.E., D.A. Peterson, and J.I. Gordon, *Ecological and Evolutionary Forces Shaping Microbial Diversity in the Human Intestine*. *Cell*, 2006. **124**(4): p. 837-848.
489. Eckburg, P.B., *et al.*, *Diversity of the Human Intestinal Microbial Flora*. *Science*, 2005. **308**(5728): p. 1635-1638.
490. Carter, D.O., E.N. Junkins, and W.A. Kodama, *A primer on microbiology*, in *Forensic Microbiology*. D.O. Carter, *et al.*, Editors. 2017, Hoboken, USA: John Wiley & Sons, Ltd. p. 1-24.